

**CHARACTERIZATION OF *MYOCBACTERIUM* SP. P450 SYSTEMS**

**Thesis submitted for the degree of  
Doctor of Philosophy  
at the University of Leicester**

**by**

**David Geraint Lewis BSc (Cardiff)  
Department of Biochemistry  
University of Leicester**

**October 2007**

## **Declaration**

The work presented in this thesis is the original work of the author, except where specific reference is made to other sources. It has not been submitted in part, or in whole for any other degree.

D. Geraint Lewis

## **Acknowledgements**

I would like to thank a number of people who have helped and supported me during this PhD. Firstly, I would like to express my deep and sincere gratitude to my supervisor, Prof. Andrew Munro. His knowledge, understanding, encouragement and personal guidance has been of great value to me. A large thank you must also go to my various lab colleagues over the years which have made the PhD enjoyable. In particular, a special mention must go to Dr Kirsty McLean (University of Manchester) and Dr Ker Marshall (University of Leicester) for ‘teaching me the ropes’.

I also wish to express my gratitude to Dr David Leys (University of Manchester) for the crystallography of the CYP121 mutants and to a number of other people including Dr Myles Cheesman at UEA for assistance with EPR and MCD, Prof Ewen Smith (University of Strathclyde) for resonance Raman, Dr Hui Hong (University of Cambridge), Prof. Stewart Cole, Dr. Mary Jackson, Dr. Laurent Marsollier (all Institut Pasteur, Paris) with identification of substrate and determination of MICs and Dr Timothy Stinear (Monash University) for the opportunity to clone CYP140A2 and for providing mycolactone C.

# Abstract

This work reports detailed structural and mechanistic characterisation of three cytochrome P450 (CYP) enzymes from diverse mycobacteria.

For *Mycobacterium tuberculosis* (Mtb) CYP121, a high resolution atomic structure revealed mutagenesis targets to explore structure/function relationships. Several mutants were generated and structurally characterised. The R386L variant disrupted heme coordination environment, producing an enzyme with shifted Soret absorption features and predominantly high-spin ferric heme iron. EPR and resonance Raman spectra confirmed the spin-state conversion. The P346L variant resulted in altered heme conformation due to perturbed interactions with the heme pyrrole D ring. Alterations to heme ligation state were observed from EPR studies. Ligand binding and thermodynamic studies were done on CYP121 mutants. Studies of the action of various azole based drugs (which bind tightly to CYP121 heme iron) showed that azoles had potent inhibitory effects on Mtb growth.

*Mycobacterium ulcerans*, the aetiological agent of Buruli ulcer, produces a human toxin (mycolactone) and encodes CYP140A2 on a plasmid, with the *CYP140A2* gene adjacent to other mycolactone biosynthetic genes. Purified oxidised CYP140A2 has a Soret absorption band at 418 nm and  $\alpha/\beta$  bands at 567/534 nm, respectively. The Fe(II)CO complex conforms to typical P450 properties, with a characteristic Soret shift to 449 nm. Resonance Raman and EPR spectra confirm the protein to be low-spin and with a typical cysteinate- and water-ligated *b*-type heme iron. Azole drugs were shown to bind CYP140A2 tightly, and to be potential therapeutics. CYP140A2 catalysed hydroxylation of mycolactone precursor molecules, consistent with its proposed role in synthesis of the toxic polyketide.

*Mycobacterium* sp HE5 CYP151A2 was shown to have a role in metabolism of secondary amines, such as morpholine. CYP151A2 was expressed and purified, and spectroscopic analyses were consistent with cysteinate- and aqua-ligated heme iron. Dithionite reduction of CYP151A2 induced non-standard spectral changes, with a blue-shifted Soret band indicative of a cysteine thiolate-to-thiol switch in heme ligation. Thiolate coordination was restored on oxidation of CYP151A2, indicating that the thiol is readily deprotonated to thiolate in the ferric form. An  $\epsilon_{419}$  of 186 mM<sup>-1</sup> cm<sup>-1</sup> was determined for oxidised CYP151A2 and (at high concentration) morpholine substrate was shown to coordinate heme iron as an inhibitor at high concentrations.

# Abbreviations

## Amino Acids

	Code	Symbol
Alanine	Ala	A
Arginine	Arg	R
Aspartate	Asp	D
Asparagine	Asn	N
Cysteine	Cys	C
Glutamate	Glu	E
Glutamine	Gln	Q
Glycine	Gly	G
Histidine	His	H
Isoleucine	Ile	I
Leucine	Leu	L
Lysine	Lys	K
Methionine	Met	M
Phenylalanine	Phe	F
Proline	Pro	P
Serine	Ser	S
Threonine	Thr	T
Tryptophan	Trp	W
Tyrosine	Tyr	Y
Valine	Val	V

## Oligonucleotides

A - Adenine, C – Cytosine, G – Guanine, T – Thymine

## Standard units

m	metre
g	gram
s	second
l	litre
Da	Dalton
°C	degrees Celsius
M	molar
V	volt
Å	Angstrom
K	degrees Kelvin

## Textual Abbreviations

Abs	absorbance
ACP	acyl carrier protein
ADR	adrenodoxin reductase
Adx	adrenodoxin
APS	ammonium persulfate
AraLAM	non-mannose capped lipoarabinomannan
ATP	adenosine triphosphate
BCG	Bacille Calmette-Guérin
BSA	bovine serum albumin
CD	circular dichroism
CIAP	calf intestinal alkaline phosphatase
CPR	cytochrome P450 reductase
CYP	cytochrome P450
dH <sub>2</sub> O	distilled water
DMSO	dimethylsulfoxide
DNA	deoxyribonucleic acid
dNTP	deoxyribonucleotide triphosphate
DOTS	directly observed treatment short-course
DTT	dithiothreitol
<i>E. coli</i>	<i>Escherichia coli</i>
EDTA	ethylenediaminetetraacetate
E	redox potential
EPR	electron paramagnetic resonance
FAD	flavin adenine dinucleotide
FAS I	fatty acid synthase I
FLD	<i>E. coli</i> flavodoxin
FLDR	<i>E. coli</i> flavodoxin reductase
FMN	flavin mononucleotide
FPLC	fast protein liquid chromatography
GdnHCl	guanidinium chloride
GPL	glycopeptidolipid
H <sub>4</sub> NADP	tetrahydronicotinamide adenine dinucleotide phosphate
Hq	hydroquinone
IPCS	International Programme on Chemical Safety
IPTG	isopropyl thiogalactoside
kb	kilobase
K <sub>d</sub>	dissociation constant
LAM	lipoarabinomannan
LB	Luria Bertani medium
ManLAM	mannose-capped Lipoarabinomannan
MCD	magnetic circular dichroism
MDR-TB	multidrug resistant tuberculosis
MOPS	3-morpholinopropanesulphonic acid
M <sub>r</sub>	relative molecular mass
Mtb	<i>Mycobacterium tuberculosis</i>
NAD	nicotinamide adenine dinucleotide
NADP	nicotinamide adenine dinucleotide phosphate

NHE	normal hydrogen electrode
NMR	nuclear magnetic resonance
OD	optical density
P450	cytochrome P450
PAGE	polyacrylamide gel electrophoresis
PCR	polymerase chain reaction
PDA	photodiode array
PILAM	Phospho- <i>myo</i> -inositol-capped Lipoarabinomannan
PMSF	phenylmethylsulfonyl fluoride
RNase	ribonuclease
SDS	sodium dodecyl sulfate
SRS	substrate recognition sequence
TACO	tryptophan-aspartate containing coat protein
TB	tuberculosis
TDM	trehalose-6,6'-dimycolate
TEMED	N,N,N',N'-tetramethylene diamine
Tris	tris(hydroxymethyl) aminomethane
UV	ultra violet
Vis	visible
WHO	World Health Organization
X-Gal	5-bromo-4-chloro-3-indolyl- $\beta$ -D-galactoside

## List of Figures

Figure 1.1	Cytochrome P450 catalysed hydroxylation reaction	4
Figure 1.2	Schematic representation of the structure of heme b (ferriprotoporphyrin IX)	5
Figure 1.3	The reaction cycle of a P450 monooxygenase catalysed hydroxylation	10
Figure 1.4	Domain organization of P450-containing monooxygenase systems	16
Figure 1.5	A ribbon representation of the P450cam structure (proximal face)	20
Figure 1.6	Structures of selected azole anti-fungal P450 inhibitors	25
Figure 1.7	Hydride donor/acceptor function of the nicotinamide moiety of NAD(P)H	26
Figure 1.8	Chemical structure of the isoalloxazine ring (oxidised and reduced states), the chemically reactive group of FAD and FMN flavin cofactors	27
Figure 1.9	Structures of common iron-sulphur clusters	29
Figure 1.10	Chemical structures of the premier anti-tuberculosis drugs	37
Figure 1.11	Schematic representation of the cell envelope of <i>M. tuberculosis</i>	41
Figure 1.12	Examples of lipophilic molecules found in the <i>M. tuberculosis</i> cell envelope	45
Figure 1.13	Geographic distribution of Buruli ulcer	50
Figure 1.14	A-D Clinical presentation of Buruli ulcer	52
Figure 1.15	Molecular structures of polyketides	53
Figure 1.16	Molecular structures of mycolactones	55
Figure 1.17	Domain and module organization of the mycolactone PKS genes	57
Figure 1.18	Chemical structure of morpholine	62
Figure 1.19	Pathway for morpholine catabolism	65
Figure 1.20	Proposed reaction of the morpholine-dependent cytochrome P450	76
Figure 3.1	PCR amplified fragments of <i>CYP121</i> mutants, P346L and R386L	103
Figure 3.2	<i>Bst</i> NI restriction digest of <i>CYP121</i> P346L (pGL1(a))	105
Figure 3.3	<i>Hga</i> I restriction digest of <i>CYP121</i> R386L (pGL2(a))	106
Figure 3.4	PCR amplification of <i>CYP121</i> S279A mutant	107
Figure 3.5	<i>Dpn</i> I digestion of <i>CYP121</i> S279A PCR product	108
Figure 3.6	Excision of wild-type <i>CYP121</i> fragment from pKM2(b)	109
Figure 3.7	<i>Nde</i> I restriction digest of histidine tagged <i>CYP121</i> (pGL3(a))	110
Figure 3.8	Time-lapsed expression of the P346L mutant of <i>CYP121</i>	112
Figure 3.9	Time-lapsed expression of the histidine tagged <i>CYP121</i>	113
Figure 3.10	SDS-PAGE analysis of <i>CYP121</i> -P346L protein purification	114
Figure 3.11	SDS-PAGE analysis of histidine tagged <i>CYP121</i> protein purification	114
Figure 3.12	UV-visible absorbance spectra of pure P346L mutant of <i>CYP121</i>	118
Figure 3.13	UV-visible absorbance spectra of pure R386L mutant of <i>CYP121</i>	119
Figure 3.14	Difference spectrum of the reduced/CO-bound form of the P346L mutant of <i>CYP121</i>	120
Figure 3.15	Electronic absorption spectra of the P346L mutant of <i>CYP121</i> with and without NO-bound.	121
Figure 3.16	Far-UV CD spectra of the P346L mutant of <i>CYP121</i>	123



Figure 3.17	Near UV-visible spectra of CYP121 P346L	124
Figure 3.18	Far-UV CD spectra of His-CYP121	127
Figure 3.19	Near UV-visible spectra of His-CYP121 and wild-type CYP121	128
Figure 3.20	X-band EPR spectrum of the P346L mutant of CYP121	131
Figure 3.21	Resonance Raman spectra of wild-type CYP121 and its P346L, R386L and S279A mutants	135
Figure 3.22	Low-frequency resonance Raman spectrum of CYP121 P346L	140
Figure 3.23	Redox titration of CYP121 P346L	143
Figure 3.24	Plot of proportion of ferrous (reduced) P450 enzyme against applied potential (vs NHE) for wild-type CYP121 and CYP121 P346L	145
Figure 3.25	Binding of ketoconazole to the P346L mutant of CYP121	149
Figure 3.26	Difference spectra for P346L mutant of CYP121 titrated with ketoconazole	150
Figure 3.27	Titration curve for the binding of ketoconazole to P346L mutant of CYP121	151
Figure 3.28	Chemical structure of the adamantane triazole derivative	153
Figure 3.29 A and B	Protein-lipid overlay assay	157
Figure 3.30	Stereo view of the heme distortions in wild-type CYP121 and the P346L mutant of CYP121	171
Figure 3.31	Stereo view of the active site of the CYP121 R386L protein	174
Figure 3.32	Putative proton relay pathways in wild-type CYP121	177
Figure 3.33	Stereo view of the active site of the CYP121 S279A protein	178
Figure 4.1	PCR amplification of <i>M. ulcerans</i> CYP140A2	183
Figure 4.2	<i>Mlu</i> I restriction digest of CYP140A2 (pGL5(a))	184
Figure 4.3	Gel analysis of time lapsed CYP140A2 expression	185
Figure 4.4	Gel analysis of soluble and insoluble CYP140A2 expression	186
Figure 4.5	SDS-PAGE analysis of histidine tagged CYP140A2 protein purification	187
Figure 4.6	Anaerobic electronic absorption spectra for CYP140A2	189
Figure 4.7	Difference spectrum of the reduced/CO-bound CYP140A2	191
Figure 4.8	Electronic absorption spectra for CYP140A2 with inhibitor ligands	192
Figure 4.9	Pyridine hemochromagen spectrum of CYP140A2	193
Figure 4.10	Amino acid alignment of <i>M. ulcerans</i> CYP140A2 and P450EryF from <i>Saccharopolyspora erythraea</i> generated by ClustalW	198
Figure 4.11	Far-UV CD spectra of CYP140A2 and P450 BM-3 heme	200
Figure 4.12	Near UV-visible spectra of CYP140A2 and P450 BM-3 heme domain	202
Figure 4.13	X-band EPR spectra of CYP140A2	203
Figure 4.14	Resonance Raman spectra of ligand-free and -bound CYP140A2	206
Figure 4.15	Redox titration of CYP140A2	209
Figure 4.16	Plot of absorption change <i>versus</i> applied potential (relative to NHE) for CYP140A2	210
Figure 4.17	Binding of mycolactone C to CYP140A2	213
Figure 4.18	Titration of econazole to CYP140A2 in complex with mycolactone C	215

Figure 4.19	Difference spectra for the CYP140A2 mycolactone C complex upon titration with econazole	216
Figure 4.20	Titration curve for the binding of econazole to the CYP140A2-mycolactone C complex	217
Figure 4.21	Binding of palmitic acid (C <sub>16</sub> , saturated fatty acid) to CYP140A2	219
Figure 4.22	Binding of clotrimazole to CYP140A2	224
Figure 4.23	Difference spectra for CYP140A2 titrated with clotrimazole	225
Figure 4.24	Titration curve for the binding of clotrimazole to CYP140A2	226
Figure 4.25	LC-MS analysis of mycolactone C turnover	228
Figure 4.26	MS spectra of mycolactone C turnover molecular ions	229
Figure 4.27	LC-MS analysis of mycolactone E turnover	231
Figure 4.28	MS spectra of mycolactone E turnover molecular ions	232
Figure 5.1	Time-lapsed expression of CYP151A2	237
Figure 5.2	SDS-PAGE analysis of CYP151A2 protein purification	238
Figure 5.3	UV-visible absorbance spectra of pure CYP151A2 in oxidised and dithionite-reduced forms	240
Figure 5.4	Spectrum of the reduced/CO-bound form of CYP151A2	241
Figure 5.5	Fe <sup>2+</sup> -CO minus Fe <sup>2+</sup> difference spectrum for CYP151A2	242
Figure 5.6	Electronic absorption spectra for CYP151A2 in oxidised form and with inhibitory ligands bounds	243
Figure 5.7	Pyridine hemochromagen absorption spectrum for CYP151A2	244
Figure 5.8	Amino acid alignment of <i>Mycobacterium</i> sp. strain HE5 CYP151A2 with other structurally characterized bacterial P450s	248
Figure 5.9	Far UV CD spectra of CYP151A2 and P450 BM-3	250
Figure 5.10	Near UV-visible spectra of CYP151A2 and P450 BM-3	251
Figure 5.11	Far-UV CD spectra of CYP151A2 in the presence and absence of morpholine and econazole	252
Figure 5.12	Near-UV-visible CD spectra for CYP151A2 in the presence and absence of morpholine and econazole	255
Figure 5.13	A-D X-band EPR spectra of CYP151A2	253
Figure 5.14	UV-visible MCD spectral properties of CYP151A2	259
Figure 5.15	Near-IR MCD spectral properties of CYP151A2	261
Figure 5.16	Resonance Raman spectrum of ligand-free and -bound forms of CYP151A2	263
Figure 5.17	Redox titration of substrate-free CYP151A2	265
Figure 5.18	Data fit for determination of heme iron reduction potential of CYP151A2	267
Figure 5.19	Redox titration of morpholine-bound CYP151A2	269
Figure 5.20	Data fit for determination of the midpoint reduction potential for morpholine-bound CYP151A2	271
Figure 5.21	Schematic representation of d-orbital (d <sup>5</sup> ) electronic occupancy in low- and high-spin forms of ferric P450 heme iron	274
Figure 5.22	The denaturation of CYP151A2 monitored by far-UV CD spectroscopy	276

Figure 5.23	Plot of change in CYP151A2 far-UV CD as a function of [GdnHCl]	277
Figure 5.24	Binding of morpholine to CYP151A2	279
Figure 5.25	Difference spectra for CYP151A2 titrated with morpholine	280
Figure 5.26	Titration curve for the binding of morpholine to CYP151A2	281
Figure 5.26	Spectral changes on binding of compound A to CYP151A2	289
Figure 5.27	Difference spectra from titration of CYP151A2 with compound A	290
Figure 5.28	Titration curve for the binding of compound A to CYP151A2	290

## List of tables

Table 1.1	Cytochrome P450 catalysed reactions	8
Table 2.1	Genotypes of expression vectors used in this study	71
Table 2.2	<i>E. coli</i> host expression strains and their genotypes (Novagen)	72
Table 2.3	Oligonucleotide primers used for gene amplification and mutation	75
Table 3.1	Summary purification table for P346L mutant of CYP121	115
Table 3.2	Summary purification table for R386L mutant of CYP121	116
Table 3.3	Summary purification table for S279A mutant of CYP121	116
Table 3.4	Purification table for histidine tagged CYP121	117
Table 3.6	Resonance Raman frequencies for the main vibrational features observed in wild-type CYP121 and its point mutants	136
Table 3.7	Dissociation constants ( $K_d$ values) for inhibitors binding to the P346L mutant of CYP121	152
Table 3.8	Azole MIC values for <i>M. tuberculosis</i> (H37Rv) and <i>M. smegmatis</i> (mc <sup>2</sup> 155)	163
Table 4.1	Purification table for histidine tagged CYP140A2	188
Table 4.2	Resonance Raman frequencies for the main peaks observed in ligand-bound and -free forms of oxidised CYP140A2	207
Table 4.3	Dissociation constants ( $K_d$ values) for inhibitor binding to CYP140A2	221
Table 5.1	Purification table for histidine-tagged CYP151A2	238
Table 5.2	Resonance Raman frequencies for the main features observed in ligand bound and -free forms of CYP151A2	264
Table 5.3	Dissociation constants ( $K_d$ values) for inhibitor binding to CYP151A2	285

# Contents

<b>Chapter 1 Introduction</b>	<b>1</b>
<b>1.0 Heme containing proteins</b>	<b>2</b>
1.0.1 Introduction	2
<b>1.1 Cytochrome P450 complement</b>	<b>2</b>
<b>1.2 Cytochrome P450</b>	<b>4</b>
1.2.1 Background to P450s	4
1.2.2 Cytochrome P450 diversity and evolution	6
1.2.3 P450 catalytic mechanism	9
1.2.4 P450 classification	15
1.2.5 Structure and function	18
1.2.5.1 Cytochrome P450 Structure	19
1.2.5.2 Substrate recognition sequence	21
1.2.6 Cytochrome P450 inhibitors	22
<b>1.3 Redox partners and electron transfer</b>	<b>26</b>
1.3.1 Pyridine nucleotide coenzymes	26
1.3.2 Flavin containing redox components	27
1.3.3 Iron-sulphur redox components	29
<b>1.4 Tuberculosis</b>	<b>31</b>
1.4.1 Introduction	31
1.4.2 Historical perspective	31
1.4.3 Tuberculosis epidemiology and transmission	32
1.4.4 <i>M. tuberculosis</i> chemotherapy	33
1.4.5 Drug-resistant TB	34
1.4.6 Chemotherapeutic agents of TB	35
1.4.6.1 Isoniazid	35
1.4.6.2 Rifampicin	37
1.4.6.3 Pyrazinamide	38
1.4.6.4 Streptomycin	38

1.4.6.5	Ethambutol	39
1.4.6.6	Second line chemotherapy	39
1.4.7	Bacteriology of <i>M. tuberculosis</i>	40
1.4.8	Mycobacterial cell wall	40
1.4.9	Cell wall structure	41
1.4.10	<i>M. tuberculosis</i> metabolism	43
1.4.10.1	Lipid metabolism	43
1.4.10.2	Fatty acid degradation	44
1.4.10.3	Fatty acid biosynthesis	44
1.4.10.4	Polyketide synthesis	45
1.4.10.5	Siderophores	46
1.4.10.6	Sterol biosynthesis	46
<b>1.5</b>	<b>Aims and objectives</b>	<b>46</b>
<b>1.6</b>	<b><i>Mycobacterium ulcerans</i></b>	<b>47</b>
1.6.1	Introduction	47
1.6.2	Bacteriology of <i>M. ulcerans</i>	47
1.6.3	Genome	48
1.6.4	Epidemiology	49
1.6.4.1	History and geographic distribution	49
1.6.4.2	Transmission	50
1.6.5	Clinical presentation and pathogenesis	51
1.6.5.1	Clinical features	51
1.6.6	Pathogenesis	53
1.6.6.1	Toxin—Mycolactone	53
1.6.7	Biosynthesis of mycolactones A and B	55
1.6.8	Therapy	58
1.6.8.1	Surgery	58
1.6.8.2	Drug treatment	58
1.6.8.3	Vaccine	59
1.6.9	Aims and objectives	59
<b>1.7</b>	<b><i>Mycobacterium</i> sp. strain HE5</b>	<b>60</b>

1.7.1	Introduction	60
1.7.2	Biodegradation and mycobacteria	60
1.7.3	Morpholine	61
1.7.3.1	Physical and chemical properties	61
1.7.3.2	Sources of human and environmental exposure	62
1.7.3.3	Evaluation of effects on human health	63
1.7.4	Morpholine biodegradation	63
1.7.4.1	Morpholine biodegradation and cytochrome P450s	64
1.7.5	Aims and objectives	69
	<b>Chapter 2 Materials and methods</b>	<b>70</b>
2.0	Materials and Methods	71
<b>2.1</b>	<b>Materials</b>	<b>71</b>
2.1.1	Vectors	71
2.1.2	<i>E. coli</i> strains	71
2.1.3	Molecular biology reagents	72
2.1.4	Other Reagents	72
<b>2.2</b>	<b>Methods</b>	<b>73</b>
2.2.1	Sterilisation of equipment and solutions	73
2.2.2	PCR amplification of <i>CYP121P346L</i> , <i>CYP121R386L</i> , <i>CYP121S279A</i> , and <i>CYP140A2</i>	73
2.2.3	DNA cloning	75
2.2.4	Agarose gel electrophoresis	76
2.2.5	Extraction and purification of DNA from agarose gels	77
2.2.6	‘A’ tailing of PCR fragments	77
2.2.7	<i>DpnI</i> digestion of <i>CYP121S279A</i>	78
2.2.8	Cloning of PCR- and restriction digest-generated fragments into pGEM-T Easy and pET15b	78
2.2.9	Transformation of competent cells	78
2.2.10	Automated DNA sequencing	79
2.2.11	Restriction digest of recombinant pGEM-T Easy vectors	79

2.2.12 Restriction digest of pKM2(b) and pET15b	80
2.2.13 Subcloning of <i>CYP121</i> P346L and <i>CYP121</i> R386L fragments into pKM2(b), and <i>CYP121</i> wild-type fragment into pET15b	80
2.2.14 Restriction digestion of pGL1, pGL2 and pGL4	81
2.2.15 Restriction digest of pGEM-T <i>CYP140A2</i>	83
2.2.16 Subcloning of the <i>CYP140A2</i> fragment into pET15b	84
2.2.17 Subcloning of <i>CYP121</i> into pGL4	84
2.2.18 Transformation of <i>E. coli</i> HMS174 (DE3) and <i>E. coli</i> BL21 (DE3) competent cells	85
<b>2.3 Protein expression studies</b>	<b>85</b>
2.3.1 SDS-PAGE analysis of protein expression	86
<b>2.4 Characterisation of CYP121</b>	<b>86</b>
2.4.1 Protein expression and purification	86
2.4.1.2 Protein expression of histidine-tagged CYP121 wild-type and CYP121 mutants	86
2.4.1.3 Protein expression of histidine tagged CYP140A2	87
2.4.1.4 Protein expression of histidine tagged CYP151A2	87
2.4.1.5 Cell Lysis	88
2.4.1.6 Protein purification of CYP121 mutants	88
2.4.1.7 Protein purification of His-CYP121	89
2.4.1.8 Protein purification of His-CYP140A2	89
2.4.1.9 Protein purification of His-CYP151A2	90
<b>2.5 Spectrophotometric and biophysical characterization</b>	<b>90</b>
2.5.1 Initial spectrophotometric analysis	90
2.5.2 Carbon monoxide and nitric oxide binding	91
2.5.3 Concentration determination	91
2.5.4 Pyridine hemochromagen method	92
2.5.5 Circular Dichroism (CD)	92
2.5.6 Electron paramagnetic resonance (EPR) spectroscopy	92
2.5.7 Magnetic circular dichroism (MCD) spectroscopy	93
2.5.8 Resonance Raman spectroscopy	93

2.5.9	Redox potentiometry	93
<b>2.6</b>	<b>Protein Denaturation</b>	<b>94</b>
2.6.1	Protein unfolding monitored by circular dichroism spectroscopy	94
<b>2.7</b>	<b>Thermostability Studies</b>	<b>95</b>
2.7.1	Heat Denaturation	95
<b>2.8</b>	<b>Inhibitor and substrate binding studies</b>	<b>95</b>
2.8.1	Inhibitor binding	95
2.8.2	Ligand binding	96
2.8.3	Competitive inhibition in substrate binding	97
<b>2.9</b>	<b>Turnover analysis of mycolactone C and E</b>	<b>97</b>
<b>2.10</b>	<b>Protein Lipid Overlay Assay</b>	<b>98</b>
<b>2.11</b>	<b>Susceptibility testing of azole drugs for <i>M. tuberculosis</i> and <i>M. ulcerans</i></b>	<b>99</b>
<b>Chapter 3</b>	<b>Cloning, expression and characterisation of CYP121 mutants</b>	<b>101</b>
<b>3.1</b>	<b>Molecular biology of CYP121 mutants P346L, R386L and S279A, and histidine tagged CYP121</b>	<b>102</b>
3.1.1	Preface	102
<b>3.2</b>	<b>Molecular biology</b>	<b>103</b>
3.2.1	Cloning of CYP121 mutants and histidine tagged CYP121	103
<b>3.3</b>	<b>Expression and purification</b>	<b>110</b>
3.3.1	Expression and purification of P346L, R386L and S279A mutants of CYP121 and histidine tagged CYP121	110
3.3.2	Protein purification of CYP121 mutants and histidine tagged CYP121	113
<b>3.4</b>	<b>Initial P450 characterisation</b>	<b>117</b>
3.4.1	Spectrophotometric analysis of CYP121 mutants	117
<b>3.5</b>	<b>Biophysical characterization</b>	<b>122</b>
3.5.1	Circular dichroism of CYP121 P346L mutant	122
3.5.2	Circular dichroism of histidine-tagged CYP121	126



3.5.3	Electron paramagnetic resonance (EPR) spectroscopy	129
3.5.4	Resonance Raman of wild-type CYP121 and mutants	132
<b>3.6</b>	<b>Redox potentiometry of CYP121 P346L</b>	<b>141</b>
<b>3.7</b>	<b>Ligand binding studies of the P346L mutant of CYP121</b>	<b>148</b>
3.7.1	Inhibitor binding	148
<b>3.8</b>	<b>Protein-lipid overlay assay</b>	<b>154</b>
<b>3.9</b>	<b>Susceptibility testing of azole drugs against <i>M. tuberculosis</i></b>	<b>160</b>
<b>3.10</b>	<b>Crystallography</b>	<b>167</b>
3.10.1	Crystal structure of P346L	169
3.10.2	Crystal structure of R386L	173
3.10.3	Crystal structure of S279A	175
<b>3.11</b>	<b>Summary</b>	<b>179</b>

## **Chapter 4 Characterisation of the P450 CYP140A2 from the Buruli ulcer**

	<b>causative agent <i>Mycobacterium ulcerans</i></b>	<b>181</b>
<b>4.1</b>	<b>Characterisation of CYP140A2</b>	<b>182</b>
4.1.1	Preface	182
<b>4.2.</b>	<b>Molecular biology</b>	<b>182</b>
4.2.1	Cloning of histidine tagged <i>CYP140A2</i>	182
<b>4.3</b>	<b>Expression and purification of histidine tagged CYP140A2</b>	<b>184</b>
4.3.1	Expression	184
4.3.2	Protein purification	187
<b>4.4</b>	<b>Initial P450 characterisation</b>	<b>189</b>
4.4.1	Spectrophotometric analysis	189
<b>4.5</b>	<b>Pyridine heme chromagen</b>	<b>192</b>
<b>4.6</b>	<b>Sequence analysis</b>	<b>193</b>
<b>4.7</b>	<b>Biophysical characterisation</b>	<b>199</b>
4.7.1	Circular dichroism (CD)	199
4.7.2	Electronic Paramagnetic Resonance (EPR)	202
4.7.3	Resonance Raman	205
<b>4.8</b>	<b>Redox potentiometry</b>	<b>208</b>

<b>4.9</b>	<b>Ligand binding</b>	<b>211</b>
4.9.1	Substrate binding assay	211
4.9.2	Inhibitor binding assays	219
<b>4.10</b>	<b>Turnover of mycolactones C and E</b>	<b>227</b>
<b>4.11</b>	<b>Summary</b>	<b>234</b>
<b>Chapter 5</b>	<b>Characterisation of the P450 CYP151A2 (P450<sub>mor</sub>)</b>	<b>235</b>
<b>5.1</b>	<b>CYP151A2</b>	<b>236</b>
5.1.1	Preface	236
5.2	Molecular biology	236
5.2.2	Expression and purification of CYP151A2	236
5.2.3	Protein purification of histidine tagged CYP151A2	238
<b>5.3</b>	<b>Initial P450 characterisation</b>	<b>239</b>
5.3.1	Spectrophotometric analysis	239
<b>5.4</b>	<b>Pyridine hemochromagen method</b>	<b>243</b>
<b>5.5</b>	<b>Sequence analysis</b>	<b>245</b>
<b>5.6</b>	<b>Biophysical characterization</b>	<b>249</b>
5.6.1	Circular dichroism	250
5.6.2	Electronic Paramagnetic Resonance (EPR)	254
5.6.3	Magnetic circular dichroism (MCD)	258
5.6.4	Resonance Raman	262
<b>5.7</b>	<b>Redox potentiometry</b>	<b>265</b>
<b>5.8</b>	<b>Thermostability studies by heat denaturation</b>	<b>273</b>
<b>5.9</b>	<b>Protein unfolding measured by circular dichroism spectroscopy</b>	<b>275</b>
<b>5.10</b>	<b>Ligand binding</b>	<b>277</b>
5.10.1	Putative substrate binding	278
5.10.2	Inhibitor binding	285
<b>5.11</b>	<b>Summary</b>	<b>291</b>
<b>Chapter 6</b>	<b>Discussion</b>	<b>293</b>

<b>6.0</b>	<b>Preface</b>	<b>293</b>
<b>6.1</b>	<b><i>Mycobacterium tuberculosis</i> CYP121</b>	<b>294</b>
<b>6.2</b>	<b><i>Mycobacterium ulcerans</i> CYP140A2</b>	<b>300</b>
<b>6.3</b>	<b><i>Mycobacterium</i> sp. strain HE5 CYP151A2</b>	<b>305</b>
	<b>Appendix</b>	<b>311</b>
	<b>Bibliography</b>	<b>315</b>

# Chapter 1

## Introduction

## **1.0 Heme containing proteins**

### **1.0.1 Introduction**

Tetrapyrrole pigments, of which hemes are an ubiquitous example, comprise a group of metabolites that function in a host of critically important biological systems. Hemes are the vital catalysts in a wide variety of vitally important physiological processes, such as photosynthesis, respiration, microsomal electron transfer, and the utilization and metabolism of oxygen and peroxides (Poulos and Finzel, 1984). Hemoproteins contain an iron complex of porphyrin, and exist as e.g. hemoglobin, myoglobin, cytochromes, catalases, peroxidases, oxygenases and oxidases. Among the hemoproteins, cytochrome P450 monooxygenases (P450s) are a particularly important group. These are a broad class of enzymes found in the vast majority of organisms, and catalyse the oxidation of a large range of organic molecules (Urachler *et al.*, 2004). They are particularly well known for their roles in human drug metabolism and detoxification (De Groot and Sies, 1989).

### **1.1 Cytochrome P450 complement**

The deciphering of the *M. tuberculosis* genome revealed the presence of twenty P450s genes, the largest number ever found in a single bacterial genome to that date (Cole *et al.*, 1998). Such an abundance of P450s represented a departure from the prokaryotic norm, as prior to the determination of the *M. tuberculosis* genome sequence, the seven P450s of *Bacillus subtilis* was the largest P450 complement in a prokaryote (Kunst *et al.*, 1997).

Subsequent genome sequencing of the actinomycetes family has revealed similar P450 complements. In *S. coelicolor* A3(2), a soil bacterium producing medically important natural products, eighteen CYPs were detected (Lamb *et al.*, 2002). Streptomycetes produce a vast array of human and veterinary antibiotics, as well as anti-parasitic agents, herbicides, and pharmacologically active metabolites (e.g. immunosuppressants). Streptomycetes also catalyse numerous biotransformations of xenobiotics of industrial and environmental importance (Hopwood, 1999).

Mycobacteria such as *M. bovis* (Garnier *et al.*, 2003) reveal almost identical P450 complements to *M. tuberculosis*, but *M. leprae*, the aetiological agent of the chronic skin and nerve disease leprosy, contains only one functional P450 gene with a few P450 pseudogenes. The presence of just one functional P450 gene, in contrast to the twenty found in *M. tuberculosis*, suggests an important physiological role for this isoform. The *M. leprosy* genome has undergone extensive genetic decay and rearrangement by reductive evolution in comparison to the *M. tuberculosis* genome and, as a result, has eliminated many important metabolic activities. This genome downsizing may define the minimal gene-set for pathogenic mycobacterial survival (Cole *et al.*, 2001).

Cytochrome P450s catalyse a wide variety of reactions, which include the biosynthesis of lipids, steroids, antibiotics, and the degradation of xenobiotics (Munro and Lindsay, 1996; Bishai, 1998; Cole *et al.*, 1998; Camus *et al.*, 2002). In line with the variety of reactions catalysed, the range of substrates varies significantly. The presence of so many P450 genes in *M. tuberculosis* indicates an important role in physiological systems, highlighting their suitability as potential drug targets. Due to the unique and complex composition of the membrane, the *M. tuberculosis* P450s are likely to be involved in the synthesis and inter-conversions of membrane lipids, polyketides and (possibly) even sterols, essential for cell integrity. To date, the product of gene *Rv0764c* has been identified as a putative sterol biosynthetic enzyme, encoding CYP51, a P450 capable of sterol 14 $\alpha$ -demethylation catalysis at low rates (Bellamine *et al.*, 1999). CYP51 is a homologue of the mammalian and fungal sterol demethylase, with the latter involved in the synthesis of the essential membrane sterol ergosterol (Aoyama *et al.*, 1998; Bellamine *et al.*, 1999). However, there is inconclusive evidence to whether CYP51 is an actual sterol demethylase *in vivo*, as there is no evidence indicating that *M. tuberculosis* can synthesise cholesterol or other sterols.

Several potent inhibitors of P450s exist, centred on functional group coordination to the heme iron of the P450, inactivating enzyme function. The most widely used inhibitors are the anti-fungal/yeast azole agents. These compounds possess an imidazole or triazole group that ligates to the ferric iron of the P450 via a

nitrogen atom. These compounds are specifically designed to prevent the synthesis of ergosterol, which is essential in membrane integrity (Aoyama *et al.*, 1998; Bellamine *et al.*, 1999, Souter *et al.*, 2000). In addition, fatty acid-linked imidazoles are also known to be potent inhibitors of lipid-metabolising P450s (Noble *et al.*, 1998). Accordingly, cytochrome P450 inhibitors may provide the new therapeutic agents required so urgently in the fight against TB, and represent an alternative strategy for combating *M. tuberculosis* and drug-resistant strains thereof.

## 1.2 Cytochrome P450

### 1.2.1 Background to P450s

The cytochrome P450s are a superfamily of heme *b*-containing monooxygenase enzymes, containing protoporphyrin IX as their prosthetic heme factor. P450 monooxygenases are ‘mixed function oxygenases’, constituting the terminal components of electron transport chains where both substrate and NAD(P)H are oxidised.

Irrespective of substrate, the general function of a P450 is the same - the activation of molecular dioxygen and subsequent insertion of a single atom of molecular oxygen into an organic molecule (Figure 1.1).

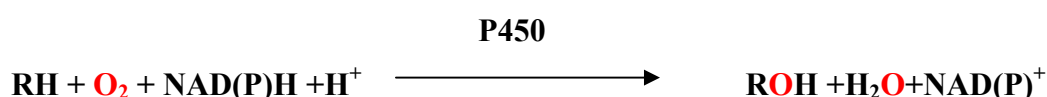


**Figure 1.1 Cytochrome P450 catalysed hydroxylation reaction.**

RH represents an oxidisable substrate and ROH the corresponding hydroxylated product.

The first experimental evidence relating to cytochromes P450 was provided in 1955 (Axelrod, 1955; Brodie *et al.*, 1955) when an enzyme system oxidising xenobiotic compounds was identified in the endoplasmic reticulum of the liver. In 1958, a carbon monoxide binding pigment with an absorption maximum at 450 nm was detected in liver microsomes (Garfinkle, 1957; Klingenberg, 1958). The microsomal carbon monoxide-binding pigment was later demonstrated to contain iron-protoporphyrin IX (Omura and Sato, 1962; Omura and Sato, 1964), which was

named cytochrome P450 after the primary characteristic feature in its absorption spectrum on complex formation with CO.

The heme structure found in P450s is a tetrapyrrole heme *b* (protoporphyrin IX) (Figure 1.2), which is a highly symmetrical and conjugated system, coordinated to an iron atom. The highly conjugated ring system leads to a strongly coloured chromophore. The surrounding tetrapyrrole structure and axial ligands modulate the chemical properties of the heme iron. Heme electron transfer involves a single electron reversible oxidation/reduction of the iron between its 2<sup>+</sup> and 3<sup>+</sup> oxidation states, although the P450 catalytic cycle also involves other oxidation states of heme iron in the short-lived intermediates responsible for substrate oxidation (4<sup>+</sup> and/or 5<sup>+</sup>). The properties of heme redox centres can be altered dramatically by changing the axial ligands. In P450s, four porphyrin central nitrogens provide the equatorial planar ligands for the heme iron, and the fifth ligand is usually a conserved cysteine sulphydryl bond (the 'proximal' distal ligand, typically considered to be in the deprotonated thiolate form). A 6<sup>th</sup> (displaceable) water ligand is generally found opposite the cystein(at)e as the distal ligand. This ligand makes way for binding of oxygen in the catalytic cycle. The heme macrocycle is typically bound non-covalently to the protein. However, recent studies of the mammalian CYP4 family of P450s indicate that covalent linkage of a peripheral heme methyl group via a glutamate residue is feasible (LeBrun *et al* 2002a; LeBrun *et al.*, 2002b).

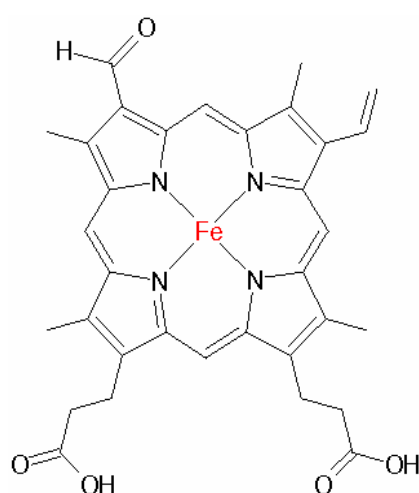


**Figure 1.2** Schematic representation of the structure of heme *b* (ferriproteoporphyrin IX)  
Drawn in Chemdraw.



Changes in electronic spectral properties occur during catalytic cycles of heme proteins and on interactions with various ligands. Spectral perturbations of the P450 heme result from the ability of various ligands to perturb the spin equilibrium or alter the coordination state of the proximal cysteinate-ligated heme iron. Substrates of P450s frequently shift the equilibrium in favour of the high-spin form, which occurs by displacement of a water molecule at the 6<sup>th</sup> ligand (distal axial ligand). Different spectral properties of the Soret band occur in the low-spin and high-spin forms, with maxima close to 420nm and 390nm, respectively (Munro *et al.*, 2000; Loew and Harris, 2000). For several P450s (particularly certain well characterised bacterial isoforms), the change in spin-state facilitates the next step in their enzymatic cycle, one-electron reduction of heme iron from the redox partner.

Alterations in spin-state are an integral part of the characteristic and functional properties of the P450s. The signature electronic properties of heme sites are primarily due to  $\pi$ - $\pi^*$  electron transitions within the protoporphyrin IX cofactor and the S $\rightarrow$ Fe ligand-to-metal charge transfer bands. Also, normally associated with substrate-induced shift in spin-state are changes in the mid-point reduction potential of the ferric heme iron. Electronic re-distribution that occurs in the low- to high-spin transition in the iron *d*-orbitals and changes in overall energy levels of the orbitals leads to a more positive heme iron reduction potential in the high-spin state (Sharrock *et al.*, 1973).

The spectroscopic properties (i.e. UV-visible and other methods) of P450s provide a means to study and characterise a number of properties associated with these diverse biological catalysts. Accordingly, substrate dissociation constants ( $K_d$ ) can be determined by the extent of the spin-state shifts induced during titration with a substrate and by using optical spectroscopy (Daff *et al.*, 1997; Loew and Harris, 2000). Binding of inhibitory ligands (e.g. azoles) can be analysed by similar methods.

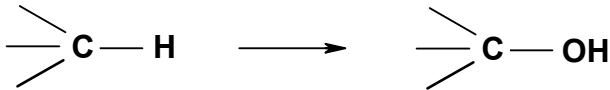
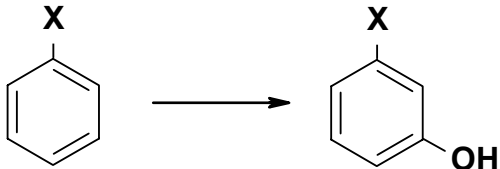
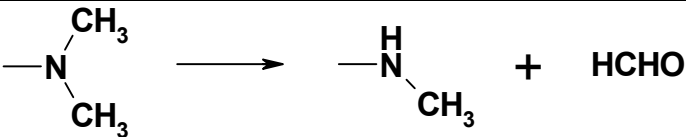
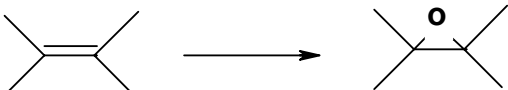
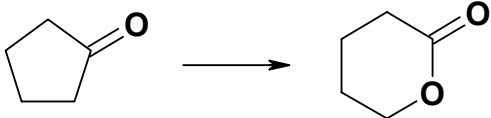
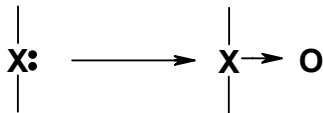
### **1.2.2 Cytochrome P450 diversity and evolution**

The cytochrome P450 super-family is one of the largest and most diverse enzyme families known. The full extent of P450 distribution has only recently become clear from the results of various genome-sequencing projects. There were

over 1,500 known P450 genes distributed at all levels of the phylogenetic tree, in archaea, bacteria, simple eukaryotes (e.g., fungi), plants, and animals according to (Nelson, 1999). The current number is significantly higher (~6,500) and continues to grow as new genome sequences are determined.

In mammals, P450s are numerous with two primary roles involving the biosynthesis of lipophilic chemicals engaged in chemical signal transmission (e.g., steroid hormones and prostanoids), and the degradation of lipophilic endobiotic or xenobiotic chemicals. Despite the relatively simple iron porphyrin-containing active site, eukaryotic P450s can catalyse a large range of chemical reactions such as hydroxylations, epoxidations, N-, S- and O-dealkylations, N-oxidations, sulfoxidations and dehalogenations (summarised in Table 1.1) (Sligar, 1999). Diversity in activities is explained by variations in active site structure of the P450s and nature of substrates, and is also influenced by factors such as nature of redox partners.

Typically, the structural change induced by P450-dependent transformation of a substrate compound also affects the biological properties of the compound, and often serves as a general method for terminating the biological activity and enhancing the clearance of foreign chemicals. This is achieved by the activities of P450s in the mammalian liver and the intestine, each with diverse and overlapping substrate specificities, although human P450s are not restricted to these organs. Action of other (phase II) enzymes such as glutathione-S-transferases and UDP-glucuronyl transferases may be required to facilitate P450 product excretion from an organism. P450s are also involved in catalysing the biosynthesis and interconversions of sterols, a vital component of eukaryotic plasma membranes (Munro *et al.*, 1999a; Noble *et al.*, 1999; Lewis, 2000;).

P450 Reaction	Reaction Example
Alkane hydroxylation	
Aromatic hydroxylation	
Demethylation	
Epoxidation	
Lactonisation	
N-, S-Oxidation	

**Table 1.1**      **Cytochrome P450 catalysed reactions**

Examples of the diverse range of reactions carried out by cytochromes P450. P450s are the only identified mammalian enzyme system with the oxidative power to effectively functionalise primary carbons using molecular oxygen (Sligar, 1999). X indicates a N or S atom, or another functional group.

The catalysis of these diverse reactions usually requires an external source of reducing equivalents, usually provided by NAD(P)H and by auxiliary proteins e.g., putidaredoxin, putidaredoxin reductase in *Pseudomonas putida* P450<sub>cam</sub> for electron transfer to the heme of P450<sub>cam</sub> to enable camphor hydroxylation (Unno *et al.*, 2002).

Interest in P450s is primarily due to their involvement in critical metabolic processes and their implication in carcinogenesis. The P450s have also been found to have biotechnological and industrial potential because they catalyse the stereo- and regio-specific oxidation of organic substrates. This potential has been demonstrated with the use of P450s in the commercial manufacture of steroids, a process continually being developed and improved. Particular interest lies in the mechanism for P450-dependent molecular scission of oxygen and the subsequent oxidation of substrate (Munro and Lindsay, 1996; Omura, 1999).

### **1.2.3 P450 catalytic mechanism**

The ultimate function of the vast majority of P450s is the cleavage of molecular oxygen for substrate oxidation, while avoiding the damaging nature of oxygen radicals that are formed on the heme iron during the catalytic cycle. The catalytic process is achieved via a complex, but flexible, cycle involving conformational and redox changes. This cycle permits substrate oxygenation whilst preventing uncoupled production of  $\text{H}_2\text{O}_2$  or superoxide, thus avoiding wastage of reducing equivalents from the NAD(P)H cofactor. The catalytic cycle of P450s has been elucidated mainly through the work carried out on cytochrome P450cam (CYP101A1) (Mueller *et al.*, 1995; Aoyama *et al.*, 1996; Wong, 1998; Omura, 1999; Miles *et al.*, 2000; Schlichting *et al.*, 2000) (Figure 1.3).

As shown schematically in Figure 1.3, the heme site of the P450 undergoes complex transformations during its enzymatic cycle. This complex pathway from the inactive resting species to the putative catalytically active ferryl  $\text{Fe}=\text{O}$  species involves sequential changes in the oxidation state, distal ligands, and spin state of the heme, forming both known and postulated transient species.

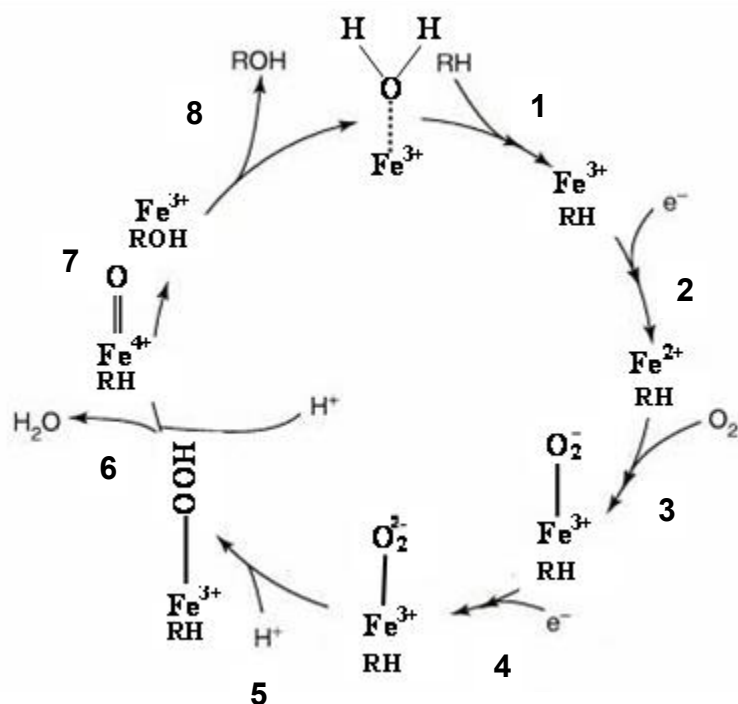


**Figure 1.3 The reaction cycle of a P450 monooxygenase catalysed hydroxylation.**

The substrate is denoted by RH and the oxygenated product ROH. The cycle starts with the binding of substrate to ferric heme (1). This allows the first electron transfer (2). Dioxygen can then bind to the ferrous heme, in turn reducing to a ferric superoxo complex (3). Delivery of the second electron results in the formation of an iron-peroxo species (4), which is then protonated to form a ferric hydroperoxy intermediate (5). A further protonation and dehydration of this intermediate produced the highly reactive oxyferryl state (6). This interacts with the bound substrate (7), resulting in the formation and release of the hydroxylated product (8). On release of product from the active site, the P450 returns to the initial resting state (Miles *et al.*, 2000).

The P450 catalytic cycle as shown in figure 1.3, begins with the enzyme in a hexacoordinate low-spin ferric state ( $S = 1/2$ ) ( $\text{Fe}^{\text{III}}$ ), step 1, with an exchangeable water ligand trans to the proximal cysteinate. In many P450s, the starting state can also be a pentacoordinate high-spin  $\text{Fe}(\text{III})$  with the water off and retaining the cysteinate as the axial ligand. In many prokaryotic systems, the low-spin form predominates. Upon substrate binding in a site close to the heme, dissociation of the weakly bound water ligand generally occurs, thus shifting the equilibrium to a five-coordinate high spin ferric state ( $S = 5/2$ ), step 2. In the case of P450cam, this

conversion of the ferric iron from low- to high-spin results in a significant increase in the redox potential of the enzyme heme (Mueller *et al.*, 1995), thus providing a thermodynamic trigger to allow electron transfer from the reductase or e.g. ferredoxin redox partner.

Thereafter, one-electron reduction of the complex to a ferrous state produces the third intermediate, a pentacoordinate high-spin species that facilitates O<sub>2</sub> binding to form the ferrous-dioxygen (oxyferrous) intermediate. Electronic reorganisation means that this species is formally considered to be a ferric superoxo complex. A number of iron-oxygen intermediates are thought to occur after the binding of oxygen to the ferrous heme in the catalytic cycle, but due to their short lifespan at least one remains to be positively identified (Waterman and Johnson, 1991; Mueller *et al.*, 1995; Wong, 1998; Omura, 1999; Sligar, 1999; Miles *et al.*, 2000; Schlichting *et al.*, 2000). At this stage CO can bind to form the ferrous-CO inhibited adduct, instead of dioxygen, inducing a shift of the Soret band to 450nm, which is characteristic for P450 enzymes (Klingenberg, 1958; Omura and Sato, 1964).

Addition of a second electron to the relatively unstable ferric-superoxo species, leads to a short-lived ferric peroxide adduct, step 4, which can then be rapidly protonated by delivery of a proton to the active site. The protonation of the distal oxygen atom results in the formation of a ferric hydroperoxy form (step 5). Reaction with a further proton leads to formation of the highly reactive oxyferryl species, together with the generation of a water molecule. Depending on the protein, the two protons may originate from the aqueous environment surrounding the protein and delivered via solvent channels that lead to the heme active site, as speculated in the case of P450cam (Schlichting *et al.*, 2000). Another proton route is possible via both the external solvent molecules and amino acid residues lining the active site, such as Thr<sup>268</sup> in P450 BM3 (Ravichandran *et al.*, 1993). The ferric hydroperoxy species loses the water molecule to make a reactive, high valent iron-oxo (oxyferryl) complex (Fe<sup>IV</sup>=O) (step 6). The diverse oxidations affected by these enzymes suggest that different types of oxidants may be involved in some specific functions (Newcomb *et al.*, 2002). There is some evidence to suggest that alternative oxidants such as hydroperoxo (and possibly even ferrous-oxy) forms are responsible for some P450 mediated reactions (Mansuy, 1998).

The P450 catalytic cycle is completed when, following double protonation, the heterolytic cleavage of the O-O bond (steps 6 and 7) allows an oxygen atom transfer from the oxyferryl ( $\text{Fe}^{\text{IV}}=\text{O}$ ) complex to the substrate to yield the oxygenated product (ROH). Thus, the proposed oxo-ferryl porphyrin radical intermediate actually carries out the monooxygenation reaction. Release of the hydroxylated product (step 8) returns the ferric heme iron of the P450 to its resting state, and the P450 catalytic cycle can be repeated (Sligar, 1999; Mueller *et al.*, 1995; Wong, 1998; Loew and Harris, 2000; Schlichting *et al.*, 2000). In the presence of external oxygenation agents, such as peracids, the ferric enzyme complex may be directly converted to the hydroperoxo complex via a "shunt" pathway. Protonation of this species then leads to formation of the oxyferryl intermediate. This pathway is rarely efficient, although a bacterial class of enzymes (typified by P450<sub>BS $\beta$</sub> ) appears to have evolved to utilise peroxide as the natural substrate (Matsunaga *et al.*, 2002).

The requirement for substrate binding before the first electron reduction is believed to be a physiological "gate" to the formation of the reactive oxygen intermediates within P450cam (and other systems such as P450 BM3), since otherwise this intermediate and subsequent breakdown products could damage the protein/heme and compromise functional activity. However, this physiological gate may not be the general case for all P450s, particularly mammalian isoforms (Guengerich and Johnson, 1997).

For well-regulated P450 systems (e.g. P450cam and P450 BM3), the changes in P450 ferric heme iron spin-state elevate (make more positive) the heme iron redox potential and act as a redox switch preventing the uncoupled consumption of NAD(P)H, i.e. electrons cannot pass to the heme until substrate is bound to the P450, controlling the process of electron transfer utilising NAD(P)H as reductant. The redox switch also prevents the production of reactive oxygen species such as  $\text{O}_2^{\bullet-}$  and  $\text{O}^{2-}$ , which are capable of causing extensive intracellular and protein damage (Munro *et al.*, 1999a; Omura, 1999; Loew and Harris, 2000; Schlichting *et al.*, 2000). However, it is known that various eukaryotic P450 isoforms are not as efficient in coupling electron

transfer to product formation, as indeed are numerous bacterial P450 isoforms (Wong, 1999; Miles *et al.*, 2000).

The iron of the heme prosthetic group is the focus of catalytic events, augmented by interaction with individual amino acids that enable reactions such as protonation. Although the previous sequence of events is the one most commonly proposed for P450 reactions, with the ferryl-oxo species driving the oxygenation chemistry, alternate mechanisms may include oxidations by hydroperoxo-iron and peroxo-iron entities (Vaz *et al.*, 1998). Distinguishing among these mechanisms is not trivial, in that the steps following oxygen binding have proven extremely difficult to study because of the unstable nature of these intermediates (Schlichting *et al.*, 2000). In particular, compelling evidence for the P450 ferryl-oxo species remains elusive.

In the absence of electron transport proteins, the substrate can be P450 hydroxylated by the addition of hydrogen peroxide or organic peroxy compound through a "peroxide shunt" mechanism (Hollenberg, 1992). Peroxides can provide protons, electrons normally supplied by NAD(P)H and molecular oxygen required for the normal P450 catalytic cycle. These oxygen donors include hydrogen peroxide ( $\text{H}_2\text{O}_2$ ), alkyl peroxides ( $\text{ROOH}$ ), peroxyacids ( $\text{R-C(O)-OOH}$ ), sodium chlorite ( $\text{NaClO}_2$ ), sodium periodate ( $\text{NaIO}_4$ ) and iodosylbenzene ( $\text{Ph-IO}$ ) (White and Coon, 1980; Porter and Coon, 1991). The oxygen donors bind to the iron to form the ferric hydroperoxy intermediate, and this is subsequently protonated to give water and the active iron-oxo species (Peterson and Graham, 1998). Developments of such systems are of interest due to the expense involved in the commercial production of NADPH (Miles *et al.*, 2000). However, these reagents do oxidatively attack the heme macrocycle and amino acid side chains. The alternative shunt pathway offers tremendous opportunity to employ cell-free P450 catalysis without requiring NAD(P)H regeneration, additional proteins, or dioxygen, and could eliminate rate-limiting electron transfer steps (Cirino and Arnold, 2003). However, the drawbacks are the slow formation of reactive intermediates with peroxide substrates and the oxidative destruction of the catalyst by their use. Exploitation of the peroxide shunt pathway would require further understanding of the peroxygenase reaction mechanism, particularly in the presence of substrate. The recent discovery of "natural" peroxygenase P450s (such as P450 B<sub>SP</sub>) clearly provides a route to such



information (Matsunaga *et al.*, 1998). Other artificial mechanisms to drive P450 reactions include the use of electrode systems, a less expensive system used to provide the required electrons to the P450 (Reipa *et al.*, 1997). However, many such systems do not yet replicate the catalytic efficiency observed for enzymes such as P450cam and P450 BM3.

The range of substrates oxidised and their varying nucleophilic or electrophilic properties are evidence of the versatility of the P450 oxygenating species. As mentioned, in addition to the ferryl-oxo species, the hydroperoxo-iron and peroxo-iron may also attack the substrate (Vaz *et al.*, 1998). The hydroperoxo-iron species may function as an electrophilic oxidant in reactions such as the decarbonylation of aldehydes and ketones, and the sulfoxidation of thioesters (Coon *et al.*, 1998).

#### **1.2.4 P450 classification**

Cytochrome P450s fall into several different classes according to how electrons are delivered from NAD(P)H to the active site. There is no recognised formal classification for these redox systems as yet, but a typical classification regime is presented below. Catalysed reactions generally require one or more accessory enzymes or redox partners to allow them to use the redox coenzymes, NADH or NADPH.

Class I and II P450s require the successive delivery of two electrons, which are provided by redox protein partners. All P450-containing monooxygenase systems of these two classes share common structural and functional domain architecture (Figure 1.4). They are composed of three functional domains: NAD(P)H-dependent FAD-containing reductase (FAD domain), an iron-sulphur protein (in class I) or FMN-binding domain (in class II), and a P450 protein (heme domain) (Degtyarenko, 1995). In class I systems these domains take the form of distinct proteins, but in class II systems the FAD- and FMN-binding domains are fused to form the protein NADPH-cytochrome P450 reductase (CPR). Class I enzymes, which include certain prokaryotic forms and some mammalian mitochondrial enzymes, take electrons from a specific ferredoxin (an iron-sulphur protein) that shuttles electrons from a NAD(P)H-dependent FAD- or FMN-containing ferredoxin reductase (Munro and Lindsay, 1996) (Figure 1.3). Class II P450s (including certain prokaryotic forms and

most eukaryotic P450s, including mammalian forms localised in the endoplasmic reticulum) receive electrons directly from NADPH–cytochrome-P450 reductase (CPR), composed of FAD-binding (C-terminal) and FMN-binding (N-terminal) domains. Both CPR and P450 components of the Class II systems are bound to eukaryotic membranes by N-terminal hydrophobic anchors. Hence they present difficulties as regards to isolation for detailed enzymology and structural studies (Narhi and Fulco, 1986; Boddupalli *et al.*, 1990; Munro *et al.*, 1995; Munro and Lindsay, 1996; Munro *et al.*, 2000; Lewis and Hlavica, 2000). However, protein engineering has been used extensively to generate soluble forms of several CPR and class II P450 enzymes, and atomic structures have been successfully determined for soluble forms of rat and yeast CPRs, and for a limited number of engineered mammalian P450s (e.g. Cosme *et al.*, 2000) (Figure 1.4).

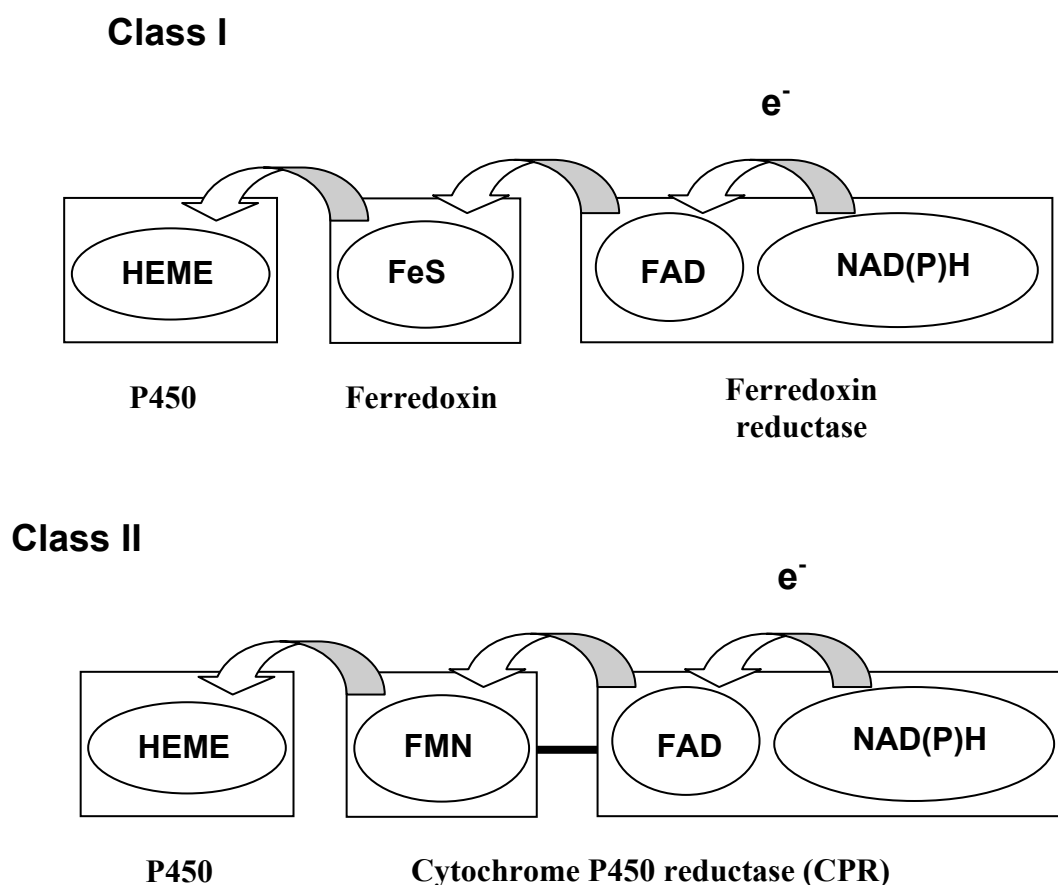


**Figure 1.4 Domain organization of P450-containing monooxygenase systems**  
Independent structural domains are shown as boxes. Cofactors and heme are shown as ellipses and labelled. Curved arrows show the electron transfer pathway.

Further classes have also been defined. Class III P450s exist as a single polypeptide chain with two functional parts, a heme and a reductase domain, as typified by the P450 BM-3 system (Narhi and Fulco, 1987). In this type of one-component system, the heme and reductase domain are expressed as a P450 fusion protein. The FMN- and FAD-containing C-terminal P450 reductase, is linked to the N-terminal P450 in one continuous polypeptide. The best characterised example of this system is the long chain fatty acid hydroxylase flavocytochrome P450 BM-3 from *Bacillus megaterium* (CYP102A1) (Nebert and Gonzales 1996; Noble *et al.*, 1998). These P450s comprise a self-sufficient one component P450 system with two linked domains (Munro and Lindsay, 1996). Although P450 BM-3 is of bacterial origin, the amino acid sequence of the heme domain has a greater sequence similarity to eukaryotic (fatty acid hydroxylase) P450s than to bacterial Class I P450s. This continuous polypeptide arrangement is a catalytically efficient system with a reductase-to-heme reduction rate 100-1000 fold over that found for most eukaryotic forms. Due to the fact that BM-3 is soluble and because of its similarity to the microsomal P450s, it provides a good structural model for the Class II P450s, which are of great medical and pharmaceutical interest (Narhi and Fulco, 1986; Boddupalli *et al.*, 1990; Munro *et al.*, 1995; Munro and Lindsay, 1996; Munro *et al.*, 2000; Lewis and Hlavica, 2000). Other examples of this class include the membrane-bound fatty acid hydroxylase P450foxy (CYP505A1) from the pathogenic fungus *Fusarium oxysporum* (Kitazume, 2000) and two additional P450 BM-3 homologues (CYP102A2 and 102A3) which were revealed from the genome of *Bacillus subtilis* (Kunst *et al.*, 1997). Further genome sequencing projects have revealed the presence of additional Class III P450 BM-3 homologues in the fungus *Fusarium verticillioides* (CYP505B1), the pathogens *Bacillus anthracis* (the causative agent of anthrax) and *Bacillus cereus* (involved in intestinal infections), the actinomycete *Actinosynnema pretiosum*, and in the heavy metal resistant *Ralstonia metallidurans* (De Mot and Parret, 2002).

Class IV enzymes use redox coenzymes, but do so directly, without the intervention of any accessory enzymes. The cytochrome P450nor (CYP55) family is the only known example to date of this P450 class. Members of this family include P450norA and P450norB from *Fusarium oxysporum*; P450nor1 and P450nor2 from *Cylindrocarpan tonkinense*; and P450nor from *Trichosporon cutaneuem* (Kaya *et al.*,

2004). The P450<sub>nor</sub> family receive electrons directly from the reduced pyridine nucleotides NAD(P)H, catalysing the reduction of two molecules of NO to N<sub>2</sub>O (Zumft, 1997).

Finally, a Class V of P450s also exists which do not require NAD(P)H or any electron donating protein. These P450 enzymes catalyse molecular rearrangements and therefore do not require molecular oxygen, reduction through a separate protein or protein domain, or a source of reducing equivalents from NAD(P)H. Members of this class include; allene oxide synthase (CYP74) which converts lipoxygenase-derived fatty acid hydroperoxides to allene epoxides (Miyata *et al.*, 1994), and thromboxane synthase (CYP5A1) which catalyses the conversion of prostaglandin H<sub>2</sub> to thromboxane A<sub>2</sub>, a potent mediator of platelet aggregation, vasoconstriction and bronchoconstriction. (Chevalier *et al.*, 2001)

Different types of P450 systems continue to be discovered. For instance, two further bacterial P450s isolated from *Sphingomonas paucimobilis* and *Bacillus subtilis* specifically require hydrogen peroxide for catalytic turnover, with no need for any exogenous redox system or molecular oxygen (Lee *et al.*, 2003). These peroxygenase P450s are discussed above in context of the artificial driving of P450 reactions by the peroxide shunt. A novel type of P450/reductase fusion enzyme has been characterised from a *Rhodococcus* sp. Strain NCIMB 9784, in which the P450 is linked to an FMN and iron sulphur-containing phthalate dioxygenase reductase-like redox partner (Roberts *et al.*, 2002). The proteobacterium *Methylococcus capsulatus* revealed another novel system where the P450 domain is naturally fused to a ferredoxin domain at the C-terminus (Jackson *et al.*, 2002). In addition, there exists a characterised prokaryotic P450 (P450<sub>cin</sub>) that uses a flavodoxin-like protein and auxiliary flavoprotein reductase that resembles a disconnected form of the two domains of NADPH-P450 reductases (Mehareenna *et al.*, 2004). Moreover, other proteins may be physiologically associated with the P450 (e.g., an acyl carrier protein with P450 BioI) and act to deliver substrate or stabilise the P450 structure (Stok and De Voss, 2000). Recently, a P450-flavodoxin fusion capable of degradation of a widely used RDX explosive (royal demolition explosive) was described (Rylott *et al.*, 2006). Further variations are likely to be revealed by genome analysis.

The genomes of plants are expected to contain more functional P450 genes than that in animals, as plants utilise P450s in so many essential metabolic pathways. Indeed, to date the mustard plant, *Arabidopsis thaliana* with 273, and the rice plant with 458, contain the highest number of P450 genes (<http://drnelson.utmem.edu/CytochromeP450.html>). Within plants cytochrome P450 monooxygenases are involved in the biosynthesis of various compounds such as phenylpropanoids, lipids and phytohormones (Inoue, 2004).

### 1.2.5 Structure and function

The first P450 to be purified and crystallised was the soluble bacterial, P450cam (CYP101A1) of *Pseudomonas putida* (Dus *et al.*, 1970; Yu *et al.*, 1974). The camphor-bound atomic structure was published in 1987 (1AKD) (Poulos *et al.*, 1987). Several other, high-resolution atomic structures of different cytochromes P450s have been determined to date, predominantly of prokaryotic origin.

Available P450 atomic structures include the heme domain of cytochrome P450 BM-3 (CYP102), a fatty acid hydroxylase from *Bacillus megaterium* (1BU7) (Ravichandran *et al.*, 1993b); cytochrome P450terp (CYP108), a terpeneol hydroxylase from a *Pseudomonas* species (1CPT) (Hasemann *et al.*, 1994); the substrate-bound form of cytochrome P450eryF (CYP107A1), a 6-deoxyerythronolide B hydroxylase from *Saccharopolyspora erythraea* involved in erythromycin biosynthesis (1OXA) (Cupp-Vickery and Poulos, 1995); the azole inhibitor-bound form of P45014DM (MTCYP51) a sterol 14 $\alpha$ -demethylase from *M. tuberculosis* (1E9X) (Podust *et al.*, 2001); and CYP154C1, a P450 from *Streptomyces coelicolor* involved in monooxygenation of macrolide ring systems (1GWI) (Podust *et al.*, 2003). More important with regard to the current work is the crystal structure of *M. tuberculosis* CYP121 (1N40) (Leys *et al.*, 2003). Crystal structures have also been determined for several P450cam catalytic cycle intermediates, although these do not provide conclusive evidence for specific postulated intermediates late in the catalytic cycle (Schlichting *et al.*, 2000).

### 1.2.5.1 Cytochrome P450 Structure

Despite low overall sequence identities, generally of less than 20%, and only three absolutely conserved amino acids across this gene superfamily, the overall P450 structural fold and topology is very similar in member P450s structurally characterized (Hasemann *et al.*, 1995) (Figure 1.5). The structures generally consist of 13  $\alpha$ -helices named A to L, although P450 BM-3 has an insertion termed the J-helix, and 5  $\beta$ -sheets that form a triangular prism-shaped molecule predominantly helical in structure. The conserved structural core of the P450 is formed by a four helix-bundle composed of three parallel helices, D, L, and I, and one antiparallel helix E in a four helix-bundle (Presnell and Cohen, 1989; Peterson and Graham, 1995; Halpert *et al.*, 1998). The heme group is confined between the highly conserved distal I-helix that spans the diameter of the protein structure, and the shorter proximal L-helix. The L-helix is attached through its N-terminus to the adjacent cysteine-thiolate ligand, which contains the P450 amino acid signature sequence FxxGx(H/R)xCxG (Peterson and Graham, 1998; Miles *et al.*, 2000).

The I-helix contains the signature sequence (A/G)Gx(E/D)T located above the heme, and because of this sequence, there is usually a kink in the middle of the helix. The highly conserved threonine preceded by an acidic residue is positioned in the active site and believed to be involved in catalysis with roles in oxygen binding and/or protonation (Imai *et al.*, 1989; Martinis *et al.*, 1989; Kimata *et al.*, 1995; Vidakovic *et al.*, 1995; Taraphder and Hummer, 2003). The conserved core also includes the helices J and K. The C-terminal part of the K-helix contains the absolutely conserved ExxR salt bridge motif that stabilises a highly structurally conserved coil termed the meander. This meander formation is found on the proximal face of the protein (the putative redox partner-binding site) and is highly conserved within P450 structure (Omura, 1999; Graham and Peterson, 1999; Miles *et al.*, 2000). There are two structurally conserved  $\beta$ -sheets:  $\beta$ 1 containing five strands and  $\beta$ 2 containing two strands. The presence of  $\beta$ 5 is variable.  $\beta$ -sheets I and II are surrounded by the less-conserved helices A, B and K. These conserved  $\beta$ -sheet regions are thought to be involved in forming the hydrophobic substrate access channel, as well as performing a function in protein folding and heme binding (Graham and Peterson, 1996; Graham and Peterson, 1999; Omura, 1999; Miles *et al.*, 2000).

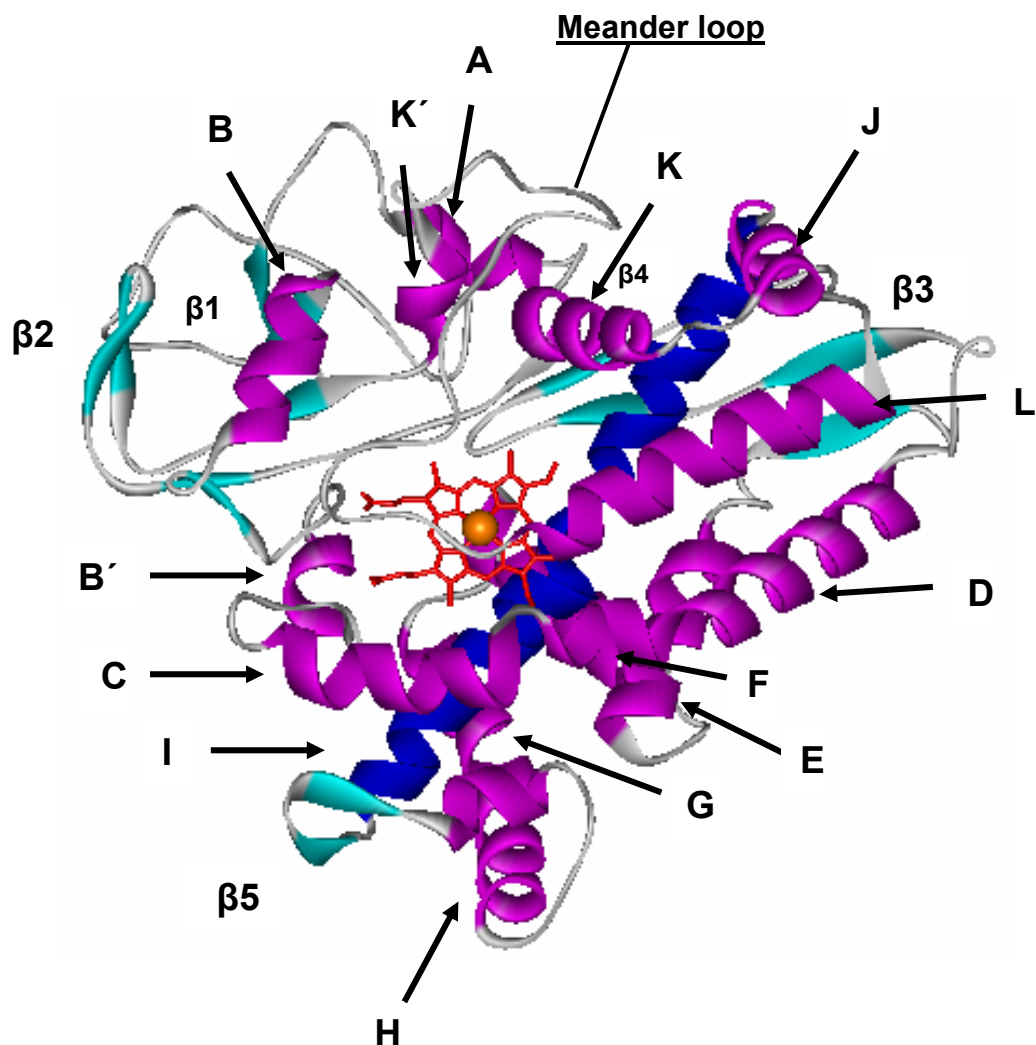


**Figure 1.5** A ribbon representation of the P450cam structure (proximal face) The  $\alpha$ -helices (purple) are labelled with capital letters,  $\beta$ -sheets (cyan) are labelled with numbers. The central I helix is in dark blue.

The prosthetic heme group lies deep within the structure, with the substrate-binding site positioned on the heme distal face. The greatest structural variability is observed in the regions associated with substrate binding and redox partner interactions. The substrate binding sites of the known P450 structures are considerably different in size, shape and chemical character, reflecting the different natures of their substrates. Although the overall  $\alpha$ -helical and  $\beta$ -sheet structures are well conserved between structurally characterised P450, it is the lengths and locations of the helices, sheets and loops that allow different P450s to accommodate different

substrates and redox partners (Boddupalli *et al.*, 1990; Graham and Peterson, 1996; Graham and Peterson, 1999; Omura, 1999; Miles *et al.*, 2000).

#### 1.2.5.2 Substrate recognition sequence

Although the structural fold is highly conserved, enough structural diversity remains within P450s to accomplish their variable functions. The variability in function lies with topological variations in the polypeptide backbone and the type of side chain lining the active site. Comparison of substrate-free and -bound structures of both P450 cam and P450 BM-3 reveals conformational changes between the two forms, indicating a degree of protein mobility important in substrate access and (possibly) catalysis, although these changes are much more marked in the P450 BM-3 enzyme. These factors explain why the overall the similar structure of P450s are able to catalyse a multitude of reactions with a varied range of substrates (Boddupalli *et al.*, 1990; Graham and Peterson, 1999; Miles *et al.*, 2000).

The most variable structural elements in P450s are the helices A, B', B, F, G, H, K', the  $\beta$  sheets  $\beta 3$  and  $\beta 4$ , and the loops, containing residues associated with substrate recognition/binding. These elements include six known substrate recognition sequences (SRS) (Figure 1.5) (Gotoh, 1992). The B'-helix region, parts of the F- and G-helices, a part of the I-helix, the K-helix  $\beta 2$  connecting region, and the  $\beta 4$  hairpin line the P450 active site and define the SRS regions. In particular, the SRS predetermine P450 substrate specificity; point mutations within SRSs significantly affect the substrate specificities (Gotoh, 1992). However, it should be noted that residues outside the SRSs can also impact on catalytic properties of the P450s.

In many instances, the resting form of an enzyme does not perfectly fit the structure of its substrate with proper molecular fit only occurring upon structural rearrangement after substrate binding to the protein. The proposed induced-fit model of substrate protein interaction (Koshland, 1958), addresses the functional importance of structural flexibility in proteins. Comparison of substrate-free and different ligand-bound P450 structures gives insight into the structural changes in P450s upon ligand binding, which can be explained by an induced-fit model (Schoch *et al.*, 2003).



### 1.2.6 Cytochrome P450 inhibitors

With respect to antifungals, there has been substantial investment by the pharmaceutical industry in the design and development of P450 inhibitors. Cytochrome P450 inhibitors can be divided into three different categories based on mechanism of action: (1) agents that bind reversibly, (2) agents that form *quasi*-irreversible complexes with the heme iron atom, and (3) agents that bind irreversibly to the active site pocket of the prosthetic heme group, or that accelerate degradation of the prosthetic heme group (Correia and Ortiz de Montellano, 1993).

The imidazoles and triazoles constitute the largest broad-spectrum class of antifungals in clinical use (Odds *et al.*, 2003) (Figure 1.6). The main target of antifungal azoles is the inhibition of CYP51, a cytochrome P450 involved in the 14 $\alpha$ -demethylation of lanosterol in the ergosterol biosynthetic pathway (Bossche *et al.*, 1995). Furthermore, in some fungal species, inhibition of the subsequent  $\Delta$ 22-desaturase step by CYP61 has been reported (Kelly *et al.*, 1997).

Ergosterol is an essential component of the fungal cell membrane, regulating membrane fluidity and permeability as well as the activity of membrane-bound enzymes. In yeast, ergosterol is also a major component of secretory vesicles and plays an important role in oxidative phosphorylation reactions (Bammert and Fostel, 2000). With ergosterol levels depleted, the normal permeability and fluidity of the fungal membrane is altered, with secondary consequences for membrane-bound enzymes, such as those involved in cell wall synthesis (Marichal *et al.*, 1995). Severe ergosterol depletion may additionally interfere with the hormone-like initiating functions of ergosterol, affecting cell growth and proliferation. Inhibition of 14 $\alpha$ -sterol demethylase leads not only to depletion of ergosterol and subsequent disruption of the integrity and function of the fungal cell membrane, but also to accumulation of toxic sterol precursors including squalene, zymosterol, lanosterol, 4,14-dimethylzymosterol, and 24-methylenedihydrolanosterol (Sanati *et al.*, 1997; Ghannoum and Kuhn, 2002). Therefore, azole-induced ergosterol depletion in the membrane severely affects cell growth and replication and may lead to irreparable damage, causing cell lysis (Rozman and Waterman, 1998; Szklarz and Halpert, 1998; Lewis *et al.*, 1999). Certain azole drugs, such as ketoconazole, not only directly

inhibit ergosterol biosynthesis but also, impair respiration and induce anaerobiosis through inhibition of mitochondrial cytochrome *c* oxidase in fungi (Georgopapadakou, 1998). This brings into focus possible problems with specificity of azole drugs for their fungal target. Not only is there potential for non-specific interactions with other P450s (Korashy *et al.*, 2007), but also the possibility of undesirable interactions with potassium channel proteins (Wu *et al.*, 2006).

The family of commercial azole anti-fungals include the compounds clotrimazole, econazole, fluconazole, ketoconazole, miconazole and voriconazole (Figure 1.6) (Correia and Ortiz de Montellano, 1993; Joseph-Horne and Hollomon, 1997). The group classification is derived from the number of nitrogen atoms in the azole ring, with two nitrogens in the case of imidazoles and three nitrogens for triazoles. The azole class of antifungal agents was first discovered in the late 1960s. The imidazole agents, miconazole and clotrimazole, were introduced for clinical use in the early 1970s, followed by ketoconazole, an orally active imidazole introduced in 1981. Triazoles constitute the second generation of azoles (Figure 1.6). The first triazoles, fluconazole and itraconazole, were introduced in the early 1990s and have found widespread use in fungal treatment, in large part due to an improved safety profile compared to alternatives (Hitchcock, 1993).

More recently new triazole antifungals have become available, including voriconazole and posaconazole. Voriconazole, enjoys a very broad spectrum of activity against several fungal species (Espinel-Ingroff *et al.*, 2001). It is structurally derived from fluconazole, with one triazole moiety replaced by a fluoropyrimidine group and a methyl group added to the propanol backbone (Girmenia *et al.*, 1998). Posaconazole has a close resemblance to itraconazole, but with the dioxolane ring altered to a tetrahydrofuran. Although the structural differences are small, they dictate antifungal potency and spectrum, bioavailability, drug interaction and toxic potential – very important considerations for compounds that bind to heme groups in P450s.

Substrate-linked imidazole derivatives, such as 12-(imidazolyl)-dodecanoate, have been shown to be potent inhibitors of the fatty acid hydroxylase P450 BM-3 and eukaryotic fatty acid hydroxylase, displaying the potential inhibitory value of substrate mimicking agents (Noble *et al.*, 1998). New imidazole compounds similar to

the azole anti-fungals, such as the bicyclic nitroimidazopyrans, inhibit the synthesis of protein and cell wall lipids in *M. tuberculosis*. The nitroimidazopyran based agent, PA-824 may inhibit an enzyme responsible for the oxidation of hydroxymycolate to ketomycolate (Bastain and Colebunders, 1999; Stover *et al.*, 2000).

Structure based *de novo* design and synthesis of non-azole inhibitors of fungal lanosterol 14 $\alpha$ -demethylases, with a view to reducing human drug toxicity, are also underway by molecular modelling with the *M. tuberculosis* CYP51 structure (Ji *et al.*, 2003). The azole anti-fungal agents, substrate mimics and non-azole agents may provide a new generation of agents required in the control of multi-drug resistant tuberculosis. Preliminary studies have indicated that azole drugs bind tightly to a number of *M. tuberculosis* P450s and that these agents prevent growth of mycobacteria and related bacteria (McLean *et al.* 2002b). The exact mechanism of action of the azoles remain to be elucidated. Azoles also alter the membrane composition of *M. smegmatis*, pointing to P450s roles in the generation of the membrane (Burguiere *et al.*, 2005).

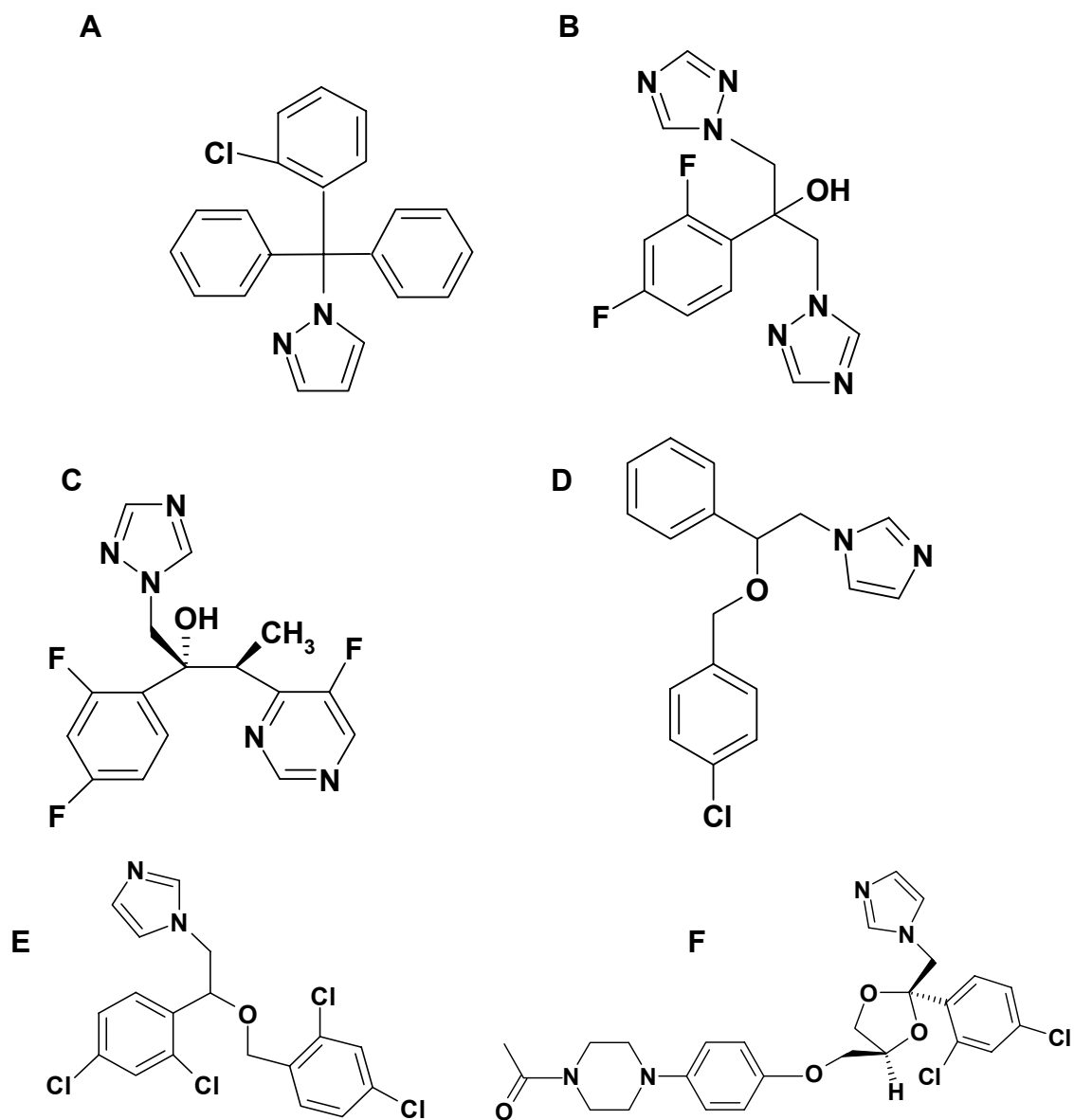


**Figure 1.6 Structures of selected azole anti-fungal P450 inhibitors**  
 (A) clotrimazole, (B) fluconazole, (C) voriconazole, (D) econazole, (E) miconazole and (F) ketoconazole. Structures were drawn with ISIS Draw.

### 1.3 Redox partners and electron transfer

For cytochrome P450s to accomplish their diverse range of chemical reactions, P450s in general receive the required reducing equivalents via interaction with one or more redox partners. Recent studies on the P450 systems, particularly those from microbial species, have revealed a great diversity in the systems used to deliver electrons to the P450s (as discussed above in section 1.2.4). In the majority of P450 systems, pyridine nucleotide coenzymes act as the initial source of hydride ions, electrons from which are delivered to the P450 via its appropriate redox partner(s).

#### 1.3.1 Pyridine nucleotide coenzymes

The nicotinamide coenzymes include  $\text{NAD}^+$  (nicotinamide adenine dinucleotide) and  $\text{NADP}^+$  (nicotinamide adenine dinucleotide phosphate). Both  $\text{NAD}^+$  and  $\text{NADP}^+$  serve as reversible initial carriers of reducing equivalents for P450s. The redox-active moiety is the nicotinamide base, which can be reduced by two electrons and protonated to generate NADH or NADPH. In effect, the nicotinamide accepts a hydride ion equivalent from the substrate. Such a reaction requires a strongly electrophilic centre, which is provided by the oxidised pyridinium ring. Specifically, the carbon atom *para*- to the hybridised nitrogen of the pyridine heterocycle is particularly active and its reactivity is enhanced by the presence of an amide group *ortho*- to it. The hydride donor and acceptor properties of the nicotinamide moiety of NAD(P)H are displayed in figure 1.7.

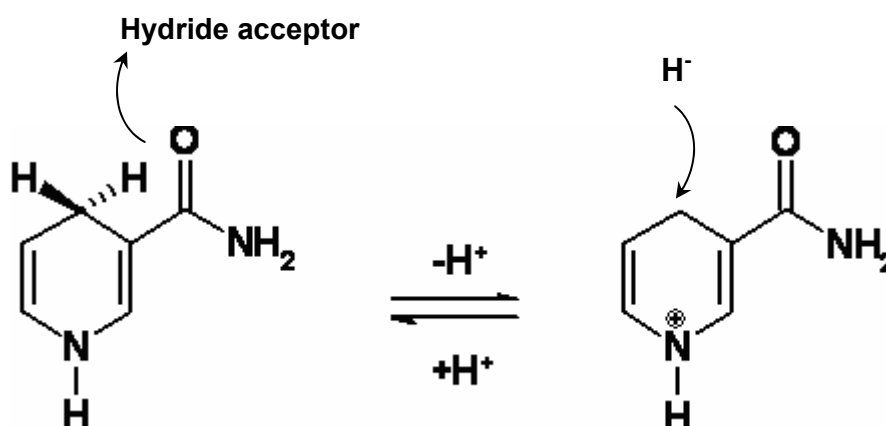


**Figure 1.7** Hydride donor/acceptor function of the nicotinamide moiety of NAD(P)H.

### 1.3.2 Flavin containing redox components

The flavin mononucleotide cofactor (FMN) provides the redox active component, whose intrinsic properties are profoundly modified by the host apoprotein. The FMN molecule is made of a fused, aromatic, triple ring (the isoalloxazine) (Figure 1.8A), a phosphate group and a linking ribityl chain chain attached to the central N-10 position of the pyrazine moiety. FMN is produced by the phosphorylation of riboflavin, at the 5' carbon of the ribityl linked group, while FAD is the adenylated version of FMN (Singer and Edmondson, 1978).

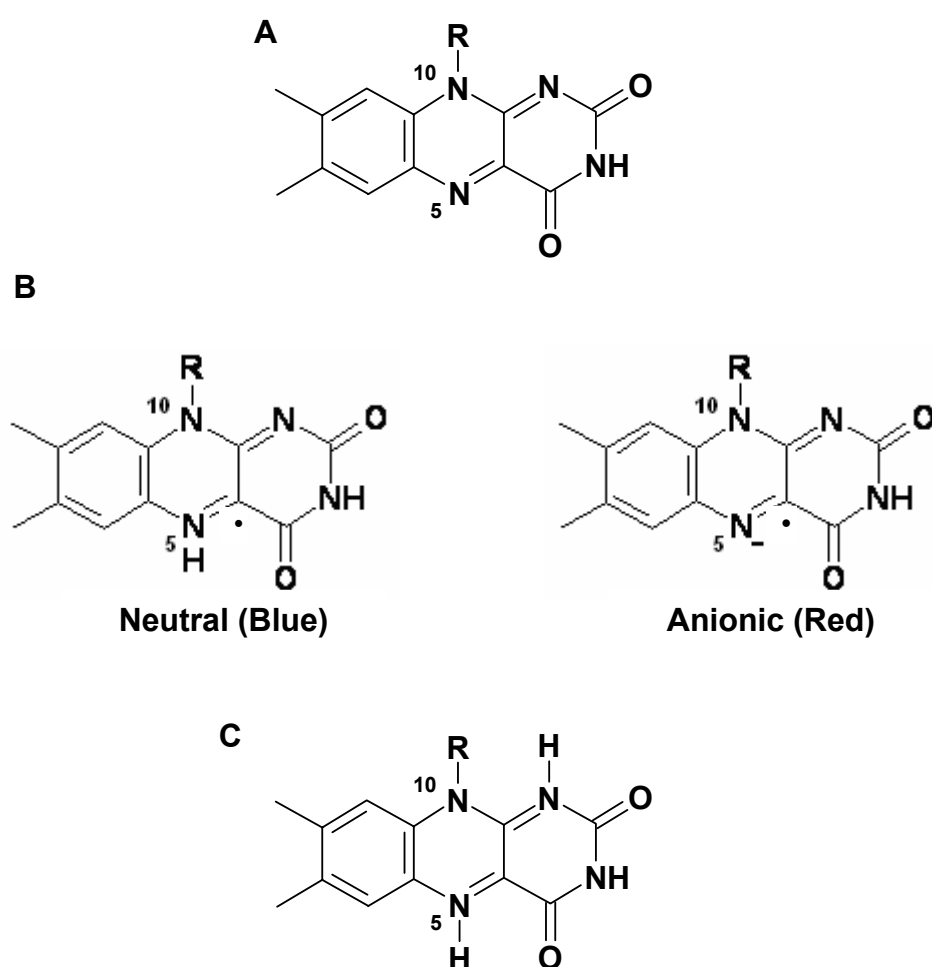


**Figure 1.8** Chemical structure of the isoalloxazine ring (oxidised and reduced states), the chemically reactive group of FAD and FMN flavin cofactors.  
(A) oxidised, (B) 1-electron reduced semiquinone form, and (C) hydroquinone.

Flavoproteins contain a flavin prosthetic group which can be bound to the protein non-covalently or, less commonly, covalently. The isoalloxazine ring provides the functional element of these cofactors, while the flavin prosthetic group side chain plays an important role in binding, and sometimes in modulation of redox properties (Sancho, 2006). Flavoproteins are typically involved in redox reactions as electron transfer enzymes, accepting one or two electrons from a reducing substrate and subsequently donating them to an oxidised substrate or electron acceptor (Sancho, 2006). Flavoproteins are often isolated in their single-electron reduced semiquinone form, e.g. the stable semiquinone forms of flavodoxins (Figure 1.8B). The isoalloxazine ring allows flavins to exist in three oxidation states; the fully oxidised quinone, one electron reduced semiquinone, and the two-electron reduced hydroquinone (Figure 1.8A, B, C). Thus, flavoproteins have the ability to mediate electron transfer between two-electron donors such as NAD(P)H and one electron acceptors such as heme or iron-sulphur centres. The oxidised form of flavin produces a yellow colour, while the fully reduced form is generally colourless. The one-electron reduced semiquinone form can be either red (anionic) or blue (neutral) in colour. The specific colour change facilitates the spectrophotometric monitoring of flavin reduction, enabling e.g. the identification of intermediates in flavoprotein catalytic cycles (Singer and Edmondson, 1978; Macheroux, 1999).

Flavoproteins are able to exist in separate reduction states due to the redox modifying properties of the apoprotein, forming complexes of different affinities with the three redox forms (Figure 1.8) and resulting in the relative stability of the oxidised, one-electron reduced (semiquinone) (Figure 1.8B) or two-electron reduced (hydroquinone) (Figure 1.8C) forms. Hydrogen-bonding as well as certain residue interactions are believed to be involved in the stabilisation of the neutral semiquinone (Simonsen and Tollin, 1980). Extensive information on identifying the residues of the polypeptide that are responsible for this differential binding has been provided by mutational work and NMR studies done mainly on flavodoxins from *Desulfovibrio vulgaris* (O'Farrell *et al.*, 1998; McCarthy *et al.*, 2002; Lohr *et al.*, 2004) and *Clostridium beijerinckii* (Kasim and Swenson *et al.*, 2000; Kasim and Swenson 2001; Lohr *et al.*, 2004), and also in those from *Anabaena* (Nogues *et al.*, 2004).

### 1.3.3 Iron-sulphur redox components

Iron-sulphur (Fe-S) clusters are a widely abundant and diversely employed class of enzymatic cofactor. These functions include direct catalysis of hydration/dehydration reactions (Beinert *et al.*, 1996), oxygen and iron sensing, regulation of gene expression (Gaudu and Weiss, 1996) and the generation and stabilisation of radical intermediates (Broderick *et al.*, 1997).

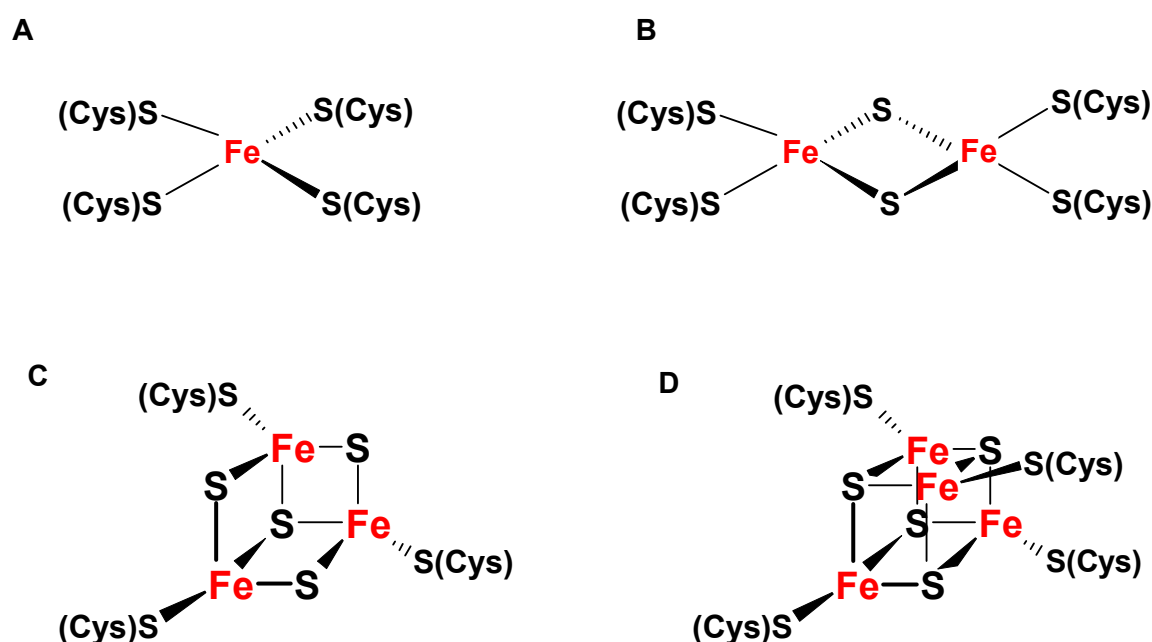


**Figure 1.9 Structures of common iron-sulphur clusters**  
A. Rubredoxin-style iron centre. (Cys)S or S(Cys) represents coordinating cysteine residues from the polypeptide backbone. B. [2Fe-2S] cluster. C [3Fe-4S] cluster. D. [4Fe-4S] cluster. S = inorganic sulphide and (Cys)S = cysteinyl-sulphur.

The basic Fe-S centre contains a single iron atom linked by four cysteine residues within a polypeptide (Figure 1.9A). Other Fe-S clusters have two, three or four iron atoms coordinated to polypeptide residues and linked by inorganic sulphide. More complex structures are assembled in specialised redox enzymes through metal substitution and/or bridges between the simpler cluster modules (Rees, 2002). The most common protein ligand is cysteine, but other residues including histidine,



aspartate and arginine have been observed (Duderstadt *et al.*, 1999; Chen *et al.*, 2002; Berkovitch *et al.*, 2004). Iron-sulphur clusters serve most prominently in redox enzymes, with the biochemical practicality of these clusters based in their ability to both accept and donate electrons. Ferredoxins are obligate one-electron carriers of low molecular weight. In addition to cysteine ligations, ferredoxins also contain acid-labile sulphide (Berkovitch *et al.*, 2004). Ferredoxins have tetrahedral coordination of the iron-sulphur cofactor, which can be in the form of inorganic sulphide or cysteine residues, and ferredoxins typically bind cofactors with 2Fe-2S, 3Fe-4S or 4Fe-4S clusters, as well as multinuclear iron clusters (Rees 2002) (Figure 1.9). Such multiple iron clusters potentially offer a greater range of oxidation states and reduction potentials.

Amongst the class I P450s, ferredoxins transfer electrons from an NAD(P)H-reduced ferredoxin reductase to the cytochrome P450. One of the best studied components of electron transfer of the Class I systems is the 2Fe-2S-cluster ferredoxin (putidaredoxin) from *Ps. putida* (Martinis *et al.*, 1996). During electron transfer, putidaredoxin operates two distinct binding sites for separate reductase (putidaredoxin reductase) and P450cam association (Lewis and Hlavica, 2000). Interaction with the reductase is facilitated via the negatively charged residues on the  $\alpha$ -helical segment of the ferredoxin as well as by hydrophobic and steric interactions; whilst specific hydrogen bonds from the surface loop near the iron sulphur cluster provide interactions with the P450 (Lewis and Hlavica, 2000). Moreover, bacterial P450s that utilise 3Fe-4S ferredoxins from *Streptomyces griseus* (Trower, 1992) and 4Fe-4S ferredoxins in the P450 BioI system (Green *et al.*, 2001) have emerged. Also observed in *Methylococcus capsulatus* is the CYP51FX sterol-demethylating enzyme, composed of a 3Fe-4S cluster-P450 fusion (Jackson *et al.*, 2003). The combination of redox partner proteins into a single polypeptide may improve the electron transfer to the terminal P450.

During evolution, various iron-sulphur cluster traits have ensured that they are redox moieties of choice. Principal among these is their wide range of reduction potentials, from -150 to +400 mV (Hunsicker-Wang *et al.*, 2003). Iron-sulphur potentials are influenced by moderate changes in protein structure that create local residue charges, dipole-dipole interactions with the polypeptide chain, and hydrogen

bonds between surrounding residues and the cluster sulphur ligands (Capozzi *et al.*, 1998; Babini *et al.*, 1999). Therefore, simple evolutionary changes can adjust iron-sulphur clusters for roles in many different redox pathways. The redox potential ( $E^\circ$ ) of putidaredoxin is -240 mV, which upon binding with P450cam increases to -197 mV (Sligar and Gunsalus, 1976). The positive increase in  $E^\circ$  is due to the iron-sulphur cluster repositioning within the interface of the two proteins (Lewis and Hlavica, 2000), consequently, improving the efficient transferral of electrons to the substrate bound P450 cam.

## **1.4 Tuberculosis**

### **1.4.1 Introduction**

*M. tuberculosis*, the aetiological agent of TB, has plagued humanity throughout recorded history. TB is a social disease that has always occurred disproportionately among disadvantaged populations such as the homeless, malnourished, and overcrowded. Within the past decade it also has become clear that both the spread of HIV infection and immigrants arriving from areas of high incidence have resulted in increased numbers of TB cases.

The knowledge gathered in the past decade about the structure of the tubercle bacillus, the epidemiology of TB, the physiological and immunological responses of the host to infection, and the physiology of *M. tuberculosis* in laboratory broth cultures is considerable. However, a large extent of the basic biology of *M. tuberculosis* in its natural setting of the infected human is unknown.

### **1.4.2 History**

TB has existed since pre-Columbian America, in the South Pacific before the arrival of Europeans, and was a likely common cause of death in Egypt some 4,000 years ago (Donoghue *et al.*, 2004). In the U.S. and Western Europe, TB was a frequent cause of adult mortality up until the 19<sup>th</sup> century (Wilson, 1990). Though TB mortality has dropped significantly in the industrialised world over the last 150 years, it remains a leading cause of death in developing countries, particularly among young adults. In contrast, TB mortality in industrialised countries is increasingly associated with older age (Pablos-Mendez *et al.* 1996; Cayla *et al.*, 2004). In 1882, Robert Koch

discovered *M. tuberculosis* (Murray, 1998). He developed staining techniques, culture media in which to grow the organism, demonstrated the mode of transmission of the illness and recommended the isolation of patients with TB (Schluger, 2005). In 1908, Albert Calmette and Camille Guérin created the BCG vaccine against tuberculosis (Murray, 1998).

The first major advance in the TB chemotherapy occurred in 1944, with the discovery of the potency of streptomycin against *M. tuberculosis* (Schatz *et al.*, 2005). Isoniazid was introduced in 1952, and was a more potent drug than streptomycin or para-aminosalicylic acid (Ryan, 1992). With this new chemotherapeutic agent, pulmonary tuberculosis could be cured with combined therapy using isoniazid, streptomycin, and para-aminosalicylic acid. Finally, the availability of rifampicin in the mid-1960s and the revival of pyrazinamide, allowed the development of modern "short-course" antituberculosis chemotherapy (Fox *et al.*, 1999). WHO eventually adopted the scheme of direct observation of medications taken orally under the DOTS (Directly Observed Therapy Short-Course) (Enarson, 1991). The DOTS strategy has proved to be an efficient, although under-used, methodology for national programs to deal with TB. However, the establishment of HIV–AIDS has negated many TB control efforts, particularly in developing countries, where the two infections often coexist (De Cock and Chaisson, 1999).

### **1.4.3 Tuberculosis epidemiology and transmission**

In sub-Saharan Africa, the overlapping HIV and TB epidemics have contributed to as much as a 200% TB case rate increase over the last 10 years, and the numbers continue to rise despite efforts to control TB (Cantwell and Binkin, 1996; Kenyon *et al.*, 1999). Current strategies, including DOTS, to deal with rising case rates in heavily HIV-afflicted countries have failed (De Cock, 1999). The continuing rise of TB in Africa and the relatively high TB incident rate in Europe highlight important limitations with current efforts to reduce TB mortality. In Eastern Europe, the emergence of multiple-drug-resistant TB (MDR-TB) is a tremendous burden on the healthcare system (Espinal *et al.*, 2001a; Odigwe, 2004).

Tuberculosis is spread from person to person through the air by droplet nuclei, particles 1 to 5 mm in diameter that contain *M. tuberculosis* (Edwards and Kirkpatrick,

1986). After inhalation, the droplet nucleus is carried down the bronchial tree and implants in a respiratory bronchiole or alveolus. Whether or not an inhaled tubercle bacillus establishes an infection in the lung depends on both the bacterial virulence and the microbicidal ability of the ingesting alveolar macrophage (Dannenberg, 1989).

#### **1.4.4 *M. tuberculosis* chemotherapy**

*M. tuberculosis* is a difficult therapeutic target, due to the organism's long generation time and low metabolic activity when in dormancy (Wayne, 1994; McKinney *et al.*, 2000). In addition, tubercle bacilli locations such as the pulmonary cavities, pleural fluid, or solid caseous material, provide difficulty for the penetration of antibiotics, or exhibit low pH to inhibit the activity of most antibiotics (Iseman and Madison., 1991). A major advance in therapy occurred in the late 1960s with the discovery of rifampicin, which enabled the development of orally administered regimens that ultimately reduced the length of therapy from 18–24 months to a mere 6 months.

The aim of TB therapy is not just to cure the patients and to prevent their relapse, but also to render them rapidly non-infectious and to prevent the emergence of drug resistance. Anti-TB agents are therefore selected to rapidly kill actively metabolizing bacilli in the lung cavities, to destroy less actively replicating bacilli in acidic and anoxic closed lesions, and to kill near-dormant bacilli that might otherwise cause a relapse of the disease (Mitchison, 2000). In this context, a distinction is drawn between agents that will kill bacilli *in vitro* (bactericidal agents) and those that will sterilize lesions *in vivo*.

The most effective agents for the destruction of tubercle bacilli in the three categories described above are, respectively, isoniazid (INH), pyrazinamide (PZA) and rifampicin. Accordingly, these three agents form the basis of modern regimens, which are divided into an initial 2-month intensive phase in which all three agents are administered together with, in most regimens, a fourth agent, usually ethambutol (WHO, 2001). These agents destroy bacilli during the initial intensive phase of treatment. This phase is followed by a 4-month course of rifampicin and isoniazid. The former kills residual dormant bacilli and the latter kills any rifampicin-resistant mutants that commence replication.

### 1.4.5 Drug-resistant TB

Drug resistance in patients with *Mycobacterium tuberculosis* infection became evident soon after the introduction of effective antituberculosis agents (Canetti, 1965). In the early 1990s, outbreaks of multidrug-resistant tuberculosis were reported in patients with HIV (Dooley *et al.*, 1992; Fischl *et al.*, 1992; Small *et al.*, 1993; Alland *et al.*, 1994). Multidrug-resistant tuberculosis (MDR-TB) is caused by *Mycobacterium tuberculosis* resistant to, at least, isoniazid and rifampicin (Espinal *et al.*, 2003), the two fundamental components of any regimen for the treatment of drug-susceptible TB.

Cases of MDR-TB are substantially more difficult to treat, with the therapy often based on pyrazinamide, to which some strains are still susceptible, or second-line drugs that are often more toxic, more expensive and less active than the standard first-line drugs (Mukherjee *et al.*, 2004). Furthermore, the therapy is of longer duration than that of standard regimens, continuing for nine to twelve months after the sputum becomes negative for *M. tuberculosis*. The problem of resistance results from treatment that is inadequate, often because of an irregular drug supply, inappropriate regimens, or poor compliance (Kochi *et al.*, 1993; O'Brien and Nunn, 2001; Espinal *et al.*, 2001b). With careful management, many patients with MDR-TB may be cured. The presence of these antimicrobial agents applies a selective pressure, enabling resistant organisms to develop. Accordingly, MDR *M. tuberculosis* strains have accumulated independent mutations in genes encoding either the drug target or the enzymes involved in drug activation (Zhang and Telenti, 2000; Wade and Zhang, 2004). However, the genetic basis of resistance to some anti-TB agents is not fully understood (Rattan *et al.*, 1998). For example, streptomycin resistance emerges through mutations in *rrs* and *rpsL* genes, leading to a change in the binding site for streptomycin in the ribosome. However, such changes have been identified in just over half the strains studied to date (Honore and Cole, 1994; Sreevatsan *et al.*, 1996). Mutations in the *pncA* gene, encoding pyrazinamidase, are thought to be the major mechanism of pyrazinamide resistance in *M. tuberculosis*, but resistant strains containing the wild-type gene have been described (Mestdagh *et al.*, 2000). Moreover, although the primary targets of activated isoniazid are enzymes involved in the biosynthesis of cell wall mycolic acids, mutations associated with changes in these targets have been shown to contribute to isoniazid resistance, but cannot entirely

account for the observed resistance (Slayden and Barry, 2000). Another factor is the low permeability of the lipid-rich mycobacterial cell wall, which presents *M. tuberculosis* with an intrinsic resistance to most antibiotics, and appears to be one of the main factors involved in restricted drug uptake (Brennan, 2003; Niederweis, 2003).

#### **1.4.6 Chemotherapeutic agents of TB**

Bacterial resistance to antibiotics typically involves drug inactivation or modification, target alteration, or decrease in drug accumulation associated with decrease in permeability and/or increase in efflux (Li and Nikaido, 2004). Other resistance mechanisms include inhibition of the activation of pro-drugs, such as the unique antitubercular compounds isoniazid and pyrazinamide, into active drugs (Raynaud *et al.*, 1999; Scior *et al.*, 2002).

Historically, mycobacterial cell wall synthesis and assembly has been thought to be the target of many effective antituberculosis agents, including isoniazid. Drugs such as isoniazid, ethionamide, and thiocarlide interfere with the synthesis of mycolic acids (Takayama *et al.*, 2005). The subsequent lack of mycolic acids has been thought to ultimately lead to a disruption of the hydrophobic barrier, resulting in a loss of cellular integrity (Barry III *et al.*, 1998). The actual cause of death of the organism may be related not simply to the production of cell wall, but instead to a dysregulation of the proteins involved in that process. The action and mechanism of resistance of the most important antituberculosis drugs are still not fully understood.

##### **1.4.6.1 Isoniazid**

Isoniazid has been a mainstay of TB chemotherapy since its discovery more than 50 years ago. It is known that isoniazid is a pro-drug, whose *in vivo* activation occurs as the result of its oxidation by the *katG*-encoded catalase-peroxidase (Zhang *et al.*, 1992; Heym *et al.*, 1993) (Figure. 1.10). Based on *in vitro* experiments, it has been proposed that the activation of isoniazid generates a number of 4-isonicotinoyl-NAD (isoniazid-NAD) adducts (Johnsson and Schultz, 1994; Nguyen *et al.*, 2003). Isoniazid resistance has been associated with mutations in several genes. The most commonly reported mutations occur at three loci: *katG*, *inhA* (Musser *et al.*, 1996), and the *oxyR-ahpC* region (Wilson and Collins, 1996).

The *inhA*-encoded, NADH-dependent enoyl-ACP protein reductase is the primary target for isoniazid. A reactive form of isoniazid inhibits InhA by reacting with the NAD(H) cofactor bound to the enzyme active site forming a covalent adduct (isonicotinic acyl NADH) that is apt to bind with high affinity (Rozwarski *et al.*, 1998). This enzyme is part of the type II fatty acid synthase complex responsible for elongating C<sub>16</sub>-C<sub>18</sub> acyl-ACPs to generate the C<sub>50</sub>-C<sub>60</sub> meromycolates (White *et al.*, 2005). These are subsequently condensed with C<sub>24</sub> fatty acids to generate the mycolic acids (Barry III *et al.*, 1998; Takyama *et al.*, 2005).

Mutation in the *katG* gene is the most common source for clinical resistance (Telenti *et al.*, 1997a; Kiepiela *et al.*, 2000; Piatek *et al.*, 2000; Ramaswamy *et al.*, 2003). Commonly, resistance is associated with a single G-to-C point mutation, revealed by gene sequencing studies, which results in a serine-to-threonine amino acid substitution at codon 315 (Ramaswamy and Musser, 1998). Mutagenesis experiments have confirmed that this nucleotide substitution confers isoniazid resistance with only a moderate reduction in catalase-peroxidase activity (Rouse *et al.*, 1996; Wengenack *et al.*, 1997). Other resistance-conferring substitutions have been reported at the same site (Bifani *et al.*, 2002).

Mutations in the *oxyR-ahpC* intergenic region have been studied less frequently (Kiepiela *et al.*, 2000; Ramaswamy *et al.*, 2003). The roles of mutations in the *oxyR-ahpC* locus are less clear. The *ahpC* gene encodes alkylhydroperoxidase, an enzyme thought to be important in the oxidative stress response (Wilson and Collins, 1996). Mutations upstream of *ahpC* have previously been reported in isoniazid-resistant isolates. There is no evidence that overexpression of alkylhydroperoxidase confers isoniazid resistance to susceptible isolates; however, mutations resulting in the upregulation of *ahpC* have been associated with the absence of catalase-peroxidase activity and are thought to be compensatory mutations important for the survival of the organism (Stretevatsan *et al.*, 1997a). A real molecular understanding of the series of events that render *M. tuberculosis* so highly sensitive to isoniazid remains elusive.

### 1.4.6.2 Rifampicin

One of the main reasons for treatment failure and fatal clinical outcome in tuberculosis patients is resistance to rifampicin (Mitchison and Nunn, 1986). In addition to a significant early bactericidal effect on metabolically active *M. tuberculosis*, rifampicin also exhibits excellent late sterilizing action on semi-dormant organisms undergoing short bursts of metabolic activity. The recognition of this late effect of rifampicin, and the additional effectiveness of pyrazinamide, has allowed for the reduction of routine tuberculosis treatment from 1 year to 6 months (Grosset, 1978; Mitchison, 1992).

Rifampicin inhibits mycobacterial transcription by targeting DNA-dependent RNA polymerase (Figure. 1.10). The development of resistance to rifampicin is due to mutations in a well-defined, 81 base pair (bp) (27 codons) central region of the gene that encodes the  $\beta$ -subunit of RNA polymerase (*rpoB*) (Telenti *et al.*, 1993). More than 96% of the rifampin-resistant strains contain a mutation in this 81 bp region of *rpoB*, thus facilitating a straightforward approach to detecting rifampicin resistance (Ramaswamy and Musser, 1998; Heep *et al.*, 2000).

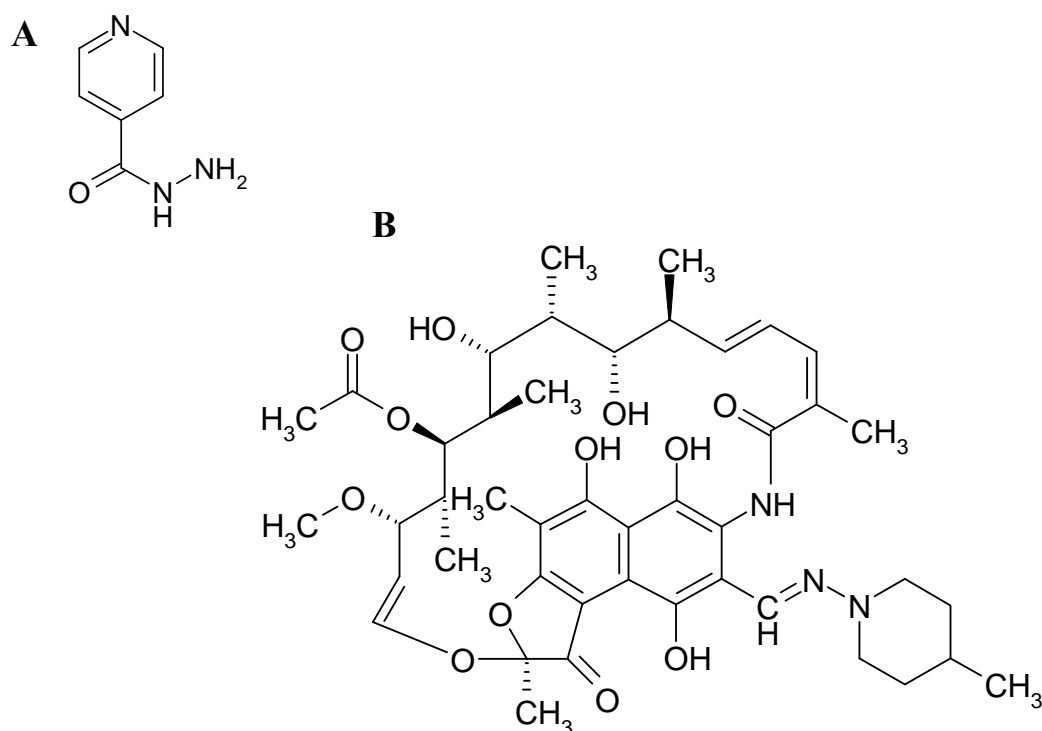


**Figure 1.10 Chemical structures of the principal anti-tuberculosis drugs**  
A: Isoniazid (isonicotinic acid hydrazide); B: Rifampicin (3-[[[4-methyl-1-piperazinyl] imino]-methyl]-rifamycin).



### 1.4.6.3 Pyrazinamide

Pyrazinamide has an excellent sterilising effect on semi-dormant tubercle bacilli and, when used in combination with isoniazid and rifampicin, shortens the duration of treatment of tuberculosis patients from 1 year to 6 months (Steele and Dez Prez., 1988; Bass *et al.*, 1994).

Pyrazinamide, a structural analogue of nicotinamide, is a pro-drug that requires amide hydrolysis by mycobacterial pyrazinamidase (a nicotinamidase) to pyrazinoic acid (Konno *et al.*, 1967). Pyrazinamide kills semi-dormant tubercle bacilli under acidic conditions (Heifets and Lindholm-Levy, 1992). The accumulation of pyrazinoic acid lowers the intracellular pH to a suboptimal level that is likely to inactivate a vital target enzyme, such as fatty acid synthase I (Zhang *et al.*, 1999; Zimhony *et al.*, 2000;).

It has been observed that the pyrazinamide-resistant *M. tuberculosis* isolates usually lose their *pncA*-encoded pyrazinamidase activity (Konno *et al.*, 1967). It was found that 72–97% of all pyrazinamide-resistant clinical isolates tested carry a mutation in the structural gene or in the putative promoter region of the gene (Scorpio and Zhang, 1996). However, the involvement of other mechanisms i.e. those that involve pyrazinamide uptake, *pncA* regulation, or pyrazinoic acid efflux is suggested by the existence of isolates that exhibit a high level of pyrazinamide resistance without mutations in the *pncA* gene (Raynaud *et al.*, 1999).

### 1.4.6.4 Streptomycin

Streptomycin is an aminocyclitol glycoside antibiotic directly targeting the ribosomal unit (Carter *et al.*, 2000). In *E. coli*, streptomycin binds to 16S rRNA, inhibiting translational initiation in the process, and resulting in detrimental effects in translation reliability (Moazed and Noller, 1987). The ribosome centre is a highly conserved component of the translational apparatus (Alksne *et al.*, 1993), comprising an rRNA domain and several polypeptides of the small subunit, including the ribosomal protein S12 (Carter *et al.*, 2000). Mutations associated with *M. tuberculosis* streptomycin resistance have been identified in the genes *rpsL* and *rrs*, which are involved in the synthesis of ribosomal proteins S12 and S16, respectively. Mutations

in these genes account for 70% of streptomycin resistant strains (Timms *et al.*, 1992; Finken *et al.*, 1993; Toivonen *et al.*, 1999).

#### **1.4.6.5 Ethambutol**

Ethambutol ([S,S']-2,2'-[ethylenediimino])di-1-butanol is a bactericidal drug that inhibits incorporation of mycolic acids into the cell wall (Takayama and Kilburn, 1989). Takayama and Kilburn (1989) showed that ethambutol inhibited the transfer of arabinogalactan into the cell wall of *M. smegmatis*, a process that led to the accumulation of mycolic acids and their cognate trehalose esters (Wolucka *et al.*, 1994). Ethambutol has been proposed to be an arabinose analogue, and the specific target is an arabinosyl transferase. To gain an insight into ethambutol resistance, a three gene locus (*embCAB*) that encodes arabinosyl transferases has been established in *M. smegmatis* (Telenti *et al.*, 1997b). It is likely that the molecular basis of ethambutol resistance involves altered interaction of the drug with one or more products of the *embCAB* operon. Mutations of the *embB* gene are associated with roughly 70% of ethambutol resistant isolates (Telenti *et al.*, 1997b; Sreevatsan *et al.*, 1997b). The cause of ethambutol resistance in many organisms lacking mutations in the *EmbB* putative arabinosyltransferase is unknown (Telenti *et al.*, 1997b).

#### **1.4.6.6 Second line chemotherapy**

By definition, chemotherapy of MDR-TB cannot rely solely upon isoniazid and rifampicin, the two most effective drugs for the treatment of TB. Depending on the individual susceptibility pattern, residual first-line drugs must be appropriately combined with additional second-line drugs.

Currently available second-line drugs used to treat MDR-TB are four to ten times more likely to fail than with the benchmark therapy for drug-susceptible tuberculosis (Telzak *et al.*, 1995; Park *et al.*, 1996; O'Brien and Vernon, 1998; Espinal *et al.*, 1999). Since the introduction of rifampicin, no notable antituberculosis drug with new mechanism(s) of action has been developed in over thirty years. Second-line drugs include agents such as pyrazinamide, amikacin/kanamycin, capreomycin, *p*-aminosalicylic acid, clarithromycin, linezolid and also some more recently discovered classes of drugs, notably the fluoroquinolones (e.g. ofloxacin, moxifloxacin) (Dincer *et al.*, 2004).

*M. tuberculosis* is naturally resistant to many antibiotics, due mainly to the highly hydrophobic cell envelope acting as a permeability barrier (Cole and Telenti, 1995). However, numerous other putative resistance mechanisms encoded within the genome await characterisation. These include hydrolytic or drug-modifying enzymes such as  $\beta$ -lactamases and aminoglycoside acetyl transferases, and numerous drug-efflux systems. Characterisation of these resistance mechanisms will facilitate the conception of new therapies and improved drug design.

#### **1.4.7 Bacteriology of *M. tuberculosis***

*M. tuberculosis* is a member of the actinobacteria and is a Gram-positive, non-motile microbe with a pleiomorphic rod structure. Distinctive features of the tubercle bacillus include its slow growth, dormancy, complex cell envelope, intracellular pathogenesis and genetic homogeneity (Wheeler and Ratledge, 1994). The generation time of *M. tuberculosis*, in synthetic medium or infected animals, is typically ~24 hours. The completed genome sequence of *M. tuberculosis* H37Rv revealed a 4,411,529 bp genome with a mean G+C content of 65.6 mol % (Cole *et al.*, 1998). The genome contains about 4000 genes (Cole *et al.*, 1998) with accurate or putative functions attributed to roughly 52 % of the genes, with the remaining genes being conserved hypotheticals or unknown (Camus *et al.*, 2002). There is a slight bias in the direction of replication with respect to the orientation of the genes, as about 59% are transcribed with the same direction as replication, compared with 75% in *Bacillus subtilis*. Genes transcribed in the same direction as the replication function are believed to be expressed more efficiently (Blattner *et al.*, 1997; Kunst *et al.*, 1997). Thus, the more balanced gene polarity distribution in *M. tuberculosis* may reflect the slow growth and infrequent replication cycles (Cole *et al.*, 1998).

#### **1.4.8 Mycobacterial cell wall**

The cell envelope of *M. tuberculosis* deserves particular consideration due to its exceptional structure, which is rich in unusual lipids, glycolipids and polysaccharides (Kolattukudy *et al.*, 1997) and has importance in many of the virulent properties of the microbe. Novel biosynthetic pathways generate cell wall components such as mycolic acids, mycocerosic acid, phenolthiocerol, lipoarabinomannan and arabinogalactan, and several of these may contribute to mycobacterial longevity, trigger inflammatory host reactions and act in pathogenesis. It is unusual in that 60%

of the envelope is composed of mycolic acids, a unique branching form of lipid, found only in mycobacteria and corynebacteria (Kolattukudy *et al.*, 1997). These are strongly hydrophobic structures and create an effective permeability barrier around the cells. Lipids play an important role in mycobacterial pathogenesis (Glickman and Jacobs, 2001). Their role in growth and persistence is not surprising, as the importance of the lipid-rich cell envelope of mycobacteria has long been suspected, and this role is supported by studies that show immunomodulatory activities of purified mycobacterial surface components on host cells and *in vivo*. Studies have shown that expression and regulation of *M. tuberculosis* lipids such as mycolic acids and phthiocerol dimycocerosate are required for *in vivo* growth and persistence (Glickman and Jacobs, 2001).

#### 1.4.9 Cell wall structure

The mycobacterial cell envelope (Figure 1.11) is important in directing host–pathogen interactions (Brennan and Nikkaido, 1995).

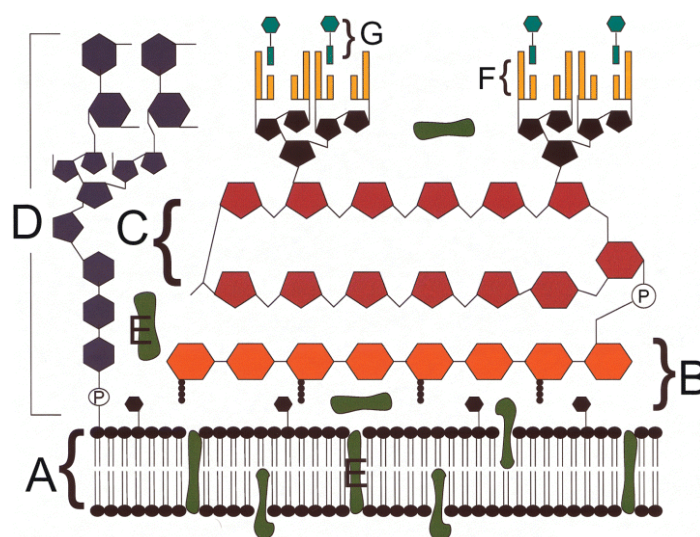


**Figure 1.11 Schematic representation of the cell envelope of *M. tuberculosis***  
 Above the plasma membrane (A) is the peptidoglycan (B) to which the arabinogalactan is attached (C) via a diglycosylphosphoryl bridge. Another major component of the cell wall is the mannose-capped lipoarabinomannan (D) that is attached to the plasma membrane via a phosphatidylinositol anchor. (E) represents the plasma membrane- and cell envelope-associated proteins (Brennan and Nikaido, 1995). The mycolic acid chains (F) are shown perpendicular to the plasma membrane, with the exposed chains interacting with the mycolic acid chains of the glycolipid surface molecule, trehalose dimycolate (G). The image was adopted from Karakousis *et al.*, 2004.

Lipoarabinomannan (LAM) is a phosphatidylinositol-anchored lipoglycan composed of a mannan core with oligoarabinosyl-containing side-chains, and has diverse biological activities (Chatterjee and Khoo, 1998; Hunter and Brennan, 1990; Chatterjee *et al.*, 1991). Structural variations in LAM occur according to mycobacterial species, and three general classes of LAM have been described. Within the *M. tuberculosis* spp., specifically the virulent strains Erdman and H37Rv and the avirulent strains of H37Ra and BCG, the cell wall is comprised of mannose-capped LAM (ManLAM) (Chatterjee *et al.*, 1992a; Prinzis *et al.*, 1993). ManLAM is characterised by extensive mannose capping of the arabinan termini. Phospho-*myo*-inositol-capped LAM (PILAM), is found in the rapidly growing *M. smegmatis* and *M. fortuitum* (Nigou *et al.*, 2003), and AraLAM, which was described in the rapidly growing *M. chelonae*, lacks mannosylation in its arabinan termini (Guerardel *et al.*, 2002). Differences in biological activity between the major classes of LAM have been attributed primarily to the heavy mannose capping of ManLAM or to differences in the phosphatidylinositol anchor (Barnes *et al.*, 1992; Chatterjee *et al.*, 1992b).

The sulpholipids of *M. tuberculosis* are mycobacterial cell envelope molecules with pleiotropic biological activities, including antitumour activity (Yarkoni *et al.*, 1979). Five structurally related sulphatides have been identified, with Sulpholipid-I (SL-I), the main sulphatide of the family, identified as a 2,3,6,6'-tetraacyl- $\alpha,\alpha'$ -D-trehalose 2'-sulphate (Goren *et al.*, 1976). Sulpholipid expression by various *M. tuberculosis* strains has been correlated with virulence in the guinea pig model (Goren, 1982). SL-I biosynthetic genes have been identified, including *pks2* (Sirakova *et al.*, 2001) and *mmpL8* (Converse *et al.*, 2003).

Mycolic acids are high-molecular-weight  $\alpha$ -alkyl,  $\beta$ -hydroxy fatty acids found in the genera *Mycobacterium*, *Nocardia*, *Corynebacterium* and *Rhodococcus* (Brennan and Nikaido, 1995). Covalently attached to arabinogalactan, mycolic acids constitute a very hydrophobic barrier (Draper, 1998) responsible for resistance to certain drugs (Nikaido, 2001). Mycolic acid-containing glycolipids exert a number of immunomodifying effects, in particular, trehalose-6,6'-dimycolate (TDM), which is the most abundant representative of this class of molecules. TDM has a number of biological activities, including high toxicity to mice (Behling *et al.*, 1993), potent adjuvant activity by stimulating cell-mediated immunity with co-administration of

protein antigen (Ribi *et al.*, 1982), and proangiogenic activities (Saita *et al.*, 2000; Sakaguchi *et al.*, 2000).

The 19 kDa lipoprotein is a member of a family of prokaryotic lipoproteins that have been found extensively in both Gram-positive and Gram-negative bacteria (Brightbill *et al.*, 1999). In the *M. tuberculosis* complex, the lipoprotein is anchored to the cell wall by its lipid moiety (Young and Garbe, 1991). Although its function remains largely unknown, the 19 kDa lipoprotein has been implicated in a range of immunological responses. The immunological activity of the lipoprotein has been attributed to the NH<sub>2</sub>-terminal triacylated lipopeptide region, as removal of the fatty acyl moieties abolishes the immunoregulatory functions of the parent molecule (Brightbill *et al.*, 1999). The pleiotropic immunological effect of the cell envelope components presents difficulty in discerning the precise mechanism by which each contributes to the vitality of tuberculosis.

#### **1.4.10 *M. tuberculosis* metabolism**

The Mtb H37Rv genome sequence has unravelled a number of putative pathways involved in the synthesis of essential amino acids and enzyme co-factors. *M. tuberculosis* can metabolise a variety of carbohydrates, hydrocarbons, alcohols, ketones and carboxylic acids (Cole *et al.*, 1998). In addition to genes involved in lipid metabolism, the genes necessary for glycolysis, the pentose phosphate pathway, and the tricarboxylic acid and glyoxylate cycles are all present (Cole *et al.*, 1998).

##### **1.4.10.1 Lipid metabolism**

A structurally diverse range of lipophilic molecules are generated by *M. tuberculosis*. These lipids range from simple fatty acids such as palmitate, through to isoprenoids, and to complex long-chain molecules such as mycolic acids (Cole *et al.*, 1998). However, with roughly 250 enzymes involved in fatty acid metabolism, the degradative fatty acid oxidation capability of *M. tuberculosis* exceeds the biosynthetic diversity (Cole *et al.*, 1998). The significance of such a high number of fatty acid metabolising genes is further highlighted by the presence of only fifty fatty acid metabolising genes in *E. coli* (Cole *et al.*, 1998).

#### 1.4.10.2 Fatty acid degradation

Mycobacteria are regarded to be largely lipolytic, rather than lipogenic, because of the quantity of genes encoding components of fatty acid oxidation systems. (Wheeler and Ratledge, 1994). This is further highlighted in *Mycobacterium tuberculosis* by the presence of 36 acyl-CoA synthases and a family of 36 related enzymes that may catalyse the first step in fatty acid degradation (Cole *et al.*, 1998).

#### 1.4.10.3 Fatty acid biosynthesis

Fatty acids are synthesised from malonyl-CoA and precursors are generated by the enzymatic carboxylation of acetyl (or propionyl)-CoA by a biotin-dependent carboxylase (Cole *et al.*, 1998). At least two discrete enzyme systems are involved in fatty acid biosynthesis in mycobacteria, fatty acid synthase (FAS) I and FAS II. FAS I is a single polypeptide with multiple catalytic activities, that is found predominantly in eukaryotes. It catalyses the formation of C<sub>16</sub>-C<sub>18</sub> and C<sub>24</sub>-C<sub>26</sub> fatty acids, subsequently released as CoA derivatives. (Petersen and Bloch, 1977; Kolattukudy *et al.*, 1997). The FAS II consists of dissociable enzyme components that exclusively use long-chain (C<sub>16</sub> to C<sub>24</sub>) primers for synthesising the extraordinarily long (C<sub>50</sub> to C<sub>60</sub>) meromycolic acids (Slayden and Barry III, 2002).

Mycolic acids are characterised by very hydrophobic C<sub>50</sub> to C<sub>60</sub> β-fatty acids with shorter C<sub>22</sub> to C<sub>26</sub> α- alkyl side chains (Brennan and Nikaido, 1995; Kolattukudy *et al.*, 1997; Schroeder *et al.*, 2002) (Figure 1.12). Synthesis of the backbone of fatty and mycolic acids in the cell is followed by extensive post-synthetic modifications and desaturations, particularly in the case of the mycolic acids (Barry III *et al.*, 1998). Much of the subsequent structural diversity in mycolic acids is generated by a family of S-adenosyl-L-methionine-dependent enzymes, which introduce *cis* and *trans* cyclopropanes into the unsaturated meromycolic acid precursor (Barry III *et al.*, 1998).

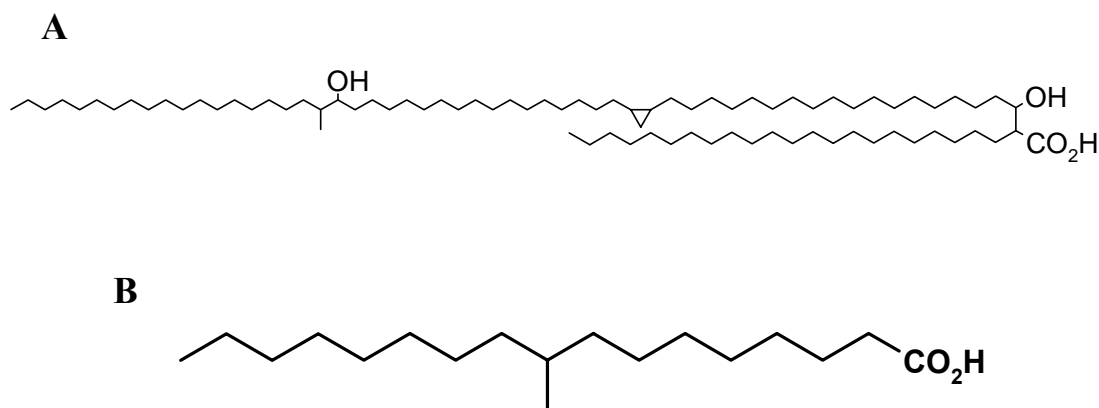


**Figure 1.12 Examples of lipophilic molecules found in the *M. tuberculosis* cell envelope**

A: mycolic acid; B: tuberculostearate

Tuberculostearic acid (10-methyl-octadecanoic acid) is a cell wall constituent of mycobacteria and has been explored as a diagnostic marker for the detection of TB (Stopforth *et al.*, 2005) (Figure 1.12). The methylation of oleic acid to form tuberculostearic acid may be performed by one of two enzymes, lipid methyltransferases (Ufa1 and Ufa2) that share homology with cyclopropane fatty acid synthase of *E. coli* (Barry III *et al.*, 1998).

#### 1.4.10.4 Polyketide synthesis

Several different polyketide synthesis mechanisms exist in mycobacteria. A modular type I system, similar to that involved in erythromycin biosynthesis (Hopwood, 1999), is encoded by a very large *pps* operon, and functions in the production of phenolphthiocerol (Kolattukudy *et al.*, 1997). The absence of a second type I polyketide synthase suggests that the related lipids phthiocerol A and B may all be synthesised by the same system.

Another large class of polyketide synthases are able to generate the multiply methyl-branched fatty acid components of mycosides and phthiocerol dimycocerosate, which are abundant cell wall-associated molecules (Hopwood, 1999). A fourth class of polyketide synthases is related to the plant enzyme superfamily that includes chalcone and stilbene synthase (Hopwood, 1999). These polyketide synthases



generate unreduced polyketides that are similar to anthocyanin pigments and flavonoids (Cole *et al.*, 1998).

#### **1.4.10.5 Siderophores**

Peptides that are not ribosomally synthesised are made by a process that is mechanistically analogous to polyketide synthesis (Hopwood, 1999). These peptides include the structurally related iron-scavenging siderophores, the mycobactins and the exochelins (Gobin *et al.*, 1995).

Mycobactins function by binding one atom of iron per molecule. Mycobactins are virtually insoluble in water because of the long alkyl chain attached to the molecule (Bosne *et al.*, 1992). The importance of mycobactin to the growth of *M. tuberculosis* has been established by a *M. tuberculosis* mutant lacking a mycobactin biosynthetic gene, which resulted in a considerably decreased ability to grow in human macrophages (De Voss *et al.*, 2000). The water soluble exochelins are able to remove iron from host sources of iron, such as transferrin and ferritin, as well as being able to solubilise it from inorganic sources such as ferric hydroxide or ferric phosphate (Dover and Ratledge, 2000).

#### **1.4.10.6 Sterol biosynthesis**

The genome sequence of *M. tuberculosis* revealed a number of genes homologous to *Saccharomyces cerevisiae* sterol biosynthetic enzymes. Sterols are universally synthesised from acetic acid via the key intermediates mevalonic acid and squalene (Mercer, 1991), found in mammals, fungi and plants. It is still unclear whether sterols are present in *M. tuberculosis*.

Further light on the obscure role of sterols was made when cholesterol was found to play a crucial role not only in entry of mycobacteria into macrophages, but also in mediating the phagosomal association of TACO, a coat protein that prevents degradation of mycobacteria in lysosomes (Gatfield and Pieters, 2000).

### **1.5 Aims and objectives**

The aim of this part of the study is to further understand the biochemical and biophysical properties of *M. tuberculosis* CYP121 (McLean *et al.*, 2002a) through

analysis of a series of mutants. Expression and biophysical studies have established that the wild-type CYP121 has properties typical for members of this class (McLean *et al.*, 2002a). Whereas the physiological role remains unclear, the enzyme binds bulky azole antifungal drugs with high affinity, and the binding constants for these drugs are perturbed by the presence of erythromycin and other large polyketides, suggesting that CYP121 may metabolizes polyketides or bulky polycyclics *in vivo* (McLean *et al.*, 2002a). The high level resolution (1.06 Å) of the CYP121 crystal structure revealed important residues for further study, including residue Pro<sup>346</sup> which is involved in the distortion of the heme macrocycle, Arg<sup>386</sup> which lies in the vicinity of the heme-substrate binding pocket and Ser<sup>279</sup>, a critical residue at the junction of proposed proton relay pathways (Leys *et al.*, 2003).

## **1.6 *Mycobacterium ulcerans***

### **1.6.1 Introduction**

Buruli ulcer, caused by the pathogen *M. ulcerans*, is a major mycobacteriosis that affects people in scattered foci around the world. *M. ulcerans* is the third most common mycobacterial human pathogen, after *M. tuberculosis* and *M. leprae*, and is amongst the most neglected of human diseases in terms of knowledge and healthcare strategies. The increasing incidence of Buruli ulcer, particularly in West Africa, has led the WHO (World Health Organisation) to recognise it as an emerging disease (WHO, 1998). Currently, the epidemiology of the disease is poorly understood, but recent advances including the unravelling of the pathogen's genome, examination of virulence mechanisms and the role of chemotherapy in disease treatment and prevention, are expanding the knowledge base of the disease.

### **1.6.2 Bacteriology of *M. ulcerans***

*M. ulcerans* is a slow-growing environmental organism that can be cultured on standard mycobacterial media at 32°C (van der Werf *et al.*, 2005). Isolation from the environment has generally been unsuccessful and success from clinical samples has varied, with some reference laboratories reporting high success rates in clinically confirmed cases, via improved transport media and decontamination methods (Palomino *et al.*, 1998).

*M. ulcerans* closely resembles *M. marinum*, which is the causative agent of fish tank or swimming pool granulomas (Chemal *et al.*, 2002). The marked differences exhibited in phenotypic properties and disease symptoms by *M. marinum* and *M. ulcerans* contrasts with the high degree of genetic similarity between the two species (Kirschner *et al.*, 1993). However, further analysis of the genomes of these two closely related species has revealed differences. The finding most used to clearly discriminate the two species is the presence of the high copy numbers of insertion sequence IS2404 in *M. ulcerans* that is absent in all *M. marinum* isolates from different geographic regions investigated to date (Stinear *et al.*, 2000). Hence, this insertion sequence is believed to be highly characteristic for the species definition of *M. ulcerans*.

Strains of *M. ulcerans* isolated from different geographical regions show variations in a type of polyketide derived macromolecule, termed mycolactone, possibly reflecting regional differences in clinical presentation and virulence of *M. ulcerans* disease (Mve-Obiang *et al.*, 2003). Other *M. ulcerans*-related strains, referred to provisionally as *M. liflandii*, (Mve-Obiang *et al.*, 2005) and *Mycobacterium* sp. MU128FXT (Stinear *et al.*, 2005), have also been isolated from frogs. In the case of the former strain, these frogs were imported from West Africa and showed signs of disease mimicking the oedematous and ulcerative forms of *M. ulcerans* disease in humans (Trott *et al.*, 2004). This mycobacterium tested positive for the IS2404 that was previously considered species-specific for *M. ulcerans*, and produces mycolactones (Mve-Obiang *et al.*, 2005). This finding may have further implications with regard to the natural reservoir of *M. ulcerans*.

### 1.6.3 Genome

At the Pasteur Institute in Paris, the project to determine the complete genome sequence of *M. ulcerans* is nearing completion. The anticipated publication of the whole *M. ulcerans* genome sequence will be a major milestone for Buruli ulcer researchers:

(<http://www.pasteur.fr/recherche/unites/Lgmb/mycogenomics.html#ulcerans>).

Knowledge of the genetic component of microbial pathogens provides an important resource for identifying pathogenesis pathways and potential drug and vaccine therapy targets.

Within the genome of interest are the unusually large numbers of two distinct types of repetitive sequences, called IS2404 and IS2606, with 100–250 copies of each (Stinear *et al.*, 1999). In effect, *M. ulcerans*, with an estimated genome size of 5000 kb, has 10% of its genome composed of these two insertional DNA elements that have no known function other than to replicate. These sequences are short 1.5 kb stretches of DNA that are present in regular intervals throughout the genome. The biological implications for such large amounts of repetitive sequences are unknown, but it is highly likely that they render the organism more susceptible to significant mutation (Stinear *et al.*, 1999).

The Pasteur project has also uncovered the presence of a large virulence plasmid that encodes mycolactone production proteins (Stinear *et al.* 2004). The assembly of this extrachromosomal segment of the *M. ulcerans* genome has been given a high priority in view of the key role that mycolactone plays in pathogenesis.

#### **1.6.4 Epidemiology**

##### **1.6.4.1 History and geographic distribution**

The first report of Buruli ulcer from Africa dates back to 1897, when Sir Albert Cook noted cases of human ulceration in Uganda (Meyers, 1994). In 1948, the first clinical description of the disease occurred in a young child in Bairnsdale, Australia (Jenkin *et al.*, 2002). The authors then called it “Bairnsdale ulcer”. Since that first case report, the disease remains prevalent in Australia and this appears to be one of the few foci of the disease in a temperate climate

Many cases have since been reported in other countries (Figure 1.13) with most cases occurring in the tropics. Disease foci have been reported from tropical areas in Asia and Latin America, but the largest numbers of patients with Buruli ulcer disease have been detected in sub-Saharan Africa (Hayman, 1991; Portaels, 1996). The earliest reports came from the Democratic Republic of the Congo, where the disease is still prevalent (Bafende, 2004). During the late 1960’s and early 1970’s, reports of large numbers of infected patients emerged in Uganda, from a regional county then called Buruli, hence “Buruli ulcer” (Barker, 1971). Currently, many countries of sub-Saharan Africa are considered endemic for Buruli ulcer disease, but the largest

number of patients has been reported from areas within regions of Benin, Ivory Coast, and Ghana (Figure 1.13).

Within these countries, prevalence estimates have varied between areas, but have been reported to be as high as 150 – 280/100,000 population in endemic regions of Ghana (Amofah *et al.*, 2002; Raghunathan *et al.*, 2005). Similar rates have been reported from the Ivory Coast (Marston *et al.*, 1995) and Benin (Debacker *et al.*, 2004). Although Buruli ulcer may be found in all age groups, the majority of patients are aged between 5–15 years, with no distinction between gender (van der Werf *et al.*, 1999).

The outbreaks, especially those in developing countries, have increased the available knowledge on Buruli infections. However, the precise mode of transmission of Buruli ulcer, both in humans and animals, remains elusive.

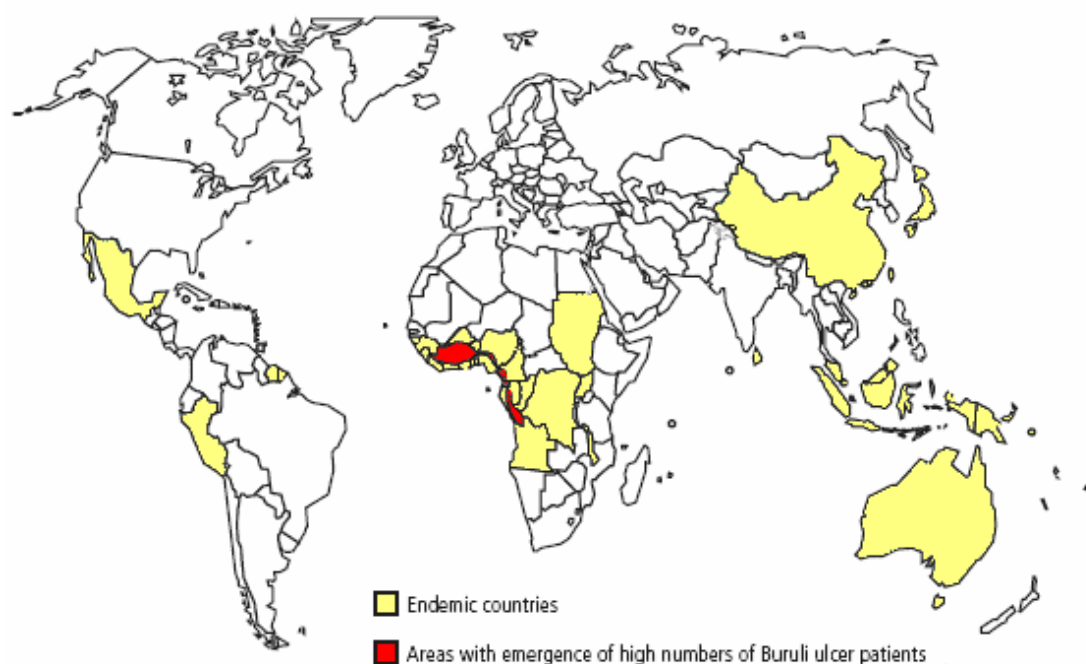


**Figure 1.13 Geographic distribution of Buruli ulcer**  
Endemic countries are shown in yellow. Areas of high prevalence rate are shown in red. Source WHO (<http://www.who.int/buruli/country/en/index.html>).

#### 1.6.4.2 Transmission

The precise mode of transmission of Buruli ulcer is unknown. Infection by *M. ulcerans* is known to commonly occur in riverine areas. (Portaels,

1995) and support for this theory was derived from clinical observations in Uganda. The high incidence of the disease in locations adjacent to swampy areas near the Nile River fell substantially when the refugees were moved elsewhere (Bradley *et al.*, 1971).

*M. ulcerans* was first detected in the environment using PCR (Ross *et al.*, 1997). Subsequent research using PCR identified *M. ulcerans* in aquatic insects obtained from endemic areas in Africa (Portaels *et al.*, 1999), leading to the hypothesis that *M. ulcerans* is possibly transmitted by biting aquatic insects of the order *Hemiptera* (*Naucoridae* and *Belostomatidae*). *M. ulcerans* has also been recovered from several other species in endemic areas, including molluscs and fish (Portaels *et al.*, 2001; Eddyani *et al.*, 2004), but in all cases these animals do not appear to develop obvious characteristics of the disease. Furthermore, certain aquatic insects, such as *Naucoridae*, are able to concentrate *M. ulcerans* within the salivary glands (Portaels *et al.*, 1999; Marsollier *et al.*, 2002). These predatory insects may feed on molluscs that in turn feed on the biofilm of water plants that appear to contain *M. ulcerans* (Marsollier *et al.*, 2002). In a laboratory experiment, *M. ulcerans*-infected *Naucoridae spp* were able to transmit *M. ulcerans* disease via bites (Marsollier *et al.*, 2002).

Patients do not normally recall being bitten by an insect prior to developing the disease. However, it is still unknown whether insect bites represent a mode of transmission to man. Infection, through skin pricks, is suspected to be acquired through contact with grasses and weeds. In a study from Ivory Coast (Marston *et al.*, 1995), the wearing of long trousers was a protective factor from Buruli ulcer in communities with a high prevalence of the disease. Only two known cases of human-to-human transmission have been reported (Exner *et al.*, 1987, Debacker *et al.*, 2002).

## **1.6.5 Clinical presentation and pathogenesis**

### **1.6.5.1 Clinical features**

In most African patients with Buruli ulcer disease, the subcutaneous tissue is the initial point of infection. The first stage of the disease is normally a firm, painless nodule (Figure.1.14A), but pre-ulcerative lesions also include plaques (Figure. 1.14B), which consist of larger areas of hardened skin, and oedema (excess fluid) (Figure.

1.14D). Progressively, the second stage involves ulceration (Figure. 1.14C). The healing process may result in complications such as scarification, ankylosis (stiffness or fusion of a joint), and contractures (Figure. 1.14E). Another presentation of Buruli ulcer infection, although rare, is osteomyelitis (acute or chronic bone infection).



**Figure 1.14 A -D Clinical presentation of Buruli ulcer**  
A. Papule, B. Nodule, C. Ulceration, D. Oedema E. Contracture (source: Buruli Ulcer Global Initiative) (<http://www.who.int/buruli/photos/nonulcerative/en/index.html>)

## 1.6.6 Pathogenesis

### 1.6.6.1 Toxin - Mycolactone

*M. ulcerans* has a unique property in that it produces a polyketide-derived macrolide toxin termed mycolactone (Figure 1.16A) (Fidanze *et al.*, 2001). *M. ulcerans* isolates from particular regions produce a distinct pattern of mycolactone variants (Mve-Obiang *et al.*, 2003) and represent the only example of a polyketide-derived virulence factor in a human pathogen (Hong *et al.*, 2005a). Until the discovery of mycolactone, polyketide macrolides had only previously been isolated from soil bacteria, such as the *Streptomyces* species, or from fungi (Katz and Donadio, 1993). Intriguingly, mycolactone shares similar structural features with potent immunosuppressive drugs such as macrolide lactone FK506, the *Streptomyces* macrocyclic rapamycin, and the soil fungi derived metabolite cyclosporin A (Figure 1.15), all of which are capable of altering the function of lymphocytes and dendritic cells (Coutanceau *et al.*, 2007).

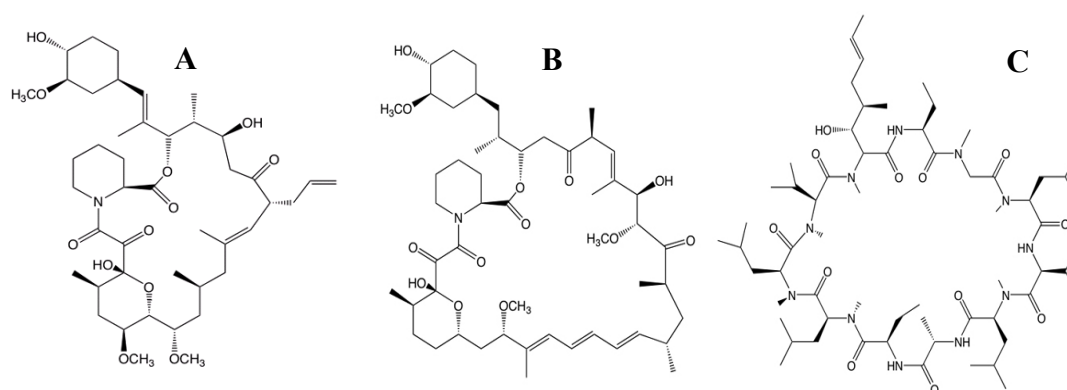
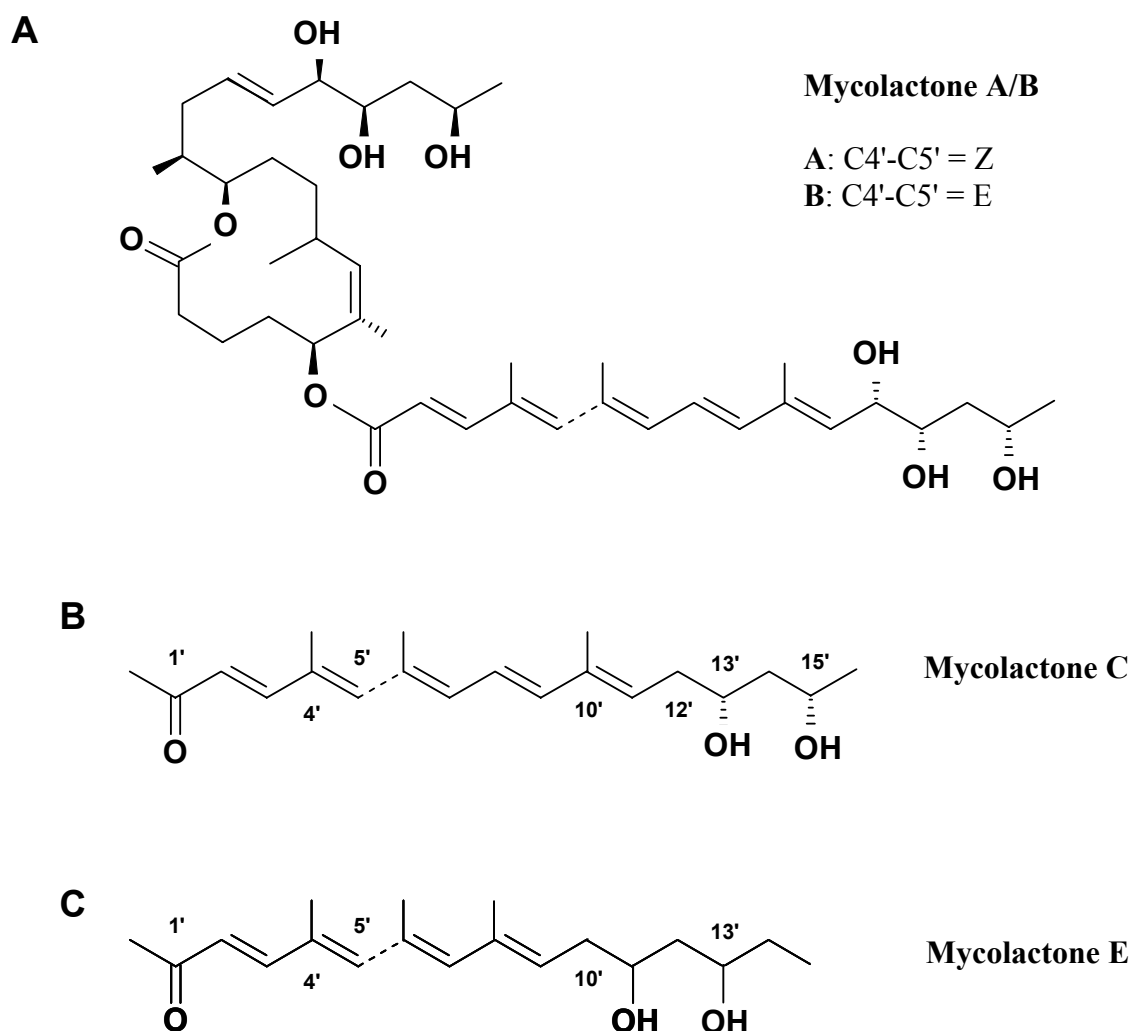


**Figure 1.15 Molecular structures of polyketides**  
FK506 (A), Rapamycin (B) and Cyclosporin A (C). Structures drawn with Chemdraw.

The increased research activity toward Buruli ulcer led to the first major breakthrough in the field when Small and colleagues isolated and identified mycolactones A and B (Figure 1.16A) as the polyketide toxins secreted by *M. ulcerans* (George *et al.*, 1999). The structures of the major mycolactones A and B were determined to be, respectively, *Z*- and *E*- isomers of a 12-membered macrocyclic polyketide, to which a highly unsaturated polyketide side chain is attached via an ester linkage (Figure 1.16A). Since then, several other mycolactones have been identified



(C, D, E and F; Figures 1.16B,C,D, respectively) all of which show conservation of the lactone core, but modifications in the side chain (Hong *et al.*, 2003; Mve-Obiang *et al.*, 2003; Mve-Obiang 2005; Hong *et al.*, 2005b). Although, the biological effects of mycolactones have been extensively studied and documented as being cytotoxic, apoptotic and immunosuppressive (George *et al.*, 1999; George *et al.*, 2000), the precise mechanisms by which they act remain largely unknown. Most recent structural analysis of mycolactones has revealed mycolactone E (Figure 1.16C) from a *M. ulcerans*-related pathogenic mycobacterium from *Xenopus* toads (Mve-Obiang *et al.*, 2005), and mycolactone F (Figure 1.15D) from a Chinese frog clinical isolate of *M. ulcerans* (Hong *et al.*, 2005b).



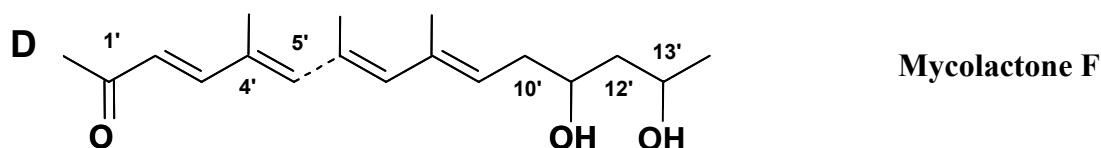


**Figure 1.16 Molecular structures of mycolactones**

A. Mycolactone A/B (George *et al.*, 1999), B. Mycolactone C (Mve-Obiang *et al.*, 2003), C. Mycolactone E (Mve-Obiang 2005), D. Mycolactone F (Hong *et al.*, 2005b). Mycolactone D has been characterised by mass, but structure is unknown and may involve an additional oxygen molecule (Mve-Obiang 2005).

The number and type of mycolactones produced have important implications for virulence. Biological evaluation shows that the lactone core in itself is sufficient for cytopathicity, but that the side chain greatly enhances its virulence factor, probably by facilitating entrance into the cell or by interaction with an intracellular target molecule (Snyder and Small, 2003). The mode of action of all mycolactone analogues would therefore appear to be identical, but the potency varies with the composition of the side chain. Australian isolates produce two mycolactones: mycolactone C, which lacks a hydroxyl group at C<sub>12</sub>, along with a trace amount of A or B. *In vitro*, mycolactone C is 10,000-fold less active than mycolactones A and B (Mve-Obiang *et al.*, 2003), suggesting that the differences in virulence that are observed between geographical strains of *M. ulcerans* can be directly correlated to their differences in mycolactone profile.

### 1.6.7 Biosynthesis of mycolactones A and B

Jenkin *et al.* (2003) were the first to identify *M. ulcerans*-specific polyketide synthase (PKS) genes using genetic subtraction experiments. Subsequent investigations led to the discovery of the 174-kb virulence plasmid pMUM001 encoding a PKS locus, whose main function appears to be mycolactone production (Stinear *et al.*, 2004). Furthermore, complete decoding and translation of the biosynthetic gene cluster revealed two PKSs responsible for assembling the macrolactone core of the toxin and a third PKS for formation of the side chain. These proteins are members of the modular class of PKSs (Cortes *et al.*, 1990, Donadio *et al.*, 1991). Efforts have led to the characterisation of many examples of these multienzymes, whose hallmarks are their comparatively large size and their linear

arrangement of catalytic domains. These domains function as an "assembly line" to polymerise and modify, by reduction and dehydration steps, simple monomer CoA esters to much higher molecular weight products. These products are richly decorated with ketone, hydroxyl, carbon–carbon double bond, and alkyl substituents at specific locations and in specific stereochemical configurations, which are "programmed" by the organisation of catalytic domains grouped into "modules" for each monomer addition (Staunton and Weissman, 2001).

Most of pMUM001 (~105 kb) consists of genes coding for proteins involved in mycolactone synthesis (Stinear *et al.*, 2004). Two polyketide synthases (PKS MLSA1 and MLSA2) are responsible for the synthesis of the mycolactone core, while a third PKS (MLSB) constructs the side chain (Stinear *et al.*, 2004). The arrangement of the three PKSs resembles an 'assembly-line' of enzymes. For the formation of the lactone core by MLSA1 and MLSA2, the growing polyketide chain is extended nine times by a ketosynthase and an acyltransferase adding either a C2- (malonate) or a C3-unit (methylmalonate). The added unit is subsequently reduced to the appropriate degree by enzymes immediately following the acyltransferase in the assembly-line (Figure 1.17). The saturated parts in the chain are obtained by the successive action of a ketoreductase, a dehydratase and an enoylreductase. When the enoylreductase is missing an olefin is formed, while a hydroxyl moiety is produced if only a ketoreductase is present.

After completion of the chain, a terminal thioesterase/cyclase releases the product as the 12-membered lactone ring. In a similar fashion, MLSB produces the side chain by seven chain extensions. The plasmid also contains three genes encoding for probable polyketide-modifying enzymes, including a P450 monooxygenase, a FabH-like type III ketosynthase and a type II thioesterase. The cytochrome P450 encoded by *mup053* and designated as CYP140A2 (Mve-Obiang *et al.*, 2005) is believed to be responsible for the additional hydroxyl moiety at carbon 12. The role of the enzyme resembling FabH, encoded by the gene *mup043*, is unclear, but it is believed to catalyse the ester bond formation between the mycolactone core and the side chain (Stinear *et al.*, 2004). Alternatively, the side chain attachment may be mediated directly by the C-terminal thioesterase on MLSB (Stinear *et al.*, 2004). The *mup045* gene has a significantly lower GC content of 52.8%, compared to the rest of

the plasmid, suggesting that it has been acquired recently by horizontal transfer. Immediately 3' of *mlsA2* is *mup037*, a gene encoding a type II thioesterase that may be required for removal of short acyl chains from the PKS loading modules, arising by decarboxylation (Stinear *et al.*, 2004).

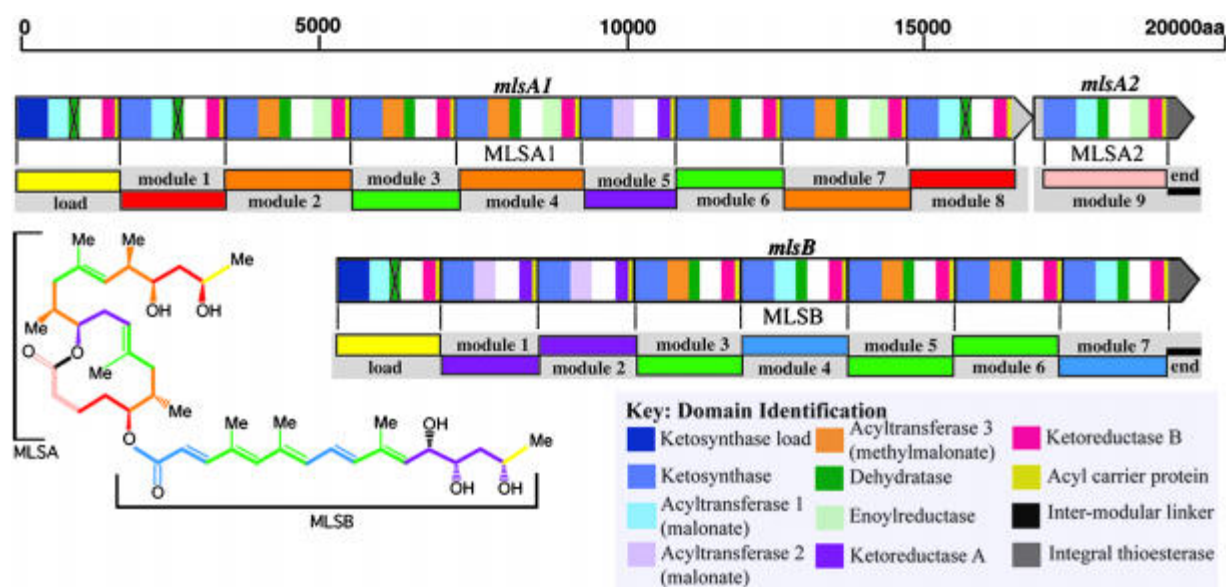


**Figure 1.17 Domain and module organization of the mycolactone PKS genes**  
Within each of the three genes (*mlsA1*, *mlsA2*, and *mlsB*), different domains are represented by a coloured block. The domain designation is described in the key. White blocks represent inter-domain regions of 100% identity. Module arrangements are depicted below each gene, and the modules are colour coded to indicate identity both in function and sequence (>98%). For example, module 5 of MLSA1 is identical to modules 1 and 2 of MLSB. The crosses through four of the dehydratase domains indicate that they are predicted to be inactive based on a point mutation in the active site sequence. The structure of mycolactone has also been colour-coded to match the module responsible for a particular chain extension (Stinear *et al.*, 2004).

The predicted sizes of the proteins involved in mycolactone synthesis places them among the largest of known proteins. The largest of these proteins is 1.8 MDa, which along with its smaller partner, at 0.26 MDa, constructs the ketolide core of mycolactone. The side chain is synthesised by the third PKS of 1.2 MDa. Secondly, the extent of similarity is exceptionally high at the gene and protein levels among domains of comparable function in all the 16 modules that carry out chain extension

chemistry, with stretches of up to 27 kb of near identical nucleotide sequence (99.7%) (Stinear *et al.*, 2004). Although amino acid sequence identities lie between 40% and 70%, the key ketosynthase domains in the mycolactone PKS, for example, are >97% identical (Stinear *et al.*, 2004). The entire 105 kb mycolactone locus contains only 9.5 kb of unique, non-repetitive DNA sequence.

The fact that the genetic machinery of mycolactone biosynthesis is housed in a plasmid, with highly conserved and repetitive DNA sequences, suggests that the acquisition of this virulence marker took place quite recently and evolved rapidly by gene recombination and duplication events (Stinear *et al.*, 2004).

### **1.6.8 Therapy**

#### **1.6.8.1 Surgery**

At present, the main treatment to remove existing large ulcers is surgery. Surgical procedures have been widely practised and involve excision of necrotic tissue and a surrounding rim of normal tissue, followed by skin grafting (van der Werf *et al.*, 1999). However, availability of surgical treatment in endemic areas is limited. No formal studies have been done on surgical efficacy, recurrence rates, and functional limitations after healing.

#### **1.6.8.2 Drug treatment**

The role of chemotherapy with anti-mycobacterial agents in the treatment of Buruli-ulcer disease has traditionally been ineffective. *M. ulcerans* is reported to be susceptible *in vitro* to rifampin (Havel *et al.*, 1975), macrolides (Portaels *et al.*, 1998), and quinolones (Thangaraj *et al.*, 2000).

Susceptibility testing of antibiotic treatment using a mouse footpad model has led to reports of smaller lesions and a decrease in the number of *M. ulcerans* cells in the tissue (Stanford and Phillips, 1972; Dega *et al.*, 2000; Bentoucha *et al.*, 2001). The combination of rifampicin with amikacin or streptomycin was most effective at preventing relapse after treatment for 12 weeks, suggesting a bactericidal effect, but treatment of cultures of *M. ulcerans* were not successful in this study (Bentoucha *et al.*, 2001). Subsequent studies showed no viable bacteria in mouse tissue after 7 weeks treatment with the combination of rifampicin plus amikacin (Marsollier *et al.*, 2003).

A further human trial has also shown that early nodular lesions may be rendered culture-negative after a minimum of four weeks therapy with rifampicin plus streptomycin (Etufal *et al.*, 2003).

Further research to identify cheap, safe, and effective oral combinations that can be used as an adjuvant to surgery, or that could even replace surgery for early lesions, is urgently required. Antimicrobial therapy may be important in certain disseminated cases, and in the prevention of osteomyelitis. At least one new compound, PA-824, appears safe for humans in early phase I trials, and has activity *in vitro* against many mycobacterial species including *M. tuberculosis* and *M. ulcerans* (Cole and Alzari, 2005).

### **1.6.8.3 Vaccine**

BCG vaccination appears to protect against disseminated *M. ulcerans* disease, including osteomyelitis (Portaels *et al.*, 2002) and re-vaccination might provide additional protection. A trial to assess this possibility is planned by the WHO. The development of new vaccines (eg, based on Ag85A) (Tanghe *et al.*, 2001) holds promise, but it is likely to be many years before a field vaccine can be introduced. If such vaccines were developed, the advantage could be much greater than for Buruli ulcer alone, because the vaccine might also cross-protect against tuberculosis and leprosy.

### **1.6.9 Aims and objectives**

The location of the cytochrome P450, CYP140A2, in the mycolactone biosynthesis cluster and its subsequent probable function in mycolactone biosynthesis indicates an enzyme of physiological and pathological importance, and presents it as a potential target in the design of new anti-BU chemotherapy agents. *M. ulcerans* strains from around the world have thus far been shown to produce a very restricted range of mycolactones. A study of thirty-four *M. ulcerans* isolates collected worldwide showed that the core lactone remained identical within these strains, with minor variations only observed in the acyl side chain (Mve-Obiang *et al.*, 2003). Some of these variations have been largely attributed to oxidation (or lack of) at C-12' of the side chain (Hong *et al.*, 2003; Mve-Obiang, 2003), and it has been proposed that this is due to the activity (or lack of activity) of the cytochrome P450 CYP140A2.

The purpose of this project is to PCR clone *CYP140A2* from cosmid libraries of *M. ulcerans* genomic DNA. Expression in *E. coli* and subsequent purification of the protein will lead to P450 characterisation by a variety of spectroscopic and other techniques. Identification of P450-catalysed product formation would further enhance the knowledge of the physiological role of this P450. Inhibitor binding studies will be performed with the view to investigating the effect of successful inhibitors on *M. ulcerans* cell growth.

## **1.7 *Mycobacterium* sp. strain HE5**

### **1.7.1 Introduction**

The various organic pollutants released by the ever increasing industrial processes is the direct cause of many environmental and human health-related problems (Spain *et al.*, 2000). Standard approaches to remediation of contaminated sites, such as land-filling, recycling and incineration, are inefficient and costly and can also lead to the formation of toxic intermediates (Dua *et al.*, 2002). As a result, biological decontamination methods are preferable to conventional methods because, in general, micro-organisms degrade numerous environmental pollutants without producing toxic intermediates (Pieper and Reineke, 2000; Furukawa, 2003).

Sites polluted with toxic chemicals and potentially harmful industrial wastes may offer biotechnological opportunities. Such sites include valuable niches for micro-organisms that have evolved the necessary enzymes to use these foreign and frequently xenobiotic compounds as their carbon and energy source. Thus, microbial biodegradative pathways for recalcitrant chemicals are not only appealing for remediation of environmental pollution (Timmis and Pieper, 1999), but also as sources of unique catalytic activities in green chemistry and white biotechnologies (Schmid *et al.*, 2001).

### **1.7.2 Biodegradation and mycobacteria**

Two-thirds of known organic chemicals contain heterocyclic structures (Kuhn and Sulfitá, 1989). Synthetic heterocyclic compounds are used as industrial solvents, dyes, explosives, pharmaceuticals, and pesticides. In addition to biological sources of heterocyclic compounds, agricultural activities introduce a wide variety of xenobiotic

heterocyclic compounds into the biosphere through the application of herbicides, insecticides, detergents and industrial waste products. Waste materials containing large amounts of heterocyclic compounds are also generated by the mining industry, coal tar- and oil shale-processing operations, wood-preserving facilities, and chemical manufacturing plants.

Despite the potentially serious consequences of such contaminants, insufficient research has been conducted to determine the environmental fate of these compounds (Bollag and Kaiser, 1991). Biodegradation of industrial organic pollutants, especially heterocyclic compounds, are of special environmental interest. Therefore gaining a clearer understanding of the processes by which degradation occurs and the types of micro-organisms involved is a crucial step. Of the heterocyclic compound class, pyrrolidine, piperidine, morpholine and derivatives form important representatives.

Recent studies have shown the biodegradative abilities of *Mycobacterium* species, with capacities to metabolise xenobiotics such as polycyclic aromatic hydrocarbons (Tiehm and Fritzsche, 1995; Dean-Ross and Cerniglia, 1996; Kleespies *et al.*, 1996), chlorophenols (Hägglom *et al.*, 1988), trichloroethylene (Wackett *et al.*, 1989), vinyl chloride (Hartmans and De Bont, 1992), amines (Emitiazi and Knapp, 1994), and isonicotinate (Kretzer and Andreesen, 1991).

### **1.7.3 Morpholine**

#### **1.7.3.1 Physical and chemical properties**

Morpholine (C<sub>4</sub>H<sub>9</sub>ON), chemically known as 1-oxa-4-azacyclohexane (Figure. 1.17), is a colourless, oily, hygroscopic, volatile liquid with a characteristic amine smell (Reinhardt and Brittelli, 1981). It is completely miscible with water, as well as with many organic solvents, but has limited solubility in alkaline aqueous solutions. The chemical structure (Figure.1.20) has both a secondary amine and an ether functional group, which forms a base, with the conjugated acid at a pK<sub>a</sub> of 8.33 (IPCS, 1996).



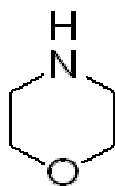


**Figure 1.18 Chemical structure of morpholine**

According to the WHO's International Programme on Chemical Safety (IPCS), under environmental and physiological conditions, the potential vertebrate carcinogen *N*-nitrosomorpholine is formed by reaction of solutions of nitrite or gaseous nitrogen oxides with dilute solutions of morpholine (IPCS, 1996).

#### **1.7.3.2 Sources of human and environmental exposure**

World-wide industrial production of morpholine is estimated at 25,000 tonnes of morpholine per year (IPCS, 1996). The main production process used is via an ammonia and diethylene glycol reaction in the presence of hydrogen and catalysts (IPCS, 1996). Industrially, morpholine is primarily used as a chemical intermediate in the rubber industry, as a corrosion inhibitor, and in the synthesis of optical brighteners, crop protection agents, dyes and drugs (IPCS, 1996). In addition, morpholine is used as a solvent for a large variety of organic materials, including resins, dyes and waxes (IPCS, 2001). Both human and environmental exposure occurs from manufacturing and chemical gaseous and aqueous emissions, and directly from some uses; for example in cosmetic formulations (IPCS, 1996). In addition, morpholine has been detected in a wide variety of foods (Singer and Lijinsky 1976; Hamano *et al.*, 1981; Mohri, 1987). The latter exposure most likely arises from the wax coatings on fruit or on packaging, but in some cases its origin is unknown (IPCS, 1996). As a result of uses in waxes and polishes, morpholine is released into the environment through volatilisation and is easily adsorbed by moisture (IPCS, 1996). Although, the hydrosphere would appear to be the main sphere for morpholine accumulation, there is no evidence to date of significant contamination of this sphere (IPCS, 1996).

Incineration is the preferred method of disposal for undiluted morpholine, but for aqueous effluents activated sludge treatment is accepted (Brown and Knapp 1990). However, several authors have reported apparent recalcitrance of the compound, or

have referred to difficulties in the treatment of morpholine-containing effluents (Tolgyessy *et al.*, 1986; Cech *et al.*, 1988).

#### **1.7.3.3 Evaluation of effects on human health**

The general population is primarily exposed to morpholine by consumption of contaminated food, through direct treatment of fruit with morpholine-containing waxes for conservation purposes (IPCS, 1996). Morpholine does not seem to create any significant risk of systemic toxic effects. However, irritation of the eyes and respiratory tract have been reported (IPCS, 1996).

Morpholine is not considered directly mutagenic or carcinogenic in animals, unless nitrosated to form *N*-nitrosomorpholine (Turcotte and Johnson, 1992), which is mutagenic and carcinogenic in several species of experimental animals. Morpholine fed to rats with nitrite caused an increase in tumours, mostly hepatocellular carcinoma and sarcomas of the liver and lungs (Mirvish *et al.* 1983), although there is inadequate evidence in experimental animals for the carcinogenicity of morpholine (IPCS, 1999). Conversion of morpholine to *N*-nitrosomorpholine is the main cause of concern, especially with respect to vertebrate populations. *N*-nitrosomorpholine has been reported in industrial wastewater and in contaminated soil (IPCS, 1996). The presence of morpholine in water destined for processing to drinking-water is a major cause for concern.

#### **1.7.4 Morpholine biodegradation**

The high water solubility and the potential for chemical and biological *N*-nitrosation, has developed environmental interest in the removal of morpholine from contaminated industrial waste waters. The *N*-nitrosation reaction forms the highly soluble carcinogenic compound, *N*-nitrosomorpholine (Suzuki and Mitsuoka, 1984; Enzmann *et al.*, 1995).

Isolated microbes capable of growing on morpholine as sole source of carbon, nitrogen and energy have been identified in most cases as mycobacteria (Cech *et al.*, 1988; Knapp and Brown, 1988; Swain *et al.*, 1991; Poupin *et al.*, 1998), with the exception of an *Arthrobacter* sp. (Dmitrenko *et al.*, 1985). Knapp and co-workers

(Knapp *et al.*, 1982) first discovered two strains of *Mycobacterium* (MorD and MorG) able to utilise morpholine as a carbon source for growth.

Further studies to understand the morpholine biodegradation process and its regulation led to the proposed hypothetical pathway for the biodegradation of morpholine by *Mycobacterium chelonae* (Figure 1.19) (Swain *et al.*, 1991). The pathway could proceed via 2-(2-aminoethoxy)acetate and glycolate and/or ethanolamine. Further work described the degradation of morpholine by *M. aurum* MO1 (Mazure and Truffaut, 1994). They proposed that *M. aurum* grown on morpholine could degrade intermediary compounds via the ethanolamine and glycolate routes. Depending on the morpholine concentration in the medium, one pathway could be used while the other was inhibited (Mazure and Truffaut, 1994). The application of  $^1\text{H}$  NMR spectroscopy for direct detection of morpholine enabled the identification of 2-(2-aminoethoxy)acetate as an intermediate of morpholine degradation, demonstrating that the initial ring cleavage occurred at the C–N bond (Fig. 1.19) (Combourieu *et al.*, 1998).

Little is known about the enzymes catalysing these initial steps (Knapp *et al.*, 1982; Cech *et al.*, 1988; Knapp and Brown, 1988; Swain *et al.*, 1991; Emtiazi and Knapp, 1994; Mazure and Truffaut, 1994). However, more evidence revealed cytochrome P450s as being putatively involved in the initial oxidation of morpholine by an environmental *Mycobacterium* strain (Poupin *et al.*, 1998).

#### **1.7.4.1 Morpholine biodegradation and cytochrome P450s**

Poupin and colleagues (Poupin *et al.*, 1998) were the first to identify the role of a P450 in morpholine degradation. The group isolated a *Mycobacterium* strain (RP1) from a contaminated activated sludge collected in a wastewater treatment unit of a chemical plant. The strain was capable of utilising morpholine and other heterocyclic compounds, pyrrolidine and piperidine, as the sole source of carbon, nitrogen, and energy. The use of *in situ*  $^1\text{H}$  NMR spectroscopy allowed the determination of two intermediates in the biodegradative pathway, 2-(2-aminoethoxy)acetate and glycolate (Figure 1.19). Furthermore, spectrophotometric analysis confirmed the presence of a cytochrome P450. Reduced cell extracts from

morpholine-grown cultures, but not succinate-grown cultures, gave rise to a characteristic carbon monoxide difference spectrum with a peak near 450 nm. Moreover, the inhibition of morpholine degradation was dependent on the metyrapone concentration. A heme-containing monooxygenase was also detected in pyrrolidine- and piperidine-grown cultures, suggesting specific induction of a P450-containing degradation system by these substrates.

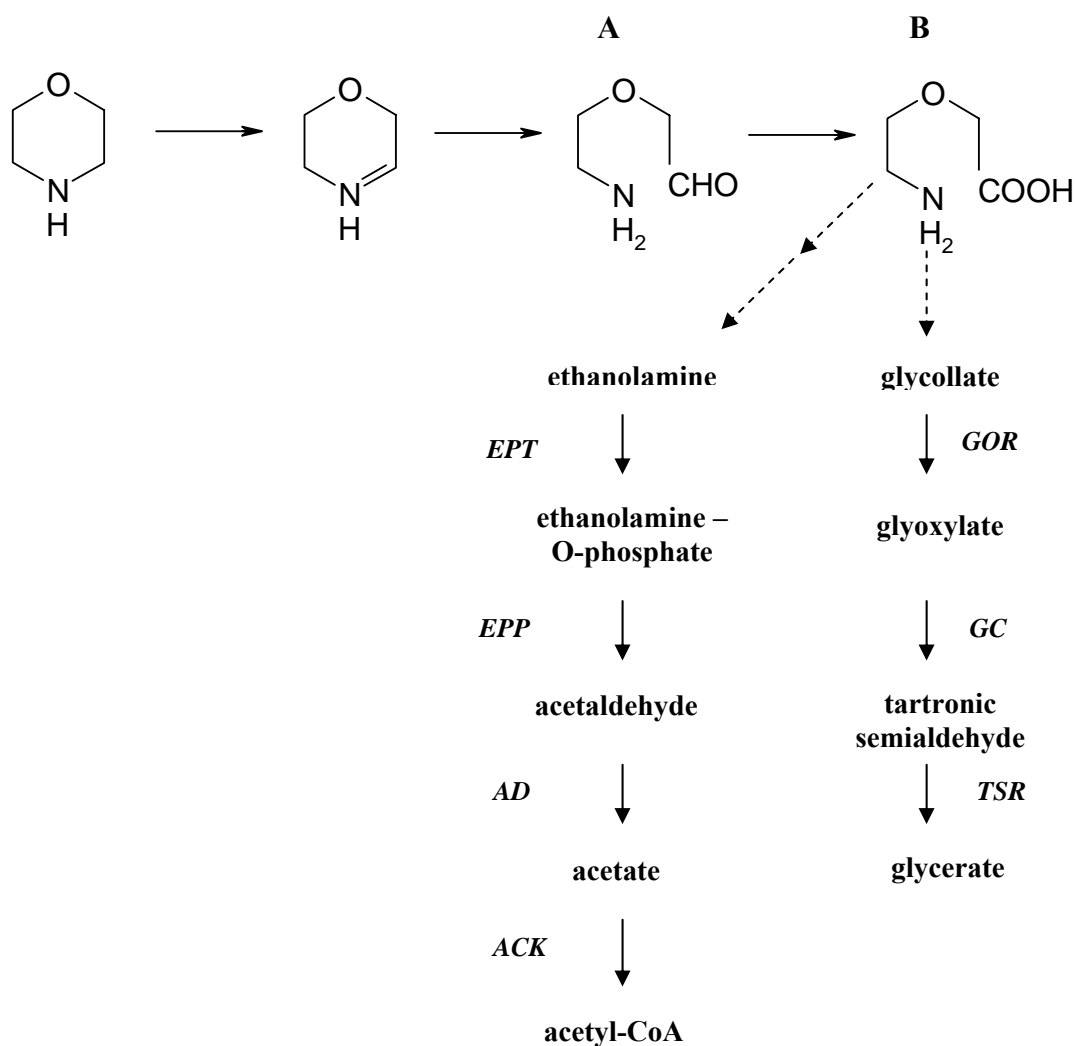


**Figure 1.19 Pathway for morpholine catabolism**

*Solid arrows* indicate established reaction steps; *dashed arrows* indicate probable reaction steps. *Italicised initials* are names of enzymes as follows: *ABD*, 4-aminobutyrate dehydrogenase; *AGAT*, 4-aminobutyraldehyde aminotransferase; *SSD*, succinic semialdehyde dehydrogenase; *EPT*, ethanolamine phosphotransferase; *EPP*, ethanolamine-O-phosphate phospholyase; *AD*, acetaldehyde dehydrogenase; *ACK*, aceto-CoA-kinase; *GOR*, glycollate oxidoreductase; *GC*, glyoxylate carbonylase; *TSR*, tartronic semialdehyde reductase. Predicted intermediates (A) and (B) are 2(2-aminoethoxy)acetaldehyde and 2(2-aminoethoxy) acetate respectively (adapted from Swain *et al.*, 1999).

Spectrophotometric assays of the *Mycobacterium aurum* MO1 strain by Combourieu *et al.*, (1998) produced further evidence of a soluble cytochrome P450, involved in the degradative pathway for morpholine. The kinetics of the biodegradation of the sulphur analogue thiomorpholine was monitored by using *in situ* NMR, allowing the identification of two intermediates: the sulfoxide of thiomorpholine resulting from S-oxidation, and thiodiglycolic acid owing to ring cleavage. The inhibitory effect of metyrapone on the thiomorpholine and morpholine degradative abilities of *M. aurum* MO1 confirmed the involvement of a cytochrome P450. These results and the decrease in the rate of formation of the first intermediate during morpholine degradation, 2-(2-aminoethoxy) acetate, proved the key role of a cytochrome P450 in the the C—N bond cleavage (Figure 1.20).

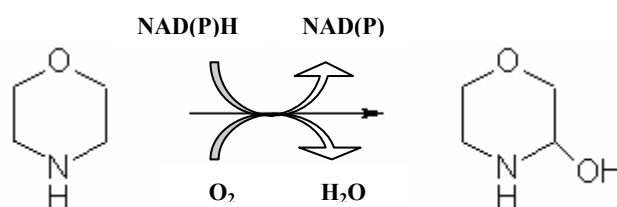


**Figure. 1.20** Proposed reaction of the morpholine-dependent cytochrome P450 (Combourieu *et al.*, 1998).

Poupin and colleagues (Poupin *et al.*, 1999a), using transposon mutagenesis, isolated the mutant strain of *Mycobacterium smegmatis* mc<sup>2</sup>155 (LGM1). This strain had altered regulation of piperidine and pyrrolidine utilisation. The complete nucleotide sequence of the gene inactivated in mutant LGM1 was determined from the wild-type strain. Discovered was a gene (*pipR*) encoding a member of the GntR family of bacterial regulatory proteins. Three additional open reading frames were found downstream. The first open reading frame (*pipA*) appeared to encode a protein identified as a cytochrome P450. This gene was the first member of a new family, *CYP151*, subsequently designated as *CYP151A1*. By a gene replacement experiment, it was demonstrated that the cytochrome P450 gene (*pipA*) was required for piperidine and pyrrolidine utilisation in *M. smegmatis* mc<sup>2</sup>155. Genes homologous to *pipA* were detected by hybridization in several, previously isolated, morpholine-degrading mycobacterial strains (Poupin *et al.*, 1999b). A gene encoding a putative 3Fe-4S ferredoxin was also found downstream of *pipA*.

Using morpholine as a sole source of carbon, nitrogen and energy, a mycobacterium strain HE5 (DSM 44238) was isolated from forest soil (Schrader *et al.*, 2000). A maximal growth rate was observed at a morpholine concentration of 30 mM and tolerated up to 100 mM. In addition to morpholine, the strain utilised pyrrolidine, piperidine and proposed intermediates in morpholine metabolism such as glycollate, glyoxylate and ethanolamine. Degradation of morpholine, piperidine and pyrrolidine was strictly dependent on the presence of oxygen. Addition of the cytochrome P450 inhibitor metyrapone to the growth medium, in the presence of heterocyclic amines as substrate, resulted in a significantly decreased growth rate. Carbon monoxide difference spectra of crude extracts from cells grown on these substrates, compared to spectra obtained for extracts of succinate-grown cells, indicated that a cytochrome P450 was specifically expressed during growth on the cyclic amines.

Further studies of the *Mycobacterium* sp. strain HE5 (DSM 44238) demonstrated the expression of a cytochrome P450 and an iron-sulfur protein. The proteins expressed were specifically induced during growth on morpholine and were directly purified from the strain (Sielaff *et al.*, 2001). The cytochrome P450, designated P450<sub>mor</sub>, was characterised as a monomer with an apparent molecular mass of 44.7 kDa. The iron-sulfur protein was characterised as a 3Fe-4S ferredoxin exhibiting a molecular mass of 6.8 kDa and named Fd<sub>mor</sub>. The data obtained during the study indicated that the isolated cytochrome P450<sub>mor</sub> and Fd<sub>mor</sub> were the putative components of a P450-dependent monooxygenase system able to catalyse the oxidation of morpholine.

Sielaff *et al.* (2005a) subsequently purified Fd<sub>mor</sub> and P450<sub>mor</sub> as recombinant proteins, as well as a ferredoxin reductase FdR<sub>mor</sub>. Production of P450<sub>mor</sub> as an N-terminal His-tag fusion protein enabled the purification of this protein in its spectrally active form. The proposed substrates morpholine, piperidine or pyrrolidine failed to produce substrate-type binding spectra of P450<sub>mor</sub>. Pyridine, metyrapone and variousazole compounds generated type II binding spectra and the determined low  $K_d$  values for these compounds suggested that P450<sub>mor</sub> might have a preference for more bulky and/or hydrophobic molecules.

*Mycobacterium* sp. strain RP1 was also found to degrade morpholine, piperidine, and pyrrolidine (Trigui *et al.*, 2004). A genomic DNA fragment, containing the gene encoding MorA, was cloned and sequenced (Trigui *et al.*, 2004). Encoded was a cytochrome P450 designated as MorA, which was the second member of the *CYP151* family and designated *CYP151A2*. The second open reading frame (*morB*) featured a 3Fe-4S type ferredoxin. A third gene (*morC*), exhibited sequence identity to known reductases, and was found downstream of *morB*. Recombinant MorA cytochrome P450 was purified to homogeneity. The purified enzyme was a monomeric soluble protein with an apparent  $M_r$  of about 45,000. *CYP151A2*, in the presence of artificial electron donors, catalysed the ring cleavage of the secondary amines and the  $V_{\max}/K_{\text{Mapp}}$  values indicated that pyrrolidine was the preferred substrate when compared to morpholine and piperidine (Trigui *et al.*, 2004).

Recently, the cloning and sequencing of the *morABC* operon from *Mycobacterium* sp. strain HE5 (DSM 44238) revealed the genes encoding the three components of a cytochrome P450 monooxygenase system, which was previously shown to be required for the degradation of the N-heterocycle morpholine (Sielaff *et al.*, 2005b). The system included cytochrome P450 (P450<sub>mor</sub> (*CYP151A2*)) and the 3Fe-4S ferredoxin (Fd<sub>mor</sub>), encoded by *morA* and *morB*, respectively, and *morC* encoding a specifically morpholine-induced ferredoxin reductase. The gene *morC* of *Mycobacterium* sp. strain HE5 was heterologously expressed. The purified recombinant protein FdR<sub>mor</sub> was characterized as a monomeric 44 kDa protein, being a strictly NADH-dependent, FAD-containing reductase. The  $K_m$  values of FdR<sub>mor</sub> for the substrate NADH (37.7 +/- 4.1  $\mu\text{M}$ ) and the artificial electron acceptors potassium ferricyanide (14.2 +/- 1.1  $\mu\text{M}$ ) and cytochrome *c* (28.0 +/- 3.6  $\mu\text{M}$ ) were determined. FdR<sub>mor</sub> was shown to interact functionally with its natural redox partner, the 3Fe-4S protein Fd<sub>mor</sub>, and with the 2Fe-2S protein adrenodoxin, albeit with a much lower efficiency, but not with spinach ferredoxin. In contrast, adrenodoxin reductase, the natural redox partner of adrenodoxin, could not use Fd<sub>mor</sub> in activity assays. These results indicated that FdR<sub>mor</sub> can utilise different ferredoxins, but that Fd<sub>mor</sub> requires the specific NADH:ferredoxin oxidoreductase FdR<sub>mor</sub> from the P450<sub>mor</sub> system for efficient catalytic function.

Kinetic analysis of the redox couple  $\text{FdR}_{\text{mor}}/\text{Fd}_{\text{mor}}$  revealed a 30-fold preference for the NADH-dependent reduction of NBT and an absolute requirement for  $\text{Fd}_{\text{mor}}$  in this reaction, compared with the NADH-dependent reduction of cytochrome *c*. (Sielaff *et al.* 2005a). The relatively low  $K_m$  value (5.6 +/- 0.3 nM) of  $\text{FdR}_{\text{mor}}$  for  $\text{Fd}_{\text{mor}}$ , measured with NBT as the electron acceptor, indicated high specificity. The purified recombinant proteins  $\text{FdR}_{\text{mor}}$ ,  $\text{Fd}_{\text{mor}}$  and  $\text{P450}_{\text{mor}}$  were used to re-establish the homologous P450-containing monooxygenase, which was shown to hydroxylate morpholine (Sielaff *et al.* 2005a).

### **1.7.5 Aims and objectives**

The previous expression of CYP151A2 ( $\text{P450}_{\text{mor}}$ ) and subsequent identification of its probable function in morpholine catabolism indicates that this is an enzyme of putative bioremedial importance. The purpose of this work done in this chapter was to further characterise CYP151A2. Expression in *E. coli* and subsequent purification of the protein enabled the more detailed characterisation of the P450 and ferredoxin by a variety of spectroscopic techniques and ligand binding assays. Protein was purified with a view to structural characterisation.



# Chapter 2

## Materials and Methods

## 2.0 Materials and Methods

### 2.1 Materials

#### 2.1.1 Vectors

The vector pGEM-T Easy (Promega) was used for initial cloning and when necessary sequencing of PCR products. Vectors pET11a, pET15b and pET28a from Novagen were used for protein production in *E. coli*. All plasmid expression vector samples used, pKM2(b), pGL1(a), pGL2(a), pGL3(a), pGL4(a), pGL5(a) and pMCN28, are based on various pET vectors, with their relevant genotypes listed in Table 2.1. The prefix “His-” indicates that the relevant gene or mutant gene is attached to a histidine linker which is encoded at the N-terminal of the protein.

Plasmid	Genotype	Reference
pKM2(b)	Ap <sup>R</sup> , <i>CYP12I</i> , pET11a	McLean <i>et al.</i> , 2002a
pGL1(a)	Ap <sup>R</sup> , <i>CYP12I</i> P346L, pET11a	This study
pGL2(a)	Ap <sup>R</sup> , <i>CYP12I</i> R386L, pET11a	This study
pGL3(a)	Ap <sup>R</sup> , <i>CYP12I</i> S279A, pET11a	This study
pGL4(a)	Ap <sup>R</sup> , His- <i>CYP12I</i> , pET15b	This study
pGL5(a)	Ap <sup>R</sup> , His- <i>CYP140A2</i> , pET15b	This study
pMCN28	Kan <sup>R</sup> , His- <i>CYP151A2</i> , pET28a	Sielaff <i>et al.</i> , 2005b

**Table 2.1 Genotypes of expression vectors used in this study**

Ap<sup>R</sup> indicates presence of  $\beta$ -lactamase gene (conferring ampicillin resistance). Kan<sup>R</sup> indicates resistance to kanamycin.

#### 2.1.2 *E. coli* strains

*E. coli* strain JM109 (F' *traD36 proA*<sup>+</sup>*B*<sup>+</sup> *lacI*<sup>f</sup>  $\Delta$ (*lacZ*)M15/  $\Delta$ (*lac-proAB*) *glnV44 e14* *gyrA96 recA1 relA1 endA1 thi hsdR17*) (Promega) was used for blue/white screening, while some screening was also performed with *E. coli* Novablue

(*endA1 hsdR17(rK12<sup>-</sup> mK12<sup>+</sup>) supE44 thi-1 recA1 gyrA96 relA1 lac F' [proA<sup>+</sup>B<sup>+</sup> lacIqZΔM15::Tn10(TetR)]*) (Novagen). Protein expression strains used are summarised in Table 2.2.

Strain	Genotype/description
BL21(DE3)	<i>F', ompT, hsdS<sub>B</sub>(r<sub>B</sub><sup>-</sup>m<sub>B</sub><sup>-</sup>), gal, dcm</i>
HMS174(DE3)	<i>F', ompT, hsdR(r<sub>K12</sub><sup>-</sup>m<sub>K12</sub><sup>+</sup>), Rif<sup>R</sup></i>
Rosetta(DE3)	<i>F', ompT, hsdS<sub>B</sub>(r<sub>B</sub><sup>-</sup>m<sub>B</sub><sup>-</sup>), gal, dcm, lacY1, pRARE (Cm<sup>R</sup>)</i>
Rosetta-Gami(DE3)	<i>Δara-leu 7697, ΔlacX74, ΔphoAPvull, phoR, araD139, ahpC, galE, galK, rspL, F'[lac<sup>+</sup>(lacI<sup>q</sup>)pro], gor522::Tn10(Tc<sup>R</sup>), trxB::kan (DE3), pRARE (Cm<sup>R</sup>)</i>
Origami(DE3)	<i>F', ompT, hsdS<sub>B</sub>(r<sub>B</sub><sup>-</sup>m<sub>B</sub><sup>-</sup>), gal, dcm, lacY1, ahpC (DE3), gor522::Tn10 trxB, (Kan<sup>R</sup>, Tet<sup>R</sup>)</i>

**Table 2.2** *E. coli* host expression strains and their genotypes

### 2.1.3 Molecular biology reagents

PCR oligonucleotide primers were obtained from the Protein and Nucleic Acid Chemistry Laboratory (University of Leicester). New England Biolabs (Hitchin UK) provided all restriction enzymes and the DNA modifying enzyme; calf intestinal alkaline phosphatase. *Taq* DNA polymerase, along with T4 DNA ligase, were obtained from Promega (Southampton, UK). KOD polymerase was obtained from Novagen (Nottingham, UK). The 1 kb DNA-marker used in agarose gel electrophoresis was obtained from NEB.

### 2.1.4 Other Reagents

All remaining reagents, unless otherwise specified, were obtained from Sigma-Aldrich (Poole, UK). Media and most solutions were made according to standard recipes (Sambrook *et al.*, 1998). Chromatography resins, ion-exchange and hydrophobic affinity resins were purchased from Amersham (Little Chalfont, UK). Ceramic hydroxyapatite was from Bio-Rad (Hemel Hempstead, UK). Nickel affinity resin was from Novagen. Azole anti-fungal drugs were obtained from ICN Biomedicals (Basingstoke, UK). Voriconazole was donated by Pfizer and all azole-antifungal inhibitor solutions were prepared as stock solutions in DMSO.

## 2.2 Methods

### 2.2.1 Sterilisation of equipment and solutions

As required, all vessels, materials, solutions and media were sterilised before usage. Sterilisation was achieved by autoclaving at 121°C, 2 bar for 30 min. Solutions which contained heat-sensitive material, such as antibiotics, were filtered through a 0.2 µm pore size sterile filter (Sartorius, Epsom, UK).

### 2.2.2 PCR amplification of *CYP121P346L*, *CYP121R386L*, *CYP121S279A*, and *CYP140A2*

The PCR reactions for the 465 bp and 353 bp fragments containing *CYP121P346L* and *CYP121R386L*, respectively, were amplified in a 50 µL reaction volume. The PCR mix was made up in a 0.5 mL thin walled tube containing 0.2 mM dNTP mix (equimolar dATP, dCTP, dGTP and dTTP) (Stratagene, Cambridge, UK), 0.35 µM of oligonucleotide primers, and ~50 ng of the pKM2(b) template containing the wild-type *CYP121* DNA. In addition, the mix contained 2.5 units of *Pfu* polymerase (Promega) and 5 µL of the 10x reaction buffer supplied by the manufacturer. PCR was performed in a 105 °C heated lid Genius Thermal Cycler (Techne) with an annealing temperature of 51 °C. The cycling parameters were 30 cycles of 94 °C for 45s, 51 °C for 1 min, followed by 72 °C for 1 min.

Oligonucleotide primers for the gene amplification and production of the relevant mutations were designed from the *M. tuberculosis* and *M. ulcerans* genomic DNA sequence (Cole *et al.*, 2001). As above, complementarity at the 3'-end and self-complementarity of primer sequences was analysed by the OligoPerfect Designer (<http://www.invitrogen.com/content.cfm?pageid=9716>) to minimise primer-dimer formation and the introduction of secondary structures such as hairpin loops. Restriction enzyme sites were engineered into the *CYP121* gene, incorporating a *SacII* site into the 5'-end, and a *HindIII* site into the 3'-end of the primer for the P346L mutation (Table 2.3). In the R386L mutation, an *MfeI* site was incorporated into the 5'-end primer, and a *HindIII* site into the 3'-end (Table 2.3).

The PCR reaction for the 6832 bp plasmid containing *CYP121S279A* was performed in a 50 µL reaction volume using the Quikchange™ mutation kit

(Stratagene). The PCR mix was made up in a 0.5 mL thin walled tube containing 0.2 mM dNTP mix (equimolar dATP, dCTP, dGTP and dTTP), oligonucleotide primers (20 picomoles), and ~15 ng of the pKM2(b) template containing wild-type *CYP121*. In addition, the mix contained 5 µL of 10 x *Pfu* buffer (Promega) and 2 units of *Pfu* polymerase enzyme. PCR was performed in a 105 °C heated lid Genius Thermal Cycler (Techne) with an annealing temperature of 55 °C. The cycling parameters were 1 cycle of 94 °C for 30 s, followed by 18 cycles of 95 °C for 30 s, 55 °C for 1 min, 68 °C for 2 min. An *AseI* restriction enzyme site was engineered into the 5'-end primer of the *CYP121* gene through a silent mutation (Table 2.3).

The 1330 bp fragment containing the *CYP140A2* gene was amplified in a 50 µL reaction volume. The mix, made up in a 0.5 mL thin walled PCR tube, contained 5 µL of 2 mM dNTP mix (containing equimolar dATP, dCTP, dGTP and dTTP), 5 µL of DMSO, forward and reverse primer solutions (20 pmol), 1 µL of *M. ulcerans* 22D03IG08 contig pDNA (from Dr. Timothy Stinear, Pasteur Institute, Paris) (~50 ng) and made up to the final volume with ddH<sub>2</sub>O. In addition, the mix contained 1 µL of 10 x KOD buffer (Roche, Welwyn Garden City, UK) and 1 µL of KOD enzyme (2.5 U/mL). PCR was performed in a Genius Thermal Cycler (Techne) with an annealing temperature of 66 °C. The cycling parameters were 95 °C for 1 min; 5 cycles of 94 °C for 30 s, 66 °C for 30 s, 72 °C for 1.5 min; 25 cycles of 94 °C for 20 s, 60 °C for 15 s, 72 °C for 1 min; followed by 72 °C for 7 min.

Gene	Oligonucleotide sequence	T <sub>m</sub> (°C)
<i>CYP121P346L</i>	forward: 5'-TTCGGCCGCGGCCAA CACTTCTGTCTTGA-3'	67
	reverse: 5'-GAAAGCTTATCATCG ATAAGCTTTAATGCGG-3'	60
<i>CYP121R386L</i>	forward: 5'- GACCAATTGGTCTGGCG CACCCGATTCCAACTACGC-3'	70
	reverse: 5'-GACAAGCTTATCA TCGATAAGCTTTAATGCGG-3'	60
<i>CYP121S279A</i>	forward: 5'- CTGCTGCGGATTAATCTCGCCTTCG CCGAC -3'	68
	reverse: 5'- GTCGGCGAAGGCGAGATTAATCC GCAGCAG -3'	68
<i>CYP140A2</i>	forward: 5'-CATATGAGG CAGAGATTGAACTGGATT -3'	57
	reverse: 5'-CGGATCCGATATGTC GTCATCGGATAGCCATCG -3'	67

**Table 2.3 Oligonucleotide primers used for gene amplification and mutation**  
Primers and corresponding melting temperatures (T<sub>m</sub>) for the engineering of *M. tuberculosis* and *M. ulcerans* P450s. The engineered restriction enzymes sites are highlighted in bold with the incorporated initiation codon underlined. Bases highlighted in red indicate the base change.

Following PCR amplification, DNA was resolved on a 1 % agarose gel and excised. The *CYP121R386L*, *CYP121P346L* and *CYP140A2* PCR fragments were cloned using the pGEM-T easy vector system. Transformation of the ligated product was then carried out using competent *E. coli* JM109 cells (Novagen). The *CYP121S279A* PCR product underwent *DpnI* digestion to confirm presence of the correctly amplified DNA.

### 2.2.3 DNA cloning

Following PCR amplification, gene products were analysed on 1 % agarose gels; PCR fragments of the expected size were excised from the gel and purified from the agarose using the QIAquick gel extraction kit (Qiagen, West Sussex, UK). The

purified DNA was cloned directly into the plasmid vector pGEM-T easy using standard ligation and transformation procedures. Transformant colonies were screened for recombinant *CYP121P346L*, *CYP121R386L* and *CYP140A2* clones directly by colour screening on X-Gal/isopropyl-thiogalactoside (IPTG) indicator plates (blue/white screen). Recombinant clones were prepared by the mini-prep spin-kit (Qiagen), following the manufacturer's guide. The resulting DNA preparations were verified by digestion with appropriate restriction enzymes.

#### **2.2.4 Agarose gel electrophoresis**

Agarose gel electrophoresis was used to fractionate the DNA samples with 1 % (w/v) gels. Size-fractionation of DNA was carried out using agarose gel electrophoresis in 1 x TBE buffer (48 mM Tris, 44 mM Boric acid, 1mM EDTA). Electrophoresis was carried out in a horizontal gel apparatus (Flowgen, Nottingham, UK).

The agarose gels were prepared by melting 0.5g of agarose in 50 mL of 1 x TBE, to which 1.3 µL of ethidium bromide (10 mg/mL) was added and mixed. This was then poured into a casting tray with combs, and allowed to set. The samples, which were prepared by the addition of one-tenth volume of bromophenol loading dye (1x TBE, 40 % v/v glycerol and 0.05 % w/v Bromophenol blue), were applied onto the gel and subjected to electrophoresis at 100 V for 20 min in a 1 x TBE buffer. Following electrophoresis, the position of the DNA fragments were visualised using a Gene Genius (Syngene, Cambridge, UK) transilluminator and the gel was photographed using a Sony video copy processor. A 1 kb molecular marker (NEB) was run alongside samples to confirm fragment size.

#### **2.2.5 Extraction and purification of DNA from agarose gels**

DNA was extracted from ethidium bromide-stained agarose gels and purified using the QIAquick Gel Extraction kit (Qiagen), according to the manufacturer's instructions. Specifically, a slice of agarose gel containing the DNA fragment of interest was excised using a clean, sharp scalpel. The gel slice was then weighed and three volumes of QG Buffer were added to one volume of gel. The mixture was then incubated for 10 min at 50 °C with occasional inversion in order to facilitate the

dissolution of the gel slice. When the gel was completely dissolved, a 1 gel volume of isopropanol was added, followed by mixing. The mixture was then transferred to a QIAquick column, which was placed in a 2 mL collection tube and centrifuged for 1 minute at maximum speed in a microcentrifuge. Following centrifugation, the eluate was discarded and 0.5 mL of Buffer QG added, and the column centrifuged for 1 minute. Thereafter, 0.75 mL of Buffer PE was added to the column, which was left to stand for 5 minutes at room temperature. The column was then subjected to centrifugation, as previously. The resultant eluate was then discarded and the column was centrifuged for an additional 1 min. Finally, the column was placed in a clean 1.5 mL tube (Eppendorf), and the DNA bound to the column membrane was eluted by applying 30  $\mu$ L of Buffer EB to the membrane followed by centrifugation, as described above. Subsequently, the fragments of *CYP12IP346L* and *CYP121R386L* were 'A' tailed.

#### **2.2.6 'A' tailing of PCR fragments**

The *CYP12IP346L* and *CYP121R386L* PCR fragments were 'A' tailed in a 10  $\mu$ L reaction volume. The mix, made up in a 0.5 mL thin walled PCR tube, contained 1  $\mu$ L of 5mM dATP and 7  $\mu$ L of fragment DNA. In addition, the mix contained 1  $\mu$ L of 10 x Taq buffer (Promega) and 1  $\mu$ L of Taq polymerase (1 U/mL). 'A' tailing was performed in a Genius Thermal Cycler (Techne) with the parameter of 70 °C for 30 min. Subsequently, the fragments were ligated into pGEM-T Easy (Promega).

#### **2.2.7 *DpnI* digestion of *CYP12IS279A***

Following PCR generation, to confirm successful amplification, the PCR product was digested with *DpnI*. 1  $\mu$ L of the *DpnI* restriction enzyme (10 U/ $\mu$ L) was added directly to the amplification reactions and each reaction mixture was gently mixed by pipetting the solution up and down several times. The reaction was incubated at 37 °C for 1 hour. Following electrophoresis, the position of the DNA fragments were visualised using a Gene Genius (Syngene) transilluminator and the gel was photographed using a Sony video copy processor. A 1 kb molecular marker (NEB) was run alongside to confirm fragment size. Subsequently, the *DpnI* digested DNA was transformed into NovaBlue cells (Novagen) (section 2.2.9).



### **2.2.8 Cloning of PCR- and restriction digest-generated fragments into pGEM-T Easy and pET15b**

Both the PCR-generated P346L and R386L *CYP121* fragments, and *CYP140A2*, were cloned using a pGEM-T Easy vector system, following the manufacturer's recommended instructions (Promega). A 10 µL ligation reaction was set up containing 1 µL of PCR product, 5 µL of 10 x T4 ligase buffer, 1 µL of pGEM-T Easy vector (50 ng) (Promega), T4 DNA ligase (3 Weiss units/µl) (Promega) and left overnight at 4 °C. Transformation of the ligated products was then carried out using competent *E. coli* JM109 cells (Promega). Successful cloning of *CYP121P346L* and *CYP121R386L* fragments was established by screening for recombinant clones (white) directly by colour selection on X-gal/isopropyl-thiogalactoside (IPTG) indicator plates (blue/white screen). Recombinant clones were prepared by the mini-prep spin kit (Qiagen), following the manufacturer's guide (Promega). The resulting DNA preparations were verified by DNA sequencing.

*CYP121* wild-type fragment was cloned into pET15b pre-digested with *NdeI* and *BamHI*. A 20 µL ligation reaction was set up containing 2 µL of 10 x Ligase buffer (200 mM Tris-HCl, 100 mM MgCl<sub>2</sub>, 250 µg/mL acetylated BSA, pH 7.6), 2 µL 100 mM DTT, 1 µL 10 mM ATP, 2 µL prepared pET15b vector (100 ng), 2 µL *CYP121* fragment (200 ng) and 1 µL T4 DNA Ligase (0.4 Weiss U/µL), and the mixture was incubated at 4 °C overnight. Transformation of the ligated products was then carried out using competent *E. coli* NovaBlue cells (Novagen). Successful cloning of the wild type *CYP121* fragment was established by screening for recombinant clones on ampicillin-containing LB agar plates. Recombinant clones were prepared by the mini-prep spin kit (Qiagen), following the manufacturer's guide. The resulting DNA preparations were verified by restriction digest.

### **2.2.9 Transformation of competent cells**

pGEM-T Easy vectors containing *CYP121P346L* and *CYP121R386L* were transformed into JM109 and in the case of *CYP121S279A* and *CYP140A2* into NovaBlue. Competent cells were removed from a -70 °C freezer and immediately placed on ice. Cells were allowed to thaw on ice for 2-5 minutes and were then "flicked" to achieve resuspension and aliquoted into pre-chilled tubes as 20 µl

amounts. 1 µl of either ligation reaction or purified plasmid DNA was added directly to the cells and stirred gently to mix, and kept on ice for 5 minutes. After ice incubation, cells were heated at 42 °C in a water bath for exactly 30 seconds, and then immediately placed on ice for 2 minutes. 80 µL of SOC medium was added to the transformation reaction. For NovaBlue cells, transformation tubes were heat-shocked at 37 °C (250 rpm) for 30-60 minutes prior to plating on selective media.

#### **2.2.10 Automated DNA sequencing**

The plasmid clones were sequenced to establish the correct DNA sequence and orientation using the services of PNACL (Protein and Nucleic Acid Chemistry Laboratory, University of Leicester). Sequencing was by the dideoxy chain termination method (Sanger *et al.* 1977), using the dye-based terminator method. Oligonucleotide primers used for sequencing of pGEM-T vectors containing relevant inserts were the T7 primer 5'-TGT AAT ACG ACT CAC TAT ACG G-3' and the Sp6 primer 5'-ATT TAG GTG ACA CTA AGA CAT A-3'. Subsequently, the clones were digested to excise the fragments. For sequencing of the S279A insert in the pET11a vector and CYP151A2 in a pET28a vector, pETFor 5'-TAA TAC GAC TCA CTA TAG GG-3' (T7 promoter) and pETRev 5'-GCT AGT TAT TGC TCA GCG G-3' (T7 terminator) were used (Appendix).

#### **2.2.11 Restriction digest of recombinant pGEM-T Easy vectors**

The pGEM-T Easy (Promega) constructs containing the *CYP12IP346L* and *CYP12IR386L* fragments were digested with complementing enzymes to excise the required fragments. For *CYP12IP346L*, a reaction mix containing 23 µL of plasmid DNA (36 ng/µL) was placed in a sterile microfuge tube and mixed with 3 µL Buffer 2 (10 mM Tris-HCl, 10 mM MgCl<sub>2</sub>, 50 mM NaCl, 1 mM dithiothreitol (pH 7.9 at 25°C)), 2 µL *SacII* (1,000 U/mL) and 2 µL *HindIII* (20,000 U/mL). The mix was incubated at 37 °C for 6 hours. For *CYP12IR386L*, a reaction mix containing plasmid DNA (~500 ng) was placed in a sterile microfuge tube and mixed with 3 µL Buffer 2, 2 µL *MfeI* (10,000 U/mL) and 2 µL *HindIII* (20,000 U/mL). The mix was incubated at 37 °C for 6 hours. In both cases, the resulting digest was run on a 1 % agarose gel to separate plasmid DNA from the insert, and the appropriate fragment

was excised and purified as described previously. This was in preparation for the subcloning of the fragments into pet11a based pKM2(b) vector.

#### **2.2.12 Restriction digest of pKM2(b) and pET15b**

The ~1200 bp fragment containing the *CYP121* gene was released through digestion of pKM2(b) by *NdeI* and *BamHI*. The digestion mix, was made in a sterile microfuge tube and contained 20 µL of pKM2(b) (50 ng/µL) mixed with 3 µL Buffer 2 (10 mM Tris-HCl, 10 mM MgCl<sub>2</sub>, 50 mM NaCl, 1 mM dithiothreitol (pH 7.9 at 25°C)), 2 µL *NdeI* (20,000 U/mL) and 2 µL *BamHI* (20,000 U/mL), and made up to a 30 µL total volume with ddH<sub>2</sub>O. The mix was incubated at 37 °C for 5 hours. The subsequent digest was run on a 1 % agarose gel to separate plasmid DNA from the insert, and the appropriate fragment was excised and purified as described previously in preparation for the subcloning into pET15b.

The pET15b expression vector was digested for the subsequent insertion of the CYP121 wild-type fragment with a digestion mix containing 15 µL of pET15(b) (Novagen) (70 ng/µL) mixed with 3 µL Buffer 2 (10 mM Tris-HCl, 10 mM MgCl<sub>2</sub>, 50 mM NaCl, 1 mM dithiothreitol (pH 7.9 at 25°C)), 0.5 µL CIAP (20,000 U/mL), 2 µL *NdeI* (20,000 U/mL) and 2 µL *BamHI* (20,000 U/mL), and made up to a 30 µL total volume with ddH<sub>2</sub>O. The mix was incubated at 37 °C for 6 hours. The resulting digest was run on a 1 % agarose gel to separate plasmid DNA from the insert, and the appropriate fragment was excised and purified as described previously in preparation for subcloning of the CYP121 wild-type fragment.

#### **2.2.13 Subcloning of *CYP121P346L* and *CYP121R386L* fragments into pKM2(b), and *CYP121* wild-type fragment into pET15b**

The vector pKM2(b), a pET11a-based expression plasmid containing the *CYP121* WT gene, was firstly linearised by restriction enzyme digestion. For the cloning of *CYP121P346L* into the pET vector, a reaction mix containing 1 µg of pKM2(b) DNA was placed in a sterile microfuge tube. One-tenth of the total volume (3 µL) of 10 x restriction Buffer 2 was added, followed by 2 µL of CIAP (10,000 U/mL). Also, 2 µL of restriction enzyme *HindIII* (20,000 U/mL) and 2 µL of *SacII* (1,000 U/mL) were added and mixed with sterile H<sub>2</sub>O to a volume of 30 µL. The

reaction mix was incubated at 37 °C for 6 hours. Subsequently, the digest was run on a 1 % agarose gel and the DNA backbone was extracted and purified. Cloning of *CYP121R386L* into the pET11a vector was performed identically to the previously mentioned reaction, except that 2 µL of *MfeI* (10000 U/mL) replaced *SacII*.

The *CYP121P346L* fragment was cloned into the pKM2(b) expression vector, previously digested with *SacII* and *HindIII*, and dephosphorylated with CIAP. A 10 µL ligation reaction was set up containing *CYP121P346L* (50 ng), 1 µL of 10 x T4 ligase buffer (Promega), 1 µL T4 ligase (10 U/µL), 4.5 µL ddH<sub>2</sub>O, and then incubated at 16 °C overnight. Transformation of the ligated products was then performed using competent *E. coli* JM109 cells (Promega). Thereafter, clones were selected that contained the insert and minipreped, and were subsequently digested and sequenced. The *CYP121R386L* fragment was cloned into the pKM2(b) expression vector previously digested with *MfeI*, *HindIII* and treated with CIAP, using the same ligation procedure previously described.

The *CYP121* wild-type fragment was also cloned as a histidine-tagged form into the pET15b vector, previously digested with *NdeI* and *BamHI*. A 10 µL ligation reaction was set up containing *CYP121P346L* (50 ng), 1 µL of 10 x T4 ligase buffer (Promega), 1 µL T4 ligase (10 U/µL), 4.5 µL ddH<sub>2</sub>O, and then incubated at 16 °C overnight. Transformation of the ligated products was then performed using competent *E. coli* JM109 cells (Promega). Thereafter, clones were selected that contained the insert and minipreped, and were subsequently digested. The *CYP121* fragment was cloned into the pET15b expression vector previously digested with *NdeI*, *BamHI* and treated with CIAP, using the same ligation procedure previously described.

#### **2.2.14 Restriction digestion of pGL1, pGL2 and pGL4**

To confirm the presence of the *CYP121P346L*, *CYP121R386L* and wild-type *CYP121* inserts, restriction digests were performed on the minipreped plasmid constructs with *BstNI*, *HgaI* and *NdeI* respectively. For *CYP121P346L* clones, a reaction mix containing the plasmid DNA (500 ng) was placed in a sterile microfuge tube. One-tenth of the total volume (3 µL) of the 10 x restriction Buffer 2, followed

by 3  $\mu$ L of Bovine Serum Albumin (BSA) (1 mg/mL) were added, and the sample mixed. 2  $\mu$ L of restriction enzyme *Bst*NI (10,000 U/mL) was added and the sample mixed again. The reaction mixture was incubated in a water bath at 60 °C overnight.

For *CYP121R386L*, a reaction mix containing plasmid DNA (700 ng) was placed in a sterile microcentrifuge tube. One-tenth of the total volume (3  $\mu$ L) of the 10 x restriction Buffer 1 (10 mM Bis Tris Propane-HCl, 10 mM  $MgCl_2$ , 1 mM dithiothreitol (pH 7.0 at 25 °C ) and 2  $\mu$ L of restriction enzyme *Hga*I (2,000 U/mL) were added and the sample mixed. The reaction mixture was incubated in a water bath at 37 °C overnight. In both cases, a control digest with pKM2(b) was performed to allow comparison.

For the histidine-tagged CYP121, a reaction mix containing plasmid DNA (400 ng) was placed in a sterile microcentrifuge tube. One-tenth of the total volume (3  $\mu$ L) of the 10 x restriction Buffer 4 (50 mM potassium acetate, 20 mM Tris-acetate, 10 mM magnesium acetate, 1 mM dithiothreitol (pH 7.9 at 25°C )) and 2  $\mu$ L of restriction enzyme *Nde*I (20,000 U/mL) were added and the sample mixed. The reaction mixture was incubated in a water bath at 37 °C for 6 hours.

The resulting digests were run on a 2 % agarose gel to allow improved resolution of the digested fragments. Positive clones containing the desired insert were designated pGL1(a) (containing *CYP121P346L*), pGL2(a) (containing *CYP121R386L*) and pGL4 (a) (containing *CYP121* wild-type). Subsequently, the constructs were transformed into the expression strain *E. coli* HMS174 (DE3).

DNA sequencing of the pGL1(a) and pGL2(a) clones was performed to fully verify each construct, using an Applied Biosystems DNA sequencer at PNACL (University of Leicester). Sequencing primers used were based on the flanking pGEM-T sequences (section 2.2.10).

### **2.2.15 Restriction digest of pGEM-T *CYP140A2***

The pGEM-T (Promega) constructs containing the *CYP140A2* fragment were digested with selected restriction enzymes to excise the P450-encoding fragment. For

pGEM- *CYP140A2*, a reaction mix containing plasmid DNA (~500 ng/μL) was placed in a sterile microfuge tube and mixed with 3 μL Buffer *Bam*H1, 2 μL *Bam*HI (20,000 U/mL) and 2 μL *Nde*I (10,000 U/mL). The mix was incubated at 37 °C for 6 hours. The resulting digest was run on a 1 % agarose gel to separate plasmid DNA from the insert, and the correct clones were sequenced. The resulting selected clone was miniprep'd in readiness for excision of the *CYP140A2* fragment with *Nde*I and *Bam*HI. The resulting digest was run on a 1 % agarose gel to separate plasmid DNA from the insert, and the appropriate fragment was excised and purified as described previously. This was done in preparation for the subcloning of the fragment into pET15b.

#### **2.2.16 Subcloning of the *CYP140A2* fragment into pET15b**

The pET15b-based expression plasmid was linearised by digestion with the enzymes *Bam*HI and *Nde*I. For the cloning of *CYP140A2* into pET15b, a reaction mix containing 1 μg of plasmid DNA was placed in a sterile microfuge tube and mixed with sterile ddH<sub>2</sub>O to a final volume of 30 μL (following the enzyme and buffer additions). One-tenth of the total volume (3 μL) of 10x restriction Buffer *Bam*HI was added, followed by 2 μL of CIAP (10,000 U/mL). Also 2 μL of restriction enzyme *Bam*HI (20,000 U/mL) and 2 μL of *Nde*I (10,000 U/mL) were added and mixed. The reaction mix was incubated at 37 °C for 6 hours. Thereafter, the digest was run on a 1 % gel and the DNA backbone was extracted and purified, in preparation for ligation of the *CYP140A2* fragment.

The *CYP140A2* fragment was cloned into the pET15b expression vector, previously digested with *Bam*HI and *Nde*I. A 10 μL ligation reaction was set up at a 1:1 ratio containing 2 μL pET15b (~100 ng), *CYP140A2* (~50 ng/μL), 1 μL of 10 x T4 ligase buffer (NEB), 1 μL T4 ligase (10 U/μL), 4.5 μL ddH<sub>2</sub>O, and then incubated at 16 °C overnight. Transformation of the ligated products was then performed using competent *E. coli* NovaBlue cells (Novagen), and thereafter colonies were miniprep'd and the plasmid DNA isolated from these colonies was digested to confirm that the correct fragment had been cloned.

A confirmation digestion of *CYP140A2* was done using a reaction mix containing the relevant plasmid DNA (600 ng) in a sterile microcentrifuge tube. One-tenth of the total volume (3  $\mu$ L) of the 10 x restriction Buffer 3 (100 mM NaCl, 50mM Tris-HCl, 10 mM MgCl<sub>2</sub>, 1mM dithiothreitol (pH7.9 at 25°C )) and 2  $\mu$ L of restriction enzyme *Mlu*I (2,000 U/mL) were added and mixed. As with the previous digests, the final volume was achieved (30  $\mu$ L) by addition of sterile distilled water. The reaction mixture was incubated in a water bath at 37 °C for 6 hours.

The resulting digest was run on a 1 % agarose gel to allow improved resolution of digested DNA fragments. Positive clones containing the correct insert were designated pGL5(a). Subsequently, the constructs were transformed into the *E. coli* expression strains.

#### **2.2.17 Subcloning of *CYP121* into pGL4**

The *CYP121* gene was cloned into the pET15b expression vector to generate a N-terminal histidine tagged protein. The pET15b vector was previously digested with *Bam*HI and *Nde*I (section 2.2.16) and, thereafter, the digest was run on a 1 % agarose gel and the *CYP121* fragment was extracted and purified, in preparation for ligation into a pET15b vector.

A 10  $\mu$ L ligation reaction was set up at a 1:1 ratio containing, pET15b (~50 ng), *CYP121* fragment (~50 ng), 1  $\mu$ L of 10 x T4 ligase buffer (NEB), 1  $\mu$ L T4 ligase (10 U/ $\mu$ L), 4.5  $\mu$ L ddH<sub>2</sub>O, and then incubated at 4 °C overnight. Transformation of the ligated products was then performed using competent *E. coli* NovaBlue cells (Novagen), and thereafter colonies were miniprepmed. Positive clones were subsequently transformed into the expression strain *E. coli* HMS174 (DE3).

A confirmation digestion for the construction of the *His*-tagged *CYP121* was performed in a reaction mix containing plasmid DNA (~700 ng) in a sterile microcentrifuge tube. One-tenth of the total volume (3  $\mu$ L) of the 10 x restriction *Eco*RI Buffer (50 mM NaCl, 100 mM Tris-HCl, 10 mM MgCl<sub>2</sub>, 0.025 % Triton X-100, pH 7.5 at 25 °C) and 2  $\mu$ L of restriction enzyme *Eco*RI (20,000 U/mL) were added and mixed. The reaction mixture was incubated in a water bath at 37°C for 3

hours. The resulting digest was run on a 1 % agarose gel. Positive clones containing the insert were designated pGL4(a). Subsequently, the constructs were transformed into the expression strain *E. coli* HMS174 (DE3).

#### **2.2.18 Transformation of *E. coli* HMS174 (DE3) and *E. coli* BL21 (DE3) competent cells**

*E. coli* HMS174 (DE3) competent cells were removed from storage at -70°C and thawed on ice and transformed. This was done as previously described for JM109, but with some alterations to the procedure. ‘Heat shock’ was performed at 42 °C for 2 minutes and the sample rapidly transferred to ice, and then incubated for a further 2 minutes. Following growth of cells on selective media, single transformed colonies were chosen and used to inoculate 5 mL LB medium containing ampicillin (30 µg/mL) and the samples incubated at 37 °C overnight, with shaking, in preparation for protein expression. *E. coli* BL21 (DE3) was transformed using the same method, as were the other strains used in the expression trials.

### **2.3 Protein expression studies**

The pGL5 recombinant expression clone was re-transformed into T7 RNA polymerase strains BL21(DE3), HMS174(DE3), Rosetta-Gami(DE3), Rosetta(DE3), and Origami(DE3). Cell cultures for investigation into protein expression were grown on a small scale (~5 mL) in Luria-Bertani (LB) medium containing ampicillin (100 µg/mL) until mid logarithmic phase ( $OD_{600}$  ~0.6), whereupon gene expression was induced by the addition of 1 mM isopropyl-thiogalactoside (IPTG).

CYP151A2 (P450<sub>mor</sub>) established in the pET15b expression vector and designated pMCN28, was transformed into Rosetta(DE3). Cell cultures for investigation into protein expression were grown on a small scale (~5 mL) in Luria-Bertani (LB) medium containing chloramphenicol (34 µg/mL), kanamycin (15 µg/mL) or ampicillin (100 µg/mL) until mid logarithmic phase ( $OD_{600}$  ~0.6), whereupon gene expression was induced by the addition of 100 µM IPTG.

Protein solubility was measured by lysing the cells with Bugbuster Protein Extraction Reagent (Novagen), and separating soluble and insoluble fractions.



Various induction times, growth temperatures and phase of growth prior to induction were investigated to optimise expression.

### **2.3.1. SDS-PAGE analysis of protein expression**

Cells were harvested by centrifugation and prepared for investigation by sodium dodecyl sulphate polyacrylamide gel electrophoresis (SDS-PAGE). The levels of expression under a variety of conditions and the molecular mass of the protein under study were measured. Samples were prepared by mixing with one-third volume of 3x Reducing SDS Loading Buffer (NEB) containing dithiothreitol (DTT), and were boiled at 95 °C for 4 minutes.

SDS-PAGE analysis was performed with a gel consisting of 10 % acrylamide resolving gel, 5% acrylamide stacking gel, and the gel was run in a Tris-glycine electrophoresis buffer. All SDS-PAGE components were prepared by standard methods (Sambrook *et al.*, 1989). Gels were initially run at 130 V through the stacking gel and the voltage increased to 170 V through the resolving gel. On completion of electrophoresis, gels were stained with a solution containing 0.25 % Coomassie Blue R-250, 50 % (v/v) methanol and 10 % acetic acid for ~5 minutes. Destaining of the gel was performed in a 10 % methanol and 5 % acetic acid solution with two solution changes.

## **2.4 Characterisation of CYP121**

### **2.4.1 Protein expression and purification**

#### **2.4.1.2 Protein expression of histidine-tagged wild-type CYP121 and CYP121 mutants**

Protein expression of CYP121 P346L, CYP121 R386L, CYP121 S279A and His-CYP121 was based on the expression protocol developed for wild-type CYP121 (McLean *et al.*, 2002a). Cell cultures of the *E. coli* strain HMS174(DE3) containing the appropriate recombinant expression plasmid were grown at 30 °C in 6 L of Terrific Broth containing 100 µg/mL ampicillin in a refrigerated shaking incubator at 250 rpm. Twenty minutes prior to induction (OD<sub>600</sub> 0.5-0.6) the temperature was reduced to 18 °C and the culture allowed to equilibrate, with shaking at 180 rpm. Gene expression was induced by the addition of 100 µM IPTG at OD<sub>600</sub> 0.8, and cells

were grown for a further 20-24 hours at 18 °C, 190 rpm. Cells were harvested by centrifugation (6,500 rpm, 25 minutes). The cell pellet was washed by resuspension in ice-cold 50 mM Tris EDTA, pH 7.2 (buffer A) and finally resuspended in a small volume of the same buffer for lysis. The protease inhibitors PMSF and benzamidine hydrochloride (both at 1 mM) were added to all buffers and the cell extract was kept on ice at all times to minimise proteolysis.

#### **2.4.1.3 Protein expression of histidine tagged CYP140A2**

Expression of N-terminal histidine tagged CYP140A2 was performed using cell cultures of the *E. coli* strain BL21(DE3) containing the pGL5 expression plasmid, with cells grown at 30 °C in 6 Litres of Terrific Broth containing 100 µg/mL ampicillin, and in a refrigerated shaking incubator at 250 rpm. Twenty minutes prior to induction (OD<sub>600</sub> 0.5-0.6) the temperature was reduced to 18 °C and the culture allowed to equilibrate, with shaking at 180 rpm. Gene expression was induced by the addition of 100 µM IPTG at OD<sub>600</sub> 0.8, and cells were grown for a further 16-20 hours at 18 °C, 180 rpm. Cells were harvested by centrifugation (6,500 rpm, 25 mins). The cell pellet was washed by resuspension in ice-cold buffer A and finally resuspended in a small volume of the same buffer for lysis that contained two protease inhibitor tablets (EDTA-free) (Roche). PMSF and benzamidine hydrochloride (1 mM) were added to all buffers and the cell extract was kept on ice at all times to minimise proteolysis.

#### **2.4.1.4 Protein expression of histidine tagged CYP151A2**

Expression of the C-terminal histidine tagged CYP151A2 was done by culture of the *E. coli* strain Rosetta(DE3) containing the CYP151A2/pET28a expression plasmid. Cultures were grown at 30 °C in 6 Litres of Terrific Broth containing kanamycin (15 µg/mL) and chloramphenicol (34 µg/mL) in a refrigerated shaking incubator at 250 rpm. Twenty minutes prior to induction (OD<sub>600</sub> 0.3-0.4) the temperature was reduced to 25 °C and the culture was allowed to equilibrate, with shaking at 200 rpm. Gene expression was induced by the addition of 100 µM IPTG at OD<sub>600</sub> 0.5-0.6, and cells were grown for a further 16-20 hours at 25 °C, 180 rpm. Cells were harvested by centrifugation (6,500 rpm, 25 min). The cell pellet was washed by resuspension in ice-cold 50 mM Tris-HCl (pH 7.2) (buffer A), and finally

resuspended in a small volume of the same buffer for lysis. PMSF and benzamidine hydrochloride (1 mM) were added to all buffers and the cell extract was kept on ice at all times to minimise proteolysis.

#### **2.4.1.5 Cell Lysis**

Cells expressing each of the proteins studied were lysed by intermittent sonication, using a Bandelin Sonoplus GM2600 sonicator with an Ultrasonic Homogeniser HG2600 probe. Sonication was performed by 8-10 x 20 second bursts at full power, with 2 minute breaks between each burst, keeping the suspension on ice at all times. The cell suspension was also subjected to further lysis using a French Press (950 lb/inch<sup>2</sup>) to improve the efficiency of cell lysis. The lysate was centrifuged (16,000 rpm, 30 mins, 4 °C) to remove cellular debris, and the supernatant was carefully removed.

#### **2.4.1.6 Protein purification of CYP121 mutants**

The purification of the mutants CYP121 P346L, CYP121 R386L, and CYP121 S279A, was as described for the wild-type (McLean *et al.*, 2002a). The soluble cell extract was directly subjected to an initial purification step of ammonium sulphate precipitation. The salt was added stepwise to 30 % saturation with stirring slowly at 4 °C, ensuring complete dissolution of the salt to produce a homogeneous solution between each addition. The precipitate was pelleted by centrifugation (8,000 rpm, 15 minutes, 4 °C) and the reddish-coloured soluble fraction retained. This fraction was subjected to a further 30-70 % ammonium sulphate cut, and the resulting protein precipitate was pelleted following centrifugation as before. Subsequent purification of the CYP121 mutants involved column chromatography using Phenyl Sepharose, Q-Sepharose and hydroxyapatite resins, as described below.

The protein precipitate from the 30-70 % ammonium sulphate fractionation was resuspended in a minimal volume of buffer A, in order to prevent a large decrease in the salt concentration, and loaded directly onto a Phenyl Sepharose (30 cm x 5 cm) column washed in buffer A containing 1.5 M ammonium sulphate. CYP121 mutants were eluted in a linear 500 mL gradient of 1.5 to 0 M ammonium sulphate in buffer A, and were eluted at ~250 mM salt. The most intensely red fractions were pooled and dialysed extensively into buffer A.

The protein solution was then loaded onto a Q-Sepharose column (30 cm x 5 cm) and the column washed extensively with buffer A. CYP121 mutants were eluted in a linear 500 mL gradient of 0 to 500 mM potassium chloride (KCl) in buffer A, eluting at 100-150 mM KCl. The most intensely red-coloured fractions were pooled and concentrated by ultrafiltration (1,500 rpm, 4 °C) to a final volume of ~5 mL using Centriprep Centrifugal Filtration Devices, with a 30 kDa  $M_r$  cut-off (Millipore).

The protein solutions collected were dialysed extensively against 25 mM potassium phosphate ( $KP_i$ ), pH 6.5 (buffer B) and then loaded onto a hydroxyapatite column (25 cm x 5 cm). Elution was achieved in a 500 mL linear gradient of buffer B to 500 mM  $KP_i$ , pH 6.5. The protein was dialysed against buffer A to remove any salts and concentrated by ultrafiltration, as before, to a final concentration of ~10-15 mg/mL. The purified proteins were dialysed overnight in buffer A containing 50 % (v/v) glycerol and then stored at -80 °C.

#### **2.4.1.7 Protein purification of His-CYP121**

For the purification of N-terminal histidine tagged CYP121, the protein solution was loaded onto a nickel affinity column (Qiagen, Valencia, CA) (25 cm x 5 cm), pre-equilibrated with 50 mM potassium phosphate ( $KP_i$ ), pH 7.5 (Buffer C). The loaded column was washed with 10 column volumes of buffer C containing 10 mM imidazole. The protein was eluted with buffer D (buffer C containing 400 mM KCl) plus 20 mM imidazole. The eluted protein was dialysed against two changes of buffer containing 2 L of 20 mM Tris-HCl, pH 7.5, 1 mM EDTA.

The most intensely red-coloured fractions were pooled and concentrated by ultrafiltration (1,500 rpm, 4 °C) to a final volume of ~15-20 mg/mL using centripreps with a 30 kDa  $M_r$  cut-off (Millipore). The purified proteins were dialysed overnight in buffer A containing 50 % (v/v) glycerol and then stored at -80 °C.

#### **2.4.1.8 Protein purification of His-CYP140A2**

For the purification of His-CYP140A2, the protein solution was loaded onto a nickel affinity column (Qiagen, Valencia, CA) (25 cm x 5 cm), pre-equilibrated with

50 mM potassium phosphate ( $\text{KP}_i$ ), pH 7.5 (Buffer C). The loaded column was washed with 10 column volumes each of buffer C containing 20 mM imidazole and 250 mM KCl. The protein was eluted with buffer D containing 50 mM imidazole. The most intensely red-coloured fractions were pooled and concentrated by ultrafiltration (1,500 rpm, 4 °C) to a final volume of <1 mL using Centripreps with a 30 kDa  $M_r$  cut-off (Millipore).

Further chromatography was performed using gel filtration. The protein solution from was loaded directly onto a gel filtration column (70 cm x 5 cm) column containing a Sephadex<sup>®</sup> G-100 Medium equilibrated in buffer D (10 mM Tris, pH7.0). The most intensely red fractions were pooled, concentrated and dialysed extensively into buffer A containing 50 % (v/v) glycerol and then stored at –80 °C.

#### **2.4.1.9 Protein purification of His-CYP151A2**

This protein solution was dialysed extensively against buffer D, and then loaded onto a nickel affinity column (Qiagen, Valencia, CA) (25 cm x 5 cm), pre-equilibrated using buffer C (50 mM potassium phosphate ( $\text{KP}_i$ ), pH 7.5) containing 20 mM imidazole and 250 mM KCl. The protein was eluted with buffer C containing 50 mM imidazole. The eluted protein was dialysed against two changes of buffer containing 2 L of 20 mM Tris-HCl, pH 7.2, 1 mM EDTA.

### **2.5 Spectrophotometric and biophysical characterisation**

#### **2.5.1 Initial spectrophotometric analysis**

UV-visible absorption spectra of the P450s were recorded at 25 °C over a wavelength range from 200-800 nm using a Cary-50 UV-visible scanning spectrophotometer (Varian) and a 1 cm pathlength quartz cuvette. Purity of protein samples was assessed by comparison of the P450 Soret band ( $\sim A_{418}$ , depending on the particular protein absorbance) to the aromatic amino acids absorption band ( $A_{280}$ ). The ratio of the two peaks  $A_{418}/A_{280}$  is a convenient indicator of P450 purity, with a ratio value of  $\sim 2.0$  (although the value can vary due to the aromatic amino acid content of the particular P450 protein) indicating highly pure P450 protein.

### 2.5.2 Carbon monoxide and nitric oxide binding

Binding of carbon monoxide (CO) to the P450 proteins was performed by initial protein reduction using a few grains of solid sodium dithionite. CO was then bubbled slowly through the ferrous P450 solution for 1 minute inside a fume hood. Spectra of the oxidised, reduced and reduced/CO-bound forms were recorded. P450 difference spectra were generated by the subtraction of the spectrum for the reduced form from that for the reduced/CO-bound adduct. Nitric oxide (NO) complexes of CYP121 were obtained by brief bubbling of the buffered enzyme solution with NO gas. Care was taken to avoid excessive addition of NO given its ability to form nitrous acid in solution with consequent effects on protein denaturation.

### 2.5.3 Concentration determination

The concentration of P450 samples was determined spectroscopically using the method of Omura and Sato (Omura and Sato, 1964).

$$A = \epsilon cl$$

#### **Equation 1 The Beer-Lambert law for the calculation of cytochrome P450 concentration**

Where **A** is absorbance;  $\epsilon$  the extinction coefficient for the protein; **c** the sample concentration; **l** is the pathlength of the sample cuvette.

The P450 concentration was calculated by subtraction of the ferrous P450 spectrum from that for the ferrous/CO-bound adduct, and the absorbance difference calculated between a peak value and a wavelength where negligible absorption change is observed ( $A_{448} - A_{490}$ ). The Beer-Lambert law ( $A = \epsilon cl$ ) was then applied, using the P450 molar extinction coefficient  $\Delta\epsilon_{448-490} = 91,000 \text{ M}^{-1} \text{ cm}^{-1}$  (Omura and Sato 1964).

Due to incomplete conversion of the P450s to the CO-adduct at 450 nm (i.e. P420 formation was typically observed and was considered likely to be due at least partially to the process involved in forming the adduct), the concentration was also estimated directly using the Soret maximum of the oxidised enzyme in the resting (low-spin state) (Noble *et al.*, 1999).

#### 2.5.4 Pyridine hemochromagen method

Calculation of heme content in any relevant protein was performed using the method of Berry and Trumpower (1987), providing an independent method for determination of protein extinction coefficient based on Soret absorption with reference to the absorption characteristics of a heme-pyridine complex of the relevant P450 protein. Protein concentration was determined using a heme *b* extinction coefficient of  $\epsilon_{556-540} = 24 \text{ mM}^{-1} \text{ cm}^{-1}$ . A P450 spectrum was collected for a sample containing 100 mM NaOH, 20 % (v/v) pyridine and 300  $\mu\text{M}$   $\text{K}_3\text{Fe}(\text{CN})_6$  in a sealed cuvette. The sample was then reduced by the addition of a few grains of sodium dithionite to the cuvette. The heme concentration was then calculated using the Beer-Lambert law, as shown in Equation 1, with the calculated extinction coefficient for CYP140A2  $\epsilon_{556-541} = 96 \text{ mM}^{-1} \text{ cm}^{-1}$  and CYP151A2  $\epsilon_{555-539} = 186 \text{ mM}^{-1} \text{ cm}^{-1}$ .

#### 2.5.5 Circular Dichroism (CD)

Circular dichroism spectra were recorded at 25 °C on a JASCO J715 spectropolarimeter (calibrated with 0.06 % d-10 camphorsulphonic acid). Far-UV CD spectra were recorded over the wavelength range 190 to 260 nm in a quartz cylindrical cell of 0.02 cm pathlength with a scan rate of 10 nm min<sup>-1</sup>. Near-UV and visible CD spectra were recorded over the wavelength range 260 to 600 nm, in cells of 0.5 cm pathlength with scan rates of 20 nm min<sup>-1</sup>. Spectra were performed in duplicate and averaged. Secondary structure content analysis was performed by the mathematical function fitting programmes Selcon (Sreerema *et al.*, 1999), accessed via Dichroweb (Lees *et al.*, 2006). Protein concentrations used were 2  $\mu\text{M}$  (far-UV CD) and 20  $\mu\text{M}$  (near UV-visible CD). Both near-UV and visible CD spectra analysis, as described previously in this section, was also performed on CYP151A2 in the presence of morpholine (5 mM) and econazole (30  $\mu\text{M}$ ).

#### 2.5.6 Electron paramagnetic resonance (EPR) spectroscopy

EPR spectra were recorded in collaboration with Dr. M. R. Cheesman, University of East Anglia. Protein samples (170  $\mu\text{M}$ ) were in 50 mM Tris-HCl (pH 7.2) and 50 % (v/v) glycerol. EPR spectra were recorded on an X-band ER-200B spectrometer (Brüker Spectrospin) interfaced to an ESP1600 computer and fitted with a liquid helium flow-cryostat (ESR-9, Oxford instruments). Spectra were recorded at

10 K with microwave power of 2.08 mW amplitude and a modulation amplitude of 1 mT. CYP151A2 analysis was also performed with included 30 mM and 100 mM morpholine, as well as 50  $\mu$ M fluconazole. CYP140A2 analysis was done in the presence of 5  $\mu$ M mycolactone C.

#### **2.5.7 Magnetic circular dichroism (MCD) spectroscopy**

MCD spectra were recorded in collaboration with Dr. M. R. Cheesman, University of East Anglia. CYP151A2 protein samples (30  $\mu$ M for UV-Vis region and 300  $\mu$ M for Near-IR region) were in 50 mM TrisHCl (pH 7.2) plus 50 % (v/v) glycerol. MCD spectra were recorded on circular dichrographs, JASCO J-500D and JASCO J-730 for the ranges 280 to 1000 nm and 800 to 2000 nm, respectively. Samples were mounted on a SM-1, 6 Tesla superconducting solenoid (Oxford Instruments) with an ambient-temperature bore for measurements at room temperature.

#### **2.5.8 Resonance Raman spectroscopy**

Resonance Raman spectra of protein samples were obtained using 15 mW, 406.7 nm radiation at the sample, from a Coherent Innova 300 krypton ion laser, and acquired using a Renishaw micro-Raman system 1000 spectrophotometer. The sample was held in a capillary under the microscope at a concentration of 100  $\mu$ M, and an extended scan was obtained from 200 to 1700  $\text{cm}^{-1}$ , with 12 x 15 s exposures. Spectra were collected at the University of Strathclyde in collaboration with Professor Ewen Smith. CYP140A2 spectra was also collected in the presence of mycolactone C (10  $\mu$ M, red) and miconazole (30  $\mu$ M). Morpholine-bound (30 mM and 60 mM) and fluconazole-bound (30  $\mu$ M) forms of CYP151A2 spectra were also collected.

#### **2.5.9 Redox potentiometry**

Redox titrations (to determine heme iron redox potentials) were performed in a Belle Technology glove-box under a nitrogen atmosphere. All solutions were degassed under vacuum with argon. Oxygen levels were maintained at less than 2 ppm. The CYP121 P346L protein was applied to a BioRad Econo-Pac 10DG desalting column in the anaerobic box, pre-equilibrated with degassed 50 mM potassium phosphate pH 7.0 buffer, to ensure removal of all traces of oxygen. The



buffer also contained glycerol at a concentration of 10 % v/v to aid stability of the protein throughout the process. The protein solution (~ 2-14  $\mu$ M in 5 mL buffer), was titrated electrochemically according to the method of Dutton (Dutton, 1978) using sodium dithionite as reductant and potassium ferricyanide as oxidant. Dithionite and ferricyanide were delivered in 0.2  $\mu$ L aliquots from concentrated stock solutions (typically 10-50 mM). Mediators were added to facilitate electrical communication between enzyme and electrode, prior to titration. Typically, 2  $\mu$ M phenazine methosulfate (PMS) (+80 mV), 7  $\mu$ M 2-hydroxy-1,4-naphthoquinone (HNQ) (-145 mV), 0.3  $\mu$ M methyl viologen (MV) (+430 mV), and 1  $\mu$ M benzyl viologen (BV) (+311 mV) were included to mediate in the range between +100 to -480 mV (Munro *et al.*, 2001; Ost *et al.*, 2001). At least 10 minutes was allowed to elapse between each addition to allow stabilisation of the electrode. Spectra (250-800 nm) were recorded using a Cary UV-50 Bio UV-Visible scanning spectrophotometer. The electrochemical potential of the solution was measured using a Hanna pH 211 meter coupled to a Pt/Calomel electrode (ThermoRussell Ltd.) at 25 °C. The electrode was calibrated using the  $\text{Fe}^{3+}/\text{Fe}^{2+}$  EDTA couple as a standard (+108 mV). A factor of +244 mV was used to correct relative to the standard hydrogen electrode. Potentiometry was also performed, as described previously in this section, with CYP151A2 in the presence/absence of morpholine (30 mM).

To determine the heme iron reduction potential from the redox titration data collected, spectral data at wavelengths maximal for the optical (Soret) transition between oxidised ( $\text{Fe}^{3+}$ ) and reduced ( $\text{Fe}^{2+}$ ) forms of P450 heme iron were plotted *versus* the applied potential, and the data fitted to the Nernst function using Origin 7.0 (OriginLab, Northampton MA).

## **2.6 Protein Denaturation**

### **2.6.1 Protein unfolding monitored by circular dichroism spectroscopy**

Far-UV circular dichroism spectra were recorded at 25 °C on a JASCO J-700 spectropolarimeter, as described in section 2.3.4. Spectra were performed in duplicate and averaged. Guanidine hydrochloride (GdnHCl) solutions at concentrations of (typically) 0, 0.25, 0.5, 0.75, 1, 1.5, 2, 3, and 6 M GdnHCl and containing approximately 2  $\mu$ M of CYP151A2 were prepared in 10 mM Tris-HCl (pH 7.5), and

incubated for 30 mins at room temperature prior to scanning (in the far-UV CD region from ~190-260 nm). The degree of unfolded protein was determined by plotting the maximal change in ellipticity (typically at ~220nm) against the appropriate GdnHCl concentration and fitting data to a hyperbolic function.

## **2.7 Thermostability Studies**

### **2.7.1 Heat Denaturation**

UV-Visible absorption spectra of both CYP140A2 and CYP151A2 were recorded between 250-750 nm using a Cary-50 (Varian) UV-visible scanning spectrophotometer and quartz cuvettes of 1 cm pathlength. A 5  $\mu$ M P450 solution was prepared and, in order to aid stabilisation of the protein and prevent aggregation, glycerol was included to a final concentration of 10 % (v/v) in the cuvette. Spectra were recorded at an initial temperature of 20 °C, and the temperature was increased in 2 °C increments, allowing 10 minutes between each scan to allow the sample to equilibrate in the cuvette. The temperature was increased until heat denaturation of the protein occurred, observed by a substantial decrease in the intensity of the Soret absorption band and/or development of turbidity due to protein aggregation.

## **2.8 Inhibitor and substrate binding studies**

The binding of substrates and heme-coordinating inhibitors to the P450s were analysed by optical titrations using a Cary UV-50 Bio scanning spectrophotometer (Varian). The spectra for the inhibitor-free P450 enzymes (typically 0.8-2  $\mu$ M protein) were recorded at 25 °C in 50 mM Tris-HCl, 1mM EDTA (pH 7.2) buffer. Additions of the inhibitors were in 0.1-0.5- $\mu$ l aliquots (using a Hamilton syringe) up to a final volume of not more than 2 % of the total volume of the solution. Spectral data collected were corrected for any dilution effects incurred through ligand addition.

### **2.8.1 Inhibitor binding**

The P450 inhibitors; imidazole, 2-phenyl imidazole, 4-phenyl imidazole, clotrimazole, econazole, ketoconazole, miconazole, fluconazole, voriconazole and 1H-1,2,4-Triazole, 1-tricyclo(3.3.1.1<sup>3,7</sup>)dec-1-yl (also known as adamant-1-yl) were used, and were prepared as stock solutions in DMSO. Additions of the inhibitors were in 0.1-0.5  $\mu$ l aliquots (using a Hamilton syringe) up to a final volume of not more than 2 % of the total volume of the solution. Spectra were recorded after each addition of

ligand, and difference spectra were computed by subtraction of the starting (ligand-free) spectrum from those generated at each point in the titration. The maximum apparent absorption change induced at each point in the titration was determined by subtraction of the minimum absorption value at the trough in each difference spectrum from the maximum value at the peak (using data at the same wavelengths in each titration). Dissociation constants ( $K_d$  values) were determined by plotting the maximum changes in absorption *versus* the relevant ligand concentration. Data were fitted either to a rectangular hyperbola (equation 3) or, where ligands bound very tightly to the P450 enzyme reflected in high standard errors (>10%) in the constants, to a quadratic function (equation 2) that accounts for the quantity of enzyme consumed in the enzyme-substrate complex at each point in the titration.

$$A = ((A_{\max}/(2 \times E)) \times (L + E + K_d)) - ((L + E + K_d)^2 - (4 \times L \times E))^{0.5}$$

**Equation 2 Quadratic function**

Where  $A$  represents the observed absorption difference at each azole addition,  $A_{\max}$  is the maximal absorption difference at azole saturation,  $E$  is the total enzyme concentration,  $L$  is the ligand concentration used and  $K_d$  the dissociation constant.

All data analysis was performed using Origin software. In the case of the weak binding imidazole, data were fitted to a standard hyperbolic function:

$$Abs = \frac{A_{\max}[L]}{K_d + [L]}$$

**Equation 3 Hyperbolic function**

Where  $A_{\max}$  is the maximal absorbance change at ligand saturation,  $K_d$  is the dissociation constant for the ligand binding to the P450,  $L$  is the ligand concentration used and  $Abs$  is the observed absorption difference generated at the ligand concentration  $[L]$ .

## 2.8.2 Ligand binding

The binding of morpholine to CYP151A2 (~1  $\mu$ M final protein concentration) was measured at 25 °C by UV-visible absorption spectroscopy, as previously described in section 2.6. Titrations of CYP140A2 were performed with the fatty acid compounds; arachidonic acid, myristic acid and lauric acid; and with the polyketides erythromycin and tylosin (stocks prepared in methanol). Small aliquots (0.1-0.4  $\mu$ L)

of substrate were added to a protein solution with the total addition less than 10  $\mu$ L. Spectra were recorded after each addition of substrate between 300 and 750 nm. In the case of CYP151A2, morpholine was titrated as previously described up to a concentration of 60  $\mu$ M.

### 2.8.3 Competitive inhibition in substrate binding

An estimation of the  $K_d$  value for mycolactone binding to CYP140A2 was made as follows. Spectral data were collected for the binding of econazole to CYP140A2 in the presence of mycolactone. These data were fitted to the following expression detailing competitive inhibition of the binding econazole by mycolactone (Equation 4). The function is derived from the Michaelis Menten equation for competitive inhibition. The P450 inhibitor econazole was titrated against the P450 as described in section 2.6.1.

$$A_{obs} = (A_{max} * S)/S + (K_d * (1 + [I]/K_i))$$

#### Equation 4 Competitive inhibition equation

Where  $A_{obs}$  is the observed absorption change at the varied ligand (econazole) concentration  $S$ ;  $A_{max}$  is the maximal change in absorption at the varied ligand saturation point;  $K_d$  is the dissociation constant for the ligand varied;  $[I]$  is the fixed concentration of the other ligand (mycolactone); and  $K_i$  is the dissociation constant for the other ligand.

Experiments were done at two different (fixed) concentrations of mycolactone C (6  $\mu$ M and 12  $\mu$ M), and the concentrations of the azole (econazole) were varied until no further optical changes were observed. The respective data sets were fitted to the relevant equation (using the  $K_d$  value determined for econazole in the absence of mycolactone) to determine the  $K_i$  value. The  $K_i$  value reported is the statistical average of the determinations made at the two different mycolactone concentrations, and the mean value presented varied by <20 % from each of the individually determined values.

## 2.9 Turnover analysis of mycolactone C and E

Product formation was measured using mass spectrometry under the guidance of Dr Hui Hong at the Department of Biochemistry, University of Cambridge in the

laboratory of Prof. Peter Leadlay. A 0.67  $\mu\text{M}$  concentration of CYP140A2 was incubated for 16 hours at room temperature with 75  $\mu\text{M}$  mycolactone C, *E. coli* flavodoxin (1.67  $\mu\text{M}$ ), *E. coli* flavodoxin NADP<sup>+</sup> oxidoreductase (189  $\mu\text{M}$ ), glucose dehydrogenase (NADP<sup>+</sup>-dependent, 16.5 units), glucose (20 mM) and 120  $\mu\text{M}$  NADPH, with stirring in 1 mL 20 mM MOPS (3-morpholinopropanesulphonic acid) (pH 7.4) +100 mM KCl assay buffer. Negative controls were also prepared identically to the above reactions, but without the addition of NADPH. A 500  $\mu\text{L}$  reaction sample was removed and the reaction was halted by the addition of 500  $\mu\text{L}$  ethyl acetate. Product was extracted from the aqueous environment and evaporated under a nitrogen atmosphere. The product was resuspended in 50  $\mu\text{L}$  of methanol and the LC-MS analyses were carried out on a Finnigan LCQ instrument (Thermo-Finnigan, Waltham, USA), coupled with a HP1100 HPLC system (Agilent, Palo Alto, USA). For mycolactone analysis, the instrument was fitted with a Phenomenex Prodigy PH-3 column (5  $\mu\text{m}$ , 100  $\text{\AA}$ ), 4.6 $\times$ 250 mm. The mass spectrometer was set to record positive- and negative-ion scans between 500 to 800  $m/z$ . Mycolactone E turnover was performed and analysed as above.

## 2.10 Protein Lipid Overlay Assay

Lipid-protein overlay assays were performed according to the protocol of Dowler *et al.* (2003) to detect interactions of His-CYP121 with potential substrate molecules. Lipids were extracted from *M. tuberculosis* (Erdman strain) and provided by Dr. Mary Jackson, Institut Pasteur, Paris. The precise composition of the lipid fractions used was unknown.

A series of 1, 5 and 10  $\mu\text{L}$  volumes of the lipids were spotted onto Hybond C extra nitrocellulose membrane (Amersham Biosciences) from various chloroform:methanol extraction stocks. The membranes were allowed to dry under vacuum for 1 hour and were then wetted by floating on purified water. The membranes were equilibrated in 50 mM Tris-buffered saline containing 0.1 % (v/v) Tween 20 (TBS-T) for 5 minutes, followed by blocking with 3 % fatty acid-free bovine serum albumin/TBS-T (blocking reagent) for 1 hour at room temperature. Purified His-CYP121 was diluted into blocking reagent to a final concentration of 10 nM. The membranes were then incubated in the presence of the enzyme overnight at 4

°C on a rocking platform. The following day the membranes were washed six times for 5 min with TBS-T. All subsequent steps were carried out at room temperature. The protein was then identified by incubating with a 1:2000 dilution of anti-His monoclonal donkey antibody (Amersham Biosciences) in blocking reagent for 1 h. This was followed by a second wash step of 6 x 5 min with TBS-T. Secondary HRP-conjugated rabbit antibody (Amersham Biosciences) was diluted 1:5000 into blocking reagent and incubated for 1 hour. This was followed by a final wash step of twelve times for 5 minutes with TBS-T. Finally, the protein was visualized using Enhanced Chemiluminescence (Amersham Biosciences) with exposure to Biomax MR film (Eastman Kodak).

### **2.11 Susceptibility testing of azole drugs for *M. tuberculosis* and *M. ulcerans***

The azole drugs econazole, miconazole, ketoconazole, and clotrimazole were dissolved in 100 % DMSO. Subsequent dilutions of these drugs were made in 100 % DMSO. All stock solutions were stored at -70 °C in small aliquots.

Radiometric azole susceptibility testing was determined by using the radiometric criteria of the BACTEC 460 system (Becton Dickinson) in conjunction with Dr Laurent Marsollier, Institut Pasteur, Paris. The standard protocol was followed (Siddiqi, 1995) and all procedures were carried out in a biological safety cabinet inside a biosafety level 3 biocontainment facility. The BACTEC vials contained Middlebrook 7H12B medium with <sup>14</sup>C-labelled palmitic acid as a carbon source. Substrate consumption generates <sup>14</sup>CO<sub>2</sub> in the airspace of the sealed vial. The BACTEC TB-460 (Becton Dickinson) instrument detects the amount of radioactivity and records it as a growth index (GI). A suspension of an actively growing culture was made in water, and 0.1 mL was transferred to a vial. These bottles were incubated until the appropriate GI was obtained, after which 0.1 mL aliquots were removed and transferred to fresh vials containing the drugs. Five different concentrations of each azole drug were tested; 2, 4, 8, 16 and 32 mg/mL. The bottles were incubated at 30 °C and analysed daily until the GI of the growth control diluted 1:100 was  $\geq 30$ .

Resistance was determined by comparing the change in GI over that of the previous day ( $\Delta$ GI) between the control vial (GI<sub>control</sub>) and the vials containing drugs (GI<sub>drugs</sub>). The results are interpreted as follows: if  $\Delta$ GI<sub>control</sub> is  $> \Delta$ GI<sub>drug</sub>, the strain is

referred to as “susceptible”; if  $\Delta GI_{\text{control}}$  is  $< \Delta GI_{\text{drug}}$ , the strain is referred to as “resistant”; and if  $\Delta GI_{\text{control}}$  is equal to  $\Delta GI_{\text{drug}}$ , the strain is referred to as “intermediate”. The MIC, determined by the procedure recommended by the manufacturer of the BACTEC 460 radiometric system, was defined as the lowest concentration of drug for which the GI of the drug-containing vial was less than the GI of the control diluted 1:100, obtained from measurements on the day when the GI of the control vial was  $\geq 30$ , and corresponded to the concentration that resulted in  $>99\%$  inhibition of the bacterial population growth.

# Chapter 3

## Cloning, expression and characterisation of CYP121 mutants



### **3.1 Molecular biology of CYP121 mutants P346L, R386L and S279A, and histidine tagged CYP121**

#### **3.1.1 Preface**

The large number of P450 genes identified in the *M. tuberculosis* genome indicates they have essential roles in the physiology and potentially the virulence of the pathogen. In addition, the P450s offer an attractive new drug target in the pathogen's control. Biochemical and biophysical characterisation of *M. tuberculosis* P450s has been limited to date to CYP51 and CYP121 (Bellamine *et al.*, 1999; McLean *et al.*, 2002a; McLean *et al.*, 2006). The structure of CYP121 has revealed many interesting features, including heterogeneity in heme conformation (i.e. the binding of the heme macrocycle in two distinct conformations, related to each other by a 180° rotation of the heme) and distortion of the heme at one of its pyrrole rings due to interaction with the residue Pro<sup>346</sup>, which is located adjacent to the cysteinate ligand of the heme iron (Leys *et al.*, 2003). Also defined is a putative bifurcated proton delivery pathway (involving H<sub>2</sub>O molecules and amino acid side chains) that converge on Ser<sup>279</sup> and could provide timed delivery of two protons to CYP121's ferric peroxy and ferric hydroperoxy catalytic cycle intermediates, in order to form compound I and to facilitate substrate hydroxylation (Leys *et al.*, 2003). Another notable amino acid identified through analysis of the region immediately above the heme plane is Arg<sup>386</sup>, which appears to control access to the active site and/or to provide substrate binding motifs in the heme environment (Leys *et al.*, 2003).

In order to understand the role of the latter residues, CYP121 mutants P346L, R386L and S279A were generated and characterised using a range of techniques, including EPR, CD and resonance Raman spectroscopy, as well as crystallography. This chapter describes the creation and cloning of the mutant genes; and expression, purification and characterisation of the mutant proteins. In addition to elucidating the role of certain residues of CYP121 through mutagenesis, a histidine tagged version of CYP121 was also created to explore possible substrates of the P450.

## 3.2 Molecular biology

### 3.2.1 Cloning of CYP121 mutants and histidine tagged CYP121

The *CYP121* P346L and *CYP121* R386L gene fragments were amplified by PCR using *Pfu* DNA polymerase with forward and reverse primers designed from the gene sequence, as described in the Materials and Methods section 2.2.2.

The PCR fragments containing the mutated genes were analysed by agarose gel electrophoresis, and verified to be of the expected size by comparison with DNA fragment standards (1 kb ladder, NEB) (Figure 3.1).

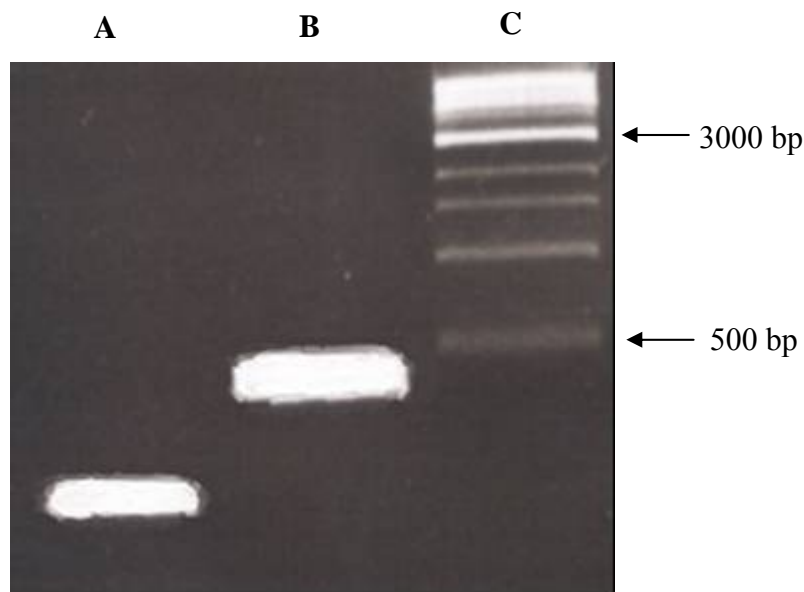


**Figure 3.1 PCR amplified fragments of *CYP121* mutants, P346L and R386L**

The PCR products were fractionated by electrophoresis on an ethidium bromide-stained 1% agarose gel. The bands displayed are those of mutants P346L (A) and R386L (B) and are consistent with the expected sizes of 353 and 465 bp, respectively. Alongside is a 1 kb DNA ladder (NEB) with relevant sizes highlighted (C).

‘A’ tailing was performed on the fragments to produce single adenosine nucleotide overhangs at the 3' ends (as described in Materials and Methods section 2.2.6). This modification was subsequently exploited to enable cloning of the fragments into the pGEM-T Easy (Promega) vector (which has single T nucleotide overhangs at the 5' ends)

(as described in Materials and Methods section 2.2.8). Following transformation of the ligation mix to *E. coli* strain JM109 (as described in Materials and Methods section 2.2.9), correct clones were identified by the  $\alpha$ -complementation colour selection method (Vieira and Messing, 1987) on LB agar media containing ampicillin, X-gal and IPTG.

The DNA insertion site of the pGEM-T Easy vector is located within the  $\alpha$ -peptide coding section of the gene (*lacZ*) for the enzyme  $\beta$ -galactosidase. Insertion of foreign DNA (i.e. PCR product) in the  $\alpha$ -peptide coding region disrupts this *lacZ* gene segment, preventing complementation of the truncated *lacZ* that is chromosomally encoded. The subsequent lack of X-gal conversion in successful clones results in white colonies. This form of insertional activation of the *lacZ* gene in the vector pGEM-T Easy provides the rationale behind the 'blue/white screen' for recombinant clones on X-gal-containing media.

Plasmid preparations were made from selected transformants, and the clones verified by DNA sequencing at the University of Leicester PNACL using T7 primer 5' – TGT AAT ACG ACT CAC TAT ACG G- 3' and the Sp6 primer 5' –ATT TAG GTG ACA CTA AGA CAT A- 3' (as described in Materials and Methods section 2.2.10).

The relevant fragments were then excised from the pGEM-T Easy vector by restriction enzyme digest, using *Sac*II and *Hind*III for *CYP121* P346L, and *Mfe*I and *Hind*III for *CYP121* R386L. The sites for these restriction enzymes were incorporated at the 5' ends of the forward and reverse primers in both cases. The fragments were isolated by gel extraction and purified using the QIAquick Gel Extraction kit (Qiagen) (Materials and Methods section 2.2.5), and then cloned into plasmid pKM2(b) (containing wild-type *CYP121*) pre-cut with the corresponding restriction enzymes (Materials and Methods section 2.2.13).

The clones were verified by restriction enzyme digestion with *Bst*NI for *CYP121* P346L and *Hga*I for *CYP121* R386L (Figures 3.2 and 3.3, respectively). To allow easier differentiation of the mutants, the wild-type pKM2(b) clone was also digested and run

alongside the mutant clones. The generated band of interest in the *Bst*NI digest of *CYP121* P346L, and differing from the identical digest of wild-type pKM2(b), is the band at 234 bp. The absence of a band at 160 bp is also diagnostic. The observed difference relates to the removal of a *Bst*NI restriction site upon the single base mutation change. In the case of *Hga*I digest of *CYP121* R386L, generated bands at 836 and 867 bp differed from the identical wild-type pKM2b digest due to the removal of the *Hga*I site by the mutation.

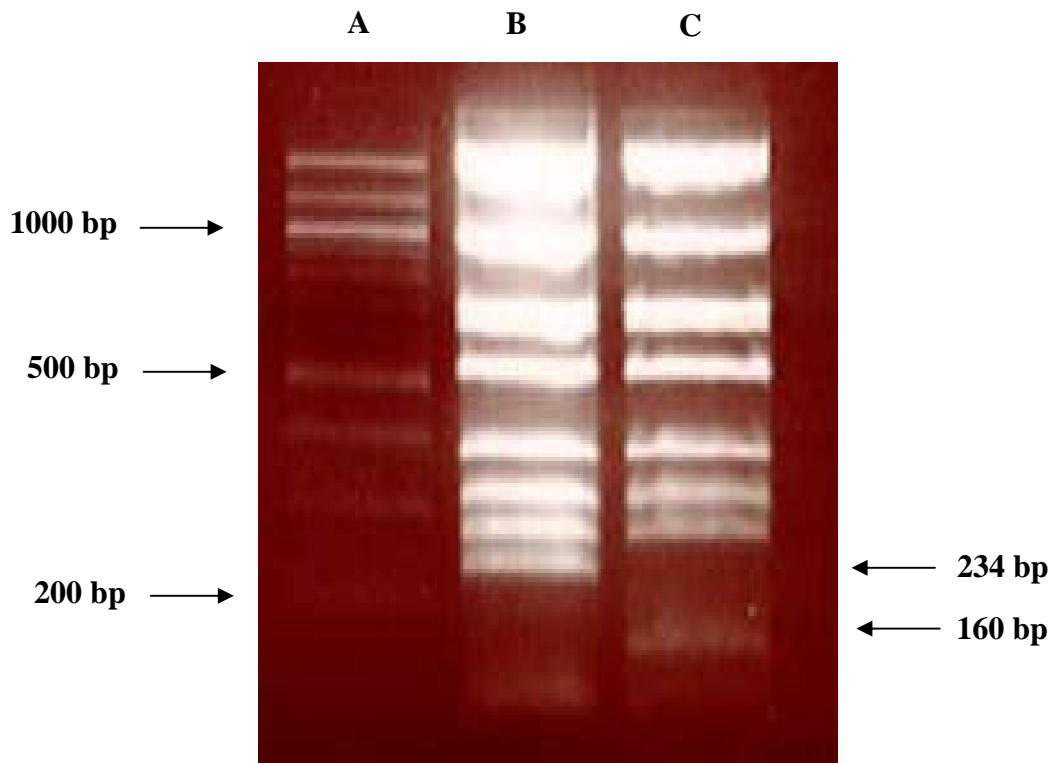


**Figure 3.2** *Bst*NI restriction digest of *CYP121* P346L (pGL1(a))

The digested DNAs were fractionated using a 2% agarose gel. The fragments of interest in the pGL1(a) clone (B) which differed from the WT clone (C) to confirm correct mutant clone isolation are arrowed and sized. Alongside is a 100 bp DNA ladder (NEB) with the 1000, 500 and 200 bp fragments highlighted (A).

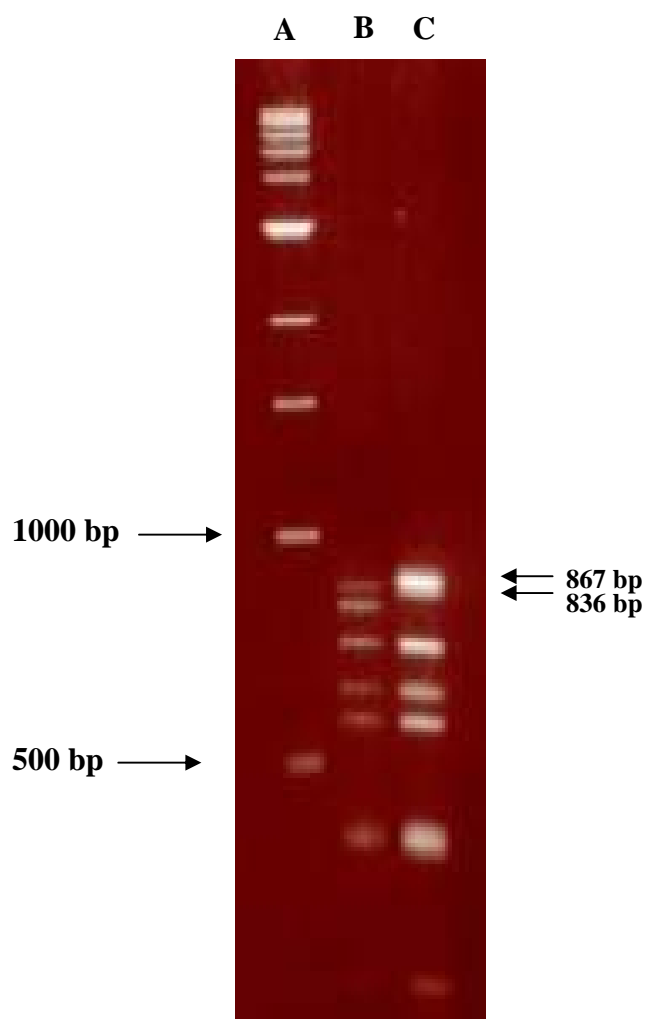


**Figure 3.3** *HgaI* restriction digest of *CYP12I* R386L (pGL2(a))  
 The digested DNAs were fractionated using a 2% agarose gel. The fragments of interest in the pGL2(a) (C) are arrowed and sized, and differed from the WT *CYP12I* (B) to confirm correct mutant clone isolation. Alongside is a 1 kb DNA ladder (NEB) with the 500 and 1000 bp fragments labelled (A).

The S279A mutant of *CYP12I* was generated by PCR amplification of the entire pKM2(b) plasmid using the QuikChange site-directed mutagenesis kit (Stratagene), using *Pfu* DNA polymerase and forward and reverse primers designed from the gene sequence, as described in section 2.2.2 of Materials and Methods.

The PCR fragments containing the mutated genes were analysed by agarose gel electrophoresis, and verified as the expected size by comparison with DNA fragment standards (1 kb ladder, NEB) (Figure 3.4)

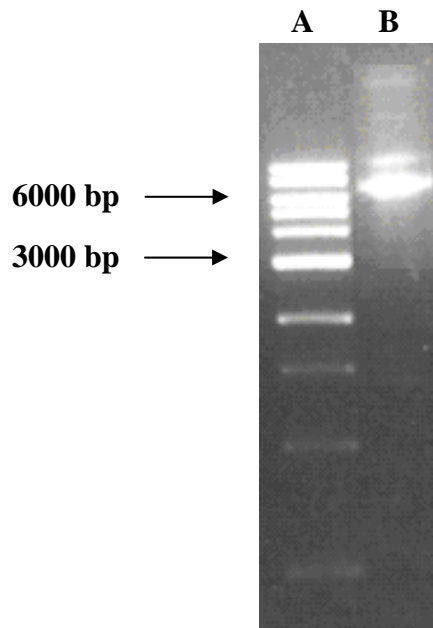


**Figure 3.4 PCR amplification of CYP121 S279A mutant**

The PCR products were fractionated by electrophoresis using an ethidium bromide stained 1% agarose gel. The main band displayed is that of S279A (B) and is consistent with the expected size of 6832 bp. Alongside is a 1 kb DNA ladder (NEB) with the 6000 bp and 3000 bp fragments labelled (A).

Following PCR amplification, restriction enzyme *DpnI* was added to the PCR reaction mix to remove methylated or hemi-methylated DNA formed by the *dam* methylase of *E. coli* (Figure 3.5) (Marinus and Harris, 1973; Geier and Modrich, 1979). This resulted in the removal of the parent template DNA or mutant/wild-type DNA heteroduplexes.

Successful clones were identified, following transformation of the ligation mixture into Nova Blue *E. coli* cells. Plasmid preparations were made from selected transformants, and the correct clones verified by DNA sequencing at the University of

Leicester PNACL using pETFor 5'-TAA TAC GAC TCA CTA TAG GG-3' (T7 promoter) and pETRev 5'-GCT AGT TAT TGC TCA GCG G-3' (T7 terminator) were used (as described in Materials and Methods section 2.2.10).

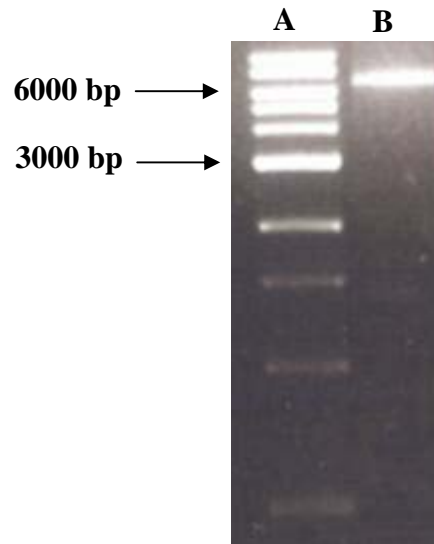


**Figure 3.5** *DpnI* digestion of *CYP121* S279A PCR product

The PCR products were fractionated by electrophoresis on an ethidium bromide stained 1% agarose gel. The band displayed is that of the S279A mutant of pKM2(b) (B) and is consistent with the expected size of 6832 bp, with no presence of methylated or parental DNA. Alongside is a 1 kb DNA ladder (NEB) with the 3000 and 6000 bp fragments labelled (A).

The histidine tagged CYP121 was created through restriction digest of pKM2(b) plasmid using the *Bam*HI and *Nde*I to release the ~1200 bp CYP121-encoding fragment (Figure 3.6). The fragments were analysed by agarose gel electrophoresis, and verified to be of the expected size by comparison with marker DNA fragments, as described in section 2.2.12.

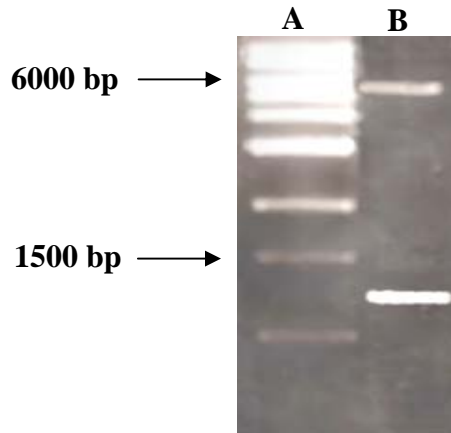


**Figure 3.6 Excision of wild-type CYP121 fragment from pKM2(b)**

The PCR products were fractionated by electrophoresis using an ethidium bromide stained 1% agarose gel. (B) The lower band displayed is that of CYP121 fragment and is consistent with the expected size of ~1200 bp and the upper band is that of the pET11a backbone of ~5680 bp. Alongside is a 1 kb DNA ladder (NEB) with the 6000 bp and 1500 bp fragments labelled (A).

No further modification was required and direct ligation of the excised fragment into a pre-digested *Bam*HI-*Nde*I pET15b vector was performed. Following transformation of the ligation mix to *E. coli* strain NovaBlue (as described in Materials and Methods section 2.2.9), correct clones were identified on LB agar media containing ampicillin. Plasmid preparations were made from selected transformants, and the clones verified by linearisation with *Nde*I (Figure 3.7) (described in Materials and Methods section 2.2.14).



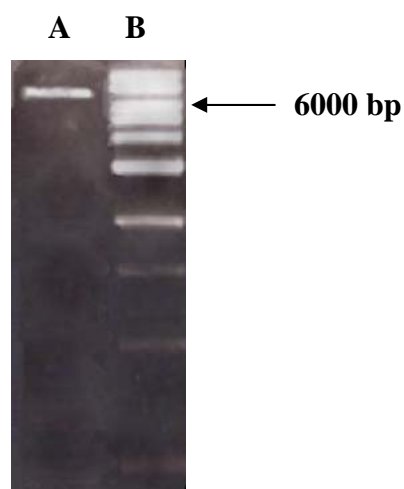


**Figure 3.7** *NdeI* restriction digest of histidine tagged CYP121 (pGL4(a))  
 (A) The band displayed is that of linearised pGL4(a) and is consistent with the expected size of 6800 bp. Alongside is a 1 kb DNA ladder (NEB) with the 6000 bp fragment labelled (B).

### 3.3 Expression and purification

#### 3.3.1 Expression and purification of P346L, R386L and S279A mutants of CYP121 and histidine tagged CYP121

Soluble protein of P346L, R386L and S279A CYP121 mutants, and the histidine tagged CYP121 was expressed under strict conditions optimised for native CYP121 (McLean *et al.*, 2002a), from the T7 RNA polymerase based promoter systems in vectors pGL1(a), pGL2(a), pGL3(a) and pGL4(a), respectively. Whereby, numerous conditions were investigated to optimise expression of soluble protein, including temperature, IPTG concentration, duration of induction, host strains and media types. Soluble CYP121 P346L production was achieved in *E. coli* HMS174 (DE3), in 12 litres of culture of Terrific Broth at 30 °C (230 rpm) until mid-log phase ( $OD_{600} \sim 0.6$ ), when the temperature was reduced to 18 °C. The culture was allowed to equilibrate before induction with 100  $\mu$ M IPTG at an  $OD_{600} = 0.8$ , with the cell culture continuing at 18 °C for 20-24 h post-induction at 180 rpm, before harvesting and subsequent lysis (McLean *et al.*, 2002a).

For both the CYP121 mutants and the histidine tagged CYP121, an efficient cell lysis process was found to be crucial to the recovery of soluble protein, as previously reported for wild-type CYP121, (McLean *et al.*, 2002a). The combination of the complementary lysis techniques of the French-press procedure and sonication was successful in extracting greater yields of soluble protein. Nonetheless, care was required as moderate warming of the cell extract during the lysis process was sufficient to induce protein aggregation and precipitation.

Despite high expression levels of the CYP121 mutants (Figure 3.8), analyses established that a significant proportion of the expressed protein was in the insoluble fraction. Expression of protein from the P346L mutant of CYP121 was measured on SDS-PAGE by comparison of soluble and insoluble fractions from lysed cells (Figure 3.8).

It is apparent that the majority of the expressed protein is insoluble, as is the case with wild-type CYP121, possibly in the form of inclusion bodies (McLean *et al.*, 2002a) (Figure 3.8). Solubilisation of these bodies for improved yield of wild-type CYP121 using either guanidinium chloride as a denaturant or Bugbuster protein extraction reagent (Novagen) resulted exclusively in the P420 form (McLean *et al.*, 2002a). However, under the previously described conditions with culture growth post-induction for up to 24 hours at 18 °C, an adequate amount of soluble protein is generated. The molecular mass of the expressed P346L mutant of CYP121, as well as the other mutants, is ~43 kDa, consistent the 43.257 kDa predicted molecular weight for the wild-type CYP121. Histidine tagged CYP121 has a predicted molecular weight of 45.437 kDa (Figure 3.9).

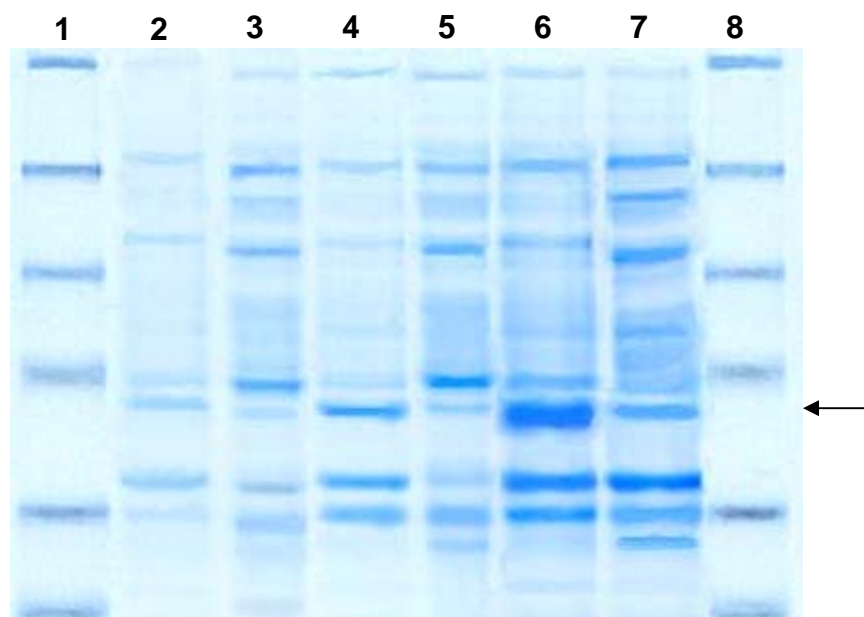


**Figure 3.8 Time-lapsed expression of the P346L mutant of CYP121**  
 SDS-PAGE gel (10%) showing expression of CYP121-P346L mutant (43.6 kDa) in HMS174(DE3) indicated by an arrow. Gel demonstrates time resolution analysis of insoluble and soluble protein fractions induced with 100  $\mu$ M IPTG and grown at 18  $^{\circ}$ C, with samples taken at 2, 4 and 24 hours. Lane 1 and 8; broad-range protein molecular weight standards (6-175 kDa) (NEB) (in descending order, kDa); 175, 83, 62, 47.5, 32.5, and 25. Insoluble (lane 2) and soluble (lane 3) fractions respectively, for 2 hours post-induction. Lanes 4 (insoluble fraction) and 5 (soluble fraction); 4 hours post induction. Lanes 6 (insoluble fraction) and 7 (soluble fraction); 24 hours post-induction.

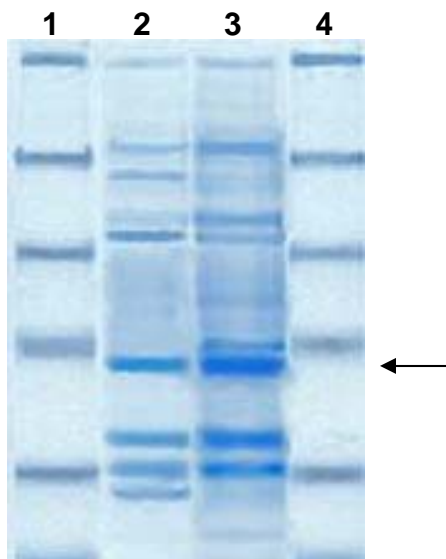


**Figure 3.9 Time-lapsed expression of the histidine tagged CYP121**  
 SDS-PAGE gel (10%) showing expression of histidine tagged CYP121 mutant (45.4 kDa) in HMS174(DE3) indicated by an arrow. Gel demonstrates time resolution analysis of insoluble and soluble protein fractions in cultures induced with 100  $\mu$ M IPTG and grown at 18  $^{\circ}$ C for 24 hours. Lanes 1 and 4; broad-range protein molecular weight standards (6-175 KDa) (NEB) (in descending order, kDa); 175, 83, 62, 47.5, 32.5, and 25. Soluble (lane 2) and insoluble (lane 3) fractions for 20 hours post-induction.

### 3.3.2 Protein purification of CYP121 mutants and histidine tagged CYP121

Purification of the proteins was followed spectrophotometrically by measuring the total protein concentration from the absorbance at 280 nm and the total P450 concentration by heme absorbance at 416.5 nm, or (in the case of the R386L mutant) at 419 nm. It was found that these values varied significantly in subsequent expression and purification runs due mainly to the relative efficiency of the cell lysis process as well as the inconsistent growth of HMS174(DE3). The  $A_{416.5/280}$  ratio ( $R386L = A_{419/280}$ ) was measured at each stage and a final ratio of  $\sim 1.9$  was considered to represent pure P450. Protein samples were removed at each stage of the purification process and analysed by SDS-PAGE for the P346L mutant of CYP121, and ultimately purified to homogeneity (Figure 3.10). The observed protein distributions observed upon the expression and purification of the R386L and S279A mutant proteins were similar to that for P346L

mutant of CYP121. During the purification of the histidine tagged CYP121 proteins, samples were removed and analysed by SDS PAGE, and are displayed in Figure 3.11.

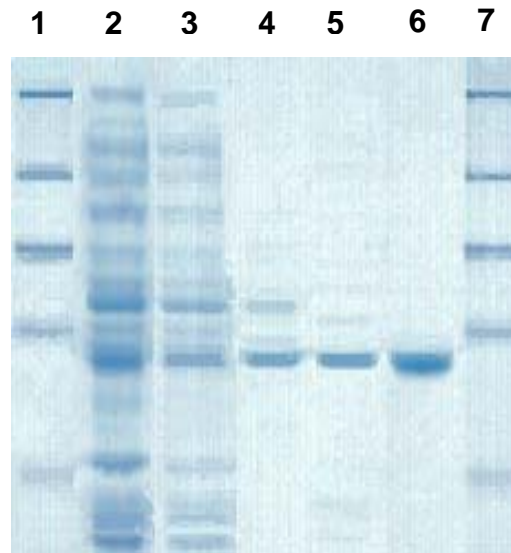


**Figure 3.10**      **SDS-PAGE analysis of CYP121-P346L protein purification**  
SDS PAGE gel (10%). Lane 1 and 7: protein molecular weight marker (NEB). Mass units (descending, kDa): 175, 83, 62, 47.5, 32.5. Lane 2: cell extract; Lane 3: 30-70% ammonium sulphate fraction; Lane 4: post-Phenyl Sepharose; Lane 5: post-Q-Sepharose; Lane 6: post-Hydroxyapatite (showing 7 mg pure CYP121-P346L protein at ~43 kDa).

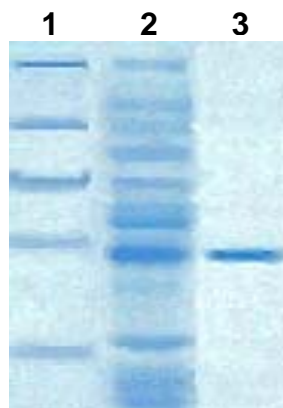


**Figure 3.11**      **SDS-PAGE analysis of histidine tagged CYP121 protein purification**  
SDS PAGE gel (10%). Lane 1: protein molecular weight marker (NEB). Mass units (descending, kDa): 175, 83, 62, 47.5, 32.5. Lane 2: cell extract; Lane 3: post-Nickel affinity (showing 5 mg pure histidine tagged CYP121 protein at ~45 kDa).

Homogenous protein purification of the histidine tagged CYP121 was achieved by nickel affinity fractionation. Purification of CYP121 P346L was measured during purification by comparing the heme-specific absorbance at 416.5 nm with the total protein concentration by absorbance at 280 nm and at different stages of purification. These data are shown in Table 3.1. Purification of the S279A mutant of CYP121 protein and the histidine tagged CYP121 protein was followed using the same chromatographic procedure as previously described, whilst R386L was followed at 419 nm and the subsequent purification data for the various proteins recorded in Tables 3.2, 3.3 and 3.4, respectively.

<b>Purification Stage</b>	<b>Total Protein (mg)</b>	<b>Total P450 (mg)</b>	<b>Ratio P450/ Protein</b>	<b>Stepwise Purification Factor</b>	<b>Overall Purification Factor</b>	<b>Stepwise Yield (%)</b>	<b>Overall Yield (%)</b>
<b>Lysate</b>	12800	128	0.01	1	1	100	100
<b>P-Sepharose</b>	6122	109	0.02	2	2	85	85
<b>Q-Sepharose</b>	678	62.5	0.09	4.5	9	57	49
<b>HA</b>	62.4	16.4	0.26	2.9	26	26	13
<b>GF</b>	11.3	5.89	0.52	2	52	36	4.6

**Table 3.1 Summary purification table for P346L mutant of CYP121**

Yields at each step of the purification (lysate, Phenyl Sepharose (P-Sepharose), Q-Sepharose ion-exchange chromatography, Hydroxyapatite affinity (HA) and Gel Filtration (GF)) were followed by the overall protein absorbance ( $A_{280} = 1 = 1 \text{ mg mL}^{-1}$ ) and the P450-specific heme absorbance ( $A_{416.5} = 95 \text{ mM}^{-1} \text{ cm}^{-1}$ ).

Purification Stage	Total Protein (mg)	Total P450 (mg)	Ratio P450/ Protein	Stepwise Purification Factor	Overall Purification Factor	Stepwise Yield (%)	Overall Yield (%)
Lysate	13100	128	0.01	1	1	100	100
P-Sepharose	6133	98	0.02	2	2	77	77
Q-Sepharose	638	58.2	0.09	4.5	9	59	45
HA	55.3	15.2	0.27	3	27	26	12
GF	9.1	5.02	0.55	2	55	33	3.9

**Table 3.2 Summary purification table for R386L mutant of CYP121**

Yields at each step of the purification (lysate, Phenyl Sepharose (P-Sepharose), Q-Sepharose ion-exchange chromatography, Hydroxyapatite affinity (HA) and Gel Filtration (GF)) were followed by the overall protein absorbance ( $A_{280} = 1 = 1 \text{ mg ml}^{-1}$ ) and the P450-specific heme absorbance ( $A_{419} = 95 \text{ mM}^{-1} \text{ cm}^{-1}$ ).

Purification Stage	Total Protein (mg)	Total P450 (mg)	Ratio P450/ Protein	Stepwise Purification Factor	Overall Purification Factor	Stepwise Yield (%)	Overall Yield (%)
Lysate	11500	118	0.01	1	1	100	100
P-Sepharose	5261	93	0.02	2	2	79	79
Q-Sepharose	501	49.3	0.1	5	10	53	42
HA	48.6	12.5	0.26	2.6	26	25	11
GF	8.3	4.03	0.49	1.9	49	32	3.4

**Table 3.3 Summary purification table for S279A mutant of CYP121**

Yields at each step of the purification (lysate, Phenyl Sepharose (P-Sepharose), Q-Sepharose ion-exchange chromatography, Hydroxyapatite affinity (HA) and Gel Filtration (GF)) were followed by the overall protein absorbance ( $A_{280} = 1 = 1 \text{ mg ml}^{-1}$ ) and the P450-specific heme absorbance ( $A_{416.5} = 95 \text{ mM}^{-1} \text{ cm}^{-1}$ ).

Purification Stage	Total Protein (mg)	Total P450 (mg)	Ratio P450/ Protein	Stepwise Purification Factor	Overall Purification Factor	Stepwise Yield (%)	Overall Yield (%)
Lysate	13200	141	0.01	1	1	100	100
Nickel affinity	18.4	16.4	0.89	89	89	12	12

**Table 3.4 Purification table for histidine tagged CYP121**

Yields at each stage of the purification (lysate, nickel affinity chromatography followed by the overall protein absorbance ( $A_{280} = 1 = 1 \text{ mg ml}^{-1}$ ) and the P450-specific heme absorbance ( $A_{416.5} = 95 \text{ mM}^{-1} \text{ cm}^{-1}$ ).

### 3.4 Initial P450 characterisation

#### 3.4.1 Spectrophotometric analysis of CYP121 mutants

UV–visible absorption spectroscopy provides an important technique for characterisation of cytochrome P450 enzymes. The UV-visible spectrum of the oxidised P346L mutant of CY121 showed typical characteristic features of a heme-containing protein. The Soret peak of the protein was located at 416.5 nm, with the smaller intensity  $\alpha$  and  $\beta$  bands at 565 nm and 533 nm (Q-region), respectively (Figure 3.12). The S279A mutant of CYP121 and histidine tagged CYP121 also generated the same heme electronic absorbance characteristics as observed for the P346L isoform, whilst the R386L mutant differed (Figure 3.13). The Soret absorbance of the R386L mutant of CYP121 had red-shifted to 419 nm in comparison to the wild-type CYP121 and the other characterised mutants, with no distinction between the  $\alpha$  and  $\beta$  bands in the Q-region (Figure 3.13).

With CYP121 mutants (except for the R386L mutant), as noted for wild-type CYP121 and CYP51, the lack of a significant absorption shoulder at  $\sim 390 \text{ nm}$  indicates that the mutant is predominantly low-spin ( $S = 1/2$ ) with minimal high-spin ( $S = 5/2$ ) ferric heme iron content (McLean *et al.*, 2002a; McLean *et al.*, 2006). In contrast the R386L mutant protein is notable for the development of a distinct shoulder at  $\sim 390 \text{ nm}$ , associated with high-spin ferric heme.



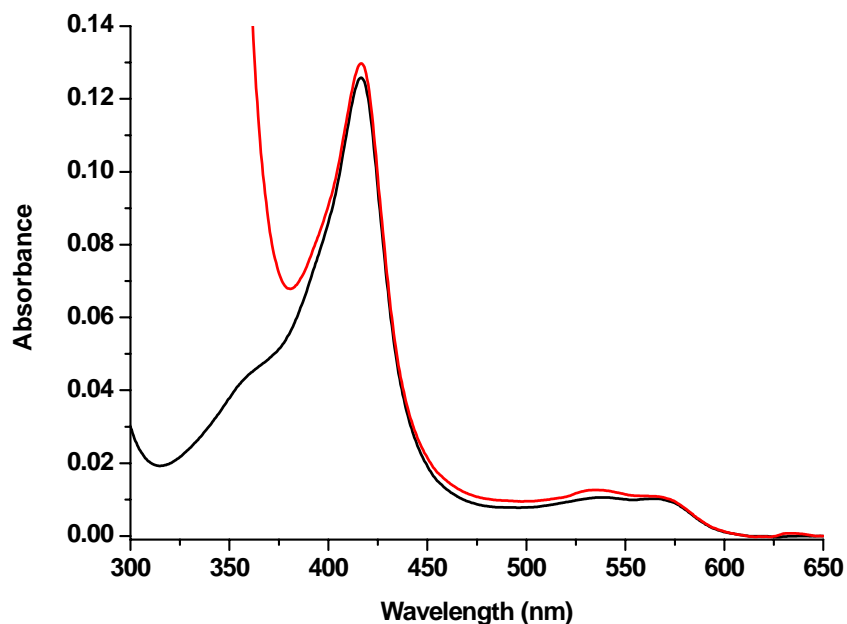


**Figure 3.12 UV-visible absorbance spectra of pure P346L mutant of CYP121**  
P346L mutant of CYP121 (~1.3  $\mu$ M) recorded in 50 mM Tris-HCl (pH 7.2). The oxidised form of the enzyme is displayed in black, while the sodium dithionite-reduced form is displayed in red.

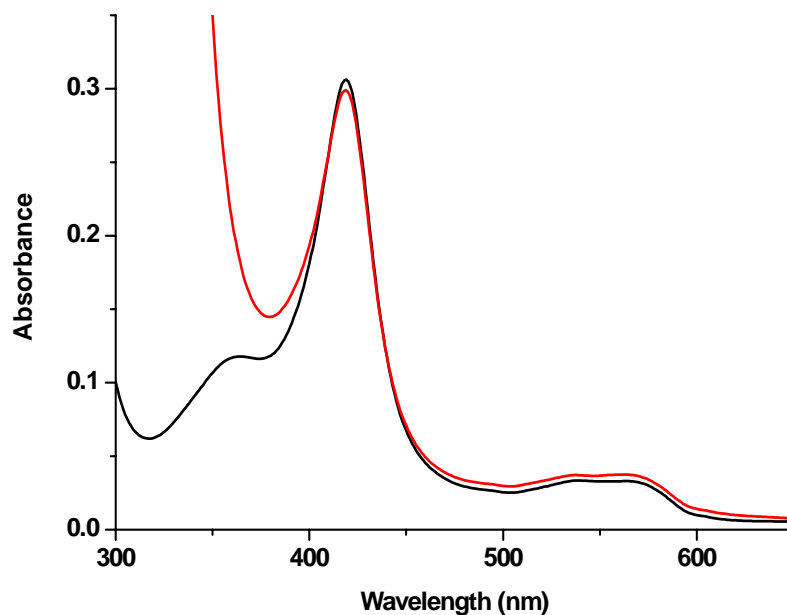


**Figure 3.13 UV-visible absorbance spectra of pure R386L mutant of CYP121**  
R386L mutant of CYP121 (~3  $\mu$ M) recorded in 50 mM Tris-HCl (pH 7.2). The oxidised form of the enzyme is displayed in black, while the sodium dithionite-reduced form is displayed in red.

Anaerobic reduction of the pure P346L enzyme with sodium dithionite resulted in no shift in the Soret band maximum (Figure 3.12), as also is the case for the S279A isoform and histidine tagged CYP121. Further changes also occurred in the Q-band region in relation to relative intensities of the  $\alpha$  and  $\beta$  bands (Figure 3.12). A similar lack of optical change was also observed for the R386L mutant of CYP121 (Figure 3.13). The lack of change in the Soret band is likely to reflect the general difficulty in reducing ferric CYP121 using dithionite, even under anaerobic conditions, rather than any specific heme properties resulting from the mutations (McLean *et al.*, 2002a). The reduction of wild-type CYP121 has been reported to be difficult to achieve and to reproduce, due mainly to the relatively rapid rate of re-oxidation of the heme iron and its rather negative heme iron reduction potential ( $<-400$  mV vs. SHE). There is also a requirement for a critical amount of dithionite to be added to effect complete heme iron reduction in wild-type CYP121, with excessive additions resulting in protein aggregation (McLean *et al.*, 2002a). Upon successful sodium dithionite reduction of wild-type CYP121, the Soret band has been reported to decrease slightly in intensity and shift to a shorter wavelength of 405 nm, and the  $\alpha$  and  $\beta$  bands fuse to form a new spectral species with intermediate wavelength (538 nm) (McLean *et al.*, 2002a).

Binding of CO to the dithionite-treated P346L, R386L and S279A mutants of CYP121 leads to formation of an Fe(II)-CO complex, with a minor absorption maximum at 446 nm, and a major Soret maximum at 420 nm (the inactive P420 form). The shift of the Soret band to 446 nm is strongly indicative of a cytochrome P450, with a cysteinate thiolate-ligated heme, whilst the peak at 420 nm denotes a P420 spectral species reflecting that a proportion of the enzyme has developed cysteine thiol ligation following dithionite reduction and exposure to the CO gas. Thus, the P420 form is believed to arise from protonation of the proximal ligand, from thiolate to thiol ligation (McIver *et al.*, 1998; Perera *et al.*, 2003). P420 formation is consistent with protonation of the cysteinate (Cys 345) to a thiol underlying the observed P450-P420 transition (McLean *et al.*, 2006). Studies of the Fe(II)-CO state of *M. tuberculosis* CYP51 and wild-type CYP121 have revealed generation of significant P420 species, presumably arising from a similar process (Ayoama *et al.*, 1998; Ogura *et al.*, 2004; McLean *et al.*, 2006). Since completion

of this PhD project, pH titration studies of wild-type CYP121 demonstrated that the thiolate/thiol conversion was reversible, with a pKa value of 7.2 for the P420/P450 transition in the CO complex (Dunford *et al.*, 2007). It is important to note that, although the ligand-free CYP121 mutants (and wild-type) are difficult to reduce with dithionite, the presence of CO enables the reduction to go to completion, with CO binding to ferrous iron trapping the iron in this state and eventually pulling the equilibrium over completely to a stable ferrous (CO-bound) form. A difference spectra was generated by the subtraction of the ferrous spectrum from that for the ferrous/CO-bound adduct for CYP121 P346L (Figure 3.14). The formation of a peak at ~450 nm confirms the protein to be the recombinant CYP121 mutant; P346L. In light of the fact that *E. coli* has no endogenous P450s, this assay can also be used to examine the behaviour of CYP121 and its mutants in CO complexation reactions in relatively crude lysates. Similar spectral shifts were obtained for the CYP121 R386L, S279A mutants and histidine tagged CYP121. It should be noted that, although the proteins are only partially reduced by dithionite in absence of CO, the difference spectra still report faithfully on the formation of P450 and P420 species.

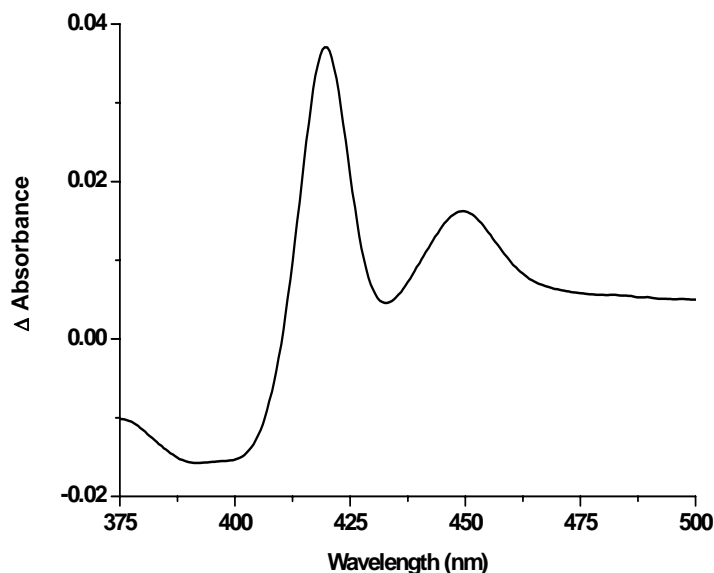


**Figure 3.14** Difference spectrum of the reduced/CO-bound form of the P346L mutant of CYP121

P346L mutant of CYP121 (~1.2  $\mu$ M) in 50 mM Tris-HCl pH 7.2. Difference spectrum generated by subtraction of the spectrum for ferrous CYP121 from the ferrous-CO form. The presence of the P450 species is evident from the peak at 450 nm. The P420 species is also present in rather larger amounts.

Nitric oxide (NO) binding to ferric P346L, R386L and S279A mutants of CYP121 resulted in a decrease in the intensity and shift of the Soret band to 437 nm, and of the  $\alpha$ - and  $\beta$ -bands to 576 nm and 545 nm, respectively (Figure 3.15). This “type II” binding spectrum is typical of strong ligand co-ordination, as also seen for the binding ofazole inhibitors to ferric heme, in this case giving rise to a Soret maximum at  $\sim$ 425 nm (section 3.15).

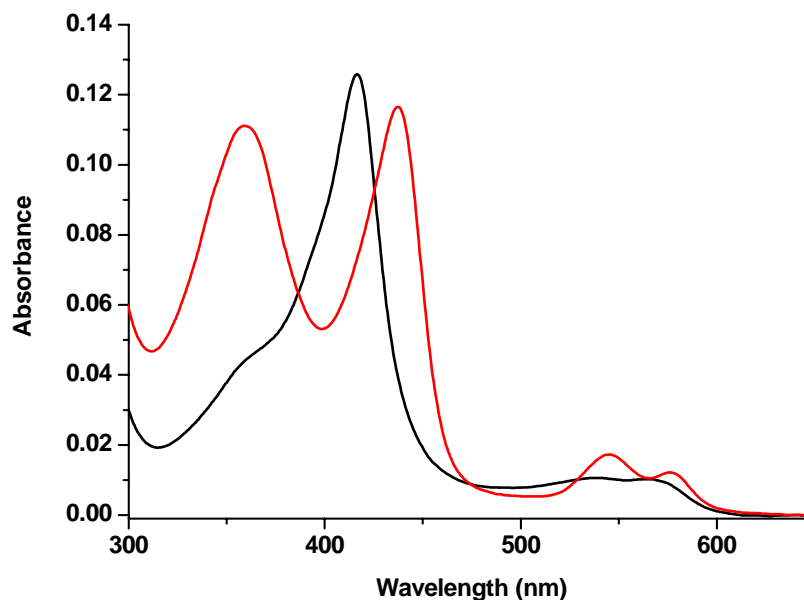


**Figure 3.15 Electronic absorption spectra of the P346L mutant of CYP121 with and without NO-bound**  
CYP121 ( $\sim$ 1.3  $\mu$ M) in 50 mM Tris-HCl pH 7.2, in the oxidised (black) and nitric oxide-bound (red) form, with Soret maxima located at 416.5 and 437 nm, respectively.

The spectral changes induced by the small molecules CO and NO are typical of distal ligations to P450 heme iron with a cysteinate proximal ligand heme (cysteine in the case of the P420 form). The ligation of NO ligand to the ferric P450 results in conversion to a single spectral species typical of those seen in other P450s, and indicating that the P420 material observed upon reduction and CO-binding is not a reflection of inactive (thiol-coordinated) enzyme existing in the ferric state of the enzyme.

### **3.5 Biophysical characterisation**

#### **3.5.1 Circular dichroism of CYP121 P346L mutant**

Circular Dichroism (CD) spectroscopy provides information on specific 3-D structural chiral-centre-containing macromolecules. CD refers to the differential absorption of the left- and right-circularly polarized components of plane polarized electromagnetic radiation (Kelly *et al.*, 2005). Experimentally, plane-polarized radiation from a Xenon lamp is split by passage through a modulator into circularly polarized components. The modulator transmits the left- and right-handed components, each in turn. Passage of the circularly polarized light through the sample of interest will generate, upon recombination, radiation polarized in the original plane and/or elliptically polarized light. The latter arises when the components are not absorbed or are absorbed at equal extents. The former case arises if one polarized component is absorbed by the sample to a greater extent than the other. The resulting CD spectrum, comprising an ellipticity plot versus wavelength, can provide important information on the secondary and tertiary structure of proteins (Kelly *et al.*, 2005).

The CD spectrum in the far-UV region (typically from 260 nm to 180 nm) can be used to provide quantitative information of the secondary structure content of a protein. The different forms of regular secondary structure found in peptides and proteins exhibit distinctive far-UV CD spectra. Analysis of a far-UV CD spectrum occurs by comparison to reference spectra of proteins for which structures have been determined to a high resolution by X-ray crystallography. Analyses of the secondary structure can be performed using algorithms such as SELCON 3 (self-consistent), VARSLC (variable selection), CDSSTR and CONTIN (Kelly *et al.*, 2005).

The far-UV CD spectrum of the *M. tuberculosis* CYP121 P346L mutant is demonstrated below with comparison to wild-type CYP121 (Figure 3.16). The CD spectra were obtained in millidegree ellipticity ( $\theta$ ) scale and, in the case of the far-UV CD spectrum, transformed to molar ellipticity  $[\theta]$  using the mean residue weight and concentration prior to the secondary structure analysis.

The near UV and visible CD spectra provide information on the heme cofactor environment as well as on the tertiary structure of the protein. Although in isolation a heme chromophore exhibits no optical activity, because of the high symmetry, when bound in an asymmetric protein environment optical activity in the visible region may arise (Myer and Pande, 1978). The spectrum in the near UV region (i.e. in the region between 260-320 nm) arises predominantly from the aromatic amino acids, phenylalanine, tryptophan and tyrosine, along with possible contributions from disulfide bonds. Aromatic CD spectral intensities are affected by protein flexibility, with the more highly mobile side-chains having lower CD intensities. In addition, interactions between aromatic side-chains in close proximity contribute to stronger signal intensity. The near UV-visible CD spectrum of the CYP121 P346L mutant is displayed below alongside the corresponding spectrum of wild-type CYP121 (Figure 3.17).

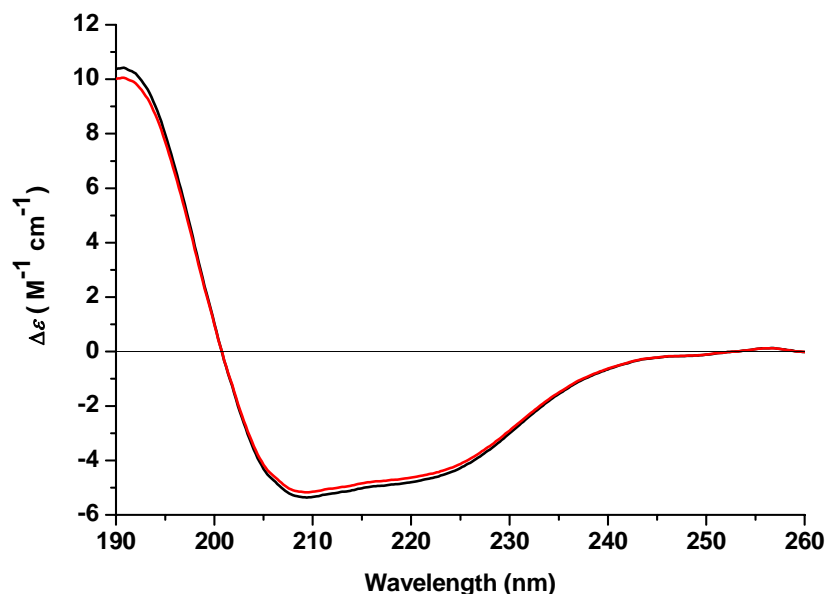


**Figure 3.16 Far-UV CD spectra of the P346L mutant of CYP121**  
P346L (2  $\mu$ M) (red) compared with wild-type CYP121 (2  $\mu$ M) (black). Both proteins were in 10 mM KPi pH 7.0, with a pathlength of 0.02 cm. Experiment was performed on a JASCO J715 spectrapolarimeter at 25 °C.

The far-UV CD spectra (190-260 nm) for P346L indicated no significant change in secondary structure compared with the wild-type. The strong similarity illustrated

between the far-UV CD spectra of P346L and wild-type CYP121 further emphasised that CYP121 is mainly composed of  $\alpha$ -helical structure (73%), consistent with all other structurally characterised P450s (McLean *et al.*, 2002a). P346L has a virtually identical far-UV CD spectrum to that of the wild-type enzyme, with double minima at 208 and 220 nm, and a maximum at 190 nm. The trough, occurring at 208 nm, corresponds to a weak but broad  $n \rightarrow \pi^*$  transition, and an intense  $\pi \rightarrow \pi^*$  transition corresponds to the peak at 190 nm (Munro *et al.*, 1999).

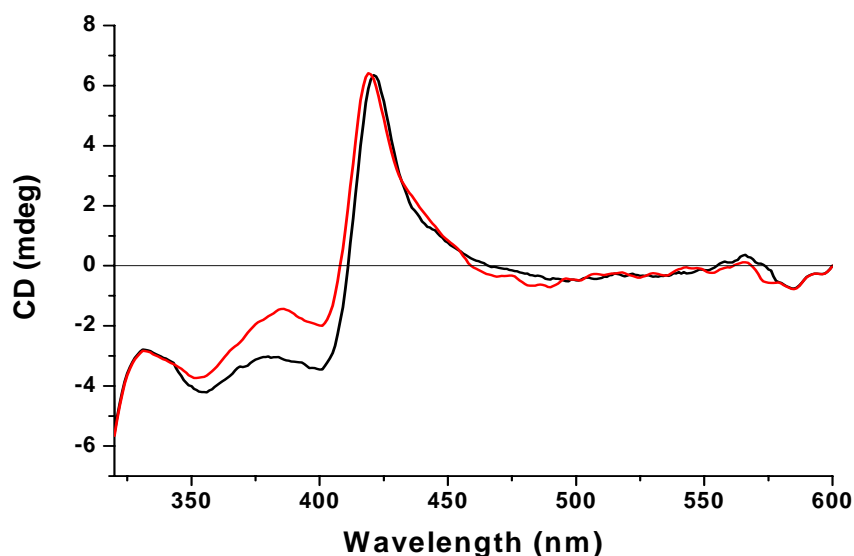


**Figure 3.17** Near UV-visible spectra of CYP121 P346L

P346L mutant of CYP121 (20  $\mu$ M) (black) compared with wild-type CYP121 (20  $\mu$ M) (red) in 10 mM Tris pH 7.0. Data were collected with a pathlength of 0.5 cm. Experiment was performed on a JASCO J715 spectropolarimeter at 25  $^{\circ}$ C.

The near UV-visible CD spectra of P346L and of wild-type CYP121 display similarities in both the aromatic amino acid and heme environment features (Figure 3.17). The near UV-visible spectrum of P346L is characterised with distinct transitions at 354 and 422 nm (delta and Soret bands, respectively) which are due to the  $\pi \rightarrow \pi^*$  transitions of the porphyrin ring (Hsu and Woody, 1971). However, in the environment of the heme group (350-450 nm), the spectrum of P346L heme in its resting ferric form is slightly different from that of the wild-type CYP121. This portion of the spectrum is dominated by a sharp Soret feature with positive ellipticity. The positive Soret feature at 421 nm for

P346L differs from that observed with wild-type CYP121. For the wild-type, this is centred at 419 nm, close to the maximum in the electronic absorption spectrum (416.5 nm) (McLean *et al.*, 2002a). In addition, the near-UV-visible CD spectrum of P346L has its delta band at 354 nm, while for wild-type CYP121 this lies at 352 nm. This difference is not mimicked (under identical data collection conditions) in the optical transition seen in the electronic absorption spectrum, where optical absorption spectra are indistinguishable for wild-type and P346L CYP121. Thus, near-UV-visible CD spectroscopy highlights differences in the spectra of the P346L and wild-type CYP121 that are not obvious from optical absorption spectroscopy. Furthermore, the intensity of the negative ellipticity transmission between ~350 and ~450 nm is also notably greater for P346L than for the wild-type CYP121.

These CD spectral changes of heme Soret and delta bands, displayed at a slightly longer wavelength for the P346L mutant than for wild-type CYP121, likely relate to alterations in the nature of the ‘kinked’ heme conformation caused by the P346L mutation. The heme is substantially distorted at one of the pyrrole groups in wild-type CYP121 as a consequence of the conformation of the side chain of P346. The removal of this residue leads to a substantial alteration in the distortion of this region of the heme in the P346L mutant structure (Section 3.10.1). In the P450 BM-3 (CYP102A1) system, a phylogenetically conserved phenylalanine residue (F393) located seven amino acids before the cysteine ligand also stacks with both the heme plane and packs with the cysteinate ligand, generating a large effect on the heme electronic properties (Ost *et al.*, 2001a). However, in this case the heme macrocycle remains predominantly planar in both wild-type and F393 variants.

The near UV-visible CD spectrum of P346L, as in the case of native CYP121, displays positive ellipticity in the heme region (a positive Cotton effect). This is in contrast to the strong negative Cotton effect found in P450 BM-3 (Andersson and Peterson, 1995; McLean *et al.*, 2002a). The negative Soret CD band feature of P450 BM-3 is shared by other P450s from various sources, including isoforms isolated from mammalian liver microsomes (Chiang and Coon, 1979), from the adrenal cortex



mitochondria (Shimizu *et al.*, 1981), and from other bacterial P450s e.g. P450cam (CYP101A1), P450 BM3 and P450terp (CYP108) (Andersson and Peterson, 1995). However, the transmission intensity varies among these different bacterial P450s (Andersson and Peterson, 1995).

This marked difference between CYP121 and P450 BM-3 indicates that the two P450s may have significantly different heme topology, as was confirmed from the atomic structure of CYP121 (Leys *et al.*, 2003). Certain histidine ligated hemoglobins from soybean leg and lamprey exhibit negative Soret CD transmissions, while mammalian myoglobins with similar tertiary structure have positive bands (Myer and Pande, 1978). Furthermore, binding of alkyl isocyanides to a deoxy-ferrous lamprey hemoglobin form converts a negative Soret CD transmission to a positive transmission in a manner that is dependent on the length (hydrophobicity) of the alkyl group (Myer and Pande, 1978). Thus, the characteristics of the Soret CD bands of heme proteins appear to be sensitive to the size and/or hydrophobicity of the heme environment (Sono *et al.*, 1995). The differing geometry of the heme for CYP121 and P450 BM-3 may also reflect in some way the distinct functions of the P450 enzymes. P450 BM-3 is a fatty-acid hydroxylase, whereas the *M. tuberculosis* CYP121 appears to be involved in lipid or polyketide metabolism peculiar to this pathogenic bacterium.

### **3.5.2 Circular dichroism of histidine-tagged CYP121**

In order, to monitor the effect of the recombinant histidine residues on the overall structure of His-CYP121, far and near UV-visible CD spectroscopy was performed and spectra compared to that for wild-type CYP121. The far UV-visible CD spectrum of the His-CYP121 is displayed below, alongside the corresponding spectrum of wild-type CYP121 (Figure 3.18).

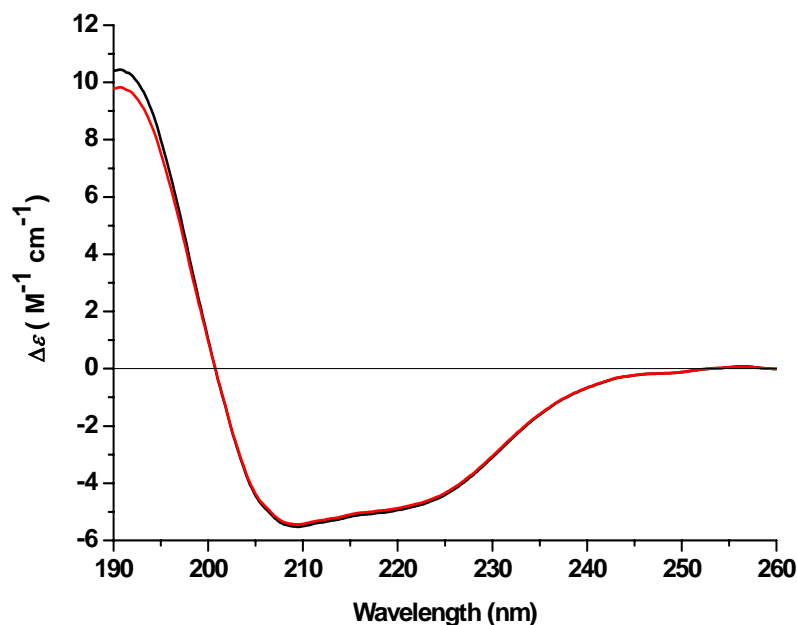


**Figure 3.18 Far-UV CD spectra of His-CYP121**

His CYP121 (2  $\mu\text{M}$ ) (black) compared with wild-type CYP121 (2  $\mu\text{M}$ ) (black). Both proteins were in 10 mM KPi pH 7.0. Spectra were recorded in cells with a path length of 0.02 cm. Experiment was performed on a JASCO J715 spectropolarimeter at 25  $^{\circ}\text{C}$ .

The far-UV CD spectra (190-260 nm) for His-CYP121 indicate no significant conformational changes in secondary structure compared with the wild-type enzyme. The strong similarity illustrated between the far-UV CD spectra of His-CYP121 and wild-type CYP121 emphasises no measurable change in the proportions of the  $\alpha$ -helical and beta sheet components of the structure. His-CYP121 has a virtually identical far-UV CD spectrum to that of the wild-type enzyme, with double minima at 220 and 208 nm and a maximum at  $\sim 190$  nm. The trough, occurring at 208 nm, corresponds to a weak but broad peptide  $n \rightarrow \pi^*$  transition, and an intense  $\pi \rightarrow \pi^*$  transition corresponds to the peak at  $\sim 190$  nm (Munro *et al.*, 1999).

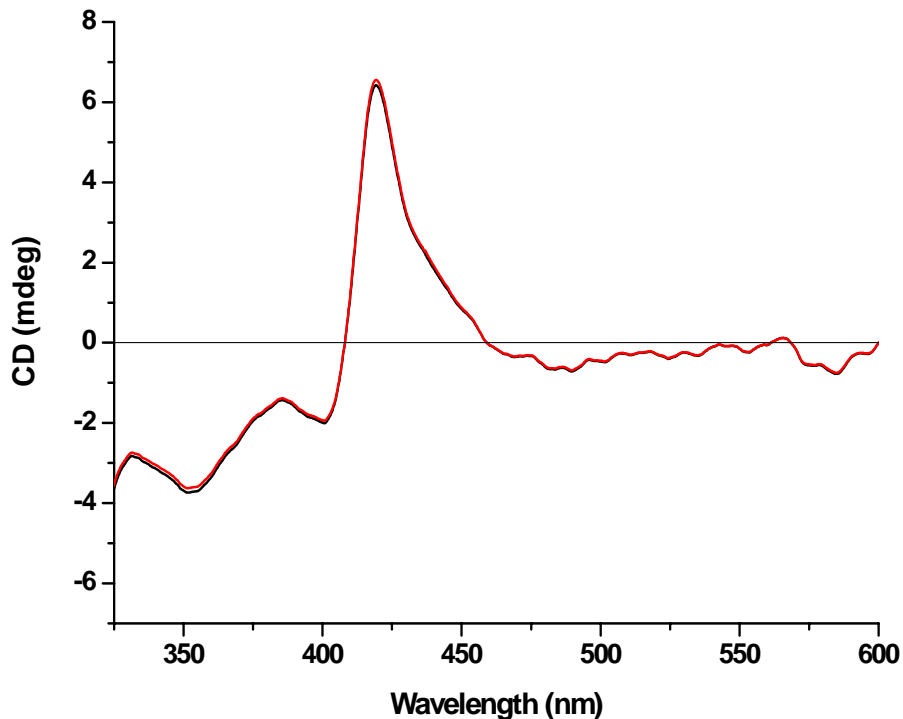


**Figure 3.19** Near UV-visible spectra of His-CYP121 and wild-type CYP121  
His-CYP121 (20  $\mu$ M) (red) compared with wild-type CYP121 (20  $\mu$ M) (black) in 10 mM Tris pH 7.0. Data were collected in quartz cells with a path length of 0.5 cm. Experiment was performed on a JASCO J715 spectropolarimeter at 25  $^{\circ}$ C.

The near UV-visible CD spectra of His-CYP121 and of wild-type CYP121 display strong similarities in both the aromatic amino acid and heme environment features (Figure 3.19). Aromatic residue signals are displayed at  $<300$  nm, and the spectra are highly similar for both forms of the P450. The near UV-visible spectrum of His-CYP121 is characterized with distinct transitions at 352 and 419 nm (delta and Soret bands, respectively) which are due to  $\pi \rightarrow \pi^*$  transitions of the porphyrin ring (Hsu and Woody, 1971). In the environment of the heme group (350-450 nm), the spectrum of His-CYP121 heme is dominated by a sharp Soret feature with positive ellipticity. The positive feature at 419 nm for His-CYP121 is identical to that observed with wild-type (non-tagged) CYP121. For the wild-type, this is centred at 419 nm, close to the maximum in the electronic absorption spectrum (416.5 nm) (McLean *et al.*, 2002a).

Thus, whilst the spectra are virtually identical to those observed for the wild-type, non-tagged CYP121 protein, the overall conformational structure of the enzyme in both the far and near-UV-visible regions has remained unchanged in the presence of the histidine residues used for the affinity tag.

### 3.5.3 Electron paramagnetic resonance (EPR) spectroscopy

An atom will generate a net magnetic moment due to the spin and orbital magnetic moments of its unpaired electrons. The spin magnetic moments of unpaired electrons are randomly orientated in the absence of a magnetic field, but the application of a field aligns the magnetic spin parallel or anti-parallel to the magnetic field orientation. In electron paramagnetic resonance (EPR) spectroscopy, the presence of an external magnetic field allows detection of unpaired electrons carrying an electron-spin magnetic moment. In a magnetic field each orbital energy level will be split into several energy levels and the transitions between them are associated with a net absorption of energy from the applied electromagnetic radiation (Hoff, 1989). Furthermore, this microwave absorption signal is also dependent on the orientation of the molecule bearing the unpaired electron with respect to the magnetic field, on the mobility of that molecule and on the presence of other unpaired electrons in the vicinity. The resulting resonance between the electron and a microwave field forms the basis of EPR, which is detected by a spectrometer to generate a signal. EPR is used in a variety of analyses including determination of molecular orientation; molecular dynamics; ligand binding; intra- and intermolecular distances and various levels of protein structure. The frequency for EPR is calibrated in the dimensionless number called the g-factor which is defined in the following equation:

$$\nu = (g\beta B)/h$$

$\nu$  = operating frequency of the spectrometer (constant)

$g$  = the g-factor

$\beta$  = electron Bohr magneton ( $9.273 \times 10^{-23}$  Tesla)

$B$  = magnetic field (Tesla) at relevant point in EPR spectrum

$h$  = Planck's constant.

In the equation,  $g\beta B$  describes interaction of electron spin with the magnetic field, characterised by the intrinsic  $g$ -factor (Zeeman interaction). The  $g$ -factor itself defines the centre of the resonance.

Specifically, EPR is an informative means in the study of cofactor ligations, such as for ferric heme in cytochromes. The  $g$ -tensor values in heme systems provide information regarding the nature of bonding between the transition-metal ion and its neighbouring ligands in biomolecules. In quantitative terms, the state of this bonding is reflected in the energy separations of the  $d$ -like orbitals and the mixing in the molecular wave functions of the  $d$ -orbitals among themselves and with the surrounding ligands (Roy *et al.*, 1989). No EPR signal can be detected for low-spin ferrous cytochromes since there are no unpaired electrons, therefore low-spin cytochromes must be in the oxidised ferric state to exhibit an EPR spectrum. However, in high-spin cytochromes, unpaired electrons exist in both the reduced (ferrous) and oxidised (ferric) states, and so generate EPR signals in both states. Discrete EPR signals are produced for different spin-states and conformations. The  $g$ -values generated differ depending on the ligation and environment of the heme iron (Hoff *et al.*, 1989; Mansuy and Renaud, 1995). The two most common types of spectra for iron-containing cytochromes are axial high spin and rhombic low spin. Axial high-spin systems have characteristic  $g$ -values of  $\sim 2$  and  $\sim 8$ , whereas rhombic low-spin systems have three distinct  $g$ -values between 1.0 and 3.8.

The X-band EPR spectrum of oxidised CYP121 P346L was recorded at 10 K with 2 mW microwave power (Figure 3.20). The major signals generated in the EPR spectrum of P346L constitute a rhombic trio of  $g$ -tensor elements. The occurrence of 3 major peaks indicates a nuclear spin state of  $\frac{1}{2}$  ( $2I + 1$ ). The resulting  $g$ -values ( $g_z$ ,  $g_y$ ,  $g_x$ ): ( $g_z$ ) 2.49, ( $g_y$ ) 2.26 and ( $g_x$ ) 1.90 are typical for low-spin ferric ( $\text{Fe}^{3+}$ ) heme (Mansuy and Renaud, 1995). Indeed, the P346L spectra is virtually identical to the native CYP121 ( $g = 2.47$ , 2.25, 1.90) (McLean *et al.*, 2002a). It is also highly similar to those of low-spin ferric forms of the well-characterised P450cam and P450 BM-3 ( $g = 2.46$ , 2.26, 1.91 and 2.42, 2.26, 1.92, respectively) (Dawson *et al.*, 1982; Miles *et al.*, 1992), and to the low-spin ferric forms of the Nitric Oxide Synthases (NOSs) in which the heme is also bound

axially by cysteinate and water (Lipscomb, 1980; Dawson *et al.*, 1982; Berka *et al.*, 1988; Salerno *et al.*, 1995; Tsai *et al.*, 1996). The signal at  $g = \sim 2.0$  is suggestive of minor radical contaminants. However, there is some disparity between P346L and wild-type CYP121, with broadening of the  $g_z$  and  $g_x$  component signals of the P346L sample. This broadening effect on the EPR signal of P346L is suggestive of some degree of perturbation of the heme ligand conformation.

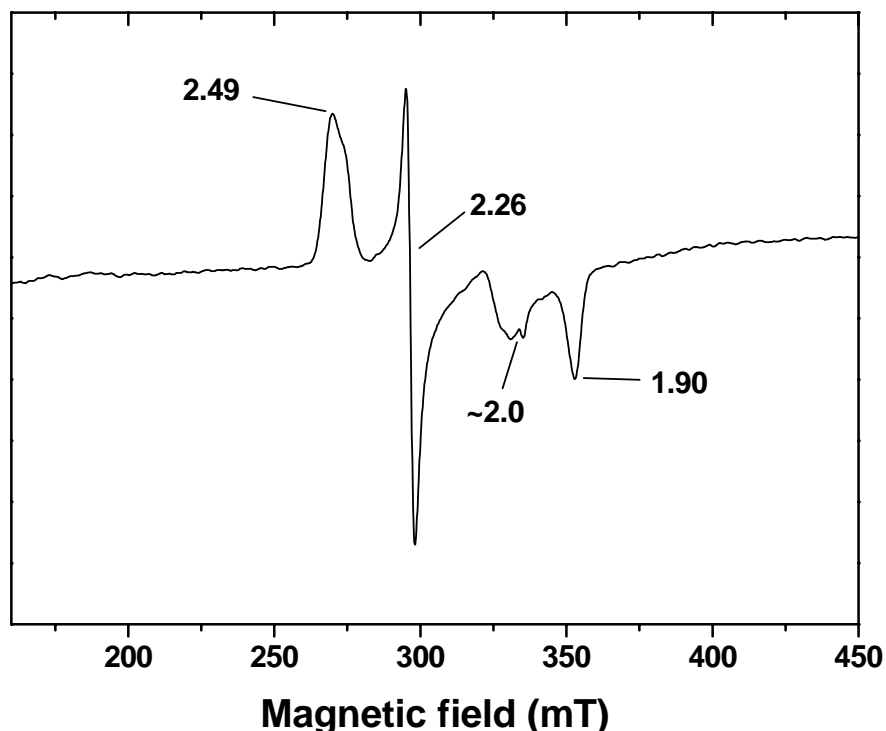


**Figure 3.20 X-band EPR spectrum of the P346L mutant of CYP121**

The protein was at a concentration of 170  $\mu\text{M}$  in 50 mM Tris-HCl pH 7.5 including 50 % (v/v) glycerol. Sample conditions were temperature 10 K, microwave power = 2.0 mW, modulation amplitude = 1 mT

In wild-type CYP121 the splitting of the  $g$ -value at  $g = 2.01$  indicates some heterogeneity of the heme species, along with the minor signals observed at  $g = 5.9$  and 4.29. This heterogeneity is thought to be due to the purity of the sample (McLean *et al.*, 2002a). The presence of the minor signals ( $g = 5.9$  and 4.29) are due to trace amounts of high-spin ferric heme and adventitious Fe (III), respectively, or may even indicate a low degree of rhombic splitting of the  $S = 5/2$  high spin ferric state, a feature observed upon

substrate, or in some cases, ligand binding (Lipscomb, 1980; Dawson *et al.*, 1983). The g-values are very sensitive to the nature of the heme axial ligands and to perturbations such as the orientations of the ligands. The fact that these values for P346L are practically identical to the wild-type CYP121, P450cam and P450 BM-3 suggests that the P346L mutation has not had major significant effects on the low-spin ferric heme-iron ligation environment of CYP121. However, as indicated in the previous paragraph, the broadening of the  $g_x$  and  $g_z$  components is suggestive of some perturbation of the conformation of one or both of the axial ligands.

#### **3.5.4 Resonance Raman of wild-type CYP121 and mutants**

The vibrational spectroscopic technique, resonance Raman (RR) spectroscopy, utilises the electronic absorption bands to enhance the magnitude of the Raman signal, thus providing a variety of information regarding the molecular structure, chemical bonding and molecular environment of a protein (Asher, 1988). In RR spectroscopy, the frequencies with which bonded atoms vibrate, relative to each other, determine the vibrational spectrum (Weaver and Schwenz, 2001).

Raman measures the photon scattering process that occurs when photons from a monochromatic source (e.g. laser) interact with a molecule. The Raman effect is an inelastic scattering process with the incident photons distorting the electron cloud of the molecular bonds (Weaver and Schwenz, 2001). The degree of electron cloud deformation relates to the polarisability of the molecule and results in the energy of the scattered photons either increasing or decreasing in energy, which corresponds to a vibrational transition (Weaver and Schwenz, 2001).

The majority of the scattered light produced by this method is known as Rayleigh scattering, which denotes the elastic process in which the photons interact and subsequently distort the electron cloud surrounding the nucleus (Weaver and Schwenz, 2001). Rayleigh scattering has a wavelength almost identical to the incident light, since there is no transfer of energy to or from the photons (Rousseau *et al.*, 1979). Raman scattering only occurs when a few photons (approximately 1 in every  $10^6$ ) are involved in

an inelastic process involving the change in inter-nuclear distances of the molecule. This motion of a nucleus in an electric field is due to the attraction of electrons and nuclei of the molecule towards opposite poles, so polarising the molecule (Weaver and Schwenz, 2001). This change in molecular polarisability results in the frequency of the scattered light collected differing from the frequency of the incident light by one vibrational unit (Rousseau *et al.*, 1979). Thus, the extent of the Raman shift corresponds to a vibrational mode and molecular information is conveyed by the frequency of the mode, the intensity and the polarisation of the scattered light.

RR spectroscopy relies on the ability to couple closely the excited vibrational transitions of the molecule with that of the excitation frequency used. Excitation into the electronic absorption band significantly enhances the Raman signal and provides greater sensitivity relative to Raman spectroscopy (Weaver and Schwenz, 2001). To increase further the magnitude of the signal, RR spectra are acquired using a laser system as the excitation source. A laser greatly facilitates the acquisition of data because of the intensity and coherence of the source, as Raman scattering itself is inherently several orders of magnitude weaker than Rayleigh elastic scattering. RR spectroscopy has been shown to be more powerful and selective than Raman, by up to  $10^4$  times (Rousseau *et al.*, 1979).

RR spectroscopy has been used to probe the intrinsic electronic and vibrational properties of metalloproteins, resulting in effective characterisation of structural changes in active sites. In the case of heme proteins, the oxidation state of the porphyrin moiety, the type of coordination of the metal ion and the spin state of the metal ion can be detected from the vibrational frequencies of the porphyrin group. The published RR spectra of the intensively studied P450cam and P450 BM-3, in particular, has enabled the identification of characteristic signals for heme iron spin and coordination state. In addition, details on heme vinyl, methyl and propionate groups related to vibrational data have been obtained, making RR an insightful method in the study of conformational and other properties of the P450 heme cofactor (Abe *et al.*, 1978; Hildebrandt and Stockburger, 1989).



Resonance Raman spectroscopy has proved to be an invaluable probe of the porphyrin conformation within proteins. In fact, it was the first technique to detect (Alden *et al.*, 1989), and the only method currently known that can quantify, the conformational equilibrium between planar and non-planar conformers of some metal porphyrins (Alden *et al.*, 1989; Alden *et al.*, 1990; Anderson *et al.*, 1993; Song *et al.*, 1996).

The resonance Raman spectrum of CYP121 and of the CYP121 P346L, R386L and S279A mutants (Figure 3.21) were obtained with excitation at 406.7 nm and bands were labelled according to previous assignments (Kitagawa and Ozaki, 1987; Parthasarathi *et al.*, 1987; Hildebrandt and Stockburger, 1989; Hudeček *et al.*, 2000). The 406.7 nm excitation length is close to the Soret transition of the heme chromophores (416.5 - 419 nm) and generates Raman scattering from the vibrational modes of the porphyrin ring. The generated spectra for wild-type CYP121 and mutants show a general strong similarity to those obtained for other P450 enzymes (Kitagawa and Ozaki, 1987; Parthasarathi *et al.*, 1987; Hildebrandt and Stockburger, 1989; Hudeček *et al.*, 2000; McLean *et al.*, 2002a).

The dominant oxidation state marker band obtained for wild-type CYP121 and mutants thereof is assigned the  $\nu_4$  mode. The observed value of 1370-1373  $\text{cm}^{-1}$  for  $\nu_4$  indicates that the heme iron is in the ferric (FeIII) state, in accordance with the data obtained from electronic absorption spectra and EPR. Bands in the range 1450 – 1650  $\text{cm}^{-1}$  are characteristic indicators of the porphyrin ring core size and, consequently, of the spin-state of the heme iron (Abe *et al.*, 1978; Hildebrandt and Stockburger, 1989). The characteristic spin-state marker in this range is  $\nu_3$  and the presence of this band located at  $\sim 1500 \text{ cm}^{-1}$  reveals wild-type CYP121 and mutants to be in a low-spin ferric heme state. Overall, the RR spectra of the CYP121 mutants are fairly typical of wild-type CYP121, indicating no major changes in spin-state and a predominantly ferric cysteinate-ligated P450 (Hudeček *et al.*, 2000). The assignments and band frequency values for the main peaks in the RR spectrum of wild-type CYP121 and mutants are summarised in Table

3.6. However, there are some significant differences for the P346L and R386L mutants compared to wild-type in the  $\nu_3$  band and in the central region of the spectra.

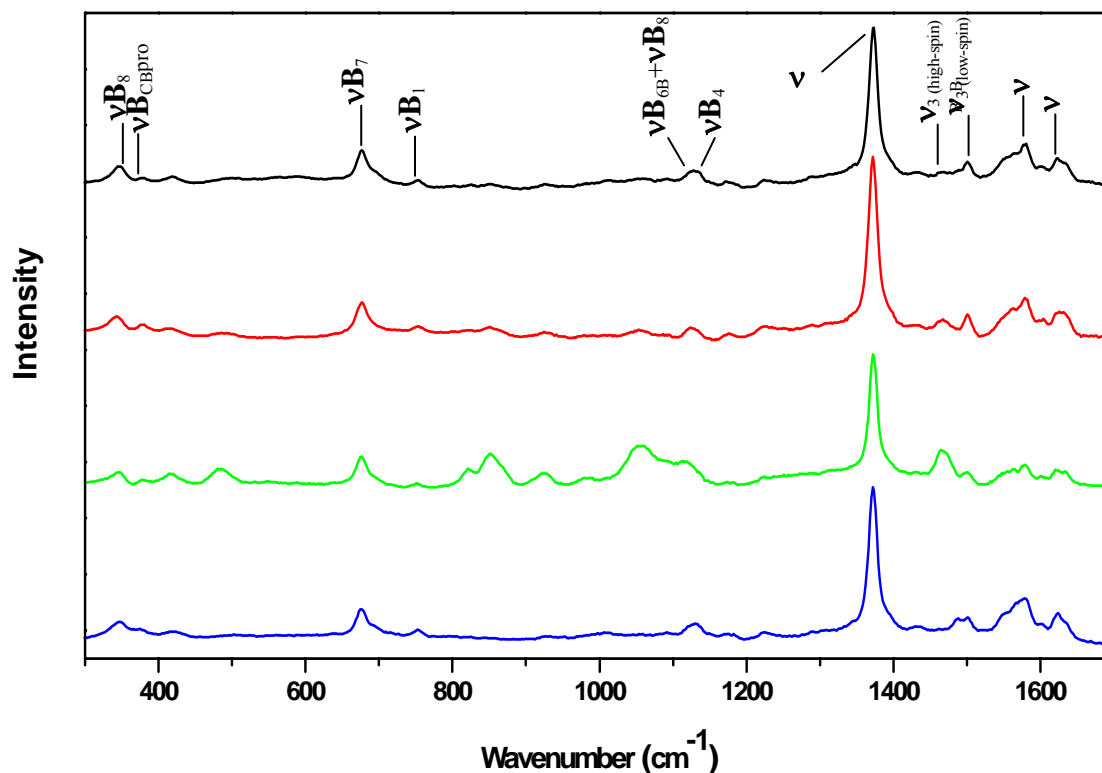


**Figure 3.21** Resonance Raman spectra of wild-type CYP121 and its P346L, R386L and S279A mutants

P450 mutant proteins (100  $\mu$ M) were in 10 mM Tris-HCL pH 7.5, and spectra were recorded between 300 and 1700  $\text{cm}^{-1}$ . Positions of assigned vibrational bands are shown, including the  $\nu_4$  marker band for oxidised ferric heme (1370  $\text{cm}^{-1}$ ), and the  $\nu_3$  feature indicating the low-spin heme. Assignments of the wild-type CYP121 spectra (black) are shown and are also representative of corresponding features in the CYP121 mutants P346L (red), R386L (green) and S279A (blue).

	Band position (cm <sup>-1</sup> )			
Assignment	Wild-type CYP121	P346L	R386L	S279A
$\nu_{\text{C}=\text{C}}$	1621	1626	1621	1623
$\nu_2$	1579	1579	1579	1580
$\nu_3$ (low-spin)	1499	1501	1500	1502
$\nu_3$ (high-spin)	1487	1487	1487	not observed
$\nu_4$	1370	1372	1373	1373
$\nu_{44}$	1131	1133	1135	1133
$\nu_6 + \nu_8$	1125	1124	1124	1127
$\nu_{16}$	753	753	751	752
$\nu_7$	674	677	676	677
$\delta(\text{C}_\beta\text{C}_\alpha\text{C}_\beta)$	417	417	415	417
$\text{C}_{\text{bprop}}$	376	380	376	378
$\nu_8$	343	343	343	347

**Table 3.6 Resonance Raman frequencies for the main vibrational features observed in wild-type CYP121 and its point mutants**

Excitation was at 406.7 nm. Protein concentrations were 100  $\mu\text{M}$ , as detailed in the legend of figure 3.21.

Strong differences in some regions of the RR spectra are seen between wild-type CYP121 and the R386L mutant (Figure 3.21). The Arg<sup>386</sup> residue is located immediately above the heme plane, dominating the local structure, and lies adjacent to the oxygen scission site. It was proposed to form part of a proton transfer pathway to the heme iron (Leys *et al.*, 2003). Of note is the difference in the relative intensity of bands in the range of 820-1150 cm<sup>-1</sup> between wild-type protein and the R386L mutant. For example, the

relative intensity of the peak at  $1051\text{ cm}^{-1}$  is increased in the R386L mutant compared to the wild-type. In contrast to the previously published RR spectrum for wild-type CYP121, the splitting of the  $\nu_3$  marker is less resolved (McLean *et al.*, 2002a). In the previously published data there is clear splitting of the  $\nu_3$  band into two well-resolved components located at  $1487$  and  $1500\text{ cm}^{-1}$  and representing high-spin and low-spin ferric heme, respectively (McLean *et al.*, 2002a). The intensity of the low-spin band is greater (McLean *et al.*, 2002a). The lack of a distinct high-spin component observed in this study of wild-type CYP121 may reflect the relatively low-intensity of this component.

The majority of bands in the  $1000\text{-}1300\text{ cm}^{-1}$  region are proposed to originate from porphyrin modes and include large contributions from the heme substituent groups (Abe *et al.*, 1978; Choi *et al.*, 1982a, b; Hu *et al.*, 1993). Indeed, previous studies have suggested that this region may provide a "fingerprint" for specific heme-protein interactions (Rospendowski *et al.*, 1991).

The crystal structure of wild-type CYP121 revealed that the distal Arg<sup>386</sup> residue is located in the immediate vicinity of the heme active site, directly above the heme plane, and dominating the local structure (Leys *et al.*, 2003). The residue also forms part of a hydrogen bonded network in the vicinity of the heme (Leys *et al.*, 2003). X-ray crystallography shows the substitution of the arginine with leucine results in alterations of positions of water molecules in the heme pocket (section 3.10.2).

The high-spin to low-spin equilibrium of ferric P450s is very sensitive to the distal pocket structure, and this is reflected in the  $\nu_3$  mode. The resonance Raman spectroscopy measurements of R386L clearly show that the protein exists in two well-resolved components relating to high-spin/low-spin forms, as seen in the splitting of the  $\nu_3$  feature. In addition, both spin-components are of approximately equal intensity. Mutations of distal pocket residues in P450cam, such as Tyr96, Thr101, Thr185, Val247 and Val295, have been noted to affect the spin-state equilibrium (Atkins and Sligar, 1988; Loida and Sligar, 1993). Small structural changes at the distal side of the heme

could be sufficient to alter the degree of occupancy of water at the iron site and, thus, the spin-state of the ferric enzyme. The UV–visible absorption spectroscopy of the R386L protein further highlighted the increased presence of high-spin protein with the observed shift of the Soret peak to lower wavelength, as compared to wild-type CYP121 (section 3.3).

The P346L mutation resulted in a shift among the internal vibrational modes of heme vinyls. The heme of wild-type CY121 is notably kinked in one pyrrole group, due to close interaction with the Pro<sup>346</sup> residue (Leys *et al.*, 2003). Specifically, the vinyl stretching ( $\nu_{C=C}$ ) mode has been shown to be sensitive to the conformation of the vinyl groups (Kalsbeck *et al.*, 1995), and is therefore often used as a heme structural indicator. The vinyls may be present in two broadly different conformations, either out-of-plane or in-plane with the heme. These two conformations in hemoproteins may be observed as distinct modes at about 1630  $\text{cm}^{-1}$  and 1620  $\text{cm}^{-1}$ , respectively (Kalsbeck *et al.*, 1995). In the wild-type CYP121, the  $\nu_{C=C}$  mode occurs at 1621  $\text{cm}^{-1}$ , and the position of this vibrational mode is suggestive of the heme vinyls being in an out-of-plane position relative to the heme. The shift in the  $\nu_{C=C}$  vibration to 1626  $\text{cm}^{-1}$  in the P346L mutant of CYP121, can be interpreted as fixation of the heme vinyls in a position more co-planar to the heme than is observed in the wild-type protein. This possibly occurs through a steric constraint imposed by the Leu<sup>346</sup> mutation. Analysis of heme peroxidase structures based on this interpretation has been previously published (Smulevich, 1998). However, it should be remembered that the Pro<sup>346</sup> residue is located immediately after the cysteinate ligand to the heme iron and that its side chain appeared responsible for a local distortion of one of the heme pyrrole groups. Overall, the X-ray crystal structure of the P346L mutant is highly similar to that of wild-type CYP121 (section 3.10.1), but reveals that the distortion of the heme pyrrole ring is reduced in comparison to the wild-type structure, and thus that the pyrrole ring is more in-plane with the rest of the heme macrocycle.

The  $\nu_3$  mode of the P346L protein clearly shows the presence of the low-spin component (1501  $\text{cm}^{-1}$ ). However, the intensity of the high-spin component is severely diminished as compared to the wild-type CYP121 protein. This alteration may reflect the

reinforcement by the P346L mutation of the low spin-form, although a high-spin component remains at  $1487\text{ cm}^{-1}$  (Figure 3. 21). Evidence for a change in the heme environment is provided by the crystal structure of the mutant where the previous degree of heme macrocycle distortion in the presence of Pro<sup>346</sup> is diminished upon the mutation with leucine, although the heme macrocycle remains notably non-planar.

The fact that the high-frequency spectral region for the P346L enzyme closely resembles that obtained for the wild-type suggested that attention should be focused on the low-frequency spectral region (specifically  $300\text{-}700\text{ cm}^{-1}$ ) of P346L, in order to look for further distinctive signals that might distinguish the wild-type and P346L enzymes. The low-frequency region (stretching from  $\sim 200\text{-}800\text{ cm}^{-1}$ ) is informative for identification of heme structural non-homogeneity and for identifying the axial ligation of the central iron atom. A number of bands in this region can be assigned to out-of-plane modes, and this is of relevance to structural comparisons between wild-type and P346L mutants. The low-frequency RR spectrum of P346L is shown in Figure 3.22, and the frequencies of the vibrational bands and their assignments are listed in Table 3.6.

The spectral pattern observed in the low-frequency region of the P346L mutation of CYP121 enzyme is quite similar to those observed for the prosthetic groups of most heme proteins (Spiro *et al.*, 1988; Hu *et al.*, 1996). The low-frequency region (Figure 3.22) is dominated by a relatively intense  $\nu_7$  heme core mode occurring at  $674\text{ cm}^{-1}$ , with all other modes being of much lower intensity. Again, it is noted that the P346L mutation has not substantially affected the frequencies, or relative intensities, of the modes as compared to wild-type CYP121. The lower intensity bands are assigned to porphyrin stretching modes at  $\nu_8$ , and  $\delta(\text{C}_\beta\text{C}_\alpha\text{C}_\beta)$  is assigned to the bending mode of a propionate group.

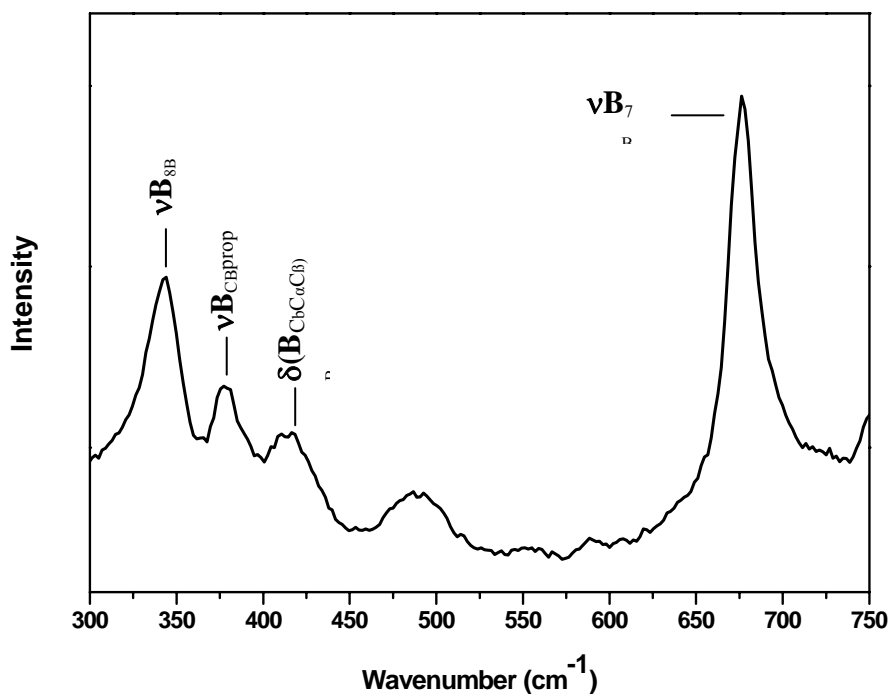


**Figure 3.22 Low-frequency resonance Raman spectrum of CYP121 P346L**  
 CYP121 P346L ( $\sim 100 \mu\text{M}$ ) was in 10 mM Tris-HCl pH 7.5. Spectra recorded between 750 and 300  $\text{cm}^{-1}$  with excitation at 406.7 nm. Positions of assigned vibrational bands are shown.

Previous Raman evidence for protein-induced out-of-plane distortion of the heme occurs in cytochrome *c* (Hu *et al.*, 1993) and mammalian lactoperoxidase within this low-frequency region (Zbylut and Kincaid, 2002). The number of vibrations within this region in cytochrome *c* is doubled compared to other heme proteins and this is considered to be an indicator of a closed heme crevice and a pronounced saddling distortion of the heme group resulting from the six-coordinate state and the existence of strong steric constraints on the heme (Hu *et al.*, 1993). The out-of-plane modes have been attributed to protein-induced distortion mediated by the covalent thioether linkages (Hu *et al.*, 1993). Furthermore, the heightened intensities of the 413 and 335  $\text{cm}^{-1}$  bands in the spectrum of mammalian lactoperoxidase, which are of near equal intensity to that of  $\nu_7$  at 678  $\text{cm}^{-1}$  in

this protein, are assigned to out-of-plane distortions of the macrocycle. These are thought to be protein-induced distortions through covalent ester linkages with the acid residues of the polypeptide (Zbylut and Kincaid, 2002). However, with similar features in both the wild-type CYP121 and CYP121 P346L mutant, this region may not reflect heme distortions in CYP121.

The residue Ser<sup>279</sup> is of interest for existing in two distinct conformations in the CYP121 structure. Each of these conformations is in contact with a different series of residues and buried water molecules that eventually lead up to the surface of the molecule, thus forming two putative proton relay pathways (Leys *et al.*, 2003). The substitution of Ser<sup>279</sup> to an alanine residue in order to disrupt the convergence point for two proposed proton relay pathways results in no significant change in the overall RR spectrum in comparison to the wild-type. An exception is observed in the  $\nu_3$  mode area of S279A, which is indicative of a low-spin component (1501  $\text{cm}^{-1}$ ). The presence of a high-spin component was not observed, which may relate to the masking effect of the apparent “double formation” of lower wavelength bands of higher intensities at 1502/1493  $\text{cm}^{-1}$ .

### **3.6 Redox potentiometry of CYP121 P346L**

The determination of redox potentials of proteins is of fundamental importance in understanding electron transfer and electron coupled reactions in a number of biological processes (Dutton, 1978; Wilson 1978). In most cases the only practical technique for determining redox potentials is potentiometry, commonly using a platinum (Pt)/calomel electrode and involving the measurement of associated changes in the electronic absorption spectrum on progressive reduction and oxidation of the enzyme using chemical reductant and oxidant (typically sodium dithionite and potassium ferricyanide, respectively). This method has been successfully applied to the study of P450 and related systems, such as the well-characterised P450 BM3, nitric oxide synthase (NOS) and cytochrome P450 reductase (CPR) (Dutton *et al.*, 1978). The Pt/calomel electrode consists of a solution of potassium chloride in contact with solid mercurous chloride (calomel) and mercury containing a platinum wire. The resulting redox potentials



measured using this electrode are expressed relative to the normal hydrogen electrode (NHE), with the correction factor being an addition of 244 mV.

The heme redox centres of proteins are frequently shielded by the protein body due to their situation near the centre of a protein molecule (Wirtz *et al.*, 2000; Garcia-Rubio *et al.*, 2007). This is particularly evident in the case of P450s, where the heme is typically buried in the hydrophobic core of the protein and well insulated. This fact in some way explains the rather poor electronic interactions of P450s with electrode surfaces and the general failure of cyclic voltammetry methods for redox cycling of this class of enzymes. To enhance communication between the heme redox centre and the measuring electrode, “bridging” with small organic or inorganic redox mediator agents is a frequently used method. In redox potentiometry (i.e. the spectroelectrochemical methods used here), mediators such as phenazine methosulphate (PMS, midpoint potential +80 mV vs. NHE), benzyl viologen (BV, -358 mV vs. NHE), methyl viologen (MV, -450 mV vs. NHE) and 2-hydroxy-1,4-naphthoquinone (HNQ, -152 mV vs. NHE) are frequently used to facilitate and expedite electrical communication between enzyme and electrode. Mediators are generally chosen to cover the redox potential range across which the redox active centre(s) in the enzyme are reduced, and are added to solutions in small (catalytic) amounts. The oxidant potassium ferricyanide, and the reductant sodium dithionite are used in titrations to reduce/oxidise the protein of interest. Dithionite and ferricyanide are often chosen for this role due to their very negative (dithionite) and positive (ferricyanide) standard midpoint reduction potentials ( $E^0$ ), which are sufficient to cover the range of reduction potentials observed for most cofactors in biological systems. Ferricyanide and dithionite often also react relatively quickly in solution with the protein under study (Dutton, 1978; Wilson, 1978).

To examine any altered thermodynamic properties from the wild-type CYP121, the reduction potential of the heme iron in the P346L mutant of CYP121 was determined by anaerobic spectroelectrochemistry of the protein solution. As previously described, the method involves the titration of the P450 with small amounts of oxidant or reductant, and recording applied potential and spectral change simultaneously when the system has

reached equilibrium. Several points are recorded across the range from oxidised to reduced cofactor (i.e. from ferric to ferrous heme iron). Data are then plotted (observed spectral change against applied potential) and fitted to the Nernst equation to derive the midpoint potential of the heme cofactor. The CYP121 P346L mutant proved to be extremely difficult to reduce to completion using dithionite even under anaerobic redox conditions (a reflection of the quite negative redox potential of the predominantly low-spin heme iron by comparison with that of dithionite (*ca.* -420 mV). The spectral changes observed during the redox titration of P346L are displayed in Figure 3.23.

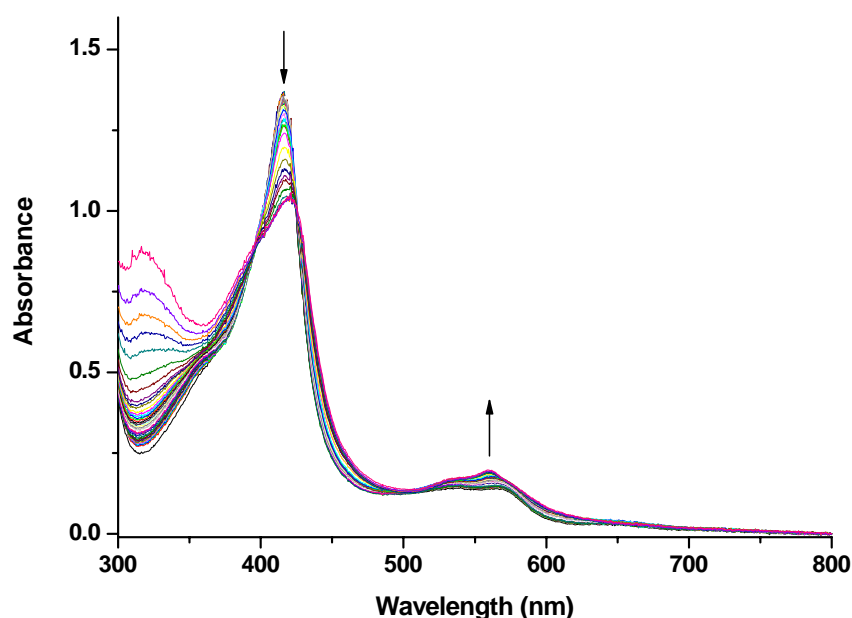


**Figure 3.23 Redox titration of CYP121 P346L**

Spectral changes observed for the CYP121 point mutant P346L ( $\sim 14 \mu\text{M}$ ) in 50 mM  $\text{KPi}$  pH 7.0 during a reductive titration. The starting spectrum is that with the most intense Soret band, and is for the oxidised, ferric form of CYP121 P346L with Soret maxima at 416.5 nm and  $\alpha$ - and  $\beta$ -bands at 565 and 533 nm, respectively. Successive spectra recorded on reduction of the P450 lead to decrease in Soret intensity. Arrows indicate direction of spectral changes during the reductive reaction. Increases in intensity are observed in the long wavelength region for the reduced enzyme. All changes were reversible (i.e. no hysteric effects observed) and upon full oxidation the spectrum returns to that almost identical to the starting form.

Titration of the CYP121 P346L mutant with dithionite resulted in decreases in the intensity of the Soret maximum at 416.5 nm with a small shift to longer wavelength (419

nm) for the ferrous enzyme. In addition, there is an increase in the absorption intensity in the visible region, where the  $\alpha$  and  $\beta$  bands absorb at 565 and 533 nm in the ferric enzyme. For the reduced form, there is development of a distinct absorption feature at 559 nm. Complete reduction of P346L proved unattainable under the reaction conditions and this is indicative of a very low redox potential. Dithionite is only capable of “driving” the reductive half-reaction to its own potential ( $\sim -420$  mV at pH 7.0) (Dutton, 1978) and is therefore unable to fully reduce the CYP121 P346L mutant since the midpoint  $\text{Fe}^{3+}/\text{Fe}^{2+}$  potential for the P450 is in the same range as that for the reductant. Figure 3.23 shows the accumulation of dithionite as a large peak forming at 300 nm towards the end of the titration (i.e. excess dithionite accumulates as the P450 reduction reaches its end point in the titration). Thus, as in the case of wild-type CYP121, it appears that full reduction of the P346L mutant cannot be achieved using dithionite, due to the relatively negative midpoint potential of the P450.

A Nernst function single electron fit (Figure 3.24) was performed by estimation and extrapolation of the reductive end-point, fixing the Nernst factor or slope ( $RT/F$  value) to 59, which corresponds to that expected for a one-electron redox couple at 25 °C. This method produced a very negative mid-point reduction potential for P346L at  $-430 \pm 28$  mV, compared to  $-440 \pm 37$  mV for wild-type CYP121. The values of P346L were thus consistent with those determined for the wild-type CYP121 and indicate the P346L mutation had relatively little effect on the redox potential of the heme iron. The relatively high errors associated with the midpoint potential estimates reflect the fact that reduction is not complete and that extrapolation is needed to obtain the estimate (Figure 3.24).

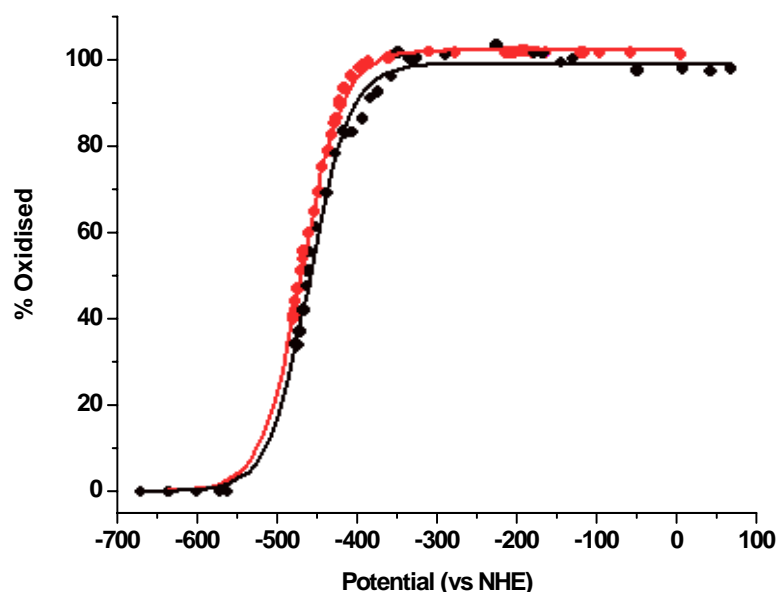


**Figure 3.24** Plot of proportion of ferrous (reduced) P450 enzyme against applied potential (vs NHE) for wild-type CYP121 and CYP121 P346L

The data at 416.5 nm (at the Soret peak for oxidised CYP121) were fitted to a single electron Nernst function and the end-point absorption values predicted to allow an estimation of the mid-point potentials for the two enzymes. The potentials determined were  $-440 \pm 37$  mV (wild-type CYP121, red) and  $-430 \pm 28$  mV (CYP121 P346L, black).

The CYP121 P346L mutant, as is the case for the wild-type CYP121, is difficult to reduce fully with dithionite in the absence of a *bona fide* substrate (which would be expected to produce a substantial amount of high-spin heme iron and thus make the reduction potential more positive). Thus, this quite negative redox potential value for wild-type CYP121 is unlikely to represent the catalytically relevant state of the P450, since it is rather more negative than the potential of its likely ultimate electron donor molecule, NAD(P)H ( $\sim -320$  mV). A similar difficulty in reduction (with dithionite) and a negative heme-iron reduction potential has also been reported for the P450 BM-3 system and for the camphor hydroxylase P450cam, although the mid-point reduction potential of CYP121 is significantly more negative than that for the P450cam system - 300 mV (Sligar, 1976), but reasonably similar to that for the substrate-free BM-3 heme domain ( $-427$  mV) (Ost *et al.*, 2001a). In the P450 BM-3 and P450cam enzymes, binding of fatty acid substrate and camphor, respectively, induces extensive shift in the heme iron

spin-state equilibrium towards the high-spin form, and an elevation of the reduction potential by ~140 and 130 mV, respectively (Sligar, 1976; Munro *et al.*, 1995). Such P450-substrate binding thus brings the systems into the redox potential range where the heme-iron can receive electrons - in the case of P450 BM-3 from the fused P450 reductase redox partner, and in the case of P450cam through the Fe<sub>2</sub>S<sub>2</sub> ferredoxin putidaredoxin. A similar mechanism may occur within the CYP121 redox system, with a shift in spin-state equilibrium occurring on binding of the natural substrate(s), enabling the P450 to be reduced effectively in the cell by its natural redox partner(s).

Substrate binding close to the heme in P450s typically displaces the aqua ligand from the 6<sup>th</sup> coordination position on heme iron, causing an electronic rearrangement in the iron d orbitals and a low- to high-spin heme iron spin-state change. There is a noted link between the modulation of P450 spin-state and redox potential in certain systems, with a more positive heme iron reduction potential expected on conversion of the heme iron to the high-spin form, as observed for potentiometric measurements in both the P450cam and P450 BM3 systems (Sligar, 1976; Dutton, 1978; Munro *et al.*, 1995).

Accordingly, there is a direct correlation between substrate binding and the perturbation favouring the shift to the high-spin heme iron state, and with positive increases in the heme-iron redox potentials of at least selected P450s (Sligar, 1976; Sligar and Gunsalus; 1976). This mechanism may act as a ‘redox switch’, checking the *in vivo* uncoupled consumption of NAD(P)H and preventing oxygen reduction at the heme iron if there is no substrate available for oxygenation.

Analysis of the Fe<sub>3</sub>S<sub>4</sub> *M. tuberculosis* ferredoxin encoded by the *Rv0763c* gene (located adjacent to the CYP51 gene in the genome) has indicated that it can support the catalytic function of CYP121, despite that fact that the protein measured in isolation has a far more positive reduction potential ( $E^0 = -31 \pm 2$  mV) than does the CYP121 heme-iron (McLean *et al.* 2006).

Such a large difference in the redox potential values between CYP121 and the ferredoxin make it difficult to rationalise how this enzyme could be an efficient redox partner for CYP121 *in vivo*, even if the binding of CYP121's natural substrate elevates the reduction potential of the heme iron by  $\sim 130$  mV. If such a redox partner was to be utilised by CYP121, a very large thermodynamic gradient would have to be overcome for the successful transfer of electrons. Such an impediment may be overcome by the interaction of the ferredoxin encoded by *Rv0763c* (or another *M. tuberculosis* ferredoxin) with wild-type CYP121. Such a redox component interaction could alter the electronic environments of both the heme and iron-sulfur cofactors, leading to favourable changes in the redox potentials of one or both centres and facilitating equilibration of electrons between the ferredoxin and the (substrate-bound) P450. For example, the P450cam redox partner, putidaredoxin, has a redox potential of  $-240$  mV, which only permits supply of electrons to P450cam upon binding camphor, with a resultant increase in the heme iron redox potential from  $-300$  mV to  $-173$  mV (Sligar 1976).

Similar events apparently occur in the microsomal P450/CPR system, although the reduction of substrate-free P450 enzymes is permissible in many cases, and a number of the microsomal P450s are extensively high-spin in their resting forms. By contrast, P450BM-3 exhibits virtually no electron transfer to its heme iron in absence of substrate, although oxidation of the flavins produces superoxide/peroxide radicals (Munro *et al.*, 1995; Guengerich and Johnson, 1997). Ultimately, the reduced P450 is required to reduce molecular dioxygen in two sequential stages (see section 1.2.3). Upon reduction of the ferric heme iron, the ferrous form rapidly binds oxygen, and the catalytic process may be irreversible at this point due to this species having a more positive potential and taking a second electron from the ferredoxin or CPR redox partner, leading to rapid progression of the P450 through the catalytic cycle. Thus, the second reduction step could involve electron transfer to a heme iron intermediate species (specifically the ferric superoxy form) that has even more positive reduction potential than the resting ferric (high-spin) form. There may also be a regulatory prerequisite in *M. tuberculosis* to strictly control this (and other) P450 redox system(s), by carefully controlling the turnover rate through the imposition of a thermodynamic barrier, which may serve to limit rate in relation with

the slow growth rate of the pathogen. The high energy demands for the generation and maintenance of the *M. tuberculosis* lipid rich cell wall has been proposed as a potential limiting factor in growth rate (Lewin and Sharbati-Tehrani, 2005).

### **3.7 Ligand binding studies of the P346L mutant of CYP121**

#### **3.7.1 Inhibitor binding**

The rising incidence of invasive tuberculosis infections and the emergence of broader *M. tuberculosis* resistance have led to the need for novel anti-tuberculosis agents (Solis *et al.*, 2005). To date, the azole-class of antifungal derived agents are a major group of drugs that have been approved for treating invasive fungal infections (Torres *et al.*, 2005). Previous studies by Munro and colleagues have noted the capability of commercially available anti-fungal azoles to bind tightly to wild-type CYP121 and to act bacteriostatically on *M. tuberculosis* (McLean *et al.*, 2002b). The activity of the compounds in *in vitro* studies (McLean *et al.*, 2002b) suggests that azoles represent a potentially important addition to the anti-TB armoury. The azole-class inhibitors comprise a nitrogen heterocyclic ring with the nitrogen atom able to co-ordinate to the P450 heme-iron via the displacement of the distal H<sub>2</sub>O molecule, thus inactivating the function of the enzyme as described in section 1.2.6. Typically, inhibitor binding is observed through an induced shift in P450 absorbance, with the Soret band displaying a red shift to ~424 nm. The commercial anti-fungal P450 inhibitors clotrimazole, econazole, ketoconazole, fluconazole, voriconazole and miconazole (Figure 1.5) were used to study interactions with the CYP121 P346L protein, as previously reported for the wild-type CYP121 (McLean *et al.*, 2002b). In light of the lack of a known substrate for wild-type CYP121, ligand binding with antifungal azoles was performed on the P346L isoform of CYP121 to characterize its active site and variations in azole affinity with the wild-type CYP121.

The azole compounds were seen to induce shifts in the absorbance maximum of the Soret band of CYP121 P346L. The binding of the selected azole inhibitors to CYP121 P346L was investigated as described previously (McLean *et al.*, 2002b). Titrations with the azole anti-fungals ketoconazole, fluconazole, miconazole,

clotrimazole and econazole indicated tight binding to CYP121 P346L. Typical azole-induced changes in absorbance of CYP121 P346L are displayed in Figure 3.25 upon addition of successive amounts of ketoconazole.

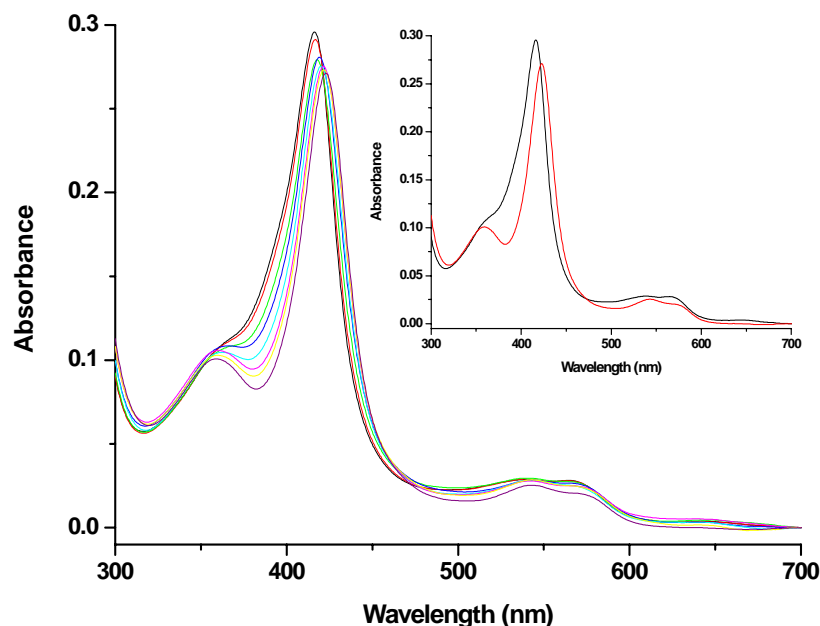


**Figure 3.25 Binding of ketoconazole to the P346L mutant of CYP121**  
 UV-visible spectra displaying a titration of CYP121 (3  $\mu$ M) in 50 mM Tris-HCl, 1mM EDTA (pH 7.2) with successive additions of ketoconazole at 0, 0.38, 1.13, 2.63, 3, 5.25, 5.62 and 7.88  $\mu$ M (black, red, green, blue, cyan, magenta, yellow and purple lines respectively). The full extent of the absorbance shift is shown (inset) with inhibitor-free (black) and inhibitor-saturated (red) forms.

Ketoconazole induced a shift in the absorbance maximum for CYP121 P346L from 416.5 nm to 425 nm. Also noted upon azole binding is the spectral fusion of the  $\alpha$ - and  $\beta$ - bands to form a new, broad spectral species with maximum at 530 nm (Figure 3.25). The red-shifted spectral perturbation upon azole ligation suggests reinforcement of the low-spin heme state of CYP121.

In order to analyse the titration with ketoconazole, a difference spectrum was constructed at each point by the subtraction of the spectrum for the inhibitor-free form



from each successive inhibitor-bound spectrum in the titration. These difference spectra are displayed in Figure 3.26.

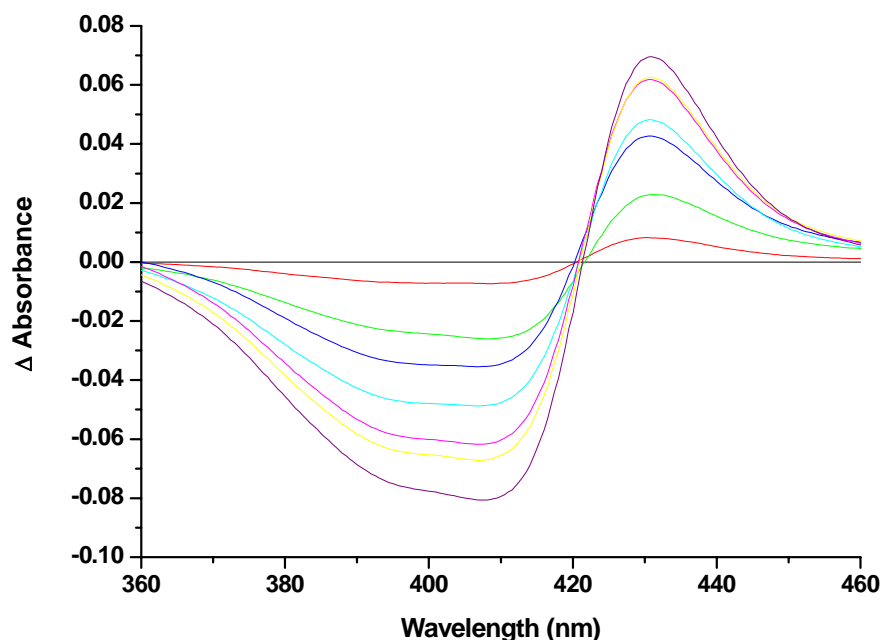


**Figure 3.26** Difference spectra for P346L mutant of CYP121 titrated with ketoconazole

Difference spectra were created by the subtraction of the spectrum for ketoconazole-free P450 from those at various other concentration of the drug: 0.38, 1.13, 2.63, 3, 5.25, 5.62 and 7.88  $\mu\text{M}$  (black, red, green, blue, cyan, magenta, yellow and purple lines respectively). Difference spectral maxima and minima are at 432 nm and 407 nm, respectively.

The difference spectra generated for the titration of the CYP121 mutant with ketoconazole display maxima and minima values at approximately 431 nm and 407 nm, respectively. The type II binding spectrum is characterised by a peak and a trough at the aforementioned wavelengths. For each concentration of ketoconazole, the maximal absorbance difference was determined by subtraction of the absorbance value at the trough from that at the peak in each difference spectrum (using the same  $\lambda$  values for each). These values were subsequently plotted against the corresponding concentration of ketoconazole, and the data fitted to a standard hyperbolic function, to determine the dissociation constants ( $K_d$ ), Figure 3.27.

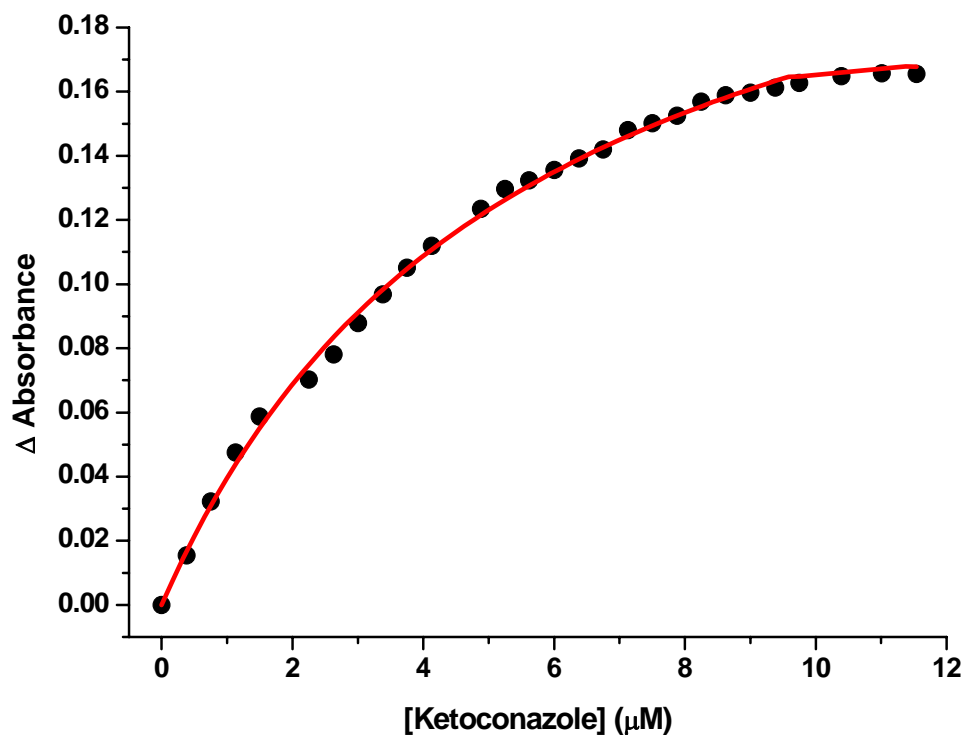


**Figure 3.27 Titration curve for the binding of ketoconazole to P346L mutant of CYP121**  
 CYP121 P346L (~3 μM). Data from the difference spectra ( $\Delta A_{430}$  minus  $\Delta A_{408}$ ) were fitted to a hyperbolic function, yielding a  $K_d = 4.20 \pm 0.23$  μM.

The  $K_d$  values were determined for all azoles as previously described, and compared with azole  $K_d$  values measured for wild-type CYP121 (Table 3.7).

<b>Inhibitor</b>	<b>P346L mutant <math>K_d \pm \text{error}</math> (<math>\mu\text{M}</math>)</b>	<b>Wild-type CYP121 <math>K_d \pm \text{error}</math> (<math>\mu\text{M}</math>)</b>
<b>Clotrimazole</b>	<b><math>0.11 \pm 0.02</math></b>	<b><math>0.07 \pm 0.03</math></b>
<b>Econazole</b>	<b><math>0.02 \pm 0.01</math></b>	<b><math>0.31 \pm 0.04</math></b>
<b>Miconazole</b>	<b><math>0.52 \pm 0.05</math></b>	<b><math>0.09 \pm 0.05</math></b>
<b>Ketoconazole</b>	<b><math>4.20 \pm 0.23</math></b>	<b><math>3.30 \pm 0.30</math></b>
<b>Fluconazole</b>	<b><math>36.2 \pm 2.5</math></b>	<b><math>9.70 \pm 0.60</math></b>
<b>1H-1,2,4-Triazole, 1-tricyclo(3.3.1.1<sup>3,7</sup>)dec-1-yl (referred to as compound A)</b>	<b>No binding</b>	<b>No binding</b>

**Table 3.7**      **Dissociation constants ( $K_d$  values) for inhibitors binding to the P346L mutant of CYP121**

Data were generated from spectral titrations using the quadratic function (equation 2, section 2.6.1) for clotrimazole, econazole and miconazole, and from fitting to the hyperbolic function (equation 3, section 2.8.1) in the case of ketoconazole, and fluconazole. No binding (by spectral perturbation) was observed with compound A. Data are compared with those for wild-type CYP121.

The azole antifungal drugs clotrimazole, econazole, fluconazole, ketoconazole and miconazole induced in the P346L mutant a shift of the Soret maximum to  $\sim 425$  nm, resulting in the reinforcement of low-spin heme iron in the azole complexes. In addition, all induced an apparent spectral fusion of  $\alpha$ - and  $\beta$ - bands, leading to a new spectral feature centred at  $\sim 554$  nm. These spectral perturbations were similar to those observed

for wild-type CYP121 upon azole titrations (McLean *et al.*, 2002b). The affinity of the azoles for CYP121 P346L followed the same pattern as that observed with wild-type CYP121, albeit in general with slightly lower affinities for the mutant. As in the case of wild-type CYP121, fluconazole titrations were also revealed to have the lowest affinity and clotrimazole the highest affinity (McLean *et al.*, 2006). The differences suggest that conformational change directly within the heme macrocycle, or indirectly in the active site, may result in some disruption of azole binding to the mutant P346L isoform, and somewhat lower azole affinities. However, the  $K_d$  values are still in the micromolar binding range indicating that any structural change is small, as also indicated by crystal structures (section 3.10.1).

In view of the apparent strong affinity of CYP121 for structurally varied azoles, and to further probe the spatial properties of CYP121, 1H-1,2,4-Triazole, 1-tricyclo(3.3.1.1<sup>3,7</sup>)dec-1-yl (referred to as compound A, Figure 3.28) was kindly provided by Dr Sandeep Modi, GlaxoSmithKline, Stevenage, for binding assays. The core structure of this molecule consists of adamantane carboxylate with a triazole side chain. Successive titrations of compound A to the P346L and CYP121 induced no perturbation of the heme spectrum, unlike in CYP151A2 (section 5.10.2). This further highlighted the specificity of the CYP121 enzyme for sterol metabolising P450-type inhibitors. It should be noted that we cannot rule out that compound A does bind to CYP121 and its P346L mutant. However, any binding cannot be in the immediate vicinity of the heme and cannot involve direct heme iron coordination.

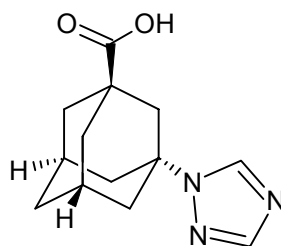


**Figure 3.28** Chemical structure of the adamantane triazole derivative 1H-1,2,4-Triazole, 1-tricyclo(3.3.1.1<sup>3,7</sup>)dec-1-yl, referred to as compound A in this study, and provided by Dr Sandeep Modi, GSK, Stevenage.

The binding of clotrimazole, econazole, and miconazole to the P346L mutant of CYP121 were too tight to analyse accurately, even at low concentrations of the enzyme ( $<1.0\ \mu\text{M}$ ) (Table 3.7). For these azoles, the optical change associated with azole ligation occurred linearly with azole concentration, sharply reaching a plateau and indicative of near-stoichiometric binding to the P450. However, to circumvent problems fitting the data, the quadratic function was used (Equation 2). This function compensates for P450 consumed in an azole-P450 complex at each point in the titration. Data fitting to the equation resulted in a rather more accurate determination of values for tight-binding ligands. At such high affinities, it should be noted that fitting clotrimazole, econazole and miconazole binding data to the described quadratic equation likely does not provide a highly accurate  $K_d$  value. However, the binding of these ligands to the P346L mutant indicates broadly similar affinity to that for wild-type CYP121. It is possible that the  $K_d$  in each case may be even lower than predicted, and at least half the enzyme concentrations, an occurrence previously described with fatty acid-linked inhibitors for P450 BM-3 (Ortiz de Montellano and Correia, 1995).

This tight azole binding observed for the P346L enzyme indicates that the mutant has not altered the apparent preference of CYP121 for interaction with bulky polycyclic type molecules (McLean *et al.*, 2002b). The noted specificity of CYP121 for the antifungal azoles highlights the potential role of the hydrophobic residues of the largely apolar active site in ligand binding, as opposed to the primary determinant of affinity being ligation of the azole group to the ferric heme iron.

### **3.8 Protein-lipid overlay assay**

Protein-targeting interactions play a central role in most biological processes. The detection and analysis of such interactions *in vitro* can provide important information on specificity, affinity and structure–function relationships that are realised via these interactions. Blotting of DNA, protein and lipids has proven to be a highly versatile technique and new applications based on it are being continually developed. Protein overlay assays are very powerful techniques for detecting and analysing the proteins or protein motifs involved in cellular-targeting processes. These methods are based on the

principle that ligands can be transferred to an immobilising matrix (e.g. nitrocellulose or nylon membrane) and can then be screened with putative binding partners, followed by subsequent appropriate detection methods to examine the complexes formed. Protein-lipid overlay assays are suitable tools for the identification of ligands for lipid-binding proteins (Dowler *et al.*, 2002).

Nitrocellulose is the most widely used matrix and in its use for blotting, nitrocellulose serves as a 'depth filter' in which the macromolecules are absorbed throughout the matrix, predominantly by chemical interaction rather than sieving (Gershoni and Palade, 1983). Despite the considerable amount of research that has been conducted since nitrocellulose was first used as a binding membrane, the exact mechanism of binding remains largely unknown (Harlow and Lane, 1988). It is known that a number of forces are involved; specifically, hydrophobic interactions, hydrogen bonding, and electrostatic interactions, of which the hydrophobic effects are believed to be a key component. However, a clear understanding of the precise effect and significance of each force has remained elusive. Grounds for the hydrophobic effect relates to protein electroelution performed at pH 8 and results in nitrocellulose being negatively charged (Gershoni and Palade, 1983). In addition, non-ionic detergents may elute proteins absorbed to nitrocellulose (Schneider, 1980; Farrah *et al.*, 1981). Direct experimental evidence for the hydrophobic effect is provided from the hydrophobic interaction of the lipid moiety of a glycoconjugate, which allows the molecule to bind to nitrocellulose (Handman and Jarvis, 1985).

An important requirement in the characterisation of CYP121 has been the need to discover the native substrate of CYP121. Indeed, given the variety and complexity of the mycobacterial envelope in terms of lipophilic compounds, the catalytic function of CYP121 may well be involved in the biosynthesis/metabolism of these important *M. tuberculosis* components. In an attempt to identify and demonstrate an interaction between CYP121 and a *M. tuberculosis* ligand(s), binding studies were carried out using the lipid-protein overlay method developed by Alessi and co-workers (Dowler *et al.*, 2002). Sequential thin layer chromatography lipid extracts from *M. tuberculosis* (Erdman

strain), based on chloroform:methanol extraction, were kindly provided by Dr. Mary Jackson, Pasteur Institute, Paris. By this simple and quick method, lipids were immobilised on a nitrocellulose membrane, and the binding assayed by incubation with His-tagged CYP121 (His-CYP121), followed by immunostaining with an anti-His tag antibody. Ultrapure non-acetylated BSA and non-ionic Tween 20 were used as blocking agents to prevent the non-specific binding of His-CYP121. His-CYP121 was probed and detected by application of a rabbit anti-His primary antibody, and this was followed by incubation with anti-rabbit horseradish peroxidase-conjugated secondary antibody.

Figure 3.29A demonstrates a physical interaction between His-CYP121 and lipid extracts named 60:40 and 96:4, representing chloroform:methanol ratios used for their isolation. His-CYP121 showed strongest interaction with the apolar lipid extract 96:4, with some weak interaction with the 60:40 lipid extract, perhaps indicative of some non-specific binding in the latter case. No interaction was observed with other immobilised lipid extracts, or with the negative control corresponding to 10  $\mu$ l of the chloroform or the chloroform:methanol extraction solution used. The negative control membrane, prepared in the same manner as the reaction membrane, but incubated without His-CYP121, produced no positive signals. This indicated that the His-CYP121 positive results observed in the membrane (Fig 3.29A) are specific to the presence of the protein and are not due to interactions involving other components used in the assay (Figure 3.29B).

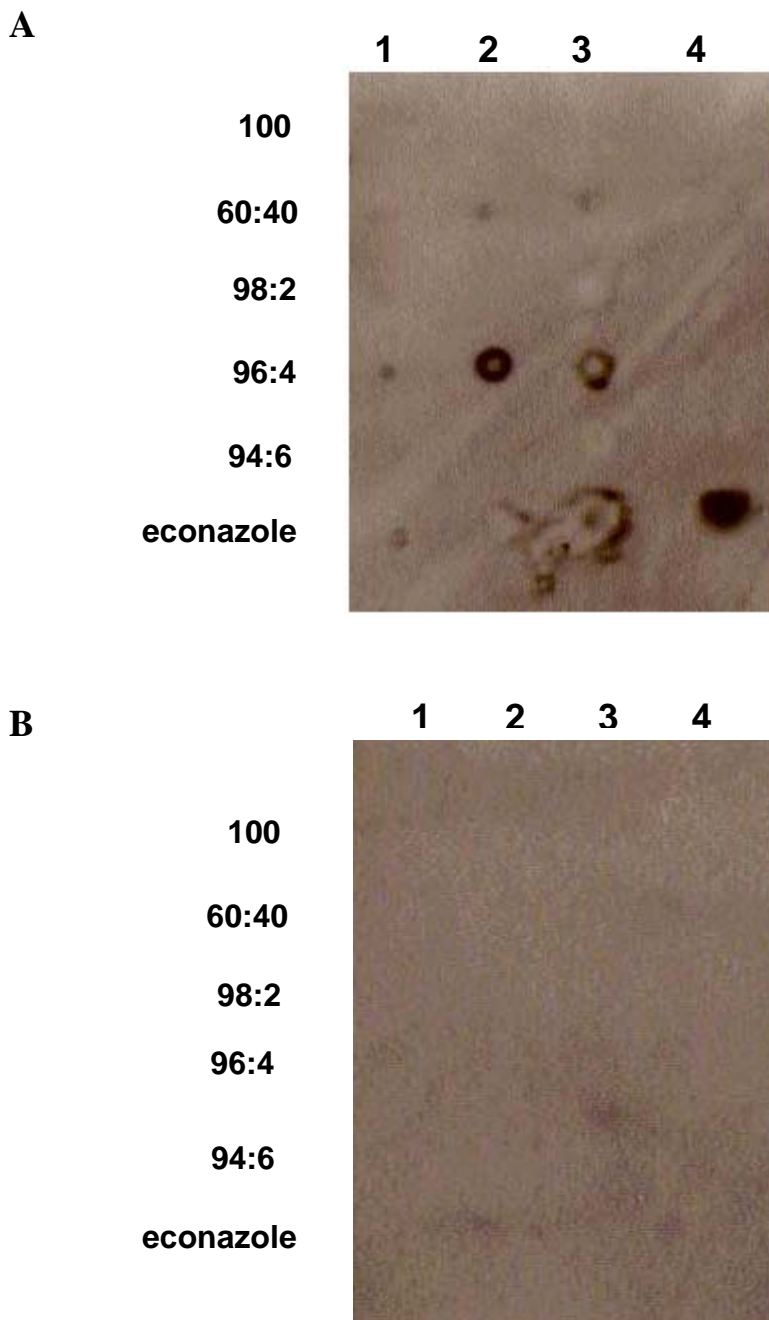


**Figure 3.29 A and B Protein-lipid overlay assay**

Assays employed CYP121-His protein. Nitrocellulose membrane strips spotted with a variety of lipid extracts were incubated with CYP121-His (Figure A). Rows 100, 60:40, 98:2, 96:4, 94:6 correspond to the chloroform:methanol ratio used to isolate the different *M. tuberculosis* lipid fractions, where 100 corresponds to 100 % chloroform. Lanes 1, 2, 3 correspond to the volume ( $\mu$ l) of each extract at 1, 5, 10  $\mu$ l of each chloroform:methanol lipid extract added, whilst 4 refers to a control of 10  $\mu$ l of the lipid solvent used for extraction. Controls were carried out without the CYP121-His (panel B). Negative controls for each extract were set-up, corresponding to the chloroform or chloroform:methanol ratio used at 10  $\mu$ l. Econazole was also used as a potential positive reaction, where lane 1 = 0.2  $\mu$ M; 2 = 1  $\mu$ M; 3 = 10  $\mu$ M econazole. The negative control for econazole was the solvent DMSO at 10  $\mu$ l.



A cautious approach must be adopted in the interpretation of the results (Fig 3.29 A). The observed weak interaction and rim binding observed with the 60:40 and 96:4 extracts, respectively, is possibly indicative of some non-specific binding. Non-specific protein binding results from an unwanted interaction between the protein and the lipid sample. Such interactions can be the result of any of the common causes of protein attachment, including charge attraction, hydrophobicity and hydrogen bonding. However, non-specific attachment to the membrane should be reduced or prevented by the blocking with BSA and the surfactant Tween 20. Titration of the lipid extracts (that resulted in positive signals with His-CYP121) caused no apparent spectral changes by UV-visible absorbance spectroscopy. However, due to the apolar nature of these lipid extracts, a UV-visible absorbance spectroscopy spectral change may be difficult to achieve in aqueous buffer.

Even though such spot assays have proven very useful in the initial identification and analysis of lipid-binding proteins, data from more specific methods, such as EPR, are required to confirm the results and confirm interactions between lipids and the P450 active site (Misra *et al.*, 2001; Lemmon, 2003). There are several aspects that need to be considered when interpreting results generated via overlays, including (a) some lipids may bind weakly to the immobilising matrix; (b) reactivity to some proteins or ligands can be lost because of the denaturing effects of absorption; and (c) some protein complexes may form only in specific microenvironments that are difficult to reproduce in *in vitro* studies.

The precise composition of the lipid extracts is unknown, but it is likely that the apolar lipophilic cell envelope components represent a large proportion of the extracts. Therefore, it is envisaged tentatively that the lipid extracts which produced the strongest signals may contain the major constituents of the lipid protective layer such as glycopeptidolipids and the highly oxygenated and adorned mycolic acids. Recent work by Besra and colleagues (Burguiere *et al.*, 2005) has established that econazole and clotrimazole inhibit glycopeptidolipid (GPL) biosynthesis in *M. smegmatis*. The aforementioned clinical azole drugs, along with other clinically applied azole drugs such

as miconazole and ketoconazole, have been demonstrated to be effective inhibitors of the *M. tuberculosis* P450s CYP51 and CYP121, with dissociation constants in the low  $\mu\text{M}$  and nM range (Hartman *et al.*, 1997; Bellamine *et al.*, 1999; Guardiola-Diaz *et al.*, 2001; McLean *et al.*, 2002b). In particular, clotrimazole was found to inhibit production of all four types of polar de-*O*-acylated GPLs (dGPLs) found in *M. smegmatis*, which vary from one to another by the presence or absence of *O*-methyl groups on the fatty acyl chain and/or the rhamnose sugar. This is suggestive of an early and common clotrimazole target within the GPL biosynthetic pathway. Altogether, the studies previously outlined suggest that an azole-specific target, possibly a cytochrome P450, may be involved in the hydroxylation of the amide-linked long-chain fatty acid in GPL biosynthesis (Burguiere *et al.*, 2005).

The composition of the outer layer varies between species of mycobacteria, but generally contains a mixture of GPLs glycolipids and phospholipids. GPLs comprise an abundant lipid of the outer-layer of several non-tuberculous mycobacteria that cause opportunistic infections (*Mycobacterium avium* complex, *M. peregrinum*, *M. chelonae*, *M. abscessus* and *M. avium paratuberculosis*) and saprophytic mycobacteria such as *M. smegmatis* (Aspinall *et al.*, 1995; Brennan and Nikkaido, 1995; Daffé and Draper, 1998). The GPLs represent surrogate markers for mycobacterial species, such as *Mycobacterium xenopi* (Besra *et al.*, 1993), as well as providing the basis for MAC serovaration (Krzywinska *et al.*, 2004). GPLs are also found in saprophytic mycobacteria, such as *M. smegmatis*, and in animal pathogens, such as *M. avium* (Camphausen *et al.*, 1988). In a recent study, the GPLs of *M. smegmatis* were shown to be involved in the inhibition of non-opsonic phagocytosis of mycobacteria by human macrophages (Villeneuve *et al.*, 2003).

The GPLs consist of a tripeptide-amino alcohol core, D-Phe-D-allo-Thr-D-Ala-L-alaninol, which is linked with a combination of 3-hydroxy and 3-methoxy C<sub>26-34</sub> fatty acids at the N-terminal D-Phe through amide linkage (Belisle *et al.*, 1993). The D-allo-Thr and the terminal L-alaninol are further linked with 6-deoxytalose (6-dTal) and *O*-methyl rhamnose, respectively, to form nsGPL (Patterson *et al.*, 2000). These apolar

GPLs are found in all members of the MAC family and *M. smegmatis* (Belisle and Brennan, 1989; Aspinall *et al.*, 1995). Although the study did not identify a specific azole-intracellular target, it would appear likely that the drugs *in vivo* inhibit P450(s), with the hydroxylated amide-linked long-chain fatty acid of nsGPLs the most apparent target.

The high molecular weight (C<sub>60</sub>–C<sub>90</sub>) mycolic acids consist of  $\alpha$ -alkyl,  $\beta$ -hydroxy fatty acids, and are produced by all known species of mycobacteria. Within the cell wall, mycolic acids are arranged in a bilayer, forming the inner low fluidity permeability barrier, separate from the plasma membrane (Liu *et al.*, 1995). Prominent mycolic acid-based features of the cell envelope are the arabinogalactan-mycolate covalently linked to the cell wall peptidoglycan via a phosphodiester bond located on the inner leaflet of the outer membrane (McNeil *et al.*, 1991), and a free glycolipid called trehalose dimycolate, which accumulates in a cord-like fashion on the surface of the cells (Takyama *et al.*, 2005). These macromolecules constitute 40–60% dry weight of the cell envelope complex (Minnikin, 1982), providing a thick layer of lipid on the outer part of the cell to protect the tubercle bacillus from noxious chemicals and the host's immune system. Significant changes in the fluidity of this inner layer, resulting in changes in permeability, have been shown to occur from alterations in the proportion and structures of mycolic acids (George *et al.*, 1995; Jackson *et al.*, 1999). Previous studies have shown inactivation of *fbpC*, a gene coding for one of the three mycoloyl transferases (Belisle *et al.*, 1997), resulted in a significant decrease in the level of all cell wall-linked mycolates, and an increase in the permeability of the cell envelope; but the inactivated strain remained viable in macrophages (Jackson *et al.*, 1999). However, econazole and clotrimazole have been reported to have no inhibitory effect on mycolic acid synthesis, with the mycolic acid profile similar to that observed typically for non-azole treated *M. smegmatis* (Burguiere *et al.*, 2005).

### **3.9 Susceptibility testing of azole drugs against *M. tuberculosis***

Development of drugs with potent anti-mycobacterial activity is crucial with TB, especially since the MDR-TB form is becoming increasingly a burden on public health

resources. No significant addition has been made to the armoury of antitubercular drugs in recent years. Previous experiments with azoles have already shown that the growth of *M. smegmatis*, which is a saprophytic strain of mycobacteria, is inhibited (Jackson *et al.*, 2000; McLean *et al.*, 2002b). Thus azoles offer potential as novel antitubercular drugs.

Testing the susceptibility of bacteria to antimicrobial agents likely to be used in treatment is an important aspect in clinical use of such agents. Three different growth-based laboratory methods have been traditionally used for determining antimicrobial susceptibility of *M. tuberculosis*: (1) the resistance ratio method, (2) the absolute concentration method, and (3) the proportion method (Inderlied and Nash, 1996). These traditional or conventional methods for mycobacterial culture utilise media containing egg or potato base (Middlebrook 7H10 or 7H11) or albumin (Lowenstein Jensen's medium, LJ). While these media effectively support the growth of mycobacteria, incubation of up to several weeks (2-8 weeks) is necessary before growth can be detected. Also, an equivalent amount of time may be required to test for the susceptibility of the isolate to anti-TB therapy.

Because anti-tuberculosis susceptibility testing on solid media requires visible growth of the organisms (requiring several weeks of incubation), testing is increasingly preferred in liquid media. A significant advance in culturing methods has been obtained with the introduction of the rapid radiometric mycobacterial detection system, BACTEC-460 TB (Becton Dickinson Diagnostic Instruments Systems). The introduction of this liquid based growth system, established more than 20 years ago, has significantly reduced the time required to obtain results (Eltringham *et al.*, 1999). The BACTEC radiometric system for mycobacterial culture is considered the gold standard for rapid identification and susceptibility testing of mycobacterial strains. The BACTEC-460TB requires less than 10 days of incubation before results are available (Siddiqi, 1995; Pfyffer *et al.*, 2002). BACTEC drug susceptibility is determined by following a modified version of the conventional proportion method (Canetti *et al.*, 1969). The critical proportion for resistance is taken as 1 % for all anti-tuberculosis drugs. This means that if 1 % or more of the test mycobacterial population is resistant, the culture is considered resistant for

laboratory reporting purposes. Resistance is determined by comparing the rate of growth in the control vial and the 12B Medium (consisting of Middlebrook 7H9 media) vials containing the test drug. The contents of the pre-grown culture vial (from the BACTEC vial) are properly homogenised with a hypodermic syringe and a needle. Homogenisation enables breaking the clumps of *M. tuberculosis* growth, thus facilitating proper dispersion of organisms in the medium. If not properly homogenised, there are fair chances of less inoculum or larger clumps being pipetted out for the assay, both of which will lead to misinterpretation of the assay results. Use of low inoculum will mean that a lower number of viable organisms will be infected and a lower number of plaques will be visible for enumeration.

The basic principle of the BACTEC radiometric susceptibility assay for mycobacteria is similar to the one utilised in the primary isolation procedure. When mycobacteria grow in B12 medium containing  $^{14}\text{C}$ -labeled substrate, they utilise the substrate and  $^{14}\text{CO}_2$  is produced. The amount of  $^{14}\text{CO}_2$  detected reflects the rate and amount of growth occurring in the vial, and is expressed in terms of the growth index. When an antituberculous drug is added to the medium, suppression of growth occurs if the test organisms are susceptible. This suppression can be detected by either a decline or a very small increase of the daily growth index as compared to the control. However, if the organisms are resistant to drugs, no suppression occurs.

To determine the 1 % proportion of resistance, the bacterial inoculum used in the control vial is one-hundred fold less than that used for the drug-containing vial. The drug and control vials are tested daily after inoculation. The rate of increase in the growth index, or the amount of change over that of the previous day, called delta ( $\Delta$ ) growth index, is compared between the control vial and the vials containing drugs. If the daily growth index increase in the drug vial is equal to or greater than that in the control vial, the test organisms are considered resistant to the drug. For a susceptible population, the daily growth index increase for the control would be higher than that of the drug vial. For example, if 1 % of the mycobacterial population is resistant to a anti-microbial agent, then 99 % of the organisms would be inhibited by the agent and only 1 % will grow in

the drug vial. The growth rate in the drug vial would be similar to the growth rate in the control vial in which the original bacterial inoculum was only 1/100 of that in the drug vial.

In collaboration with Dr. Laurent Marsollier, Unite de Genetique Moleculaire Bacterienne, Institut Pasteur, Paris, the susceptibility of *M. tuberculosis* to azole drugs was analysed using the BACTEC-460TB radiometric method. The azole drug susceptibility results on *M. tuberculosis* (H37Rv) are summarised in Table 3.8.

<b>Azole drugs and control</b>	<b>MIC value for <i>M. tuberculosis</i> (H<sub>37</sub>Rv) in <math>\mu\text{M}</math> (<math>\mu\text{g ml}^{-1}</math>)</b>	<b>MIC value for <i>M. smegmatis</i> (mc<sup>2</sup>155) in <math>\mu\text{M}</math> (<math>\mu\text{g ml}^{-1}</math>) (McLean <i>et al.</i>, 2002b)</b>	<b>CYP121 <math>K_d</math> value in <math>\mu\text{M}</math> (<math>\mu\text{g ml}^{-1}</math>) (McLean <i>et al.</i>, 2006)</b>
<b>Econazole</b>	<b>21 (8)</b>	<b>&lt;0.2 (&lt;0.1)</b>	<b>0.03 (0.01)</b>
<b>Miconazole</b>	<b>19 (8)</b>	<b>2.6 (1.1)</b>	<b>0.09 (0.04)</b>
<b>Ketoconazole</b>	<b>30 (16)</b>	<b>38 (20)</b>	<b>3.57 (1.89)</b>
<b>Clotrimazole</b>	<b>32 (11)</b>	<b>0.3 (&lt;0.1)</b>	<b>0.07 (0.02)</b>

**Table 3.8** Azole MIC values for *M. tuberculosis* (H37Rv) and *M. smegmatis* (mc<sup>2</sup>155)

The azole susceptibility assay with *M. tuberculosis* H37Rv indicated that the strain was susceptible to a range of azole antifungal drugs, and these were compared with the MIC values obtained for *M. smegmatis* (McLean *et al.*, 2002b). According to the results achieved for BACTEC-460TB in this study, the critical concentrations were lowest for miconazole (19  $\mu\text{M}$ ; 8  $\mu\text{g ml}^{-1}$ ) and econazole (21  $\mu\text{M}$ ; 8  $\mu\text{g ml}^{-1}$ ). The MICs of ketoconazole (30  $\mu\text{M}$ ; 16  $\mu\text{g ml}^{-1}$ ) and clotrimazole (32  $\mu\text{M}$ ; 11  $\mu\text{g ml}^{-1}$ ) were higher. Fluconazole was not tested due to previously poor MIC results for *M. smegmatis* (McLean *et al.*, 2002b). Therefore, for these four azole drugs a break-point for the critical MIC concentration was established, which varied significantly from the previous azole drug susceptibility tests on *M. smegmatis* (McLean *et al.*, 2002b). DMSO, used as the

solvent for the azoles, had no effect on cellular growth at the concentrations used (<0.1%). The data clearly established the working critical concentrations of the test drugs in the BACTEC-460 TB system, which yielded dissimilar set of results from those obtained with the plate proportion method for *M. smegmatis* (McLean *et al.*, 2002b) (Table 3.8). Overall, the *M. tuberculosis* MICs were significantly higher than observed with *M. smegmatis* (>80-fold in the case of econazole). In contrast, the first line antituberculosis drugs, rifampicin and isoniazid have significantly lower reported MIC values of 0.4 µg ml<sup>-1</sup> (0.5 µM) and 0.2 µg ml<sup>-1</sup> (1.5 µM) by the proportion method (Chanwong *et al.*, 2007). Furthermore, the order of the azole drugs' strength did not correlate with the  $K_d$  values of binding to the CYP121 enzyme (Table 3.8), as was observed in the case of *M. smegmatis*. However, in both *M. tuberculosis* and *M. smegmatis*, econazole was a leading azole drug, while ketoconazole was the least effective inhibitor.

A recent study determined that the MIC of the intravenous tolerated ketoconazole against virulent *M. tuberculosis* H37Rv in 7H9 liquid medium was 8–16 µg ml<sup>-1</sup> (Byrne *et al.*, 2007), which supports the result obtained in this study. Ketoconazole was also found to have enhanced activity against dormant, non-growing bacilli *in vitro* when combined with pyrazinamide and rifampicin. The *in vivo* activity of ketoconazole was evaluated in established pulmonary TB in the murine model, compared alone and in combination with isoniazid, pyrazinamide and rifampicin. Ketoconazole alone exhibited little effect after short-term treatment, with a very limited bacteriostatic effect on spleen colony counts, but not on lung counts. Ketoconazole, in combination with isoniazid, pyrazinamide and rifampicin, significantly improved the treatment outcome in the lungs when compared with treatment with isoniazid, pyrazinamide and rifampicin alone. The bacilli count in lungs was lowest in mice treated with a combinatorial therapy of ketoconazole, pyrazinamide and rifampicin (Byrne *et al.*, 2007).

Prior studies by Khuller and colleagues (Ahmad *et al.*, 2005), demonstrated the antimycobacterial potential of azole drugs against *M. tuberculosis* H37Rv under *in vitro* and *ex vivo* conditions. Within this study, econazole and clotrimazole were found to be

potent inhibitors of *M. tuberculosis* with MIC values of  $0.125 \mu\text{g ml}^{-1}$ , and similar to that for *M. smegmatis* (McLean *et al.*, 2002b). The study was carried out as a colony forming units (cfu) enumeration via percent growth inhibition of *M. tuberculosis* on Middlebrook 7H10 agar. In addition, the study highlighted the synergistic potency of econazole and clotrimazole in various combinations with isoniazid and rifampicin, and the apparent *ex vivo* potency of the azoles in TB affected Laca mice. In a separate study miconazole, 2-nitroimidazole, and clotrimazole were found to have significant antituberculosis activity, with MICs in the range of 1 to  $10 \mu\text{g ml}^{-1}$  (Sun and Zhang, 1999). Of particular note was the activity of 2-nitroimidazole against stationary phase tubercle bacilli (Sun and Zhang, 1999).

Several published studies have reported that results obtained by the BACTEC susceptibility method compared well with the conventional proportion method (employing 7H10/7H11 media) or the resistance ratio method (employing Lowenstein-Jensen egg medium) (Siddiqi *et al.*, 1981; Snider *et al.*, 1981; Vincke *et al.*, 1982; Roberts *et al.*, 1983; Siddiqi *et al.*, 1985). The accuracy and reproducibility of the BACTEC susceptibility method has also been evaluated, with positive results often achieved within 4 to 6 days (Terrand, 1985; Woodley, 1986; Heifets, 1991). Given the fact that MICs, as a whole, are highly dependent on a large array of different factors such as medium composition, pH, inoculum size, and incubation time, a variation in results would be anticipated. In addition, considerable variation in antibiotic susceptibility is found among the different species of mycobacteria, such that whereas *M. tuberculosis* is highly susceptible to isoniazid, *M. smegmatis* and other fast-growing mycobacteria are resistant to the drug (Zhang *et al.*, 1996). As a result, the *M. smegmatis* results should be considered only as an initial establishment of tentative MIC concentrations for further azole analyses in mycobacteria.

The non-pathogenic and fast-growing soil bacterium *M. smegmatis* shares many features with the pathogenic *M. tuberculosis*, and is particularly useful as a model mycobacterial system in studying basic cellular processes. However, physiological and metabolic differences between the two species employed would have a putative bearing



on the disparity of the MIC results observed. For example, polyprenyl phosphates are involved in the biosynthesis of bacterial cell walls and their availability is rate limiting for several aspects of cell wall synthesis (Crick *et al.*, 2000). *M. smegmatis* has been shown to contain two forms of polyprenyl phosphate, while *M. tuberculosis* contains only one (Crick *et al.*, 2000). With specific regard to this study, an important consideration is the approximately forty CYP genes within the genome of *M. smegmatis* (Jackson *et al.*, 2003), thus offering a potentially far greater number of azole targets than in *M. tuberculosis*.

It is well established that azole antifungal agents are potent inhibitors of cytochrome P450-monooxygenases (Lamb *et al.*, 1999; McLean *et al.*, 2002b). The identification of econazole as a lead drug is further supported with the reported alteration in the nsGPL expression in *M. tuberculosis* during treatment with azoles (Burguiere *et al.*, 2005). In the latter work, GPL biosynthesis was inhibited by the azole antifungal econazole and clotrimazole drugs at sub-MIC concentrations; the proportion of the different deacylated GPLs (dGPLs) changed significantly upon treatment with econazole but with clotrimazole the production of all dGPLs was decreased strikingly (Burguiere *et al.*, 2005). The overall synthesis of total dGPLs remained unchanged in *M. smegmatis* treated with econazole ( $10\text{ }\mu\text{g ml}^{-1}$ ) in comparison to the control cultures. However, the relative abundance of dGPL-I and dGPL-II decreased by 65 and 23 % respectively, whereas the amounts of dGPL-III and dGPL-IV increased by 28 and 78 % respectively (Burguiere *et al.*, 2005). The effect of clotrimazole ( $10\text{ }\mu\text{g ml}^{-1}$ ) was more dramatic; with the biosynthesis of all four dGPLs being strongly inhibited (Burguiere *et al.*, 2005). These data suggest that econazole and clotrimazole may act as inhibitors at different points in the synthesis pathways of the dGPLs.

Successful treatment of TB involves targeting the multiple populations of bacteria that reside in the host. Currently, TB is treated with a combination of drugs including isoniazid, rifampicin, pyrazinamide and ethambutol given for 2 months, followed by a 4 month treatment with isoniazid and rifampicin (American Thoracic Society *et al.*, 2003). The lengthy therapy often results in poor patient compliance and the emergence of drug

resistance. A compound that targets this subset of cells may be able to shorten the duration of therapy.

*In vitro* studies in murine models have already demonstrated the effectiveness of ketoconazole in combination with standard front-line anti-tuberculosis drugs (Byrne *et al.*, 2007). *In vitro* methods such as radiometric techniques are important to determine the minimal inhibitory concentration of antimicrobial agents. Effective doses of azole inhibitors should also be evaluated in a macrophage model to ensure intracellular drug effectiveness. Guinea pig macrophages have previously been utilised for such intracellular drug susceptibility testing of *M. tuberculosis* H37Rv, with MIC values of isoniazid and rifampicin towards intracellular H37Rv both reported as 0.1 µg/ml, respectively (Chanwong *et al.*, 2007).

Another alternative, as a line of investigation that deserves to be developed, is therapy combining two or more antifungal agents. Itraconazole combined with terbinafine has a synergic effect against clinical isolates of a fungus (Meletiadiis *et al.*, 2000), and there is clearly potential for such studies aimed at inhibiting growth of *M. tuberculosis*. Furthermore, the antimycobacterial MIC values may be lower for the newer clinically effective azole drugs like voriconazole, ravuconazole, albaconazole and posaconazole.

### **3.10 Crystallography**

An ongoing challenge of cytochrome P450 protein chemistry is to understand how the different sets of substrate specificities and metabolic transformations are controlled by the precise nature of the heme-iron oxygen and protein structure. Therefore, the valuable properties of biological macromolecules such as P450s cannot be fully understood without detailed knowledge of their 3D structure. Owing to the increasing number of P450 crystal structures solved in recent years, our understanding of P450 structure-function relationships has been considerably advanced (Cojocaru *et al.*, 2007). The P450s are now recognised to be widespread in nature and it is also clear that they have an enormous range of substrate specificity and physiological functions. These variations in metabolic profile and substrate specificity are ultimately dictated by the

bioinorganic chemistry of heme iron and oxygen, as controlled by the protein environment.

Typically, experimental techniques such as X-ray crystallography and nuclear magnetic resonance (NMR) spectroscopy are used to determine the 3D-structure of proteins at the atomic level. In X-ray crystallography, the electric field of the X-ray photons induce an in-phase electron dipole oscillation, which in turn gives rise to coherently diffracted radiation from the protein crystal under study (Drenth, 1999). In order to resolve atomic structural features it is essential to employ radiation with a wavelength of the order of atomic spacing or smaller (Drenth, 1999). However, the interaction between X-rays and electrons is weak, and such energetic radiation causes ionisation of the constituent atoms of the molecule, damaging the molecule under study. Thus it is necessary to examine a vast number of molecules simultaneously, through the use of a crystal containing many copies of a molecule in a regular lattice (Drenth, 1999).

Upon exposure of crystals to X-rays, the radiation is scattered into what is referred to as a diffraction pattern. The X-rays are scattered from all loci in the crystal, with the intensity in proportion to the electron concentration at a particular point (Drenth, 1999). All the scattered X-rays along any particular direction interfere with each other, giving rise to detailed features in the diffraction pattern that depend on the arrangement of atoms in the crystal (Terwillinger and Berenzden, 1999). Analysis of the subsequent diffraction pattern can allow the organisation of atoms to be deduced.

CYP121 mutants; P346L, R386L and S279A were generated by PCR and cloned as described in section 2.2.2. Purified protein samples of P346L and R386L mutants for the initial crystallisation experiments were prepared as described in section 2.4.1. X-ray crystallographic studies on the CYP121 mutants; P346L, R386L and S279A were performed by Dr Kirsty McLean and Dr David Leys (both Faculty of Life Sciences, University of Manchester). Conditions used for the generation of CYP121 mutants were as used for wild-type CYP121 (Leys *et al.*, 2003). Data collection was carried out at the European Synchrotron Radiation Facility (Grenoble, France) and structures were solved

via molecular replacement using the structure of wild-type CYP121 (PDB code 1N40) as base model.

### 3.10.1 Crystal structure of P346L

Generally in cytochrome P450 proteins, the heme is fully buried in the protein interior and its heme iron is ligated to the protein through a proximal cysteine residue (Denisov *et al.*, 2005). In some cases, the P450 heme is also covalently linked to the protein through the vinyl groups, although this modification appears restricted to eukaryotic CYP4 family proteins and to involve a catalysis-dependent reaction of the heme side chain with a conserved glutamate residue in the I helix (LeBrun *et al.*, 2002a; Baer *et al.*, 2005). The protein environment may influence the heme structure and chemical properties such that a specific function can be achieved by multiple ways, including constraining the access of substrate/oxygen to the distal (sixth) ligation site on the heme (Ludermann *et al.*, 2000; Wade *et al.*, 2004), influencing the strength of the proximal ligand bond (Ost *et al.*, 2001b), altering the electrostatic properties of the heme surface (Moore *et al.*, 1986), and distorting the heme geometry away from planarity (Leys *et al.*, 2003). Without this “tuning” of the heme properties by the protein, most P450s and other heme proteins would be incapable of performing their function. Despite the considerable structural and catalytic data available on a large number of cytochrome P450 proteins, the means by which the considerable functional diversity observed is actually achieved remains largely unknown in most cases. Often, the level of resolution of P450 structures is not high enough to enable detailed description of the heme binding site. However, in the case of CYP121 the 1.06 Å structure reveals detailed features of the heme and its binding site (Leys *et al.* 2003).

An unusual feature in wild-type CYP121 was the out-of-plane distortion of one of the four pyrrole rings of the heme due to the close interaction with the side-chain of a proline residue (Pro<sup>346</sup>) (Leys *et al.*, 2003). Pro<sup>346</sup> immediately follows the cysteinate heme ligand (Cys<sup>345</sup>). Munro and colleagues (Leys *et al.*, 2003) have proposed that structural perturbation of heme planarity may therefore be a common characteristic in other P450 enzymes but previously unrecognised due to the absence of a proline residue

adjacent to the proximal cysteine ligand in P450 structures solved to date (Figure 3.30) and, as previously mentioned, due to the much lower level of structural resolution achieved in most of the other available P450 structures (typically  $\geq 2.0$  Å) (Nagano *et al.*, 2003; Oku *et al.*, 2003).

Such distortions of heme structure are potentially very important to the specific electronic properties of the heme. In the P450 BM3 system a phylogenetically conserved Phe residue (Phe<sup>393</sup> located 7 amino acids before the cysteine ligand) interacts with the cysteinate ligand and the heme, and exerts a large effect on the heme electronic properties (Ost *et al.*, 2002a). Mutation of the residue has profound effects on heme iron redox potential and a substantial effect on catalytic efficiency of the enzyme. The effect of the Pro<sup>346</sup> residue in CYP121 on the P450 heme appears to be even greater than seen for Phe<sup>393</sup> in P450 BM3, and the residue could thus have a substantial impact on the heme catalytic and thermodynamic properties.

In order to deduce the heme properties associated with the Pro<sup>346</sup> interaction, a leucine mutation was introduced in attempts to alter the degree of distortion of the heme macrocycle at this position (Figure 3.30), whilst maintaining the general hydrophobic properties of the original proline residue.

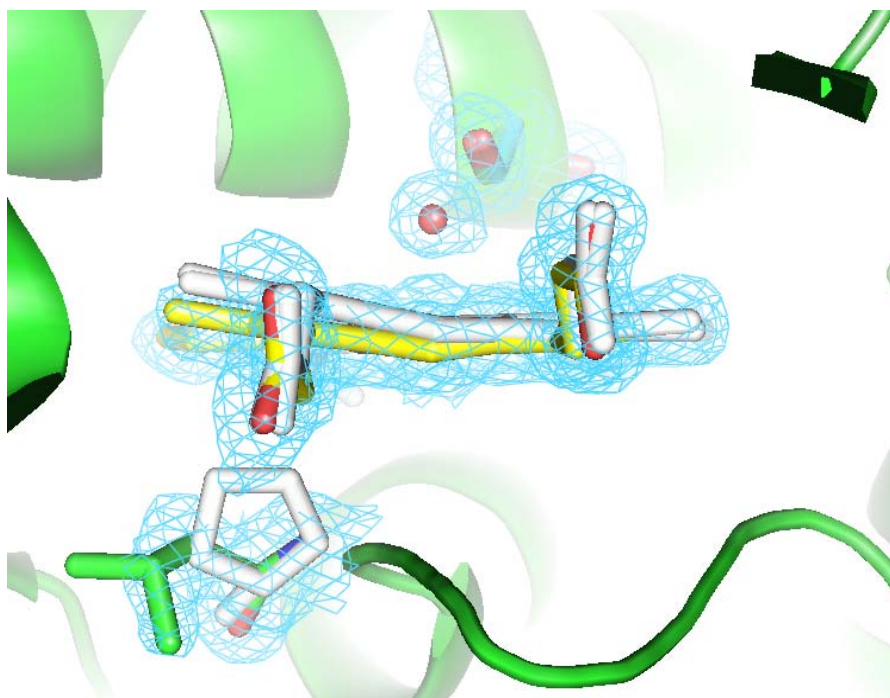


**Figure 3.30 Stereo view of the heme distortions in wild-type CYP121 and the P346L mutant of CYP121**

The figure shows a view of the heme site of CYP121 (centre of figure) in wild-type and P346L CYP121 protein structures. The heme is notably kinked due to the close interaction with Pro<sup>346</sup> in the wild-type CYP121 and is shown in white. The Leu<sup>346</sup> mutation is shown in green. The resulting distortion of the heme in the P346L mutant is shown in yellow along with the related electron density (blue). The Ser<sup>237</sup> residue, in close proximity to the heme, has been proposed to pass protons to dioxygen bound to the heme iron during catalysis in order to facilitate its scission and to enable formation of the reactive compound I species (Leys *et al.*, 2003). The red atom immediately above the heme centre represents the position of the oxygen atom of the 6<sup>th</sup> water ligand, with corresponding electron density shown (blue).

In most six-coordinate porphyrin systems, the macrocycle is generally planar in the absence of bulky peripheral substituents (Shelnutt *et al.*, 1998). In comparison with other published P450 structures (e.g. Cupp-Vickery and Poulos, 1995; Li and Poulos, 1997; Park *et al.*, 1997; Cupp-Vickery *et al.*, 2000; Park *et al.*, 2000; Podust *et al.*, 2001; Zerbe *et al.*, 2002; Williams *et al.*, 2003; Pylypenko *et al.*, 2003; Podust *et al.*, 2003; Jano *et al.*, 2003; Nagano *et al.*, 2003; Rowland *et al.*, 2006), the heme of CYP121 is in a

considerably ‘kinked’ orientation, Figure 3.30. As discussed above, though, absence of apparent heme distortions in some of these P450s could be a consequence of rather low structural resolution. In CYP121, the P346L heme macrocycle is still markedly non-planar, but the heme is distorted to a lesser degree than in the wild-type enzyme. The replacement of a proline for the Leu<sup>346</sup> residue (Figure 3.30, yellow) thus appears not to be the major reason for the distortion of the heme macrocycle. It thus appears likely that other structural factors also contribute to the kinking of the heme in CYP121. In the majority of other P450s much smaller, less bulky residues such as isoleucine, leucine and valine are located at this position, immediately following the heme-ligating cysteine, in the structure. The significance of the Pro<sup>346</sup> thus remains to be determined.

A proline residue immediately adjacent to the proximal cysteine is found in other *M. tuberculosis* P450s; CYP128 and CYP141, both of unknown function. This rare motif also occurs in CYP105R1 from *Streptomyces avermitilis*, the producer of the antiparasitic avermectins. The genome contains 33 open reading frames (ORFs) which encode cytochrome P450 enzymes (Lamb *et al.*, 2002). *CYP105R1* lies in a polyketide synthase (pks4) gene cluster and is proposed to be involved in the formation of simple polyketides (Lamb *et al.*, 2002). This signature motif also occurs in the structurally characterised P450epoK, which is involved in epothilone biosynthesis in the myxobacterium *Sorangium cellulosum*. However, no apparent distortion of the heme-plane was noted, which may be due to the lower structural resolution of the protein (~2.0 Å) (Nagano *et al.*, 2003).

Many previous studies have reported (Renner *et al.*, 1994; Fukuzumi *et al.*, 1999; Raman *et al.*, 2000) the effects resulting from loss of planarity in porphyrins. The distortion of the porphyrin ring results in changes in the energies of the iron d orbitals, as well as the porphyrin  $\pi$  orbitals, and as a consequence the electronic properties and redox potentials of the heme protein are changed. In the case of a P450 protein, the thermodynamic change in the heme would affect the electron transfer rate from its partner protein, and also likely impact on the P450’s ability to reductively activate molecular oxygen. Factors that have been proposed as important for poisoning the heme reduction

potential include the electrostatic environment of the cofactor, the nature and general properties of the proximal and distal ligands, and distortion of the porphyrin ring. Nonetheless, a direct link between reduction potential and heme distortion in proteins has yet to be described in any hemoprotein. Furthermore, no major change in the electronic properties of the P346L protein was observed from either redox potentiometry or resonance Raman studies (sections 3.54 and 3.6). Thus, mutation of the unusual Cys-Pro motif in CYP121 does not appear to have a major impact on the heme redox properties or on the heme distortion.

### 3.10.2 Crystal structure of R386L

Analysis of the active site of CYP121 provides important clues to key residues that could be involved in dictating structural features and defining substrate binding and subsequent catalytic functions. Of these residues, Arg<sup>386</sup> dominates the local structure immediately above the CYP121 heme plane (Figure 3.31).

The presence of the bulky and positively charged Arg<sup>386</sup> residue above the heme plane and adjacent to the oxygen scission site appears to be unique to CYP121 among structurally resolved P450 proteins and thus appears to restrict access of azole drugs to the heme. The side chain of Arg<sup>386</sup> is hydrogen bonded to Ser<sup>237</sup>, Gln<sup>385</sup> and two water molecules in the active site cavity (Leys *et al.*, 2003). The proximity of the arginine and serine residues may define a binding site for a negatively charged substrate functional group, e.g. a carboxylate, as observed previously for P450 BM3 with its fatty acid substrates (Li *et al.*, 1997; Noble *et al.*, 1999). Arg<sup>386</sup> is also proposed to form part of a putative proton relay pathway, either by donating protons to heme-bound oxygen directly or via Ser<sup>237</sup> (Leys *et al.*, 2003).

Several azole antifungal agents have been shown to bind tightly to wild-type CYP121 in solution (McLean *et al.*, 2002b), but obtaining crystallographic complexes with these compounds has, until very recently, been unsuccessful. This is highly likely due to a combination of the extreme insolubility of the polycyclic azoles (e.g. clotrimazole, ketoconazole, miconazole) in the ammonium sulfate mother liquor used for



CYP121 crystallization, and also due to restricted access of the azoles to the heme due to obstruction by Arg<sup>386</sup>. In order to investigate the role of Arg<sup>386</sup> in the CYP121 structure and in attempts to improve azole access to the heme binding pocket to facilitate isolation of an azole-CYP121 crystal complex, an arginine-to-leucine mutation was introduced, and the R386L mutant enzyme was purified and crystallized for structural analysis.

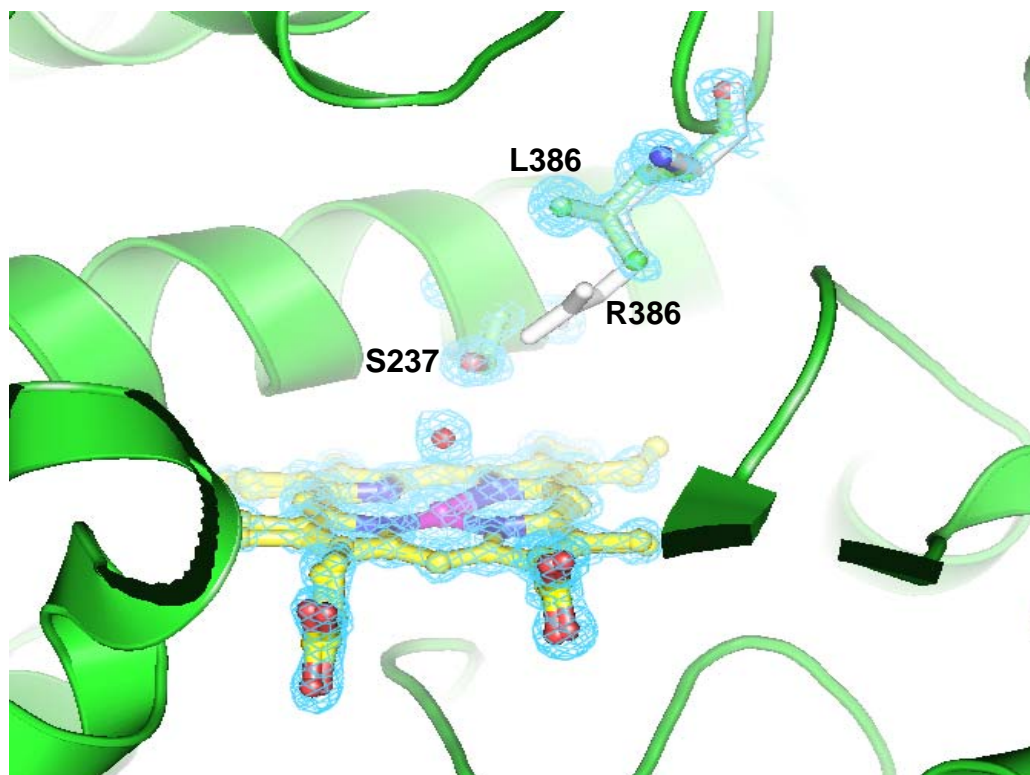


**Figure 3.31 Stereo view of the active site of the CYP121 R386L protein**  
Stereo view of the active site of CYP121 with the superimposed R386L mutation. At the centre of figure is the heme macrocycle (in CPK colouring with carbons shown in yellow) with the surrounding electron density (blue). The red atom immediately above the heme centre represents the position of the oxygen atom in the 6<sup>th</sup> water ligand, with the corresponding electron density (blue). Ligand/substrate access to the heme cavity is restricted due to the presence of the Arg<sup>386</sup> (white). The position of Leu<sup>386</sup> in the R386L mutant is shown in green with the related electron density.

The R386L mutation resulted in the opening of the area immediately above the heme plane and the disruption of the hydrogen bond with S237 that has been proposed to be a substrate contact point and/or part of the putative proton relay pathway in catalysis (Leys *et al.*, 2003). Further evidence for increased ligand access to the heme locality in the R386L mutant was obtained, with lower dissociation constants ( $K_d$  values) achieved with azole-R386L complexes in solution than were determined previously with wild-type CYP121 (section 3.7.1). Co-crystallization or soaking experiments of R386L crystals with azole drugs have proved unsuccessful to date. However, in recent work a fluconazole complex was successfully crystallized for wild-type CYP121 (Seward *et al.*, 2006). The complex was obtained by co-crystallization of CYP121 crystals with the azole. The data revealed a unique mode of fluconazole co-ordination to the CYP121 heme iron via a bridging water molecule in the majority of molecules in the structure, and underlined the importance of hydrophobic interactions with I helix residues and the position of the I helix itself in controlling the fluconazole coordination to the heme iron. Also of note in the study was the formation of a direct hydrogen bond between a carbon hydroxyl group of the indirectly-ligating triazole and Arg<sup>386</sup> (Seward *et al.*, 2006).

Thus, the R386L mutation caused some structural alterations above the heme plane but did not lead directly to isolation of an azole complex CYP121 crystal structure and disrupted the key interaction with Ser<sup>237</sup> seen in the wild-type CYP121.

### 3.10.3 Crystal structure of S279A

The initial steps of the catalytic cycle in P450s require both electrons and protons to be consecutively passed to the heme iron oxy species in order to split the dioxygen bond and to create the reactive oxidising intermediate(s) (i.e. compound 0 and compound 1). Upon initial reduction of the heme iron by the redox partner, it is converted from the ferric to the ferrous form, and can then bind dioxygen. The further reduction of the ferrous oxy complex leads to formation of the ferrous peroxy form, in which (for CYP121) the bound dioxygen molecule could either accept a proton from proximal water molecules or from Ser<sup>237</sup> (Leys *et al.*, 2003). However, when complexed with substrate, the active site could be mainly devoid of water molecules in the vicinity of the heme

plane, suggesting that Ser237 may be highly relevant to proton relay under the catalytically relevant condition. Ser<sup>237</sup>, in turn, can easily receive a proton from Arg<sup>386</sup> (Leys *et al.*, 2003). This residue contacts a water molecule buried in the protein interior. At this point, there are several other residues contacting this water molecule that could provide a proton. The most notable is Ser<sup>279</sup>, which occupies two distinct conformations in the CYP121 structure. Both of these conformations are in contact with a different series of residues and buried water molecules that ultimately lead up to the solvent surface of the molecule, providing routes for replenishing protons to active site residues (Figure 3.32) (Leys *et al.*, 2003).

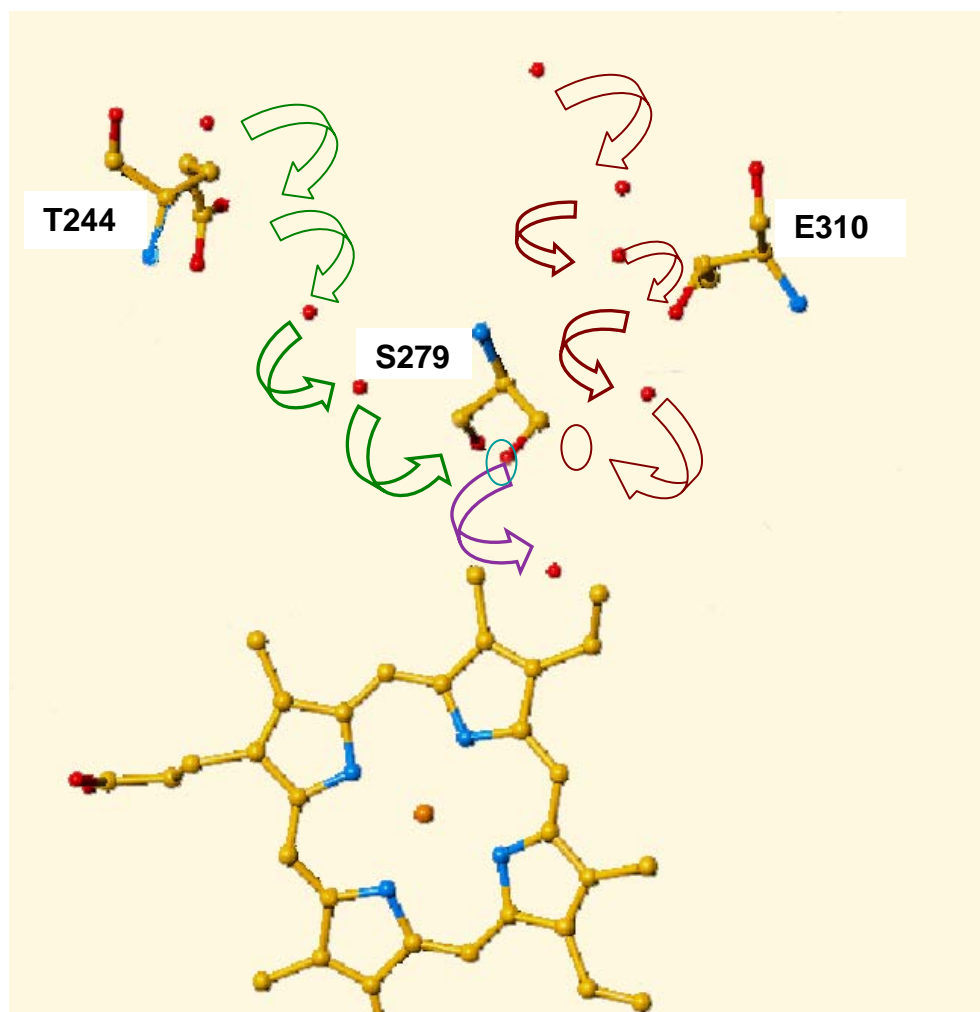


**Figure 3.32 Putative proton relay pathways in wild-type CYP121**

View of two putative proton pathways leading from the solvent into the active site, shown in green and brown, to the vicinity of the heme. Both pathways involve buried water molecules (red) in addition to a single amino acid (Thr<sup>244</sup> and Glu<sup>310</sup>, respectively) in the two pathways. These pathways merge at Ser<sup>279</sup>, which occupies two distinct conformations, each contacting a water molecule. The purple arrow indicates the transfer of a proton to the Ser<sup>279</sup> contacted water molecule that is hydrogen-bonded to Arg<sup>386</sup> (not shown). The green arrows indicate proton delivery to Ser<sup>279</sup> via ordered water molecules and the side chain of Thr<sup>244</sup> in one of two channels leading to the protein surface. On the right hand side of the scheme, the putative second proton delivery pathway from the protein surface to Ser<sup>279</sup> via Glu<sup>310</sup> is shown, with Ser<sup>279</sup> predicted to accept the proton with its side chain located in its second crystallographically determined position (indicated by a brown circle). Following proton transfer to Arg<sup>386</sup>, Ser<sup>279</sup> is proposed to donate protons either directly, or via Ser<sup>237</sup> (not shown), to the iron-oxygen intermediates.

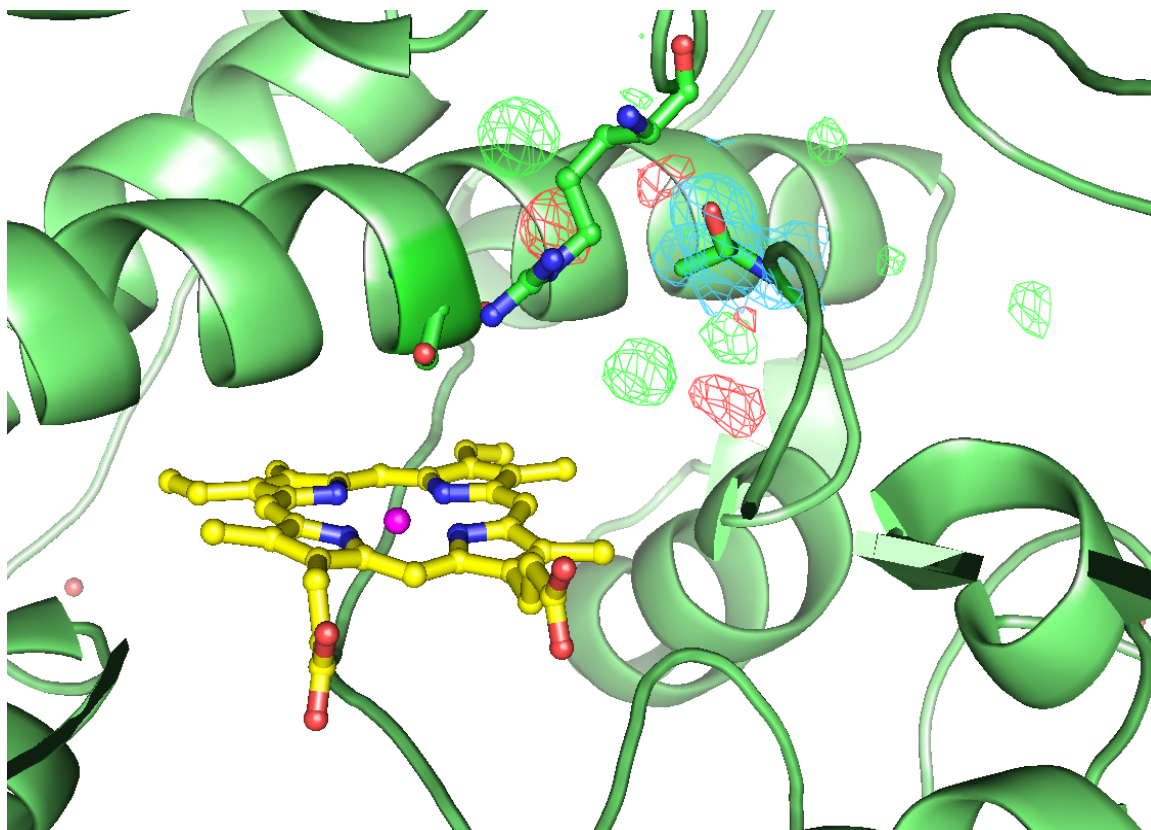


**Figure 3.33 Stereo view of the active site of the CYP121 S279A protein**  
 The heme macrocycle is shown in CPK colouring with carbons in yellow. The Ala<sup>279</sup> with the related electron density is shown top right in the structure with the new surrounding water molecules shown in red. Water molecules located in the wild-type CYP121 with the native Ser<sup>279</sup> are shown in green.

In the S279A mutant, it is interesting to note that the hydrogen bond network with Arg<sup>386</sup> and Ser<sup>237</sup> was not disrupted. However, the mutation does disrupt the well structured water network (Figure 3.33). The altered positions of water molecules in the S279A mutant structure could reflect the disruption of the “natural” proton relay pathway seen in wild-type CYP121, which in turn would reinforce the importance of Ser<sup>279</sup> in the catalytic process of CYP121. Confirmation of such a role awaits the definition of a substrate for CYP121, and the analysis of catalysis and product formation in wild-type and S279A CYP121 forms.

Folding, stability, and function of protein molecules are all likely to be influenced by their interactions with water molecules. Despite the importance of these interactions, the precise role of water in structure and function is often difficult to elucidate. Ordered water molecules are nearly universally observed in macromolecular crystallographic analysis (Badger and Casper, 1991; Karplus and Faerman, 1994), and biologically important functions for these observed water molecules have been identified in many cases, including roles in substrate specificity (e.g. Quioco *et al.*, 1989) and catalysis (e.g. Singer *et al.*, 1993). However, despite the reorganisation of active site water molecule in the S279A mutant, there was otherwise no significant conformational change observed in the overall mutant CYP121 P450 structure.

### 3.11 Summary

The previous high resolution structure of the *M. tuberculosis* CYP121 allowed recognition of several residues with apparent functional importance, including Pro<sup>346</sup>, Arg<sup>386</sup> and Ser<sup>279</sup>. Mutation of the Pro<sup>346</sup> residue (to leucine) implicated in the distortion of the heme macrocycle resulted in a decrease in the extent of the ‘out-of-plane’ pyrrole ring disruption and highlighted the important role that this residue plays in the control of the heme macrocycle conformation. Biophysical characterisation of the P346L mutant (by comparison to wild type CYP121) revealed changes in the EPR and CD spectroscopic features, indicative of some perturbation of the heme environment, as confirmed subsequently by the atomic structure. The greatest overall changes, in terms of the structural and biophysical characteristics of CYP121, occurred with the replacement of Arg<sup>386</sup> with leucine. The R386L mutant protein structure resulted in some expected structural alterations above the heme plane, with the opening of the heme to the active site, as well as the disruption of the hydrogen bonding interaction with Ser<sup>237</sup>. UV-visible absorption spectroscopy revealed a major Soret band at 419 nm, which reflected a blue-shift in the wavelength maximum compared to wild-type CYP121 and was indicative of an alteration in the spin state of one component of the protein, forcing it almost completely low-spin. However, the UV-visible spectrum of the R386L mutant also revealed the presence of a large shoulder at ~390 nm, indicating that the mutant had a proportion of the protein in the high-spin state. Both these UV-visible absorption bands

(low-spin and high-spin) are probably a result of altered interactions of heme iron with the distal water ligand, either reinforcing its binding (low-spin component) or weakening its interaction (high-spin component). However, the nature of these interactions is not clear from structural analysis. Further evidence for an increase in the high-spin component of this mutant was also observed from resonance Raman analysis. The  $\nu_3$  marker band is split into high-spin and low-spin features in P450s, and the high-spin species is dominant for R386L, whereas the opposite was the case for wild-type (the low-spin  $\nu_3$  marker was dominant). These changes in spin-state populations in the R386L variant are likely to relate directly to the structural changes associated with the disruption of the hydrogen bond between Arg<sup>386</sup> and Ser<sup>237</sup> in wild-type CYP121.

An important step in the characterisation of CYP121 is the identification of the true endogenous substrate of the protein. To this end, a lipid-protein overlay assay was performed using lipid extracts from *M. tuberculosis*, with results indicating a physical interaction between CYP121 and apolar lipid fractions. However, the molecular composition of these fractions remains to be identified. Furthermore, The MICs of various anti-fungal azole drugs were determined, showing that some of these had relatively high potency against *M. tuberculosis*. The same azoles bound tightly to CYP121, suggesting a link between CYP121 inhibition and antitubercular action of these drugs. Recent studies have further highlighted the chemotherapeutic potential of azole anti-fungal against *M. tuberculosis* (Ahmad *et al.*, 2007; Byrne *et al.*, 2007).

## Chapter 4

# Characterisation of the P450 CYP140A2 from the Buruli ulcer causative agent *Mycobacterium ulcerans*



## **4.1 Characterisation of CYP140A2**

### **4.1.1 Preface**

*Mycobacterium ulcerans*, the causative agent of Buruli ulcer, produces a macrolide toxin, mycolactone A/B (Figure 1.18), which is thought to play a major role in virulence of the bacterium. Each isolate of *M. ulcerans* produces a characteristic mixture of mycolactone congeners (Cadapan *et al.*, 2001; Hong *et al.*, 2003; Mve-Obiang *et al.*, 2003). *M. ulcerans* strains from different geographic areas produce distinct patterns of mycolactone congeners. The structural heterogeneity in mycolactones is due to variations in the fatty acid side chain (Mve-Obiang *et al.*, 2005).

Genes for mycolactone biosynthesis form a contiguous 110 kb cluster on a large plasmid (Stinear *et al.*, 2004). The lactone core is encoded by two polyketide synthase (Pks) genes, *mlsA1* and *mlsA2*, and a third polyketide synthase gene, *mlsB*, encodes the fatty acid side chain. Three accessory genes are found in the mycolactone cluster. One of these, *mup053*, encodes a P450 monooxygenase that is thought to produce the hydroxyl at C'-12 on the fatty acid side chain. Furthermore, the related bacterium *M. liflandii* produces a novel plasmid-encoded mycolactone, mycolactone E. *M. liflandii* contains all of the genes in the mycolactone cluster with the exception of that encoding the homologue of CYP140A2 (Mve-Obiang *et al.*, 2005).

This chapter describes the cloning of the *M. ulcerans* CYP140A2 gene (also known as *mup053*) and the expression, purification and characterisation of the CYP140A2 protein.

## **4.2. Molecular biology**

### **4.2.1 Cloning of histidine tagged CYP140A2**

A blunt ended CYP140A2-containing fragment was amplified by PCR using KOD Hi-Fi DNA polymerase (Novagen) with forward and reverse primers designed from the gene sequence, as described in the Materials and Methods section 2.2.2.

The PCR fragment containing the *CYP140A2* gene was resolved by agarose gel electrophoresis, and verified to be of the expected size by comparison with DNA fragment standards (1-kb ladder, NEB) (Figure 4.1).

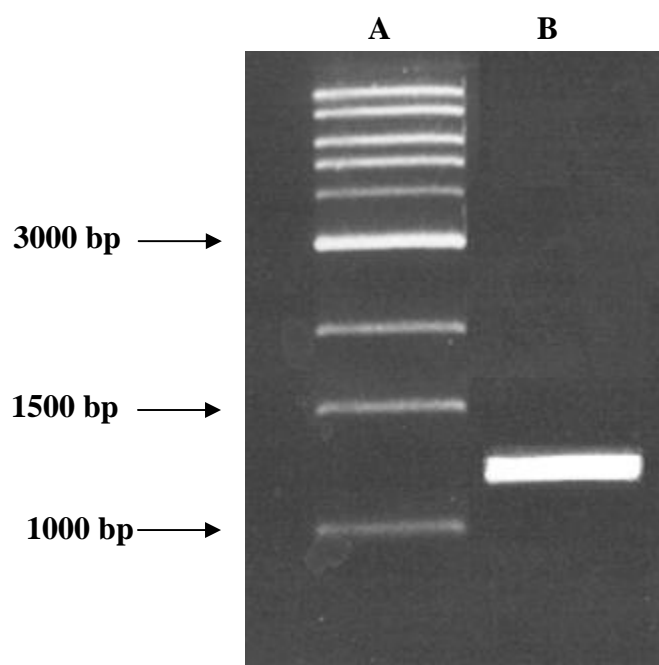


**Figure 4.1** PCR amplification of *M. ulcerans CYP140A2*

The PCR product was resolved by electrophoresis using an ethidium bromide stained 1 % agarose gel. The band displayed is consistent with the expected size of the 1383 bp *CYP140A2* gene (B). Alongside is a 1 kb DNA ladder (NEB) with the 1000, 1500 and 3000 bp fragments labelled (A).

‘A’ tailing was performed (as described in Materials and Methods section 2.2.6), on the PCR amplified *CYP140A2* gene to produce single adenosine nucleotide overhangs at the 3' ends, and the gene was then ligated into the pGEM-T easy vector (Materials and Methods section 2.2.8). Successful clones were identified, following transformation of the ligation mixture into *E. coli* strain Nova Blue, by the blue/white colour selection method on LB agar media containing ampicillin, X-gal and IPTG.

Plasmid preparations were made from selected transformants, and the *CYP140A2* clones verified by DNA sequencing at the University of Leicester PNACL using T7 primer 5' -TGT AAT ACG ACT CAC TAT ACG G- 3' and the Sp6 primer 5' -ATT TAG GTG ACA CTA AGA CAT A- 3' (as described in Materials and Methods section 2.2.10).

The *CYP140A2* gene was then excised from the pGEM-T easy vector by restriction enzyme digestion, using *NdeI* and *BamHI* restriction enzymes, the sites for which were incorporated at the 5' ends of the forward and reverse primers used for amplification of *CYP140A2*. The *CYP140A2* gene was then cloned into pET15b pre-cut with the previously mentioned restriction enzymes, and the pET clone (named pGL5(a)) verified by restriction enzyme digestion with *MluI* (Figure 5.2).

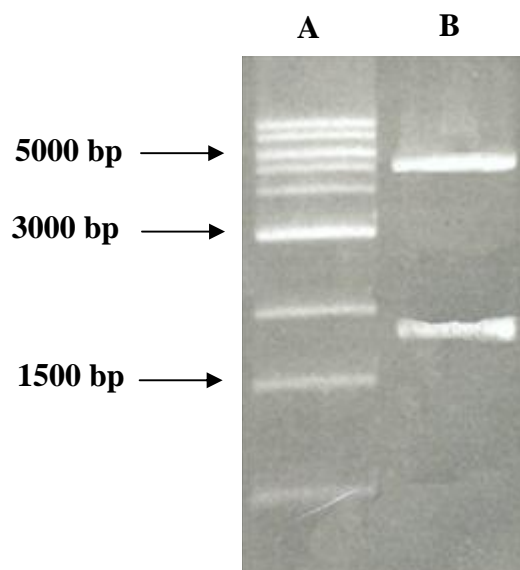


**Figure 4.2** *MluI* restriction digest of *CYP140A2* (pGL5(a))

The digested *CYP140A2* clone fragments were resolved by electrophoresis using a 1 % agarose gel. The pGL5(a) bands displayed (B) are consistent with the expected sizes of ~1770 bp and ~5310 bp, respectively, from a *MluI* digest. Alongside is a 1 kb DNA ladder (NEB) (A).

### 4.3 Expression and purification of histidine tagged CYP140A2

#### 4.3.1 Expression

Several different vector/host combinations were tested to obtain the best possible yield of protein in its desired form. Expression trials of the recombinant plasmid pGL5a containing the P450 CYP140A2 encoding gene were performed with *E. coli* expression hosts BL21(DE3), HMS174(DE3), as well as the specialist expression hosts Rosetta (DE3), Origami (DE3) and Rosetta-gami (DE3). Rosetta (DE3) overcomes the codon bias of *E. coli* by expressing the rarely used codons; AUA, AGG, AGA, CUA, CCC, GGA, thus leading to the improved expression of proteins whose genes contain these codons. Origami has mutations in both the

thioredoxin reductase (*trxB*) and glutathione reductase (*gor*) genes, which enhances disulfide bond formation in the cytoplasm. The Rosetta-gami (DE3) *E. coli* host strain (Novagen) combines the features of Rosetta and Origami strains. All the host expression strains contain chromosomal copies of the T7 RNA polymerase gene and a fragment containing the *lacI* gene and the *lacUV5* promoter (Studier *et al.*, 1990). Once the expression plasmid is transferred to the DE3 lysogen host, the IPTG-induced *lacUV5* promoter elevates transcription of the T7 RNA polymerase gene. IPTG functions by binding to the lac repressor protein, preventing association with the operator to allow transcription of the T7 polymerase to proceed (Studier, 1991). Levels of protein expression of the clone pGL5 (pET15b/CYP140A2) were studied using a variety of conditions and measured by SDS-PAGE (Figure 4.3). Initial experiments found expression levels at a relatively high level, especially in the BL21 (DE3) strain. Plasmid stability tests indicated that the pET15b clones were indeed stable.

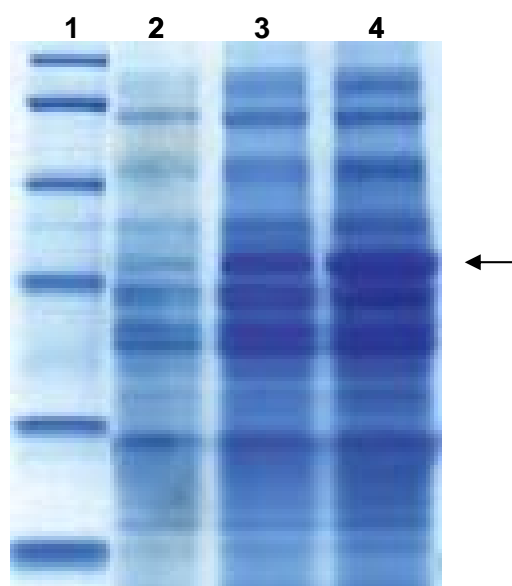


**Figure 4.3 Gel analysis of time lapsed CYP140A2 expression**

The gel displays the high level of protein expression of the *CYP140A2* gene product. The SDS-PAGE gel (10 %) shows production of CYP140A2 in BL21(DE3) indicated by the arrow. Lane 1: protein molecular weight standards (NEB) (in descending order, kDa): 175, 83, 62, 47.5, 32.5 and 25. Lanes 2-4 display the accumulation of a protein at 25 °C taken at 1, 3 and 6 hours, respectively, after induction with 1mM IPTG.

Despite high levels of expression (Figure 4.3), further analysis revealed that the majority of the expressed CYP140A2 protein was in the insoluble form. Numerous conditions were investigated to optimise expression of soluble protein, including temperature, host strains, IPTG concentration, duration of induction, and media types. Expression of soluble protein from the *CYP140A2* construct was measured on SDS-PAGE by comparison of soluble and insoluble fractions of lysed cells. Figure 4.4, displays examples of gels demonstrating protein expression and analysis of soluble and insoluble fractions from BL21(DE3).

It is evident in Figure 4.4 that the majority of the expressed protein is insoluble, possibly in the form of inclusion bodies. However, under conditions of growth at 18 °C, particularly 24 hours after induction, a small degree of soluble protein is present. The molecular mass of the expressed histidine tagged CYP140A2 is ~51 kDa, as indicated by the arrows on Figure 4.4, and consistent with the predicted molecular weight of 50.561 kDa.

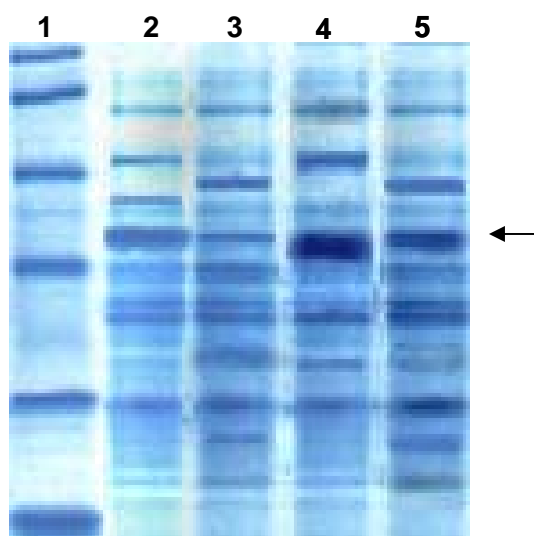


**Figure 4.4** Gel analysis of soluble and insoluble CYP140A2 expression SDS-PAGE gel (10 %) showing expression of CYP140A2 (50.6 kDa) in BL21(DE3), indicated by an arrow. Gel demonstrates time resolved analysis of insoluble and soluble protein fractions from cells induced with 100  $\mu$ M IPTG and grown at 18 °C, with samples taken at 8 and 20 hours. Lane 1; broad-range protein molecular weight standards (6-175 kDa) (NEB) (in descending order, kDa); 175, 83, 62, 47.5, 32.5, and 25. Insoluble (lane 2) and soluble (lane 3) fractions, respectively, for 8 hours post-induction. Lanes 4 (insoluble fraction) and 5 (soluble fraction), for 20 hours post-induction.

### 4.3.2 Protein purification

Purification of the N-terminal histidine tagged CYP140A2 was spectrophotometrically tracked through the measurement of the total protein concentration through the absorbance at 280 nm, and the total P450 concentration by heme absorbance at 418 nm. The  $A_{418/280}$  ratio was measured at each stage, and at each purification stage protein samples were taken and analysed by SDS-PAGE for the relative purity of the protein (Figure 4.5).

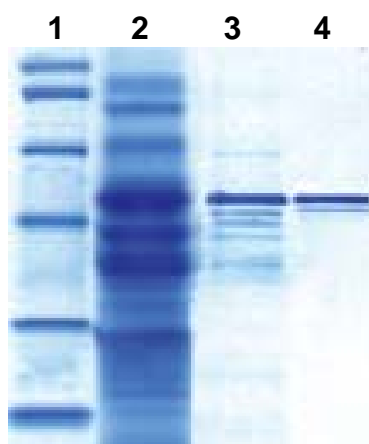


**Figure 4.5** **SDS-PAGE analysis of histidine tagged CYP140A2 protein purification**

SDS PAGE gel (10 %). Lane 1: broad range protein molecular weight marker (NEB). Mass units (descending, kDa): 175, 83, 62, 47.5, 32.5. Lane 2: cell extract; Lane 3: post-nickel affinity column fraction; Lane 4: post-gel filtration (showing 3 mg pure CYP140A2 protein at ~ 51 kDa).

Protein purification of the CYP140A2 protein was achieved by nickel affinity fractionation and gel filtration. Purification of CYP140A2 was measured during purification by comparing the heme-specific absorbance at 418 nm, with the total protein concentration absorbance at 280 nm at different stages of purification. The data are shown in Table 4.1.

Purification Stage	Total Protein (mg)	Total P450 (mg)	Ratio P450/ Protein	Stepwise Purification Factor	Overall Purification Factor	Stepwise Yield (%)	Overall Yield (%)
Lysate	14500	78	0.01	1	1	100	100
Nickel affinity	29.7	5.4	0.18	18	18	6.9	6.9
Gel Filtration	13.3	3.6	0.27	1.5	27	66	4.6

**Table 4.1 Purification table for histidine tagged CYP140A2**

Yields at each stage of the purification (lysate, nickel affinity chromatography and gel filtration step) were followed by the overall protein absorbance ( $A_{280} = 1 = 1 \text{ mg/ml}$ ) and the P450 specific heme absorbance ( $A_{418} = 96 \text{ mM}^{-1} \text{ cm}^{-1}$ ). Data presented relate to protein purified from 12 litres of transformant cells.

Homogeneous purification of CYP151A2 was achieved with difficulty due to the presence of lower molecular weight proteins/contaminants shown on SDS-polyacrylamide gel. An improved purification procedure for the expressed CYP151A2 was attempted with anion exchange chromatography, through the use of DEAE cellulose and the stronger anion resin Q-Sepharose in this purification protocol. Based on the calculated isoelectric point of 8.75 for CYP140A2, both the aforementioned matrices were equilibrated in 50 mM Tris-HCl (pH 7.2, at 4 °C) buffer. However, the P450 was eluted under very low ionic strength conditions (<60 mM) in fractions contaminated by numerous other proteins. Decreasing the pH of the buffer to 6.5 did not result in stronger binding. Further chromatography was attempted on hydroxyapatite equilibrated in buffer ranging from 20-100 mM potassium phosphate (pH 6.5, at 4 °C), CYP140A2 protein did not bind to the column under these conditions.

## 4.4 Initial P450 characterisation

### 4.4.1 Spectrophotometric analysis

UV-visible absorption spectroscopy provides the primary technique for recognition and characterisation of P450s. The UV-visible spectrum of the oxidised form of CYP140A2 (black line) showed characteristic features of a heme-containing protein (Figure 4.6). The major Soret peak of the P450 in its oxidised state was located at 418 nm, with the smaller  $\alpha$  and  $\beta$  bands of the Q-region at 567 nm and 534 nm, respectively. The  $\alpha$  and  $\beta$  bands were of roughly equal intensity. In CYP140A2, as remarked for CYP121 and CYP51 (McLean *et al.*, 2002a; McLean *et al.*, 2006), the absence of an absorption shoulder at  $\sim 390$  nm indicates that the P450 is predominantly low-spin ( $S = 1/2$ ) with minimal high-spin ( $S = 5/2$ ) ferric heme iron content under these conditions. On reduction of CYP140A2 with sodium dithionite, the Soret band shifted to 416 nm and diminished slightly in intensity whilst the  $\alpha$  and  $\beta$  bands merge to form a new spectral species with an intermediate maximum at 536 nm (Figure 4.6). It is clear that substantial reduction of the heme iron has occurred, although a slightly larger shift in the Soret band might have been expected for complete conversion to the ferrous state.

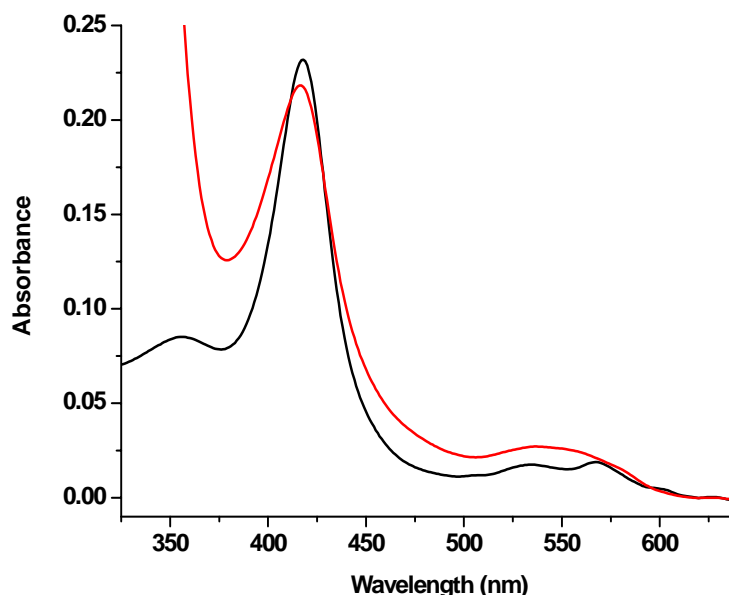


**Figure 4.6** Anaerobic electronic absorption spectra for CYP140A2  
The UV-visible absorption spectrum for pure CYP140A2 ( $\sim 2.4 \mu\text{M}$ ). The oxidised (black) and sodium dithionite-reduced (red) forms are shown, with Soret absorption maxima located at 418 nm and 416 nm, respectively.



These features are similar to other well characterised P450s, such as the P450cam (CYP101) and P450 BM3 (CYP102A1) enzymes (Sligar, 1976; Miles *et al.*, 1992). However, this conversion to the reduced form of CYP140A2 required anaerobic conditions, due to the rapid reaction of the ferrous P450 with oxygen. Interestingly, the extent of anaerobic conversion of CYP140A2 to the ferrous form is less than observed for either P450cam or P450 BM-3, with the peak maximum wavelength of 416 nm for the Soret band of the ferrous form being ~10 nm longer than that observed for P450cam and P450 BM-3 (Daff *et al.*, 1997; Miles *et al.*, 2000). This likely indicates a partial reduction due to an unstable CYP140A2 ferrous-oxy complex, in turn due to the relatively fast re-oxidation of the heme iron (compared to the reduction rate of the ferric heme by dithionite) due to scavenging of traces of oxygen. Addition of large excesses of dithionite promoted aggregation and precipitation of CYP140A2, and it is impossible to achieve near-complete reduction of the P450 under aerobic conditions.

Slow bubbling of carbon monoxide (CO) through the dithionite-treated CYP140A2 generated a Fe(II)-CO complex with a mixture of new spectral features; a peak at 449 nm, and a minor shoulder at 422 nm. The shift of the Soret band to 449 nm is strongly indicative of a cytochrome P450, with a cysteine thiolate-ligated heme iron; whilst the shoulder at 422 nm is indicative of a P420 spectral species in which a proportion of the enzyme has lost cysteinate ligation following dithionite reduction and exposure to the CO gas. The electronic transition that characterises the P450 species arises from proximal heme iron coordination by a cysteinate (Cys 350 in CYP140A2). The P420 form is considered to result from loss of thiolate coordination and, specifically, from the protonation of the ligand to a thiol (McIver *et al.*, 1998; Perera *et al.*, 2003). Studies of the Fe(II)-CO forms of both *M. tuberculosis* P450s CYP121 and CYP51 showed them to form mainly the thiol-coordinated P420 species rather than the cysteinate-coordinated P450 form. In the case of CYP51, the P450 CO complex collapses in favour of the P420 form over a few minutes, demonstrating that the thiolate-coordinated form is present initially, but is unstable in this form and converts to thiol-coordination (Ayoama *et al.*, 1998; Ogura *et al.*, 2004; McLean *et al.*, 2006). A difference spectrum was generated by the subtraction of the ferrous spectrum from that for the ferrous/CO-bound adduct (Figure 4.7). Formation of a peak

at 450 nm confirms the protein to be the recombinant P450, CYP140A2, in a predominantly thiolate-coordinated CO-bound state.

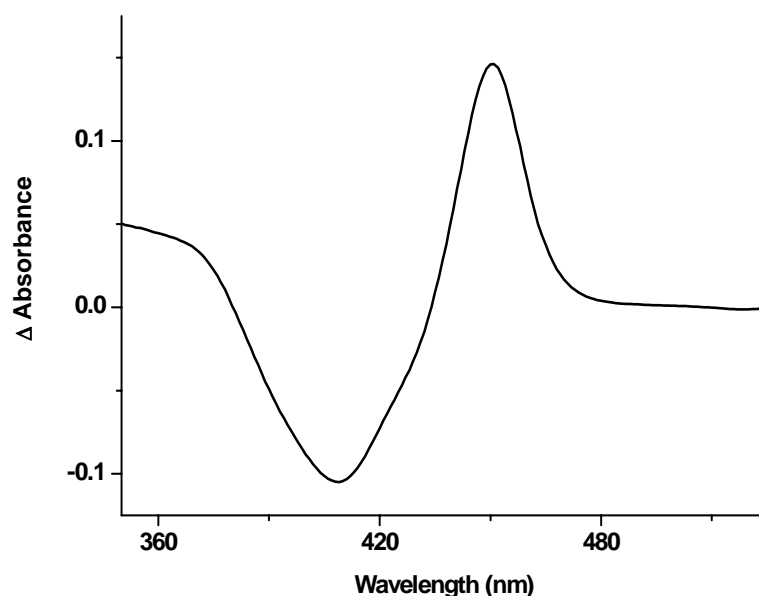


**Figure 4.7** **Difference spectrum of the reduced/CO-bound CYP140A2**  
CYP140A2 (~2.5  $\mu$ M) in 50 mM Tris-HCl, pH 7.2. Difference spectrum generated by subtraction of the spectrum for ferrous CYP140A2 from that for the ferrous-carbon monoxy form. The presence of the predominant P450 form is evident from the spectral maximum at 451nm.

Gentle bubbling of nitric oxide (NO) into a solution of ferric CYP140A2 was also performed. NO induced a reduction in the intensity and a shift of the Soret band to 431 nm, and a shift of the  $\alpha$ - and  $\beta$ -bands to 573 nm and 543 nm, respectively (Figure 4.8, red). This “type II” binding spectrum is typical of co-ordination of a strong ligand to the ferric heme iron. The spectral properties of the nitrosyl complex are similar to those observed for e.g. CYP121 mutants (see section 3.4) and for other P450 enzymes. Ligation of cyanide ( $\text{CN}^-$ ) to ferric CYP140A2 (Figure 4.8, green) induces complete conversion to another 6-coordinated heme adduct with a significant decrease in the Soret maximum at 432 nm, and spectral fusion of the  $\alpha$ - and  $\beta$ -bands to a species of intermediate wavelength (552 nm).

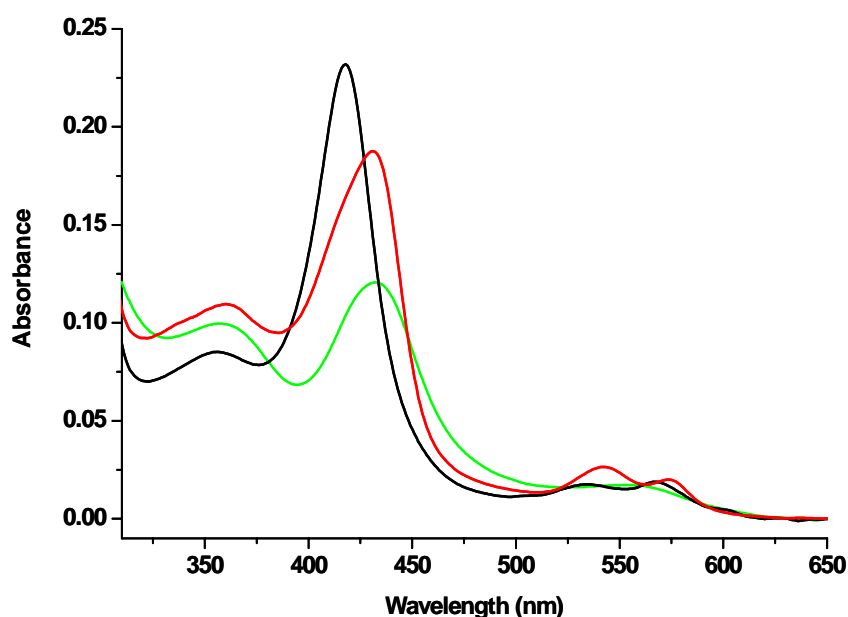


**Figure 4.8**      **Electronic absorption spectra for CYP140A2 with inhibitor ligands**

CYP121 (~2.4  $\mu\text{M}$ ) in 50 mM Tris-HCl, pH 7.5, in the oxidised form (black line), nitric oxide-bound form (red) and cyanide-bound form (green). Soret maxima are located at 418, 431 and 432 nm, respectively.

The spectral changes induced by the small molecules CO, NO and  $\text{CN}^-$  are typical of distal ligations to P450 heme iron with a cysteinate proximal heme iron ligand. The ligation of NO and  $\text{CN}^-$  inhibitor molecules to the ferric P450 results in conversion to a single spectral species, suggesting that the small amount of P420 material observed upon CO-binding reflects a minor proportion of thiolate-to-thiol ligand switch form that occurs in the ferrous (and/or ferrous-CO complex) form, and that the ferric state of this enzyme is exclusively thiolate-coordinated in its resting state.

#### 4.5 Pyridine heme chromagen

P450 concentrations can be determined via a stable Fe(II)-CO adduct, and the subsequent application of the extinction coefficient  $\epsilon_{450-490}$  of  $91 \text{ mM}^{-1} \text{ cm}^{-1}$  for data from the reduced/CO-bound *minus* reduced P450 difference spectrum (Correia, 2005). The instability of the CO complex for CYP140A2 prevented accurate use of the

previous method. Therefore, CYP140A2 heme concentration was determined by the pyridine hemochromagen technique (Berry and Trumpower, 1987) (Figure 4.9).

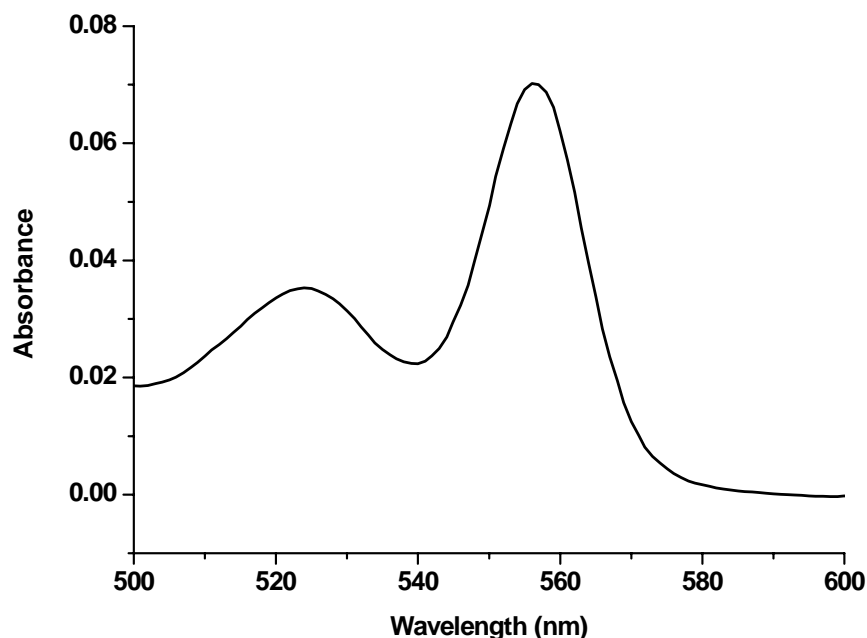


**Figure 4.9 Pyridine hemochromagen spectrum of CYP140A2**  
CYP140A2 in 50 mM Tris-HCl, pH 7.2, 100 mM NaOH, 20 % (v/v) pyridine and 300  $\mu$ M  $K_3Fe(CN)_6$ . In the Q-band region (alpha and beta region), an absorption maximum was generated at 556 nm, which is typical of heme *b*. Protein concentration was determined using a heme *b* extinction coefficient of  $\epsilon_{556-540} = 24 \text{ mM}^{-1} \text{ cm}^{-1}$ .

An average  $\epsilon_{418}$  coefficient of  $96 \text{ mM}^{-1} \text{ cm}^{-1}$  was determined for oxidised CYP140A2 at the Soret peak using data from the hemochromagen method. This value is in the typical range of P450s coefficients of between 90-150 (Hawkes *et al.*, 2002; McLean *et al.*, 2002a; McLean *et al.*, 2006). For example, the Soret coefficient of the cineole-degrading P450cin (CYP176A) from *Citrobacter braakii* was determined by the same method to be  $\epsilon_{415} = 150 \text{ mM}^{-1} \text{ cm}^{-1}$  (Hawkes *et al.*, 2002).

#### 4.6 Sequence analysis

The P450 protein superfamily is distributed widely throughout the evolutionary kingdoms, suggesting an early origin of this superfamily (Deng *et al.*, 2007). The gene evolution within the P450 superfamily has been proposed to correlate

with organism evolution and atmosphere oxygen concentration flux (Lewis *et al.*, 1998).

As the classification name of CYP140A2 suggests, the protein is defined within the CYP140 family, which currently is comprised of P450s based within the *Mycobacterium* genus (<http://drnelson.utmem.edu/P450.stats.2006.htm>); CYP140A1 (*M. tuberculosis*), CYP140A1 (*M. bovis* subsp. *bovis* AF2122/97), CYP140A2 (*M. ulcerans*), CYP140A3P (*M. leprae* TN), CYP140A4 (*M. avium* subsp. *paratuberculosis*), CYP140A5 (*M. marinum*), CYP140A5 (*M. ulcerans*) and CYP140A6 (*M. vanbaalenii* PYR-1). The amino acid sequence of *M. ulcerans* CYP140A2 was submitted for a PSI- and PHI-BLAST analysis at NCBI to identify proteins with the highest sequence identity. CYP140A2 was found to be 61 and 62% identical to CYP140A5 from *M. ulcerans* and CYP140A1 from *M. tuberculosis*, respectively. To date the functions of these P450s remain unknown. Highest identity with a characterised P450 was observed with the erythromycin biosynthetic protein, P450 EryF (CYP107A1) from *Saccharopolyspora erythraea*, with a 38 % identity match (Cupp-Vickery and Poulos, 1995). The soluble 45 kDa P450 EryF has been structurally determined in complexes with both the natural substrate 6-deoxyerythronolide B (6-DEB) and alternative ligands (Cupp-Vickery and Poulos, 1995; Cupp-Vickery *et al.*, 2000). However, caution must be adopted in using amino acid sequence identity deductions alone, as it is well reported that single amino acid changes in P450s can significantly alter catalytic properties such as substrate specificity (Munro and Lindsay, 1996). The amino acid alignment programme ClustalW (<http://www.ebi.ac.uk/clustalw/>) was used for the amino acid comparative study of CYP140A2 with P450 EryF (Figure 4.10).

P450eryF exhibits homotropic (Cupp-Vickery *et al.*, 2001; Davydov *et al.*, 2002) and heterotropic (Khan *et al.*, 2003) cooperativity with a variety of substrates such as androstenedione, testosterone and 7-benzoxoquinoline (Davydov *et al.*, 2002; Khan *et al.*, 2003). Of particular note in the structure of P450 EryF was the large active site, as expected from the size of its macrocyclic substrate, and secondly the replacement of the highly conserved threonine, Thr<sup>252</sup> in P450cam (CYP101A1) (Aikens and Sligar, 1994) (Thr<sup>271</sup> in CYP140A2), with Ala<sup>245</sup> in P450 EryF (Cupp-Vickery and Poulos, 1995; Cupp-Vickery *et al.*, 2000) (Figure 4.10). The conserved

threonine is a catalytically important residue believed to play a role in proton transfer during dioxygen bond cleavage in the activation of molecular oxygen (Aikens and Sligar, 1994; Cupp-Vickery *et al.*, 2000). The crystal structure of P450 EryF shows that the threonine-hydrogen bonding interactions are replaced by hydrogen bonding interactions with the 5-hydroxyl group of the substrate (Cupp-Vickery *et al.*, 2000). Other highly conserved characteristic amino acids across the P450 superfamily include phenylalanine 373, which is implicated in thermodynamic control of the heme iron (Ost *et al.*, 2001a), and cysteine 380, likely to provide the proximal sulfur ligand to the CYP140A2 heme iron (Figure 4.10, red highlight) (Poulos *et al.*, 1995; Peterson and Graham, 1996; Graham and Peterson, 1996).

Despite low sequence identities at the amino acid level within the P450 superfamily, the overall protein fold and topologies are very similar and certain sequence motifs corresponding to the conserved tertiary structure and enzyme functions are identifiable. In general, P450 structures form a triangular prism-shaped molecule consisting of 14  $\alpha$ -helices designated A to L and 5  $\beta$ -sheets (Pylypenko and Schlichting, 2004). Within the P450 structural core is a conserved four-helix bundle composed of three parallel helices, D, L, and I, and an antiparallel helix E (Presnell and Cohen, 1989). Located between the I-helix and the L-helix is the heme group which is attached to the adjacent Cys-heme-ligand loop which contains the P450 signature amino acid sequence FxxGx(H/R)xCxG (Cys<sup>380</sup> in CYP140A2) (Denisov *et al.*, 2005). The flanking amino acids of the heme-binding motif (Cys-pocket) are involved in formation of  $\beta$ -turns (Berman *et al.*, 2000). The amino acid in the +2 position from Cys to the C-terminus (Gly) allows a sharp turn from the Cys-pocket into the L-helix. The Phe which dominates in the -7 position completes the hydrophobic shielding of the Cys-iron bond (Buchatskii *et al.*, 2001). The kinked I-helix contains the signature sequence (A/G)Gx(E/D)T located above the heme (Pylypenko and Schlichting, 2004). The conserved core of the protein also contains the helices J and K (Pylypenko and Schlichting, 2004). There are two structurally conserved  $\beta$ -sheets:  $\beta$ 1 containing five strands and  $\beta$ 2 containing two strands (Pylypenko and Schlichting, 2004).

Although the P450 fold is highly conserved, sufficient structural diversity exists to achieve the required diverse functions. The most variable structural elements

in P450s are considered to be the helices A, B', B, F, G, H, K' and their adjacent loops, and the  $\beta$  sheets  $\beta 3$  and  $\beta 4$  (Gotoh, 1992; Pylypenko and Schlichting, 2004). Amino acid mutations within these regions have been shown to confer new substrate specificities onto P450s, or to alter stereo- and regioselectivity of substrate oxidation (Negishi *et al.*, 1996).

The aforementioned variable regions contain residues associated with substrate recognition/binding and include six designated substrate recognition sequences (SRS) (Gotoh, 1992). The SRS predetermine P450 substrate specificity although point mutations within SRS significantly affect such specificities (Gotoh, 1992). The B'-helix region (SRS1), parts of the F- and G-helices (SRS 2 and SRS 3), a part of the I-helix (SRS4), the K-helix  $\beta 2$  connecting region (SRS 6), and the  $\beta 4$  hairpin (SRS 5) line the P450 active site (Pylypenko and Schlichting, 2004). In many cases, the resting form of an enzyme does not perfectly fit the structure of its substrate and so the SRSs are considered flexible protein regions, which move upon substrate binding so as to favour binding and, subsequently, the catalytic reaction. Studies of P450cam using bound ruthenium-linker substrates show large changes in peripheral enzyme structure, specifically the F and G helices, are coupled to conformational changes in the I helix of the active site residues (Dunn *et al.*, 2001). Further work on the binding of ketoconazole in P450 EryF has been noted to induce conformational changes in the I-helix. The P450eryF/ketoconazole crystal structure indicates that the I-helix cleft near the active site is a flexible structure able to collapse upon ligand binding (Cupp-Vickery *et al.*, 2001). Based on significant changes in the hydrogen bonding and water structure within this region, it has been proposed that movement of the peptide backbone in the region of the I-helix cleft during catalysis could assist in proton shuttling to the oxygen atom (Cupp-Vickery *et al.*, 2001). The I-helix also provides residues for interactions with the substrate 6-DEB in EryF (Cupp-Vickery and Poulos 1995). This induced-fit model of substrate-protein interaction addresses the functional importance of structural flexibility in proteins (Koshland, 1958). Such structural flexibility in P450s is thought to be the reason for their ability to bind and oxidise extremely structurally diverse substrates.





highlight), D (violet), H (pink), I (blue), K (bright green), K' (yellow), L (turquoise), E (teal), as well as the Cys-pocket (red highlight) and meander (brown highlight). Other regions also found to be relatively well conserved structurally are located in the  $\beta$ 1-4 (orange font),  $\beta$ 2-1 (red),  $\beta$ 2-2, (light blue) and  $\beta$ 3-2 (lime) sheets regions. Of particular note in the CYP140A2/EryF sequence alignment is the highly conserved sequence in the K-helix. The C-terminal section of the CYP140A2 K-helix contains the highly conserved sequence E/D-X-X-R. This region sequence contains Glu and Arg residues which are believed to stabilise the meander through salt bridge interactions and hydrogen bonds (Pylypenko and Schlichting, 2004).

Alignment studies by Gotoh (Gotoh, 1992) defined six putative substrate recognition sites (SRS) that occur in common regions of primary sequence for prokaryotic and eukaryotic P450s (Hasemann *et al.*, 1995). Site-directed mutagenesis studies with CYP2 family members and with other mammalian P450 families (Schalk and Croteau, 2000) have largely supported this concept by localising, in the predicted SRS, the contact residues that direct substrate specificity. Sequence alignments in the present study reveal that the residues residing in these regions are not well conserved between P450EryF and CYP140A2 (Figure 4.10, with SRS regions having dashed underline marking). This should reflect the difference in substrate selectivity between these isoforms.

A number of specific active site residues involved in ligand binding have been identified in P450EryF and are highlighted in Figure 4.10. These include the active-site residues Phe<sup>78</sup>, Gly<sup>91</sup>, Ser<sup>171</sup>, Ile<sup>174</sup>, and Leu<sup>175</sup> (Khan *et al.*, 2002). Phe<sup>78</sup>, Ser<sup>171</sup>, Ile<sup>174</sup>, and Leu<sup>175</sup> (retained as Leu<sup>200</sup> in CYP140A2) are located near the distal ligand in the two-ligand-bound P450EryF crystal structures, and possibly play a significant role in cooperative binding of substrate (Khan *et al.*, 2002). On the other hand, Gly-91 (not conserved in CYP140A2) lies in close proximity to the ligand and heme and could be important for substrate binding and/or oxidation (Khan *et al.*, 2002).

Residues of further interest in P450EryF are Cys<sup>154</sup> (Cys<sup>176</sup> in CYP140A2, located in a possible E-helix) and Arg<sup>164</sup> (Arg<sup>186</sup> in CYP140A2), in which ligand-induced conformational rearrangement in the vicinity of Cys<sup>154</sup> has been associated

with changes in the accessibility and hydration of the heme pocket (Davydov *et al.*, 2005). The distance between the sulfur atom of Cys<sup>154</sup> and the epsilon nitrogen atom of Arg<sup>164</sup> is within 3.5–4.0 Å, suggesting the formation of a salt bridge (Davydov *et al.*, 2005). This ligand-induced transition is accompanied by possible dissociation or rearrangement of several salt bridges in the proximity of Cys<sup>154</sup> (Davydov *et al.*, 2005). The conservation of these important residues in CYP140A2 suggests that similar roles in structural maintenance and rearrangement may be played by these residues in the *M. ulcerans* P450.

On the basis of the crystal structures of substrate-bound P450EryF, it has been proposed that hydrogen bonds are formed between the C-5 hydroxyl group of erythromycin and Ser<sup>246</sup> of the enzyme with active site water molecules (Kim *et al.*, 2001). Ser<sup>246</sup> has been shown to indirectly participate in the proton shuttling pathway, and supports the role of the C-5 hydroxyl group of the substrate in the acid-catalysed cleavage of the dioxygen bond (Kim *et al.*, 2001). In CYP140A2, Thr<sup>274</sup> is located in this position in CYP140A2, and is the more widely conserved hydroxyl group-containing residue in this position in the P450s.

The majority of protein-ketoconazole interactions in P450EryF are hydrophobic and involve the side-chains of residues Phe<sup>72</sup>, Val<sup>237</sup> (Val<sup>325</sup> in CYP140A2, located in the I-helix region), Ala<sup>241</sup>, Ala<sup>245</sup>, and Leu<sup>391</sup> (Cupp-Vickery *et al.*, 2001). Pro<sup>288</sup> (Pro<sup>315</sup> in CYP140A2) lies in the active site and has been proposed to bind with 9-aminophenanthrene and androstenedione (Cupp-Vickery *et al.*, 2000). Thus, further key residues in P450EryF are conserved in CYP140A2, and suggest that similar roles in structural motifs and interactions with substrate may be played in this P450.

## **4.7 Biophysical characterisation**

### **4.7.1 Circular dichroism (CD)**

Circular dichroism is the differential absorption of the left- and right-circularly polarised components of plane-polarised electromagnetic radiation. The technique provides structural and dynamic information about proteins quickly and conveniently, and is increasingly recognised as a valuable technique for examining the structure of proteins in solution.

The far-UV CD spectra (190-260 nm) for CYP140A2 indicate no major differences in overall secondary structure by comparison with the *Bacillus megaterium* P450 BM-3 heme domain (Figure 4.11). Some differences in spectral magnitude are illustrated between the far-UV CD spectra of CYP140A2 and P450 BM-3, but these may relate mainly to small deviations in protein concentration. Overall the data emphasise that CYP140A2 is mainly composed of  $\alpha$ -helical structure (74 % predicted), consistent with all other P450s structurally characterised to date.

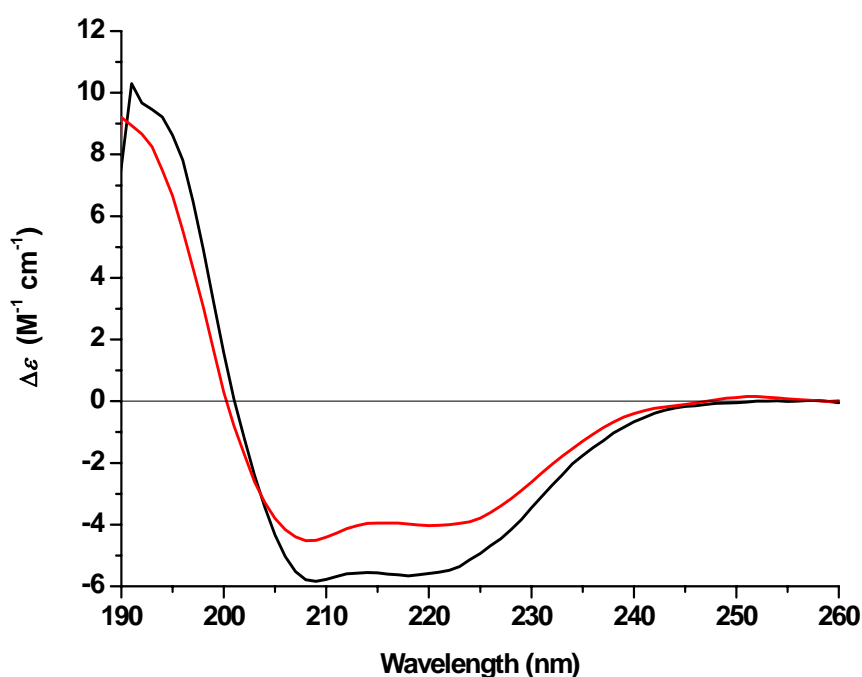


**Figure 4.11 Far-UV CD spectra of CYP140A2 and P450 BM-3 heme domain**  
CYP140A2 (2  $\mu$ M) (black) compared with P450 BM3 heme domain (2  $\mu$ M) (red), in 10 mM KPi, pH 7.0, and in quartz cuvettes with a pathlength of 0.02 cm. Experiments were performed using a JASCO J-715 spectropolarimeter at 25 °C.

In this region of the CD spectrum, the absorbing chromophore is principally the peptide bond. The absorption of CYP140A2 displays typical  $\alpha$ -helical-rich protein characteristics, with minima occurring at 208 and 218 nm, corresponding to a weak, but broad,  $n \rightarrow \pi^*$  transition, and an intense  $\pi \rightarrow \pi^*$  transition corresponding to the peak at 190 nm (Kelly *et al.*, 2005).

The near UV-visible CD spectrum of CYP140A2 is displayed in Figure 4.12 alongside the corresponding spectrum of P450 BM-3. The near UV-visible CD spectra of CYP140A2 and P450 BM-3 display differences in both the aromatic amino acid and heme environment signals. Signals corresponding to the environment of the heme group (350-450 nm) are significantly different (as is the Q-band region between 500-600 nm, although the signal intensity in this region is much lower and prone to distortion by lower signal-to-noise ratios). For CYP140A2, this range of the spectrum is dominated by a sharp Soret feature with negative ellipticity centred at 420 nm, and a particularly prominent delta band with negative ellipticity centred at 345 nm. These features are both due to the  $\pi \rightarrow \pi^*$  transitions of the porphyrin ring (Hsu and Woody, 1971). In the near-UV-visible CD region (260-600 nm), the spectrum of CYP140A2 in its resting oxidised form is rather different from that of the BM3 heme domain. Although both spectra display minima at ~420 nm and ~350 nm (Soret and delta bands, respectively), the Soret/delta ratio is not identical for the different P450s. In particular, the delta band of CYP140A2 is more intense than that observed for P450 BM-3 and other P450s analysed in this study. Furthermore, literature spectra of ferric P450s also display variations in the intensity for the two bands. An example is P450 BM-1 (Andersson and Peterson, 1995). In CD spectra, enhancement of the Soret band relative to the delta band has been hypothesised to indicate a more “open” active site structure (Wang and Kimura, 1976).

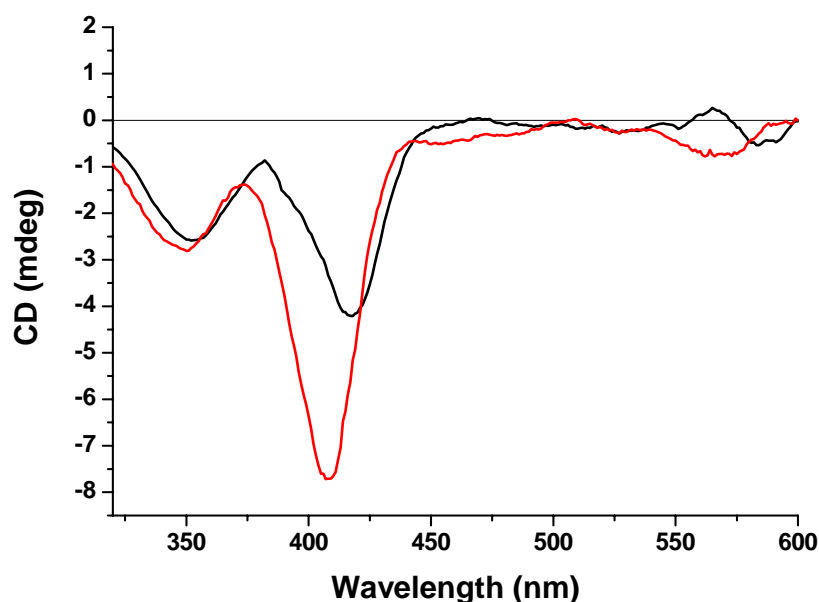


**Figure 4.12** Near UV-visible spectra of CYP140A2 and P450 BM-3 heme domain

CYP140A2 (20  $\mu$ M) (black) compared with P450 BM-3 (20  $\mu$ M) (red) in 10 mM KPi, pH 7.0. Data were recorded in quartz cuvettes with a sample pathlength of 0.5 cm. Experiment was performed on a JASCO J-715 spectropolarimeter at 25°C. The spectral minima for the Soret/delta bands are located at 417/352 nm and 408/349 nm for CYP140A2/P450 BM-3, respectively.

Although there is a current lack of understanding on the precise basis of positive and negative ellipticity and intensity changes with respect to general cofactor structure and conformation in proteins, differing geometry of the heme macrocycle for CYP140A2 and P450 BM-3 likely reflects the differences in CD spectra. This, in turn, possibly reflects in some way the distinct functions of the P450 enzymes. P450 BM-3 is a fatty-acid hydroxylase, whereas CYP140A2 is involved in polyketide biosynthesis.

#### 4.7.2 Electronic Paramagnetic Resonance (EPR)

To further characterise substrate binding of CYP140A2 and in attempts to elucidate the molecular mechanism for this specific binding, the EPR spectra for the substrate-free and mycolactone C-bound forms of the CYP140A2 were examined. Figures 4.13 A and B show the EPR spectra of the substrate-free and mycolactone C-bound forms of CYP140A2, recorded at 10.5K.

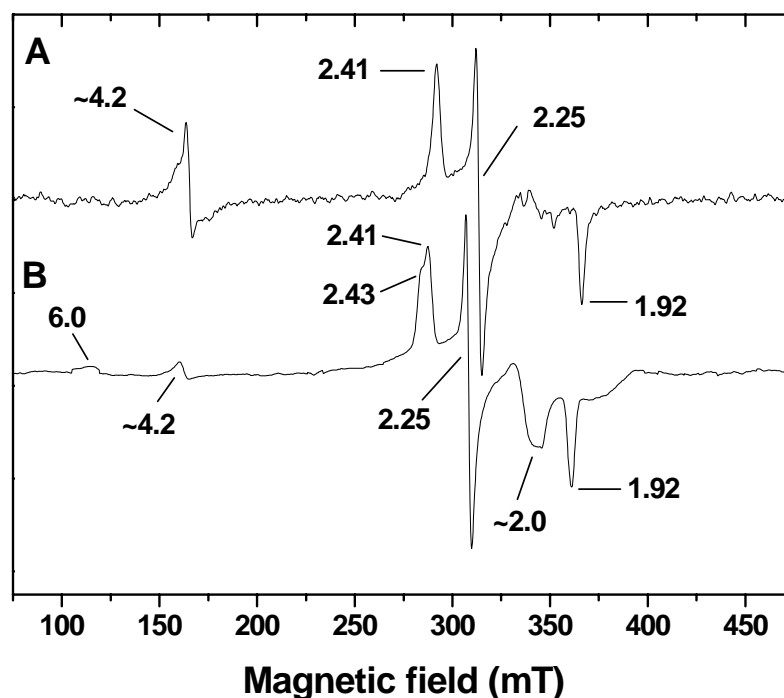


**Figure 4.13 X-band EPR spectra of CYP140A2**

The protein was at a concentration of 150  $\mu\text{M}$  in 50 mM Tris-HCl, pH 7.5 including 50 % (v/v) glycerol. Sample conditions were temperature 10.5 K, microwave power = 2.0 mW, modulation amplitude = 1 mT. Panel A: resting, oxidised CYP140A2; Panel B: CYP140A2 with 5  $\mu\text{M}$  mycolactone C. The g-values are indicated on the two spectra.

The major signals generated in the EPR spectrum of CYP140A2 constitute a rhombic trio of g-tensor elements ( $g_z$ ,  $g_y$ ,  $g_x$ ) (Figure 4.13A). The occurrence of these three major peaks indicates a nuclear spin state of  $\frac{1}{2} (2I + 1)$ . The resulting g-values of 2.41 ( $g_z$ ), 2.25 ( $g_y$ ) and 1.92 ( $g_x$ ) are reflective of a low-spin ferric (FeIII) heme (Mansuy and Renaud, 1995; Lipscomb, 1998). Indeed, the resting oxidised CYP140A2 spectra is similar to the wild-type CYP121 ( $g = 2.47, 2.25, 1.90$ ) (McLean *et al.*, 2002), along with those of low-spin ferric forms of the well-characterised P450cam and P450 BM-3 proteins ( $g = 2.46, 2.26, 1.91$  and  $2.42, 2.26, 1.92$ , respectively) (Dawson *et al.*, 1982; Miles *et al.*, 1992). In addition, there is similarity with the low-spin ferric form of Nitric Oxide Synthases (NOSs), in which the heme is also bound axially by cysteinate and water (Lipscomb, 1980; Dawson *et al.*, 1982; Berka *et al.*, 1988; Salerno *et al.*, 1995; Tsai *et al.*, 1996). The g-values are very sensitive to the nature of the heme axial ligands and to perturbations such as the orientations of the ligands. The fact that these values for CYP140A2 are very similar

to wild-type CYP121, P450cam and P450 BM-3 suggests the heme ligation environment is very similar in all of these P450s.

In the presence of 5  $\mu$ M mycolactone C, the  $g_z$  heme iron signal showed the formation of a shoulder with a  $g$ -value of 2.43, while the  $g_x$  heme iron signal remained completely shifted to a lower ( $g$  value = 1.92) field, with no apparent heterogeneity (Figure 4.13B). These signal shifts can be interpreted as decreased heme rhombicity due to a change in the heme ligation environment. A similar decreased rhombicity was also reported in the 4-phenylimidazole-bound form of P450cam (2.45/2.5, 2.25, 1.89) (Uchida *et al.*, 2004). The signals at  $g_z$  2.43/2.41 and  $g_x$  1.92 indicate a proportion of the sample retains a distal water ligand, although substrate binding causes some heterogeneity in the  $g_z$  signal, as reported previously for other P450s (Girvan *et al.*, 2004; Lawson *et al.*, 2004). The latter heterogeneity appears in the EPR spectra with minor features at  $g$  = 6.00 and  $\sim$ 4.2. The presence of the minor signals ( $g$  = 6.0 and  $\sim$ 4.2) are either due to trace amounts of high-spin ferric heme and adventitious Fe (III), respectively, or possibly indicate a low degree of rhombic splitting of the  $S = 5/2$  high spin ferric state, a feature typically observed upon P450 substrate (or ligand) binding (Lipscomb *et al.*, 1980; Dawson *et al.*, 1982). These high-spin signals are consistent with those reported previously for the camphor hydroxylase P450cam and for other P450s (Lewis, 1996). Although the amplitude of the features pertaining to a high spin-state shift are small, they are in agreement with the small high-spin shift observed in the absorption spectroscopy experiments upon binding of mycolactone C to CYP140A2. The derivative feature at  $g$  =  $\sim$ 2.0 is likely to be due to adventitious copper.

Furthermore, substrate binding induces slight broadening of the  $g_z$  and  $g_x$  components' signals, suggesting that there may be a split population of two conformers, as previously indicated for azole-bound P450 BM-3 (Girvan *et al.*, 2004). This broadening effect on the EPR signal is indicative of formation of a CYP140A2-mycolactone C complex, and the concomitant perturbation of the heme ligand environment.

### 4.7.3 Resonance Raman

As discussed previously in studies of other P450s analysed in this thesis, a strong signal enhancement is observed when resonant radiation is used to excite the sample in resonance Raman spectroscopy (RR). The sensitivity of the technique lies in the excitation of an electronic absorption band of a chromophore (the Soret band of the P450 in this case) and allows the analysis of specific vibrational modes and electronic states of the chromophore. Since chromophores generally have a key importance in biological activities, RR is a valuable tool for probing such activity, leading to a better understanding of the molecular composition of the cofactor and its environment in the protein.

The RR spectrum of substrate-free CYP140A2 was obtained with excitation at 406.7 nm and labelled according to previous assignments (Kitagawa and Ozaki, 1987; Parthasarathi *et al.*, 1987; Hildebrandt and Stockburger, 1989; Hudeček *et al.*, 2000). The 406.7 nm excitation band lies relatively close to the 418 nm Soret transition of the heme chromophore and thus generates Raman scattering from the vibrational modes of the heme porphyrin ring. The ligand-free CYP140A2 generated a spectrum with overall strong similarity to those obtained for other P450 enzymes, including wild-type CYP121 (Kitagawa and Ozaki, 1987; Parthasarathi *et al.*, 1987; Hildebrandt and Stockburger, 1989; Hudeček *et al.*, 2000; McLean *et al.*, 2002a).

The dominant oxidation state marker band obtained for wild-type CYP140A2 is assigned the  $\nu_4$  mode (Figure 4.14). The observed value of  $1372\text{ cm}^{-1}$  for  $\nu_4$  indicates that the heme iron is in the ferric (FeIII) state, in accordance with the data obtained from electronic absorption spectra and from EPR spectroscopy. Resonance Raman bands in the range  $1450\text{--}1650\text{ cm}^{-1}$  are characteristic indicators of the porphyrin ring core size and, accordingly, of the spin-state of the heme iron (Abe *et al.*, 1978; Hildebrandt and Stockburger, 1989). The characteristic spin-state marker in this range is  $\nu_3$  and the presence of this band located at  $1503\text{ cm}^{-1}$  reveals CYP140A2 to be in a predominantly low-spin ferric heme state (i.e. there is little sign of a  $\nu_3$  feature at lower wavenumber indicative of the high-spin form, as is observed in certain CYP121 mutants. In general, the RR spectrum of CYP140A2 is thus indicative of a predominantly ferric, cysteinate-ligated P450 (Hudeček *et al.*, 2000). The assignments and band frequency values for the main features in the RR spectrum of



ligand-free and ligand-bound CYP140A2 are summarised in Table 4.2. The quality of the spectra for CYP140A2 is not as high as for some of the other P450s analysed in this thesis, due in part to the relatively poor performance of the RR equipment at the time of collection of these data. Notwithstanding this issue, the data collected clearly define the major, diagnostic P450 heme bands.

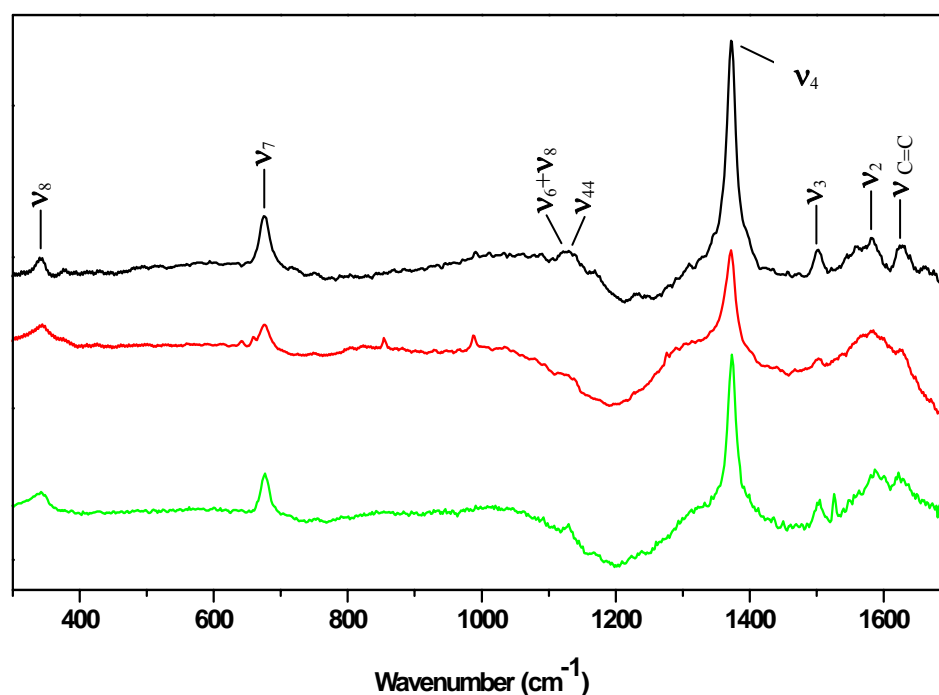


**Figure 4.14 Resonance Raman spectra of ligand-free and -bound CYP140A2**  
Protein samples (100  $\mu\text{M}$ ) were in 10 mM Tris-HCl, pH 7.5, and spectra were recorded between 300 and 1700  $\text{cm}^{-1}$ . Positions of assigned vibrational bands are shown, including the  $\nu_4$  marker band for oxidised ferric heme ( $\sim 1372 \text{ cm}^{-1}$ ), and the  $\nu_3$  feature indicating the predominantly low-spin heme ( $\sim 1503 \text{ cm}^{-1}$ ). Assignments made for the ligand-free CYP140A2 spectrum (black) are shown, and are also representative of corresponding peaks in the mycolactone C-bound (30  $\mu\text{M}$ , red) and miconazole-bound (30  $\mu\text{M}$ , green) forms.

Assignment	Band position (cm <sup>-1</sup> )		
	CYP140A2	Mycolactone C bound	Miconazole bound
$\nu_{C=C}$	1625	1623	1623
$\nu_2$	1581	1584	1586
$\nu_3$	1503	1503	1505
$\nu_4$	1372	1372	1374
$\nu_6 + \nu_8$	1125	1124	1125
$\nu_7$	674	676	674
$\nu_8$	344	344	344

**Table 4.2**      **Resonance Raman frequencies for the main peaks observed in ligand-bound and -free forms of oxidised CYP140A2**

RR excitation was at 406.7 nm. Samples were prepared and spectra recorded as described in the legend to figure 4.14.

The relatively low frequencies of spin-state-sensitive modes, such as  $\nu_2$  (1581 cm<sup>-1</sup>) and  $\nu_3$  (1503 cm<sup>-1</sup>), are also consistent with CYP140A2 having a predominantly low-spin, ferric heme iron.

For mycolactone C-bound CYP140A2 protein (Figure 4.14, red), the absence of a high-energy shoulder (or discrete band) for  $\nu_3$  is further indicative of the P450 retaining a low-spin state upon the binding of mycolactone C. The oxidation state marker band  $\nu_4$  is unaltered in frequency and, to a large extent, in intensity. This is also indicative of retention of a low-spin species in which the iron-coordinated water molecule has not been expelled as the 6<sup>th</sup> ligand to the heme iron. In addition, the up-shift in the frequency of the spin-state-sensitive mode  $\nu_2$  (1584 cm<sup>-1</sup>) adds further support to the retention of a low-spin ferric heme in the mycolactone C-bound P450. Further, changes are observed upon mycolactone-C binding, with regard to the formation of two new peaks with low intensities located at 854 and 999 cm<sup>-1</sup>. Bands in this region may originate from porphyrin modes and include contributions from substituent groups (Choi *et al.*, 1982a, b; Abe *et al.*, 1978; Hu *et al.*, 1993). Thus,

these bands provide evidence for the binding of the mycolactone C in the heme pocket of CYP140A2 and suggest that the molecule may induce some reorientation of the heme substituents (e.g. propionate or vinyl groups), even though the spin-state of the P450 heme iron is apparently unaltered in the complex.

The miconazole-bound CYP140A2 RR spectrum is also highly similar to that for the ligand-free form. The major  $\nu_2$  in-plane bands also has a frequency dissimilar to those for the ligand-free and mycolactone C-bound proteins, and is illustrative of a low-spin species. The oxidation state marker band  $\nu_4$  is up-shifted slightly in frequency, and this is indicative of reinforcement of the low-spin species. In this case, the reason for this phenomenon is the displacement of the water ligand to the heme iron in favour of the miconazole drug, as opposed to the retention of the aqua ligand.

The recorded data for the CYP140A2 RR spectra (above  $\sim 900\text{ cm}^{-1}$ ) suffer from a fluorescence background (Figure 4.14), which has been removed for clarity. This is observed frequently in studies of hemoproteins, and can be due to buffer, contaminant proteins or other fluorescent impurities. In the case of CYP140A2 it is possible that some fluorescence appears due to low level contamination of the samples with other proteins. However, the software used allows for accurate removal of the fluorescent background and thus the positions of the RR bands remain accurate. The problem with background fluorescence was peculiar to the CYP140A2 protein and was not observed for either of the two other P450s studied (i.e. CYP121 mutants and CYP151A2).

#### **4.8 Redox potentiometry**

Research on the electrochemistry of enzymes is partly motivated by the fundamental need to understand the details of electron transport in proteins. Early studies involving direct electron transfer between an electrode and protein were pioneered in the late 1970s (Eddowes and Hill, 1977; Yeh and Kuwana, 1977). This early research demonstrated that the problem of slow electron transfer between an electrode and a metalloprotein could be overcome by use of electron shuttles (or mediators). Since then, much effort has been directed into developing suitably mediated or modified electrode systems that facilitate biological electrochemistry.

However, in many cases the only viable technique for determining redox potentials of cofactors bound to proteins is by solution-state potentiometry (Dutton, 1978).

To examine further the electronic properties of CYP140A2, the reduction potential of the P450 was determined using anaerobic spectroelectrochemistry. The P450 was progressively reduced and oxidised, via the titration of small amounts of reductant or oxidant to a CYP140A2 enzyme solution. Subsequent spectral alterations were monitored at a specific (equilibrated) potential value, as described in section 3.6. The spectral changes observed during the redox titration of CYP140A2 are displayed in Figure 4.15.

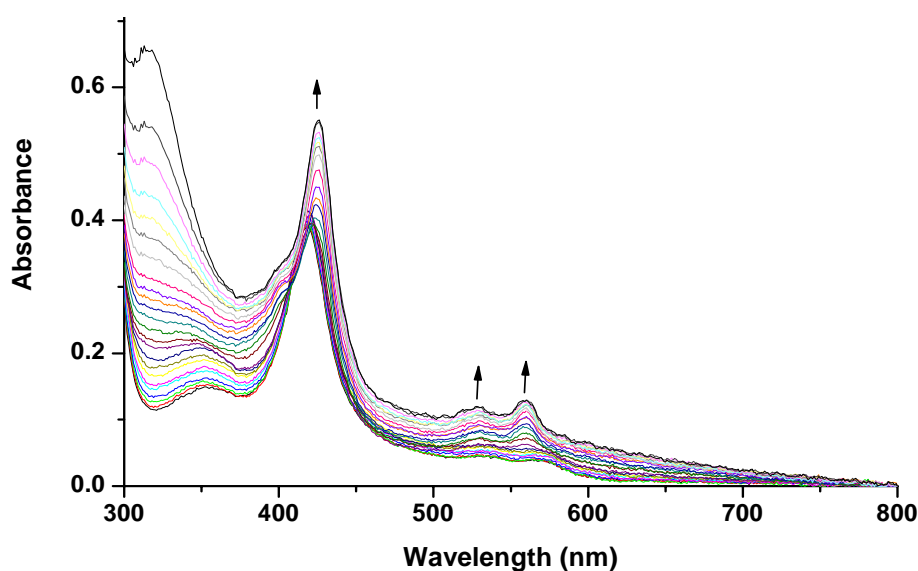


**Figure 4.15 Redox titration of CYP140A2**

Spectral changes were recorded for CYP140A2 ( $\sim 5.8 \mu\text{M}$ ) in 50 mM  $\text{KPi}$ , pH 7.0 and those displayed were recorded during the reductive titration. The oxidised, ferric form of CYP140A2 has its Soret maximum at 418 nm and  $\alpha$ - and  $\beta$ -bands at 567 and 534 nm, respectively. Reduction with dithionite increases the intensity of the Soret maximum and also increases the absorption in the longer wavelength visible region at 567 and 534 nm. Upon oxidation the spectrum is returned to that resembling the starting ferric form. Arrows indicate the direction of absorbance changed during the reductive titration. All changes were reversible (i.e. no hysteretic effects were observed).

Titration of CYP140A2 with sodium dithionite resulted in an increase in the intensity in the region of the Soret maximum (418 nm for the oxidised P450) with a shift to longer wavelength (426 nm) seen for the reduced form. In addition, there was

increased absorption in the visible region, with elevated intensity of absorption bands observed at 567 and 534 nm. Complete reduction of CYP140A2 proved to be attainable. Figure 4.15 also shows the accumulation of excess dithionite as a peak forming at 300 nm as the titration approached completion. The development of turbidity due to enzyme aggregation occurred somewhat during the course of the redox titration, but did not prevent accurate estimation of the redox potential for the heme iron. The titration was completely reversible in reductive and oxidative directions, and with no sign of hysteretical behaviour (i.e. the spectra collected at similar potentials during oxidative and reductive titrations were essentially identical).

Absorption *versus* potential data were plotted at 561 nm (i.e. at the maximum for a new feature in the reduced enzyme spectrum and in a spectral region minimally affected by turbidity) and were fitted to a 1-electron Nernst equation to define the midpoint reduction potential for the CYP140A2 heme iron in the absence of substrate (mycolactone C). Fixing the Nernst factor or slope ( $RT/F$  value) to 59 mV, which corresponds to the slope of a one-electron redox couple at 25 °C, yielded a mid-point reduction potential of  $-264 \pm 4$  mV (Figure 4.16).

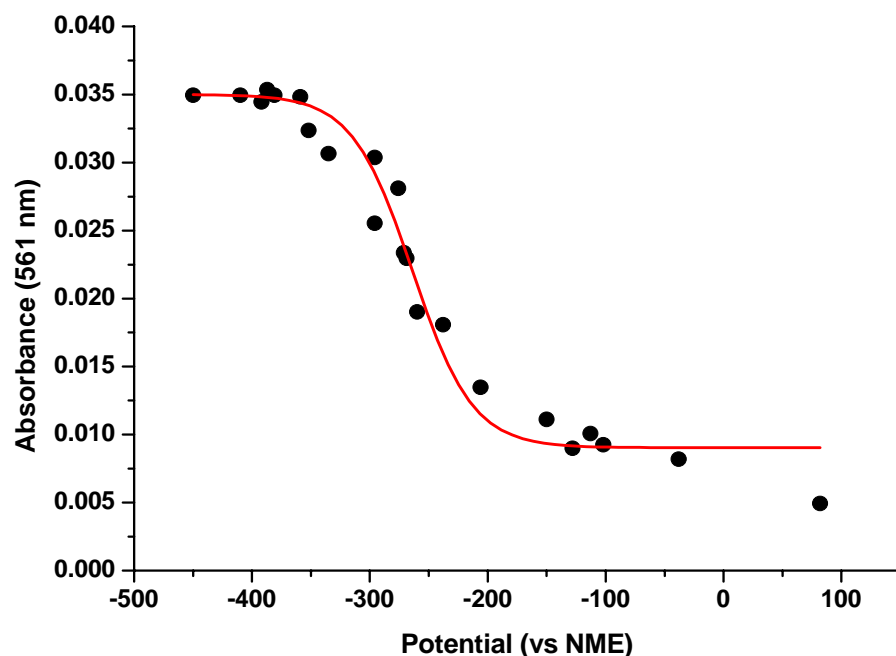


**Figure 4.16** Plot of absorption change *versus* applied potential (relative to NHE) for CYP140A2

The data at 561 nm were fitted to a single electron Nernst function to allow an estimation of the mid-point heme iron reduction potential for the CYP140A2 enzyme. The potential determined is  $-264 \pm 8$  mV.

The redox potential value for substrate-free CYP140A2 is relatively positive compared to that for CYP121 and its P346L mutant. It is also substantially more positive than seen for P450 BM-3 and P450cam in their substrate-free forms, at ~-350 to -400 mV (Sligar, 1976, Munro *et al.*, 1995). Indeed, the potential is rather more positive than that for NAD(P)H and indicates that there is a positive driving force for electron transfer from this coenzyme(s) to the P450 (via redox partners), even for the P450 in its substrate-free form (Kazlauskaite *et al.*, 1996). However, the nature of the optical changes observed on CYP140A2 reduction is distinct from those seen for e.g. CYP121, P450cam and P450 BM-3. The long wavelength shift of the heme Soret band and the sharpening/increase in intensity of the visible region features on reduction likely reflects the protonation of the cysteine thiolate to the thiol in the reduced form of the enzyme. This, in turn, likely reflects the conversion of the P450 form of the enzyme to the “inactive” P420 state. The fact that the redox titration was fully reversible on oxidation, importantly, suggests that any inactivation to the thiol-coordinated form on reduction is reversible, and that the thiolate-coordinated species is re-formed on oxidation of the heme iron. This type of phenomenon has been observed in recently published studies on the *M. tuberculosis* CYP51 enzyme (McLean *et al.*, 2006). Potentiometry analysis in the presence of mycolactone C was not successful due to the low solubility of the substrate, which induced a large amount of turbidity in the protein solution.

## **4.9 Ligand binding**

### **4.9.1 Substrate binding assay**

The presence of the CYP140A2 encoding gene (*mup053*) within the mycolactone biosynthetic locus has led to the suggestion that the proposed function of the P450 is in the synthesis of the hydroxylated macrocyclic polyketide designated mycolactone A/B (Stinear *et al.*, 2004). Furthermore, the absence of the CYP140A2 gene from the mycolactone locus in an Australian *M. ulcerans* (94-1325) strain led to the generation of a less polar lipid molecule as the major mycolactone species (Mve-Obiang *et al.*, 2003). The new mycolactone species corresponded to a mycolactone A/B lacking oxygen, and was designated mycolactone C (Mve-Obiang *et al.*, 2003). *M. liflandii*, a genetically close relative, also produces a novel mycolactone, called mycolactone E. *M. liflandii* contains the previously identified plasmid borne genes for the mycolactone cluster, as was identified for CYP140A2, with the exception of

the gene encoding CYP140A2 (Mve-Obiang *et al.*, 2005). Although the core lactone structure of mycolactone E is identical to that of mycolactone A/B and C, variation does occur in the number of hydroxyl groups and double bonds of the fatty acid side chain (Mve-Obiang *et al.*, 2005). In light of the strong circumstantial evidence for the role of CYP140A2 in the modification of the mycolactone fatty acyl side chain, UV-visible absorption spectroscopy was performed to observe the biophysical interaction of the P450 with mycolactone.

Binding of mycolactone C to CYP140A2 was measured by spectral titration (Figure 4.17). Mycolactone C, the proposed substrate of the P450, did not induce any clear perturbation of the heme Soret peak at up to 40  $\mu\text{M}$  of substrate. However, some form of interaction with the heme pocket was induced upon the binding of mycolactone C, as indicated by minor increases in intensity of the  $\beta$  absorption band (534 nm) relative to the  $\alpha$  band (567 nm). Titrations, with as little as 0.02  $\mu\text{M}$  of mycolactone C, were sufficient to induce very small perturbations of the  $\beta$  band. However, no subsequent significant changes occurred with further increases in the mycolactone concentration. The lack of a shift in the Soret peak, at apparent near-saturating substrate concentrations, is atypical of P450s. However, as shown in (Figure 4.17), the addition of the hydrophobic mycolactone does also result in some turbidity in the solution, making it very difficult to discern true optical changes from non-specific light-scattering. Further evidence for the interaction of morpholine with CYP140A2 was also provided by EPR and resonance Raman studies.

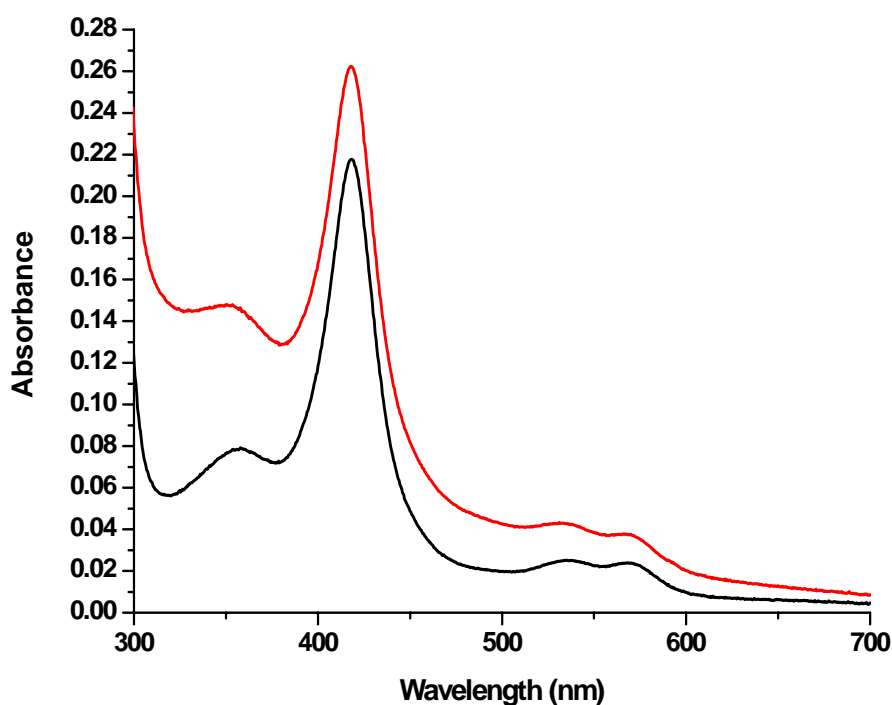


**Figure 4.17 Binding of mycolactone C to CYP140A2**  
 UV-visible spectra displaying oxidised CYP140A2 (~2.2 μM, black) in 50 mM Tris, pH 7.2 (20°C), and following the addition of 2 μM mycolactone C (red).

With such minor heme spectral perturbations upon addition of the proposed substrate, it becomes impossible to use spectral changes to determine binding coefficient ( $K_d$ ) values. The apparent absence of perturbation of the Soret peak could simply reflect a lack of spin-state change on the addition of the mycolactone C, a phenomenon which is quite common on substrate binding to P450s. In general, binding of substrates to the P450 enzymes induces a shift of the heme iron spin state towards the high-spin form, leading to a change in the Soret region of the P450 absorption spectrum. Typical substrates induce low-to-high spin transformation in the electronic ground state of P450s, and this was first reported for ferric P450cam, (Sharrock *et al.*, 1973) and subsequently has been found to be a characteristic feature of many other P450s. This occurs through the displacement of the weakly bound water molecule coordinated to the iron, resulting in electronic reorganisation of the heme iron d-orbitals and thereby an increased high-spin population (Li and Poulos, 1997; Cupp-Vickery *et al.*, 2000). This is typically indicated by a shift of the Soret



band towards ~392 nm, as observed, for example, with the alkane hydroxylase CYP153A6 (Funhoff *et al.*, 2006) upon saturation with substrates. The binding of estriol to *M. tuberculosis* CYP51, produces a heme spectral change towards 392 nm, consistent with formation of a high-spin species (McLean *et al.*, 2006). For P450cam, the binding of the camphor substrate is a prerequisite for initiation of the catalytic cycle (Sligar and Gunsalus, 1976). However, substrate-induced high-spin heme iron formation is not always observed in P450s.

Atypical substrate-induced spectral changes (or lack of these) have been previously reported in a number of P450s. For example, the steroid 15 $\beta$ -hydroxylase (CYP106A2) from *Bacillus megaterium* ATCC 13368 is a prokaryotic P450 which exhibits only a very minor spectral change towards the high-spin form upon addition of substrate (Simgen *et al.*, 2000). Fourier transform infrared spectroscopy of the stretch vibration of the heme-iron CO ligand, as a spectroscopic probe, demonstrated that the substrate deoxycorticosterone bound in the heme pocket. Moreover, the sterols lanosterol and obtusifoliol are oxidatively demethylated by *M. tuberculosis* CYP51, whilst titrations with these compounds produce only marginal spectral shifts within their solubility range in aqueous buffer (Bellamine *et al.*, 1999; Mclean *et al.*, 2006). Further evidence, of unusual characteristics is provided in CYP153A6, with variation in the degree of spin-state change induced by different alkanes (Funhoff *et al.* 2006). In this study octane and nonane induced the largest optical change, while undecane and hexane generated only small changes in the position of the Soret band. However, the extent of perturbation did not reflect the turnover activity, whereby undecane and hexane had the highest turnover numbers. The low solubility of these alkanes may explain the decreased degree of high-spin formation (Funhoff *et al.*, 2006) and a similar situation may partly explain the atypical absorption spectroscopy of CYP140A2 in complex with the highly apolar mycolactone C.

In light of this difficulty in deducing a dissociation constant ( $K_d$ ) for mycolactone C with CYP140A2, competitive inhibition was investigated as a possible method of determining the  $K_d$  upon titration of a CYP140A2/mycolactone C complex with econazole. Econazole titrations in the presence of a specific amount of mycolactone C allowed the estimation of the  $K_d$  value. Although no changes in the Soret peak of CYP140A2 were observed upon binding of mycolactone C within a

reasonable solubility range, a minor increase in the intensity of the  $\beta$ -band absorption reflected some form of substrate-heme interaction. Therefore, titration of the inhibitor econazole to the CYP140A2-mycolactone C complex was followed by observing changes in the Soret band absorption, and resulted in a spectral change in this region similar to that found for azole binding to the inhibitor-free form of CYP140A2 (Figure 4.18). The observed spectral change data were consistent with competitive inhibition behaviour, with displacement of the mycolactone C from the active site upon the binding of econazole. In the reciprocal experiment, no significant level of displacement of econazole in complex with CYP140A2 by mycolactone C was observed. However, this is likely due to a combination of the relatively low solubility of the mycolactone C and the tight binding for econazole to the substrate-free CYP140A2 ( $K_d = 1.85 \mu\text{M}$ , see Table 4.3). Based on a competitive inhibition function (Equation 4), a dissociation constant for mycolactone C was determined through monitoring the change in absorbance of the Soret peak of CYP140A2 once in complex with a specific concentration of mycolactone C, and subsequent to titration with econazole Figure 4.18.

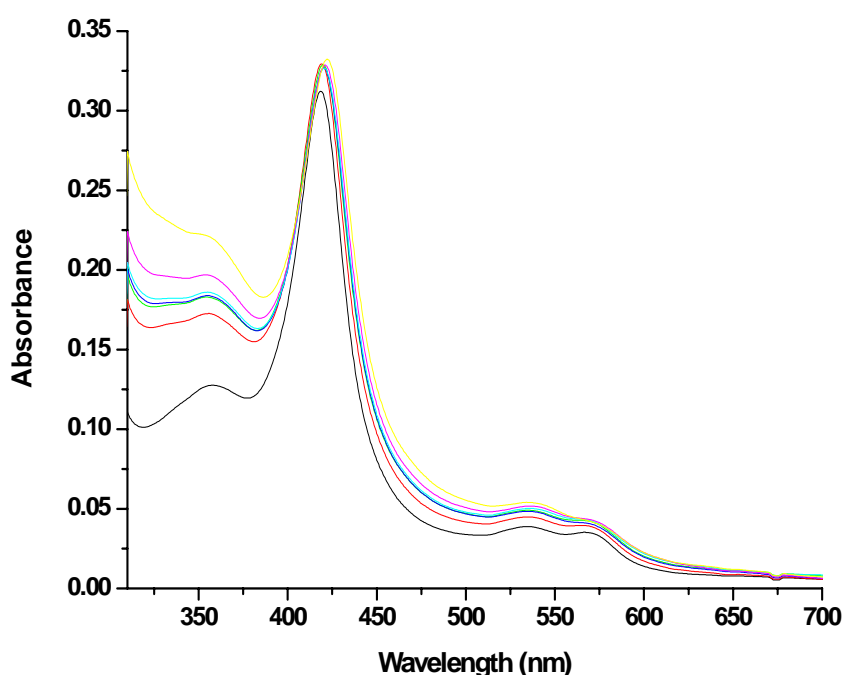


**Figure 4.18 Titration of econazole with CYP140A2 in complex with mycolactone C**

UV-visible spectra displaying a titration of CYP140A2 ( $\sim 3 \mu\text{M}$ , black) in 50 mM Tris-HCl, pH 7.2 with successive additions of econazole at 1.08, 1.62, 2.7, 3.24, 4.86 and  $10.25 \mu\text{M}$  (red, green, blue, cyan, magenta and yellow lines respectively). Mycolactone C was at a concentration of  $6 \mu\text{M}$ .

In order to deduce the  $K_d$ , a difference spectrum was constructed at each point by the subtraction of the spectrum for the CYP140A2-mycolactone C complex from each successive econazole-bound spectrum in the titration. The difference spectra are displayed in Figure 4.19.

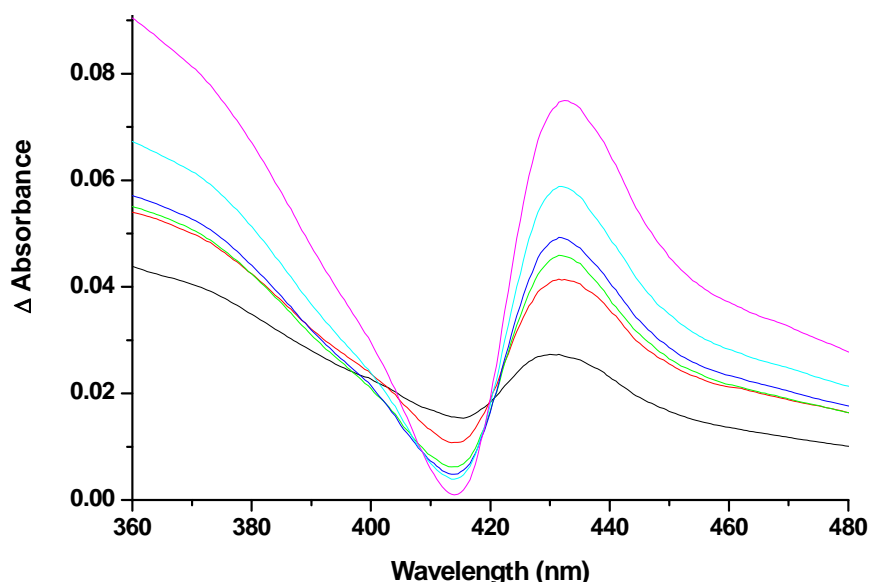


**Figure 4.19** Difference spectra for the CYP140A2 mycolactone C complex upon titration with econazole

Econazole at concentrations at 1.08, 1.62, 2.7, 3.24, 4.86 and 10.25  $\mu\text{M}$ , represented by black, red, green, blue, cyan, and magenta lines, respectively. Mycolactone C was at a concentration of 6  $\mu\text{M}$ . Enzyme was at 3  $\mu\text{M}$  concentration.

The difference spectra generated for the titration of the CYP140A2-mycolactone C complex with econazole display maxima and minima values at approximately 435 nm and 415 nm, respectively. The type II binding spectrum (forazole drugs) is characterised by a peak and a trough, respectively, at the aforementioned wavelengths. For each concentration of econazole, the maximal absorbance difference was determined by subtraction of the absorbance value at the trough from that at the peak in each difference spectrum (using the same wavelength values for each). These values were subsequently plotted against the corresponding concentration of econazole, and the data fitted to a competitive inhibitor function, to determine the inhibition coefficient ( $K_i$ ) for the binding of mycolactone C, Figure 4.20.

The titration curve generated a binding constant;  $K_i = 3.27 \pm 0.31 \mu\text{M}$  for mycolactone C.

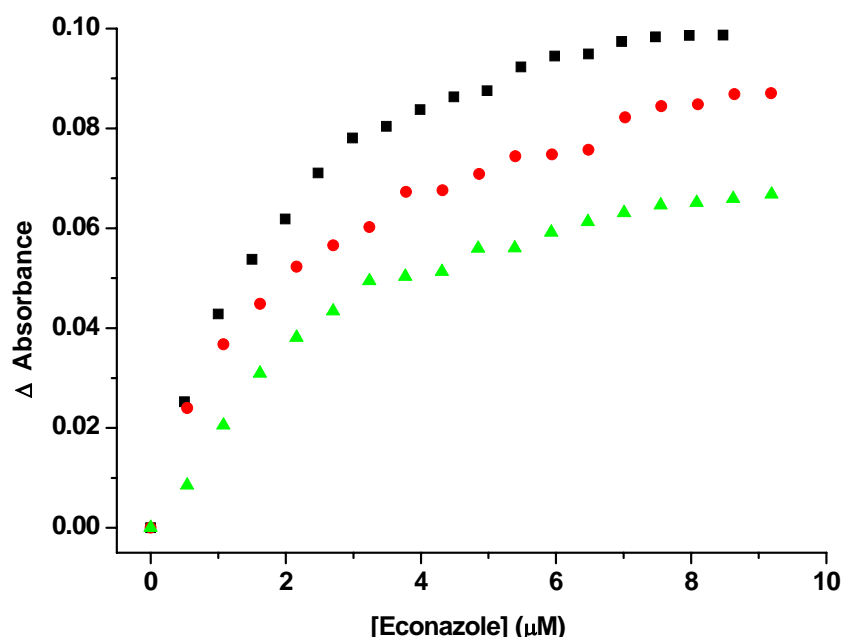


**Figure 4.20 Titration curve for the binding of econazole to the CYP140A2-mycolactone C complex**

Titration of CYP140A2 was done in the presence of 6  $\mu\text{M}$  (red circles) and 12  $\mu\text{M}$  (green triangles) mycolactone C, with the subsequent data fitted to a competitive inhibitor function (Equation 4), yielding a mycolactone C  $K_d = 3.27 \pm 0.31 \mu\text{M}$ ,  $4.07 \pm 0.42 \mu\text{M}$ , respectively. Econazole titration (black squares) was fitted to a hyperbolic function (Equation 3), yielding a  $K_d = 1.85 \pm 0.06 \mu\text{M}$ .

Binding of mycolactone C to CYP140A2 did not induce spectral changes in the Soret peak of CYP140A2, as described previously. However, addition of econazole to the mycolactone-complexed P450 induced a type II spectral change with a shift of the Soret peak to 425 nm. This is associated with reinforcement of the low-spin state of the heme macrocycle and the coordination of the heme iron by an azole nitrogen atom. Changes were also observed in the visible region of the spectrum, but these are smaller and are obscured somewhat by the turbidity in the spectrum on addition of the two hydrophobic molecules (mycolactone C and econazole). The observed spectral changes were similar to those for the azole titrated mycolactone C-free CYP140A2, discussed in section 4.7.1, which produced a  $K_d$  value of  $0.36 \mu\text{M}$  for econazole. In order to further verify the  $K_d$  estimate for mycolactone C, the econazole titration experiment was repeated with the same concentration of

CYP140A2 in the presence of 12  $\mu\text{M}$  of mycolactone C. A fit of econazole-induced absorption shift data (as shown in Figures 4.18-4.20 above) yielded a very similar  $K_d$  value of  $4.07 \pm 0.42 \mu\text{M}$  as that determined in presence of 6  $\mu\text{M}$  mycolactone C ( $3.27 \pm 0.31 \mu\text{M}$ ).

The capability of CYP140A2 to bind to other bulky polyketides was investigated through titration of the P450 with up to 10 mM of the antibiotics erythromycin and tylosin. However, no optical changes were detected. Furthermore, in view of the apparent strong affinity for a macrolide comprising a long-chain fatty acyl side chain, and the proposed role of CYP140A2 in the hydroxylation of the side chain; a number of long chain fatty acid compounds were also tested for binding to CYP140A2. Binding of a number saturated fatty acids; lauric ( $\text{C}_{12}$ ), myristic ( $\text{C}_{14}$ ), palmitic ( $\text{C}_{16}$ ), as well as the unsaturated fatty acids myristoleic ( $\text{C}_{14}$ ), palmitoleic ( $\text{C}_{16}$ ) and arachidonic acid ( $\text{C}_{20}$ ) were performed. This study was also done to obtain some indication as to whether the major driving force for binding of mycolactone C to CYP140A2 is due to the fatty acyl side chain or to the contribution of the core lactone ring.

The long chain saturated and unsaturated fatty acids did not induce any significant substrate-like high-spin shifts in the heme iron spin-state equilibrium (i.e. optical Soret shifts towards  $\sim 394 \text{ nm}$  or other notable spectral changes to the heme absorption) with up to 50  $\mu\text{M}$  of these putative substrate-like molecules (Figure 4.21).

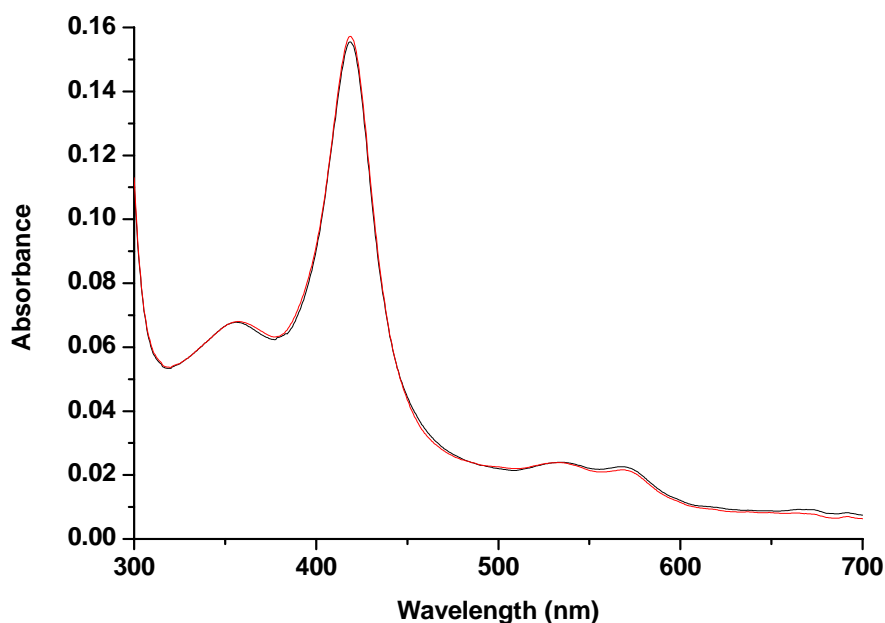


**Figure 4.21 Binding of palmitic acid (C<sub>16</sub>, saturated fatty acid) to CYP140A2**  
 UV-visible spectra for oxidised, ligand-free CYP140A2 (~1.5 μM, black) in 50 mM Tris-HCl, pH 7.2 (20 °C), with the same P450 following the addition of 20 μM palmitic acid (red).

The lack of any significant spectral changes following the addition of the long-chain fatty acids does not necessarily indicate no binding in the heme pocket. The fatty acids could be located some distance from the heme iron, and only very minor changes in the Q-band region were observed previously upon binding of the likely substrate mycolactone C. However, in the case of addition of the fatty acids there are no obvious spectral effects in the CYP140A2 Q-band region. The evidence likely suggests that the core lactone ring has an important role in controlling the binding of the mycolactone C, and enabling its fatty acid side chain to approach close to the heme macrocycle of the P450. Studies with the precise structural side chain component would be required to confirm this suggestion, however.

#### 4.9.2 Inhibitor binding assays

The usual first sign of the severe skin infection that is Buruli ulcer is a small painless swelling in the skin (Marsollier *et al.*, 2007). This usually heals, but the resultant scar can severely restrict limb movement. Consequently, 25% of people affected by Buruli ulcers, who are predominantly children, are permanently disabled

(Marsollier *et al.*, 2007). If the disease is caught early, antibiotics can prevent ulcer formation. However, there is a need to identify more robust drugs for treatment. But most patients do not seek help until the later stages when the only treatment is to cut out the infection and to do a skin graft; a costly and lengthy treatment (Marsollier *et al.*, 2007).

Azole antifungal compounds are used as systemic fungicides. Of particular interest is the effect of these agents on ergosterol biosynthesis and the subsequent effect on the fungal cell membrane and cell wall synthesis and composition, which are obvious points of chemotherapeutic attack (Fromtling, 1998). Application of these azoles in Buruli ulcer treatment may lead to interference with cellular permeability and result in deregulation of the *M. ulcerans* envelope synthesis. This may serve as a means for selective cytotoxicity to *M. ulcerans*, as previously suggested for *M. tuberculosis* infections (McLean *et al.*, 2002b). The antifungal activity is based on the inhibition of fungal CYP51 (lanosterol-14 $\alpha$ -demethylase) and thus inhibition of sterol biosynthesis (Pfaffler *et al.*, 1990). The mode of inhibition by azoles is based on coordination to the heme iron site, and by displacement of the distal H<sub>2</sub>O to the heme iron by the azole ring nitrogen. This prevents the binding of oxygen during catalysis, and likely even the preceding reduction of the heme iron. Potentially, the azole-based inhibition of CYP140A2 would lead to prevention of the formation of the mycolactone toxin, and could thus be a useful medical treatment.

The binding of structurally diverse azole-based inhibitors to CYP140A2 was evaluated to further probe the spatial properties of the CYP140A2 active site and the effects of aromatic and alkyl substitutions on affinity for azole derivatives. As described,  $K_d$  values were determined from optical titrations with the azole drugs (Table 4.3).

Inhibitor	CYP140A2 $K_d$ ( $\mu$ M)	CYP121 $K_d$ ( $\mu$ M)
Miconazole	$0.11 \pm 0.02$	$0.09 \pm 0.05$
Clotrimazole	$0.36 \pm 0.15$	$0.07 \pm 0.03$
Ketoconazole	$1.15 \pm 0.05$	$3.30 \pm 0.30$
Econazole	$1.85 \pm 0.06$	$0.31 \pm 0.04$
Fluconazole	No binding	$9.70 \pm 0.60$
Voriconazole	No binding	ND
Imidazole	$147.2 \pm 4.9$ mM	$64 \pm 3$ mM
1-phenylimidazole	$6.47 \pm 0.05$	ND
4-phenylimidazole	$2.13 \pm 0.12$	$53 \pm 3$
ImC10	$0.86 \pm 0.14$	ND
ImC11	$0.21 \pm 0.12$	ND
ImC12	$0.19 \pm 0.06$	ND
1H-1,2,4-Triazole, 1-tricyclo(3.3.1.1 <sup>3,7</sup> )dec-1-yl	No binding	No binding

**Table 4.3** Dissociation constants ( $K_d$  values) for inhibitor binding to CYP140A2

Data generated from the quadratic equation (Equation 4) A for clotrimazole, ketoconazole, miconazole, econazole, ImC10, ImC11 and ImC12, or from fitting to a hyperbolic function (equation 2) in the case of imidazole, 1-PIM (1-phenylimidazole) and 4-PIM (4-phenylimidazole). CYP121 data obtained from McLean *et al.*, 2006. ImC10, ImC11 and ImC12 are  $\omega$ -imidazolyl alkanolic acid derivatives of indicated carbon chain length. ND: not determined.

Binding of imidazole and the substituted imidazoles, 1-phenylimidazole (1-PIM) and 4-phenylimidazole (4-PIM) to CYP140A2 was shown to induce a type II inhibitor-like spectral change, with a decrease in the intensity of the original Soret feature and a shift of the Soret maximum to ~425 nm at saturation; spectral features characteristic of the reinforcement of low-spin heme iron and imidazole coordination to heme iron. Also noted upon imidazole and PIM binding is the merger of  $\alpha$  (originally at 566 nm) and  $\beta$  (originally at 535 nm) bands into a new spectral feature



at 537 nm. Spectral titrations with imidazoles and the PIMs were performed and  $K_d$  values determined by fitting induced absorption change *versus* ligand concentration data to a hyperbolic function, producing values of  $147.2 \pm 4.9$  mM,  $6.47 \pm 0.05$   $\mu$ M and  $2.13 \pm 0.12$   $\mu$ M for imidazole, 1-PIM and 4-PIM, respectively. The addition of a hydrophobic phenyl moiety to the imidazole (for 1- PIM and 4-PIM compared to imidazole) is sufficient to increase the affinity (i.e. lower the  $K_d$  value) by a factor of more than  $10^4$ . No spectral perturbations were observed on titration of CYP140A2 with up to 20 mM of 1H-1,2,4-Triazole, 1-tricyclo(3.3.1.1<sup>3,7</sup>)dec-1-yl, an azole-based inhibitor provided by GSK for use in these studies.

In view of the likely affinity of CYP140A2 for long chain saturated and/or unsaturated fatty acids (given the alkyl chain component of the mycolactone substrate), the  $K_d$  values for the binding of  $\omega$ -imidazolyl alkanolic acid derivatives were determined from optical titrations, in order to probe further the spatial and chemical properties of the CYP140A2 active site. The imidazole derivatives used were those of decanoic acid (ImC10,  $C_{13}H_{23}N_2O_2$ ), undecanoic acid (ImC11,  $C_{14}H_{25}N_2O_2$ ) and lauric (dodecanoic) acid (ImC12,  $C_{15}H_{27}N_2O_2$ ) (Lu *et al.*, 1997). Binding of these azoles induced a type II shift in the heme spectrum, associated with reinforcement of low-spin heme iron and azole coordination to heme iron; and the Soret band shifted to a maximum at a longer wavelength (425 nm). The spectral perturbations upon saturation were identical to those previously described with the imidazole and PIM titrations.

The binding of imidazole itself was relatively weak ( $K_d = 147.2 \pm 4.9$  mM), whilst 4-PIM bound significantly more tightly ( $K_d = 2.13 \pm 0.55$   $\mu$ M). However, attachment of an alkyl chain ( $C_{10}$ - $C_{12}$ ) to the imidazole resulted in a  $>10^6$ -fold improvement in binding for these molecules, taking the  $K_d$  values into the nanomolar range (Table 4.3). Evaluation of the binding of  $\omega$ -imidazolyl alkanolic acid compounds to the fatty acid binding P450 BioI also revealed tight binding, although not quite as tight as that observed here with CYP140A2. The P450 BioI  $K_d$  values were determined as ImC10 ( $2.6 \pm 0.2$   $\mu$ M), ImC11 ( $1.5 \pm 0.2$   $\mu$ M) and ImC12 ( $1.0 \pm 0.2$   $\mu$ M) at 30°C, pH 7.0 (Lawson *et al.*, 2004). In view of the likely affinity of CYP140A2 for the alkyl side chain of mycolactone C, the extremely tight binding of the  $\omega$ -imidazolyl alkanolic acid derivatives to CYP140A2 is perhaps to be expected.

The binding of  $\omega$ -imidazolyl alkanoic acid derivatives to CYP140A2 proved too tight to analyse accurately, even at low concentrations of the enzyme ( $<1.0\ \mu\text{M}$ ) (Table 4.3). The optical changes associated with these azole ligations occur linearly with azole concentration, sharply reaching a plateau and representing near-stoichiometric binding to the P450. However, it must be noted that fitting to the described quadratic equation (Equation 2) may not provide a highly accurate solution, due to the extremely tight binding observed. This suggests that the true  $K_d$  values for binding these inhibitors may actually be even lower than predicted, an occurrence previously described for polycyclic azole binding to wild-type CYP121 (McLean *et al.*, 2002b), and for fatty acid-linked inhibitors binding to P450 BM-3 (Ortiz de Montellano *et al.*, 1995).

The binding of selected anti-fungal azole inhibitors to CYP140A2 was investigated to further probe the spatial and chemical properties of the active site. The binding of clotrimazole to the CYP140A2 ferric heme iron, as for the other azole complexes, induced a shift in the absorbance maximum from 418.5 nm to 425 nm (Figure 4.22). The azole-induced type II binding spectrum occurs as a result of binding of the azole nitrogen to the sixth coordination position of the heme iron. Also noted upon azole binding is the apparent fusion of the  $\alpha$ - and  $\beta$ - bands to form a new spectral species at 537 nm (Figure 4.22). The changes in absorbance of CYP140A2 upon titration with clotrimazole are displayed in Figure 4.22.

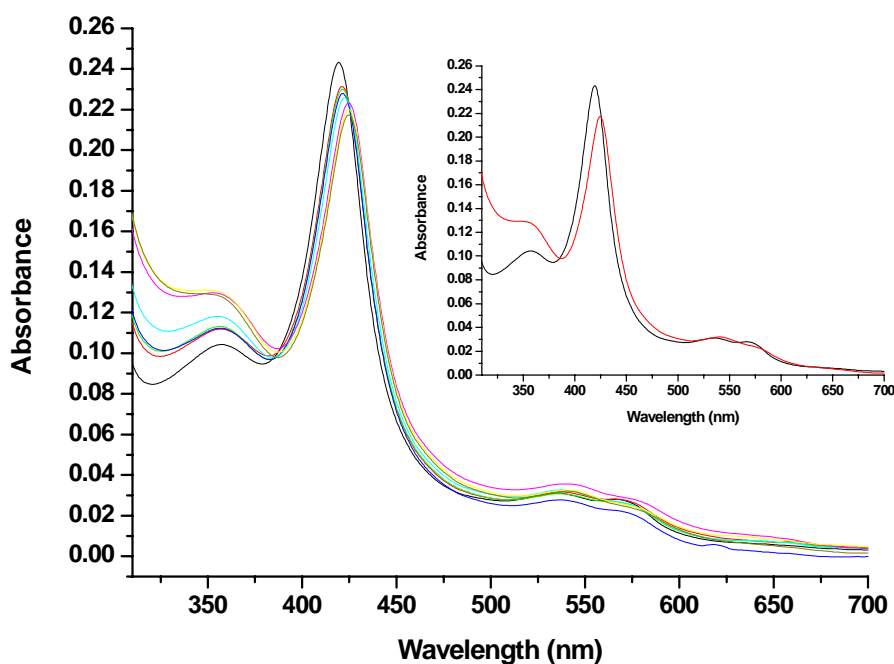


**Figure 4.22 Binding of clotrimazole to CYP140A2**  
 UV-visible spectra displaying a titration of CYP140A2 ( $\sim 2.5 \mu\text{M}$ , black spectrum) in 10 mM Tris-HCl, pH 7.5 with successive additions of clotrimazole at 0.13, 0.16, 0.19, 0.23, 0.32, 0.96 and  $2.57 \mu\text{M}$  (red, green, blue, cyan, magenta, yellow and dark yellow lines, respectively). The full extent of the absorbance shift is shown (inset) with inhibitor-free (black) and inhibitor-saturated (red) forms.

In order to analyse the titration with clotrimazole, a difference spectrum was constructed at each point by the subtraction of the spectrum for the inhibitor-free form from each successive inhibitor-bound spectrum in the titration. The generated difference spectra are displayed in Figure 4.23.

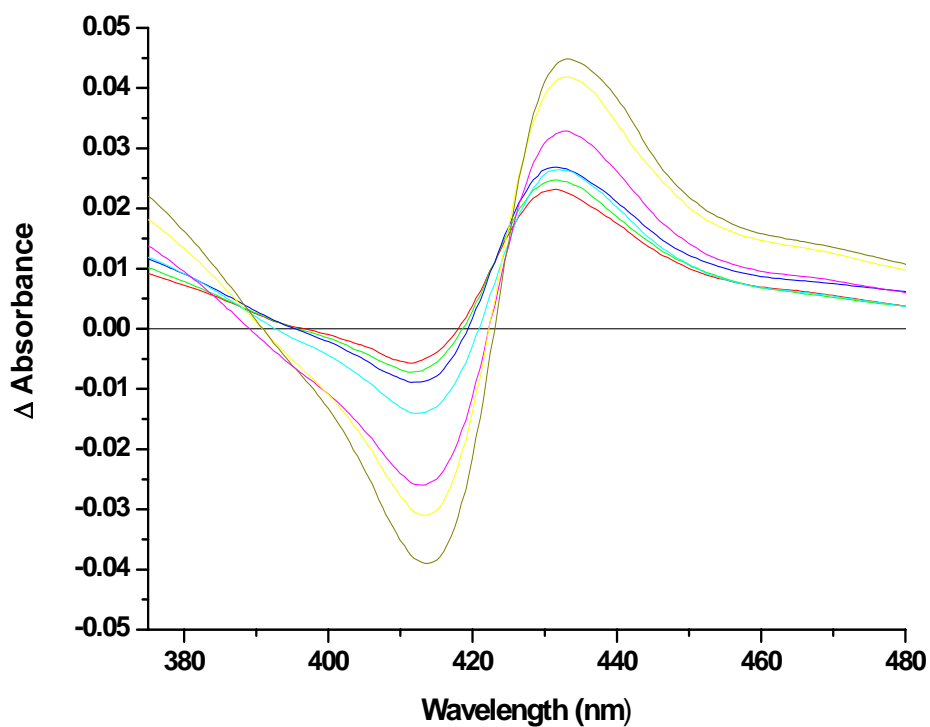


**Figure 4.23 Difference spectra for CYP140A2 titrated with clotrimazole**  
 Difference spectra for CYP140A2 titrated with clotrimazole at concentrations of 0.13, 0.16, 0.19, 0.23, 0.32, 0.96 and 2.57  $\mu\text{M}$  (red, green, blue, cyan, magenta, yellow and dark yellow lines, respectively).

The difference spectra are characterised by a peak at 434 nm and a trough at 414 nm (Figure 4.23). The clotrimazole binding constant for CYP140A2 was measured as described previously (Figure 4.24). The affinity of CYP140A2 for clotrimazole was very tight, and the binding constant ( $K_d$ ) was determined as  $0.36 \pm 0.15 \mu\text{M}$ .

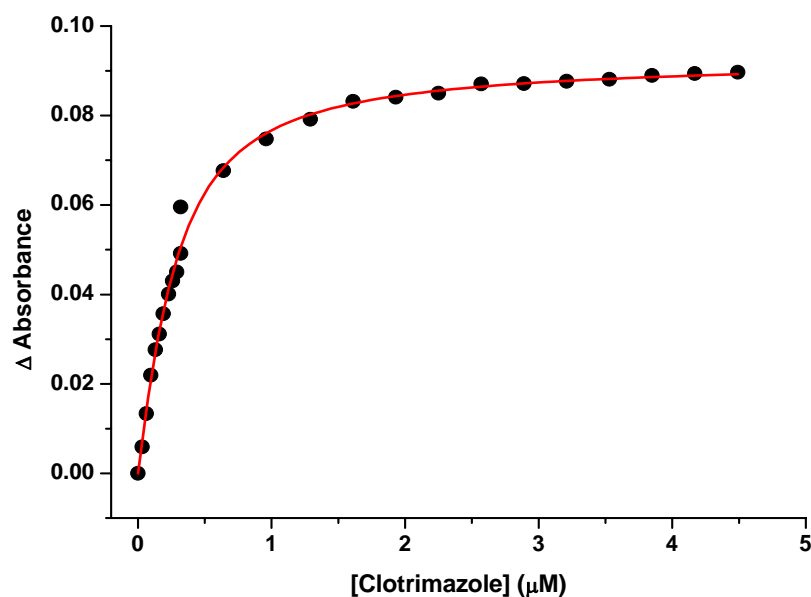


**Figure 4.24 Titration curve for the binding of clotrimazole to CYP140A2**  
Data were processed as described above. CYP140A2 concentration was 2.5  $\mu\text{M}$ . Data were fitted to the quadratic function, yielding a  $K_d = 0.36 \pm 0.15 \mu\text{M}$ .

The binding of miconazole, clotrimazole, ketoconazole and econazole to CYP140A2 proved too tight to analyse accurately using standard hyperbolic fits to the data, even at low concentrations of the enzyme ( $<1.0 \mu\text{M}$ ) (Table 4.3). The heme optical change associated with binding of the antifungal azole drugs occurred linearly with azole concentration, sharply reaching a plateau and indicative of near-stoichiometric binding to the P450 (Figure 4.24). The quadratic equation (Equation 2) accounts for the quantity of ligand complexed with the P450 and thus is an improved measure of tight ligand binding processes compared to a conventional hyperbolic function. Clearly, the  $K_d$  values for these azoles are very low. However, it is possible that even the quadratic fits do not describe the  $K_d$  values with sufficient accuracy. As with the  $\omega$ -imidazolyl alkanoic acid derivatives, the  $K_d$  may be lower than predicted, as also was described for polycyclic azole binding to wild-type CYP121 (McLean *et al.*, 2002b). Optical titrations with up to 10 mM fluconazole and voriconazole revealed no spectral perturbation. Fluconazole and its structurally derived partner voriconazole are polar compounds used clinically as systematically-tolerated antifungals. The apparent lack of binding for these drugs may reflect the very low affinity of these azoles for the apolar environment of the P450 active site, and could indicate the clear preference of CYP141A2 for hydrophobic compounds.

Evidently, CYP140A2 has a high affinity for polycyclic azoles, although the affinity of CYP140A2 for these azoles is apparently slightly lower than that noted for CYP121 (Table 4.3) (McLean *et al* 2006). The characterised polyketide metabolising P450EryF, involved in the synthesis of erythromycin, is also noted for its high affinity for anti-fungal azoles (Cupp-Vickery *et al.*, 2001). This tight binding observed for the polycyclic azoles is strongly indicative of a relatively large and flexible active site in this P450 enzyme. The strong CYP140A2 binding interactions with both bulky polycyclic type molecules and with long alkyl chain-containing inhibitors are consistent with the role of this P450 in the hydroxylation of the large polycyclic molecule mycolactone.

#### **4.10 Turnover of mycolactones C and E**

The *M. ulcerans* gene *mup053*, encoding CYP140A2, is located within the mycolactone biosynthetic locus and CYP140A2 has been proposed to participate in the synthesis of a mixture of *cis/trans* isomers designated mycolactone A and mycolactone B (Figure 1.16) (Stinear *et al.*, 2004). The absence of the CYP140A2 encoding gene from this locus has been reported in an Australian *M. ulcerans* (94-1325) strain, resulting in a less polar lipid molecule as the major mycolactone species. This mycolactone species corresponds to mycolactone A/B lacking oxygen and was designated as mycolactone C (Mve-Obiang *et al.*, 2003). Furthermore, *M. liflandii* produces a novel plasmid-encoded mycolactone, mycolactone E. *M. liflandii* contains all of the genes in the mycolactone cluster, with the exception of that encoding CYP140A2 (Mve-Obiang *et al.*, 2005). Although the core lactone structure is conserved in mycolactone E, the fatty acid side chain differs from that of mycolactone A/B in the number of hydroxyl groups and double bonds (Mve-Obiang *et al.*, 2005).

In order to obtain direct evidence of the involvement of CYP140A2 in the hydroxylation of mycolactone, the enzyme was incubated for 20 hours with 10  $\mu$ M mycolactone C or E and a redox partner system comprising *E. coli* flavodoxin and flavodoxin NADP<sup>+</sup> oxidoreductase, as well as NADPH (as described in section 2.7).

Preliminary LC-MS analysis of the reaction mixture (i.e. prospectively a mycolactone A/B-like oxidised product together with any unconverted mycolactone C) enabled comparison of the relative retention times of molecules eluting from the

column with  $m/z$  values the same as those of mycolactone C substrate (749.49, Figure 4.25B) and the expected product containing an additional oxygen atom ( $m/z$  765.47, Figure 4.25C). The post-turnover analysis showed that major peaks relating to the expected  $m/z$  of the hydroxylated product eluted at different retention times (*ca* 20-23 min) from that of the substrate mycolactone C (*ca* 26-31 min).

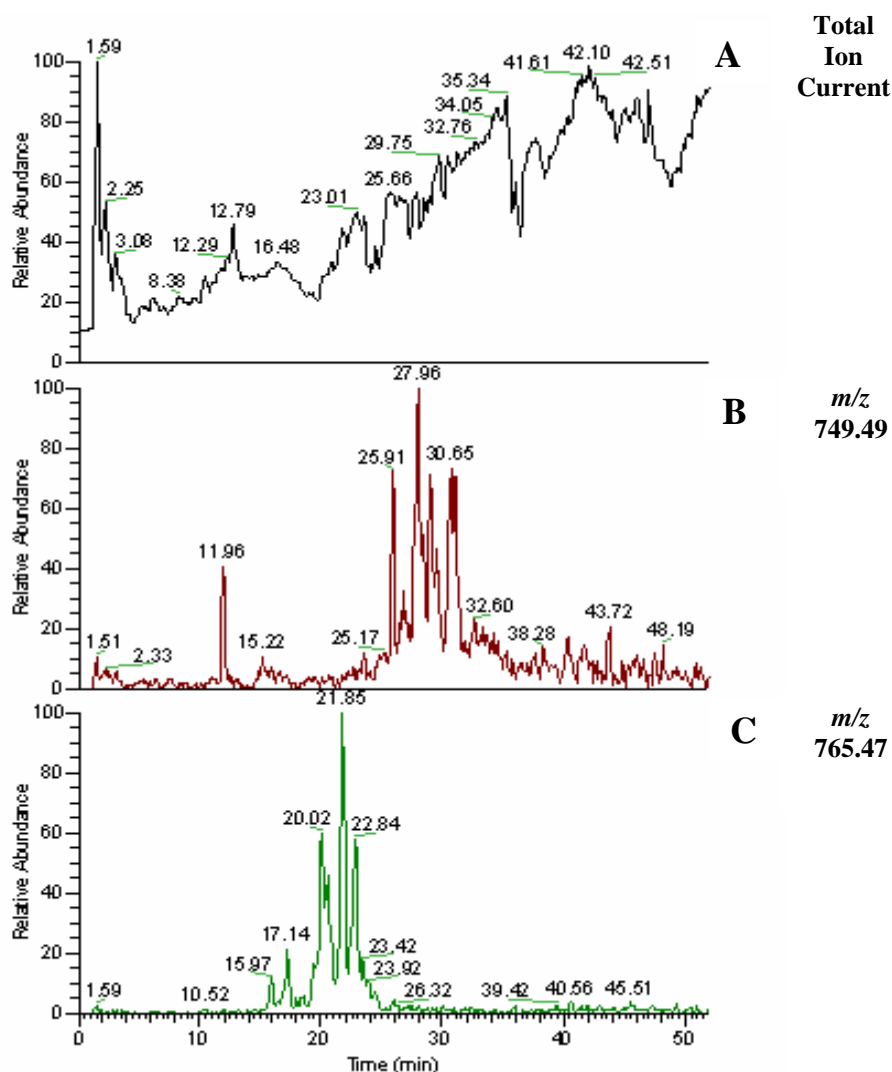


**Figure 4.25** LC-MS analysis of mycolactone C turnover (A) total ion current; (B) ion trace at  $m/z$  749.49 (mycolactone C); and (C) ion trace at  $m/z$  765.47 (postulated hydroxylated mycolactone C). Preliminary mass spectrometry data thus indicate that CYP140A2 likely catalyses oxidation of mycolactone C.

The LC-MS analysis of the turnover extracts clearly showed the presence of molecules of the appropriate  $m/z$  (765.47) (Figure 4.25 B) to be a *bona fide* product

derived from CYP140A2-dependent oxidation of mycolactone C, i.e. 16 mass units higher than mycolactone C (substrate,  $m/z$  749.49) (Figure 4.25 C). The difference in the retention times between mycolactone C ( $m/z$  749.49) and the putative hydroxylated product ( $m/z$  765.47), was consistent with the more polar nature of the likely product (i.e. containing a hydroxyl group) and its likely lower affinity for the hydrophobic LC column matrix.

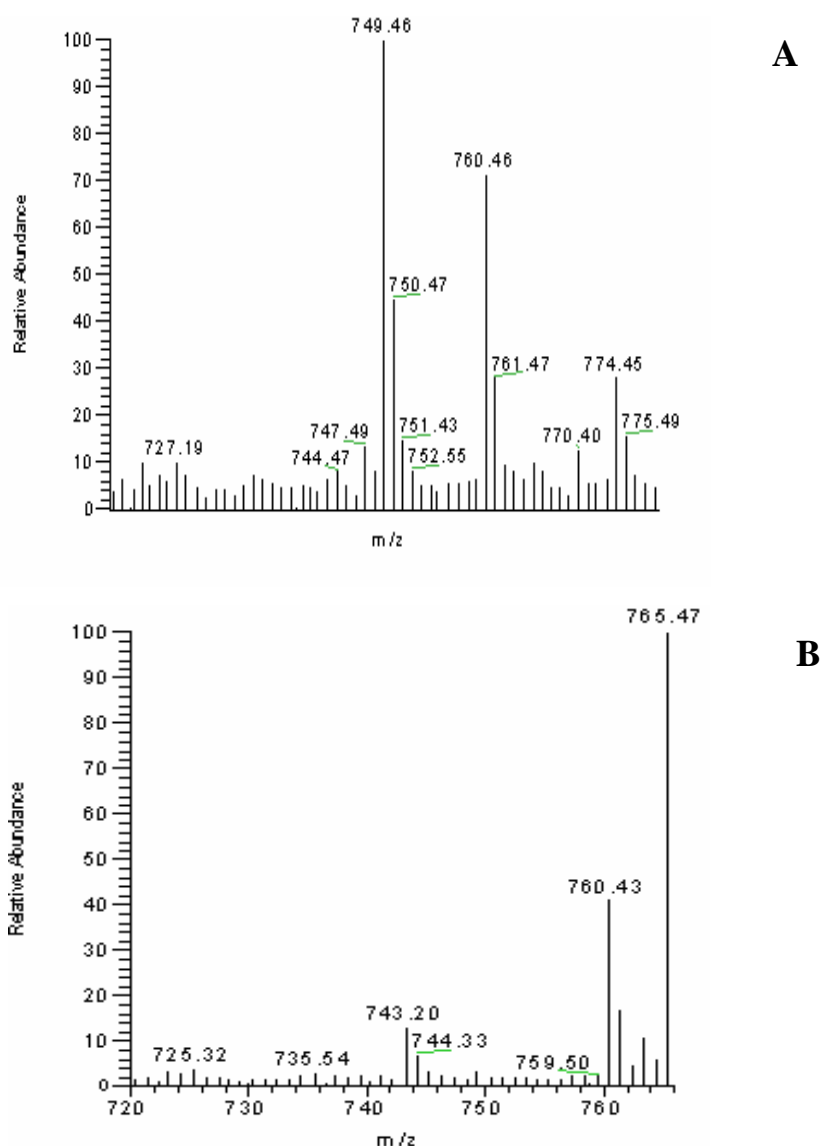


**Figure 4.26 MS spectra of mycolactone C turnover molecular ions**  
 Mycolactone molecular ions (A) at retention time range 27-32 min ( $m/z$  749.49 = mycolactone C) and (B) retention time range 19-23 min ( $m/z$  765.47 = hydroxylated mycolactone C). Some minor contaminants are also observed. Data confirm CYP140A2-catalysed oxidation of mycolactone C.



Having identified the retention times of the major peaks in the turnover assay relating to the expected mass of the hydroxylated product ( $m/z$  765.47) and the residual substrate ( $m/z$  749.49) (Figures 4.25C, B respectively), MS analysis was performed on the spectrum of molecules eluting within these time windows in order to resolve the specific  $m/z$  values of the eluted ions (Figure 4.26A, B).

MS of the ions eluted at the retention time range of 27-32 min are shown in Figure 4.26A. The major ion in the spectrum has a  $m/z$  of 749.49, indicating the presence of the non-hydroxylated substrate. Identical MS analysis of the ions eluted at the retention time range of 19-23 min (Figure 4.26B) revealed a predominant molecular ion species of  $m/z$  765.47, suggestive of the addition of an oxygen atom (+16) to the mycolactone C substrate.

It is thus concluded that the  $m/z$  765.47 species indicates the successful P450-dependent oxidation of mycolactone C leading to the formation of a mycolactone A/B like molecule. The current method of analysis, however, was not able to distinguish between the different possible geometric (E/Z) isomers of the new hydroxylated mycolactone. Previous LC-MS analysis reported C12 as the likely site for the hydroxylation on mycolactone C (Hong *et al.*, 2003). Product-to-substrate ratio in the experiment reported in my work was of the order of 3:1, indicating a good level of turnover of the substrate, even using a non-physiological redox partner system.

Although the core lactone structure is conserved in mycolactone E ( $C_{43}H_{70}O_8Na$ ,  $m/z$  737.46), the lipid side chain differs from that of mycolactone C in the number of double bonds of the side chain and in that it lacks a terminal methyl group (Mve-Obiang *et al.*, 2005, Figure 1.16). The data for mycolactone E turnover (performed as described above for mycolactone C) are shown in Figures 4.27 and 4.28.

Initial LC-MS analysis of the mycolactone E reaction mixture (prospectively containing substrate and oxidised product, as for mycolactone C) again enabled comparison of the relative retention times of molecules eluting from the column with  $m/z$  values the same as those of mycolactone E substrate ( $m/z$  737.46, Figure 4.27B) and the expected product containing an additional oxygen atom ( $m/z$  753.48, Figure 4.27C). The post-turnover analysis again showed that major peaks relating to the

expected  $m/z$  of the hydroxylated product eluted at different retention times (*ca* 19-24 min) from that of the substrate mycolactone E (*ca* 28-33 min).

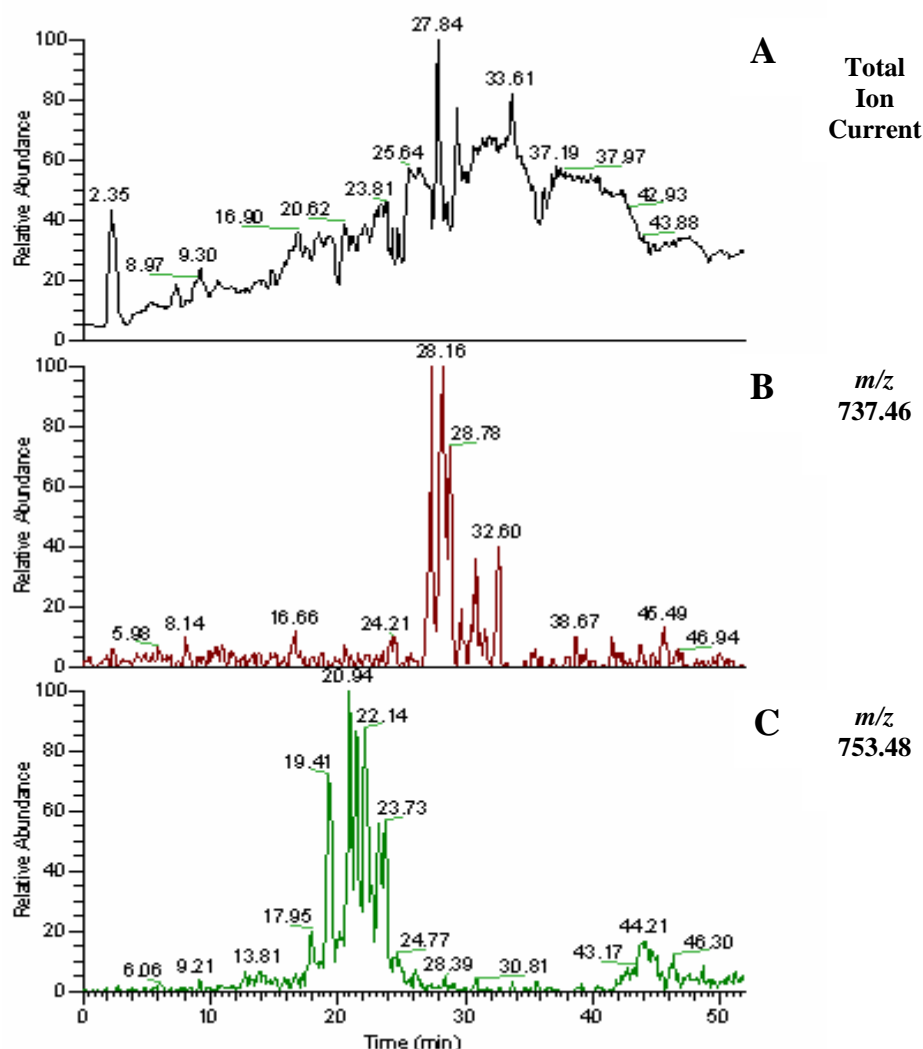


**Figure 4.27 LC-MS analysis of mycolactone E turnover**  
 (A) total ion current; (B) ion trace at  $m/z$  737.46 mycolactone E; and  
 (C) ion trace for  $m/z$  753.48 (postulated hydroxylated mycolactone E).  
 Preliminary mass spectrometry data thus indicate that CYP140A2  
 likely catalyses oxidation of mycolactone E.

The LC-MS analysis of the turnover extracts again clearly showed the presence of molecules of the appropriate  $m/z$  (753.48), 16 mass units higher than that for the mycolactone E substrate ( $m/z$  737.46), as anticipated following insertion of an oxygen atom into the substrate. As for mycolactone C, the difference in the retention times between mycolactone E and the putative hydroxylated product is likely a

consequence of the greater polarity of the latter and its lower affinity for the hydrophobic LC column matrix.

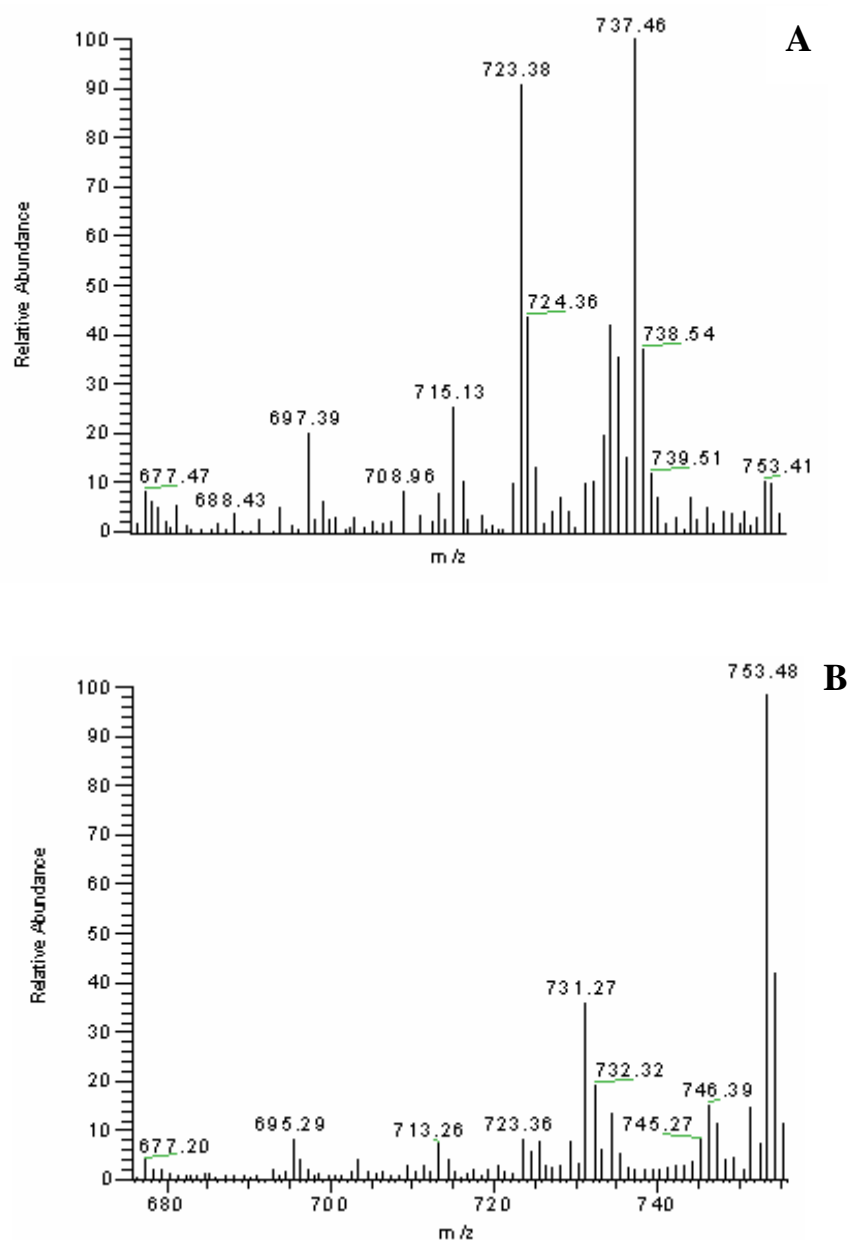


**Figure 4.28 MS spectra of mycolactone E turnover molecular ions**  
 Mycolactone molecular ions (A) at retention time range 27-29 min ( $m/z$  737.46 = mycolactone E) and (B) retention time range 19-25 min ( $m/z$  753.48 = hydroxylated mycolactone E). Some minor contaminants are also observed. Data confirm CYP140A2-catalysed oxidation of mycolactone E.

Having identified the retention times of the major peaks in the turnover assay relating to the expected mass of the hydroxylated product ( $m/z$  753.48) and the

residual substrate ( $m/z$  737.46) (Figures 4.27C, B respectively), MS analysis was performed on the spectrum of molecules eluting within these time windows in order to resolve the specific  $m/z$  values of the eluted ions (Figure 4.28A, B).

MS of the ions eluted at the retention time range of 27-29 min are shown in Figure 4.28A. The major ion in the spectrum has a mass of 737.46  $m/z$ , indicating the presence of the non-hydroxylated substrate. Identical MS analysis of the ions eluted at the retention time range at 19-25 min (Figure 4.28B), revealed a predominant molecular ion species of  $m/z$  753.48, indicative of the addition of an oxygen atom (+16) to the mycolactone E substrate. Clearly the formation of the  $m/z$  753.48 molecular ion reveals the successful turnover (i.e. hydroxylation) of mycolactone E. Product-to-substrate ratio for the mycolactone E turnover was of the order of 2:1, slightly less than for the mycolactone C oxidation analysed here.

In summary, the findings presented demonstrate the capability of CYP140A2 (in the presence of NADPH and a non-mycobacterial, class I-type P450 redox partner system) to mediate the hydroxylation of mycolactones C and E; molecules which share the same core lactone structure, but have different linear polyketide chain structures. The higher level of product formation with mycolactone C is possibly indicative that mycolactone C is the preferred substrate. Thus, the one fewer C=C bond in the side-chain of mycolactone E and/or the absence of a terminal methyl group in its side chain could result in its weaker binding to CYP140A2. However, given that an extended period of time is required for any extensive oxidation of either mycolactone substrates, it is also quite likely that the redox partner system is considerably less efficient in CYP140A2 reduction than is the homologous redox partner system from *M. ulcerans*.

#### 4.11 Summary

The *mup053* gene from pathogenic *Mycobacterium ulcerans*, the aetiological agent of Buruli ulcer was found to encode a P450 that displayed characteristic electronic absorption features in the oxidised form, with the major Soret absorption band at 418 nm, and with  $\alpha$  and  $\beta$  bands at 567 and 534 nm, respectively. Carbon monoxide binding gave rise to the characteristic Soret band shift to 449 nm.

Resonance Raman and EPR and MCD spectra show the protein to be predominantly low-spin and to have a typical cysteinate- and water-ligated *b*-type heme iron, whilst CD spectra in the far-UV region indicate a predominantly alpha helical conformation. Studies of substrate binding to CYP140A2 using EPR and resonance Raman indicated binding of mycolactone C in the vicinity of the heme pocket, and reported on its influence on the heme macrocycle. CYP140A2 was also found to bind very tightly to a range of azole antifungal drugs, suggesting that it may represent a novel target for these antibiotics in the *M. ulcerans* pathogen, and that this strategy could provide an avenue for future treatment of the disease. Reconstitution of an artificial redox system enabled electron transfer to CYP140A2 and demonstrated that this P450 was competent in the hydroxylation of both mycolactone C and mycolactone E.

# Chapter 5

## Characterisation of the P450 CYP151A2 (P450mor)

## **5.1 CYP151A2**

### **5.1.1 Preface**

Biodegradation of industrial organic pollutants is of special environmental interest and thus gaining a clearer understanding of the processes by which degradation occurs and the types of micro-organisms involved is a crucial step. According to the WHO's International Programme on Chemical Safety (IPCS), under certain environmental and physiological conditions, the potential vertebrate carcinogen *N*-nitrosomorpholine is formed by reaction of solutions of nitrite or gaseous nitrogen oxides with dilute solutions of morpholine (IPCS, 1996).

## **5.2 Molecular Biology of CYP151A2**

### **5.2.1 Cloning**

Sielaff and Andreessen kindly provided the construct of CYP151A2 (P450<sub>mor</sub>) as an N-terminal histidine-tagged fusion protein which enabled the purification of this protein in its spectrally active form, which has previously not been possible for wild-type P450<sub>mor</sub> (Sielaff and Andreessen, 2005a). Generation of the construct by PCR and cloning involved incorporation of a *Spe*I site in the N-terminal primer 5'-TATGTGACTAGTTCCTCGCCCTCGGGCCTGTC-3' to allow for an in-frame ligation in the *Nhe*I treated vector pET28b. In the C-terminal primer 5'-GATTACGAATTCAGCGCGCCGGAGTGAAACCG-3' an *Eco*RI site was incorporated (restriction sites underlined). The single 1.2 kb PCR product was digested with *Spe*I and *Eco*RI restriction enzymes, gel extracted (Qiagen Gel Extraction Kit, Hilden, Germany) and ligated in *Nhe*I/*Eco*RI digested pET28b(+) to generate the plasmid pMCN28 (Sielaff and Andreessen, 2005a). *Spe*I cleaves to leave a 5' CTAG end which can be ligated to fragments generated by *Nhe*I. Resulting recombinant cells were screened by PCR and plasmids of positive clones were purified and sequenced to confirm that no PCR errors were incorporated (Sielaff and Andreessen, 2005a).

### **5.2.2 Expression and purification of CYP151A2**

Soluble CYP151A2 was expressed from the T7 RNA polymerase based promoter system of pET28b. The fusion protein was expressed as a N-terminal His-tag in *E. coli* Rosetta(DE3) cells, in 12 Litres of culture of Terrific Broth at 30 °C

(240 rpm) until mid-log phase ( $OD_{600} \sim 0.4$ ) when the temperature was reduced to 25 °C. The culture was allowed to equilibrate to this temperature before induction with 100  $\mu$ M IPTG at an  $OD_{600} = 0.5-0.6$ , with the cell culture continuing at 25°C for 6 h post-induction at 200 rpm, before harvesting and subsequent lysis. Sonication proved to be an efficient cell lysis process. However, care was required as moderate warming of the cell extract during the lysis process was sufficient to induce protein aggregation and precipitation. Within a short time-frame high expression levels of CYP151A2 protein were achieved (Figure 5.1), and analyses indicated that a significant proportion of the expressed protein was in the soluble form, with no apparent inclusion bodies. Expression of CYP151A2 protein was measured by SDS-PAGE with comparison of P450 content in soluble and insoluble fractions of lysed cells (Figure 5.1). The apparent molecular mass of the expressed, histidine tagged CYP151A2 is  $\sim 45$  kDa, conforming with the 44.801 kDa predicted molecular weight (Figure 5.1).

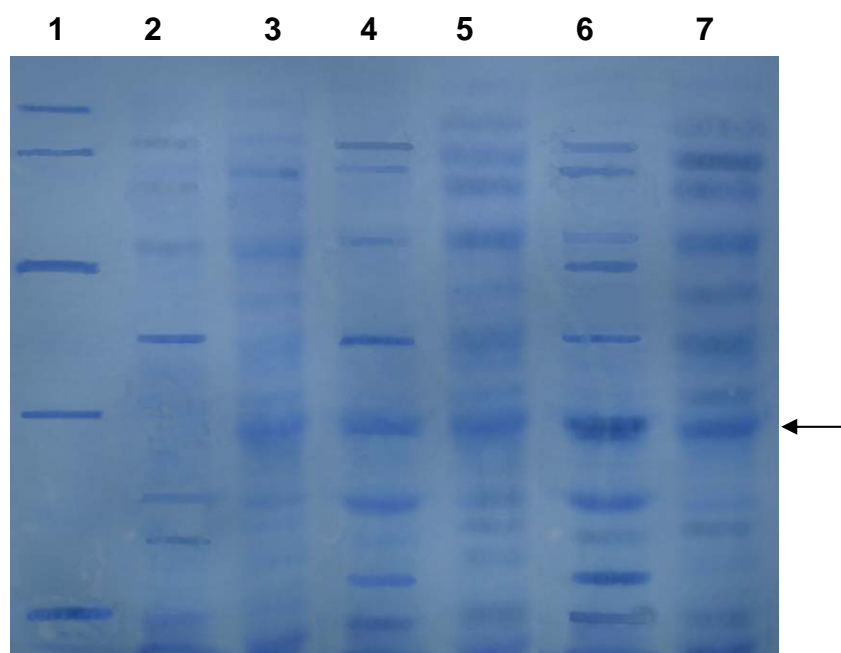


**Figure 5.1 Time-lapsed expression of CYP151A2**  
SDS-PAGE gel (10 %) showing expression of CYP151A2 (44.8 kDa) in Rosetta (DE3) indicated by an arrow. Gel demonstrates time resolution analysis of insoluble and soluble protein fractions induced with 100  $\mu$ M IPTG and grown at 25 °C taken at 0, 3 and 6 hours. Lane 1; broad-range protein molecular weight standards (6-175 kDa) (NEB) (in descending order, kDa); 175, 83, 62, 47.5, and 32.5. Soluble (lane 2) and insoluble (lane 3) fractions respectively, for 0 hours post-induction. Lanes 4 (soluble fraction) and 5 (insoluble fraction); 3 hours post-induction. Lanes 6 (soluble fraction) and 7 (insoluble fraction); 6 hours post-induction.



### 5.2.3 Protein purification of histidine tagged CYP151A2

Purification of the protein was followed spectrophotometrically by measuring the total protein concentration by the absorbance at 280 nm and the total P450 concentration by heme-specific absorbance at 419 nm at different stages of purification. These data are shown in Table 5.1. Protein samples were removed at each stage of the purification process and analysed by SDS-PAGE (Figure 5.2).

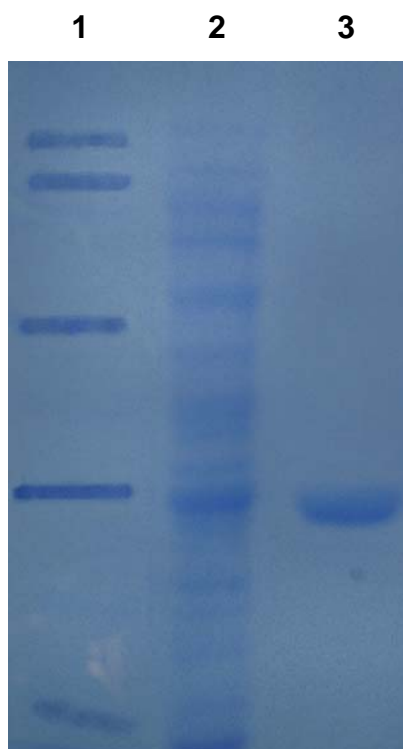


**Figure 5.2** **SDS-PAGE analysis of CYP151A2 protein purification**  
SDS PAGE gel (10 %). Lane 1; broad-range protein molecular weight marker (NEB). Mass units (descending, kDa): 175, 83, 62, 47.5, and 32.5. Lane 2: cell extract; Lane 3: post Nickel-affinity (showing 4 mg pure CYP151A2 protein at ~45 kDa).

Purification Stage	Total Protein (mg)	Total P450 (mg)	Ratio P450/ Protein	Stepwise Purification Factor	Overall Purification Factor	Stepwise Yield (%)	Overall Yield (%)
Lysate	14900	228	0.02	1	1	100	100
Nickel affinity	55.4	52.5	0.89	45	45	23	23

**Table 5.1** **Purification table for histidine-tagged CYP151A2**  
Yields at each stage of the purification (lysate, nickel affinity chromatography followed by the overall protein absorbance ( $A_{280} = 1 = 1 \text{ mg/ml}$ ) and P450-specific heme absorbance ( $A_{419} = 186 \text{ mM}^{-1}\text{cm}^{-1}$ ).

### 5.3 Initial P450 characterisation

#### 5.3.1 Spectrophotometric analysis

An important technique in the characterisation of P450 enzymes is UV-visible absorption spectroscopy, which is an exquisite reporter of the spin-state of the heme iron and of perturbations of redox and ligand-bound status of the enzyme. The UV-visible spectrum of the oxidised form of CYP151A2 showed characteristic features of a heme-containing protein. The Soret peak of the protein was located at 419 nm, with the smaller intensity  $\alpha$  and  $\beta$  bands at 566 nm and 537 nm, respectively. As noted for CYP121 and CYP51 (McLean *et al.*, 2002a; McLean *et al.*, 2006), the absence of any significant absorption shoulder at ~390 nm for oxidised CYP151A2 indicated that the P450 is predominantly low-spin ( $S = 1/2$ ) with minimal high-spin ( $S = 5/2$ ) ferric heme iron content.

Anaerobic reduction of CYP151A2 with sodium dithionite produces no significant change in the Soret maximum at 419 nm, and (at most) only very minor changes in the wavelengths of the Q-bands (Figure 5.3). These characteristics are dissimilar to other well characterised P450s, such as the P450cam (CYP101) and P450 BM-3 (CYP102A1) systems, and CYP121 (Sligar, 1976; Miles *et al.*, 1992, McLean *et al.*, 2002a). The reason is likely the rapid autoxidation of the CYP151A2 heme iron, which leads to predominance of the ferric form. Addition of large excesses of dithionite (that might be required to effect complete reduction of the CYP151A2) promoted aggregation and precipitation of CYP151A2, as also observed for other P450s characterised in this thesis.

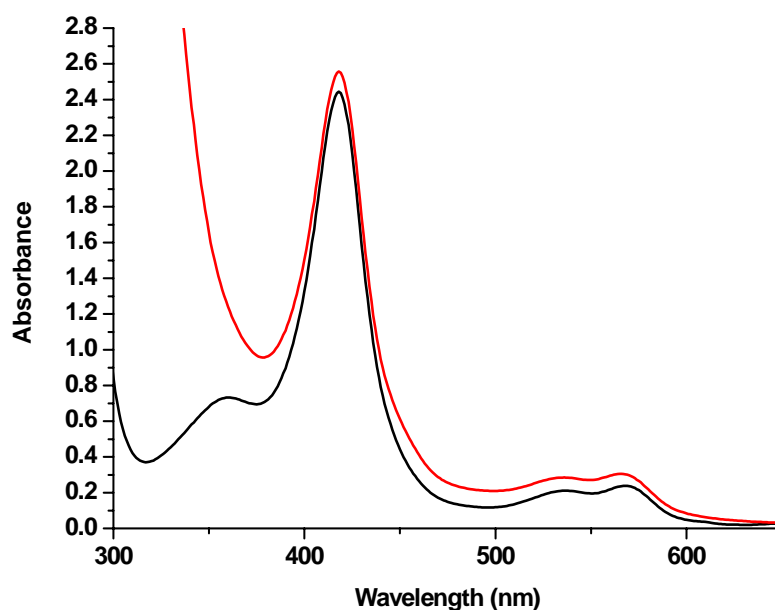


**Figure 5.3** UV-visible absorbance spectra of pure CYP151A2 in oxidised and dithionite-reduced forms

CYP151A2 (~13  $\mu$ M) in 50 mM Tris-HCl, pH 7.2. The oxidised form of the enzyme is displayed in black, while the sodium dithionite-reduced form is displayed in red.

Difficulty in the reduction of CYP151A2, even under near-anaerobic conditions, likely arises from the fast re-oxidation of the ferrous-oxy heme iron (regenerating ferric iron and forming superoxide), compared to the relatively slow reduction rate of the ferric heme by dithionite, as previously discussed (Section 3.31 and section 4.31). Atypical features have been reported for dithionite-reduced ferrous *M. tuberculosis* CYP51, in which the Soret maximum is red-shifted ( $A_{\text{max}} = 421.5$  nm) with respect to that for the ferric form (419 nm) (McLean *et al.*, 2006). This suggests that, in this isoform, heme thiolate protonation occurs directly as a result of iron reduction, and that CO ligation merely serves to provide a convenient spectral signal for this heme thiolate protonation event.

Reduction of CYP151A2 in the presence of CO leads to formation of an Fe(II)-CO complex with a minor absorption maximum at 446 nm (the P450 form), and a major Soret maximum at 424 nm (the inactive P420 form) (Fig 5.4). The shift of the Soret band to 446 nm is strongly indicative of cytochrome P450 species, with a cysteine thiolate ligated heme iron, whilst the peak at 424 nm denotes a P420 species in which thiol coordination has occurred as a consequence of protonation of the heme thiolate, either directly following dithionite reduction of heme iron, or after CO

binding to the ferrous heme (McIver *et al.*, 1998; Perera *et al.*, 2003). P420 formation in CYP151A2 is consistent with protonation of the cysteinate (Cys 351) to a thiol underlying the P450-P420 transition (Perera *et al.*, 2003; McLean *et al.*, 2006). As discussed above, studies of the Fe(II)-CO state of *M. tuberculosis* CYP51 and CYP121 have showed significant generation of P420 species, and in the former case this results from instability of the ferrous state to heme thiolate protonation, regardless of CO binding (Aoyama *et al.*, 1998; Ogura *et al.*, 2004; Mclean *et al.*, 2006).

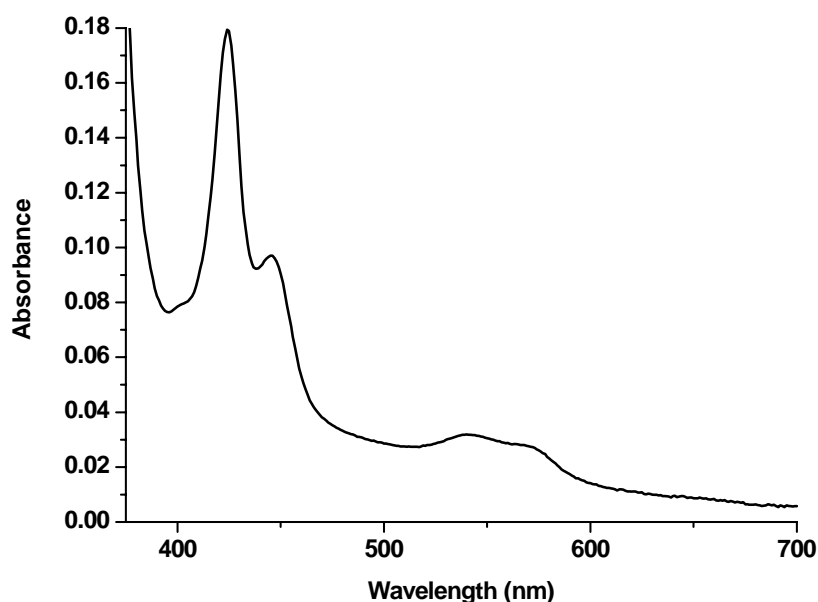


**Figure 5.4** Spectrum of the reduced/CO-bound form of CYP151A2 CYP151A2 (~0.9  $\mu$ M) in 50 mM Tris-HCl, pH 7.2. The presence of the predominant species at 424 nm (the P420 form) is evident, with a smaller amount of the P450 form also present at 446 nm.

Difference spectra were generated by the subtraction of the ferrous spectrum from that for the ferrous/CO-bound adduct (Figure 5.5). The formation of a peak at 450 nm confirms a proportion of the protein to be the thiolate-coordinated recombinant P450, CYP151A2. The secondary peak at 425 nm indicates the presence of some P420 form.

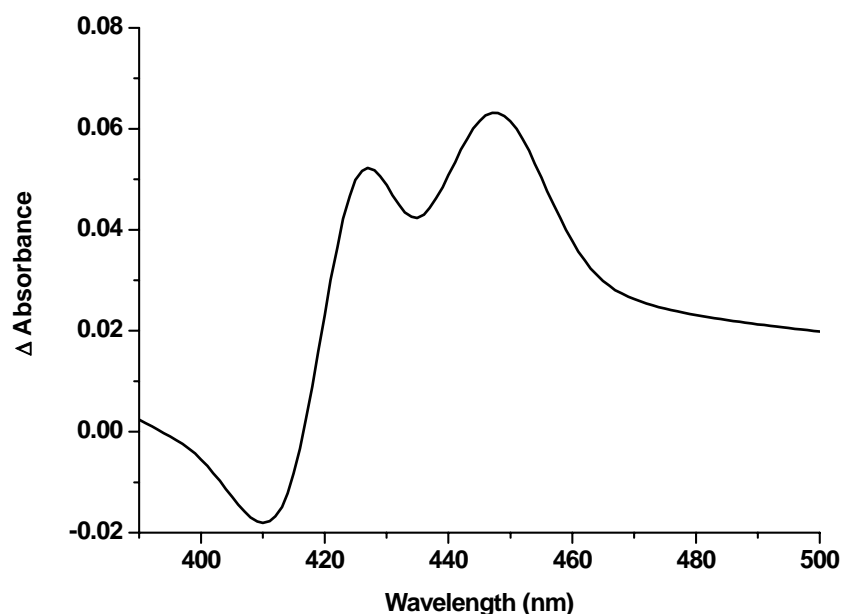


**Figure 5.5**  $\text{Fe}^{2+}\text{-CO}$  minus  $\text{Fe}^{2+}$  difference spectrum for CYP151A2  
CYP151A2 ( $\sim 0.9 \mu\text{M}$ ) in 50 mM Tris-HCl, pH 7.2. Difference spectrum generated by subtraction of the spectrum for ferrous CYP151A2 from that for the ferrous-carbon monoxy form. The presence of both the P450 and P420 forms of the protein is clear.

The native forms of low-spin ferric P450s are cysteinate-ligated (the ligand is Cys 351 in CYP151A2), with a weakly bound water molecule (or possibly hydroxide ion in some enzymes) as the other heme iron axial ligand. The water is displaced by stronger ligands, leading to optical perturbations. NO binding to ferric CYP151A2 resulted in a significant decrease in the intensity of the Soret band, and a shift of the spectral maximum to 431 nm, and of the  $\alpha$ - and  $\beta$ -bands to 574 nm and 542 nm, respectively (Figure 5.6, green). As discussed previously, this is a typical “type II” binding spectrum, reflecting replacement of the P450 distal water by a stronger ligand – in this case nitric oxide (with coordination via the nitrogen atom). Ligation of cyanide ( $\text{CN}^-$ ) to ferric CYP151A2 (Figure 5.6, red) induces complete conversion to an adduct in which there is a significant decrease in the intensity of the Soret maximum at 429 nm, and an apparent spectral fusion of the  $\alpha$ - and  $\beta$ -bands.

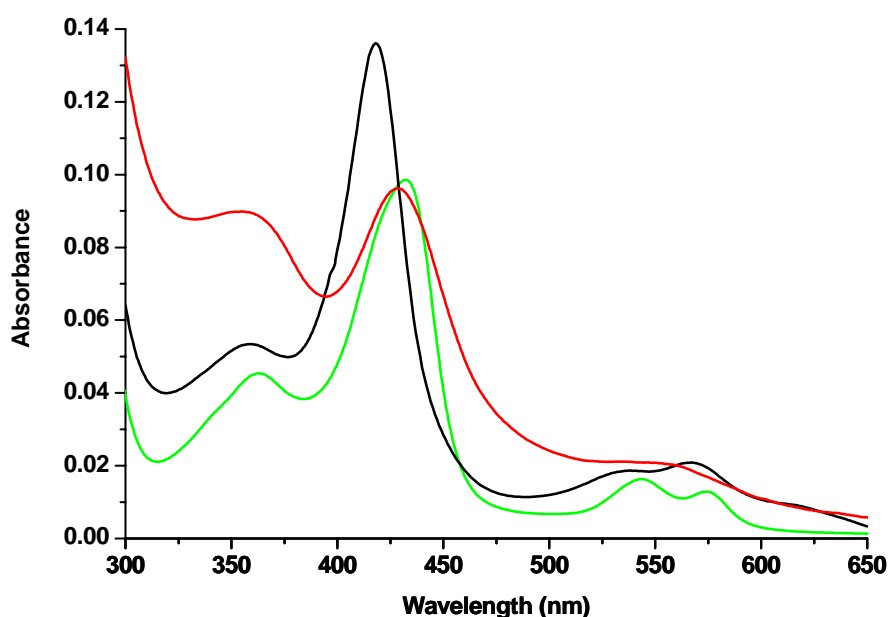


**Figure 5.6 Electronic absorption spectra for CYP151A2 in oxidised form and with inhibitory ligands bound**

CYP151A2 ( $\sim 0.75 \mu\text{M}$ ) in 50 mM Tris-HCL, pH 7.5, in the oxidised form (black line), nitric oxide-bound (green) and cyanide-bound (red) forms, with Soret maxima located at 419, 431 and 429 nm, respectively.

The spectral changes induced by the small molecules CO, NO and  $\text{CN}^-$  are typical of distal ligations to P450 heme iron with a cysteinate proximal ligand heme. In the case of the ferrous-CO complex of CYP151A2, the presence of some P420 species likely results from either the reduction process *per se*, or the reduction followed by binding of CO *trans* to the thiolate (with substantial conversion to thiol). The spectral features of the complexes with the NO and  $\text{CN}^-$  inhibitor molecules are typical of those formed by thiolate-coordinated P450s and thus confirm (as for other P450 enzymes studied in this thesis) that the ferric P450 is almost certainly near-exclusively purified in a thiolate-coordinated, low-spin form.

#### 5.4 Pyridine hemochromagen method

A commonly used method for determining P450 concentrations is dependent on the generation of a stable  $\text{Fe(II)-CO}$  adduct, and the subsequent application of the extinction coefficient  $\Delta\epsilon_{450-490} = 91 \text{ mM}^{-1} \text{ cm}^{-1}$  for data from the reduced/CO-bound *minus* reduced P450 difference spectrum (Correia, 2005). For CYP151A2, the instability of the CO complex at  $\sim 450 \text{ nm}$  hinders accurate use of the aforementioned method. Alternatively, the heme concentration was determined by the pyridine

hemochromagen technique (Berry and Trumpower, 1987) (Figure 5.7). A P450 spectrum was collected for a sample containing 100 mM NaOH, 20% (v/v) pyridine and 300  $\mu$ M.  $K_3Fe(CN)_6$  in a sealed cuvette. The sample was then reduced by the addition of a few grains of sodium dithionite to the cuvette. The heme concentration was then calculated using the Beer-Lambert law as detailed in section 2.5.3.

This indicated an average  $\epsilon_{419}$  coefficient of  $186 \text{ mM}^{-1} \text{ cm}^{-1}$  for oxidised CYP151A2 at the Soret peak. The deduced coefficient is similar to the previously reported CYP151A2 value of  $181 \text{ mM}^{-1} \text{ cm}^{-1}$  (Sielaff and Andreessen, 2005), which is unusually high for a P450, with typical range of the coefficients between  $90\text{-}150 \text{ mM}^{-1} \text{ cm}^{-1}$  (Hawkes *et al.*, 2002; McLean *et al.*, 2002a; McLean *et al.*, 2006). For example, the Soret coefficient of the cineole-degrading P450cin (CYP176A) from *Citrobacter braakii* was determined by the same method to be  $\epsilon_{415} = 150 \text{ mM}^{-1} \text{ cm}^{-1}$  (Hawkes *et al.*, 2002).

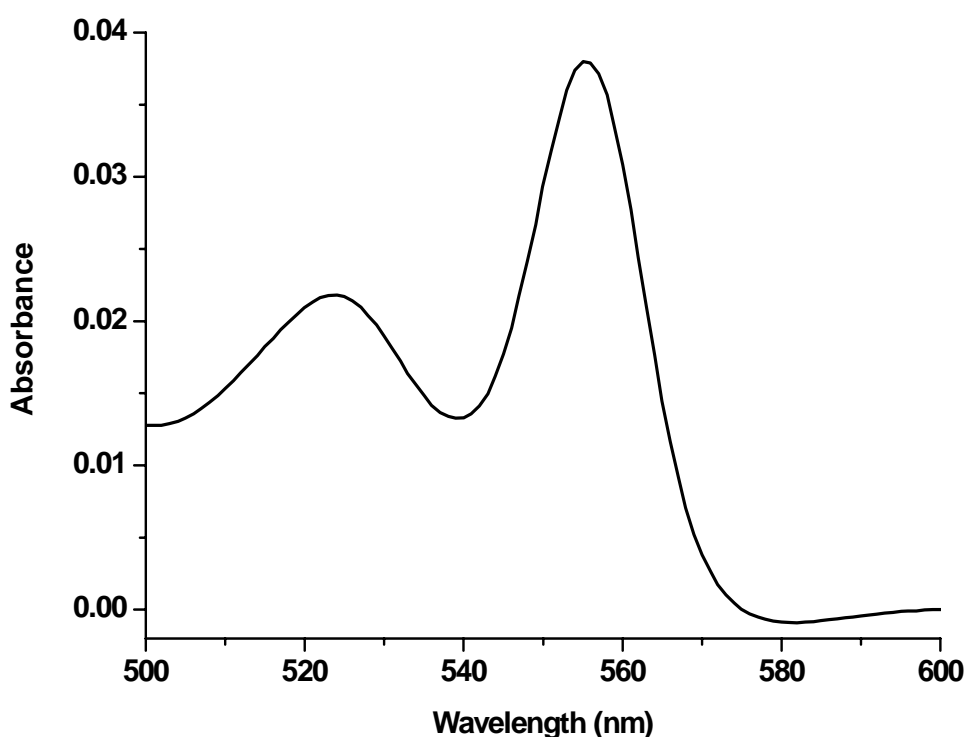


**Figure 5.7** Pyridine hemochromagen absorption spectrum for CYP151A2 CYP151A2 in 50 mM Tris-HCl, pH 7.2, 100 mM NaOH, 20% (v/v) pyridine and 300  $\mu$ M  $K_3Fe(CN)_6$ . Protein has maxima in the Q-band, which is indicative of heme *b*. Extinction coefficient of CYP151A2 was calculated using the extinction coefficient of  $24 \text{ mM}^{-1} \text{ cm}^{-1}$  for the absorption difference between 555 nm and 539 nm.

## 5.5 Sequence analysis

The P450-containing monooxygenase systems play an important role in a myriad of hydroxylation and oxidation processes leading to degradation, detoxification and syntheses of a vast array of compounds, many of which are critical for physiology and viability of the relevant organism. The CYP151A2 enzyme (and potentially the CYP151 family) may play an invaluable role as the terminal oxidases involved in a secondary amine detoxification system.

The CYP151 family is dominated by P450s based within the *Mycobacterium* genus (<http://drnelson.utmem.edu/P450.stats.2006.htm>). CYP151A1 (*M. smegmatis* strain mc<sup>2</sup>155), is 86 % identical to CYP151A2. The amino acid sequence of CYP151A2 was submitted for a NCBI PSI- and PHI-BLAST analysis to identify proteins with the highest amino acid sequence identity. Highest identities were observed with P450s from a series of environmental mycobacteria with potential roles in degradation of a range of organic molecules. A 100% match occurs with a P450 from *Mycobacterium* sp. strain RP1 (Trigui *et al.*, 2004), the originally classified CYP151A2 itself. Results detailing the turnover characteristics of CYP151A2 from strain RP 1 demonstrated that the purified recombinant P450 catalysed the biotransformation of the cyclic amines morpholine, pyrrolidine and piperidine (Trigui *et al.*, 2003). The binding affinities for these substrates indicate that CYP151A2 has relatively similar affinities for each compound in the range of 0.45-0.6 mM (Trigui *et al.*, 2004). The maximum rate of catalysis and tightest binding affinity was observed for pyrrolidine (Trigui *et al.*, 2004). In contrast, Sielaff and colleagues noted no UV-visible spectroscopic changes for CYP151A2 from *Mycobacterium* sp. strain HE5 during spectral titrations with the proposed substrates pyrrolidine, piperidine and morpholine, up to a final concentration of 50 mM (Sielaff and Andreesen, 2005a). However, the turnover (i.e. oxidation) of morpholine did occur (Sielaff and Andreesen, 2005a). An identical amino acid sequence was also observed over a 380 amino acid stretch with an uncharacterised P450 from *M. chlorophenolicum* PCP-1. *M. chlorophenolicum* PCP-1 is a close relative of the aforementioned strains, with 98.4 % identity to *Mycobacterium* sp. strain HE5 and 97.3 % to *Mycobacterium* sp. strain RP1, based on 16S rDNA, and is known to be capable of degrading polychlorinated phenols (Apajalahti and Salkinoja-Salonen, 1987; Häggblom *et al.*,



1994). Furthermore, studies have demonstrated that *M. chlorophenolicum* PCP-1 is also able to use the secondary amines morpholine, piperidine and pyrrolidine as sole carbon, nitrogen and energy sources, and that a cytochrome P450 is induced during growth on morpholine (Sielaff and Andreesen, 2005b).

Sequence analysis of the *CYP151A2* genes (Sielaff and Andreesen, 2005b), revealed that the gene from *Mycobacterium* sp. strain HE5 was identical to the corresponding gene from *Mycobacterium* sp. strain RP1 and almost identical to the same gene in *Mycobacterium chlorophenolicum* PCP-1, suggesting horizontal gene transfer (Sielaff and Andreesen, 2005b). The identification of these identical and near-identical *CYP151A2* genes in different mycobacterial strains suggests that this P450 system is more widely distributed within this genus, and thus may play an important role in the viability of the strains. This is further reinforced by the ability of a number of different mycobacteria to specifically express a cytochrome P450 during growth on morpholine, piperidine and pyrrolidine (Poupin *et al.*, 1999). It would seem likely that a proportion of these enzyme systems are also identical or exhibit high levels of identity to CYP151A2 (Sielaff and Andreesen, 2005b). Evidence for such a theory has been obtained for five distinct haloalkane-utilizing *Rhodococcus* strains, which contain the absolutely conserved *dhaA* gene encoding a haloalkane dehalogenase. The highly conserved gene region is detected on both the chromosomes and the plasmids of all these strains (Poelarends *et al.*, 2000). It has been suggested that such a wide distribution of the *dhaA* gene may have resulted from the transfer of an ancestral plasmid and subsequent integration into the chromosome. Such a plasmid-mediated horizontal gene transfer in morpholine-degrading mycobacterial strains could be possible, although no evidence for the plasmid was found in *Mycobacterium* sp. strain HE5 (Sielaff and Andreesen, 2005b).

CYP151A2 has no considerable level of amino acid sequence identity with any well characterised P450 (other than its close homologues, mentioned above). However, caution must be adopted in using amino acid sequence identity deductions in isolation, as it is well reported that single amino acid changes in P450s can significantly alter catalytic properties such as substrate specificity (Munro and Lindsay, 1996). The amino acid alignment programme Clustal W (<http://www.ebi.ac.uk/clustalw/>) was used for the amino acid comparative study of

CYP151A2 (P450<sub>mor</sub>) with P450 EryF, and also with other structurally characterised bacterial P450 systems: P450<sub>cam</sub> and the heme domain of P450 BM-3 (Figure 5.8).

Deciphering structural elements in CYP151A2 was difficult due to the extremely low sequence identities with model P450s used. Despite the generally low sequence identities at the amino acid level between non-family members in the P450 superfamily, the overall protein fold and topologies are usually very similar and certain sequence motifs corresponding to the conserved tertiary structure and enzyme functions are generally identifiable (Pylypenko and Schlichting, 2004).

Despite considerable divergence between CYP151A2 and P450<sub>eryF</sub> (CYP107A1), some regions of weak similarity exist between the two proteins. As an example, similarities are seen in the areas of the I- and K-helices in CYP151A2 and CYP170A1 (highlighted in cyan and green in Figure 5.8). These regions of P450 structure are known to be critical in controlling P450 substrate selectivity and in conformational transitions during substrate binding events (Dunn *et al.*, 2001; Pylypenko and Schlichting, 2004). Although the precise roles of any residues in these elements in CYP151A2 remain to be uncovered, studies on the binding of ketoconazole in P450 EryF have revealed major conformational changes in the I-helix. The P450<sub>eryF</sub>/ketoconazole complex crystal structure indicates that the I-helix cleft near the active site is a flexible structure able to collapse upon ligand binding (Cupp-Vickery *et al.*, 2001). Based on major alterations, changes in the hydrogen bonding and water structure network within this area, it has been proposed that that movement of the peptide backbone in the region of the I-helix cleft during catalysis could promote proton shuttling to the oxygen atom (Cupp-Vickery *et al.*, 2001).

```

Mor      -----MSSLALGPVAAFVADPSFSITSN---EVHAARER----SWYATTPYGIA 43
cam      -----TTETIQSNANLAPLPPHVPEHLVDFDMDYNPSNLSAGVQE----AWAVLQESNPV 51
eryF     -----MTTPDLESDFHVDWYRTYAELRETAPVTPVRFLGQD----AWLVTG-YDEA 48
BM3      TIKEMPQPKTFGELKNLPLNTDKPVQALMKIADDELGEIFKFEAPGRVTRYLSSQRLIKE 60
          .      .      :      :

Mor      VLRYEQFSR----LLKHPKLRQGSVAWPAHN-----GVTEGPFAEWFASWILNKEGEEHH 94
cam      DLVWTRCNGGHWIATRGQLIREAYEDYRHSSEC--PFIPREAGEAYDFIPTSMDPPEQR 109
eryF     KAALSDLRLSSDPKKKYPGVEVEFPAYLGFP-----EDVRNYFATNMGTSDPPTHT 99
BM3      ACDESRFDKNLSQALKFVRDFAGDGLFTSWTHEKNWKAHNILLPSFSQAMKGYHAMMV 120
          :      :      :      .

Mor      RLRLLMNPAFSPKLIGSLVPRFQALANELVDNFAEPYRCEFMSEFAEPYAARVIAIMLGI 154
cam      QFRALANQVVGMPVVDKLENRIQELACSLIESLRPQGQCNTEDYAEFPPIRIFMLLAGL 169
eryF     LRLKLVSQEFTVRRVEAMRPRVEQITAELELDEVGDSGVVDIVDRFAHPLPIKVICELGV 159
BM3      DIAVQLVQKWERLNADEHIEVPEMDTRLTLDITGLCGFNRYFNSFYRDQPHFITSMVRA 180
          :      : :      : .      . : . . : :

Mor      PEDEWKVISTEATMGLCLGVTGLKDLPKIEAALQRLYEYCDALITDRRA--NPREDFVT 212
cam      PEEDIPLKYLTDQMTRPDGSMT-----FAEAKEALYDYLPIIEQRRQ--KPGTDAIS 221
eryF     DEKYRGEFGRWSSEILVMDPERAE---QRGQAAREVNVNFIIDLVERRRT--EPGDDLSS 213
BM3      LD EAMNKLQRANPDDPAYDENKQ-----FQEDIKVMNDLVDKI IADRKASGEQSDDLLT 235
          : .      :      . : :      : * :      * : :

Mor      ALVEASREEDGR-LSDTELRDAMVLLIFGGFDTRNQLGLAMQTFMAHPDQWRLLAERPE 271
cam      IVANG-QVNGRP-ITSDEAKRMCGLLLVGGLDVTVNFLSFSMEFLAKSPEHRQELIERPE 279
eryF     ALIRVQDDDDGR-LSADELTSIALVLLAGFEASVSLIGIGTYLLI THPDQLALVRRDPS 272
BM3      HMLNGKDPETGEPLDDENIRYQIITFLIAGHETTSGLLSFALYFLVKNPHVLQKAAEEAA 295
          : .      :      : : : : : * : . .

Mor      -----LGGKAVEEVMRVNPTVRWVTREVLEDFEYEG-VLLKAGTTVHL 313
cam      -----RIPAAACEELLRR-FSLVADGRILTSDYEFHG-VQLKKGDQIIL 320
eryF     -----ALNAVEEILRYIAPPETTTTFAAAEEVEIGG-VAIPQYSTVLV 314
BM3      RVLVDPVPSYKQVKQLKYVGMVLNEALRLWPTAPAFSLYAKEDTVLGGEYPLEKGDELMV 355
          . : * : * .      . :      * :      : :

Mor      YSESAGTDPR-----VFDGSFDIT--AERKPHFGGGGAHHGLGHFVARSDMSEALP 363
cam      PQMLSGLDEREN-----ACPMHVDFS--RQKVSHTTGHGSHLGLGQHLARREIIVTLK 372
eryF     ANGAANRDPKQF-----PDPHRFVDVT--RDTRGHLSGGGIHFMMGRPLAKLEGEVALR 366
BM3      LIPQLHRDKTIWGDDVEEFRPERFENPSAIPQHAFKPGNGQRAIGQQFALHEATLVLG 415
          *      . : .      . ** * : * : : . * : . *

Mor      LLARRMRDP-----QALPGATWLPDSGNT-GPIQLPIGFTPAR----- 400
cam      EWLTRIPDF-----SIAPGAQIQHKSIGIVSGVQALPLVWDPATTKAV-- 414
eryF     ALFGRFPALSL-----GIDADDVWRRSLLLRGIDHLPVRLDG----- 404
BM3      MMLKHFD FEDHTNYELDIKETLT LKPEGFVVKAKSKKIPLGGIPSPSTEQSAKKVRK 472
          : :      .      .      : *

```

**Figure 5.8 Amino acid alignment of *Mycobacterium sp.* strain HE5 CYP151A2 with other structurally characterized bacterial P450s**

Alignments of the CYP151A2 amino acid sequence (Mor) were made with *Saccharopolyspora erythraea* P450 EryF (EryF), *Ps. putida* P450cam (cam) and *B. megaterium* P450 BM-3 heme domain (BM3) sequences, using the ClustalW program. The highly conserved C348 (in CYP151A2) and F341 of the heme-binding motif are highlighted in red. The former is the conserved cysteine heme iron ligand. The latter is a highly conserved residue likely to be important in the thermodynamic regulation of the heme iron. The “\*” indicates residues that are identical, “:” and “.” indicate conserved and semi-conserved residues (e.g basic, acid etc). Structural elements are highlighted; helices I (cyan) and K (green), (Hasemann *et al.*, 1995).

Residues involved in interactions with the EryF substrate 6-DEB also reside in the I-helix (e.g. Val<sup>237</sup>) (Cupp-Vickery *et al.*, 2001). A similar induced-fit model of substrate protein conformational change may well occur upon substrate binding in CYP151A2, although recognised substrates for this P450 (to date) are rather smaller than the bulky antibiotic precursor substrate for P450 EryF (Koshland, 1958). The C-terminal section of the CYP151A2 K-helix contains the highly conserved sequence E/D-X-X-R. This region of the sequence in CYP151A2 contains Glu<sup>279</sup> and Arg<sup>282</sup> residues which may stabilise the meander through salt bridge interactions and hydrogen bonds (Pylypenko and Schlichting, 2004).

In Figure 5.8, the completely conserved cysteine residue in P450s is indicated in red (Cys<sup>348</sup>). This provides the cysteinate proximal ligand to the heme iron in the P450. Seven amino acids before this comes a highly conserved phenylalanine residue (Phe<sup>341</sup>), which is implicated in the poise of heme iron reduction potential to facilitate efficient reduction and activation of dioxygen bound to P450 heme iron (Ost *et al.*, 2001a). A major deviation between the two aligned sequences is that P450 eryF is known to lack a highly conserved Ser/Thr P450 residue implicated in oxygen binding/proton transfer, with this role instead played by the substrate (6-deoxyerythronolide B) in this isoform (so-called “substrate-assisted catalysis”) (Xiang *et al.*, 2000). Well-defined roles for this conserved residue have been established in other structurally resolved P450s, e.g. Thr252 in P450cam and Thr268 in P450 BM-3 (Imai *et al.*, 1989; Yeom *et al.*, 1995). The sequence alignment of CYP151A2 with P450cam (CYP101A1) and P450 BM-3 (CYP102A1) suggests that Thr244 in CYP151A2 corresponds to the relevant hydroxyl group-containing residue in P450cam and P450 BM-3, which is important for the binding activation of molecular oxygen, and for the coupling of electron transport to substrate oxygenation (Imai *et al.*, 1989; Yeom *et al.*, 1995).

## **5.6 Biophysical characterisation**

### **5.6.1 Circular dichroism**

Circular dichroism is the differential absorption of the left- and right-circularly polarized components of plane-polarised electromagnetic radiation. The technique provides structural and dynamic information about proteins quickly and conveniently,

and thus is increasingly recognised as a valuable technique for examining the structure of proteins in solution.

The far-UV CD spectrum of CYP151A2 is shown below with comparison to the well characterized P450 BM-3 heme domain (Figure 5.9). The relative similarity illustrated between the far-UV CD spectra of CYP151A2 and P450 BM-3 emphasizes that CYP151A2 is mainly composed of  $\alpha$ -helical structure (69 %), consistent with all other characterized P450s. In this region, the absorbing chromophore is principally the peptide bond. CYP151A2 shows typical  $\alpha$ -helical protein characteristics with a spectrum that consists of an intense positive band at 193 nm and negative minima at 208 and 223 nm. The troughs at 208 nm and 223 nm corresponds to a broad amide  $n \rightarrow \pi^*$  transition, and an intense  $\pi \rightarrow \pi^*$  transition corresponds to the peak at 190 nm (Kelly *et al.*, 2005).

The near UV-visible CD spectra of CYP151A2 and P450 BM-3 display similarities in the aromatic amino acid region, but differences in the heme environments. Signals corresponding to the environment of the heme group (350-650 nm) are slightly different in terms of the Soret trough wavelength (Figure 5.10).

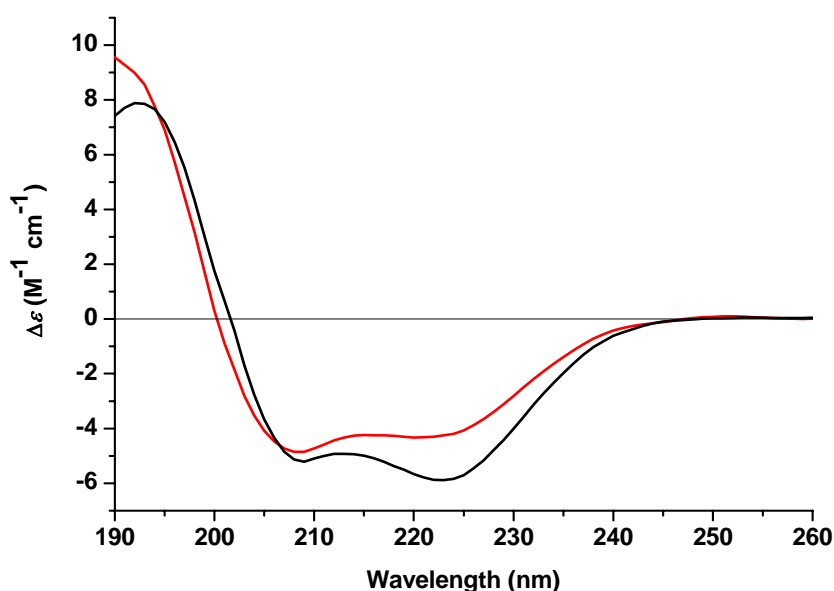


**Figure 5.9** Far UV CD spectra of CYP151A2 and P450 BM-3  
CYP151A2 (black, 2  $\mu$ M) CD spectrum compared with P450 BM-3 (red, 2  $\mu$ M), in 10 mM Tris-HCl, pH 7.0. Spectra were collected using a 0.02 cm pathlength cell. Experiments were performed on a JASCO J-715 spectropolarimeter at 25°C.

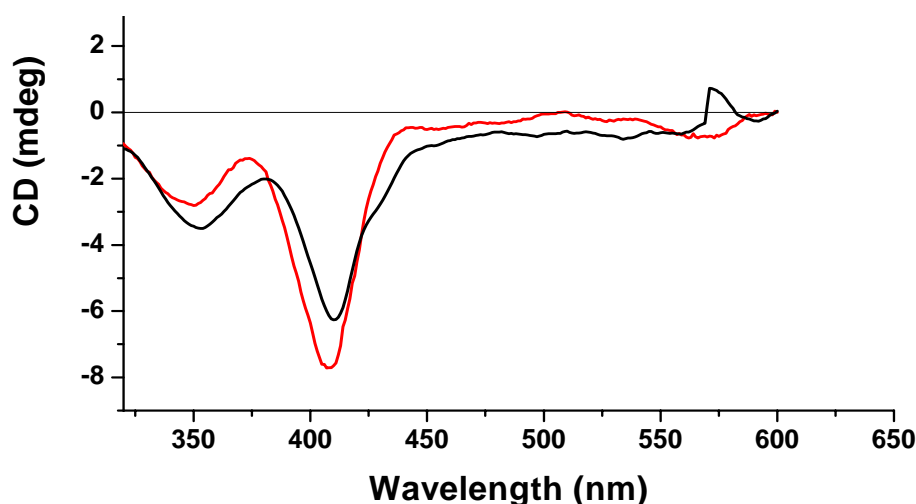


**Figure 5.10** Near UV-visible spectra of CYP151A2 and P450 BM-3

CD spectrum for CYP151A2 (20  $\mu$ M) (black) is compared with that for P450BM-3 (20  $\mu$ M) (red) in 10 mM KPi, pH 7.0. Spectra recorded in quartz cell with a pathlength of 0.5 cm. Experiment was performed on a JASCO J-715 spectropolarimeter at 25°C.

Signals corresponding to the heme group (350-450 nm) are slightly different for the two P450s. For CYP151A2, this range of the spectrum is characterised by a sharp Soret feature with negative ellipticity centred at 410 nm and a delta band with negative ellipticity centred at 350 nm, both of which are due to the  $\pi \rightarrow \pi^*$  transitions of the porphyrin ring (Hsu and Woody, 1971). The negative feature at 410 nm, close to the maximum in the electronic absorption spectrum for CYP151A2, slightly differs from that observed with the P450 BM-3 heme domain.

The near UV-visible CD spectrum of both CYP151A2 and P450BM-3 displays negative ellipticity in the heme region (negative Cotton effect). The dissimilar CD spectra for the hemes in CYP140A2 and P450 BM-3 in this region may reflect different heme geometries and in some way the dissimilar functions of the P450 enzymes. P450 BM-3 is a fatty-acid hydroxylase, whereas CYP151A2 is a morpholine hydroxylase.

Changes in CD spectra can also provide information on ligand-protein interactions. CD spectra were collected for substrate- and inhibitor-bound forms of CYP151A2, using morpholine and econazole, respectively, to assess any structural changes when compared to the substrate-free form. The far UV-visible CD spectrum

of the morpholine- and econazole-bound forms of CYP151A2 are displayed below, alongside the corresponding spectrum of the ligand-free CYP151A2 (Figure 5.11).

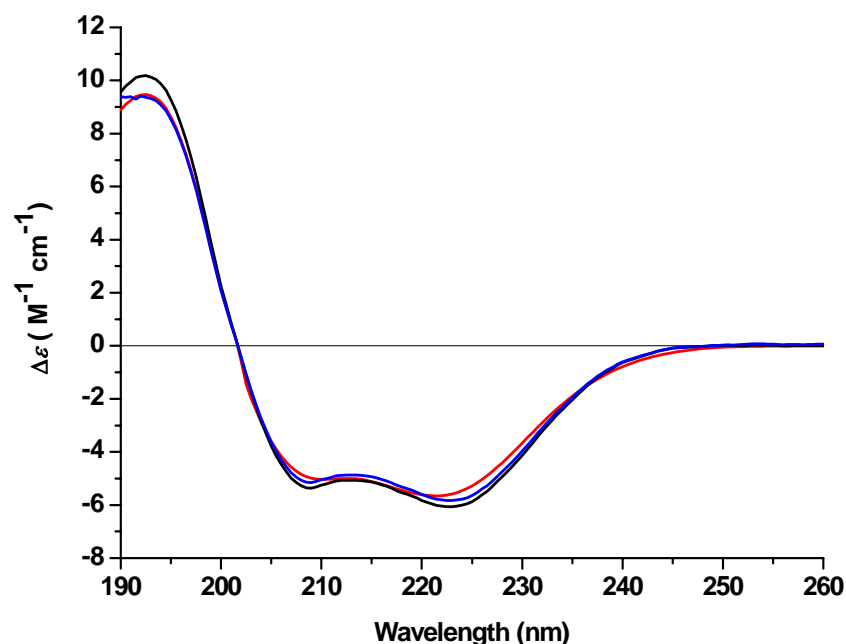


**Figure 5.11 Far-UV CD spectra of CYP151A2 in the presence and absence of morpholine and econazole**

The spectrum is shown for substrate-free CYP151A2 (2  $\mu$ M) (black), and compared with those for morpholine- (5 mM, red) and econazole- (30  $\mu$ M, blue) bound forms. All proteins were in 10 mM KPi, pH 7.0. Spectra were collected using quartz cells with a pathlength of 0.02 cm. The experiment was performed on a JASCO J-715 spectropolarimeter at 25°C.

The far-UV CD spectra (190-260 nm) for CYP151A2 indicate no major detectable changes in the secondary structure in the presence of the substrate morpholine and the inhibitor econazole. The substrate-bound and inhibitor-bound spectra of CYP151A2 are indicative of a predominantly  $\alpha$ -helical structure, and are virtually identical to that of the ligand-free enzyme, with minima at 223 and 209 nm and an abscissa at 202 nm. The fact that far-UV CD spectrum for CYP151A2 was not significantly altered by the addition of morpholine is consistent with previous P450 studies, which have indicated lack of change in secondary structural content upon the binding of arachidonic acid substrate by P450 BM-3 (Girvan *et al.*, 2004). However, upon the addition of morpholine to CYP151A2, the 223 nm negative feature, assigned to a peptide  $n \rightarrow \pi^*$  transition, is shifted slightly to 222 nm. In addition, the binding

of morpholine results in the negative peak at 209 nm, which corresponds to a  $\pi \rightarrow \pi^*$  transition parallel to a helix axis, decreasing in intensity and shifting to 210 nm.

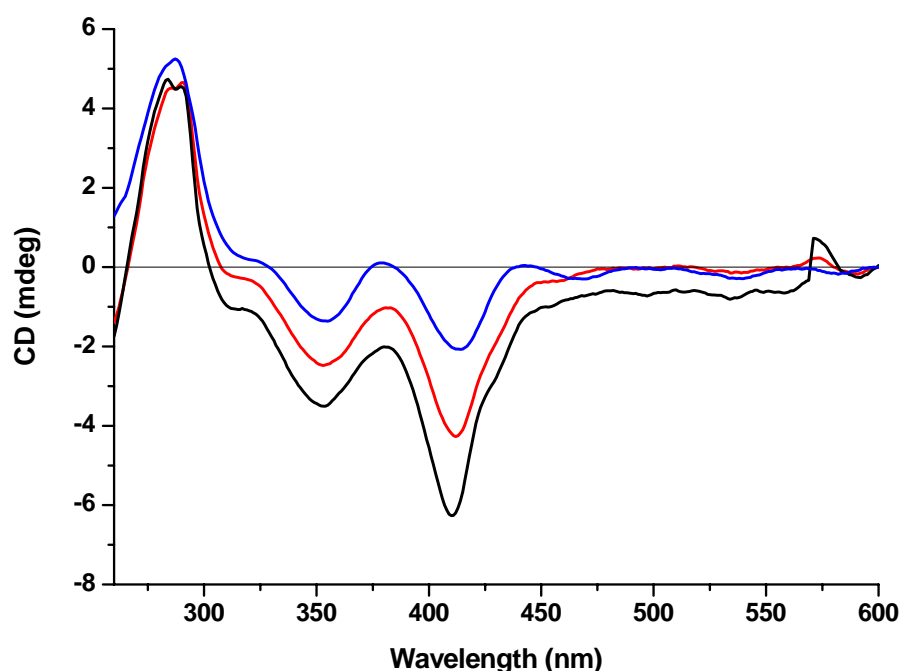


**Figure 5.12** Near-UV-visible CD spectra for CYP151A2 in the presence and absence of morpholine and econazole

Substrate-free CYP151A2 (2  $\mu$ M) (black) is compared with wild-type CYP151A2 (2  $\mu$ M) bound to morpholine (5 mM, red) and econazole (30  $\mu$ M, blue). All samples were in 10 mM KPi, pH 7.0, and spectra were recorded in a quartz cuvette with a pathlength of 0.5 cm.

The far-UV CD spectrum for CYP151A2 was not significantly altered by the addition of ligands, showing that secondary structural content is not significantly altered upon the binding of substrate and ligand. However, in the near-UV-visible CD region (260–600 nm), the spectrum of the CYP151A2 in its resting oxidised form is rather different from that of the ligand-bound forms (Figure 5.12). The near-UV region of the CD spectrum reports on the protein aromatic residues, and changes seen with econazole may be partially due to the inhibitor, rather than to any significant change in the enzyme tertiary structure itself. The visible region reports on changes in the heme environment. This portion of the spectrum is dominated by a sharp Soret feature with negative ellipticity. For the substrate-free wild-type heme domain, this is centred at 410 nm and shifts to 412 nm and 414 nm upon morpholine and econazole binding, respectively (Figure 5.12). Thus, the direction of movement of the Soret band (to longer wavelengths) mimics the optical transition seen in the electronic



absorption spectrum. This small spectral change seen between the UV-visible CD spectra of the econazole-free and -bound forms of CYP151A2 differs somewhat from that seen in optical absorption, wherein (under identical conditions) a large shift of ~7 nm occurs in the Soret band (from 419 nm to 425 nm) on econazole binding. The spectra suggest that the two molecules bind to the enzyme to induce similar changes in chirality and/or electronic properties of the CYP151A2 heme environment. However, what must be taken into account is that the protein is only partially saturated with morpholine, unlike in the case of econazole (where optical titrations indicate that the P450 is almost completely ligand-bound at 30  $\mu$ M azole). Prior to the CD spectra being collected, the states of the enzyme were verified by UV-visible spectroscopy to determine levels of ligand saturation. This further confirmed near-complete saturation with econazole.

The most apparent difference between the ligand-bound and ligand-free forms of CYP151A2 (Figure 5.12) is in the relative intensities of the Soret (~410 nm) and  $\delta$ -bands (353 nm), with a negative sign in all cases, but significantly lower CD extinction coefficient in the case of the morpholine- and econazole-bound forms. In addition, the intensity of the quite prominent  $\alpha$ -band (571 nm in the ligand-free form) lowers upon partial saturation with morpholine, and decreases further still on saturation of the P450 with econazole. The decrease in the intensity of the  $\delta$ -band also mimics the optical transition seen in the electronic absorption spectra (section 5.10.1).

### 5.6.2 Electronic Paramagnetic Resonance (EPR)

To further characterise the morpholine and azole binding in CYP151A2, and to elucidate the molecular mechanism for the specific azole binding, the EPR spectra for the substrate-free, morpholine-bound and azole-bound forms of CYP151A2 were examined. Figure 5.12 A,B,C,D shows the EPR spectra of the substrate-free, 30 mM morpholine-bound, 100 mM morpholine-bound and fluconazole-bound forms of CYP151A2 at 10.5K, respectively.

The major signals generated in the EPR spectrum of substrate-free CYP151A2 constitute a rhombic trio of g-tensor elements ( $g_z$ ,  $g_y$ ,  $g_x$ ) (Figure 5.12A). The resulting g-values of 2.42 ( $g_z$ ), 2.25 ( $g_y$ ) and 1.93 ( $g_x$ ) indicates a nuclear spin state of

$\frac{1}{2}(2I + 1)$  and are reflective of a low-spin ferric (FeIII) heme (Mansuy and Renaud, 1995; Lipscomb, 1998). Indeed, the CYP151A2 spectra is similar to the wild-type CYP121 ( $g = 2.47, 2.25, 1.90$ ) (McLean *et al.*, 2002), along with those of low-spin ferric forms of the well-characterised P450cam and P450 BM-3 ( $g = 2.46, 2.26, 1.91$  and  $2.42, 2.26, 1.92$ , respectively) (Dawson *et al.*, 1982; Miles *et al.*, 1992). In addition, there is similarity with the low-spin ferric forms of Nitric Oxide Synthases, in which the heme is also bound axially by cysteinate and water (Lipscomb, 1980; Dawson *et al.*, 1982; Berka *et al.*, 1988; Salerno *et al.*, 1995; Tsai *et al.*, 1996). The  $g$ -values are very sensitive to the nature of the heme axial ligands and to perturbations such as the orientations of the ligands. The fact that these values for CYP151A2 are very similar to wild-type CYP121, P450cam and P450 BM-3 suggests the heme ligation environment is very similar in all these P450s.

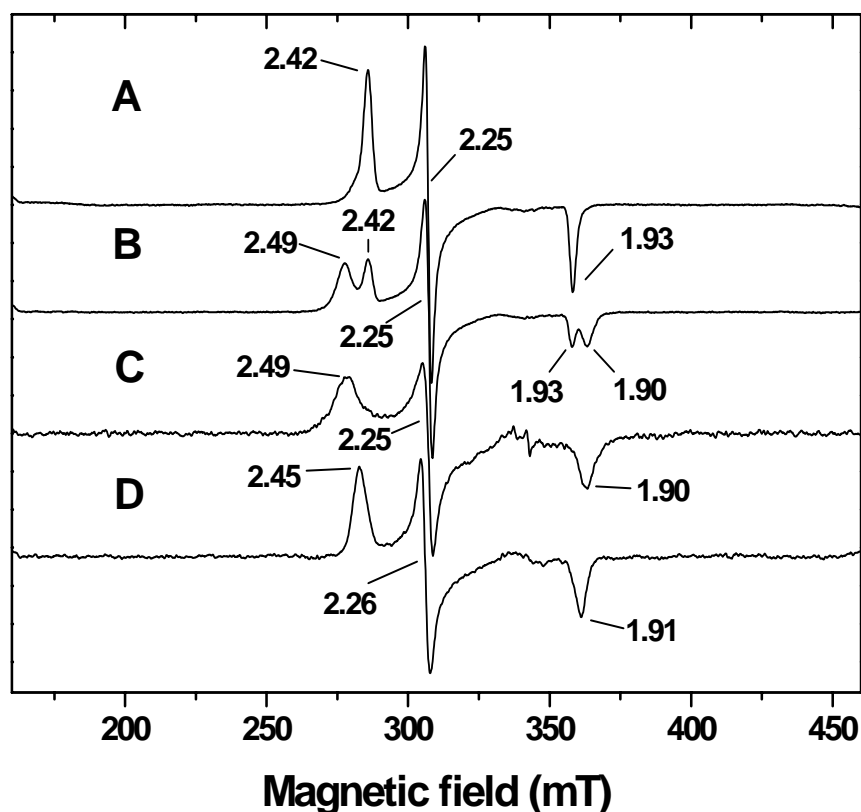


**Figure 5.13 A-D X-band EPR spectra of CYP151A2**

The protein was at a concentration of 170  $\mu\text{M}$  in 50 mM Tris-HCl, pH 7.5 including 50 % (v/v) glycerol. Sample conditions were temperature 10.5 K, microwave power = 2.0 mW, modulation amplitude = 1 mT. Panel A: resting, oxidised CYP151A2; panel B: CYP151A2 with 30 mM morpholine; panel C: CYP151A2 with 60 mM morpholine; panel D: CYP151A2 with 50  $\mu\text{M}$  fluconazole. The  $g$ -values are indicated on the individual panels.

The binding of morpholine results in significant shifts in the EPR signals. In the presence of 30 mM morpholine, heterogeneity of the low-spin heme of CYP151A2 was observed, with  $g_z$  (2.42 and 2.49) and  $g_x$  (1.93 and 1.90) at higher and lower fields, respectively (Figure 5. 13B). In previous studies, some heterogeneity in the low-spin  $g_x$  signal has been observed in P450cam with signals at both  $g = 1.97$  and 1.91 (Green *et al.*, 2001; Lawson *et al.*, 2004).

In the presence of 60 mM morpholine, the CYP151A2  $g_z$  and  $g_x$  heme iron signals were completely shifted to high (2.49) and low (1.90) field, respectively, with no apparent heterogeneity (Figure 5.13C). These shifts can be interpreted as decreased heme rhombicity because of the coordination of the nitrogen atom of the pyrrole ring (Dawson *et al.*, 1983; Tsai *et al.*, 1996; Berka *et al.*, 1996; Uchida *et al.*, 2004), resulting in perturbation of the heme ligation environment. The decreased rhombicity was also reported in the 4-phenylimidazole bound form of P450cam (2.45/2.5, 2.25, 1.89) (Uchida *et al.*, 2004). On the other hand, the addition of morpholine did not induce significant changes in the high-spin region of the EPR spectrum, which is derived from the  $S = 5/2$  species (Lipscomb, 1980; Dawson *et al.*, 1983, Tsai *et al.*, 1996; Berka *et al.*, 1996). Furthermore, at higher morpholine levels, the amplitudes of the low-spin CYP151A2 EPR transitions decrease significantly, and there is also significant signal broadening. The fact that the  $g_z$ ,  $g_y$  and  $g_x$  components' signals are broadened suggests that there may be a split population of two conformers, as previously suggested for an azole-bound form of P450BM-3 (Girvan *et al.*, 2004). This large effect on the EPR signal amplitude is suggestive of CYP151A2-morpholine complex formation and subsequent perturbation of the heme ligand environment, as also observed by absorption and CD spectroscopy for morpholine-bound CYP151A2.

EPR studies reveal spectral heterogeneity in the low-spin form of CYP151A2 in the presence of 30 mM morpholine (Figure 5.13B). An explanation for the presence of a second, low-spin form of CYP151A2 is that bound morpholine at lower concentrations interacts with the heme ligand or heme iron in a proportion of CYP151A2 molecules in the “typical” low-spin (cys-aqua ligated) form, as observed in the substrate-free form (Figure 5.13A). The fact that addition of higher concentrations of morpholine results in the loss of the “typical” P450 low-spin signal suggests that this is a possible scenario. At the higher (60 mM) concentration of

morpholine, the apparent homogeneity of the EPR spectrum is likely due to the complete ligation of the morpholine to the heme iron, thus removing the residual aqua-ligated components, as seen in the 30 mM morpholine-bound spectrum (Figure 5.13B/C). A similar explanation has been postulated previously for the heterogeneity of the low-spin BioI P450 (Lawson *et al.*, 2004). However, the signals at  $g = 2.42$  and  $1.93$  may also reflect a proportion of unligated enzyme in CYP151A2.

Carbon monoxide-binding studies show that the CYP151A2 preparation contained a limited amount of the P450 component (i.e. the cysteinate-coordinated form), with the majority of the enzyme forming the cysteine-coordinated P420 species. This does not necessarily reflect the presence of cysteine-coordinated enzyme in the resting state, however, since the process of heme iron reduction and CO binding frequently results in loss of cysteinate coordination. When CYP151A2 is bound to the higher concentration of morpholine (60 mM), a single EPR low-spin species is formed without heterogeneity (Figure 5.13C). This latter species is distinct from that of the low-spin EPR species, demonstrating heterogeneity at the lower morpholine concentration (30 mM) (Figure 5.13B). The EPR data for both the substrate-free CYP151A2 (typical of cysteinate-coordinated heme iron) and the ligand-bound forms are thus inconsistent with the presence of an inactive “P420” component as an explanation for the heterogeneity of the low-spin form at the lower morpholine concentration.

The X-band EPR for the fluconazole-bound form of CYP151A2 is shown in Figure 5.12D. The  $g$ -tensor values of the fluconazole bound form are substantially different from the substrate-free (Figure 5.12A) and morpholine-bound forms (Figure 5.12C). The resulting  $g$ -values of  $2.45$  ( $g_z$ ),  $2.26$  ( $g_y$ ) and  $1.91$  ( $g_x$ ) are reflective of a low-spin ferric ( $\text{Fe}^{3+}$ ) heme (Mansuy and Renaud, 1995; Lipscomb, 1998) and are slightly different to those of the substrate-free and morpholine-bound forms of CYP151A2 (Figure. 5.13A and C, respectively). The  $g_z$ ,  $g_y$  and  $g_x$  components signal are broadened, suggesting that there may be a split population due to two orientations of the pyrrole ring relative to the heme plane, as previously suggested for azole-bound P450 BM-3 (Girvan *et al.*, 2004). The homogeneity of the spectrum for fluconazole-bound CYP151A2 is due to the apparently complete ligation of the azole to the heme iron in this sample, thus removing the residual aqua-ligated components seen in the

substrate-free CYP151A2 spectrum. In the fluconazole-bound form of CYP151A2, a significant decrease in the amplitude of the EPR signal is observed (Figure 5.13D), further highlighting perturbation of the heme ligation environment. This is again supported by observations from absorption and CD spectroscopy (see sections 5.10.2 and 5.6.1).

### 5.6.3 Magnetic circular dichroism (MCD)

A variation on CD is magnetically induced circular dichroism (MCD), which also involves the differential absorption of left and right circularly polarized light in the presence of a longitudinal magnetic field. The magnetic field leads to the lifting of the degeneracy of energy levels and spin states and to the mixing of electronic states causing differential absorbance of left and right circularly polarised light.

The magnetic field can induce three contributive modes to the MCD spectrum, each giving rise to a characteristic band shape, which can be distinguished according to different states of origin. These MCD terms are defined as *A*, *B* and *C* (Stephens, 1974). The *A*-band causes a sigmoid or derivative-shaped MCD curve due to Zeeman splitting by the magnetic field to excited transition states, and is temperature independent. The *B*-band, with absorption-like band shapes, independent of temperature, arises due to complex field-induced mixing of different energy states, but these are generally weak for symmetric hemes such as the *b*-type in P450s. Finally, the *C*-band occurs in paramagnetic material, due to splitting of the Zeeman sub-levels of a paramagnetic ground state. The temperature dependent *C*-band has an absorption-like band shape, and becomes intense at low temperatures. The *C*-band variation with field and temperature can be analysed to provide magnetic parameters of the ground state, such as spin, *g*-factor, and zero-field splitting. The net difference in absorption between the left and right circularly polarised light derives the spectroscopic measurement (Cheesman *et al.*, 1991).

The UV-visible MCD spectrum is particularly diagnostic of the spin and oxidation states of metal ions. The optical bands of the heme porphyrin macrocycle are sensitive to iron properties and accordingly diagnostic in MCD of the spin and oxidation states of the iron. The generated spectra, diagnostic of the spin and oxidation state of the heme, occur upon mixing of porphyrin- $\pi$  with iron- $\delta$  levels

(Dawson *et al.*, 1982; Cheesman *et al.*, 1991). Features appearing between the wavelengths 300-600 nm are typically due to  $\pi$ - $\pi^*$  transitions of the porphyrin ring. As a result, MCD is a practical probe of heme active site and ligation, complementing EPR-generated data.

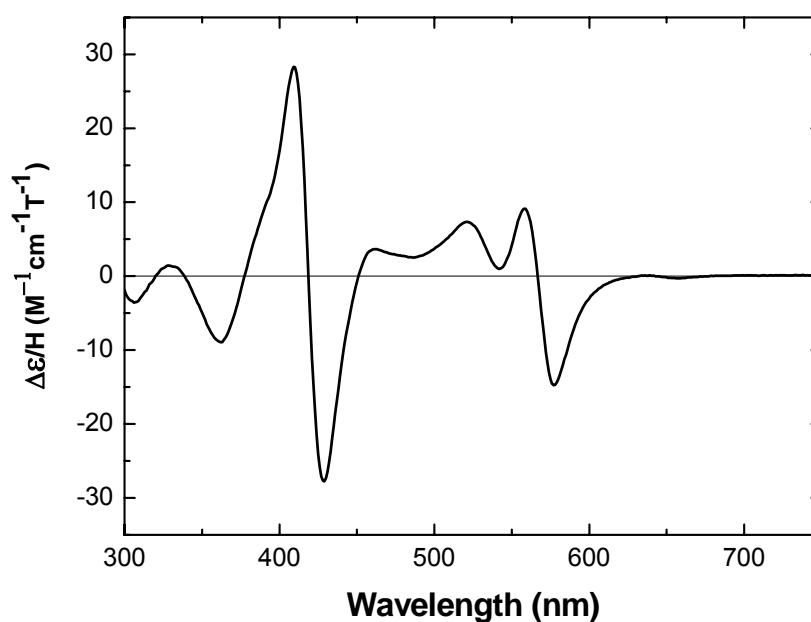


**Figure 5.14 UV-visible MCD spectral properties of CYP151A2**

Protein concentration was 30  $\mu$ M in 50 mM Tris-HCl, pH 7.5 including 50 % (v/v) glycerol.

The UV-visible and near-IR MCD spectra for oxidised CYP151A2 are shown in Figures 5.14 and 5.15, respectively. The room temperature UV-visible MCD spectrum of CYP151A2 shows a pattern of bands typical of low-spin ferric heme. From low to high energy, the MCD features of CYP151A2 are as follows with intensities in  $\text{M}^{-1} \text{cm}^{-1} \text{T}^{-1}$  ( $\epsilon_M^3$ ): 306 nm (-3.6); 362 nm (-8.9); 409 nm (+28.3); and the crossover at 417 nm (0). Subsequent bands are generated at 429 nm (-27.7); 461 nm (+3.6); 521 nm (+7.3); 558 nm (+9.1); 567 nm (0) and 577 nm (-14.7). The 417 nm crossover (zero point of the derivative-shaped feature) in the Soret region of the MCD spectrum is particularly close to the position of the Soret band in the electronic spectrum at 419 nm. This prominent Soret feature is characteristic of a MCD *A*-term with a degenerate excited state. A second *A*-term is also observed in the  $\alpha/\beta$ -region (500-600 nm), with the zero point of the derivative shaped feature at 567 nm, and

with the *A*-band trough at 577 nm ( $-14.7 \text{ M}^{-1} \text{ cm}^{-1} \text{ T}^{-1}$ ). Similar corresponding features are observed in P450cam (Andersson *et al.*, 1997), CYP121 (McLean *et al.*, 2002a), P450terp, P450 BM-3 and P450 BM-1 (Shimizu *et al.*, 1981; Cheesman *et al.*, 1991), and the liver microsomal P450 LM-2 (CYP2B4) (McKnight *et al.*, 1993). It is of interest to note the extremely close correspondence of the peak positions and band shapes between CYP151A2 and other MCD-characterised P450s.

Furthermore, in the visible region of the MCD spectrum of CYP151A2, a second derivative-shaped feature is also present with a peak at 558 nm and a trough at 577 nm, with a crossover at 567 nm. Comparable features are observed in other characterised P450s but the band positions are more similar to those of P450cam, CYP121 and P450 BM-1. The corresponding MCD band positions within P450terp, BM-3 and LM-2 are blue-shifted by  $\sim 1\text{-}3$  nm, relative to P450cam. The relatively low MCD intensity of the major features in the MCD spectra in both the Soret band region (400-420 nm) ( $56 \text{ M}^{-1} \text{ cm}^{-1} \text{ T}^{-1}$  peak to trough) and the  $\alpha/\beta$ -region (500-600 nm) ( $-14.7 \text{ M}^{-1} \text{ cm}^{-1} \text{ T}^{-1}$  for the *A*-band trough at 577nm) are also characteristic of thiolate-ligated hemes (e.g. Vickery *et al.*, 1975; Vickery *et al.*, 1976; Dawson *et al.*, 1983; Cheesman *et al.*, 1991; Berka *et al.*, 1998; Rux and Dawson, 1991; Sigman *et al.*, 1999; Girvan *et al.*, 2004.). At higher wavelengths there is a small trough at 665 nm in the MCD spectrum which corresponds to the weak broad absorption observed at 620-680 nm in the electronic absorption spectrum. This band is most likely due to a weak charge transfer band arising from a small population ( $\sim 1\%$ ) of high spin thiolate-coordinated ferric heme.

The observed discrepancy in the MCD spectra between P450terp, BM-3, LM-2 and P450cam has been reported by Peterson and colleagues (1997) to be derived from differences in distal heme pocket polarity (Andersson *et al.* 1997). The P450 enzymes P450terp and BM-3 are known to have ‘more polar’ distal pocket environments and/or hydrogen bonding between the axial  $\text{H}_2\text{O}$  ligand of the heme and the I-helix, compared to other bacterial P450s. The P450cam enzyme lacks the H-bond between the I- helix and the heme bound  $\text{H}_2\text{O}$  and also has a less polar binding pocket (Andersson *et al.*, 1997). Studies on BM-1 have indicated similar features to P450cam (Andersson *et al.*, 1997). The similarities in the MCD spectra between

CYP151A2 and P450cam suggest that a similar distal pocket environment exists in these proteins. However, CYP121, like P450cam and CYP151A2, has a corresponding blue-shifted MCD spectrum, although structural studies show H-bonding between the I-helix and the heme-bound H<sub>2</sub>O in CYP121 (Leys *et al.*, 2003).

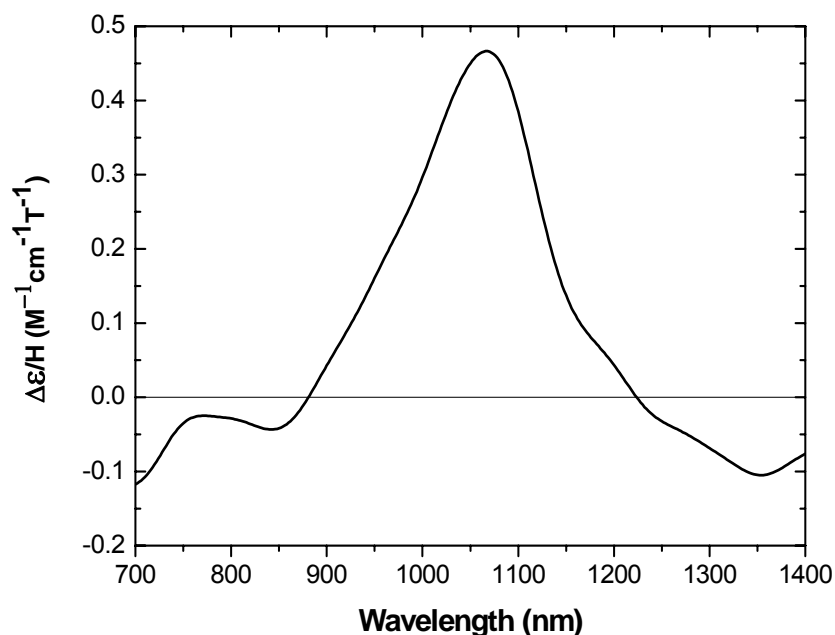


**Figure 5.15 Near-IR MCD spectral properties of CYP151A2**  
Protein concentration was 300  $\mu$ M in 50 mM Tris-HCl, pH 7.5 including 50 % (v/v) glycerol.

The MCD spectrum of CYP151A2 at near-IR wavelengths is displayed in Figure 5.14. In the near-IR region, low-spin ferric heme generate a porphyrin ( $\pi$ )-to-ferric iron (3d) charge-transfer transition which appears as a positively signed band in the MCD spectrum (Salerno *et al.*, 1995; Cheesman *et al.*, 1991). The precise energy of the observed band of the iron 3d orbitals varies systematically according to changes in axial ligation, and is thus diagnostic of the type of heme ligation (Cheesman *et al.*, 1991).

In the room temperature near-IR MCD spectrum, the charge-transfer band for CYP151A2 occurs at approximately 1062 nm (Figure 5.15). In P450 BM-3 and BioI, the NIR charge-transfer band occurs at 1060 nm and 1090 nm, respectively. This has provided evidence for cysteinate-water ligation (Shimizu *et al.*, 1981; Dawson *et al.*,



1982). The comparable wavelengths of CYP151A2, P450 BM-3 and BioI suggest similar cysteinate-water ligation in CYP151A2 (McKnight *et al.*, 1993).

#### 5.6.4 Resonance Raman

Resonance Raman (RR) spectroscopy has an important role in the study of hemoproteins because of the strong signal enhancement and detailed vibrational spectrum generated by the heme group in varied protein settings (Wood and McNaughton, 2006). The generated spectra are rich and variable with a number of useful marker bands for the porphyrin core size, for the electron density of the frontier orbitals, and for the vibrations of specific axial ligands (Aono *et al.*, 2002). The effects of peripheral substituents and of distortions imposed by the protein as well as ligands are of considerable interest with respect to heme protein structure and function relationships.

The resonance Raman spectrum of substrate-free CYP151A2 was obtained with excitation at 406.7 nm and labelled according to previous assignments (Hildebrandt and Stockburger, 1989; Kitagawa and Ozaki, 1987; Parthasarathi *et al.*, 1987; Hudeček *et al.*, 2000). The excitation line used (406.7 nm) is close to the Soret transition of the heme chromophore (419 nm) and generated Raman scattering from the vibrational modes of the porphyrin ring. The ligand-free CYP151A2 generated a spectrum with general strong similarity to those obtained for other P450 enzymes, including wild-type CYP121 (Kitagawa and Ozaki, 1987; Parthasarathi *et al.*, 1987; Hildebrandt and Stockburger, 1989; Hudeček *et al.*, 2000; McLean *et al.*, 2002a).

The dominant oxidation state marker band obtained for wild-type CYP151A2 was assigned the  $\nu_4$  mode (Figure 5.15). The observed value of  $1373\text{ cm}^{-1}$  for  $\nu_4$  indicated that the heme iron is in the ferric (FeIII) state, in accordance with the data obtained from electronic absorption spectra and EPR. Bands in the range  $1450 - 1650\text{ cm}^{-1}$  are characteristic indicators of the porphyrin ring core size and, accordingly, of the spin-state of the heme iron (Abe *et al.*, 1978; Hildebrandt and Stockburger, 1989). The characteristic spin-state marker in this range is  $\nu_3$  and the presence of this mode at  $\sim 1502\text{ cm}^{-1}$  revealed both ligand-free and -bound forms of CYP151A2 to be in a predominantly low-spin ferric heme state. In general, the RR spectrum of CYP151A2 is indicative of a ferric cysteinate-ligated P450 (Hudeček *et al.*, 2000). The

assignments and band frequency values for the main peaks in the RR spectrum of ligand-free and ligand-bound CYP151A2 are summarised in Table 5.2.

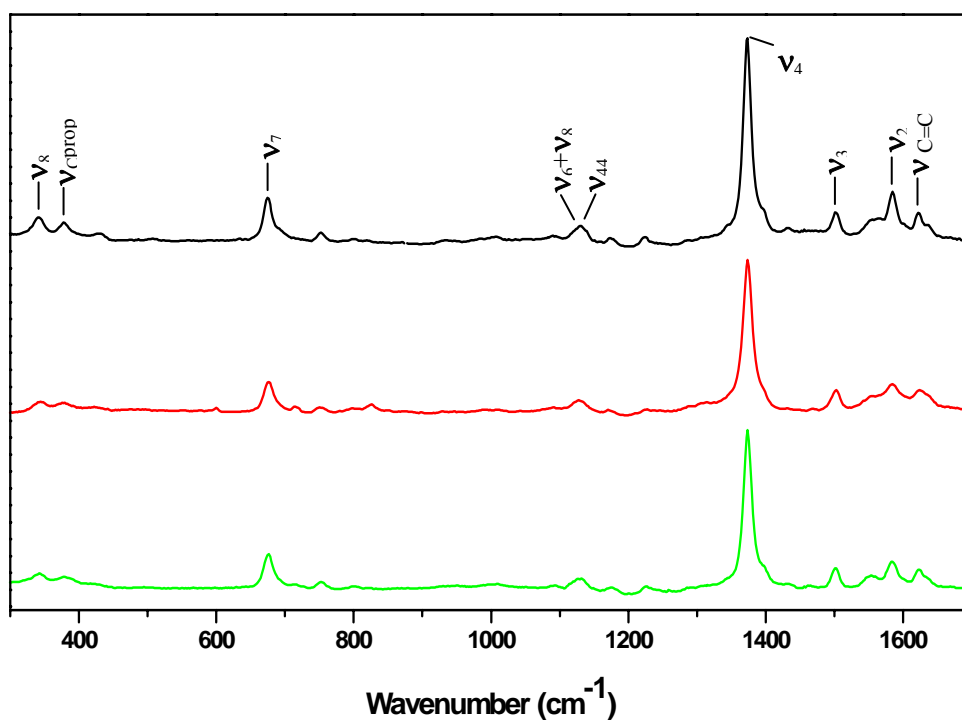


**Figure 5.16 Resonance Raman spectrum of ligand-free and -bound forms of CYP151A2**

Protein (100  $\mu\text{M}$ ) was in 10 mM Tris, pH 7.5 and spectra were recorded between 300 and 1700  $\text{cm}^{-1}$ . Positions of assigned vibrational bands are shown, including the  $\nu_4$  marker band for oxidised ferric heme (1373  $\text{cm}^{-1}$ ) and the  $\nu_3$  feature indicating the low-spin heme (at  $\sim 1502 \text{ cm}^{-1}$ ). Assignments of the CYP151A2 spectra (black) are shown and are also representative of corresponding peaks in the morpholine-bound (30 mM, red) and fluconazole-bound (30  $\mu\text{M}$ , green) forms.

	Band position (cm <sup>-1</sup> )		
Assignment	CYP151A2	Morpholine bound	Fluconazole bound
$\nu_{C=C}$	1622	1623	1623
$\nu_2$	1585	1584	1584
$\nu_3$	1502	1503	1502
$\nu_4$	1373	1374	1373
$\nu_{44}$	1130	1128	1132
$\nu_6 + \nu_8$	1125	1124	1127
$\nu_{16}$	753	750	753
$\nu_7$	674	676	676
$C_{bprop}$	378	377	379
$\nu_8$	343	345	343

**Table 5.2**      **Resonance Raman frequencies for the main features observed in ligand-bound and -free forms of CYP151A2**  
Excitation was at 406.7 nm, protein concentrations and conditions were as described in the legend to Figure 5.15.

The frequencies of the spin-state-sensitive modes such as  $\nu_2$  (1585 cm<sup>-1</sup>) and  $\nu_3$  (1502 cm<sup>-1</sup>) are consistent with CYP151A2 binding a low-spin ferric heme. For morpholine-bound protein (Figure. 5.15, red), the absence of a high-energy shoulder for  $\nu_3$  and the decrease in the intensity of this band confirms a reinforcement of the

low-spin species upon morpholine binding. At the concentration of morpholine used (and based on assignments from UV-visible absorption spectral data) it is expected that the morpholine is predominantly coordinated to the heme iron in the distal (6<sup>th</sup>) position. This would certainly be expected to maintain and reinforce the low-spin state of the heme iron, as would the coordination of the heme iron by the azole nitrogen in the inhibitor fluconazole. Thus (unlike the situation seen for CYP121 and its mutants in section 3.5.4), the RR data for CYP151A2 indicate that the ligand-free and ligand-bound forms are all nearly completely low-spin, with no evidence for any splitting of the  $\nu_3$  signal. In the morpholine-bound form, the oxidation state marker band  $\nu_4$  is slightly up-shifted in frequency with respect to that for the wild-type CYP151A2. While it is feasible that this is a species in which the iron-coordinated water molecule has not been expelled, it appears likely that at least a proportion of this low-spin species has morpholine directly coordinated to the heme iron. In the fluconazole-bound form of CYP151A2 (Figure 5.16, green), the fact that spectra are highly similar to the ligand-free form is likely due to the near-complete coordination of the heme iron by fluconazole. The major  $\nu_3$  and  $\nu_2$  in-plane bands have frequencies identical to that of morpholine-bound protein and are also illustrative of a low-spin species. The frequency of  $\nu_4$  remains unaltered at 1373 cm<sup>-1</sup>.

## 5.7 Redox potentiometry

Determining the mid-point redox potential of proteins involved in redox reactions is a valuable technique in understanding the energetics of biological electron transfer processes and the subsequent reactions coupled to electron transfer. In the case of P450 enzymes, the binding of a substrate frequently results in the dehydration of the heme iron (i.e. the loss of the 6<sup>th</sup> aqua ligand to the heme iron) and the resultant positive shift in heme iron redox potential that enables electron transfer from the redox partner and the progression of oxidative catalysis.

To examine the thermodynamic properties of the heme iron of CYP151A2, the reduction potential of CYP151A2 was determined anaerobically by spectroelectrochemistry of the protein solution, as described previously for CYP121 (section 3.6) and CYP140A2 (section 4.6). The spectral changes observed during the redox titration of CYP151A2 are displayed in Figure 5.17.

Titration of CYP151A2 with dithionite resulted in reduction in the intensity of the Soret maximum at 419 nm with a shift to longer wavelength (425 nm), as well as an increase in the absorption intensity in the visible region. There was development of a strong new spectral species at 559 nm, as well as generation of a smaller feature at 532 nm. Complete reduction of CYP151A2 was achieved using dithionite as reductant. The redox titration was completely reversible in reductive and oxidative directions, with the final spectrum for the reoxidised enzyme being essentially indistinguishable from that of the starting species. There was negligible development of turbidity due to enzyme aggregation, and no sign of hysteretical behaviour (i.e. spectra recorded at the same potential in oxidative and reductive directions were near identical).

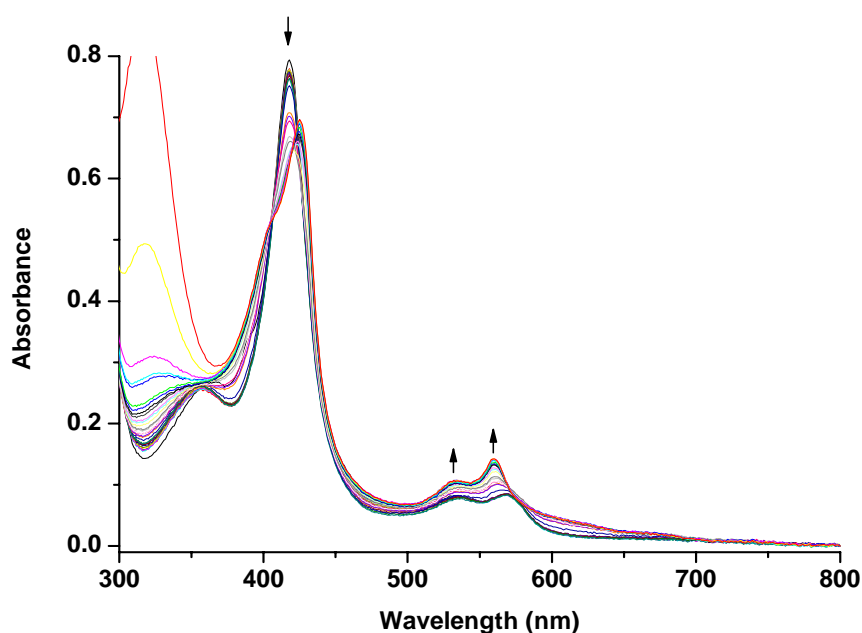


**Figure 5.17 Redox titration of substrate-free CYP151A2**

Selected spectra are shown for CYP151A2 (4.3  $\mu\text{M}$ ) at various stages of its redox titration. The starting (most intense) spectrum, shown in black, is for the oxidised ferric form of CYP151A2, with Soret maximum at 419 nm and  $\alpha$ - and  $\beta$ -bands at 569 and 535 nm, respectively. Complete reduction is represented with a red line. Arrows indicate the direction of absorbance change during the reductive titration at different wavelengths. Upon oxidation the spectrum is returned to that for the starting ferric form. All changes were reversible (i.e. no hysteretic effects observed). The redox titration was performed in 50 mM  $\text{KPi}$ , pH 7.0.

The nature of the optical change that occurs for CYP151A2 on reduction is non-characteristic of P450s. Rather than a Soret shift to a shorter wavelength on reduction, the CYP151A2 Soret band moves to a longer wavelength. Moreover, distinct spectral changes are seen in the Q-band region, particularly with respect to the increased intensity at 559 nm. The observed spectral changes are similar to those seen for CYP51 (McLean *et al.*, 2006) and the H93G variant of sperm whale myoglobin, for which cyclopentanethiol and tetrahydrothiophene sulfur donors were used to generate thiol-ligated ferrous forms (Perera *et al.*, 2003). Thus, spectral changes for ferrous CYP151A2 appear to be consistent with protonation of the thiolate ligand (Cys 394) to a thiol, a transition that likely underlies conversion of P450 to the inactivated P420 form. As discussed further below, CYP51 undergoes rapid conversion of the Fe(II)-CO complex from P450 to P420, probably as a result of protonation of the Cys 394 thiolate in this enzyme.

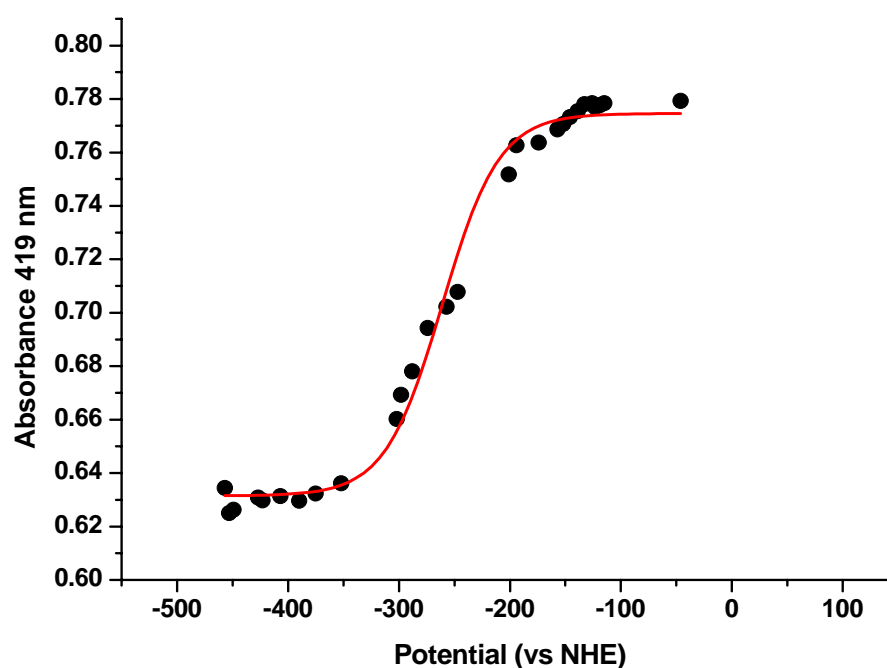


**Figure 5.18 Data fit for determination of heme iron reduction potential of CYP151A2**

The absorption data at 419 nm (near the Soret absorption maximum for the oxidised enzyme) were plotted against the applied potential. Data were fitted to a single electron Nernst function and yielded a mid-point reduction potential of  $-261 \pm 9$  mV.

Absorption *versus* potential data were plotted at 419 nm and fitted to a one electron Nernst equation to define the midpoint potential for CYP151A2 heme iron in the absence of morpholine. A mid-point heme iron reduction potential of  $-261 \pm 9$  mV was determined (Figure 5.18). The reduction potential of CYP151A2 was more positive than those reported previously for the model P450 enzymes P450 BM-3 and P450cam (Sligar, 1976; Munro *et al.*, 1991; Ost *et al.*, 2001a). However, it was similar (in fact, indistinguishable within error) to that for CYP140A2 reported in section 4.8 ( $-264 \pm 8$  mV). In addition, the long wavelength shift of the heme Soret band on reduction and the increased intensity of the visible bands on heme iron reduction are also similar to that observed for CYP140A2, and to that observed recently for *M. tuberculosis* CYP51 (McLean *et al.*, 2006). In the case of CYP51 on reduction, the Soret band loses intensity and shifts to  $\sim 423$  nm and new spectral features develop in the Q-band region with higher intensity at 559 nm.

Thus, it is concluded that in the case of CYP151A2 (as for CYP140A2) the reduction of the heme iron is associated with protonation of the heme thiolate and the conversion from thiolate- to thiol-ligation of the heme iron in the ferrous enzyme. As with CYP140A2 (and CYP51), the protonation is reversible and the enzyme converts back to thiolate ligation in the ferric form.

Substrate binding to P450s has (in many cases) been observed to alter the heme iron redox potential such that reduction from its immediate redox partner becomes more energetically favourable. In view of the marked effect of substrate binding to P450s (Sligar, 1976; Ost *et al.*, 2001a) a potentiometric study of the morpholine-bound form of CYP151A2 was undertaken to establish whether there was any shift in heme iron reduction potential, and to establish whether thiolate protonation still occurs in CYP151A2 when the enzyme is bound to a substrate molecule (Figure 5.19).

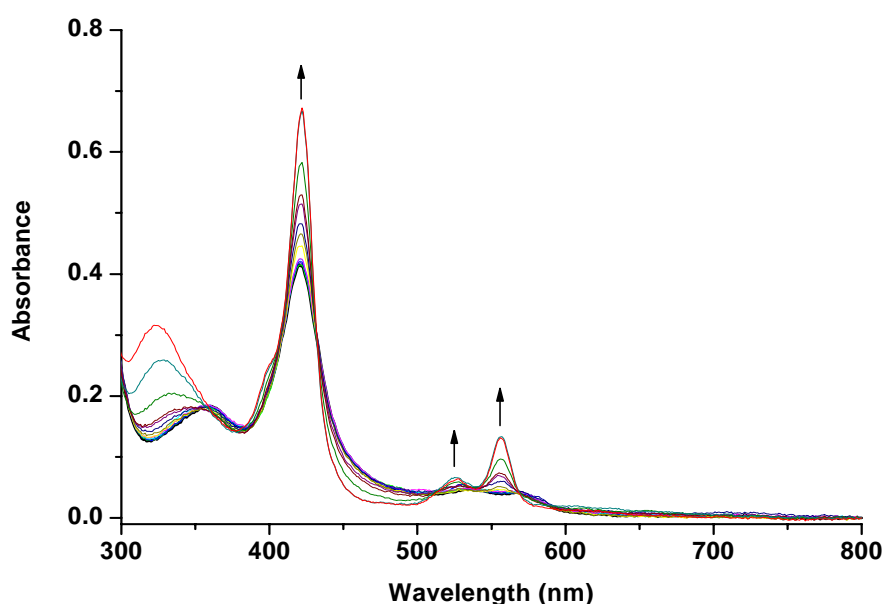


**Figure 5.19 Redox titration of morpholine-bound CYP151A2**

Spectral changes for morpholine (30 mM)-bound CYP151A2 ( $\sim 2.3 \mu\text{M}$ ) are shown at different stages in its reductive potentiometric titration. The starting (least intense) spectrum, shown in black, is for the CYP151A2-morpholine complex, with Soret maximum at 421 nm and  $\alpha$ - and  $\beta$ -bands at 557 and 525 nm, respectively. The titration was performed in 50 mM  $\text{KP}_i$ , pH 7.0. Addition of 30 mM morpholine causes a small Soret shift to 420 nm (black line). On complete reduction with dithionite, shown in red, there is an increase in the intensity of the Soret band at 422 nm along with an increase in absorbance at 531 and 560 nm. Arrows show direction of absorption change at selected wavelengths during redox titration in the reductive direction.

Dithionite-mediated reduction of CYP151A2 in the presence of morpholine resulted in an increase in the intensity of the Soret peak at 422 nm. There were also further changes in the visible region with the formation of a sharp band of strong intensity at 566 nm, and a smaller band at 531 nm. The observed spectral changes in morpholine bound CYP151A2 are also similar to the reduced form of estriol-bound *M. tuberculosis* CYP51 (McLean *et al.*, 2006). In the case of estriol-bound CYP51, the Soret band increases in intensity and is red shifted to  $\sim 423$  nm, and there is development of further features at 558.5 and 530 nm, with the former of higher intensity (McLean *et al.*, 2006). With both CYP151A2 and CYP51 the spectral changes are similar to those seen for the H93G variant of sperm whale myoglobin, for



which cyclopentanethiol and tetrahydrothiophene sulfur donors were used to generate thiol-ligated ferrous forms (Perera *et al.*, 2003). As previously noted for CYP51 (McLean *et al.*, 2006), spectral changes for ferrous CYP151A2 are suggestive of protonation of the thiolate ligand (Cys 348) which likely underlies the conversion of P450 to the inactivated P420 form. The observed spectral changes in morpholine-bound CYP151A2 are also quite similar to those for the reduced forms of various cytochromes *c*, which generally have a methionine-ligated heme iron (Miller *et al.*, 2000). A large sharp increase in the absorption in the visible (long wavelength) region is also observed in these proteins on reduction. A large band typically develops at around 550 nm occurs upon reduction (Kavanagh *et al.*, 1999; Miller *et al.*, 2000; Lett and Guillemette, 2001; Cheesman *et al.*, 2001).

The overall magnitude of the spectral change on reduction was much larger in the morpholine-bound form (Figure 5.19), compared to ligand-free CYP151A2. However, morpholine binding data (section 5.10.1) suggested that morpholine binding at saturation causes a long wavelength shift in Soret absorption, consistent with coordination of the CYP151A2 heme iron by the morpholine nitrogen atom. Thus, ligation by morpholine would maintain and reinforce the low-spin heme state of CYP151A2, and this would suggest that the reduction potential of the heme iron might become more negative in the morpholine-bound form of CYP151A2. In the morpholine-bound CYP151A2, spectra recorded towards the end of the titration (i.e. for the reduced form of the enzyme) show a small absorption feature at 396 nm, which was not obvious in the redox spectra for the substrate-free form. This feature is likely due to the reduction of methyl viologen mediator present in this titration, which was at a slightly higher concentration than in the titration in the absence of morpholine and which has absorption in this region when reduced.

It was established in earlier UV-visible spectroscopy studies that morpholine titration does cause spectral perturbations to the heme (section 5.10.1). Due to the strongly basic nature of morpholine (and hence effects on pH of the system if a near-saturating amount of morpholine was added), it was decided that morpholine would be added to a final concentration of 30 mM for the redox titration of CYP151A2. At this concentration, morpholine induced conversion of the Soret band from 419 nm to 420 nm. In addition, the  $\alpha$ -band (556 nm) showed a marked increase in intensity.

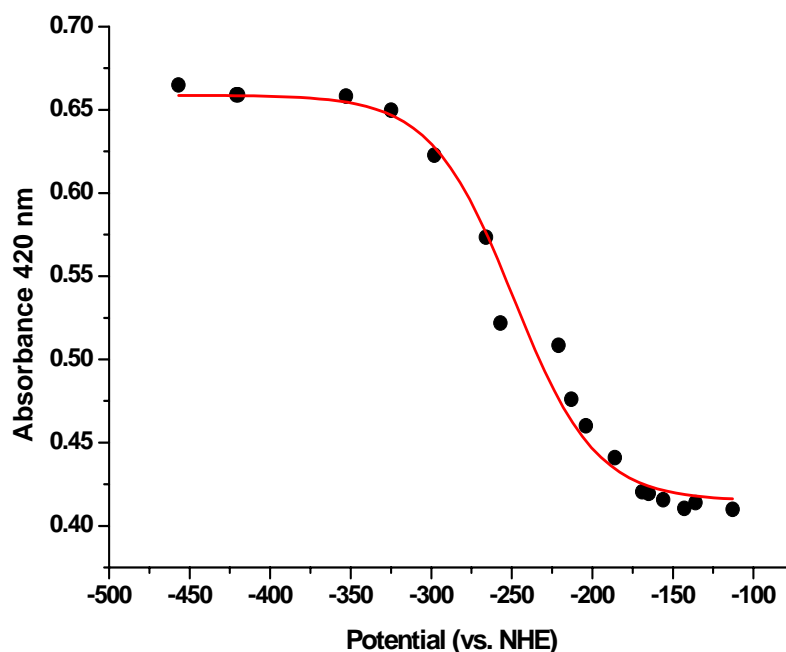


**Figure 5.20 Data fit for determination of the midpoint reduction potential for morpholine-bound CYP151A2**

Data shown are for absorption at 420 nm (near the Soret peak in the oxidised form of the enzyme) during redox titration of CYP151A2 in its morpholine (30 mM)-bound form. Data are plotted *versus* the applied potential, relative to the hydrogen electrode (NHE). Data are fitted to the single electron Nernst function yielding a mid-point reduction potential of  $-249 \pm 8$  mV.

Absorption *versus* potential data were plotted at 420 nm and were fitted to a 1-electron Nernst equation to define the mid-point potential for morpholine-bound CYP151A2 heme iron. Fixing the Nernst factor ( $RT/F$  value) to 59 mV, which corresponds to the slope of a one-electron redox couple at 25 °C, yielded a mid-point reduction potential of  $-249 \pm 8$  mV (Figure 5.18). The binding of morpholine to CYP151A2 results in a very similar heme iron redox potential ( $-249$  mV) to that determined for the ligand-free form ( $-261$  mV). Thus, substrate binding (which does not increase the high-spin content in the CYP151A2 enzyme at the concentration used) does not induce any major alteration of the reduction potential in the CYP151A2 enzyme.

In the P450 BM-3 system and in P450cam, binding of fatty acid substrate and camphor, respectively, results in the loss of the aqua ligand to the heme iron, inducing

extensive shift in the heme iron spin-state equilibrium towards the high-spin form, and causing an elevation of the reduction potential by ~140 mV and 130 mV, respectively (Sligar 1976, Ost *et al.*, 2001a). As discussed previously, such substrate-mediated effects on heme iron coordination and potential favour the reduction of the heme iron, and brings the heme iron into the range where it can receive electrons from the redox partner. In the case of P450 BM-3 this occurs from the FMN cofactor in its fused P450 reductase redox partner, and in P450cam from an iron sulfur cluster in its redox partner putidaredoxin. A similar mechanism may occur in the CYP151A2 enzyme, with a shift in spin-state equilibrium towards high-spin occurring on binding of the natural substrate(s), enabling the P450 to be reduced effectively in the cell by its redox partner. While morpholine is a *bona fide* substrate for this enzyme, it appears unlikely to be a “normal” substrate for the P450. At lower concentrations it induces a small amount of shift to high-spin (and likely some small positive shift in potential), but at higher concentrations it becomes an inhibitory ligand. Rather different characteristics might be expected of a physiologically more relevant P450 substrate. However, it should also be remembered that (for both substrate-free and morpholine-bound CYP151A2), anaerobic reduction with dithionite leads to the conversion of the enzyme to a ferrous form with a spectral signature typical of a thiol-coordinated heme iron. This likely means that, in this equilibrium method, both reduced forms of the enzyme (i.e. substrate-free and morpholine-bound) have predominantly the same heme iron coordination (and spin) states. In the oxidised enzymes, both forms of CYP151A2 are predominantly low-spin. Thus, it might be expected that similar heme iron redox potentials would be determined (as was found). It may be the case that protonation to the thiol is a consequence of the persistence of the ferrous enzyme in absence of oxygen and/or an appropriate substrate, and reflects a physiological adaptation. It may be the case that, if a faster mode of enzyme reduction/oxidation cycling could be used (e.g. protein film voltammetry, PFV), the thiol-coordinated species would not accumulate and a morpholine-induced shift in redox potential would be observed for the thiolate-coordinated enzyme (at least at lower morpholine concentrations).

However, substrate-induced redox potential shifts may be absent in some types of P450 chemistry. It has been reported for P450cin (CYP176A) (Aguey-Zinsou *et al.*, 2003) that, despite a complete low-to-high spin conversion of ferric P450cin

upon addition of cineole, the heme redox potential is unchanged. Slessor and colleagues (Aguey-Zinsou *et al.*, 2003), have proposed that the absence of an anodic shift indicated that ferric and ferrous P450cin have an equal affinity for cineole, whereas the shifts observed in other P450s reflect tighter substrate binding by the reduced form of the enzyme (Aguey-Zinsou *et al.*, 2003). However, this observation does not account for the fact that high-spin ferric heme iron is known to have a more positive reduction potential than low-spin heme iron. Moreover, this study involved immobilisation of the P450 on a pyrolytic graphite electrode and although it was hoped that the electrode surfaces used avoid the inactivation of the P450, this scenario cannot be ruled out. Also, in light of the results of this study whereby CYP151A2 naturally adopts a protonated thiolate (i.e. thiol) on reduction in an anaerobic environment, which is not prevented by substrate binding, then variation between the potentials of the substrate-bound and -free form might be unlikely.

## **5.8 Thermostability studies by heat denaturation**

The ferric iron spin-state in the heme system in P450s exists in a thermal equilibrium. As such, the proportion of the high-spin and low-spin forms can be altered by modulation of temperature in a typical physiological range, with elevated temperature leading to greater proportions of the high-spin form (Sligar and Gunsalus, 1976).

It appears that the porphyrin system and axial ligands of many hemoproteins have evolved with the heme iron near to the 'cross-over' points between the two spin states, and that this is modulated upon substrate binding. This substrate-dependent modulation is an important facet in the P450 catalytic cycle and oxygenation mechanism, in order to prevent production of harmful reactive oxygen species and to trigger electron transfer only when substrate is bound in the P450 active site. In the typical resting state of a P450, the heme moiety consists of low-spin, six-coordinate Fe(III). In both the P450 BM-3 and P450cam systems, a shift in the spin-state equilibrium from low towards high had been noted upon an increase in temperature, and this has proved useful in determining the thermodynamics and energetics of the P450 heme system (Lewis, 1996). The shift in spin-state is an electronic reorganisation that occurs in the iron d-orbitals, and results in vacation of lower

energy orbitals (Figure 5.21). This leads to easier reduction of the heme iron in the high-spin form due to a more positive heme iron reduction potential.

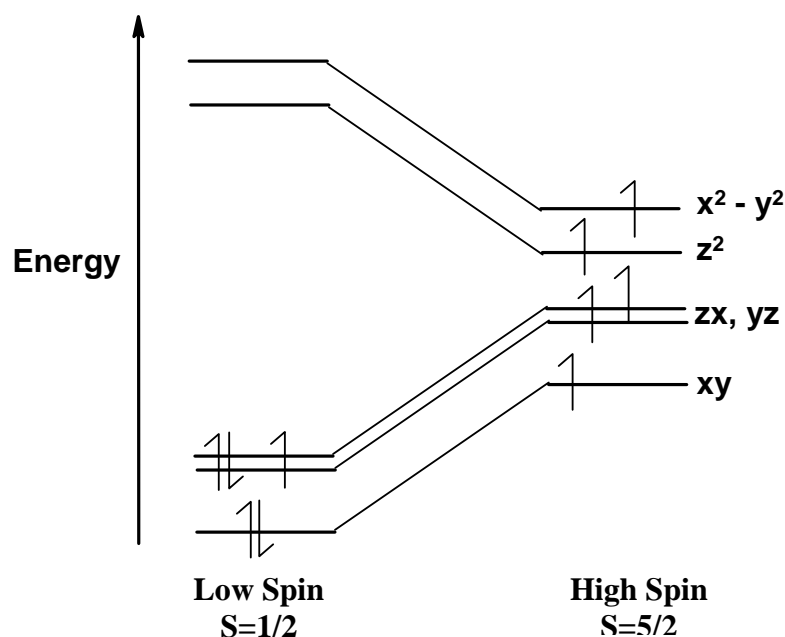


**Figure 5.21 Schematic representation of d-orbital ( $d^5$ ) electronic occupancy in low- and high-spin forms of ferric P450 heme iron**

Electronic reorganisation in P450 ferric heme iron d-orbitals ( $d^5$ ) from low- to high-spin may occur as a result of substrate binding, and give rise to changes in the mid-point reduction potential. Figure generated in ISIS Draw.

CYP151A2 was subjected to a gradual increase in temperature at increments of 2°C to observe any shift in the spin-state equilibrium in the UV-Vis absorption spectrum, until the point where thermal denaturation of the P450 occurred. Elevation of the temperature above 40°C resulted in increased turbidity of the CYP151A2 solution, producing high baseline shifts of the spectra and progressive aggregation and precipitation of the protein. As P450 denaturation occurred, loss of heme from the protein matrix was observed as marked decreases in magnitude of the Soret band. The experiment was repeated in the presence of 10 % glycerol in order to improve protein stability. Under these conditions, the temperature could be increased up to 44°C until the protein denatured as before. No significant shift in spin-state equilibrium (i.e. alteration in the equilibrium of the Soret absorption components at ~390 nm and ~420 nm) was observed before denaturation occurred in either absence or presence of glycerol.

The observed lack of any spin-state shift upon elevation of temperature within the reported range may be based on the relatively low thermostability of the protein, with protein aggregation preceding any significant change in spin-state. In addition, the water ligand may be tightly bound to the P450 even at high temperatures, possibly through a network of hydrogen bonds with amino acid side chains and other water molecules. In the penta-coordinate high-spin conformation of the heme moiety, the ionic radius of iron is greater than that for low-spin, thus, the iron will favourably move out of the porphyrin ring plane as the central cavity is too small to accommodate the increased cationic size (Lewis, 1996).

Perhaps a small disruption of the heme environment through the positioning of the iron in the absence of a substrate is enough to effect the relative stability of the low-spin form of CYP151A2. Structural changes induced by binding of the substrate (and/or direct dehydration of the iron through substrate binding in the immediate vicinity of the heme) could then lead to perturbation of the heme iron spin-state equilibrium. However, it is also possible that CYP151A2 may not easily undergo substrate-independent (i.e. thermally-induced) spin-state conversions that have been noted in certain other P450s.

## **5.9 Protein unfolding measured by circular dichroism spectroscopy**

Circular Dichroism (CD) of P450s (and indeed any protein molecule) in the far-UV region provides quantitative information on their secondary structure. The disruption of the secondary and tertiary structure of proteins can be achieved by a variety of methods, including the addition of chemical chaotropes such as guanidine hydrochloride (GdnHCl) or urea (Kelly *et al.*, 2005). Measuring chaotrope-induced perturbations in secondary structure provides information on protein stability, and can facilitate identification of any intermediates in the unfolding process. To examine the structural stability of CYP151A2, GdnHCl-induced far-UV CD spectral changes were monitored across a range of chaotrope concentrations. The data for CYP151A2, and at a variety of GdnHCl concentrations, are displayed in Figure 5.22.

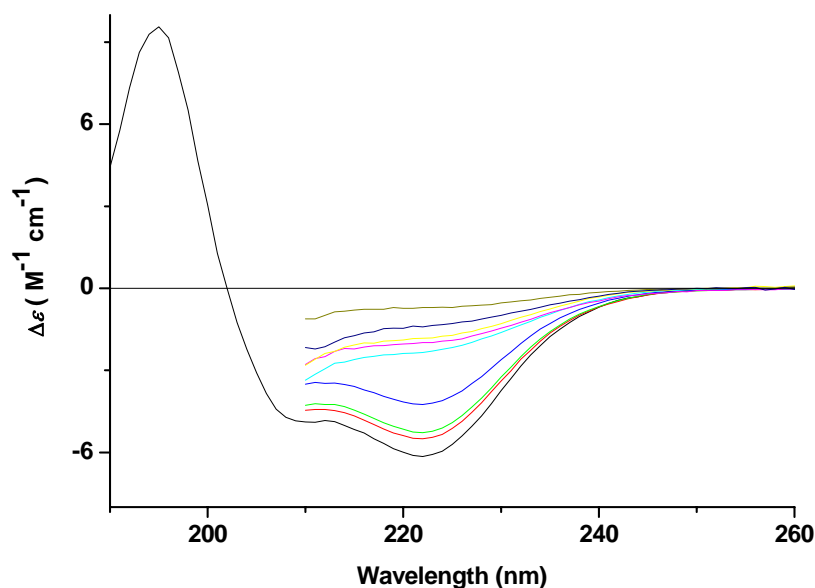


**Figure 5.22 The denaturation of CYP151A2 monitored by far-UV CD spectroscopy**

The far-UV CD spectra of CYP151A2 (6  $\mu$ M) in 10 mM Tris-HCl, pH 7.5 were collected at GdnHCl concentrations of 0, 0.25, 0.5, 0.75, 1.0, 1.25, 1.75, 2, 6 M, indicated by the black, red, green, blue, cyan, magenta, yellow, navy and dark yellow lines, respectively. Spectra were collected from samples in a quartz cuvette of path length 0.02 cm.

In the far-UV region (Figure 5.22), any differences in the spectra are indicative of changes in the secondary structure of the protein. Significant changes are noted in the overall far-UV CD spectrum upon increases in the GdnHCl concentration. With low GdnHCl concentrations (<0.75 M), small spectral changes are observed, which are largely manifested as decreases in the intensity of the CD spectrum between ~210-250 nm, without substantial changes in the overall shape of the spectrum. Data collected below 210 nm in the presence of the chaotrope are not shown, because of spectral contamination from the GdnHCl itself). More substantial changes in the CD spectrum are observed at higher GdnHCl concentrations, as evident from sharper decreases in intensity and alterations in the shape of the CD spectra. The secondary structure content is all but lost by ~4 M GdnHCl. To determine the extent of unfolding of the protein through the determined change in the secondary structure (by CD), the value for ellipticity at the spectral minimum (222 nm for the native CYP151A2) was plotted against the appropriate GdnHCl concentration (Figure 5.23). The data plot resembled a hyperbola and the data was thus fitted to a

standard hyperbolic function to obtain an estimate for the midpoint concentration of GdnHCl at which 50 % of the CYP151A2 secondary structure was lost.

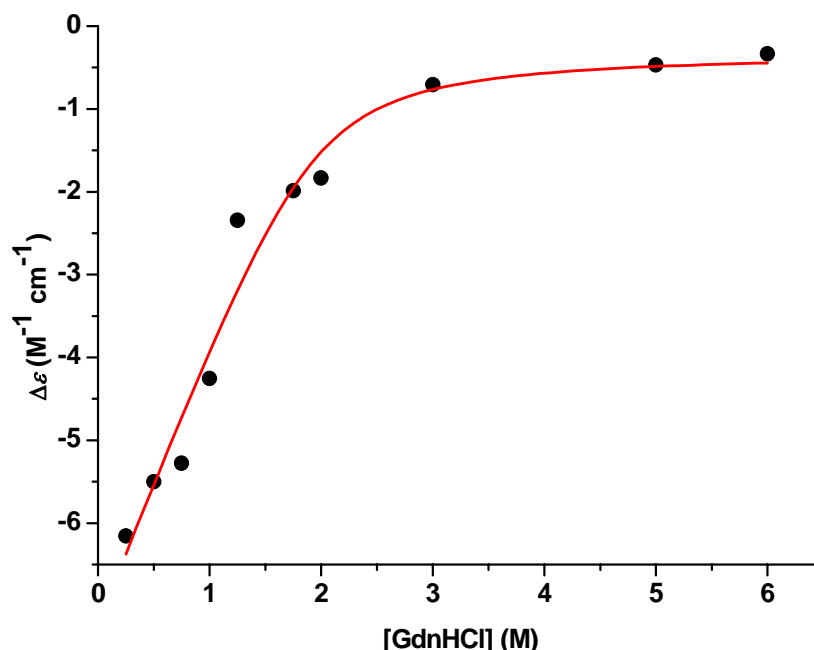


**Figure 5.23 Plot of change in CYP151A2 far-UV CD as a function of [GdnHCl]**  
The ellipticity (recorded at 222 nm) was plotted against GdnHCl concentration for CYP121. Data points are fitted to a hyperbolic function.

From Figure 5.23, CYP151A2 is 50 % unfolded at  $1.43 \pm 0.09$  M GdnHCl, as determined by the GdnHCl-induced change in ellipticity of the far-UV CD spectrum. Incubation of CYP151A2 with increasing concentrations of GdnHCl resulted in a progressive loss of the secondary structure, with the protein being almost completely unfolded at 4 M GdnHCl. The ease of denaturation may indicate a protein that has a globule like molecular structure.

## 5.10 Ligand binding

Cytochrome P450 (P450) enzymes are heme protein monooxygenases that play a crucial role in the metabolism of different substrates, both hydrophobic and hydrophilic. They sometimes simultaneously bind more than one substrate molecule (Cupp-Vickery *et al.*, 2000), and the specificity varies widely across the P450s. The visible spectrum of a ligand-bound cytochrome P450 is often used to determine the nature of the interaction between the ligand and the P450. P450s may be inhibited by the binding of compounds in the active site (McLean *et al.*, 2002b). The specificity



for such ligands can be influenced not only by the interactions made in the active site, but also by accessibility to and from the active site.

#### 5.10.1 Putative substrate binding

The amine heterocyclic compounds; morpholine (C<sub>4</sub>H<sub>9</sub>ON), pyrrolidine (C<sub>4</sub>H<sub>9</sub>N), and piperidine (C<sub>5</sub>H<sub>11</sub>N) are three heterocyclic compounds found in the environment as chemical products mainly derived from human activities, such as industrial plants and agricultural applications (Trigui *et al.*, 2004). Environmental release of these amines can result in their conversion to potent mutagenic and carcinogenic *N*-nitroso compounds (WHO, 1995). Consequently, it is important to eliminate these molecules from the environment. Growth on morpholine, pyrrolidine and piperidine as the sole source of carbon, nitrogen, and energy has been reported for different *Mycobacterium* species (Poupin *et al.*, 1999a, b; Schrader *et al.*, 2000; Sielaff *et al.*, 2001; Trigui *et al.*, 2004; Kim *et al.*, 2006).

Previous studies indicated that the initial oxidation of morpholine, pyrrolidine, and piperidine is catalysed by a cytochrome P450 monooxygenase (Combourieu *et al.*, 1998; Poupin *et al.*, 1998; Poupin *et al.*, 1999). The proposed amine degrading CYP151A2 was purified for the first time from *Mycobacterium* sp. strain HE5 (Sielaff *et al.*, 2001) and more recently from *Mycobacterium* sp. strain RP1 (Trigui *et al.*, 2004). Subsequent studies of CYP151A2 have revealed its capability to oxidise morpholine (Sielaff *et al.*, 2001; Trigui *et al.*, 2004).

Binding of the proposed substrate morpholine to CYP151A2 was shown to induce a type II spectral change, with a decrease in the intensity of the Soret band in the morpholine complex and a shift of the Soret maximum to 421 nm. The generated final visible spectrum was similar to those ofazole P450 complexes, with some perturbations also noted in the Q-band region. However, the extent of the Soret band shift at apparent saturation (to ~421 nm) is not as great as that obtained forazole drugs (Figure 5.10.2). Thus, from the type II spectral shift induced, morpholine appears to act in an inhibitory fashion and to coordinate to the CYP151A2 heme iron, reinforcing the low-spin state of the heme iron. Spectral titration with morpholine was performed and the  $K_d$  value determined by fitting induced absorption change *versus* ligand concentration data to a hyperbola, producing a value of  $18.2 \pm 0.1$  mM.

Thus, while producing a type II inhibitor-like shift in the heme spectrum, morpholine does not bind as tightly to CYP151A2 as do variousazole and triazole compounds (Table 5.3). No CYP151A2 spectral change could be observed upon addition of piperidine or pyrrolidine (up to 60 mM each). The changes in absorbance of CYP151A2 upon addition of successive amounts of morpholine are displayed in Figure 5.24.

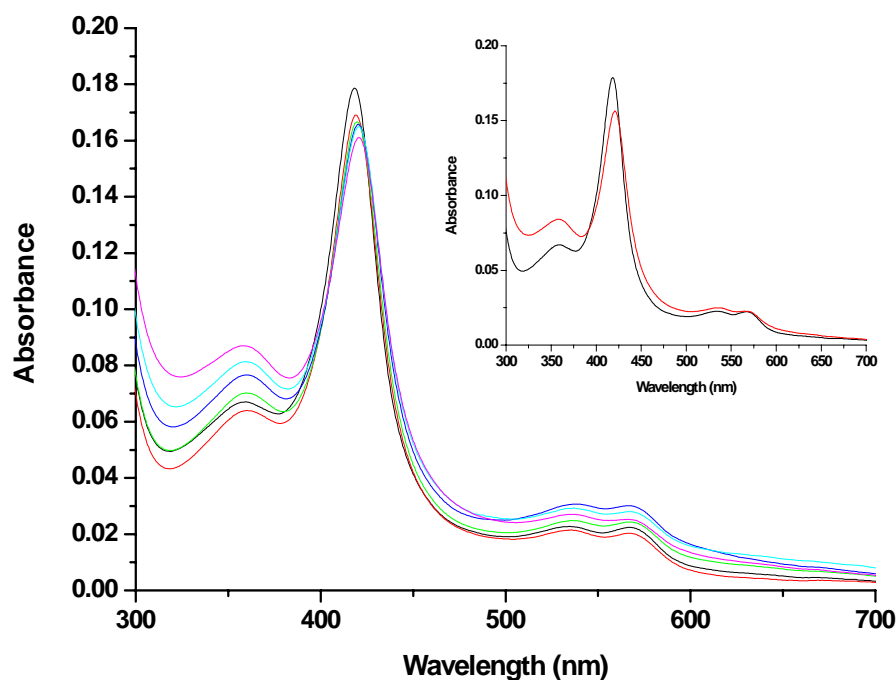


**Figure 5.24 Binding of morpholine to CYP151A2**  
UV-visible spectra displaying a titration of CYP151A2 (1.1 μM) in 50 mM Tris-HCl, 1mM EDTA (pH 7.2) with successive additions of morpholine at 0, 7.6, 12.66, 25.29, 37.89, and 50.46 mM (black, red, green, blue, cyan, and magenta lines respectively). The ultimate extent of the absorbance shift is shown (inset) with inhibitor-free (black) and inhibitor-saturated (50.46 mM, red) forms.

In order to analyse the titration with morpholine, a difference spectrum was constructed at each point by the subtraction of the spectrum for the inhibitor-free form from each successive inhibitor-bound spectrum in the titration. These difference spectra are displayed in Figure 5.25.

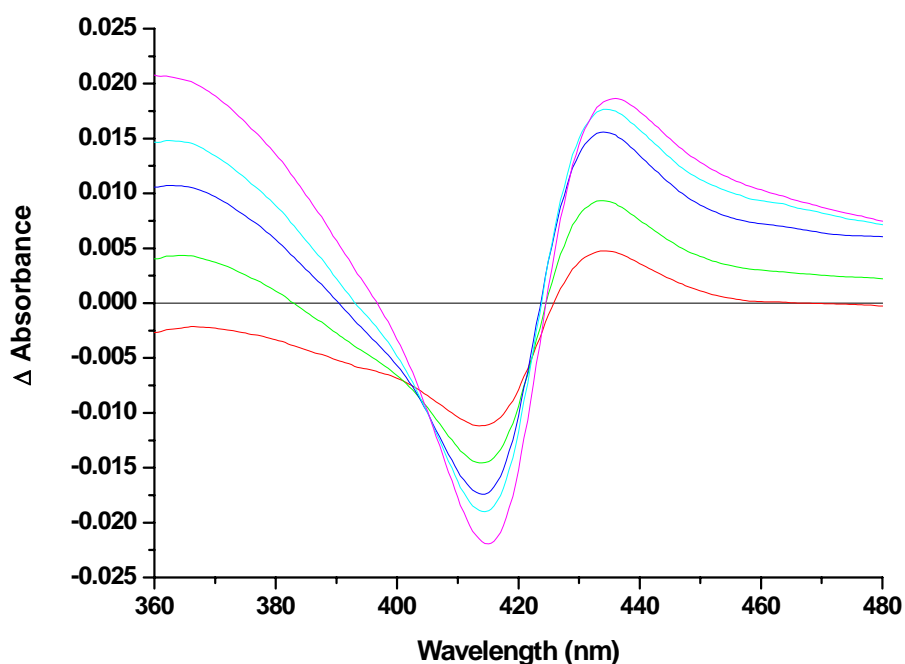


**Figure 5.25 Difference spectra for CYP151A2 titrated with morpholine**  
 Difference spectra corresponding to morpholine concentrations of 7.6, 12.66, 25.29, 37.89, and 50.46 mM are shown as red, green, blue, cyan, and magenta lines, respectively. Difference spectra were generated from absolute spectra shown in Figure 5.22.

The difference spectra generated for the titration of CYP151A2 with morpholine display maxima and minima values at approximately 435 nm and 415 nm, respectively. The type II binding spectrum is characterized by a peak and a trough at the aforementioned wavelengths. For each concentration of morpholine, the maximal absorbance difference was determined by subtraction of the absorbance value at the trough from that at the peak in each difference spectrum (using the same  $\lambda$  values for each). These values were subsequently plotted against the corresponding concentration of morpholine, and the data fitted to a hyperbolic equation, to determine a binding coefficient ( $K_d$ ) for the binding of this substrate, Figure 5.26. The titration curve generated for morpholine binding to CYP151A2 revealed a  $K_d = 18.2 \pm 0.8$  mM.

In contrast to the spectral perturbations observed for the binding of morpholine, no observable spectral change occurred upon binding of piperidine and pyrrolidine (up to 60 mM each). Previous studies of ligand binding to CYP151A2 revealed no spectral perturbations with morpholine, piperidine or pyrrolidine (Sielaff

and Andreesen, 2005a). Further optical titration studies were done using the proposed native recombinant ferredoxin and binding this protein to CYP151A2 in attempts to induce spin-state change within CYP151A2, in both the presence and absence of the described secondary amines. However, no spectral effects were noted (Sielaff and Andreesen, 2005a). The binding of adrenodoxin has previously been noted to facilitate the binding of cholesterol to CYP11A1 (Uhlmann *et al.*, 1994).

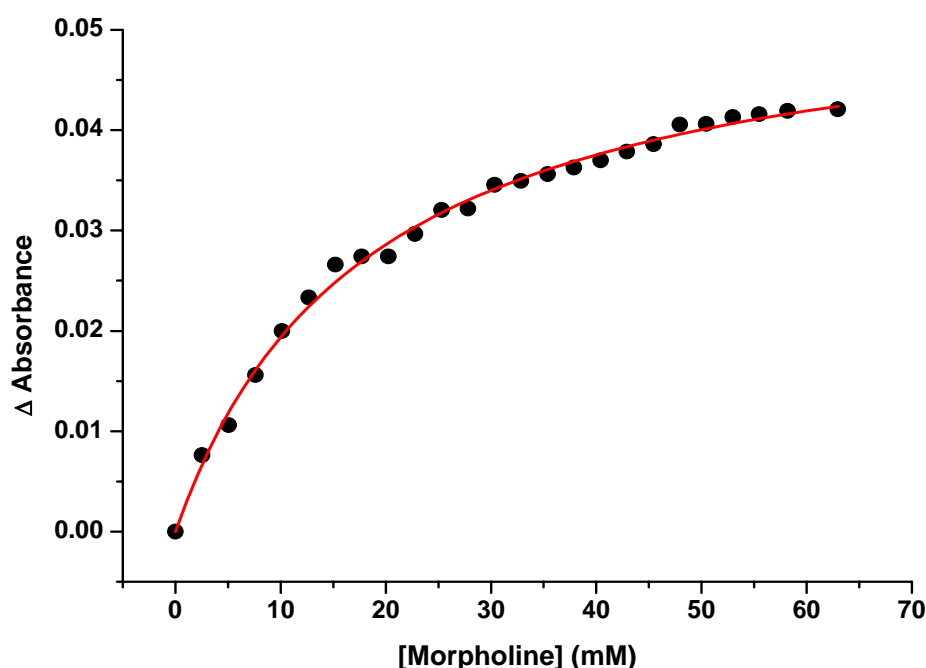


**Figure 5.26 Titration curve for the binding of morpholine to CYP151A2**  
CYP151A2 concentration was 0.97  $\mu$ M. Data (absorption difference between 435 nm and 415 nm) were fitted to a hyperbolic function, yielding a  $K_d = 18.2 \pm 0.8$  mM.

The data reported here for the interactions of the isolated bacterial CYP151A2 with morpholine raise important questions regarding substrate-heme interaction. The proposed substrate morpholine induces a non-characteristic type II spectrum and reinforcement of the low-spin ferric P450 species, as reflected in a chromic shift of Soret maximum to longer wavelength at high concentrations of morpholine.

Substrates typically bind in the P450 active site distal to the heme iron and displace the water molecule weakly bound to the iron, resulting in electronic reorganisation of the heme iron d-orbitals and an increased high-spin population.

Substrate-induced low-to-high spin transformation in the electronic ground state of P450s was first reported for ferric P450cam, (Sharrock *et al.*, 1973) and subsequently this has been found to be a characteristic feature of many other P450s. For example estriol produces a substantial heme spectral change in *M. tuberculosis* CYP51 toward 392 nm, consistent with formation of a high-spin species (McLean *et al.*, 2006). For P450cam it has been shown that the binding of substrate is a prerequisite for the beginning of the catalytic cycle (Sligar, 1976). This is typically accompanied by replacement of the heme-coordinated water molecule and subsequent reorganisation of the other active site water molecules (Li and Poulos, 1997; Cupp-Vickery *et al.*, 2000). In a previous study, morpholine, piperidine and pyrrolidine did not induce any observable change in the spectrum of CYP151A2 (Sielaff and Andreeson, 2005). This observation was proposed to be due to the polarity and hydrophilicity of these compounds in contrast to the majority of known substrates of cytochromes P450 (Sielaff and Andreeson, 2005a). Further binding studies were also performed with pyridine and metyrapone, which produced type II (inhibitory) spectral shifts from which were generated binding constants of  $7.99 \pm 0.72$  mM and  $24.6 \pm 1.6$   $\mu$ M, respectively (Sielaff and Andreeson, 2005a).

Atypical spectral perturbations have been previously observed upon substrate binding to P450s. The steroid 15 $\beta$ -hydroxylase (CYP106A2) from *B. megaterium* ATCC 13368 is another interesting prokaryotic P450, with only a minor UV-Vis spectral change observed, indicating a minor shift towards the high-spin form upon the addition of substrate (Simgen *et al.*, 2000). Fourier Transform InfraRed (FTIR) spectroscopy of the stretch vibration of the heme-iron CO ligand (as a spectroscopic probe) demonstrated that the substrate deoxycorticosterone binds in the heme pocket. Furthermore, the sterols lanosterol and obtusifolliol are oxidatively demethylated by *M. tuberculosis* CYP51, whilst titrations with these compounds produce only marginal spectral shifts within their solubility range in aqueous buffer (Bellamine *et al.*, 1999; McLean *et al.*, 2005).

Typically, distal coordination of P450 ferric heme iron by an azole/triazole inhibitor leads to a shift of the Soret absorbance band to ~423-425 nm (section 5.10.2). In CYP151A2, the Soret band for the morpholine complex is centred at ~421 nm at apparent saturation, suggesting an altered mode of ligation from that of the

azole/triazole inhibitors and the formation of a low-spin heme iron complex that might involve some indirect iron-nitrogen ligation. Incomplete ligand binding as the origin of the observed 421 nm Soret shift can be dismissed due to the fact that normal saturation behaviour occurs for the binding of morpholine to CYP151A2 (*i.e.* a hyperbolic dependence of observed spectral shift on ligand concentration, reaching a defined plateau) (Figure 5.24), as well as the lack of any notable amount of ligand-free species contributing to the final spectrum (Figure 5.22). An atypical mode of binding has been proposed for the binding of fluconazole to CYP121 where the Soret band for the fluconazole complex upon saturation is centred at ~422 nm (Seward *et al.*, 2006). In the case of CYP121, structural data suggested that the azole bound indirectly to the heme iron via a bridging water molecule. In the case of the interaction between morpholine and CYP151A2, we cannot rule out a similar binding mechanism in absence of structural data for the complex. Similarly we cannot rule out the (perhaps more likely) scenario that there is direct nitrogen coordination to CYP151A2 heme iron, with the Soret maximum position affected by the peculiar nature of the N-Fe interaction. Since very high concentrations of morpholine are required to form this complex, it is likely that activity in morpholine oxidation occurs with morpholine binding in a different mode in the active site at much lower substrate concentration.

EPR spectra of ligand-free CYP151A2 have  $g$ -values at 2.42 ( $g_z$ ), 2.25 ( $g_y$ ) and 1.93 ( $g_x$ ), as reported previously (section 5.6.2), and are comparable with those previously reported for other P450s, including the *M. tuberculosis* CYP121 (2.48 ( $g_z$ ), 2.25 ( $g_y$ ), and 1.90 ( $g_x$ )), and the *M. tuberculosis* sterol demethylase CYP51 (2.44, 2.25, and 1.91) enzymes (McLean *et al.*, 2006; Seward *et al.*, 2006). Thus, the spectrum of CYP151A2 in the absence of morpholine has a typical rhombic triplet of signals arising from low spin cysteinate-coordinated ferric heme iron. The well resolved  $g_z$  feature is relatively broad and possibly suggests a degree of heterogeneity within the low-spin heme. On binding of fluconazole to CYP151A2, a rhombic spectrum is obtained that is shifted and broadened with amplitudes of much lower intensities by comparison with the ligand-free enzyme. The  $g$ -values for this complex are 2.49, 2.25, and 1.90 (section 5.6.2). Typical  $g_z$  values for histidine- or imidazole-coordinated P450s lie in the range 2.65-2.50 (Dawson *et al.*, 1982), although  $g_z$  values outside this range are recognised. The EPR spectral features are thus consistent with a

complex that has a substantial proportion of heme iron axially coordinated by cysteinate and an azole nitrogen donor ligand. The  $g_z$  values for such complexes in other P450s are typically in the range from ~2.43 to 2.48 (Dawson *et al.*, 1982). In the CYP121-fluconazole complex the  $g_z$  value was shifted to 2.45. In addition, the peak widths were narrower, and amplitudes were more intense than that for the ligand-free CYP121 (Seward *et al.*, 2006). The EPR spectrum from CYP121-Flu complex crystals were proposed to reveal multiple species and can be interpreted as containing a mixture of ligand-free CYP121, and CYP121 with heme iron both directly and indirectly coordinated by fluconazole. These EPR spectral features were suggestive of a fluconazole complex with a considerable proportion of heme iron axially coordinated by a cysteinate and by an oxygen donor ligand. Consistent with this conclusion, the CYP121-fluconazole crystal structure contains a mixture of species with (predominantly) heme iron indirectly ligated via water, and also heme ligated directly by the azole (Seward *et al.*, 2005).

Assays with the native CYP151A2 reductase system (FdRmor/Fdmor/CYP151A2) and morpholine have demonstrated a relatively efficient hydroxylase activity (28.6 nmol morpholine/nmol/min (Sielaff *et al.*, 2005a). A prior study with CYP151A2 also revealed its capability to turn over morpholine, piperidine and pyrrolidine (Trigui *et al.*, 2004). In this study CYP151A2 exhibited  $K_M$  (apparent) values for morpholine (0.69 mM), piperidine (0.66 mM) and pyrrolidine (0.45 mM) (Trigui *et al.*, 2004).

Furthermore, the high affinity of CYP151A2 for a series of azole drug compounds suggests a binding capability and preference for more bulky and/or hydrophobic compounds (section 5.10.2). Structural studies of CYP121, which also has an extremely high affinity for various polycyclic azole drugs, revealed the presence of a large active site comprised predominantly of hydrophobic residues (Leys *et al* 2003). Therefore, it is possible that morpholine may not be the true physiological substrate of CYP151A2, but instead an adventitious activity by which it was recognised.

### 5.10.2 Inhibitor binding

In light of the of the apparent binding of the cyclic amine-based morpholine structure to CYP151A2 by direct coordination to heme iron at high concentration, binding of structurally diverse azole-based inhibitors was performed. This was done to further probe the spatial properties of the CYP151A2 active site and to explore the effects of aromatic and alkyl substitutions on affinity for azole derivatives. All azoles, upon binding, induced a type II shift in the UV-visible heme spectrum, with the Soret band shifting to a longer maximum wavelength (between 421 and 426 nm). As previously described,  $K_d$  values were determined from optical titrations with the azole drugs (Table 5.3).

<b>Inhibitor</b>	<b>CYP151A2 <math>K_d \pm \text{error}</math> (<math>\mu\text{M}</math>)</b>	<b>CYP121 <math>K_d \pm \text{error}</math> (<math>\mu\text{M}</math>)</b>
<b>Clotrimazole</b>	<b><math>&lt;0.02 \pm 0.01</math></b>	<b><math>0.07 \pm 0.03</math></b>
<b>Ketoconazole</b>	<b><math>0.02 \pm 0.01</math></b>	<b><math>3.30 \pm 0.30</math></b>
<b>Miconazole</b>	<b><math>0.02 \pm 0.01</math></b>	<b><math>0.09 \pm 0.05</math></b>
<b>Econazole</b>	<b><math>0.15 \pm 0.07</math></b>	<b><math>0.31 \pm 0.04</math></b>
<b>Fluconazole</b>	<b><math>1.15 \pm 0.06</math></b>	<b><math>9.70 \pm 0.60</math></b>
<b>Voriconazole</b>	<b><math>0.48 \pm 0.02</math></b>	<b>No data</b>
<b>2-phenylimidazole</b>	<b><math>62.11 \pm 4.89</math></b>	<b>No data</b>
<b>4-phenylimidazole</b>	<b><math>2.13 \pm 0.12</math></b>	<b><math>29.6 \pm 4.3</math></b>
<b>1H-1,2,4-Triazole, 1-tricyclo(3.3.1.1<sup>3,7</sup>)dec-1-yl (referred to as compound A)</b>	<b><math>7.03 \pm 0.18</math></b>	<b>No binding</b>

**Table 5.3**      **Dissociation constants ( $K_d$  values) for inhibitor binding to CYP151A2**

Data were generated from spectral binding data using the quadratic equation (Equation 2) for clotrimazole, ketoconazole, miconazole and econazole, or from fitting to a hyperbolic function (Equation 3) in the case of voriconazole, fluconazole, 2-PIM, 4-PIM and compound A.

Binding of the substituted imidazoles, 2-phenylimidazole (2-PIM) and 4-phenylimidazole (4-PIM), to CYP151A2 was shown to induce an inhibitor-like (type II) spectral change, with a decrease in the intensity of the Soret band in the 2-PIM and



4-PIM complexes and a shift of the Soret maximum to ~425 nm; spectral features associated with the reinforcement of low-spin heme iron in an azole complex. These features were similar to those for other azole-based complexes of CYP151A2 and other P450s. Also noted upon binding of 2-PIM and 4-PIM, and as observed upon morpholine binding to CYP151A2, is the apparent increase in the intensity of the  $\beta$ -band at 437 nm. Spectral titrations with the phenylimidazoles were performed and  $K_d$  values determined by fitting induced absorption change *versus* ligand concentration data to hyperbolae, producing values of ,  $62.11 \pm 4.89 \mu\text{M}$  and  $2.13 \pm 0.12 \mu\text{M}$  for 2-PIM and 4-PIM, respectively (Table 5.3).

In previous ligand-binding studies, the affinity of CYP151A2 for imidazole was determined as  $1.23 \pm 0.02 \text{ mM}$ , whereas the affinity of CYP151A2 for 1-PIM was significantly higher ( $K_d = 48.1 \pm 2.0 \mu\text{M}$ ) (Sielaff and Andreesen, 2005). It is interesting to note that even the addition of a hydrophobic phenyl moiety to the azoles (for 4-PIM c.f. imidazole) is sufficient to reduce the  $K_d$  value by a factor of ~580.

All of the azole antifungal drugs tested in this study (clotrimazole, econazole, fluconazole, ketoconazole, miconazole and voriconazole (Figure 1.5)) were found to bind tightly to CYP151A2, inducing a shift of the Soret maximum to ~424-426 nm, associated with the formation of low-spin heme iron. In addition, an apparent increase in the intensity of the  $\beta$ -band at 537 nm was also observed. The binding of clotrimazole, econazole, ketoconazole and miconazole to CYP151A2 proved too tight to analyse accurately, even at low concentrations of the enzyme ( $<1.0 \mu\text{M}$ ). For these four azoles, the induced optical change associated with azole ligation occurred linearly with azole concentration, sharply reaching a plateau and indicative of near-stoichiometric binding to the P450. However, to overcome problems fitting the data, the quadratic function was used, which compensates for P450 consumed in an azole-P450 complex at each point in the titration. Data fitting to the equation resulted in a rather more accurate description of  $K_d$  values for tight-binding ligands than would have been possible using a standard hyperbolic function. However, even quadratic fits could not describe the  $K_d$  with sufficient accuracy in certain cases, especially in the case of clotrimazole. The quadratic equation accounts for the quantity of ligand complexed with the P450 and thus is an improved measure of tight binding processes

compared to conventional hyperbolic functions. The equation is  $A = ((A_{\max}/(2E)) \times (I+E+K_d)) - ((I+E+K_d))^2 - (4IE))^{0.5}$ , where A is the observed absorption difference at each azole addition,  $A_{\max}$  is the maximal absorption at azole saturation, E is the total enzyme concentration and I is the azole inhibitor concentration used. However, it must be noted that fitting data for clotrimazole binding to the described quadratic equation does not provide a completely satisfactory solution for the  $K_d$ , due to the extremely tight binding of this drug. This suggests that the  $K_d$  value may actually be lower than predicted.

Clearly, the  $K_d$  value for these azoles is very low. Optical titrations with voriconazole revealed slightly weaker binding of this azole to CYP121, with a  $K_d$  value of  $0.47 \pm 0.02 \mu\text{M}$ , as determined from a hyperbolic fit of the absorption change versus the voriconazole concentration. Fluconazole-complexed CYP151A2 had the weakest affinity, with a  $K_d$  value of  $1.15 \pm 0.06 \mu\text{M}$ , as determined from a hyperbolic fit. Titrations of CYP151A2 with the azole antifungal drugs clotrimazole, econazole and miconazole indicated near-stoichiometric binding of each of these drugs until saturation was approached. The  $K_d$  values determined thus should be treated with caution and likely indicate an upper limit of the  $K_d$  range for these inhibitors.

As in the case of wild-type CYP121, fluconazole was also the weakest binding of the azoles tested for coordination to CYP151A2 (McLean *et al* 2006). The  $K_d$  values for azole drugs tested on CYP151A2 are compared (in Table 5.3) with azole  $K_d$  values measured for *M. tuberculosis* CYP121, a structurally characterised P450. Clearly, both mycobacterial P450 isoforms have a high affinity for polycyclic azoles, although the affinity of CYP151A2 for these azoles is clearly higher than that noted for CYP121 for all the azoles tested on both these P450s (Table 5.3) (McLean *et al* 2006). The results of the azole binding in this work were consistent with observations made in previous work (Sielaff and Andreessen, 2005a). In Sielaff and Andreessen's study, the binding of the azole antifungal drugs clotrimazole, econazole and miconazole to CYP151A2 was considered too tight to allow determination of accurate  $K_d$  values, and to indicate stoichiometric binding to CYP151A2 (Sielaff and Andreessen, 2005a). The work in this thesis extends previous studies in this area and defines upper limits for the affinity ( $K_d$  value) of these azoles for CYP151A2.

The tight binding observed for these azoles is an important indicator of the nature of the active site, and also of the natural substrate selectivity and function of the CYP151A2 P450 enzyme. This P450 may favour interactions with bulky polycyclic types of molecule, and CYP151A2 may also discriminate strongly against interactions with small polar molecules, as is also the case for CYP121 (McLean *et al.*, 2002b).

In view of the apparent strong affinity of CYP151A2 for structurally varied azoles, and to further probe the spatial properties of the CYP151A2 active site, 1H-1,2,4-Triazole, 1-tricyclo(3.3.1.1<sup>3,7</sup>)dec-1-yl (referred to as compound A, Figure 3.28) was kindly provided by Dr Sandeep Modi, GlaxoSmithKline, Stevenage, for binding assays. The core structure of this molecule consists of adamantanecarboxylate with a triazole side chain. Oxidation of adamantane to 1-adamantanol by P450cam has been reported previously (White *et al.*, 1984), albeit with very low catalytic activity. Site-directed mutagenesis of P450cam by Wong and colleagues has created mutants that hydroxylate adamantane with nearly 5-fold increased activity compared to the wild-type enzyme (Stevenson *et al.*, 2000). More recently *Streptomyces griseoplanus* was shown to convert adamantane to 1-adamantanol. Addition of the P450 inhibitors 1-aminobenzotriazole or menadione significantly reduced the hydroxylation activity, suggesting the possible involvement of a cytochrome P450 oxidation system in this hydroxylation reaction (Mitsukura *et al.*, 2005). Hydroxylated adamantane derivatives are viewed as promising pharmaceutical intermediates, polymers, and electronic industry materials (Mitsukura *et al.*, 2005). Furthermore adamantane derivatives have long been recognised as inhibitors of human P450s (Chan *et al.*, 1996; Strobel *et al.*, 1999; Stiborova *et al.*, 2002).

Binding of Compound A allowed further probing of the spatial properties of the CYP151A2 active site. Titration of compound A with CYP151A2 induced a type II shift in the heme spectrum, with the Soret maximum decreasing in intensity and shifting to a longer wavelength of 421 nm (Figure 5.26). As discussed previously, spectral shifts of this type are usually associated with the reinforcement of the low-spin state of the P450 heme iron and with the coordination of the heme iron by exogenous ligands. The generated spectral features were similar to those observed for binding of anti-fungal azole drugs, and an increase in the intensity of the  $\beta$  band at 537 nm was also observed for compound A binding to CYP151A2. The changes in

absorbance spectrum of CYP151A2 upon titration with compound A are displayed in Figure 5.26.

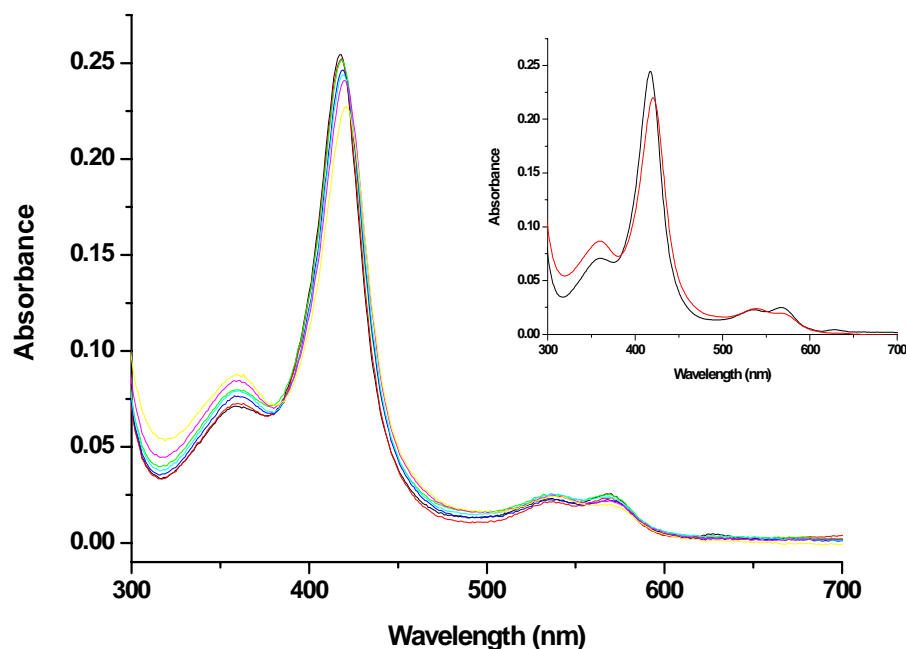


**Figure 5.26 Spectral changes on binding of compound A to CYP151A2**

UV-visible spectra displaying a titration of CYP151A2 (1.3 μM) in 50 mM Tris-HCl, 1 mM EDTA (pH 7.2) with successive additions of compound A (1H-1,2,4-Triazole, 1-tricyclo(3.3.1.1<sup>3,7</sup>)dec-1-yl) at 0, 0.81, 2.42, 4.84, 5.45, 17.71, and 158.27 μM (black, red, green, blue, cyan, magenta, and yellow lines, respectively). The full extent of the absorbance shift is shown (inset) with inhibitor-free (black) and inhibitor-saturated (158.27 μM, red) forms.

In order to analyse the titration with compound A, a difference spectrum was constructed at each point by the subtraction of the spectrum for the inhibitor-free form from each successive inhibitor-bound spectrum in the titration. These difference spectra are displayed in Figure 5.27.

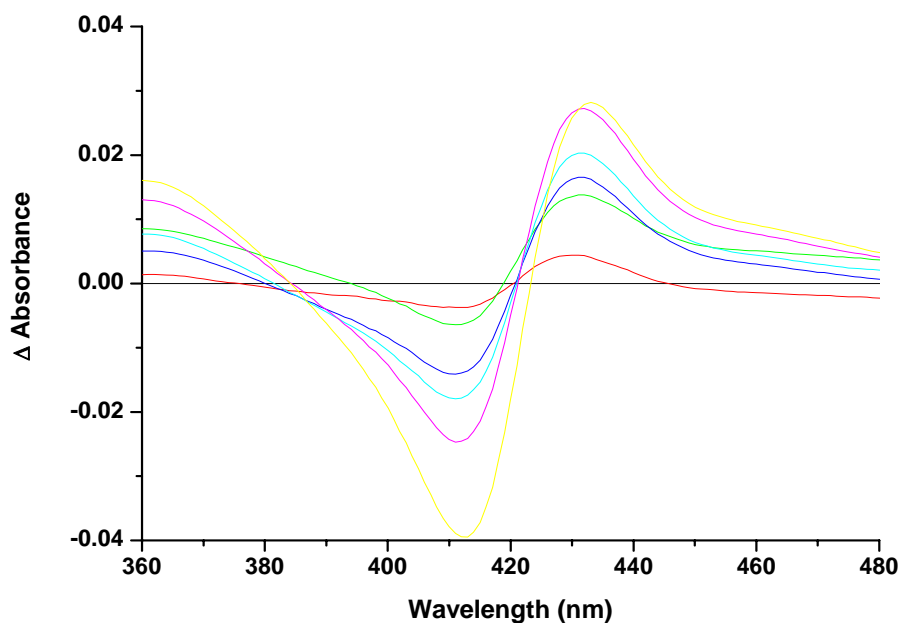


**Figure 5.27** Difference spectra from titration of CYP151A2 with compound A  
 Difference spectra for CYP151A2 titrated with compound A (1H-1,2,4-Triazole, 1-tricyclo(3.3.1.1<sup>3</sup>,7)dec-1-yl) are shown at concentrations of 0.81, 2.42, 4.84, 5.45, 17.71, and 158.27  $\mu\text{M}$  (red, green, blue, cyan, magenta and yellow lines, respectively).

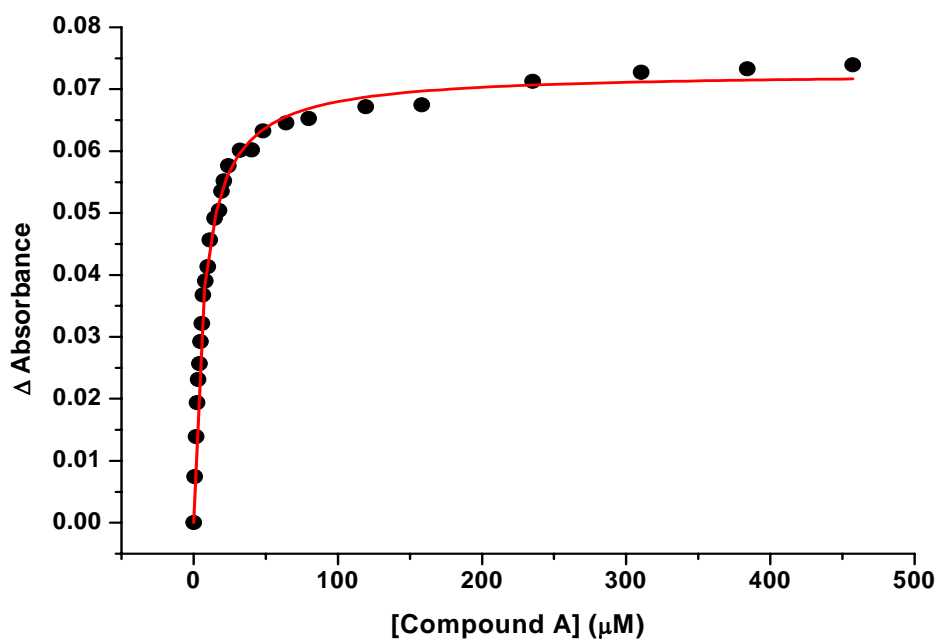


**Figure 5.28** Titration curve for the binding of compound A to CYP151A2  
 CYP151A2 was at a concentration of  $\sim 1.3 \mu\text{M}$ .  $\Delta\text{Absorbance}$  refers to the absorption difference between 434 nm and 413 nm in the difference absorption spectra (Figure 5.26). Data were fitted to a hyperbolic function, yielding a  $K_d = 7.03 \pm 0.18 \mu\text{M}$ .

The difference spectra generated for the titration of CYP151A2 with compound A display maxima and minima values at approximately 434 nm and 413 nm, respectively. The type II binding spectrum is characterised by a peak and a trough at the aforementioned wavelengths. For each concentration of compound A, the maximal absorbance difference was determined by subtraction of the absorbance value at the trough from that at the peak in each difference spectrum (using the same  $\lambda$  values for each). These values were subsequently plotted against the corresponding concentration of compound A, and the data fitted to a standard hyperbolic function, to determine a binding coefficient ( $K_d$ ), Figure 5.28.

The binding of compound A generated a binding constant  $K_d = 7.03 \pm 0.18$   $\mu\text{M}$ , which was significantly weaker than that for the antifungal azole drugs (Table 5.3). These data further indicate that the active site of CYP151A2 is relatively large and flexible and can accommodate favourably large polycyclic molecules.

## 5.11 Summary

*Mycobacterium* sp. strain HE5 encodes a CYP151A2 that catalyses the hydroxylation of different N-heterocycles. The enzyme was expressed and purified to homogeneity. Detailed spectroscopic analyses of the P450 by UV-Visible absorption, EPR, MCD and resonance Raman spectroscopy were done and the data obtained were consistent with a cysteinate- and aqua-ligated heme iron protein. UV-visible absorption titrations with N-heterocycles revealed no detectable binding with pyrrolidine or piperidine, while morpholine at high concentrations behaved as a heme iron-coordinating inhibitor. EPR and CD spectroscopy were suggestive of the formation of a CYP151A2-morpholine complex, and confirmation of the reinforcement of the low-spin species of CYP151A2 upon morpholine binding was obtained by Resonance Raman. Determination of the heme extinction coefficient of CYP151A2 using the hemochromagen method revealed an unexpectedly high value of  $\epsilon_{419} = 186 \text{ mM}^{-1} \text{ cm}^{-1}$  for oxidised CYP151A2. These data were consistent with a number of previous studies on distinct P450 enzymes, and indicate that the “traditional” method of P450 quantification based on absorption characteristics of the  $\text{Fe}^{2+}$ -CO complex are not sound and lead to an overestimation of P450 concentration (i.e. the extinction coefficient is too low). Upon CYP151A2 reduction by sodium

dithionite, protonation of the Cys<sup>348</sup> thiolate to a thiol is readily achieved, indicating instability of the ferrous enzyme to inactivation by heme ligand protonation. Potentiometric studies revealed that the midpoint potential for heme iron in ligand-free CYP151A2 is  $-261 \pm 9$  mV; a quite positive potential for a P450 enzyme.

# Chapter 6

## Discussion



## 6.0 Preface

The advent of genome sequencing has provided researchers with unparalleled insights into the metabolic complexities of microbes. Such efforts have led to the realisation that P450 enzymes are numerous and widespread in prokaryotes, and increasingly the characterisation of these P450s is leading to the elucidation of their functional roles and significance in microbial metabolism.

The work presented in this thesis relates to the expression, purification and characterisation of three distinct P450 enzymes derived from different mycobacterial strains. The data presented indicate important differences in the structural, thermodynamic, ligand-binding and spectroscopic properties of the enzymes analysed. These data highlight the diversity of P450 structure and function in general, and the different properties and substrate binding characteristics within the mycobacterial isoforms. The major experimental findings from the work on the three individual proteins (*M. tuberculosis* CYP121 and mutants; *M. ulcerans* CYP140A2; and *Mycobacterium* sp. strain HE5 CYP151A2) are summarised at the ends of the relevant chapters describing the experimental work on these enzymes. In this final discussion section, the main relevant details are examined in a wider context, leading to plans for future work in these areas.

### 6.1 *Mycobacterium tuberculosis* CYP121

The high-resolution crystal structure of wild-type CYP121 revealed some unique and interesting structural elements present in the active site and in close proximity to the heme environment (Leys *et al.*, 2003). In particular, distortion of one of the four pyrrole rings of the heme macrocycle was observed due to the close interaction with the Cys<sup>345</sup>-Pro<sup>346</sup> motif, a common structural element in other *M. tuberculosis* P450s and present also in some other prokaryotic and eukaryotic forms (Leys *et al.*, 2003). The properties of the heme relating to the Pro<sup>346</sup> interaction were investigated through a Leu<sup>346</sup> (P346L) mutation, in an attempt to establish whether the proline was the major cause of the structural disruption of the heme macrocycle, and to evaluate heme conformation and general properties of the P346L variant. The significance of the heme distortion in wild-type CYP121 is uncertain, but may potentially have an important influence on the electronic environment of the heme and

subsequently the catalytic and thermodynamic properties of the protein; for example the rather negative heme iron redox potential.

A further structural characteristic of note from the wild-type CYP121 atomic structure is the presence of Arg<sup>386</sup> above the heme plane in the active site and adjacent to the oxygen scission site. Moreover, crystallography revealed that Arg<sup>386</sup> is hydrogen bonded to Ser<sup>237</sup>, Gln<sup>385</sup> and two water molecules in the active site cavity (Leys *et al.*, 2003). The close proximity of the arginine and serine residues may define a binding site for a negatively charged substrate functional group. Arg<sup>386</sup> is also proposed to form part of a putative proton relay pathway, either by donating protons to heme-bound oxygen directly, or via Ser<sup>237</sup> (Leys *et al.*, 2003). All these features associated with Arg<sup>386</sup> indicated a notable role for the residue in the function of the P450. The aim of the generation of the R386L mutant was to disrupt the hydrogen bonded network and to improve azole access to the heme binding pocket to facilitate isolation of an azole-CYP121 crystal complex.

The CYP121 structure also revealed that a series of hydrogen-bonded amino acid and water molecules which define two potential proton delivery pathways to the heme iron, which seemingly converge at Ser<sup>279</sup> (Leys *et al.*, 2003). Ser<sup>279</sup> has two distinct conformations aligned with the different proton relay pathways. The mutant protein S279A was created to disrupt the hydrogen bond network centred on Ser<sup>279</sup> and to establish the resulting effects on structural and biophysical properties of the P450.

The CYP121 mutations; P346L, R386L and S279A were generated by PCR and cloned into the pET11a vector, which exploits a strong T7 promoter-driven expression system. The expression protocol used for variant protein isolation was identical to the one devised for the optimised production of wild type CYP121, which involved low growth temperature and mild IPTG induction in order to promote soluble protein production (McLean *et al.*, 2002a), and is described in section 2.3. As noted previously for wild-type CYP121 (McLean *et al.*, 2002a), the majority of the expressed mutated proteins were in the form of insoluble inclusion bodies. Proteins were purified to homogeneity by ammonium sulphate fractionation, followed by four chromatographic steps. The proteins were purified to homogeneity on average ~55-

fold from the cell extract and overall expression of soluble proteins was found to be ~4.5 % of the total cell protein, with the exception of S279A, in which the overall purification and yield values were 49 % and 3.4 %, respectively. This variation in the purification of the S279A mutant protein was found to be primarily due to the differences in yields obtained from the cell lysis procedure. The isolated mutant CYP121 proteins were found to be stable and were determined to be >95 % pure from spectroscopic studies. SDS-PAGE analysis indicated that the mutated proteins had been purified to homogeneity after 4 chromatography steps, and that each had a molecular mass of ~43 kDa, consistent with the predicted mass the proteins.

The first atomic resolution structure of a P450 (to 1.06 Å) was solved for CYP121 from *Mycobacterium tuberculosis* (Leys *et al.*, 2003). The crystal structures of the CY121 mutants generated here were also solved to a high resolution (~1.6 Å). The elucidation of these structures revealed distinct conformational changes from that of wild-type CYP121. The structure of the P346L mutant showed that the degree of out-of-plane distortion of one of the pyrrole groups of the heme had decreased by some 50 %, but that a notable ‘kink’ of the heme was still visible at this part of the macrocycle. This indicates that the Pro<sup>346</sup> does have a direct role in the distortion of the heme, but obviously other steric factors also have an important influence on the heme environment. The R386L mutant protein structure resulted in some expected structural alterations above the heme plane, with the opening of the heme to the active site.

The S279A mutant structure, maintained the hydrogen bond network with Arg<sup>386</sup> and Ser<sup>237</sup>, although unexpectedly the mutation did disrupt the structured water network of the active site. The altered positions of water molecules in the S279A mutant structure could reflect the disruption of the “natural” proton relay pathway seen in wild-type CYP121, which in turn would reinforce the importance of Ser<sup>279</sup> in the catalytic process of CYP121. In the longer term, it is foreseen that laser flash photolysis studies will be done with CYP121 to investigate proton relay to the heme iron and the role of the identified pathway in wild-type CYP121. The S279A mutant will be an ideal variant for comparison with wild-type CYP121 given that the predicted proton route to the heme iron is disrupted in this mutant.

Biophysical studies of the CYP121 mutant enzymes indicate that they display many characteristics typical of the P450 class. As shown by electronic absorption, resonance Raman, EPR and MCD spectroscopy, the CYP121 mutants are predominantly low-spin in the oxidised state. In general, there is a small high-spin component, as evident from the resonance Raman spectrum (splitting of  $\nu_3$  component) and from the minor absorbance shoulder near 390 nm in the electronic absorption spectrum of these mutants. EPR, MCD and resonance Raman spectroscopy all indicate that CYP121 has typical P450 cysteinate- and water-ligation to the heme iron, and that there is negligible P420 content in the ferric forms of these enzymes. Some minor changes from wild-type CYP121 were observed in the EPR of the P346L mutant, where broadening of the  $g_x$  and  $g_z$  components were indicative of some conformational perturbation of one or both of the axial heme ligands. As discussed above the P346L mutant enzyme structure revealed a less distorted heme, and the EPR data may be indicative of some resultant change in the nature of the axial heme iron coordination by the Cys<sup>345</sup> residue.

Some notable spectroscopic differences were observed in the R386L mutant of CYP121, where the UV-visible absorption spectroscopy shows a major Soret band at 419 nm; a longer wavelength than for the wild-type CYP121 (Soret peak = 416.5 nm) and indicative of a change in the nature of the low-spin state of the protein, possibly as a result of altered interactions with the distal water ligand. In contrast, the UV-visible spectra of the R386L mutant also presented the development of a large shoulder at ~390 nm, reflecting the high-spin component of the protein. Further evidence for an increase in the high-spin component of this mutant was also seen in Resonance Raman, studies with the  $\nu_3$  marker band of the high-spin species becoming dominant, whereas the opposite was the case for wild-type (where the low-spin  $\nu_3$  marker was dominant). These spectral changes are likely to relate directly to the structural changes associated with the disruption of the hydrogen bond made from Arg<sup>386</sup> to the Ser<sup>237</sup> in wild-type CYP121. The heme water (6<sup>th</sup>) ligand in the resting state of the enzyme is hydrogen bonded to Ser<sup>237</sup>. A hydroxyl-containing amino acid (more often a threonine) is widely conserved in P450s at this position, and is considered to be important in oxygen binding and/or proton delivery to iron-oxo species (Yeom *et al.*, 1995). In turn, Ser<sup>237</sup> hydrogen-bonds to the side chain of Arg<sup>386</sup>, although it is not clear from crystal structures whether this has an indirect effect on

the heme aqua ligand. Spectral and resonance Raman data suggest that there is such an effect, and that the R386L mutant likely alters the interaction with the heme-bound water molecule such that a greater degree of high-spin heme iron can accumulate. Despite local changes to active site structure, the overall conformations of the CYP121 mutant enzymes is not significantly disrupted by comparison to the wild-type enzyme, indicating that the structure is robust and tolerant to mutations.

An important step in the future characterisation of CYP121 will be the identification of the true endogenous substrate. Previous trials with a range of potential substrate molecules failed to induce a significant shift in heme iron spin-state equilibrium towards the high-spin form in CYP121 (McLean *et al.*, 2002a). Such an optical shift is normally a good indicator for the binding of a *bona fide* substrate molecule. *M. tuberculosis* is known to have a very complex lipid metabolism, and much remains to be learned about the nature of many of the lipids in this organism. The large CYP121 active site cavity (approx. 1350 Å<sup>3</sup>) and bioinformatics analysis suggests that the substrate should be a bulky lipid or polyketide. Binding studies presented here for wild-type and mutant CYP121 enzymes indicates that the active site also creates sufficient space for binding of a number of bulky azole drugs. In view of the failure to induce heme iron spin-state change, a new approach to identify CYP121 substrates was adopted, using lipid extracts from *M. tuberculosis* and with binding studies performed using the lipid-protein overlay method (Dowler *et al.*, 2002). Results from this study indicated a physical interaction between CYP121 and apolar lipid fractions.

The precise molecular composition of the lipid extracts remains unknown, although the general classes of lipids present in the individual fractions are known. Apolar lipophilic cell envelope components represent a large proportion of these cellular extracts. Major constituent of the lipid protective layer in *M. tuberculosis* are glycopeptidolipids, and evidence for the involvement of P450s in the synthesis of these components was presented by Besra and colleagues (Burguiere *et al.*, 2005), who established that azole inhibitors of CYP121 and other P450s inhibit glycopeptidolipid biosynthesis in *M. smegmatis*. Given that several distinct P450s have been shown to have affinity for long chain fatty acids (e.g. P450 BM3) and sterols (e.g. CYP51), it is plausible that CYP121 (and other *M. tuberculosis* P450s)

catalyses oxygenation reactions with substrates of similarly complex chemical structure, and that these types of substrates may be peculiar to the mycobacterium genus (or even the *M. tuberculosis* species) and could be involved in cell envelope biogenesis.

Findings that anti-fungal azole drugs have high potency against *M. smegmatis* indicate that P450 systems are feasible drug target enzymes, and a natural progression of this work was the testing of these compounds against the virulent *M. tuberculosis* H37Rv strain. Minimal inhibitory concentrations were deduced as miconazole (19  $\mu$ M), econazole (21  $\mu$ M), ketoconazole (30  $\mu$ M) and clotrimazole (32  $\mu$ M). While the MIC's of standard front line TB drugs, rifampicin and pyrazinamide have been reported lower (at 0.5 and 1.5  $\mu$ M, respectively), it is possible that other azole compounds and future ones are even more potent than those tested here. Drug companies possess vast libraries of azole drugs that could be tested for antitubercular activity. The chemotherapeutic potential of free and encapsulated econazole against murine tuberculosis was found to reduce *M. tuberculosis* bacilli by more than 90 % in the lungs and spleen of mice (Ahmad *et al.*, 2007). Moreover, studies have shown that ketoconazole in combination with standard anti-TB drugs improve the efficiency of the treatment regime in murine models (Byrne *et al.*, 2007).

Although, the deduced azole MICs in this study are higher than those for the primary anti-TB drugs, the results do offer an encouraging basis for the screening and/or development of other azole-based compounds with greater inhibitory effect. Although there are some problems with cross-reactivity (and subsequent toxicity) of certain azoles with human P450 isoforms, research is ongoing to create systemically tolerated azole drugs, and voriconazole is an example of a new generation of such a tolerated triazole derivatives (Hoffman and Rothbun, 2002).

Although the exact target of the azole drugs in *M. tuberculosis* has not been identified, CYP121 may be a major target, in light of the low azole  $K_d$  values and structural information that demonstrates the mode of binding of an azole (fluconazole) to CYP121 (Seward *et al.*, 2006). Furthermore, recent work on P450 gene knock-outs in *M. tuberculosis* has identified CYP121 as being essential for viability of *M. tuberculosis* H37Rv (McLean *et al.*, in preparation).

In future work on the CYP121 system, a key need is the identification of the natural substrate(s) of CYP121 and the definition of its catalytic reaction with the substrate(s). To this end, further screening against *M. tuberculosis* cellular extracts would be a sensible option, and could be complemented by systematic library screens. Identification of a substrate will also allow reconstitution of a native redox system, comprising CYP121, the ferredoxin reductase FprA, and the ferredoxin Fdx, in order to facilitate electron transfer from NADPH to the P450 and to enable substrate turnover. This type of redox system has already been demonstrated to be functional in transporting electrons to CYP121 (McLean *et al.*, 2006). Longer term there is a need to evaluate other residues of structural and catalytic importance that were identified by analysis of the wild-type CYP121 atomic structure. These include Phe<sup>338</sup> and Ser<sup>237</sup>, which are implicated in heme iron potential regulation and in the proton relay pathway, respectively.

## **6.2 *Mycobacterium ulcerans* CYP140A2**

An increasingly common disease in equatorial Africa is the debilitating disease termed Buruli ulcer, the causative agent of which is the bacterium *Mycobacterium ulcerans*. The clinical characteristics and virulence of the disease are due to the generation by the bacterium of a structurally diverse group of macrolide toxins termed mycolactones (Mve-Obiang *et al.*, 2005). The P450 CYP140A2 is of particular interest as it has been implicated in the synthesis of mycolactone, and appears to be a key enzyme in the generation of the structural diversity of mycolactone (Stinear *et al.*, 2004; Mve-Obiang *et al.*, 2005). However, little is currently known about the enzymology or biophysical features of this enzyme. Inhibition of the synthesis of the mycolactone via disruption of the activity of this P450 may lead to improved therapy and outcomes in the treatment of Buruli ulcer.

Initial expression studies of CYP140A2 demonstrated that it could be produced at moderately high levels in *E. coli*, but that normal growth temperatures (25-37°C) resulted in the majority of CYP140A2 forming insoluble inclusion bodies, as previously reported for *M. tuberculosis* CYP121 mutants. This problem was overcome by lowering growth temperature, thus slowing bacterial growth, and by decreasing IPTG inducer concentration. The difficulty in obtaining soluble CYP140A2 may in part be related to the relatively high GC-content of the gene (62 %)

and possibly also via its association with the cell membrane through hydrophobic interactions. There are stretches of hydrophobic amino acids that dominate long sequences in the protein and that might mediate such interactions with a lipid membrane (e.g. the region from Val 52 to Leu 101). The relative ease with which the enzyme aggregates and precipitates on heating and reduction suggests that such regions might facilitate self-aggregation and could also be important in promoting adhesion to membrane surfaces. However, it should be emphasised that CYP140A2 can be isolated as a soluble, intact protein, and thus that any membrane association would be as a peripheral interaction. Overall total expression of the CYP140A2 protein was the lowest of all the proteins reported in this study. The protein was purified on average 27-fold from the cell extract and overall expression of soluble protein was found to be ~5 % of the total cell protein in the *E. coli* system.

UV-visible absorption spectroscopy revealed the purified CYP140A2 gene product to be a heme-containing protein isolated in the oxidised form and with a major (Soret) peak at 419 nm, and additional  $\alpha$  and  $\beta$  bands in the visible region at 567 nm and 534 nm, respectively. Carbon monoxide binding to the sodium dithionite-reduced (ferrous) form of the protein displayed a stable spectral shift of the Soret band to 449 nm, indicative of a thiolate-coordinated cytochrome P450 enzyme. Ligation of oxidised enzyme with the small molecules nitric oxide and cyanide induce typical “type II” binding spectra, with Soret maxima shifting to ~430 nm in both cases. In light of these spectral properties, the protein was further confirmed to be a fairly typical cytochrome P450, giving rise to optical shifts consistent with a cysteinate-ligated heme iron protein.

At the amino acid level, CYP140A2 is reasonably distinct from other well characterised P450s, although P450EryF displays considerable levels of amino acid sequence similarity to CYP140A2 (38 % identity), perhaps suggesting common structural features that extend beyond the basic "core" P450 structure. Attempts to solve the structure of CYP140A2 by molecular replacement modelling would appear to be possible, although definitive description of its structure would require crystallisation trials (in both the presence and absence of ligands) to enable determination of the atomic structure by x-ray crystallography. This is clearly a major aim of future work on this protein.



In the absence of a structure for CYP140A2, further spectroscopic studies enabled elucidation of some aspects of its structural properties. Biophysical studies of the CYP140A2 enzyme indicate that it exhibits many properties that are typical of the P450 class. As shown in resonance Raman and EPR spectroscopy, CYP140A2 is low-spin in its resting oxidised state, with cysteinate- and water-ligations to the heme iron. The EPR of the substrate-bound protein generated a degree of heterogeneity in the spectrum, with a decrease and broadening of the rhombic heme signal, as well as the development of small amounts of a high-spin ferric heme. These data clearly indicate that substrate-binding modulates the heme ligand environment. Resonance Raman spectroscopy also revealed small changes upon binding of mycolactone C to CYP140A2, with the formation of new bands associated with porphyrin modes and heme substituent groups; again indicative of binding of mycolactone C in the vicinity of the heme pocket and influence on the heme peripheral groups. However, no evidence for the development of high spin heme iron in presence of substrate was observed using resonance Raman spectroscopy in this case. Circular dichroism spectroscopy revealed the secondary structure of CYP140A2 was predominantly  $\alpha$ -helical, a typical feature of all characterised P450s to date.

Potentiometric studies reported here have provided the first description of the redox potential of the CYP140A2 heme iron, and revealed a midpoint reduction potential of  $-264 \pm 4$  mV. The heme iron potential is in a range similar to that observed for many other bacterial P450s. For example, substrate-free P450cam has a potential of -300 mV (Sligar, 1976).

Due to the aggregation of CYP140A2 in complex with mycolactone C, the determination of a heme iron potential for the substrate-bound form proved unobtainable. It is likely that thermodynamically, as seen for the well-characterized P450 BM-3 and P450cam systems, substrate binding leads to displacement of the weakly bound aqua ligand at the distal coordination position on the heme iron, whilst generating a change in heme iron spin-state equilibrium in favour of the high-spin form. This will likely lead to an elevation in the heme iron reduction potential. The high-spin form can then be readily reduced by the physiological redox partner, so activating electron transfer and productive catalysis. The nature of the optical change

on reduction of CYP140A2 is somewhat unusual, with the Soret band shifting to 426 nm in the ferrous form. The spectral changes observed for ferrous CYP140A2 appear to be consistent with protonation of the thiolate ligand (Cys 380) to a thiol, a transition that likely underlies conversion of P450 to the inactivated P420 form. This type of phenomenon has been observed in recently published studies of the *M. tuberculosis* CYP51 enzyme (McLean *et al.*, 2006) and is becoming an increasingly frequent observation in P450s. It is plausible that the reason for such a phenomenon is that the enzyme inactivates itself when reduced in the absence of substrate; possibly to avoid production of damaging oxygen radicals if substrate is not available.

The physiological substrate of CYP140A2 is considered to be mycolactone C, although only very minor spectral perturbation of the heme was observed on addition of this molecule to a solution of the P450. It is thus not possible to use spectral changes directly to determine a binding coefficient ( $K_d$ ) value for this substrate. In view of this difficulty in deducing  $K_d$  value directly, competitive inhibition was investigated as a method for determining the  $K_d$  of mycolactone C upon titration with the azole drug econazole. Econazole titrations in the presence of fixed amounts of mycolactone C allowed the estimation of the  $K_d$  value for the substrate, by comparing the affinity for the drug in the presence and absence of mycolactone C and by using a competitive binding equation to solve the algorithms. Although no changes in the Soret peak of CYP140A2 were observed upon binding of mycolactone C alone within its solubility range, minor changes in absorption spectrum were noted, reflecting some form of substrate-heme interaction. These data were supported by EPR and RR spectroscopy of the CYP140A2/mycolactone C complex. Using the competitive binding optical titration method, a  $K_d$  value of  $3.27 \pm 0.31 \mu\text{M}$  was determined for the binding of mycolactone C to CYP140A2.

The binding of azole drugs was tested and many were found to exhibit tight binding to CYP140A2 and to have  $K_d$  values comparable to those for CYP121. Typical spectral perturbations occurred on binding the azoles, with conversion to a low-spin species with Soret maximum at  $\sim 425$  nm. The high affinity of CYP140A2 for azole drugs suggests a flexible active site with preference for bulky polycyclics and long-chain type molecules, which is in agreement with the role of CYP140A2 in the hydroxylation of the large polycyclic mycolactone C. Potentially, the azole drugs,

which are predominantly topically applied, may offer a new alternative or additional course of therapy for the Buruli ulcer skin disease. Their tight binding to CYP140A2, and the fact that this P450 is likely to be critical for the production of a potent toxin, would appear to make the likelihood of an effective azole-based topical treatment a possibility.

CYP140A2 proved to be active in the turnover of both mycolactone C and, to lesser degree, mycolactone E from the frog pathogen *M. lifandii*, which has one less double bond on the fatty acid side chain (Mve-Obiang *et al.*, 2005). Turnover was greatest for mycolactone C, as this would be suspected to be the physiological substrate. The low turnover of mycolactone E reflects the fact that this mycolactone is not the natural substrate of CYP140A2, a fact underlined by the absence of the CYP140A2 encoding genes in *M. lifandii* (Mve-Obiang *et al.*, 2005).

An artificial redox system, comprising *E. coli* flavodoxin, flavodoxin NADP<sup>+</sup> oxidoreductase and NADPH was sufficient to support the functional turnover of mycolactone by CYP140A2, although it would be likely that the natural redox partners would improve the efficiency of electron transfer to the P450, leading to greater substrate turnover. However, a functional P450 system was reconstituted and the activity of CYP140A2 in mycolactone hydroxylation clearly demonstrated.

With regards to future work, the most immediate aim is to implement a purification process to isolate homogeneous CYP140A2. A more detailed investigation of substrate and product interactions could then be undertaken with the various structurally diverse mycolactones. In addition it would be beneficial to identify the natural redox partners of CYP140A2, and to reconstitute a native redox system to enable further studies of the catalytic parameters of CYP140A2 ( $k_{\text{cat}}$  and  $K_{\text{m}}$  values). It is likely that a native redox system would be more effective in transporting electrons to the P450, and thus more efficient substrate turnover might be expected. Optimisation of conditions such as pH and ionic strength also require refinement to enhance catalytic activity. Ultimately, crystallographic trials of ligand-free and substrate/azole-bound forms of the enzyme should lead to crystals suitable for x-ray diffractions studies, and ultimately to an atomic structure for CYP140A2. This would

obviously allow for far greater insights into the structure-function relationship of the protein.

### **6.3 *Mycobacterium* sp. strain HE5 CYP151A2**

Biodegradation of industrial organic pollutants is of special environmental interest and thus gaining a clearer understanding of the enzymatic processes by which degradation occurs is important. World-wide industrial production of morpholine is estimated at 25,000 tonnes of morpholine *per* year with human and environmental exposure occurring primarily from manufacturing and chemical gaseous and aqueous emissions, and directly from some uses; for example in cosmetic formulations and fruit wax coatings (IPCS, 1996). Under specific environmental and physiological conditions, the reaction of nitrite or nitrogen oxide with dilute solutions of morpholine can form the human carcinogen *N*-nitrosomorpholine (IPCS, 1996). Thus, there are good reasons for characterizing enzymes and microorganisms able to degrade morpholine and its congeners, so removing them from the biosphere.

Biodegradation studies of morpholine led to the identification of a mycobacterium strain HE5 (DSM 44238), and implicated a novel P450 in the degradation of morpholine, through catalysis of the cleavage of the C-N bond of morpholine (Schrader *et al.*, 2000). This P450 was subsequently termed P450mor (CYP151A2) and was purified as a N-terminal His-tag fusion protein (Sielaff *et al.*, 2005a). In previous work, binding studies of CYP151A2 with the proposed substrates morpholine, piperidine or pyrrolidine apparently failed to produce typical substrate-binding spectra, whilst CYP151A2 association with differentazole compounds generated type II binding spectra (Sielaff *et al.*, 2005a). Moreover recombinant proteins FdRmor, Fdmor and CYP151A2 were used to reconstitute a functional P450mor redox system, which was shown to turn over morpholine (Sielaff *et al.*, 2005a). In more detailed studies of the CYP151A2 system reported in this thesis, high levels of expression from a pET28b T7 RNA polymerase/promoter system revealed that the majority of the target protein was in the soluble form at 25°C, and that expression of soluble CYP151A2 protein was robust over a variety of temperatures and induction strengths. Sonication proved to be an efficient *E. coli* cell lysis method, with no evidence for any P450 aggregation or adventitious hydrophobic interactions with the cell membrane fraction. The final yield of soluble CYP151A2 protein was

found to be ~23 % of the total cell protein and the isolated protein was determined to be >95 % pure spectroscopically. SDS-PAGE analysis indicated that the protein had been purified to homogeneity after a one step nickel affinity column regime, and that the isolated CYP151A2 had a molecular mass of ~45 kDa, consistent with the predicted mass. Following nickel column chromatography, thorough dialysis of the eluted CYP151A2 protein was required to remove imidazole, which was an adventitious ligand to the P450 heme iron. Thus, a highly efficient expression and purification system for CYP151A2 was developed, and the protein was highly soluble in the *E. coli* expression system used.

UV-visible absorption spectroscopy of the purified CYP151A2 showed that, upon carbon monoxide binding to the sodium dithionite-reduced (ferrous) form of the protein, the Soret maximum shifted to 424 nm (the inactive P420 form, in which thiol-coordinate heme iron occurs) and there was a minor absorption maximum at 446 nm (the thiolate-coordinated P450 form). EPR and MCD spectroscopic analysis demonstrates that thiolate ligation is in place for the oxidised CYP151A2, and thus the protonation of the cysteinate ligand was shown to be a consequence of heme iron reduction and/or CO binding. Further evidence for the ready conversion to the P420 form was observed in redox potentiometry. Anaerobic equilibrium titrations with dithionite (in the absence of CO) produced a ferrous CYP151A2 species in which the Soret maximum is red-shifted ( $A_{\text{max}} = 425 \text{ nm}$ ) with respect to that for the ferric form (419 nm). As in the case of CYP140A2, CYP151A2 thiolate protonation may therefore occur as a consequence of iron reduction, irrespective of subsequent CO ligation.

Determination of the extinction coefficient of CYP140A2 via the pyridine hemochromagen method indicated a rather large Soret coefficient of  $186 \text{ mM}^{-1} \text{ cm}^{-1}$ . This result serves to further highlight the discrepancies that are becoming increasingly apparent by comparing values determined from the “traditional” reduced/CO-binding assay (which indicates that most P450s have an extinction coefficient of  $90\text{-}100 \text{ mM}^{-1} \text{ cm}^{-1}$  at their Soret peak in the oxidised form) and assays such as the hemochromagen or EPR analysis, which usually predict a rather larger coefficient. These results highlight that the reliance on the old coefficient derived from partial conversion of a crude enzyme to a CO complex in membranes is unlikely to be a robust method for all

P450s, and thus a major error in quantifying P450s in general occurs through the continued use of this method (Omura and Sato, 1964). Alterations in heme environment, spin-state, strength and nature of ligations all have influential roles in controlling the heme absorption. A more accurate quantification of the extinction coefficients could be achieved through the combined use of EPR and hemochromagen methods, which should provide consistent quantitative values. The recommendation is thus that the CO-based assay should be used as only a qualitative tool, and that better quantitative methods are available for P450 analysis.

At the amino acid level CYP151A2 proves to be distinct from other well characterised P450s. A 100 % amino acid sequence identity is noted with a P450 from *Mycobacterium* sp. strain RP1 which has also has the capability to turn over the cyclic amines morpholine, pyrrolidine and piperidine (Trigui *et al.*, 2004). CD analyses in both the far-UV and near-UV regions revealed some structural deviations from the BM3 heme domain spectrum, although the negative ellipticity of the Soret band was a feature of both P450 proteins. However interesting changes were noted upon ligand binding, specifically with mycolactone and econazole in the near-UV-visible region. This portion of the spectrum is dominated by the sharp Soret feature with negative ellipticity centred at 410 nm. Addition of morpholine/econazole shifts the Soret CD feature to longer wavelengths of 412 nm/414 nm, respectively. In addition, they produce a decrease in the intensity of the Soret feature. Thus, the direction of movement of the Soret band (to longer wavelengths) and the decrease in the intensity observed mimics the transitions seen in the electronic absorption spectra following binding of the substrate/ligand to CYP151A2. It should be noted that while morpholine is a substrate for this P450, it is shown to induce very little substrate-like optical change. However, at millimolar concentrations, it induces a type II spectral shift, indicating that it can occupy a low affinity binding mode whereby it may act as an inhibitor and coordinate to the heme iron.

Further analysis of the effects of ligand binding to CYP151A2 was performed through EPR studies. The EPR spectrum for substrate-free CYP151A2 constitutes a rhombic trio of g-tensor elements reflective of a low-spin ferric ( $\text{Fe}^{3+}$ ) heme iron. Morpholine binding (at millimolar concentrations) resulted in decreased heme rhombicity through the coordination of the heme iron by the nitrogen atom of the

morpholine, as previously reported for interaction of various azole drugs with P450s, e.g. the 4-phenylimidazole-P450cam bound complex (Uchida *et al.*, 2004). As mentioned above, no high-spin heme species was detected upon binding of morpholine, as might be expected with a natural substrate. Binding of fluconazole was detected in EPR through the maintenance of a low-spin ferric ( $\text{Fe}^{3+}$ ) heme, with broadening of the rhombic trio signals suggestive of a split population, perhaps due to two orientations of a pyrrole ring relative to the heme plane, as previously suggested for an azole-bound form of P450 BM-3 (Girvan *et al.*, 2004). The similarities in the MCD spectra between CYP151A2 and P450cam suggest the absence of a hydrogen-bond between the I-helix and the heme-bound  $\text{H}_2\text{O}$ , and a less polar distal binding pocket than in P450cam.

Resonance Raman data for CYP151A2 indicated that the ligand-free and ligand-bound forms are all completely low-spin, with no evidence for the splitting of the  $\nu_3$  marker of low and high-spin species. In the morpholine-bound form, the oxidation state marker band  $\nu_4$  is slightly up-shifted in frequency with respect to that for the wild-type CYP151A2, and it appears likely that at least a proportion of this low-spin species has morpholine directly coordinated to the heme iron. As stated, further evidence for this form of interaction was also observed by EPR and UV-visible absorption spectroscopy. This likely indicates that, at high concentrations, the substrate morpholine can adopt a second (weaker) binding mode (or modes) that involves direct coordination of the P450 heme by a nitrogen atom; and thus this molecule appears to switch from substrate to inhibitor as its concentration is increased.

Attempts to thermally induce a spin-state change in CYP151A2 led to aggregation at higher temperatures. This may indicate that a thermally- or substrate-induced spin-state switch is not a feature of this P450 isoform, and perhaps that catalysis does not require a high-spin heme iron? The protein was not particularly stable to chaotrope either, with relatively mild denaturing conditions (<2 M GdnHCl) sufficient to cause substantial loss of secondary structure, as monitored by CD. Tertiary structure is similarly disrupted at low concentrations of the chaotrope, and slightly higher concentration of GdnHCl lead to the aggregation and precipitation of the protein. Disruption of the heme structure and loss of the heme moiety also occurs at relatively low concentrations of GdnHCl, and this also appears to be detrimental to

the overall stability of the P450, leading to further protein denaturation and indicating that heme binding is an important factor in the conformation and stability of CYP151A2.

The  $K_d$  of the proposed CYP151A2 substrate morpholine was deduced, by optical titration, as  $18.2 \pm 0.1$  mM. However, this very weak binding was calculated from an inhibitory type II coordination spectrum, and this, as discussed, is a non-characteristic feature of substrate binding to P450s. It is likely that morpholine at lower concentrations adopts a different binding mode in the active site, and one that is evidently compatible with turnover. Only at much higher concentrations is it able to adopt a different binding mode that is inhibitory. Binding of various azole antifungal drugs were tighter to CYP151A2 than reported for other P450s in this study, which suggests an active site distinct from the other P450s and able to bind tightly to bulky polycyclic azole drugs. This is an important finding and one that may ultimately facilitate the determination of atomic structures of CYP151A2 in different azole complexes.

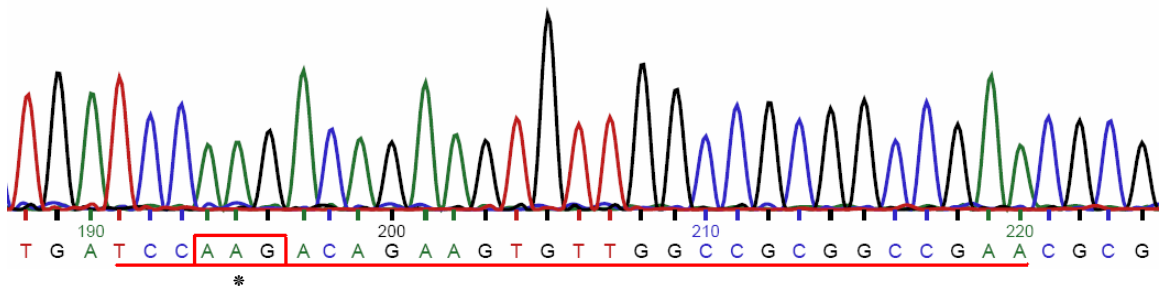
Clearly, with substantial information now gathered on the biophysical aspects of CYP151A2, including catalysis and thermodynamics, as well as  $K_d$  values from ligand binding assays, the immediate priority is the determination of an atomic structure of CYP151A2 both in isolation and in complex with substrate (morpholine) and with one or more tight-binding azole inhibitors. Since the amino acid sequence is quite distinctive among P450s, the structure could reveal novel structural motifs. Moreover, obtaining a ferrous P450 structure could also be important, since it might highlight any structural rearrangements that occur and that are involved in the heme iron protonation and P420 formation. Generation of atomic structures would also enable mutagenesis to probe structure-function relationships in greater detail.

In conclusion, the work presented in this thesis has detailed the expression and characterisation of three distinct types of mycobacterial P450 enzymes that have roles (potential or proven) in pathogenic bacterial virulence and survival (CYP121 and CYP140A2), or in the adaptation of a mycobacterium to survive and thrive in the presence of an unusual carbon source (morpholine) (CYP151A2). The data generated



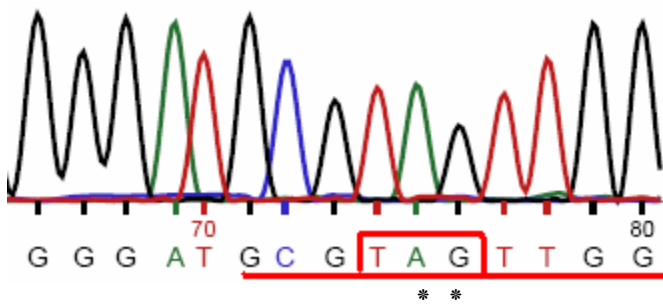
have led to (i) a more detailed understanding of the active site architecture and molecular properties of a P450 system essential for viability of *M. tuberculosis* (CYP121), and have pointed towards its role in lipid metabolism in this pathogen; (ii) the first expression and spectroscopic characterisation of a *M. ulcerans* P450 (CYP140A2) and the demonstration of its role in mycolactone toxin metabolism; and (iii) Spectroscopic, thermodynamic, ligand-binding and stability studies on another mycobacterial P450 (CYP151A2) involved in morpholine degradation, including demonstration of its proximal ligand switch from thiolate to thiol in the reduced state. Collectively, these studies have added considerably to the general understanding of structure and functional diversity in the mycobacterial P450s, and have provided important information and resources that will enable more detailed structural and other studies to be done to enable the potential exploitation of these systems as drug targets (CYP121, CYP140A2) or biotechnological tools (CYP151A2).

# Appendix



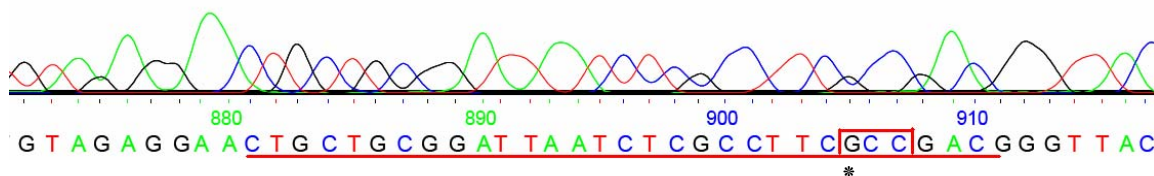
#### Chromatogram data for P346L sequencing

The Leu<sup>346</sup> codon is highlighted with red box. The PCR oligonucleotide is underlined in red. The reverse complement sequence corresponds to the wild-type sequence with the exception of the desired mutations. The specific base mutation is highlighted with a star.



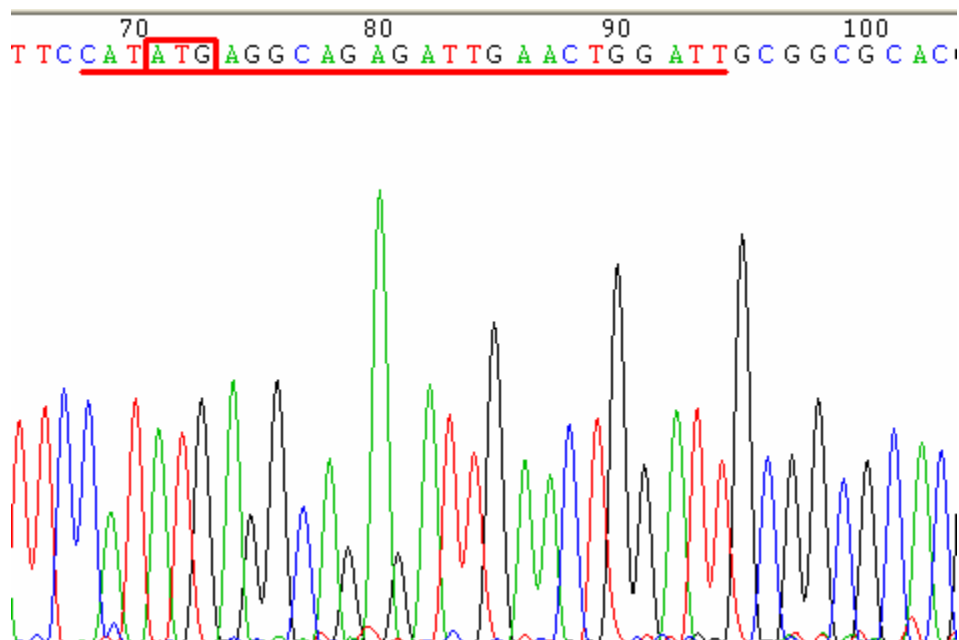
#### Chromatogram data for R386L sequencing

The Leu<sup>386</sup> codon is highlighted with red box. The oligonucleotide is underlined in red. The reverse complement sequence corresponds to the wild-type sequence with the exception of the desired mutations. The specific base mutation is highlighted with a star.



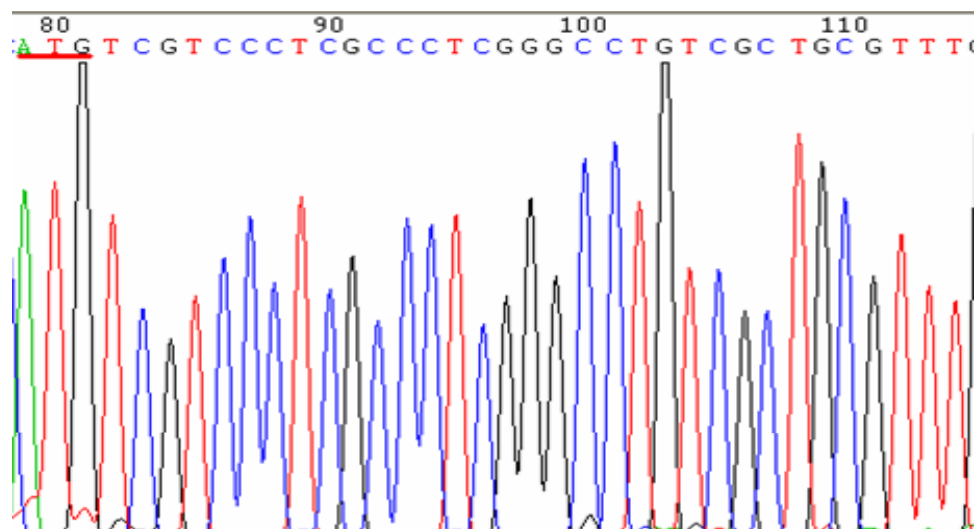
### Chromatogram data for S279A sequencing

The Ala<sup>279</sup> codon is highlighted with red box. The oligonucleotide is underlined in red. The sequence corresponds to the wild-type sequence with the exception of the desired mutations. The specific base mutation is highlighted with a star.



### Chromatogram data for CYP140A2 sequencing

Methionine (ATG) start codon for CYP140A2 is highlighted with red box. The oligonucleotide is underlined in red. The sequence corresponds to the wild-type sequence with the exception of the desired mutations.



### Chromatogram data for CYP151A2 sequencing

Methionine (ATG) start codon for CYP151A2 is underlined in red. The sequence corresponds to the expected sequence.

## Bibliography

- Abe, M., Kitagawa, T. and Kyogoku, Y. (1978) Resonance Raman-Spectra of Octaethylporphyrinato-Ni(II) and Meso-Deuterated and N-15 Substituted Derivatives .2. Normal Coordinate Analysis. *Journal of Chemical Physics* **69**, 4526-4534.
- Aguey-Zinsou, K. F., Bernhardt, P. V., De Voss, J. J. and Slessor, K. E. (2003) Electrochemistry of P450cin: new insights into P450 electron transfer. *Chemical Communications* **2003**, 418-419.
- Ahmad, Z., Sharma, S. and Khuller, G. K. (2005) In vitro and ex vivo antimycobacterial potential of azole drugs against *Mycobacterium tuberculosis* H(37)Rv. *Fems Microbiology Letters*. **251**, 19-22.
- Ahmad, Z., Sharma, S. and Khuller, G. K. (2007) Chemotherapeutic evaluation of alginate nanoparticle-encapsulated azole antifungal and antitubercular drugs against murine tuberculosis. *Nanomedicine*. **3**, 239-243.
- Aikens, J. and Sligar, S. G. (1994) Kinetic Solvent Isotope Effects during Oxygen Activation by Cytochrome P-450cam. *Journal of the American Chemical Society*. **116**, 1143-1144.
- Alden, R. G., Crawford, B. A., Doolen, R., Ondrias, M. R. and Shelnutt, J. A. (1989) Ruffling of Nickel(II) Octaethylporphyrin in Solution. *Journal of the American Chemical Society*. **111**, 2070-2072.
- Alden, R. G., Ondrias, M. R. and Shelnutt, J. A. (1990) Influences of Pi-Pi-Complex Formation, Dimerization, and Binding to Hemoglobin on the Planarity of Nickel(II) Porphyrins. *Journal of the American Chemical Society* **112**, 691-697.
- Alksne, L. E., Anthony, R. A., Liebman, S. W. and Warner, J. R. (1993) An Accuracy Center in the Ribosome Conserved over 2 Billion Years. *Proceedings of the National Academy of Sciences of the United States of America*. **90**, 9538-9541.
- Alland, D., Kalkut, G. E., Moss, A. R., Mcadam, R. A., Hahn, J. A., Bosworth, W., Drucker, E. and Bloom, B. R. (1994) Transmission of Tuberculosis in New-York-City - an Analysis by DNA-Fingerprinting and Conventional Epidemiologic Methods. *New England Journal of Medicine*. **330**, 1710-1716.
- American Thoracic Society, CDC and Infectious Diseases Society of America (2003). Treatment of tuberculosis. *MMWR Recomm Rep*. **52**, 1-77.
- Amofah, G., Bonsu, F., Tetteh, C., Okrah, J., Asamoah, K., Asiedu, K., and Addy, J. (2002) Buruli ulcer in Ghana: results of a national case search. *Emerg Infect Dis*. **8**, 167-170.
- Anderson, K. K., Hobbs, J. D., Luo, L., Stanley, K. D., Quirke, J. M. E. and Shelnutt, J. A. (1993) Structural Heterogeneity of Octaethylporphyrins Probed by Resonance Raman-Spectroscopy. *Biophysical Journal*. **64**, A156-A156.
- Andersson, L. A., and Peterson, J. A. (1995) Active-Site Analysis of Ferric P450 Enzymes - Hydrogen-Bonding Effects on the Circular-Dichroism Spectra. *Biochemical and Biophysical Research Communications*. **211**, 389-395.

- Andersson, L. A., Johnson, A. K. and Peterson, J. A. (1997) Active site analysis of P450 enzymes: Comparative magnetic circular dichroism spectroscopy. *Archives of biochemistry and biophysics*. **345**, 79-87.
- Aono, S., Kato, T., Matsuki, M., Nakajima, H., Ohta, T., Uchida, T. and Kitagawa, T. (2002) Resonance Raman and ligand binding studies of the oxygen-sensing signal transducer protein HemAT from *Bacillus subtilis*. *Journal of Biological Chemistry*. **277**, 13528-13538.
- Aoyama, Y., Horiuchi, T., Gotoh, O., Noshiro, M., and Yoshida, Y. (1998) CYP51-like gene of *Mycobacterium tuberculosis* actually encodes a P450 similar to eukaryotic CYP51. *Journal of Biochemistry*. **124**, 694-696.
- Aoyama, Y., Noshiro, M., Gotoh, O., Imaoka, S., Funae, Y., Kurosawa, N., Horiuchi, T., and Yoshida, Y. (1996) Sterol 14-demethylase P450 (P45014DM\*) is one of the most ancient and conserved P450 species. *Journal of Biochemistry*, **119**, 926-933.
- Apajalahti, J. H. and Salkinoja-Salonen, M. S. (1987) Dechlorination and para-hydroxylation of polychlorinated phenols by *Rhodococcus chlorophenolicus*. *J Bacteriol* **169**, 675-681.
- Asher, S. A. (1988) UV resonance Raman studies of molecular structure and dynamics: applications in physical and biophysical chemistry. *Annual review of physical chemistry*. **39**, 537-588.
- Aspinall, G. O., Chatterjee, D. and Brennan, P. J. (1995). The variable surface glycolipids of mycobacteria: structures, synthesis of epitopes, and biological properties. *Advanced Carbohydrate Chemical Biochemistry*. **51**, 169-242.
- Atkins, W. M. and Sligar, S. G. (1988) The Roles of Active-Site Hydrogen-Bonding in Cytochrome P-450Cam as Revealed by Site-Directed Mutagenesis. *Journal of Biological Chemistry*. **263**, 18842-18849.
- Axelrod, J. (1955) The Enzymatic Demethylation of Ephedrine. *Journal of Pharmacology and Experimental Therapeutics*. **114**, 430-438.
- Babini, E., Borsari, M., Capozzi, F., Eltis, L. D., and Luchinat, C. (1999) Experimental evidence for the role of buried polar groups in determining the reduction potential of metalloproteins: the S79P variant of *Chromatium vinosum* HiPIP. *Journal of Biological Inorganic Chemistry* **4**, 692-700.
- Badger, J. and Caspar, D. L. D. (1991) Water-Structure in Cubic Insulin Crystals. *Proceedings of the National Academy of Sciences of the United States of America*. **88**, 622-626.
- Baer, B. R., Schuman, J. T., Campbell, A. P., Cheesman, M. J., Nakano, M., Moguilevsky, N., Kunze, K. L. and Rettie, A. E. (2005) Sites of covalent attachment of CYP4 enzymes to heme: evidence for microheterogeneity of P450 heme orientation. *Biochemistry*. **44**, 13914-13920.
- Bafende, A. E., Phanzu, M. D., and Imposo, B. B. (2004) Buruli ulcer in the Democratic Republic of Congo: epidemiology, presentation and outcome. *Trop Doct* **34**, 82-84.

- Bammert, G. F., and Fostel, J. M. (2000) Genome-wide expression patterns in *Saccharomyces cerevisiae*: Comparison of drug treatments and genetic alterations affecting biosynthesis of ergosterol. *Antimicrobial Agents and Chemotherapy*. **44**, 1255-1265.
- Barker, D. J. (1971) Buruli disease in a district of Uganda. *J Trop Med Hyg*. **74**, 260-264.
- Barnes, P. F., Chatterjee, D., Abrams, J. S., Lu, S. H., Wang, E., Yamamura, M., Brennan, P. J. and Modlin, R. L. (1992) Cytokine Production Induced by *Mycobacterium-Tuberculosis* Lipoarabinomannan - Relationship to Chemical-Structure. *Journal of Immunology*. **149**, 541-547.
- Barry, C. E., 3rd, Lee, R. E., Mdluli, K., Sampson, A. E., Schroeder, B. G., Slayden, R. A. and Yuan, Y. (1998) Mycolic acids: structure, biosynthesis and physiological functions. *Prog Lipid Res* **37**, 143-179.
- Bass, J. B., Farer, L. S., Hopewell, P. C., O'Brien, R., Jacobs, R. F., Ruben, F., Snider, D. E. and Thornton, G. (1994) Treatment of Tuberculosis and Tuberculosis Infection in Adults and Children. *American Journal of Respiratory and Critical Care Medicine*. **149**, 1359-1374.
- Bastian, I., and Colebunders, R. (1999). Treatment and prevention of multidrug-resistant tuberculosis. *Drugs*. **58**, 633-661.
- Behling, C. A., Perez, R. L., Kidd, M. R., Staton, G. W. and Hunter, R. L. (1993) Induction of Pulmonary Granulomas, Macrophage Procoagulant Activity, and Tumor-Necrosis-Factor-Alpha by Trehalose Glycolipids. *Annals of Clinical and Laboratory Science*. **23**, 256-266.
- Beinert, H., Kennedy, M. C. and Stout, C. D. (1996) Aconitase as iron-sulfur protein, enzyme, and iron-regulatory protein. *Chemical Reviews*. **96**, 2335-2373.
- Belisle, J. T. and Brennan, P. J. (1989) Chemical Basis of Rough and Smooth Variation in *Mycobacteria*. *Journal of Bacteriology*. **171**, 3465-3470.
- Belisle, J. T., Mcneil, M. R., Chatterjee, D., Inamine, J. M. and Brennan, P. J. (1993) Expression of the Core Lipopeptide of the Glycopeptidolipid Surface-Antigens in Rough Mutants of *Mycobacterium avium*. *Journal of Biological Chemistry*. **268**, 10510-10516.
- Belisle, J. T., Vissa, V. D., Sievert, T., Takayama, K., Brennan, P. J. and Besra, G. S. (1997) Role of the major antigen of *Mycobacterium tuberculosis* in cell wall biogenesis. *Science*. **276**, 1420-1422.
- Bellamine, A., Mangla, A. T., Nes, W. D. and Waterman, M. R. (1999) Characterization and catalytic properties of the sterol 14 alpha-demethylase from *Mycobacterium tuberculosis*. *Proceedings of the National Academy of Sciences of the United States of America*. **96**, 8937-8942.
- Bentoucha, A., Robert, J., Dega, H., Lounis, N., Jarlier, V., and Grosset, J. (2001) Activities of new macrolides and fluoroquinolones against *Mycobacterium ulcerans* infection in mice. *Antimicrob Agents Chemother*. **45**, 3109-3112.
- Berka, V., Palmer, G., Chen, P. F., and Tsai, A. L. (1998) Effects of various imidazole ligands on heme conformation in endothelial nitric oxide synthase. *Biochemistry*, **37**, 6136-6144.



- Berkovitch, F., Nicolet, Y., Wan, J. T., Jarrett, J. T. and Drennan, C. L. (2004) Crystal structure of biotin synthase, an S-adenosylmethionine-dependent radical enzyme. *Science* **303**, 76-79.
- Berman, H. M., Westbrook, J., Feng, Z., Gilliland, G., Bhat, T. N., Weissig, H., Shindyalov, I. N. and Bourne, P. E. (2000) The Protein Data Bank. *Nucleic Acids Res.* **28**, 235-242.
- Berry, E.A., and Trumpower B.L. (1987). Simultaneous determination of hemes a,b, and c from pyridine hemochrome spectra. *Analytical Biochemistry*. **161**, 1-15.
- Besra, G. S., Mcneil, M. R., Rivoire, B., Khoo, K. H., Morris, H. R., Dell, A. and Brennan, P. J. (1993) Further Structural Definition of a New Family of Glycopeptidolipids from *Mycobacterium xenopi*. *Biochemistry*. **32**, 347-355.
- Bifani, P. J., Mathema, B., Kurepina, N. E. and Kreiswirth, B. N. (2002) Global dissemination of the *Mycobacterium tuberculosis* W-Beijing family strains. *Trends in Microbiology* **10**, 45-52.
- Bishai, W. (1998) The *Mycobacterium tuberculosis* genomic sequence: anatomy of a master adaptor. *Trends in Microbiology* **6**, 464-465.
- Blattner, F. R., Plunkett, G., Bloch, C. A., Perna, N. T., Burland, V., Riley, M., ColladoVides, J., Glasner, J. D., Rode, C. K., Mayhew, G. F., Gregor, J., Davis, N. W., Kirkpatrick, H. A., Goeden, M. A., Rose, D. J., Mau, B. and Shao, Y. (1997) The complete genome sequence of *Escherichia coli* K-12. *Science* **277**, 1453
- Boddupalli, S. S., Estabrook, R. W., and Peterson, J. A. (1990) Fatty-Acid Monooxygenation by Cytochrome-P-450Bm-3. *Journal of Biological Chemistry* **265**, 4233-4239.
- Bollag, J. M., and Kaiser, J. P. (1991) The Transformation of Heterocyclic Aromatic-Compounds and Their Derivatives under Anaerobic Conditions. *Critical Reviews in Environmental Control*. **21**, 297-329.
- Bossche, H. V., Koymans, L., and Moereels, H. (1995) P450 Inhibitors of Use in Medical-Treatment - Focus on Mechanisms of Action. *Pharmacology and Therapeutics*. **67**, 79-100.
- Bradley D. J., (1971) Epidemiology of *Mycobacterium-Ulcerans* Infection (Buruli Ulcer) at Kinyara, Uganda. *Transactions of the Royal Society of Tropical Medicine and Hygiene*. **65**, 763-and.
- Brennan, P. J. (2003) Structure, function, and biogenesis of the cell wall of *Mycobacterium tuberculosis*. *Tuberculosis* **83**, 91-97.
- Brennan, P. J. and Nikaido, H. (1995) The Envelope of Mycobacteria. *Annual Review of Biochemistry*. **64**, 29-63.
- Brightbill, H. D., Libraty, D. H., Krutzik, S. R., Yang, R. B., Belisle, J. T., Bleharski, J. R., Maitland, M., Norgard, M. V., Plevy, S. E., Smale, S. T., Brennan, P. J., Bloom, B. R., Godowski, P. J., and Modlin, R. L. (1999) Host defense mechanisms triggered by microbial lipoproteins through toll-like receptors. *Science* **285**, 732-736.

- Broderick, J. B., Duderstadt, R. E., Fernandez, D. C., Wojtuszewski, K., Henshaw, T. F. and Johnson, M. K. (1997) Pyruvate formate-lyase activating enzyme is an iron-sulfur protein. *Journal of the American Chemical Society*. **119**, 7396-7397
- Brodie, B. B., Axelrod, J., Cooper, J. R., Gaudette, L., Ladu, B. N., Mitoma, C., and Udenfriend, S. (1955) Detoxication of Drugs and Other Foreign Compounds by Liver Microsomes. *Science* **121**, 603-604.
- Brown, V. R., and Knapp, J. S. (1990) The Effect of Withdrawal of Morpholine from the Influent and Its Reinstatement on the Performance and Microbial Ecology of a Model Activated-Sludge Plant Treating a Morpholine-Containing Influent. *Journal of Applied Bacteriology*. **69**, 43-53.
- Buchatskii, A. G., Kazachenko, K. and Alexandrov, A. A. (2001) Cytochrome P450 pattern revision. *J Biomol Struct Dyn*. **19**, 273-277.
- Burguiere, A., Hitchen, P. G., Dover, L. G., Dell, A. and Besra, G. S. (2005) Altered expression profile of mycobacterial surface glycopeptidolipids following treatment with the antifungal azole inhibitors econazole and clotrimazole. *Microbiology (Reading, England)*. **151**, 2087-2095.
- Byrne, S. T., Denkin, S. M., Gu, P., Nuermberger, E. and Zhang, Y. (2007) Activity of ketoconazole against *Mycobacterium tuberculosis* in vitro and in the mouse model. *Journal of medical microbiology*. **56**, 1047-1051.
- Cadapan, L. D., R. L. Arslanian, J. R. Carney, S. M. Zavala, P. L. Small, and P. Licari. (2001). Suspension cultivation of *Mycobacterium ulcerans* for the production of mycolactones. *FEMS Microbiol. Lett*. **205**, 385-389.
- Camphausen, R. T., Jones, R. L. and Brennan, P. J. (1988) Antigenic relationship between *Mycobacterium paratuberculosis* and *Mycobacterium avium*. *American Journal of Veterinary Research*. **49**, 1307-1310.
- Camus, J. C., Pryor, M. J., Medigue, C., and Cole, S. T. (2002). Re-annotation of the genome sequence of *Mycobacterium tuberculosis* H37Rv. *Microbiology-Sgm*. **148**, 2967-2973.
- Canetti, G. (1965) Present aspects of bacterial resistance in tuberculosis. *Am Rev Respir Dis*. **92**, 687-703.
- Canetti, G., Fox, W., Khomenko, A., Mahler, H. T., Menon, N. K., Mitchiso.Da, Rist, N. and Smelev, N. A. (1969) Advances in Techniques of Testing Mycobacterial Drug Sensitivity, and Use of Sensitivity Tests in Tuberculosis Control Programmes. *Bulletin of the World Health Organization*. **41**, 21-25.
- Cantwell, M. F., and Binkin, N. J. (1996) Tuberculosis in sub-Saharan Africa: a regional assessment of the impact of the human immunodeficiency virus and National Tuberculosis Control Program quality. *Tuber Lung Dis*. **77**, 220-225.
- Capozzi, F., Ciurli, S., and Luchinat, C. (1998) Coordination sphere versus protein environment as determinants of electronic and functional properties of iron-sulphur proteins. *Metal Sites in Proteins and Models*. **90**, 127-160.

- Carter, A. P., Clemons, W. M., Brodersen, D. E., Morgan-Warren, R. J., Wimberly, B. T., and Ramakrishnan, V. (2000) Functional insights from the structure of the 30S ribosomal subunit and its interactions with antibiotics. *Nature* **407**, 340-348.
- Cayla, J. A., Caminero, J. A., Rey, R., Lara, N., Valles, X., and Galdos-Tanguis, H. (2004) Current status of treatment completion and fatality among tuberculosis patients in Spain. *Int J Tuberc Lung Dis*. **8**, 458-464.
- Cech, J. S., Hartman, P., Slosarek, M., and Chudoba, J. (1988) Isolation and identification of a morpholine-degrading bacterium. *Appl Environ Microbiol*. **54**, 619-621.
- Chan, F. C., Potter, G. A., Barrie, S. E., Haynes, B. P., Rowlands, M. G., Houghton, J. and Jarman, M. (1996) 3- and 4-pyridylalkyl adamantanecarboxylates: inhibitors of human cytochrome P450(17  $\alpha$ ) (17  $\alpha$ -hydroxylase/C17,20-lyase). Potential nonsteroidal agents for the treatment of prostatic cancer. *J Med Chem*. **39**, 3319-3323.
- Chanwong, S., Maneekarn, N., Makonkawkeyoon, L. and Makonkawkeyoon, S. (2007) Intracellular growth and drug susceptibility of *Mycobacterium tuberculosis* in macrophages. *Tuberculosis (Edinburgh, Scotland)*. **87**, 130-133.
- Chatterjee, D., and Khoo, K. H. (1998) Mycobacterial lipoarabinomannan: an extraordinary lipoheteroglycan with profound physiological effects. *Glycobiology* **8**, 113-120.
- Chatterjee, D., Bozic, C. M., Mcneil, M., and Brennan, P. J. (1991) Structural Features of the Arabinan Component of the Lipoarabinomannan of *Mycobacterium-Tuberculosis*. *Journal of Biological Chemistry*. **266**, 9652-9660.
- Chatterjee, D., Lowell, K., Rivoire, B., Mcneil, M. R., and Brennan, P. J. (1992a) Lipoarabinomannan of *Mycobacterium-Tuberculosis* - Capping with Mannosyl Residues in Some Strains. *Journal of Biological Chemistry*. **267**, 6234-6239.
- Chatterjee, D., Roberts, A. D., Lowell, K., Brennan, P. J., and Orme, I. M. (1992b) Structural Basis of Capacity of Lipoarabinomannan to Induce Secretion of Tumor-Necrosis-Factor. *Infection and Immunity*. **60**, 1249-1253.
- Cheesman, M. R., Greenwood, C. and Thomson, A. J. (1991) Magnetic Circular-Dichroism of Hemoproteins. *Advances in Inorganic Chemistry*. **36**, 201-255.
- Cheesman, M. R., Little, P. J. and Berks, B. C. (2001). Novel heme ligation in a c-type cytochrome involved in thiosulfate oxidation: EPR and MCD of SoxAX from *Rhodovulum sulfidophilum*. *Biochemistry*, **40**, 10562-10569.
- Chemlal, K., Huys, G., Laval, F., Vincent, V., Savage, C., Gutierrez, C., Laneelle, M. A., Swings, J., Meyers, W. M., Daffe, M., and Portaels, F. (2002). Characterization of an unusual *Mycobacterium*: a possible missing link between *Mycobacterium marinum* and *Mycobacterium ulcerans*. *J Clin Microbiol*. **40**, 2370-2380.
- Chen, K. S., Jung, Y. S., Bonagura, C. A., Tilley, G. J., Prasad, G. S., Sridhar, V., Armstrong, F. A., Stout, C. D., and Burgess, B. K. (2002) Azotobacter vinelandii ferredoxin I - A sequence and structure comparison approach to alteration of [4Fe-4S]<sub>2</sub>(+/+) reduction potential. *Journal of Biological Chemistry* **277**, 5603-5610.

Chevalier, D., Lo-Guidice, J. M., Sergent, E., Allorge, D., Debuysere, H., Ferrari, N., Libersa, C., Lhermitte, M. and Broly, F. (2001) Identification of genetic variants in the human thromboxane synthase gene (CYP5A1). *Mutation Research-Genomics* **432**, 61-67.

Chiang, Y. L., and Coon, M. J. (1979) Comparative-Study of 2 Highly Purified Forms of Liver Microsomal Cytochrome-P-450 - Circular-Dichroism and Other Properties. *Archives of Biochemistry and Biophysics*, **195**, 178-187.

Choi, S., Spiro, T. G., Langry, K. C. and Smith, K. M. (1982a) Vinyl Influences on Protoheme Resonance Raman-Spectra - Nickel(II) Protoporphyrin-Ix with Deuterated Vinyl Groups. *Journal of the American Chemical Society* **104**, 4337-4344.

Choi, S., Spiro, T. G., Langry, K. C., Smith, K. M., Budd, D. L. and Lamar, G. N. (1982b) Structural Correlations and Vinyl Influences in Resonance Raman-Spectra of Protoheme Complexes and Proteins. *Journal of the American Chemical Society*. **104**, 4345-4351.

Cirino, P. C., and Arnold, F. H. (2003) A self-sufficient peroxide-driven hydroxylation biocatalyst. *Angewandte Chemie-International Edition*. **42**, 3299-3301.

Cojocaru, V., Winn, P. J. and Wade, R. C. (2007) The ins and outs of cytochrome P450s. *Biochim Biophys Acta*. **1770**, 390-401.

Cole, S. T. (1999). Learning from the genome sequence of *Mycobacterium tuberculosis* H37Rv. *Febs Letters*. **452**, 7-10.

Cole, S. T., and Alzari, P. M. (2005) Microbiology. TB--a new target, a new drug. *Science* **307**, 214-215.

Cole, S. T., and Telenti, A. (1995). Drug-Resistance in *Mycobacterium-Tuberculosis*. *European Respiratory Journal*. **8**, S701-S713.

Cole, S. T., Brosch, R., Parkhill, J., Garnier, T., Churcher, C., Harris, D., Gordon, S. V., Eiglmeier, K., Gas, S., Barry, C. E., Tekaiia, F., Badcock, K., Basham, D., Brown, D., Chillingworth, T., Connor, R., Davies, R., Devlin, K., Feltwell, T., Gentles, S., Hamlin, N., Holroyd, S., Hornby, T., Jagels, K., Krogh, A., McLean, J., Moule, S., Murphy, L., Oliver, K., Osborne, J., Quail, M. A., Rajandream, M. A., Rogers, J., Rutter, S., Seeger, K., Skelton, J., Squares, R., Squares, S., Sulston, J. E., Taylor, K., Whitehead, S., and Barrell, B. G. (1998) Deciphering the biology of *Mycobacterium tuberculosis* from the complete genome sequence. *Nature*. **393**, 537-544.

Cole, S. T., Eiglmeier, K., Parkhill, J., James, K. D., Thomson, N. R., Wheeler, P. R., Honore, N., Garnier, T., Churcher, C., Harris, D., Mungall, K., Basham, D., Brown, D., Chillingworth, T., Connor, R., Davies, R. M., Devlin, K., Duthoy, S., Feltwell, T., Fraser, A., Hamlin, N., Holroyd, S., Hornsby, T., Jagels, K., Lacroix, C., Maclean, J., Moule, S., Murphy, L., Oliver, K., Quail, M. A., Rajandream, M. A., Rutherford, K. M., Rutter, S., Seeger, K., Simon, S., Simmonds, M., Skelton, J., Squares, R., Squares, S., Stevens, K., Taylor, K., Whitehead, S., Woodward, J. R., and Barrell, B. G. (2001) Massive gene decay in the leprosy bacillus. *Nature* **409**, 1007-1011.

Combourieu, B., Besse, P., Sancelme, M., Veschambre, H., Delort, A. M., Poupin, P. and Truffaut, N. (1998) Morpholine degradation pathway of *Mycobacterium aurum* MO1: direct evidence of intermediates by in situ <sup>1</sup>H nuclear magnetic resonance. *Applied and environmental microbiology*. **64**, 153-158.

Converse, S. E., Mougous, J. D., Leavell, M. D., Leary, J. A., Bertozzi, C. R., and Cox, J. S. (2003) MmpL8 is required for sulfolipid-1 biosynthesis and *Mycobacterium tuberculosis* virulence. *Proceedings of the National Academy of Sciences of the United States of America* **100**, 6121-6126.

Coon, M. J., Vaz, A. D. N., McGinnity, D. F., and Peng, H. M. (1998) Multiple activated oxygen species in P450 catalysis - Contributions to specificity in drug metabolism. *Drug Metabolism and Disposition* **26**, 1190-1193.

Correia MA (2005) Human and rat liver cytochromes P450: functional markers, diagnostic inhibitor probes, and parameters frequently used in P450 studies. In: Ortiz de Montellano PR (ed) *Cytochrome P450 - structure, mechanism and biochemistry*, 3rd edn. Plenum, New York, pp 619-657.

Correia, M.A., and Ortiz de Montellano, P.R. (1993) Inhibitors of cytochrome P450 and possibilities for their therapeutic application, in *Medicinal Implications in cytochrome P450 catalysed biotransformations*, ed by Ruckpaul, K and Rein, H., Akademie Verlag, Berlin. pp. 74-146.

Cortes, J., Haydock, S. F., Roberts, G. A., Bevitt, D. J., and Leadlay, P. F. (1990) An unusually large multifunctional polypeptide in the erythromycin-producing polyketide synthase of *Saccharopolyspora erythraea*. *Nature*. **348**, 176-178.

Cosme, J. and Johnson, E. F. (2000) Engineering microsomal cytochrome P450C5 to be a soluble, monomeric enzyme - Mutations that alter aggregation, phospholipid dependence of catalysis, and membrane binding. *Journal of Biological Chemistry*. **275**, 2545-2553.

Coutanceau, E., Decalf, J., Martino, A., Babon, A., Winter, N., Cole, S. T., Albert, M. L. and Demangel, C. (2007) Selective suppression of dendritic cell functions by *Mycobacterium ulcerans* toxin mycolactone. *The Journal of experimental medicine*. **204**, 1395-1403.

Crick, D. C., Schulbach, M. C., Zink, E. E., Macchia, M., Barontini, S., Besra, G. S. and Brennan, P. J. (2000) Polyprenyl phosphate biosynthesis in *Mycobacterium tuberculosis* and *Mycobacterium smegmatis*. *Journal of bacteriology*. **182**, 5771-5778.

Cupp-Vickery J., Anderson R., Hatziris Z. (2000) Crystal structures of ligand complexes of P450eryF exhibiting homotropic cooperativity, *Proceedings of the National Academy of Sciences. USA* **97**, 3050-3055.

Cupp-Vickery, J. R., and Poulos, T. L. (1995). Structure of Cytochrome P450Eryf Involved in Erythromycin Biosynthesis. *Nature Structural Biology*. **2**, 144-153.

Cupp-Vickery, J. R., Garcia, C., Hofacre, A. and McGee-Estrada, K. (2001) Ketoconazole-induced conformational changes in the active site of cytochrome P450eryF. *Journal of Molecular Biology*. **311**, 101-110.

Daff S.N., Chapman S.K., Turner K.L., and Holt R.A., Govindaraj S., Poulos T.L., Munro A.W. (1997) Redox control of the catalytic cycle of flavocytochrome P450 BM-3, *Biochemistry* **36** , 13816-13823.

Daffé, M. and Draper, P. (1998). The envelope layers of mycobacteria with reference to their pathogenicity. *Advance Microbiology and Physiology* **39**, 131-201.

Dannenbergh, A. M., Jr. (1989). Immune mechanisms in the pathogenesis of pulmonary tuberculosis. *Rev Infect Dis* **11**, 369-378.

Davydov, D. R., Botchkareva, A. E., Davydova, N. E. and Halpert, J. R. (2005) Resolution of two substrate-binding sites in an engineered cytochrome P450eryF bearing a fluorescent probe. *Biophysical Journal*. **89**, 418-432.

Davydov, D. R., Botchkareva, A. E., Kumar, S., He, Y. Q. and Halpert, J. R. (2004) An electrostatically driven conformational transition is involved in the mechanisms of substrate binding and cooperativity in cytochrome P450eryF. *Biochemistry*. **43**, 6475-6485.

Davydov, D. R., Kumar, S. and Halpert, J. R. (2002) Allosteric mechanisms in P450eryF probed with 1-pyrenebutanol, a novel fluorescent substrate. *Biochemical and biophysical research communications*. **294**, 806-812.

Dawson, J. H., Andersson, L. A., and Sono, M. (1983). The diverse spectroscopic properties of ferrous cytochrome P-450-CAM ligand complexes. *The Journal of Biological Biochemistry*. **258**, 13637-13645.

Dawson, J. H., Andersson, L. A., and Sono, M. (1982) Spectroscopic Investigations of Ferric Cytochrome P-450-Cam Ligand Complexes - Identification of the Ligand Trans to Cysteinate in the Native Enzyme. *Journal of Biological Chemistry*. **257**, 3606-3617.

De Cock, K. M., and Chaisson, R. E. (1999). Will DOTS do it? A reappraisal of tuberculosis control in countries with high rates of HIV infection. *Int J Tuberc Lung Dis*. **3**, 457-465.

De Groot, H., and Sies, H. (1989). Cytochrome P-450, reductive metabolism, and cell injury. *Drug metabolism review*. **20**, 275-284.

De Mot, R., and Parret, A. H. A. (2002). A novel class of self-sufficient cytochrome P450 monooxygenases in prokaryotes. *Trends in Microbiology*, **10**, 502-508.

De Voss, J. J., Rutter, K., Schroeder, B. G., Su, H., Zhu, Y. and Barry, C. E., 3rd. (2000) The salicylate-derived mycobactin siderophores of *Mycobacterium tuberculosis* are essential for growth in macrophages. *Proceedings of the National Academy of Sciences of the United States of America*. **97**, 1252-1257.

Dean-Ross, D., and Cerniglia, C. E. (1996). Degradation of pyrene by *Mycobacterium flavescens*. *Appl Microbiol Biotechnol*. **46**, 307-312.

Debacker, M., Aguiar, J., Steunou, C., Zinsou, C., Meyers, W. M., Scott, J. T., Dramaix, M., and Portaels, F. (2004). *Mycobacterium ulcerans* disease: role of age and gender in incidence and morbidity. *Trop Med Int Health*. **9**, 1297-1304.

Dega, H., Robert, J., Bonnafous, P., Jarlier, V., and Grosset, J. (2000). Activities of several antimicrobials against *Mycobacterium ulcerans* infection in mice. *Antimicrob Agents Chemother* **44**, 2367-2372.

- Degtyarenko, K. N. (1995) Structural Domains of P450-Containing Monooxygenase Systems. *Protein Engineering* **8**, 737-747.
- Deng, J., Carbone, I. and Dean, R. A. (2007) The evolutionary history of cytochrome P450 genes in four filamentous Ascomycetes. *BMC Evol Biol.* **7**, 30.
- Denisov, I. G., Makris, T. M., Sligar, S. G. and Schlichting, I. (2005) Structure and chemistry of cytochrome P450. *Chem Rev.* **105**, 2253-2277.
- Dincer, I., Ergin, A., and Kocagoz, T. (2004) The vitro efficacy of beta-lactam and beta-lactamase inhibitors against multidrug resistant clinical strains of *Mycobacterium tuberculosis*. *International Journal of Antimicrobial Agents.* **23**, 408-411.
- Dmitrenko, G. N., Udod V. M., and Gvozdyak, P. I. (1985) Destruction of morpholine by fixed bacteria. *Khim. Teknol. Vody.* **7**, 97-99.
- Donadio, S., Staver, M. J., McAlpine, J. B., Swanson, S. J., and Katz, L. (1991) Modular organization of genes required for complex polyketide biosynthesis. *Science.* **252**, 675-679.
- Donoghue, H. D., Spigelman, M., Greenblatt, C. L., Lev-Maor, G., Bar-Gal, G. K., Matheson, C., Vernon, K., Nerlich, A. G., and Zink, A. R. (2004). Tuberculosis: from prehistory to Robert Koch, as revealed by ancient DNA. *Lancet Infect Dis.* **4**, 584-592.
- Dooley, S. W., Jarvis, W. R., Martone, W. J., and Snider, D. E., Jr. (1992) Multidrug-resistant tuberculosis. *Ann Intern Med*, **117**, 257-259.
- Dowler, S., Kular, G. and Alessi, D. R. (2002) Protein lipid overlay assay. *Sci. STKE.* **129**, PL6
- Draper, P. (1998) The outer parts of the mycobacterial envelope as permeability barriers. *Front Biosci.* **3**, D1253-1261.
- Drenth J (1999) *The theory of X-ray diffraction by a crystal. Principles of Protein X-ray Crystallography*, 2nd edn. New York: Springer Verlag.
- Dua, M., Singh, A., Sethunathan, N., and Johri, A. K. (2002) Biotechnology and bioremediation: successes and limitations. *Appl Microbiol Biotechnol* **59**, 143-152.
- Duderstadt, R. E., Staples, C. R., Brereton, P. S., Adams, M. W. W., and Johnson, M. K. (1999). Effects of mutations in aspartate 14 on the spectroscopic properties of the [Fe<sub>3</sub>S<sub>4</sub>](+,0) clusters in *Pyrococcus furiosus* ferredoxin. *Biochemistry* **38**, 10585-10593.
- Dunford, A. J., McLean, K. J., Sabri, M., Seward, H. E., Heyes, D. J., Scrutton, N. S. and Munro, A. W. (2007) Rapid P450 heme iron reduction by laser photoexcitation of *Mycobacterium tuberculosis* CYP121 and CYP51B1. Analysis of CO complexation reactions and reversibility of the P450/P420 equilibrium. *The Journal of biological chemistry.* **282**, 24816-24824.
- Dunn, A. R., Dmochowski, I. J., Bilwes, A. M., Gray, H. B. and Crane, B. R. (2001) Probing the open state of cytochrome P450cam with ruthenium-linker substrates. *Proc Natl Acad Sci U S A.* **98**, 12420-12425.

Dus, K., Katagiri, M., Yu, C. A., Erbes, D. L., and Gunsalus, I. C. (1970) Chemical Characterization of Cytochrome-P-450Cam. Biochemical and Biophysical Research Communications **40**, 1423-1430.

Dutton P.L. (1978) Redox potentiometry: determination of midpoint potentials of oxidation-reduction components of biological electron transfer systems. Methods in Enzymology. **54**, 411-435.

Eddowes, M. J. and Hill, H. A. O. (1977) Novel Method for Investigation of Electrochemistry of Metalloproteins - Cytochrome-C. Journal of the Chemical Society-Chemical Communications, 771-772

Eddyani, M., Ofori-Adjei, D., Teugels, G., De Weirtdt, D., Boakye, D., Meyers, W. M., and Portaels, F. (2004) Potential role for fish in transmission of *Mycobacterium ulcerans* disease (Buruli ulcer): an environmental study. Appl Environ Microbiol. **70**, 5679-5681.

Edwards, D., and Kirkpatrick, C. H. (1986) The immunology of mycobacterial diseases. Am Rev Respir Dis. **134**, 1062-1071.

Eltringham, I. J., Wilson, S. M. and Drobniewski, F. A. (1999) Evaluation of a bacteriophage-based assay (phage amplified biologically assay) as a rapid screen for resistance to isoniazid, ethambutol, streptomycin, pyrazinamide, and ciprofloxacin among clinical isolates of *Mycobacterium tuberculosis*. Journal of Clinical Microbiology. **37**, 3528-3532.

Emitiazi, G., and Knapp, J. S. (1994) The biodegradation of piperazine and structurally-related linear and cyclic amines. Biodegradation. **5**, 83-92.

Enarson, D. A. (1991). Principles of IUATLD collaborative tuberculosis programmes. Bull Int Union Tuberc Lung Dis. **66**, 195-200.

Enzmann, H., Zerban, H., Koppschneider, A., Loser, E., and Bannasch, P. (1995). Effects of Low-Doses of N-Nitrosomorpholine on the Development of Early Stages of Hepatocarcinogenesis. Carcinogenesis **16**, 1513-1518.

Espinal, M. A. (2003) The global situation of MDR-TB. Tuberculosis (Edinb) **83**, 44-51.

Espinal, M. A., Dye, C., Raviglione, M., and Kochi, A. (1999) Rational 'DOTS Plus' for the control of MDR-TB. International Journal of Tuberculosis and Lung Disease. **3**, 561-563.

Espinal, M. A., Laserson, K., Camacho, M., Fusheng, Z., Kim, S. J., Tlali, R. E., Smith, I., Suarez, P., Antunes, M. L., George, A. G., Martin-Casabona, N., Simelane, P., Weyer, K., Binkin, N., and Raviglione, M. C. (2001b) Determinants of drug-resistant tuberculosis: analysis of 11 countries. Int J Tuberc Lung Dis. **5**, 887-893.

Espinal, M. A., Laszlo, A., Simonsen, L., Boulahbal, F., Kim, S. J., Reniero, A., Hoffner, S., Rieder, H. L., Binkin, N., Dye, C., Williams, R., Raviglione, M. C., Org, W. H., and. (2001a) Global trends in resistance to antituberculosis drugs. New England Journal of Medicine. **344**, 1294-1303.



Espinel-Ingroff, A., Boyle, K., and Sheehan, D. J. (2001) In vitro antifungal activities of voriconazole and reference agents as determined by NCCLS methods: Review of the literature. *Mycopathologia* **150**, 101-115.

Etuaful S, Carbonnelle B, Grosset J, Lucas S, Horsefield C *et al.* (2003) Bactericidal activity of rifampicin and streptomycin treatment for early human *M. ulcerans* lesions. In: Report of the 6th WHO advisory group meeting on Buruli ulcer; 2003 March 10–13; Geneva, Switzerland. Geneva: World Health Organization. Available: [http://www.who.int/gtb-buruli/activities/PDF/Report\\_6th\\_Meeting\\_BU\\_ENGpdf.pdf](http://www.who.int/gtb-buruli/activities/PDF/Report_6th_Meeting_BU_ENGpdf.pdf). Accessed 3 March 2006.

Exner, K., and Lemperle, G. (1987) Buruli ulcer--necrotizing infection of the hand of a plastic surgeon. *Handchir Mikrochir Plast Chir.* **19**, 230-232.

Farrah, S. R., Shah, D. O. and Ingram, L. O. (1981) Effects of chaotropic and antichaotropic agents on elution of poliovirus adsorbed on membrane filters. *Proceedings of the National Academy of Sciences of the United States of America.* **78**, 1229-1232.

Fidanze, S., Song, F., Szlosek-Pinaud, M., Small, P. L., and Kishi, Y. (2001) Complete structure of the mycolactones. *J Am Chem Soc.* **123**, 10117-10118.

Finken, M., Kirschner, P., Meier, A., Wrede, A., and Bottger, E. C. (1993) Molecular-Basis of Streptomycin Resistance in Mycobacterium-Tuberculosis - Alterations of the Ribosomal-Protein S12 Gene and Point Mutations within a Functional 16S Ribosomal-Rna Pseudoknot. *Molecular Microbiology*, **9**, 1239-1246.

Fischl, M. A., Uttamchandani, R. B., Daikos, G. L., Poblete, R. B., Moreno, J. N., Reyes, R. R., Boota, A. M., Thompson, L. M., Cleary, T. J., and Lai, S. (1992) An outbreak of tuberculosis caused by multiple-drug-resistant tubercle bacilli among patients with HIV infection. *Ann Intern Med*, **117**, 177-183.

Fox, W., Ellard, G. A., and Mitchison, D. A. (1999) Studies on the treatment of tuberculosis undertaken by the British Medical Research Council tuberculosis units, 1946-1986, with relevant subsequent publications. *Int J Tuberc Lung Dis.* **3**, S231-279.

Fromtling, R. A. (1997) Current developments in antibacterial and antifungal chemotherapy. *Drug News and Perspectives.* **10**, 557-572.

Fukuzumi, S., Nakanishi, I., Barbe, J. M., Guillard, R., Van Caemelbecke, E., Guo, N. and Kadish, K. M. (1999) Decreased electron transfer rates of manganese porphyrins with conformational distortion of the macrocycle. *Angewandte Chemie-International Edition.* **38**, 964-966.

Funhoff, E. G., Bauer, U., Garcia-Rubio, I., Witholt, B. and van Beilen, J. B. (2006) CYP153A6, a soluble P450 oxygenase catalyzing terminal-alkane hydroxylation. *Journal of bacteriology.* **188**, 5220-5227.

Furukawa, K. (2003). 'Super bugs' for bioremediation. *Trends Biotechnol.* **21**, 187-190.

Garcia-Rubio, I., Braun, M., Gromov, I., Thony-Meyer, L. and Schweiger, A. (2007) Axial coordination of heme in ferric CcmE chaperone characterized by EPR spectroscopy. *Biophysical journal.* **92**, 1361-1373.

Garfinkel, D. (1957). Isolation and Properties of Cytochrome-B5 from Pig Liver. Archives of Biochemistry and Biophysics. **71**, 111-120.

Garnier, T., Eiglmeier, K., Camus, J. C., Medina, N., Mansoor, H., Pryor, M., Duthoy, S., Grondin, S., Lacroix, C., Monsempe, C., Simon, S., Harris, B., Atkin, R., Doggett, J., Mayes, R., Keating, L., Wheeler, P. R., Parkhill, J., Barrell, B. G., Cole, S. T., Gordon, S. V., and Hewinson, R. G. (2003). The complete genome sequence of *Mycobacterium bovis*. Proceedings of the National Academy of Sciences of the United States of America. **100**, 7877-7882.

Gatfield, J. and Pieters, J. (2000) Essential role for cholesterol in entry of mycobacteria into macrophages. Science. **288**, 1647-1650

Gaudu, P. and Weiss, B. (1996) SoxR, a [2Fe-2S] transcription factor, is active only in its oxidized form. Proceedings of the National Academy of Sciences of the United States of America. **93**, 10094-10098.

Geier, G. E. and Modrich, P. (1979) Recognition Sequence of the Dam Methylase of Escherichia-Coli-K12 and Mode of Cleavage of Dpn-I Endonuclease. Journal of Biological Chemistry. **254**, 1408-1413.

George, K. M., Chatterjee, D., Gunawardana, G., Welty, D., Hayman, J., Lee, R., and Small, P. L. C. (1999) Mycolactone: A polyketide toxin from *Mycobacterium ulcerans* required for virulence. Science. **283**, 854-857.

George, K. M., Pascopella, L., Welty, D. M., and Small, P. L. (2000) A *Mycobacterium ulcerans* toxin, mycolactone, causes apoptosis in guinea pig ulcers and tissue culture cells. Infect Immun **68**, 877-883.

George, K. M., Yuan, Y., Sherman, D. R. and Barry, C. E. (1995) The Biosynthesis of Cyclopropanated Mycolic Acids in *Mycobacterium tuberculosis* - Identification and Functional-Analysis of Cmas-2. Journal of Biological Chemistry. **270**, 27292-27298.

Georgopapadakou, N. H. (1998) Antifungals: mechanism of action and resistance, established and novel drugs. Current Opinion in Microbiology. **1**, 547-557.

Gershoni, J. M. and Palade, G. E. (1983) Protein Blotting - Principles and Applications. Analytical Biochemistry. **131**, 1-15.

Ghannoum, M. A., and Kuhn, D. M. (2002). Voriconazole - Better chances for patients with invasive mycoses. European Journal of Medical Research. **7**, 242-256.

Girmenia, C., Luzi, G., Monaco, M. and Martino, P. (1998) Use of voriconazole in treatment of *Scedosporium apiospermum* infection: case report. Journal of clinical microbiology. **36**, 1436-1438.

Girvan, H. M., Marshall, K. R., Lawson, R. J., Leys, D., Joyce, M. G., Clarkson, J., Smith, W. E., Cheesman, M. R. and Munro, A. W. (2004) Flavocytochrome P450BM3 mutant A264E undergoes substrate-dependent formation of a novel heme iron ligand set. Journal of Biological Chemistry. **279**, 23274-23286.

- Glickman, M. S., and Jacobs, W. R. (2001) Microbial pathogenesis of *Mycobacterium tuberculosis*: Dawn of a discipline. *Cell* **104**, 477-485.
- Gobin, J., Moore, C. H., Reeve, J. R., Jr., Wong, D. K., Gibson, B. W. and Horwitz, M. A. (1995) Iron acquisition by *Mycobacterium tuberculosis*: isolation and characterization of a family of iron-binding exochelins. *Proceedings of the National Academy of Sciences of the United States of America*. **92**, 5189-5193.
- Goren, M. B. (1982) Immunoreactive Substances of Mycobacteria. *American Review of Respiratory Disease*. **125**, 50-69.
- Goren, M. B., Hart, P. D., Young, M. R., and Armstrong, J. A. (1976) Prevention of Phagosome-Lysosome Fusion in Cultured Macrophages by Sulfatides of Mycobacterium-Tuberculosis. *Proceedings of the National Academy of Sciences of the United States of America*, **73**, 2510-2514.
- Gotoh O. (1992) Substrate recognition sites in cytochrome P450 family 2 (CYP2) proteins inferred from comparative analyses of amino acid and coding nucleotide sequences. *Journal of Biological Chemistry* **267**, 83-90.
- Gotoh, O. (1992). Substrate Recognition Sites in Cytochrome-P450 Family-2 (Cyp2) Proteins Inferred from Comparative Analyses of Amino-Acid and Coding Nucleotide-Sequences. *Journal of Biological Chemistry* **267**, 83-90.
- Graham S.E. and Peterson J.A. (1996) P450s: structural similarities and functional differences. *FASEB Journal*. **10**, 206-214.
- Graham S.E., and Peterson J.A. (1999) How similar are P450s and what can their differences teach us, *Archives of Biochemistry and Biophysics*. **369**, 24-29.
- Green, A. J., Rivers, S. L., Cheesman, M., Reid, G. A., Quaroni, L. G., Macdonald, I. D. G., Chapman, S. K., and Munro, A. W. (2001) Expression, purification and characterization of cytochrome P450 Biol: a novel P450 involved in biotin synthesis in *Bacillus subtilis*. *Journal of Biological Inorganic Chemistry*. **6**, 523-533.
- Grosset, J. (1978) Sterilizing Value of Rifampicin and Pyrazinamide in Experimental Short Course Chemotherapy. *Tubercle* **59**, 287-297.
- Guardiola-Diaz, H. M., Foster, L. A., Mushrush, D. and Vaz, A. D. N. (2001) Azole-antifungal binding to a novel cytochrome P450 from *Mycobacterium tuberculosis*: implications for treatment of tuberculosis. *Biochemical Pharmacology*. **61**, 1463-1470.
- Guengerich, F. P. and Johnson, W. W. (1997) Kinetics of ferric cytochrome P450 reduction by NADPH-cytochrome P450 reductase: rapid reduction in the absence of substrate and variations among cytochrome P450 systems. *Biochemistry*. **36**, 14741-14750.
- Guerardel, Y., Maes, E., Ellass, E., Leroy, Y., Timmerman, P., Besra, G. S., Loch, C., Strecker, G., and Kremer, L. (2002) Structural study of lipomannan and lipoarabinomannan from *Mycobacterium chelonae* - Presence of unusual components with alpha 1,3-mannopyranose side chains. *Journal of Biological Chemistry* **277**, 30635-30648.

Hägglblom, M. M., Nohynek, L. J., and Salkinoja-Salonen, M. S. (1988) Degradation and O-methylation of chlorinated phenolic compounds by *Rhodococcus* and *Mycobacterium* strains. *Appl Environ Microbiol.* **54**, 3043-3052.

Hägglblom, M. M., Nohynek, L. J., Palleroni, N. J., Kronqvist, K., Nurmiaho-Lassila, E. L., Salkinoja-Salonen, M. S., Klatte, S., Kroppenstedt, R. M. and Hägglblom, M. M. (1994) Transfer of polychlorophenol-degrading *Rhodococcus chlorophenolicus* (Apajalahti et al. 1986) to the genus *Mycobacterium* as *Mycobacterium chlorophenolicum* comb. nov. *Int J Syst Bacteriol.* **44**, 485-493.

Halpert, J. R., Domanski, T. L., Adali, O., Biagini, C. P., Cosme, J., Dierks, E. A., Johnson, E. F., Jones, J. P., de Montellano, P. O., Philpot, R. M., Sibbesen, O., Wyatt, W. K., and Zheng, Z. P. (1998) Structure-function of cytochromes P450 and flavin-containing monooxygenases - Implications for drug metabolism. *Drug Metabolism and Disposition.* **26**, 1223-1231.

Hamano, T., Mitsuhashi, Y. and Matsuki, Y. (1981) Glass capillary gas chromatography of secondary amines in foods with flame photometric detection after derivatization with benzenesulfonyl chloride. *Agric Biol Chem* **45**, 2237-2243.

Handman, E. and Jarvis, H. M. (1985) Nitrocellulose-Based Assays for the Detection of Glycolipids and Other Antigens - Mechanism of Binding to Nitrocellulose. *Journal of Immunological Methods.* **83**, 113-123.

Harlow, E. and Lane D. (1988) *Antibodies: A Laboratory Manual* (Cold Spring Harbor, NY: CSHL Press).

Hartman, P. G. and Sanglard, D. (1997) Inhibitors of ergosterol biosynthesis as antifungal agents. *Current Pharmaceutical Design.* **3**, 177-208.

Hartmans, S., and De Bont, J. A. (1992). Aerobic vinyl chloride metabolism in *Mycobacterium aurum* L1. *Appl Environ Microbiol.* **58**, 1220-1226.

Hasemann, C. A., Kurumbail, R. G., Boddupalli, S. S., Peterson, J. A. and Deisenhofer, J. (1995) Structure and function of cytochromes P450: a comparative analysis of three crystal structures. *Structure.* **3**, 41-62.

Hasemann, C. A., Ravichandran, K. G., Peterson, J. A., and Deisenhofer, J. (1994) Crystal-Structure and Refinement of Cytochrome P450(Terp) at 2-Center-Dot-3 Angstrom Resolution. *Journal of Molecular Biology* **236**, 1169-1185.

Havel, A. and S. R. Pattyn (1975) "Activity of rifampicin on *Mycobacterium ulcerans*." *Ann Soc Belg Med Trop.* **55**, 105-108.

Hawkes, D. B., Adams, G. W., Burlingame, A. L., Ortiz de Montellano, P. R. and De Voss, J. J. (2002) Cytochrome P450(cin) (CYP176A), isolation, expression, and characterization. *The Journal of biological chemistry.* **277**, 27725-27732.

Hayman, J. (1991) Postulated epidemiology of *Mycobacterium ulcerans* infection. *Int J Epidemiol.* **20**, 1093-1098.

Heep, M., Rieger, U., Beck, D., and Lehn, N. (2000) Mutations in the beginning of the *rpoB* gene can induce resistance to rifamycins in both *Helicobacter pylori* and *Mycobacterium tuberculosis*. *Antimicrobial Agents and Chemotherapy*. **44**, 1075-1077.

Heifets, L. B. (1991). Antituberculosis drugs: antimicrobial activity in vitro. In *Drug Susceptibility*

Heifets, L., and Lindholmlevy, P. (1992) Pyrazinamide Sterilizing Activity Invitro against Semidormant *Mycobacterium-Tuberculosis* Bacterial-Populations. *American Review of Respiratory Disease*. **145**, 1223-1225.

Heym, B., Zhang, Y., Poulet, S., Young, D., and Cole, S. T. (1993). Characterization of the KatG Gene Encoding a Catalase-Peroxidase Required for the Isoniazid Susceptibility of *Mycobacterium-Tuberculosis*. *Journal of Bacteriology*. **175**, 4255-4259.

Hildebrandt, P. and Stockburger, M. (1989) Cytochrome-C at Charged Interfaces .2. Complexes with Negatively Charged Macromolecular Systems Studied by Resonance Raman-Spectroscopy. *Biochemistry*. **28**, 6722-6728.

Hitchcock, C. A. (1993) Resistance of *Candida-Albicans* to Azole Antifungal Agents. *Biochemical Society Transactions* **21**, 1039-1047.

Hoff, A. J. (Ed.) (1989) *Advanced EPR in Application in Biology and Biochemistry*, Elsevier Science, Amsterdam.

Hoffman, H. L. and Rathbun, R. C. (2002) Review of the safety and efficacy of voriconazole. *Expert Opin Investig Drugs* **11**, 409-429.

Hollenberg, P. F. (1992) Mechanisms of cytochrome P450 and peroxidase-catalyzed xenobiotic metabolism. *Faseb J*. **6**, 686-694

Hong, H., Gates, P. J., Staunton, J., Stinear, T., Cole, S. T., Leadlay, P. F., and Spencer, J. B. (2003) Identification using LC-MSn of co-metabolites in the biosynthesis of the polyketide toxin mycolactone by a clinical isolate of *Mycobacterium ulcerans*. *Chem Commun (Camb)*. **22**, 2822-2823.

Hong, H., Spencer, J. B., Porter, J. L., Leadlay, P. F., and Stinear, T. (2005a) A novel mycolactone from a clinical isolate of *Mycobacterium ulcerans* provides evidence for additional toxin heterogeneity as a result of specific changes in the modular polyketide synthase. *Chembiochem*. **6**, 643-648.

Hong, H., Stinear, T., Skelton, P., Spencer, J. B., and Leadlay, P. F. (2005b) Structure elucidation of a novel family of mycolactone toxins from the frog pathogen *Mycobacterium* sp. MU128FXT by mass spectrometry. *Chem Commun (Camb)*. **34**, 4306-4308.

Honore, N., and Cole, S. T. (1994) Streptomycin resistance in mycobacteria. *Antimicrob Agents Chemother*. **38**, 238-242.

Hopwood, D. A. (1999) Forty years of genetics with *Streptomyces*: from in vivo through in vitro to in silico. *Microbiology-Sgm* **145**, 2183-2202.

Hsu, M. C. and Woody, R. W. (1971) The origin of the heme Cotton effects in myoglobin and hemoglobin. *Journal of the American Chemical Society*. **93**, 3515-3525

<http://drnelson.utmem.edu/CytochromeP450.html>. P450 classification list. Accessed 30/06/06.

Hu, S. Z., Smith, K. M. and Spiro, T. G. (1996) Assignment of protoheme Resonance Raman spectrum by heme labeling in myoglobin. *Journal of the American Chemical Society*. **118**, 12638-12646.

Hu, S., I. K. Morris, J. P. Singh, K. M. Smith, and T. G. Spiro. (1993) Complete assignment of cytochrome *c* resonance Raman spectra in enzymatic reconstitution with isotopically labeled hemes. *Journal of the American Chemical Society*. **115**, 12446-12558.

Hudecek, J., Anzenbacherova, E., Anzenbacher, P., Munro, A. W. and Hildebrandt, P. (2000) Structural similarities and differences of the heme pockets of various P450 isoforms as revealed by resonance Raman spectroscopy. *Archives of Biochemistry and Biophysics*. **383**, 70-78.

Hunsicker-Wang, L. M., Heine, A., Chen, Y., Luna, E. P., Todaro, T., Zhang, Y. M., Williams, P. A., McRee, D. E., Hirst, J., Stout, C. D., and Fee, J. A. (2003) High-resolution structure of the soluble, respiratory-type Rieske protein from *Thermus thermophilus*: analysis and comparison. *Biochemistry*. **42**, 7303-7317.

Hunter, S. W., and Brennan, P. J. (1990) Evidence for the Presence of a Phosphatidylinositol Anchor on the Lipoarabinomannan and Lipomannan of *Mycobacterium-Tuberculosis*. *Journal of Biological Chemistry*. **265**, 9272-9279.

Imai, M., Shimada, H., Watanabe, Y., Matsushimahibiya, Y., Makino, R., Koga, H., Horiuchi, T., and Ishimura, Y. (1989) Uncoupling of the Cytochrome P-450Cam Monooxygenase Reaction by a Single Mutation, Threonine-252 to Alanine or Valine - a Possible Role of the Hydroxy Amino-Acid in Oxygen Activation. *Proceedings of the National Academy of Sciences of the United States of America*. **86**, 7823-7827.

Inderlied C. B., and Nash K., A. Antimicrobial agents: In vitro susceptibility testing, spectra of activity, mechanisms of action and resistance, and assays for activity in biologic fluids. In: *Antibiotics in Laboratory Medicine*. Baltimore, Md: Williams and Wilkins; 1996;127-175.

Inoue, K. (2004) Carotenoid hydroxylation - P450 finally! *Trends in Plant Science*. **9**, 515-517

Institut Pasteur, *Mycobacterium ulcerans* (<http://www.pasteur.fr/recherche/unites/Lgmb/mycogenomics.html#ulcerans>) (accessed March 15, 2006).

International Program on Chemical Safety (1996). Morpholine. <http://www.inchem.org/documents/ehc/ehc/ehc179.htm> (accessed 25/09/06).

Iseman, M. D., and Madsen, L. A. (1991) Chronic tuberculous empyema with bronchopleural fistula resulting in treatment failure and progressive drug resistance. *Chest*. **100**, 124-127.

Jackson, C. J., Lamb, D. C., Kelly, D. E. and Kelly, S. L. (2000) Bactericidal and inhibitory effects of azole antifungal compounds on *Mycobacterium smegmatis*. *Fems Microbiology Letters*. **192**, 159-162.

Jackson, C. J., Lamb, D. C., Marczylo, T. H., Parker, J. E., Manning, N. L., Kelly, D. E. and Kelly, S. L. (2003) Conservation and cloning of CYP51: a sterol 14 alpha-demethylase from *Mycobacterium smegmatis*. *Biochemical and Biophysical Research Communications*. **301**, 558-563.

Jackson, C. J., Lamb, D. C., Marczylo, T. H., Warrilow, A. G. S., Manning, N. J., Lowe, D. J., Kelly, D. E., and Kelly, S. L. (2002). A novel sterol 14 alpha-demethylase/ferredoxin fusion protein (MCCYP51FX) from *Methylococcus capsulatus* represents a new class of the cytochrome P450 superfamily. *Journal of Biological Chemistry*. **277**, 46959-46965.

Jackson, M., Raynaud, C., Laneelle, M. A., Guilhot, C., Laurent-Winter, C., Ensergueix, D., Gicquel, B. and Daffe, M. (1999) Inactivation of the antigen 85C gene profoundly affects the mycolate content and alters the permeability of the *Mycobacterium tuberculosis* cell envelope. *Molecular Microbiology*. **31**, 1573-1587.

Jano J.K., Blasco F., Li H., Schmid R.D., Henne A., Poulos T.L. (2003) Preliminary characterisation and crystal structure of a thermostable cytochrome P450 from *Thermus thermophilus*, *Journal of Biological Chemistry*. **278**, 608-616.

Jenkin, G. A., Smith, M., Fairley, M., and Johnson, P. D. (2002) Acute, oedematous *Mycobacterium ulcerans* infection in a farmer from far north Queensland. *Med J Aust*. **176**, 180-181.

Jenkin, G. A., Stinear, T. P., Johnson, P. D., and Davies, J. K. (2003) Subtractive hybridization reveals a type I polyketide synthase locus specific to *Mycobacterium ulcerans*. *J Bacteriol*. **185**, 6870-6882.

Ji, H. T., Zhang, W. N., Zhang, M., Kudo, M., Aoyama, Y., Yoshida, Y., Sheng, C. Q., Song, Y. L., Yang, S., Zhou, Y. J., Lu, J. G., and Zhu, J. (2003) Structure-based de novo design, synthesis, and biological evaluation of non-azole inhibitors specific for lanosterol 14 alpha-demethylase of fungi. *Journal of Medicinal Chemistry*. **46**, 474-485.

Johnsson, K., and Schultz, P. G. (1994) Mechanistic Studies of the Oxidation of Isoniazid by the Catalase Peroxidase from *Mycobacterium-Tuberculosis*. *Journal of the American Chemical Society*. **116**, 7425-7426.

Joseph Horne, T., and Hollomon, D. W. (1997). Molecular mechanisms of azole resistance in fungi. *Fems Microbiology Letters*. **149**, 141-149.

Kalsbeck, W. A., Ghosh, A., Pandey, R. K., Smith, K. M. and Bocian, D. F. (1995) Determinants of the Vinyl Stretching Frequency in Protoporphyrins - Implications for Cofactor-Protein Interactions in Heme-Proteins. *Journal of the American Chemical Society* **117**, 10959-10968.

Karakousis, P. C., Bishai, W. R., and Dorman, S. E. (2004). *Mycobacterium tuberculosis* cell envelope lipids and the host immune response. *Cellular Microbiology* **6**, 105-116.

Karplus, P. A. and Faerman, C. (1994) Ordered Water in Macromolecular Structure. *Current Opinion in Structural Biology*. **4**, 770-776.

Kasim, M., and Swenson, R. P. (2000) Conformational energetics of a reverse turn in the *Clostridium beijerinckii* flavodoxin is directly coupled to the modulation of its oxidation-reduction potentials. *Biochemistry*. **39**, 15322-15332.

Kasim, M., and Swenson, R. P. (2001) Alanine-scanning of the 50's loop in the *Clostridium beijerinckii* flavodoxin: Evaluation of additivity and the importance of interactions provided by the main chain in the modulation of the oxidation-reduction potentials. *Biochemistry* **40**, 13548-13555.

Katz, L., and Donadio, S. (1993). Polyketide synthesis: prospects for hybrid antibiotics. *Annu Rev Microbiol* **47**, 875-912.

Kavanagh, K. Y., Murphy, E. J., Harmey, M., Farrell, M. A., Hardimann, O., Perryman, R. and Walsh, J. E. (1999) Microspectrophotometric analysis of respiratory pigments using a novel fibre optic dip probe in microsamples. *Physiological Measurement*. **20**, 303-311.

Kaya, M., Matsumura, K., Higashida, K., Hata, Y., Kawato, A., Abe, Y., Akita, O., Takaya, N. and Shoun, H. (2004) Cloning and enhanced expression of the cytochrome P450<sub>nor</sub> gene (nicA; CYP55A5) encoding nitric oxide reductase from *Asperillus oryzae*. *Bioscience Biotechnology and Biochemistry*. **68**, 2040-2049

Kazlauskaitė, J., Westlake, A. C. G., Wong, L. L. and Hill, H. A. O. (1996) Direct electrochemistry of cytochrome P450<sub>cam</sub>. *Chemical Communications*. **21**, 89-2190.

Kelly, S. L., Lamb, D. C., Baldwin, B. C., Corran, A. J., and Kelly, D. E. (1997). Characterization of *Saccharomyces cerevisiae* CYP61, sterol Delta(22)-desaturase, and inhibition by azole antifungal agents. *Journal of Biological Chemistry*. **272**, 9986-9988.

Kelly, S. M., Jess, T. J. and Price, N. C. (2005) How to study proteins by circular dichroism. *Biochimica Et Biophysica Acta-Proteins and Proteomics* **1751**, 119-139.

Kenyon, T. A., Mwasekaga, M. J., Huebner, R., Rumisha, D., Binkin, N., and Maganu, E. (1999) Low levels of drug resistance amidst rapidly increasing tuberculosis and human immunodeficiency virus co-epidemics in Botswana. *Int J Tuberc Lung Dis*. **3**, 4-11.

Khan, K. K., He, Y. A., He, Y. Q. and Halpert, J. R. (2002) Site-directed mutagenesis of cytochrome P450<sub>eryF</sub>: Implications for substrate oxidation, cooperativity, and topology of the active site. *Chemical Research in Toxicology*. **15**, 843-853.

Khan, K. K., Liu, H. and Halpert, J. R. (2003) Homotropic versus heterotopic cooperativity of cytochrome P450<sub>eryF</sub>: a substrate oxidation and spectral titration study. *Drug Metab Dispos*. **31**, 356-359.

Kiepiela, P., Bishop, K. S., Smith, A. N., Roux, L., and York, D. F. (2000) Genomic mutations in the *katG*, *inhA* and *aphC* genes are useful for the prediction of isoniazid resistance in *Mycobacterium tuberculosis* isolates from Kwazulu Natal, South Africa. *Tubercle and Lung Disease*. **80**, 47-56.

Kim, C., Kim, H. and Han, O. (2001) The role of serine-246 in cytochrome P450<sub>eryF</sub>-catalyzed hydroxylation of 6-deoxyerythronolide B. *Bioscience Biotechnology and Biochemistry*. **65**, 752-757.



Kim, Y. H., Kang, I., Bergeron, H., Lau, P. C., Engesser, K. H. and Kim, S. J. (2006) Physiological, biochemical, and genetic characterization of an alicyclic amine-degrading *Mycobacterium* sp. strain THO100 isolated from a morpholine-containing culture of activated sewage sludge. *Arch Microbiol.* **186**, 425-434.

Kimata, Y., Shimada, H., Hirose, T., and Ishimura, Y. (1995) Role of Thr-252 in Cytochrome P450(Cam) - a Study with Unnatural Amino-Acid Mutagenesis. *Biochemical and Biophysical Research Communications.* **208**, 96-102.

Kirschner, P., Springer, B., Vogel, U., Meier, A., Wrede A., Kiekenbeck, M., Bange, F. C., and Böttger E. C. (1993). Genotypic identification of mycobacteria by nucleic acid sequence determination: report of a 2-year experience in a clinical laboratory. *J. Clin. Microbiol.* **31**, 2882-2889.

Kitagawa T. and Ozaki Y. (1987) Infrared and Raman spectra of metalloporphyrins. *Structure and Bonding.* **64**, 71-114.

Kitazume, T., Takaya, N., Nakayama, N., and Shoun, H. (2000) *Fusarium oxysporum* fatty-acid subterminal hydroxylase (CYP505) is a membrane-bound eukaryotic: Counterpart of *Bacillus megaterium* cytochrome P450BM3. *Journal of Biological Chemistry* **275**, 39734-39740.

Kleespies, M., Kroppenstedt, R. M., Rainey, F. A., Webb, L. E., and Stackebrandt, E. (1996) *Mycobacterium hodleri* sp. nov., a new member of the fast-growing mycobacteria capable of degrading polycyclic aromatic hydrocarbons. *Int J Syst Bacteriol.* **46**, 683-687.

Klingenberg, M. (1958) Pigments of Rat Liver Microsomes. *Archives of Biochemistry and Biophysics.* **75**, 376-386.

Knapp, J. S., Callely, A. G., and Mainprize, J. (1982). The Microbial-Degradation of Morpholine. *Journal of Applied Bacteriology.* **52**, 5-13.

Kochi, A., Vareldzis, B., and Styblo, K. (1993). Multidrug-resistant tuberculosis and its control. *Res Microbiol.* **144** 104-110.

Kolattukudy, P. E., Fernandes, N. D., Azad, A. K., Fitzmaurice, A. M., and Sirakova, T. D. (1997). Biochemistry and molecular genetics of cell-wall lipid biosynthesis in mycobacteria. *Molecular Microbiology* **24**, 263-270.

Konno, K., Feldmann, F. M., and McDermot, W. (1967) Pyrazinamide Susceptibility and Amidase Activity of Tubercle Bacilli. *American Review of Respiratory Disease* **95**, 461.

Korashy, H. M., Shayeganpour, A., Brocks, D. R. and El-Kadi, A. O. (2007) Induction of cytochrome P450 1A1 by ketoconazole and itraconazole but not fluconazole in murine and human hepatoma cell lines. *Toxicol Sci.* **97**, 32-43.

Koshland, D. E. (1958) Application of a Theory of Enzyme Specificity to Protein Synthesis. *Proceedings of the National Academy of Sciences of the United States of America.* **44**, 98-104.

Kretzer, A., and Andreesen, J. R. (1991) A New Pathway for Isonicotinate Degradation by *Mycobacterium* Sp Ina1. *Journal of General Microbiology.* **137**, 1073-1080.

Krzywinska, E., Krzywinski, J. and Schorey, J. S. (2004) Phylogeny of *Mycobacterium avium* strains inferred from glycopeptidolipid biosynthesis pathway genes. *Microbiology-Sgm.* **150**, 1699-1706.

Kuhn, E. P., and Suflita, J. M. (1989). Microbial-Degradation of Nitrogen, Oxygen and Sulfur Heterocyclic-Compounds under Anaerobic Conditions - Studies with Aquifer Samples. *Environmental Toxicology and Chemistry.* **8**, 1149-1158.

Kunst, F., Ogasawara, N., Moszer, I., Albertini, A. M., Alloni, G., Azevedo, V., Bertero, M. G., Bessieres, P., Bolotin, A., Borchert, S., Borriss, R., Boursier, L., Brans, A., Braun, M., Brignell, S. C., Bron, S., Brouillet, S., Bruschi, C. V., Caldwell, B., Capuano, V., Carter, N. M., Choi, S. K., Codani, J. J., Connerton, I. F., Cummings, N. J., Daniel, R. A., Denizot, F., Devine, K. M., Dusterhoft, A., Ehrlich, S. D., Emmerson, P. T., Entian, K. D., Errington, J., Fabret, C., Ferrari, E., Foulger, D., Fritz, C., Fujita, M., Fujita, Y., Fuma, S., Galizzi, A., Galleron, N., Ghim, S. Y., Glaser, P., Goffeau, A., Golightly, E. J., Grandi, G., Guiseppi, G., Guy, B. J., Haga, K., Haiech, J., Harwood, C. R., Henaut, A., Hilbert, H., Holsappel, S., Hosono, S., Hullo, M. F., Itaya, M., Jones, L., Joris, B., Karamata, D., Kasahara, Y., KlaerrBlanchard, M., Klein, C., Kobayashi, Y., Koetter, P., Koningstein, G., Krogh, S., Kumano, M., Kurita, K., Lapidus, A., Lardinois, S., Lauber, J., Lazarevic, V., Lee, S. M., Levine, A., Liu, H., Masuda, S., Mauel, C., Medigue, C., Medina, N., Mellado, R. P., Mizuno, M., Moestl, D., Nakai, S., Noback, M., Noone, D., O'Reilly, M., Ogawa, K., Ogiwara, A., Oudega, B., Park, S. H., Parro, V., Pohl, T. M., Portetelle, D., Porwollik, S., Prescott, A. M., Presecan, E., Pujic, P., Purnelle, B., Rapoport, G., Rey, M., Reynolds, S., Rieger, M., Rivolta, C., Rocha, E., Roche, B., Rose, M., Sadaie, Y., Sato, T., Scanlan, E., Schleich, S., Schroeter, R., Scoffone, F., Sekiguchi, J., Sekowska, A., Seror, S. J., Serror, P., Shin, B. S., Soldo, B., Sorokin, A., Tacconi, E., Takagi, T., Takahashi, H., Takemaru, K., Takeuchi, M., Tamakoshi, A., Tanaka, T., Terpstra, P., Tognoni, A., Tosato, V., Uchiyama, S., Vandenbol, M., Vannier, F., Vassarotti, A., Viari, A., Wambutt, R., Wedler, E., Wedler, H., Weitzenegger, T., Winters, P., Wipat, A., Yamamoto, H., Yamane, K., Yasumoto, K., Yata, K., Yoshida, K., Yoshikawa, H. F., Zumstein, E., Yoshikawa, H., and Danchin, A. (1997) The complete genome sequence of the Gram-positive bacterium *Bacillus subtilis*. *Nature.* **390**, 249-256.

Lamb, D. C., Skaug, T., Song, H. L., Jackson, C. J., Podust, L. M., Waterman, M. R., Kell, D. B., Kelly, D. E., and Kelly, S. L. (2002) The cytochrome p450 complement (CYPome) of *Streptomyces coelicolor* A3(2). *Journal of Biological Chemistry.* **277**, 24000-24005.

Lamb, D., Kelly, D. and Kelly, S. (1999) Molecular aspects of azole antifungal action and resistance. *Drug Resist Updat.* **2**, 390-402.

Lawson, R. J., Leys, D., Sutcliffe, M. J., Kemp, C. A., Cheesman, M. R., Smith, S. J., Clarkson, J., Smith, W. E., Haq, I., Perkins, J. B. and Munro, A. W. (2004) Thermodynamic and biophysical characterization of cytochrome p450 BioI from *Bacillus subtilis*. *Biochemistry.* **43**, 12410-12426.

LeBrun L.A., Xu F.Y., Kroetz D.L., and de Montellano P.R.O (2002b) Covalent attachment of the heme prosthetic group in the CYP4F cytochrome p450 family. *Biochemistry* **41**, 5931-5937.

LeBrun, L. A., Hoch, U., and de Montellano, P. R. O. (2002a) Autocatalytic mechanism and consequences of covalent heme attachment in the cytochrome P4504A family. *Journal of Biological Chemistry* **277**, 12755-12761.

- Lee, D. S., Yamada, A., Sugimoto, H., Matsunaga, I., Ogura, H., Ichihara, K., Adachi, S., Park, S. Y., and Shiro, Y. (2003) Substrate recognition and molecular mechanism of fatty acid hydroxylation by cytochrome P450 from *Bacillus subtilis* - Crystallographic, spectroscopic, and mutational studies. *Journal of Biological Chemistry*. **278**, 9761-9767.
- Lees, J. G., Miles, A. J., Wien, F. and Wallace, B. A. (2006) A reference database for circular dichroism spectroscopy covering fold and secondary structure space. *Bioinformatics*. **22**, 1955-1962.
- Lemmon, M. A. (2003) Phosphoinositide recognition domains. *Traffic*. **4**, 201-213.
- Lett, C. M. and Guillemette, J. G. (2002) Increasing the redox potential of isoform 1 of yeast cytochrome c through the modification of select haem interactions. *Biochemical Journal*. **362**, 281-287.
- Lewin, A. and Sharbati-Tehrani, S. (2005) Slow growth rate of mycobacteria. Possible reasons and significance for their pathogenicity. *Bundesgesundheitsblatt, Gesundheitsforschung, Gesundheitsschutz*. **48**, 1390-1399.
- Lewis D.F.V. (1996) *Cytochrome P450 – Structure function and Mechanism* (Taylor and Francis, Basingstoke).
- Lewis, D. F. V. (2000) On the recognition of mammalian microsomal cytochrome P450 substrates and their characteristics - Towards the prediction of human P450 substrate specificity and metabolism. *Biochemical Pharmacology*. **60**, 293-306.
- Lewis, D. F. V., and Hlavica, P. (2000) Interactions between redox partners in various cytochrome P450 systems: functional and structural aspects. *Biochimica Et Biophysica Acta-Bioenergetics*. **1460**, 353-374.
- Lewis, D. F. V., Wiseman, A., and Tarbit, M. H. (1999) Molecular modelling of lanosterol 14 alpha-demethylase (CYP51) from *Saccharomyces cerevisiae* via homology with CYP102, a unique bacterial cytochrome P450 isoform: Quantitative structure-activity relationships (QSARs) within two related series of antifungal azole derivatives. *Journal of Enzyme Inhibition* **14**, 175-183.
- Lewis, D. F., Watson, E. and Lake, B. G. (1998) Evolution of the cytochrome P450 superfamily: sequence alignments and pharmacogenetics. *Mutat Res*. **410**, 245-270.
- Leys, D., Mowat, C. G., McLean, K. J., Richmond, A., Chapman, S. K., Walkinshaw, M. D., and Munro, A. W. (2003) Atomic structure of *Mycobacterium tuberculosis* CYP121 to 1.06 Å reveals novel features of cytochrome P450. *Journal of Biological Chemistry*. **278**, 5141-5147.
- Li, H. Y. and Poulos, T. L. (1997) The structure of the cytochrome P450BM-3 haem domain complexed with the fatty acid substrate, palmitoleic acid. *Nature Structural Biology*. **4**, 140-146.
- Li, X. Z. and Nikaido, H. (2004) Efflux-mediated drug resistance in bacteria. *Drugs*. **64**, 159-204
- Lipscomb, J. D. (1980) Electron paramagnetic resonance detectable states of cytochrome P-450cam. *Biochemistry*. **19**, 3590-3599.

- Liu, J., Rosenberg, E. Y. and Nikaido, H. (1995) Fluidity of the Lipid Domain of Cell-Wall from *Mycobacterium chelonae*. Proceedings of the National Academy of Sciences of the United States of America. **92**, 11254-11258.
- Loew G.H., and Harris D.L. (2000) Role of the heme active site and protein environment in structure, spectra and function of the cytochrome P450s, Chemical Reviews. **100**, 407-419.
- Lohr, F., Yalloway, G. N., Mayhew, S. G., and Ruterjans, H. (2004) Cofactor-apoprotein hydrogen bonding in oxidized and fully reduced flavodoxin monitored by trans-hydrogen-bond scalar couplings. Chembiochem. **5**, 1523-1534.
- Loida, P. J. and Sligar, S. G. (1993) Molecular Recognition in Cytochrome-P-450 - Mechanism for the Control of Uncoupling Reactions. Biochemistry **32**, 11530-11538.
- Lu, P., Alterman, M. A., Chaurasia, C. S., Bambal, R. B. and Hanzlik, R. P. (1997) Heme-coordinating analogs of lauric acid as inhibitors of fatty acid omega-hydroxylation. Archives of biochemistry and biophysics. **337**, 1-7.
- Ludemann, S. K., Lounnas, V. and Wade, R. C. (2000) How do substrates enter and products exit the buried active site of cytochrome P450cam? 1. Random expulsion molecular dynamics investigation of ligand access channels and mechanisms. J Mol Biol. **303**, 797-811.
- Macheroux P. (1999) UV-visible spectroscopy as a tool to measure flavoproteins in *Flavoprotein Protocols* (Chapman S.K., Reid G.A. eds.) 131, pp 1-7. Humana Press Inc. Totowa, New Jersey.
- Mansuy, D. (1998) The great diversity of reactions catalyzed by cytochromes P450. Comparative Biochemistry and Physiology C-Toxicology and Pharmacology. **121**, 5-14.
- Mansuy, D., and Renaud, J. (1995) Heme- thiolate proteins different from cytochromes P450 catalysing monooxygenations, in Cytochrome P450: Structure, mechanism and specificity (Ortiz de Montellano P.R., ed), Plenum press, New York. pp. 537-574.
- Marichal, P., Gorrens, J., and Vandenbossche, H. (1985) The Action of Itraconazole and Ketoconazole on Growth and Sterol Synthesis in *Aspergillus-Fumigatus* and *Aspergillus-Niger*. Sabouraudia-Journal of Medical and Veterinary Mycology. **23**, 13-21.
- Marinus, M. G. and Morris, N. R. (1973) Isolation of Deoxyribonucleic Acid Methylase Mutants of *Escherichia-Coli* K-12. Journal of Bacteriology. **114**, 1143-1150.
- Marsollier, L., Deniaux, E., Brodin, P., Marot, A., Wondje, C. M., Saint-Andre, J. P., Chauty, A., Johnson, C., Tekiaia, F., Yeramian, E., Legras, P., Carbonnelle, B., Reyssset, G., Eyangoh, S., Milon, G., Cole, S. T. and Aubry, J. (2007) Protection against *Mycobacterium ulcerans* lesion development by exposure to aquatic insect saliva. Plos Medicine. **4**, 288-296.
- Marsollier, L., Honore, N., Legras, P., Manceau, A. L., Kouakou, H., Carbonnelle, B., and Cole, S. T. (2003) Isolation of three *Mycobacterium ulcerans* strains resistant to rifampin after experimental chemotherapy of mice. Antimicrobial Agents and Chemotherapy. **47**, 1228-1232.
- Marsollier, L., Robert, R., Aubry, J., Saint Andre, J. P., Kouakou, H., Legras, P., Manceau, A. L., Mahaza, C., and Carbonnelle, B. (2002). Aquatic insects as a vector for *Mycobacterium ulcerans*. Appl Environ Microbiol. **68**, 4623-4628.

Marston, B. J., Diallo, M. O., Horsburgh, C. R., Jr., Diomande, I., Saki, M. Z., Kanga, J. M., Patrice, G., Lipman, H. B., Ostroff, S. M., and Good, R. C. (1995) Emergence of Buruli ulcer disease in the Daloa region of Cote d'Ivoire. *Am J Trop Med Hyg.* **52**, 219-224.

Martinis, S. A., Atkins, W. M., Stayton, P. S., and Sligar, S. G. (1989) A Conserved Residue of Cytochrome-P-450 Is Involved in Heme-Oxygen Stability and Activation. *Journal of the American Chemical Society.* **111**, 9252-9253.

Martinis, S. A., Blanke, S. R., Hager, L. P., Sligar, S. G., Hoa, G. H. B., Rux, J. J., and Dawson, J. H. (1996) Probing the heme iron coordination structure of pressure-induced cytochrome P420(cam). *Biochemistry.* **35**, 14530-14536.

Matsunaga, I., Yamada, A., Lee, D. S., Obayashi, E., Fujiwara, N., Kobayashi, K., Ogura, H. and Shiro, Y. (2002) Enzymatic reaction of hydrogen peroxide-dependent peroxxygenase cytochrome P450s: Kinetic deuterium isotope effects and analyses by resonance Raman spectroscopy. *Biochemistry.* **41**, 1886-1892.

Matsunaga, I., Yamada, M., Kusunose, E., Miki, T. and Ichihara, K. (1998) Further characterization of hydrogen peroxide dependent fatty acid alpha-hydroxylase from *Sphingomonas paucimobilis*. *Journal of Biochemistry.* **124**, 105-110.

Mazure, N., and Truffaut, N. (1994). Degradation of morpholine by *Mycobacterium aurum* MO1. *Can J Microbiol* **40**, 761-765.

McCarthy, A. A., Walsh, M. A., Verma, C. S., O'Connell, D. P., Reinhold, M., Yalloway, G. N., d'Arcy, D., Higgins, T. M., Voordouw, G., and Mayhew, S. G. (2002). Crystallographic investigation of the role of aspartate 95 in the modulation of the redox potentials of *Desulfovibrio vulgaris* flavodoxin. *Biochemistry.* **41**, 10950-10962.

McIver, L., Leadbeater, C., Campopiano, D. J., Baxter, R. L., Daff, S. N., Chapman, S. K., and Munro, A. W. (1998) Characterisation of flavodoxin NADP<sup>+</sup> oxidoreductase and flavodoxin: Key components of electron transfer in *Escherichia coli*. *Eur. J. Biochem.* **257**, 577-585.

McKinney, J. D., Honer zu Bentrup, K., Munoz-Elias, E. J., Miczak, A., Chen, B., Chan, W. T., Swenson, D., Sacchettini, J. C., Jacobs, W. R., Jr., and Russell, D. G. (2000). Persistence of *Mycobacterium tuberculosis* in macrophages and mice requires the glyoxylate shunt enzyme isocitrate lyase. *Nature.* **406**, 735-738.

Mcknight, J., Cheesman, M. R., Thomson, A. J., Miles, J. S. and Munro, A. W. (1993) Identification of Charge-Transfer Transitions in the Optical-Spectrum of Low-Spin Ferric Cytochrome-P-450 *Bacillus-Megaterium*. *European Journal of Biochemistry.* **213**, 683-687.

McLean, K. J., Cheesman, M. R., Rivers, S. L., Richmond, A., Leys, D., Chapman, S. K., Reid, G. A., Price, N. C., Kelly, S. M., Clarkson, J., Smith, W. E. and Munro, A. W. (2002a) Expression, purification and spectroscopic characterization of the cytochrome P450 CYP121 from *Mycobacterium tuberculosis*. *Journal of inorganic biochemistry.* **91**, 527-541.

McLean, K. J., Marshall, K. R., Richmond, A., Hunter, I. S., Fowler, K., Kieser, T., Gurcha, S. S., Besra, G. S. and Munro, A. W. (2002b) Azole antifungals are potent inhibitors of cytochrome P450 mono-oxygenases and bacterial growth in mycobacteria and streptomycetes. *Microbiology (Reading, England).* **148**, 2937-2949.

McLean, K. J., Warman, A. J., Seward, H. E., Marshall, K. R., Girvan, H. M., Cheesman, M. R., Waterman, M. R. and Munro, A. W. (2006) Biophysical characterization of the sterol demethylase P450 from *Mycobacterium tuberculosis*, its cognate ferredoxin, and their interactions. *Biochemistry*. **45**, 8427-8443.

McNeil, M., M. Daffe, and P. J. Brennan (1991) Location of the mycolyl ester substituent in the cell walls of mycobacteria. *Journal of Biology and Chemistry*. **266**, 13217-13223.

Mehareenna, Y. T., Li, H. Y., Hawkes, D. B., Pearson, A. G., De Voss, J., and Poulos, T. L. (2004) Crystal structure of P450cin in a complex with its substrate, 1,8-cineole, a close structural homologue to D-camphor, the substrate for P450cam. *Biochemistry*. **43**, 9487-9494.

Meletiadiis, J., Mouton, J. W., Rodriguez-Tudela, J. L., Meis, J. F. G. M. and Verweij, P. E. (2000) In vitro interaction of terbinafine with itraconazole against clinical isolates of *Scedosporium prolificans*. *Antimicrobial Agents and Chemotherapy*. **44**, 470-472.

Mercer, E. I. (1991) Sterol biosynthesis inhibitors: their current status and modes of action. *Lipids*. **26**, 584-597.

Mestdagh, M., Realini, L., Fonteyne, P. A., Rossau, R., Jannes, G., Mijs, W., KA, D. E. S., Portaels, F., and Van den Eeckhout, E. (2000) Correlation of *pncA* sequence with pyrazinamide resistance level in BACTEC for 21 *Mycobacterium tuberculosis* clinical isolates. *Microb Drug Resist*. **6**, 283-287.

Meyers, W. M., Shelly, W. M., Connor, D. H., and Meyers, E. K. (1974). Human *Mycobacterium-Ulcerans* Infections Developing at Sites of Trauma to Skin. *American Journal of Tropical Medicine and Hygiene*,. **23**, 919-923.

Miles, C. S., Ost, T. W. B., Noble, M. A., Munro, A. W., and Chapman, S. K. (2000) Protein engineering of cytochromes P-450. *Biochimica Et Biophysica Acta-Protein Structure and Molecular Enzymology*. **1543**, 383-407.

Miles, J. S., Munro, A. W., Rospendowski, B. N., Smith, W. E., McKnight, J. and Thomson, A. J. (1992) Domains of the catalytically self-sufficient cytochrome P-450 BM-3. Genetic construction, overexpression, purification and spectroscopic characterization. *The Biochemical Journal*. **288**, 503-509.

Miller, G. T., Zhang, B. L., Hardman, J. K. and Timkovich, R. (2000) Converting a c-type to a b-type cytochrome: Met61 to His61 mutant of *Pseudomonas* cytochrome c-551. *Biochemistry*. **39**, 9010-9017.

Minnikin, D. E., Minnikin, S. M., Goodfellow, M. and Stanford, J. L. (1982) The Mycolic Acids of *Mycobacterium chelonae*. *Journal of General Microbiology*. **128**, 817-822.

Mirvish, S. S., Salmasi, S., Cohen, S. M., Patil, K., and Mahboubi, E. (1983). Liver and Forestomach Tumors and Other Forestomach Lesions in Rats Treated with Morpholine and Sodium-Nitrite, with and without Sodium Ascorbate. *Journal of the National Cancer Institute*. **71**, 81-85.

- Misra, S., Miller, G. J. and Hurley, J. H. (2001) Recognizing phosphatidylinositol 3-phosphate. *Cell*. **107**, 559-562.
- Mitchison, D. A. (1992). Understanding the Chemotherapy of Tuberculosis - Current Problems. *Journal of Antimicrobial Chemotherapy*. **29**, 477-493.
- Mitchison, D. A. (2000). Role of individual drugs in the chemotherapy of tuberculosis. *Int J Tuberc Lung Dis*. **4**, 796-806.
- Mitchison, D. A., and Nunn, A. J. (1986). Influence of Initial-Drug Resistance on the Response to Short-Course Chemotherapy of Pulmonary Tuberculosis. *American Review of Respiratory Disease*. **133**, 423-430.
- Mitsukura, K., Kondo, Y., Yoshida, T. and Nagasawa, T. (2006) Regioselective hydroxylation of adamantane by *Streptomyces griseoplanus* cells. *Appl Microbiol Biotechnol* **71**, 502-504.
- Miyata, A., Hara, S., Yokoyama, C., Inoue, H., Ullrich, V., and Tanabe, T. (1994) Molecular-Cloning and Expression of Human Prostacyclin Synthase. *Biochemical and Biophysical Research Communications*. **200**, 1728-1734.
- Moazed, D., and Noller, H. F. (1987). Interaction of Antibiotics with Functional Sites in 16S Ribosomal-Rna. *Nature*. **327**, 389-394.
- Mohri, T. (1987). Dietary intakes of nitrosamines precursors. *Kyusha Yakugakki Katho*. **41**, 105-112.
- Moore, G. R., Pettigrew, G. W. and Rogers, N. K. (1986) Factors influencing redox potentials of electron transfer proteins. *Proc Natl Acad Sci U S A*. **83**, 4998-4999.
- Mueller E.J., Loida P.J., and Sligar S.G. (1995) Twenty-five years of P450cam research: mechanistic insights into oxygenase catalysis, in *Cytochrome P450: Structure, mechanism and specificity* (Ortiz de Montellano P.R., ed), Plenum press, New York. pp. 83-124.
- Mukherjee, J. S., Rich, M. L., Socci, A. R., Joseph, J. K., Viru, F. A., Shin, S. S., Furin, J. J., Becerra, M. C., Barry, D. J., Kim, J. Y., Bayona, J., Farmer, P., Smith Fawzi, M. C., and Seung, K. J. (2004) Programmes and principles in treatment of multidrug-resistant tuberculosis. *Lancet*. **363**, 474-481.
- Munro A.W., Kelly S.M., Price N.C. (1999) Circular dichroism studies of flavoproteins, in *Methods in Enzymology 131: Flavoproteins protocols* (Chapman S.K., Reid G.A., ed), Humana Press Inc, Totowa, NJ.
- Munro A.W., Noble M.A., Ost T.W.B., Green A.J., McLean K.J., Robledo L., Miles C.S., Murdoch J., and Chapman S.K. (2000) Flavocytochrome P450 BM-3 – substrate selectivity and electron transfer in a model cytochrome P450, *Subcellular Biochemistry* **35**: Enzyme catalysed electron and radical transfer (ed. Holzenburg and Scrutton) Plenum publishers, New York.
- Munro, A. W., and Lindsay, J. G. (1996) Bacterial cytochromes P-450. *Molecular Microbiology*. **20**, 1115-1125.

Munro, A. W., Lindsay, J. G., Coggins, J. R., Kelly, S. M. and Price, N. C. (1995) NADPH oxidase activity of cytochrome P-450 BM3 and its constituent reductase domain. *Biochimica et biophysica acta*. **1231**, 255-264.

Munro, A. W., Noble, M. A., Miles, C. S., Daff, S. N., Green, A. J., Quaroni, L., Rivers, S., Ost, T. W., Reid, G. A. and Chapman, S. K. (1999) Flavocytochrome P-450 BM3: a paradigm for the analysis of electron transfer and its control in the P-450s. *Biochem Soc Trans*. **27**, 190-196.

Munro, A.W., Noble, M.A., Robledo, L., Daff, S.N. and Chapman, S.K. (2001). Determination of the redox properties of human NADPH-cytochrome P450 reductase. *Biochemistry*. **40**, 1956-1963.

Murray, J. F. (1998) Tuberculosis and HIV infection: a global perspective. *Respiration*. **65**, 335-342.

Musser, J. M., Kapur, V., Williams, D. L., Kreiswirth, B. N., vanSoolingen, D., and vanEmbden, J. D. A. (1996). Characterization of the catalase-peroxidase gene (*katG*) and *inhA* locus in isoniazid-resistant and -susceptible strains of *Mycobacterium tuberculosis* by automated DNA sequencing: Restricted array of mutations associated with drug resistance. *Journal of Infectious Diseases*. **173**, 196-202.

Mve-Obiang, A., Lee, R. E., Portaels, F., and Small, P. L. (2003) Heterogeneity of mycolactones produced by clinical isolates of *Mycobacterium ulcerans*: implications for virulence. *Infect Immun*. **71**, 774-783.

Mve-Obiang, A., Lee, R. E., Umstot, E. S., Trott, K. A., Grammer, T. C., Parker, J. M., Ranger, B. S., Grainger, R., Mahrous, E. A., and Small, P. L. (2005) A newly discovered mycobacterial pathogen isolated from laboratory colonies of *Xenopus* species with lethal infections produces a novel form of mycolactone, the *Mycobacterium ulcerans* macrolide toxin. *Infect Immun*. **73**, 3307-3312.

Myer, Y. P., and Pande, A. J. (1978). In *The Porphyrins* (Dolphin, D., ed.), Academic Press, New York, Vol. 3, pp. 271–322.

Nagano, S., Li, H. Y., Shimizu, H., Nishida, C., Ogura, H., de Montellano, P. R. O. and Poulos, T. L. (2003) Crystal structures of epothilone D-bound, epothilone B-bound, and substrate-free forms of cytochrome P450epoK. *Journal of Biological Chemistry*. **278**, 44886-44893.

Narhi, L. O., and Fulco, A. J. (1986) Characterization of a Catalytically Self-Sufficient 119,000-Dalton Cytochrome-P-450 Monooxygenase Induced by Barbiturates in *Bacillus-Megaterium*. *Journal of Biological Chemistry*. **261**, 7160-7169.

Narhi, L. O., and Fulco, A. J. (1987). Identification and Characterization of 2 Functional Domains in Cytochrome-P-450Bm-3, a Catalytically Self-Sufficient Monooxygenase Induced by Barbiturates in *Bacillus-Megaterium*. *Journal of Biological Chemistry*. **262**, 6683-6690.

Nebert, D. W., and Gonzalez, F. J. (1987) P450 Genes - Structure, Evolution, and Regulation. *Annual Review of Biochemistry*. **56**, 945-993.

Negishi, M., Uno, T., Darden, T. A., Sueyoshi, T. and Pedersen, L. G. (1996) Structural flexibility and functional versatility of mammalian P450 enzymes. *Faseb J*. **10**, 683-689



- Newcomb, M., Shen, R. N., Lu, Y., Coon, M. J., Hollenberg, P. F., Kopp, D. A., and Lippard, S. J. (2002) Evaluation of norcarane as a probe for radicals in cytochrome P450-and soluble methane monooxygenase-catalyzed hydroxylation reactions. *Journal of the American Chemical Society* **124**, 6879-6886.
- Nguyen, M., Claparols, C., Bernadou, J., and Meunier, B. (2001) A fast and efficient metal-mediated oxidation of isoniazid and identification of isoniazid - NAD(H) adducts. *Chembiochem.* **2**, 877-883.
- Niederweis, M. (2003) Mycobacterial porins--new channel proteins in unique outer membranes. *Mol Microbiol.* **49**, 1167-1177.
- Nigou, M., Gilleron, M., and Puzo, G. (2003) Lipoarabinomannans: from structure to biosynthesis. *Biochimie.* **85**, 153-166.
- Nikaido, H. (2001) Preventing drug access to targets: cell surface permeability barriers and active efflux in bacteria. *Seminars in cell and developmental biology.* **12**, 215-223.
- Noble, M. A., Miles, C. S., Chapman, S. K., Lysek, D. A., Mackay, A. C., Reid, G. A., Hanzlik, R. P., and Munro, A. W. (1999). Roles of key active-site residues in flavocytochrome P450 BM3. *Biochemical Journal* **339**, 371-379.
- Noble, M. A., Quaroni, L., Chumanov, G. D., Turner, K. L., Chapman, S. K., Hanzlik, R. P., and Munro, A. W. (1998). Imidazolyl carboxylic acids as mechanistic probes of flavocytochrome P-450 BM3. *Biochemistry.* **37**, 15799-15807.
- Nogues, I., Campos, L. A., Sancho, J., Gomez-Moreno, C., Mayhew, S. G., and Medina, M. (2004) Role of neighboring FMN side chains in the modulation of flavin reduction Potentials and in the energetics of the FMN: Apoprotein interaction in *Anabaena* flavodoxin. *Biochemistry.* **43**, 15111-15121.
- O'Brien, R. J. and Vernon, A. A. (1998) New tuberculosis drug development - How can we do better? *American Journal of Respiratory and Critical Care Medicine.* **157**, 1705-1707.
- O'Brien, R. J., and Nunn, P. P. (2001) The need for new drugs against tuberculosis. Obstacles, opportunities, and next steps. *American Journal of Respiratory and Critical Care Medicine.* **163**, 1055-1058.
- Odds, F. C., Brown, A. J. P., and Gow, N. A. R. (2003) Antifungal agents: mechanisms of action. *Trends in Microbiology.* **11**, 272-279.
- Odigwe, C. (2004) Drug resistant tuberculosis soars in eastern Europe. *British Medical Journal.* **328**, 663.
- O'Farrell, P. A., Walsh, M. A., McCarthy, A. A., Higgins, T. M., Voordouw, G., and Mayhew, S. G. (1998) Modulation of the redox potentials of FMN in *Desulfovibrio vulgaris* flavodoxin: Thermodynamic properties and crystal structures of glycine-61 mutants. *Biochemistry.* **37**, 8405-8416.

- Ogura, H., Nishida, C. R., Hoch, U. R., Perera, R., Dawson, J. H. and Ortiz de Montellano, P. R. (2004) EpoK, a cytochrome P450 involved in biosynthesis of the anticancer agents epothilones A and B. Substrate-mediated rescue of a P450 enzyme. *Biochemistry*. **43**, 14712-14721.
- Oku, Y., Ohtaki, A., Kamitori, S., Nakamura, N., Yohda, M., Ohno, H. and Kawarabayasi, Y. (2004) Structure and direct electrochemistry of cytochrome P450 from the thermoacidophilic crenarchaeon, *Sulfolobus tokodaii* strain 7. *J Inorg Biochem*. **98**, 1194-1199.
- Omura, T. (1999) Forty years of cytochrome P450. *Biochemical and Biophysical Research Communications*. **266**, 690-698.
- Omura, T., and Sato, R. (1962) A New Cytochrome in Liver Microsomes. *Journal of Biological Chemistry*. **237**, 1375-1376.
- Omura, T., and Sato, R. (1964) Carbon Monoxide-Binding Pigment of Liver Microsomes.I. Evidence for Its Hemoprotein Nature. *Journal of Biological Chemistry*. **239**, 2370-2378.
- Ortiz de Montellano P.R., and Corriereia M.A. (1995) Inhibition of cytochrome P450 enzymes, in *Cytochrome P450: Structure, mechanism and specificity* (Ortiz de Montellano P.R., ed), Plenum press, New York. pp. 305-366.
- Ost, T. W. B., Miles, C. S., Munro, A. W., Murdoch, J., Reid, G. A., and Chapman, S. K. (2001a) Phenylalanine 393 exerts thermodynamic control over the heme of flavocytochrome P450BM3. *Biochemistry*. **40**, 13421-13429.
- Ost, T. W., Munro, A. W., Mowat, C. G., Taylor, P. R., Pessegueiro, A., Fulco, A. J., Cho, A. K., Cheesman, M. A., Walkinshaw, M. D. and Chapman, S. K. (2001b) Structural and spectroscopic analysis of the F393H mutant of flavocytochrome P450 BM3. *Biochemistry*. **40**, 13430-13438.
- Pablos-Mendez, A., Sterling, T. R., and Frieden, T. R. (1996) The relationship between delayed or incomplete treatment and all-cause mortality in patients with tuberculosis. *Jama*. **276**, 1223-1228.
- Palomino, J. C., and F., Portaels (1998) Effects of decontamination methods and culture conditions on viability of *Mycobacterium ulcerans* in the BACTEC system. *J Clin Microbiol*. **36**, 402-8.
- Park S., Shimizu H., Adachi S., Shuro Y, Nakagawa A., Tanaka I., Sloun H., Hori H (1997) Crystallisation and preliminary diffraction and electron paramagnetic resonance studies of a single crystal of cytochrome P450 nor, *FEBS Letters*. **412**, 346-5.
- Park S.Y., Yamane K., Adachiis S., Shiro Y., Weis K.E.,Sligar S.G. (2000) Crystallisation and preliminary X-ray diffraction analysis of a cytochrome P450 (CYP119) form *Solfolobus solfataricus*, *ACTA crystallographica D*. **56** , 1173-1175.
- Park, M. M., Davis, A. L., Schluger, N. W., Cohen, H., and Rom, W. N. (1996). Outcome of MDR-TB patients, 1983-1993 - Prolonged survival with appropriate therapy. *American Journal of Respiratory and Critical Care Medicine*. **153**, 317-324.

Parthasarathi, N., Hansen, C., Yamaguchi, S. and Spiro, T. G. (1987) Metalloporphyrin Core Size Resonance Raman Marker Bands Revisited - Implications for the Interpretation of Hemoglobin Photoproduct Raman Frequencies. *Journal of the American Chemical Society*. **109**, 3865-3871.

Patterson, J. H., McConville, M. J., Haites, R. E., Coppel, R. L. and Billman-Jacobe, H. (2000) Identification of a methyltransferase from *Mycobacterium smegmatis* involved in glycopeptidolipid synthesis. *Journal of Biological Chemistry*. **275**, 24900-24906

Perera R., Sono M., Sigman J.A, Pfister J.A, Lu Y., and Dawson J.H. (2003) Neutral thiol as a proximal ligands to ferrous heme iron: Implications for heme proteins that lose cysteine thiolate ligation on reduction, *PNACL*. **100**, 3641-3646.

Peterson J.A., Graham S.E. (1995) Bacterial P450s: structural similarities and functional differenced, in *Cytochrome P450: Structure, mechanism and specificity* (Ortiz de Montellano P.R., ed.), Plenum press, New York. pp 151-182.

Peterson, D. O., and Bloch, K. (1977). *Mycobacterium-Smegmatis Fatty-Acid Synthetase - Long-Chain Transacylase Chain-Length Specificity*. *Journal of Biological Chemistry*. **252**, 5735-5739.

Peterson, J. A., and Graham, S. E. (1998) A close family resemblance: the importance of structure in understanding cytochromes P450. *Structure with Folding and Design*. **6**, 1079-1085.

Pfaller, M. A., Riley, J. and Koerner, T. (1990) Effects of Terconazole and Other Azole Antifungal Agents on the Sterol and Carbohydrate-Composition of *Candida-Albicans*. *Diagnostic Microbiology and Infectious Disease*. **13**, 31-35.

Pfyffer, G. E., Palicova, F. and Rusch-Gerdes, S. (2002) Testing of susceptibility of *Mycobacterium tuberculosis* to pyrazinamide with the nonradiometric BACTEC MGIT 960 system. *Journal of Clinical Microbiology*. **40**, 1670-1674.

Piatek, A. S., Telenti, A., Murray, M. R., El-Hajj, H., Jacobs, W. R., Kramer, F. R., and Alland, D. (2000) Genotypic analysis of *Mycobacterium tuberculosis* in two distinct populations using molecular beacons: Implications for rapid susceptibility testing. *Antimicrobial Agents and Chemotherapy*. **44**, 103-110.

Pieper, D. H., and Reineke, W. (2000) Engineering bacteria for bioremediation. *Curr Opin Biotechnol*. **11**, 262-270.

Podust L.M., Kim Y., Arase M., Neely B.A., Beck B.J., Bach H., Sherman D.H., Lamb D.C., Kelly S.L., Waterman M.R. (2003) The 1.92-angstrom structure of *Streptomyces coelicolor* A3(2) CYP154C1 - A new monooxygenase that functionalizes macrolide ring systems *Journal of Biological Chemistry*. **278**, 12214-12221.

Podust L.M., Poulos T.L., Waterman M.R. (2001) Crystal structure of cytochrome P450 14 alpha-sterol demethylase (CYP51) from *Mycobacterium tuberculosis* in complex with azole inhibitors, *Proceedings of the National Academy of Sciences. USA*. **98**, 3068-3073.

Podust, L. M., Kim, Y., Arase, M., Neely, B. A., Beck, B. J., Bach, H., Sherman, D. H., Lamb, D. C., Kelly, S. L., and Waterman, M. R. (2003) The 1.92-angstrom structure of *Streptomyces coelicolor* A3(2) CYP154C1 - A new monooxygenase that functionalizes macrolide ring systems. *Journal of Biological Chemistry*. **278**, 12214-12221.

- Podust, L. M., Poulos, T. L. and Waterman, M. R. (2001) Crystal structure of cytochrome P450 14alpha -sterol demethylase (CYP51) from *Mycobacterium tuberculosis* in complex with azole inhibitors. *Proceedings of the National Academy of Sciences of the United States of America*. **98**, 3068-3073.
- Poelarends, G. J., Zandstra, M., Bosma, T., Kulakov, L. A., Larkin, M. J., Marchesi, J. R., Weightman, A. J. and Janssen, D. B. (2000) Haloalkane-utilizing *Rhodococcus* strains isolated from geographically distinct locations possess a highly conserved gene cluster encoding haloalkane catabolism. *J Bacteriol* **182**, 2725-2731.
- Polous T.L., Cupp-Vickery J., and Li H. (1995) Structural studies on prokaryotic cytochromes P450, in *Cytochrome P450: Structure, mechanism and specificity* (Ortiz de Montellano P.R., ed.), Plenum press, New York. pp 125-150.
- Portaels, F. (1995) Epidemiology of Mycobacterial Diseases. *Clinics in Dermatology*. **13**, 207-222.
- Portaels, F., Aguiar, J., Debacker, M., Steunou, C., Zinsou, C., Guedenon, A., and Meyers, W. M. (2002). Prophylactic effect of mycobacterium bovis BCG vaccination against osteomyelitis in children with *Mycobacterium ulcerans* disease (Buruli Ulcer). *Clin Diagn Lab Immunol* **9**, 1389-1391.
- Portaels, F., Chemlal, K., Elsen, P., Johnson, P. D., Hayman, J. A., Hibble, J., Kirkwood, R., and Meyers, W. M. (2001) *Mycobacterium ulcerans* in wild animals. *Rev Sci Tech*. **20**, 252-264.
- Portaels, F., Elsen, P., Guimaraes-Peres, A., Fonteyne, P. A., and Meyers, W. M. (1999) Insects in the transmission of *Mycobacterium ulcerans* infection. *Lancet*. **353**, 986.
- Portaels, F., Fonteyne, P. A., de Beenhouwer, H., de Rijk, P., Guedenon, A., Hayman, J., and Meyers, W. M. (1996). Variability in 3' end of 16S rRNA sequence of *Mycobacterium ulcerans* is related to geographic origin of isolates. *J Clin Microbiol*. **34**, 962-965.
- Portaels, F., Traore, H., De Ridder, K., and Meyers, W. M. (1998) In vitro susceptibility of *Mycobacterium ulcerans* to clarithromycin. *Antimicrob Agents Chemother*. **42**, 2070-2073.
- Porter, T. D., and Coon, M. J. (1991) Cytochrome-P-450 - Multiplicity of Isoforms, Substrates, and Catalytic and Regulatory Mechanisms. *Journal of Biological Chemistry*. **266**, 13469-13472.
- Poulos T. L., and Finzel B. C., (1984). Heme enzyme structure and function. *Peptide and Protein Review*. **4**, 115-171.
- Poulos, T. L., Finzel, B. C., and Howard, A. J. (1987) High-Resolution Crystal-Structure of Cytochrome-P450Cam. *Journal of Molecular Biology*. **195**, 687-700.
- Poupin, P., Ducrocq, V., Hallier-Soulier, S., and Truffaut, N. (1999). Cloning and characterization of the genes encoding a cytochrome P450 (PipA) involved in piperidine and pyrrolidine utilization and its regulatory protein (PipR) in *Mycobacterium smegmatis* mc(2)155. *Journal of Bacteriology*. **181**, 3419-3426.

- Poupin, P., Truffaut, N., Combourieu, B., Besse, P., Sancelme, M., Veschambre, H., and Delort, A. M. (1998). Degradation of morpholine by an environmental Mycobacterium strain involves a cytochrome P-450. *Appl Environ Microbiol.* **64**, 159-165.
- Presnell, S. R. and Cohen, F. E. (1989) Topological distribution of four-alpha-helix bundles. *Proc Natl Acad Sci U S A.* **86**, 6592-6596.
- Prinzis, S., Chatterjee, D., and Brennan, P. J. (1993) Structure and Antigenicity of Lipoarabinomannan from Mycobacterium-Bovis Bcg. *Journal of General Microbiology.* **139**, 2649-2658.
- Pylypenko, O. and Schlichting, I. (2004) Structural aspects of ligand binding to and electron transfer in bacterial and fungal P450s. *Annu Rev Biochem.* **73**, 991-1018.
- Pylypenko, O., Vitali, F., Zerbe, K., Robinson, J. A. and Schlichting, I. (2003) Crystal structure of OxyC, a cytochrome P450 implicated in an oxidative C-C coupling reaction during vancomycin biosynthesis. *Journal of Biological Chemistry.* **278**, 46727-46733.
- Quijcho, F. A., Wilson, D. K. and Vyas, N. K. (1989) Substrate-Specificity and Affinity of a Protein Modulated by Bound Water-Molecules. *Nature.* **340**, 404-407.
- Raghunathan, P. L., Whitney, E. A., Asamoah, K., Stienstra, Y., Taylor, T. H., Jr., Amofah, G. K., Ofori-Adjei, D., Dobos, K., Guarner, J., Martin, S., Pathak, S., Klutse, E., Etuafu, S., van der Graaf, W. T., van der Werf, T. S., King, C. H., Tappero, J. W., and Ashford, D. A. (2005) Risk factors for Buruli ulcer disease (*Mycobacterium ulcerans* Infection): results from a case-control study in Ghana. *Clin Infect Dis.* **40**, 1445-1453.
- Raman, C. S., Martasek, P., and Masters, B. S. (2000) in *The Porphyrin Handbook* (Kadish, K. M., Smith, K. M., and Guillard, R., eds) Vol. 4, pp. 293-339, Academic Press, New York.
- Ramaswamy S. and Musser J. M. (1998) Molecular genetic basis of antimicrobial agent resistance in *Mycobacterium tuberculosis*: 1998 update. *Tuber Lung Dis.* **79**, 3-29.
- Ramaswamy, S. V., Reich, R., Dou, S. J., Jasperse, L., Pan, X., Wanger, A., Quitugua, T., and Graviss, E. A. (2003) Single nucleotide polymorphisms in genes associated with isoniazid resistance in *Mycobacterium tuberculosis*. *Antimicrobial Agents and Chemotherapy.* **47**, 1241-1250.
- Ratledge, C. and Dover, L. G. (2000) Iron metabolism in pathogenic bacteria. *Annual review of microbiology.* **54**, 881-941.
- Rattan, A., Kalia, A., and Ahmad, N. (1998). Multidrug-resistant *Mycobacterium tuberculosis*: molecular perspectives. *Emerg Infect Dis.* **4**, 195-209.
- Ravichandran, K. G., Boddupalli, S. S., Hasemann, C. A., Peterson, J. A., and Deisenhofer, J. (1993) Crystal-Structure of the Hemoprotein Domain of P450 Bm-3, a Prototype for Class-II P450s. *Biophysical Journal.* **64**, A350-a350.
- Raynaud, C., Laneelle, M. A., Senaratne, R. H., Draper, P., Laneelle, G., and Daffe, M. (1999). Mechanisms of pyrazinamide resistance in mycobacteria: importance of lack of uptake in addition to lack of pyrazinamidase activity. *Microbiology* **145**, 1359-1367.

- Rees, D. C. (2002) Great metalloclusters in enzymology. *Annual Review of Biochemistry*. **71**, 221-246.
- Reipa, V., Mayhew, M. P., and Vilker, V. L. (1997) A direct electrode-driven P450 cycle for biocatalysis. *Proceedings of the National Academy of Sciences of the United States of America*. **94**, 13554-13558.
- Renner, M. W., Barkigia, K. M., Zhang, Y., Medforth, C. J., Smith, K. M. and Fajer, J. (1994) Consequences of Oxidation in Nonplanar Porphyrins - Molecular-Structure and Diamagnetism of the Pi-Cation-Radical of Copper(II) Octaethyltetraphenylporphyrin. *Journal of the American Chemical Society*. **116**, 8582-8592.
- Ribi, E., Granger, D. L., Milner, K. C., Yamamoto, K., Strain, S. M., Parker, R., Smith, R. W., Brehmer, W., and Azuma, I. (1982). Induction of Resistance to Tuberculosis in Mice with Defined Components of Mycobacteria and with Some Unrelated Materials. *Immunology* **46**, 297-305.
- Roberts, G. A., Grogan, G., Greter, A., Flitsch, S. L., and Turner, N. J. (2002) Identification of a new class of cytochrome P450 from a *Rhodococcus* sp. *Journal of Bacteriology*. **184**, 3898-3908.
- Rospendowski, B. N., Kelly, K., Wolf, C. R. and Smith, W. E. (1991) Surface-Enhanced Resonance Raman-Scattering from Cytochromes-P-450 Adsorbed on Citrate-Reduced Silver Sols. *Journal of the American Chemical Society* **113**, 1217-1225.
- Ross, B. C., Johnson, P. D., Oppedisano, F., Marino, L., Sievers, A., Stinear, T., Hayman, J. A., Veitch, M. G., and Robins-Browne, R. M. (1997). Detection of *Mycobacterium ulcerans* in environmental samples during an outbreak of ulcerative disease. *Appl Environ Microbiol*. **63**, 4135-4138.
- Rouse, D. A., DeVito, J. A., Li, Z. M., Byer, H., and Morris, S. L. (1996) Site-directed mutagenesis of the *katG* gene of *Mycobacterium tuberculosis*: Effects on catalase-peroxidase activities and isoniazid resistance. *Molecular Microbiology*. **22**, 583-592.
- Rousseau D.L., and Friedman J.M, Williams I.T. (1979) Resonance Raman spectroscopy, *Topics in Current Physics*. **2**, 203-210.
- Rowland, P., Blaney, F. E., Smyth, M. G., Jones, J. J., Leydon, V. R., Oxbrow, A. K., Lewis, C. J., Tennant, M. G., Modi, S., Eggleston, D. S., Chenery, R. J. and Bridges, A. M. (2006) Crystal structure of human cytochrome P450 2D6. *Journal of Biological Chemistry*. **281**, 7614-7622.
- Rozman, D., and Waterman, M. R. (1998) Lanosterol 14 alpha-demethylase (CYP51) and spermatogenesis. *Drug Metabolism and Disposition*. **26**, 1199-1201.
- Roy, J. N., Mishra, K. C., Mishra, S. K., and Das, T. P. (1989) Variational theory for g tensor in electron paramagnetic resonance experiments: application to ferricytochrome c and azidomyoglobin. *Journal of Physical Chemistry* **93**, 194-200.
- Rozwarski, D. A., Grant, G. A., Barton, D. H. R., Jacobs, W. R., and Sacchettini, J. C. (1998). Modification of the NADH of the isoniazid target (InhA) from *Mycobacterium tuberculosis*. *Science*. **279**, 98-102.

- Rux, J. J., and Dawson, J. H. (1991) Magnetic Circular-Dichroism Spectroscopy as a Probe of Axial Heme Ligand Replacement in Semisynthetic Mutants of Cytochrome-C. *Febs Letters*. **290**, 49-51.
- Rylott, E. L., Jackson, R. G., Edwards, J., Womack, G. L., Seth-Smith, H. M. B., Rathbone, D. A., Strand, S. E. and Bruce, N. C. (2006) An explosive-degrading cytochrome P450 activity and its targeted application for the phytoremediation of RDX. *Nature Biotechnology*. **24**, 216-219.
- Saita, N., Fujiwara, N., Yano, I., Soejima, K., and Kobayashi, K. (2000). Trehalose 6,6 '-dimycolate (cord factor) of *Mycobacterium tuberculosis* induces corneal angiogenesis in rats. *Infection and Immunity*. **68**, 5991-5997.
- Sakaguchi, I., Ikeda, N., Nakayama, M., Kato, Y., Yano, I., and Kaneda, K. (2000) Trehalose 6,6 '-dimycolate (cord factor) enhances neovascularization through vascular endothelial growth factor production by neutrophils and macrophages. *Infection and Immunity*. **68**, 2043-2052.
- Salerno, J. C., Frey, C., McMillan, K., Williams, R. F., Masters, B. S. and Griffith, O. W. (1995) Characterization by electron paramagnetic resonance of the interactions of L-arginine and L-thiocitrulline with the heme cofactor region of nitric oxide synthase. *The Journal of biological chemistry*. **270**, 27423-27428.
- Sambrook J., Fritsch E.F., and Maniatis T. (Eds) (1989) *Molecular Cloning, a laboratory manual*, 2<sup>nd</sup> Edition, Cold Spring Harbor Laboratory Press.
- Sanati, H., Belanger, P., Fratti, R., and Ghannoum, M. (1997) A new triazole, voriconazole (UK-109,496), blocks sterol biosynthesis in *Candida albicans* and *Candida krusei*. *Antimicrobial Agents and Chemotherapy* **41**, 2492-2496.
- Sancho J. (2006) Flavodoxins: sequence, folding, binding, function and beyond. *Cell Mol Life Sci* **63**, 855-64.
- Sanger, F., Nicklen, S. and Coulson, A. R. (1977) DNA sequencing with chain-terminating inhibitors. *Proceedings of the National Academy of Sciences of the United States of America*. **74**, 5463-5467.
- Schalk, M. and Croteau, R. (2000) A single amino acid substitution (F363I) converts the regiochemistry of the spearmint (-)-limonene hydroxylase from a C6- to a C3-hydroxylase. *Proc Natl Acad Sci U S A*. **97**, 11948-11953.
- Schatz, A., Bugie, E. and Waksman, S. A. (2005) Streptomycin, a substance exhibiting antibiotic activity against gram-positive and gram-negative bacteria. 1944. *Clinical orthopaedics and related research*, 3-6.
- Schatz, A., Bugie, E., and Waksman, S. A. (2005) Streptomycin, a substance exhibiting antibiotic activity against gram-positive and gram-negative bacteria. 1944. *Clin Orthop Relat Res*. **437**, 3-6.
- Schluger, N. W. (2005) The pathogenesis of tuberculosis - The first one hundred (and twenty-three) years. *American Journal of Respiratory Cell and Molecular Biology*. **32**, 251-256.
- Schmid, A., Dordick, J. S., Hauer, B., Kiener, A., Wubbolts, M., and Witholt, B. (2001). Industrial biocatalysis today and tomorrow. *Nature*. **409**, 258-268.

Schneider, Z. (1980) Aliphatic alcohols improve the adsorptive performance of cellulose nitrate membranes--application in chromatography and enzyme assays. *Analytical biochemistry*. **108**, 96-103.

Schoch, G. A., Attias, R., Belghazi, M., Dansette, P. M. and Werck-Reichhart, D. (2003) Engineering of a water-soluble plant cytochrome P450, CYP73A1, and NMR-based orientation of natural and alternate substrates in the active site. *Plant Physiology*. **133**, 1198-1208.

Schrader, T., Schuffenhauer, G., Sielaff, B., and Andreesen, J. R. (2000) High morpholine degradation rates and formation of cytochrome P450 during growth on different cyclic amines by newly isolated *Mycobacterium* sp strain HE5. *Microbiology-Uk* **146**, 1091-1098.

Schroeder, E. K., de Souza, N., Santos, D. S., Blanchard, J. S. and Basso, L. A. (2002) Drugs that inhibit mycolic acid biosynthesis in *Mycobacterium tuberculosis*. *Current pharmaceutical biotechnology*. **3**, 197-225.

Scior, T., Meneses Morales, I., Garces Eisele, S. J., Domeyer, D., and Laufer, S. (2002) Antitubercular isoniazid and drug resistance of *Mycobacterium tuberculosis*--a review. *Arch Pharm (Weinheim)*. **335**, 511-525.

Schlichting I., BenendzenJ., Chu K., Stock A.M., Maves S.A., Beson D.E., Sweet R.M., Ringe D., PetskoG.A., and Sligar S.G. (2000) The catalytic pathway of cytochrome P450cam at atomic resolution, *Science*. **287**, 1615-1622.

Scorpio, A., and Zhang, Y. (1996) Mutations in *pncA*, a gene encoding pyrazinamidase/nicotinamidase, cause resistance to the antituberculous drug pyrazinamide in tubercle bacillus. *Nature Medicine*. **2**, 662-667.

Seward, H. E., Roujeinikova, A., McLean, K. J., Munro, A. W. and Leys, D. (2006) Crystal structure of the *Mycobacterium tuberculosis* P450 CYP121-fluconazole complex reveals newazole drug-P450 binding mode. *J Biol Chem*. **281**, 39437-39443.

Sharrock, M., Munck, E., Debrunner, P. G., Marshall, V., Lipscomb, J. D. and Gunsalus, I. C. (1973) Mossbauer studies of cytochrome P-450 cam. *Biochemistry*. **12**, 258-265.

Shelnutt, J. A., Song, X. Z., Ma, J. G., Jia, S. L., Jentzen, W. and Medforth, C. J. (1998) Nonplanar porphyrins and their significance in proteins. *Chemical Society Reviews*. **27**, 31-41.

Shimizu, T., Iizuka, T., Mitani, F., Ishimura, Y., Nozawa, T., and Hatano, M. (1981) Magnetic and Natural Circular-Dichroism Spectra of Cytochromes P-45011-Beta and P-450scc Purified from Bovine Adrenal-Cortex. *Biochimica et Biophysica Acta*, **669**, 46-59.

Shimizu, T., Iizuka, T., Shimada, H., Ishimura, Y., Nozawa, T. and Hatano, M. (1981) Magnetic Circular-Dichroism Studies of Cytochrome P-450cam Characterization of Axial Ligands of Ferric and Ferrous Low-Spin Complexes. *Biochimica et biophysica acta*. **670**, 341-354.

Siddiqi SH. BACTEC 460 TB System. Product and Procedure Manual. MA-0029. Sparks, Md: Becton Dickinson Diagnostic Instrument Systems; 1995.



Siddiqi, S. H., Hawkins, J. E. and Laszlo, A. (1985) Interlaboratory Drug Susceptibility Testing of Mycobacterium-Tuberculosis by a Radiometric Procedure and 2 Conventional Methods. *Journal of Clinical Microbiology*. **22**, 919-923.

Siddiqi, S. H., Libonati, J. P. and Middlebrook, G. (1981) Evaluation of a Rapid Radiometric Method for Drug Susceptibility Testing of Mycobacterium-Tuberculosis. *Journal of Clinical Microbiology*. **13**, 908-912.

Sielaff, B., and Andreessen, J. R. (2005a). Kinetic and binding studies with purified recombinant proteins ferredoxin reductase, ferredoxin and cytochrome P450 comprising the morpholine monooxygenase from Mycobacterium sp. strain HE5. *Febs Journal*. **272**, 1148-1159.

Sielaff, B., and Andreessen, J. R. (2005b). Analysis of the nearly identical morpholine monooxygenase-encoding *mor* genes from different Mycobacterium strains and characterization of the specific NADH: ferredoxin oxidoreductase of this cytochrome P450 system. *Microbiology*. **151**, 2593-2603.

Sielaff, B., Andreessen, J. R., and Schrader, T. (2001). A cytochrome P450 and a ferredoxin isolated from Mycobacterium sp. strain HE5 after growth on morpholine. *Appl Microbiol Biotechnol*. **56**, 458-464.

Sigman, J. A., Pond, A., Dawson, J. H., and Lu, Y. (1999) Engineering cytochrome c peroxidase into cytochrome P450: The proximal effect on heme-thiolate ligation. *Journal of Inorganic Biochemistry*. **74**, 297-297.

Simgen, B., Contzen, J., Schwarzer, R., Bernhardt, R. and Jung, C. (2000) Substrate binding to 15 beta-hydroxylase (CYP106A2) probed by FT infrared spectroscopic studies of the iron ligand CO stretch vibration. *Biochemical and Biophysical Research Communications*. **269**, 737-742.

Simonsen, R. P. and Tollin, G. (1980) Structure-function relations in flavodoxins. *Mol Cell Biochem*. **33**, 13-24

Singer T.P., and Edmundson D.E., (1978) Flavoproteins (Overview) in *Methods in Enzymology* **53**, Academic Press, London.

Singer, G. M., and Lijinsky, W. (1976). Naturally occurring nitrosatable amines. II. Secondary amines in tobacco and cigarette smoke condensate. *J Agric Food Chem*. **24**, 553-555.

Singer, P. T., Smalas, A., Carty, R. P., Mangel, W. F. and Sweet, R. M. (1993) The Hydrolytic Water Molecule in Trypsin, Revealed by Time-Resolved Laue Crystallography. *Science*. **259**, 669-673.

Sirakova, T. D., Thirumala, A. K., Dubey, V. S., Sprecher, H., and Kolattukudy, P. E. (2001) The *Mycobacterium tuberculosis* *pks2* gene encodes the synthase for the hepta- and octamethyl-branched fatty acids required for sulfolipid synthesis. *Journal of Biological Chemistry*. **276**, 16833-16839.

Slayden, R. A. and Barry, C. E. (2000) The genetics and biochemistry of isoniazid resistance in *Mycobacterium tuberculosis*. *Microbes and Infection*. **2**, 659-669.

Sligar S.G. (1999) Natures Universal Oxygenases: the Cytochromes P450, in *Essays in Biochemistry – Metalloproteins* 34, (Ballou D.P ed.) Princeton University Press, New Jersey.  
Sligar, S. G. (1976) Coupling of spin, substrate, and redox equilibria in cytochrome P450. *Biochemistry*. **15**, 5399-5406.

Sligar, S. G. and Gunsalus, I. C. (1976) A thermodynamic model of regulation: modulation of redox equilibria in camphor monooxygenase. *Proceedings of the National Academy of Sciences of the United States of America*. **73**, 1078-1082.

Small, P. M., Shafer, R. W., Hopewell, P. C., Singh, S. P., Murphy, M. J., Desmond, E., Sierra, M. F., and Schoolnik, G. K. (1993) Exogenous reinfection with multidrug-resistant *Mycobacterium tuberculosis* in patients with advanced HIV infection. *N Engl J Med*. **328**, 1137-1144.

Smulevich, G. (1998) Understanding heme cavity structure of peroxidases: Comparison of electronic absorption and resonance Raman spectra with crystallographic results. *Biospectroscopy*. **4**, S3-S17.

Snider, D. E., Good, R. C., Kilburn, J. O., Laskowski, L. F., Lusk, R. H., Marr, J. J., Reggiardo, Z. and Middlebrook, G. (1981) Rapid Drug-Susceptibility Testing of *Mycobacterium-Tuberculosis*. *American Review of Respiratory Disease*. **123**, 402-406.

Snyder, D. S., and Small, P. L. (2003) Uptake and cellular actions of mycolactone, a virulence determinant for *Mycobacterium ulcerans*. *Microb Pathog*. **34**, 91-101.

Song, X., Jentzen, W., Jia, S., Jaquinod, L. A., Nurco, D. J., Medforth, G. J., Smith, K. M. and Shelnutt, J. A. (1996) Nonplanar distortions of nickel(II) dialkylporphyrins along combinations of the lowest-frequency out-of-plane normal coordinates. *Biophysical Journal*. **70**, Mpmg4-Mpmg4.

Sono, M., Stuehr, D. J., Ikeda-saito, M., and Dawson, J. H. (1995) Identification of Nitric-Oxide Synthase as a Thiolate-Ligated Heme Protein Using Magnetic Circular-Dichroism Spectroscopy - Comparison with Cytochrome P-450-Cam and Chloroperoxidase. *Journal of Biological Chemistry*. **270**, 19943-19948.

Souter, A., McLean, K. J., Smith, W. E., and Munro, A. W. (2000) The genome sequence of *Mycobacterium tuberculosis* reveals cytochromes P450 as novel anti-TB drug targets. *Journal of Chemical Technology and Biotechnology*. **75**, 933-941.

Spain, J C, Hughes E J, and Knackmuss H-J. (2000). *Biodegradation of nitroaromatic compounds and explosives*. Boca Raton, Fla: Lewis Publishers.

Spiro, T. G.; and Li, X.-Y. In *Biological Applications of Raman Spectroscopy*; Spiro, T., Ed.; Wiley: New York, 1988; **3**, pp 1-37.

Springer, B., Kidan, Y. G., Prammananan, T., Ellrott, K., Bottger, E. C., and Sander, P. (2001) Mechanisms of streptomycin resistance: Selection of mutations in the 16S rRNA gene conferring resistance. *Antimicrobial Agents and Chemotherapy*. **45**, 2877-2884.

Sreerema, N., Venyaminov, S.Y., and Woody, R.W. (1999) Estimation of the number of helical and strand segments in proteins using CD spectroscopy. *Protein Sci*. **8**, 370-380.

- Sreevatsan, S., Pan, X., Stockbauer, K. E., Williams, D. L., Kreiswirth, B. N., and Musser, J. M. (1996) Characterization of *rpsL* and *rrs* mutations in streptomycin-resistant *Mycobacterium tuberculosis* isolates from diverse geographic localities. *Antimicrob Agents Chemother.* **40**, 1024-1026.
- Sreevatsan, S., Pan, X., Zhang, Y., Deretic, V., and Musser, J. M. (1997a) Analysis of the oxyR-ahpC region in isoniazid-resistant and -susceptible *Mycobacterium tuberculosis* complex organisms recovered from diseased humans and animals in diverse localities. *Antimicrobial Agents and Chemotherapy.* **41**, 600-606.
- Sreevatsan, S., Stockbauer, K. E., Pan, X., Kreiswirth, B. N., Moghazeh, S. L., Jacobs, W. R., Telenti, A., and Musser, J. M. (1997b) Ethambutol resistance in *Mycobacterium tuberculosis*: Critical role of *embB* mutations. *Antimicrobial Agents and Chemotherapy.* **41**, 1677-1681.
- Stanford, J. L., and Phillips, I. (1972) Rifampicin in Experimental *Mycobacterium-Ulcerans* Infection. *Journal of Medical Microbiology.* **5**, 39-45.
- Staunton, J., and Weissman, K. J. (2001). Polyketide biosynthesis: a millennium review. *Nat Prod Rep* **18**, 380-416.
- Steele, M. A., and Des Prez, R. M. (1988) The Role of Pyrazinamide in Tuberculosis Chemotherapy. *Chest* **94**, 845-850.
- Stephens, P. J. (1974) Magnetic Circular-Dichroism. *Annual Review of Physical Chemistry.* **25**, 201-232.
- Stevenson, J. A., Jones, J. P. and Wong, L. L. (2000) Mutations of phenylalanine-193 in the putative substrate access channel alter the substrate specificity of cytochrome P450(cam). *Israel Journal of Chemistry.* **40**, 55-62.
- Stiborova, M., Borek-Dohalska, L., Hodek, P., Mraz, J. and Frei, E. (2002) New selective inhibitors of cytochromes P450 2B and their application to antimutagenesis of tamoxifen. *Arch Biochem Biophys.* **403**, 41-49.
- Stinear, T. P., Hong, H., Frigui, W., Pryor, M. J., Brosch, R., Garnier, T., Leadlay, P. F. and Cole, S. T. (2005) Common evolutionary origin for the unstable virulence plasmid pMUM found in geographically diverse strains of *Mycobacterium ulcerans*. *Journal of bacteriology.* **187**, 1668-1676
- Stinear, T. P., Jenkin, G. A., Johnson, P. D., and Davies, J. K. (2000) Comparative genetic analysis of *Mycobacterium ulcerans* and *Mycobacterium marinum* reveals evidence of recent divergence. *J Bacteriol* **182**, 6322-6330.
- Stinear, T. P., Mve-Obiang, A., Small, P. L., Frigui, W., Pryor, M. J., Brosch, R., Jenkin, G. A., Johnson, P. D., Davies, J. K., Lee, R. E., Adusumilli, S., Garnier, T., Haydock, S. F., Leadlay, P. F., and Cole, S. T. (2004) Giant plasmid-encoded polyketide synthases produce the macrolide toxin of *Mycobacterium ulcerans*. *Proc Natl Acad Sci U S A.* **101**, 1345-1349.
- Stinear, T., Ross, B. C., Davies, J. K., Marino, L., Robins-Browne, R. M., Oppedisano, F., Sievers, A., and Johnson, P. D. R. (1999). Identification and characterization of IS2404 and

IS2606: Two distinct repeated sequences for detection of *Mycobacterium ulcerans* by PCR. *Journal of Clinical Microbiology*. **37**, 1018-1023.

Stok, J. E., and De Voss, J. J. (2000) Expression, purification, and characterization of biol: A carbon-carbon bond cleaving cytochrome P450 involved in biotin biosynthesis in *Bacillus subtilis*. *Archives of Biochemistry and Biophysics*. **384**, 351-360.

Stopforth, A., Tredoux, A., Crouch, A., van Helden, P. and Sandra, P. (2005) A rapid method of diagnosing pulmonary tuberculosis using stir bar sorptive extraction-thermal desorption-gas chromatography-mass spectrometry. *Journal of chromatography*. **1071**, 135-139.

Stover, C. K., Warrener, P., VanDevanter, D. R., Sherman, D. R., Arain, T. M., Langhorne, M. H., Anderson, S. W., Towell, J. A., Yuan, Y., McMurray, D. N., Kreiswirth, B. N., Barry, C. E., and Baker, W. R. (2000) A small-molecule nitroimidazopyran drug candidate for the treatment of tuberculosis. *Nature*. **405**, 962-966.

Strobel, S. M., Szklarz, G. D., He, Y., Foroozesh, M., Alworth, W. L., Roberts, E. S., Hollenberg, P. F. and Halpert, J. R. (1999) Identification of selective mechanism-based inactivators of cytochromes P-450 2B4 and 2B5, and determination of the molecular basis for differential susceptibility. *J Pharmacol Exp Ther*. **290**, 445-451.

Studier F.W. and Moffat B.A. (1986) Use of a bacteriophage T7 RNA polymerase to direct selective high-level expression of cloned genes. *Journal of Molecular Biology*. **189**, 113-130.

Sun, Z., and Zhang, Y., (1999) Antitubercular activities of certain antifungal and antihelminthic drugs. *Tuber Lung Dis*. **79**, 319-320.

Suzuki, K., and Mitsuoka, T. (1984) N-nitrosamine formation by intestinal bacteria. *IARC Sci Publ*. **57**, 275-281.

Swain, A., Waterhouse, K. V., Venables, W. A., Callely, A. G., and Lowe, S. E. (1991) Biochemical-Studies of Morpholine Catabolism by an Environmental *Mycobacterium*. *Applied Microbiology and Biotechnology*. **35**, 110-114.

Szklarz, G. D., and Halpert, J. R. (1998) Molecular basis of P450 inhibition and activation - Implications for drug development and drug therapy. *Drug Metabolism and Disposition*. **26**, 1179-1184.

Takayama, K., and Kilburn, J. O. (1989) Inhibition of Synthesis of Arabinogalactan by Ethambutol in *Mycobacterium-Smegmatis*. *Antimicrobial Agents and Chemotherapy*. **33**, 1493-1499.

Takayama, K., Wang, C. and Besra, G. S. (2005) Pathway to synthesis and processing of mycolic acids in *Mycobacterium tuberculosis*. *Clinical Microbiology Reviews*. **18**, 81-101.

Tanghe, A., Content, J., Van Vooren, J. P., Portaels, F., and Huygen, K. (2001) Protective efficacy of a DNA vaccine encoding antigen 85A from *Mycobacterium bovis* BCG against Buruli ulcer. *Infect Immun*. **69**, 5403-5411.

Taraphder, S., and Hummer, G. (2003). Protein side-chain motion and hydration in proton-transfer pathways. Results for cytochrome P450cam. *Journal of the American Chemical Society*. **125**, 3931-3940.

- Telenti, A., Honore, N., Bernasconi, C., March, J., Ortega, A., Heym, B., Takiff, H. E., and Cole, S. T. (1997a) Genotypic assessment of isoniazid and rifampin resistance in *Mycobacterium tuberculosis*: A blind study at reference laboratory level. *Journal of Clinical Microbiology*. **35**, 719-723.
- Telenti, A., Imboden, P., Marchesi, F., Lowrie, D., Cole, S., Colston, M. J., Matter, L., Schopfer, K., and Bodmer, T. (1993b) Detection of Rifampicin-Resistance Mutations in *Mycobacterium-Tuberculosis*. *Lancet* **341**, 647-650.
- Telenti, A., Philipp, W. J., Sreevatsan, S., Bernasconi, C., Stockbauer, K. E., Wieles, B., Musser, J. M., and Jacobs, W. R. (1997) The emb operon, a gene cluster of *Mycobacterium tuberculosis* involved in resistance to ethambutol. *Nature Medicine*. **3**, 567-570.
- Telzak, E. E., Sepkowitz, K., Alpert, P., Mannheimer, S., Medard, F., Elsadr, W., Blum, S., Gagliardi, A., Salomon, N., and Turett, G. (1995) Multidrug-Resistant Tuberculosis in Patients without HIV-Infection. *New England Journal of Medicine*. **333**, 907-911.
- Terrand, J. J. (1985) Evaluation of the BACTEC radiometric method for detection of 1% resistant populations of *Mycobacterium tuberculosis*. *Journal of clinical microbiology*. **21**, 941-6.
- Terwillinger T.C., and Berenzdon J. (1999) Automated MAD and MIR structure solution. *Acta Crystallographica*. **D55**, 849-861.
- Thangaraj, H. S., Adjei, O., Allen, B. W., Portaels, F., Evans, M. R., Banerjee, D. K., and Wansbrough-Jones, M. H. (2000) In vitro activity of ciprofloxacin, sparflaxacin, ofloxacin, amikacin and rifampicin against Ghanaian isolates of *Mycobacterium ulcerans*. *J Antimicrob Chemother*. **45**, 231-233.
- Tiehm, A., and Fritzsche, C. (1995). Utilization of Solubilized and Crystalline Mixtures of Polycyclic Aromatic-Hydrocarbons by a *Mycobacterium* Sp. *Applied Microbiology and Biotechnology*. **42**, 964-968.
- Timmis, K. N., and Pieper, D. H. (1999). Bacteria designed for bioremediation. *Trends Biotechnol*. **17**, 200-204.
- Timms, A. R., Steingrimsdottir, H., Lehmann, A. R., and Bridges, B. A. (1992) Mutant Sequences in the RpsL Gene of *Escherichia-Coli* B/R - Mechanistic Implications for Spontaneous and Ultraviolet-Light Mutagenesis. *Molecular and General Genetics*. **232**, 89-96.
- Toivonen, J. M., Boocock, M. R., and Jacobs, H. T. (1999) Modelling in *Escherichia coli* of mutations in mitoribosomal protein S12: novel mutant phenotypes of rpsL. *Molecular Microbiology*. **31**, 1735-1746.
- Tolgyessy, P., Kollar, M., Vanco, D., and Piatrik, M. (1986). The Effect of Gamma-Radiation on Biodegradability of Morpholine in Aqueous-Solution. *Journal of Radioanalytical and Nuclear Chemistry-Letters*. **107**, 291-295.
- Trigui, M., Pulvin, S., Poupin, P. and Thomas, D. (2003) Biodegradation of cyclic amines by a *Pseudomonas* strain involves an amine mono-oxygenase. *Canadian Journal of Microbiology*. **49**, 181-188.

Trigui, M., Pulvin, S., Truffaut, N., Thomas, D., and Poupin, P. (2004). Molecular cloning, nucleotide sequencing and expression of genes encoding a cytochrome P450 system involved in secondary amine utilization in *Mycobacterium* sp. strain RP1. *Res Microbiol* **155**, 1-9.

Trott, K. A., Stacy, B. A., Lifland, B. D., Diggs, H. E., Harland, R. M., Khokha, M. K., Grammer, T. C., and Parker, J. M. (2004) Characterization of a *Mycobacterium ulcerans*-like infection in a colony of African tropical clawed frogs (*Xenopus tropicalis*). *Comp Med* **54**, 309-317.

Trower, M. K., Lenstra, R., Omer, C., Buchholz, S. E., and Sariaslani, F. S. (1992) Cloning, Nucleotide-Sequence Determination and Expression of the Genes Encoding Cytochrome P-450Soy (Soyc) and Ferredoxinsoy (Soyb) from *Streptomyces-Griseus*. *Molecular Microbiology*. **6**, 2125-2134.

Tsai, A. L., Berka, V., Chen, P. F., and Palmer, G. (1996) Characterization of endothelial nitric-oxide synthase and its reaction with ligand by electron paramagnetic resonance spectroscopy. *The Journal of Biological Chemistry*. **271**, 32563-32571.

Turcotte, M.G. and Johnson T.A. (1992). Amines (Lower aliphatic), in *Kirk-Othmer Encyclopedia of Chemical Technology*. **2**, 369-386.

Uchida, T., Mogi, T., Nakamura, H. and Kitagawa, T. (2004) Role of Tyr-288 at the dioxygen reduction site of cytochrome bo studied by stable isotope labeling and resonance Raman spectroscopy. *Journal of Biological Chemistry*. **279**, 53613-53620.

Uhlmann, H., Kraft, R. and Bernhardt, R. (1994) C-terminal region of adrenodoxin affects its structural integrity and determines differences in its electron transfer function to cytochrome P-450. *J Biol Chem*. **269**, 22557-22564.

Unno, M., Christian, J. F., Sjodin, T., Benson, D. E., Macdonald, I. D., Sligar, S. G. and Champion, P. M. (2002) Complex formation of cytochrome P450cam with Putidaredoxin. Evidence for protein-specific interactions involving the proximal thiolate ligand. *The Journal of biological chemistry*. **277**, 2547-2553.

Urlacher, V. B., Lutz-Wahl, S. and Schmid, R. D. (2004) Microbial P450 enzymes in biotechnology. *Applied microbiology and biotechnology*. **64**, 317-325.

Van der Werf, T. S., Stienstra, Y., Johnson, R. C., Phillips, R., Adjei, O., Fleischer, B., Wansbrough-Jones, M. H., Johnson, P. D., Portaels, F., van der Graaf, W. T., and Asiedu, K. (2005). *Mycobacterium ulcerans* disease. *Bull World Health Organ* **83**, 785-791.

Van der Werf, T. S., van der Graaf, W. T. A., Tappero, J. W., and Asiedu, K. (1999). *Mycobacterium ulcerans* infection. *Lancet*. **354**, 1013-1018.

Vaz, A. D. N., McGinnity, D. F., and Coon, M. J. (1998) Epoxidation of olefins by cytochrome P450: Evidence from site-specific mutagenesis for hydroperoxo-iron as an electrophilic oxidant. *Proceedings of the National Academy of Sciences of the United States of America*. **95**, 3555-3560.

Vickery, L., Nozawa, T., and Sauer, K. (1976) Magnetic Circular-Dichroism Studies of Low-Spin Cytochromes - Temperature-Dependence and Effects of Axial Coordination on Spectra of Cytochrome-C and Cytochrome B5. *Journal of the American Chemical Society*. **98**, 351-357.

Vickery, L., Salmon, A., and Sauer, K. (1975) Magnetic Circular-Dichroism Studies on Microsomal Aryl-Hydrocarbon Hydroxylase - Comparison with Cytochrome B5 and Cytochrome P-450Cam. *Biochimica Et Biophysica Acta.* **386**, 87-98.

Vidakovic, M., Sligar, S. G., Li, H. Y., and Poulos, T. L. (1998) Understanding the role of the essential Asp251 in cytochrome P450cam using site-directed mutagenesis, crystallography, and kinetic solvent isotope effect. *Biochemistry.* **37**, 9211-9219.

Vieira J, Messing J. (1987) Production of single-stranded plasmid DNA, *Methods in Enzymology* **153**, 3-11. Academic Press, UK.

Villeneuve, C., Etienne, G., Abadie, V., Montrozier, H., Bordier, C., Laval, F., Daffe, M., Maridonneau-Parini, I. and Astarie-Dequeker, C. (2003) Surface-exposed glycopeptidolipids of *Mycobacterium smegmatis* specifically inhibit the phagocytosis of mycobacteria by human macrophages - Identification of a novel family of glycopeptidolipids. *Journal of Biological Chemistry.* **278**, 51291-51300.

Vincke, G., Yegers, O., Vanachter, H., Jenkins, P. A. and Butzler, J. P. (1982) Rapid Susceptibility Testing of Mycobacterium-Tuberculosis by a Radiometric Technique. *Journal of Antimicrobial Chemotherapy.* **10**, 351-354.

Wackett, L. P., Brusseau, G. A., Householder, S. R., and Hanson, R. S. (1989). Survey of microbial oxygenases: trichloroethylene degradation by propane-oxidizing bacteria. *Appl Environ Microbiol.* **55**, 2960-2964.

Wade, M. M., and Zhang, Y. (2004) Mechanisms of drug resistance in *Mycobacterium tuberculosis*. *Front Biosci.* **9**, 975-994.

Wade, R. C., Winn, P. J., Schlichting, I. and Sudarko. (2004) A survey of active site access channels in cytochromes P450. *J Inorg Biochem.* **98**, 1175-1182.

Wang, H. P., and Kimura, T. (1976) Purification and Characterization of Adrenal-Cortex Mitochondrial Cytochrome-P-450 Specific for Cholesterol Side-Chain Cleavage Activity. *Journal of Biological Chemistry.* **251**, 6068-6074.

Waterman M.R., and Johnson E.F. (1991) Cytochrome P450, in *Methods in Enzymology* **206**, Academic Press, UK.

Wayne, L. G. (1994) Dormancy of *Mycobacterium tuberculosis* and latency of disease. *Eur J Clin Microbiol Infect Dis* **13**, 908-914.

Weaver, G. C., Schwenz, R. W. (2001) The Raman Effect: A Large-Scale Lecture Demonstration. *Chemical Educator.* **6**, 164-167.

Wengenack, N. L., Uhl, J. R., Amand, A. L. S., Tomlinson, A. J., Benson, L. M., Naylor, S., Kline, B. C., Cockerill, F. R., and Rusnak, F. (1997). Recombinant *Mycobacterium tuberculosis* KatG(S315T) is a competent catalase-peroxidase with reduced activity toward isoniazid. *Journal of Infectious Diseases.* **176**, 722-727.

Wheeler, P. R. and Ratledge, C. in *Tuberculosis: Pathogenesis, Protection, and Control* (ed. Bloom, B. R.) 353-385 (Am. Soc. Microbiol., Washington DC, (1994).

White, R. E., and Coon, M. J. (1980) Oxygen Activation by Cytochrome-P-450. *Annual Review of Biochemistry*. **49**, 315-356.

White, R. E., McCarthy, M. B., Egeberg, K. D. and Sligar, S. G. (1984) Regioselectivity in the cytochromes P-450: control by protein constraints and by chemical reactivities. *Arch Biochem Biophys*. **228**, 493-502.

White, S. W., Zheng, J., Zhang, Y. M., and Rock, C. O. (2005). The structural biology of type II fatty acid biosynthesis. *Annual Review of Biochemistry*. **74**, 791-831.

WHO (1998), World Health Organisation targets untreatable ulcer: report from the first international conference on Buruli ulcer control and research, Inter Press Service, Yamoussoukro, Ivory Coast.

Williams P.A., Cosme J., Ward A., Angove H.C., Matak Vinkovic D., Jhoti, H. (2003) Crystal Structure of Human Cytochrome P450 2C9 with Bound Warfarin, *Nature*. **424**, 464-470.

Wilson G. S. (1978) Determination of oxidation-reduction potentials, *Methods in Enzymology* **54**, 396-410. Academic Press, UK.

Wilson, L. G. (1990). The historical decline of tuberculosis in Europe and America: its causes and significance. *J Hist Med Allied Sci*. **45**, 366-396.

Wilson, T. M., and Collins, D. M. (1996). *ahpC*, a gene involved in isoniazid resistance of the *Mycobacterium tuberculosis* complex. *Molecular Microbiology*. **19**, 1025-1034.

Wirtz, M., Oganessian, V., Zhang, X., Studer, J. and Rivera, M. (2000) Modulation of redox potential in electron transfer proteins: effects of complex formation on the active site microenvironment of cytochrome b5. *Faraday discussions*, 221-234; discussion 257-268.

Wolucka, B. A., Mcneil, M. R., Dehoffmann, E., Chojnacki, T., and Brennan, P. J. (1994). Recognition of the Lipid Intermediate for Arabinogalactan Arabinomannan Biosynthesis and Its Relation to the Mode of Action of Ethambutol on Mycobacteria. *Journal of Biological Chemistry*. **269**, 23328-23335.

Wong, L. L. (1998) Cytochrome P450 monooxygenases. *Current Opinion in Chemical Biology*. **2**, 263-268.

Woodley, C. L. (1986) Evaluation of streptomycin and ethambutol concentrations for susceptibility testing of *Mycobacterium tuberculosis* by radiometric and conventional procedures. *Journal of clinical microbiology*. **23**, 385-386.

World Health Organization (WHO) (1995). *Morpholine: Health and Safety Guide*, World Health Organization, Geneva, Switzerland.

World Health Organization. (2001) *Global tuberculosis control: WHO report*. Geneva, Switzerland, WHO/CDS/TB/2001.287; 1-2.



Wu, S. D., Fluxe, A., Janusz, J. M., Sheffer, J. B., Browning, G., Blass, B., Cobum, K., Hedges, R., Murawsky, M., Fang, B., Fadayel, G. M., Hare, M. and Djandjighian, L. (2006) Discovery and synthesis of tetrahydroindolone derived semicarbazones as selective Kv1.5 blockers. *Bioorganic and Medicinal Chemistry Letters*. **16**, 5859-5863.

Xiang, H., Tschirret-Guth, R. A. and Ortiz De Montellano, P. R. (2000) An A245T mutation conveys on cytochrome P450eryF the ability to oxidize alternative substrates. *The Journal of biological chemistry*. **275**, 35999-36006.

Yarkoni, E., Goren, M. B., and Rapp, H. J. (1979). Effect of Sulfolipid-I on Trehalose-6,6'-Dimycolate (Cord Factor) Toxicity and Anti-Tumor Activity. *Infection and Immunity*. **24**, 586-588.

Yeh, P. and Kuwana, T. (1977) Reversible Electrode-Reaction of Cytochrome-C. *Chemistry Letters*, 1145-1148.

Yeom, H., Sligar, S. G., Li, H., Poulos, T. L. and Fulco, A. J. (1995) The role of Thr268 in oxygen activation of cytochrome P450BM-3. *Biochemistry*. **34**, 14733-14740.

Young, D. B., and Garbe, T. R. (1991) Lipoprotein Antigens of *Mycobacterium-Tuberculosis*. *Research in Microbiology*. **142**, 55-65.

Yu, C. A., Gunsalus, I. C., Katagiri, M., Suhara, K., and Takemori, S. (1974) Cytochrome P-450Cam.1. Crystallization and Properties. *Journal of Biological Chemistry*. **249**, 94-101.

Zbylut, S. D. and Kincaid, J. R. (2002) Resonance Raman evidence for protein-induced out-of-plane distortion of the heme prosthetic group of mammalian lactoperoxidase. *Journal of the American Chemical Society*. **124**, 6751-6758.

Zerbe K., Pylypenko O., Vitali F., Zhang W., Rouset S., Heck M., Vrijbloed J.W., Bischoff D., Bister B., Sussmuth R.D., Pelzer S., Wohlleben W., Robinson J.A., Schlichting I. (2002) Crystal Structure of Oxyb, a Cytochrome P450 Implicated in an Oxidative Phenol Coupling Reaction During Vancomycin Biosynthesis. *Journal of Biological Chemistry*. **277**, 47476-47485.

Zhang Y and Telenti A (2000) Genetics of drug resistance in *Mycobacterium tuberculosis*. *Molecular Genetics of Mycobacteria* (Hatfull GF and Jacobs WR Jr, eds), ASM Press, Washington, DC.

Zhang, Y., Dhandayuthapani, S. and Deretic, V. (1996) Molecular basis for the exquisite sensitivity of *Mycobacterium tuberculosis* to isoniazid. *Proceedings of the National Academy of Sciences of the United States of America*. **93**, 13212-13216.

Zhang, Y., Heym, B., Allen, B., Young, D., and Cole, S. (1992). The Catalase Peroxidase Gene and Isoniazid Resistance of *Mycobacterium-Tuberculosis*. *Nature*. **358**, 591-593.

Zhang, Y., Scorpio, A., Nikaido, H., and Sun, Z. H. (1999) Role of acid pH and deficient efflux of pyrazinoic acid in unique susceptibility of *Mycobacterium tuberculosis* to pyrazinamide. *Journal of Bacteriology*. **181**, 2044-2049.

Zimhony, O., Cox, J. S., Welch, J. T., Vilcheze, C., and Jacobs, W. R. (2000) Pyrazinamide inhibits the eukaryotic-like fatty acid synthetase I (FASI) of *Mycobacterium tuberculosis*. *Nature Medicine*. **6**, 1043-1047.

Zumft, W. G. (1997) Cell biology and molecular basis of denitrification. *Microbiology and Molecular Biology Reviews.* **61**, 533-616.